

Elucidation of Imamoto's Organocerium Reagent

DISSERTATION

der Mathematisch-Naturwissenschaftlichen Fakultät
der Eberhard Karls Universität Tübingen
zur Erlangung des Grades eines
Doktors der Naturwissenschaften
(Dr. rer. nat.)

vorgelegt von
M. Sc. Tassilo Berger
aus Waiblingen

Tübingen
2022

Gedruckt mit Genehmigung der Mathematisch-Naturwissenschaftlichen Fakultät der Eberhard Karls Universität Tübingen.

Tag der mündlichen Qualifikation:

20.12.2022

Dekan:

Prof. Dr. Thilo Stehle

1. Berichterstatter:

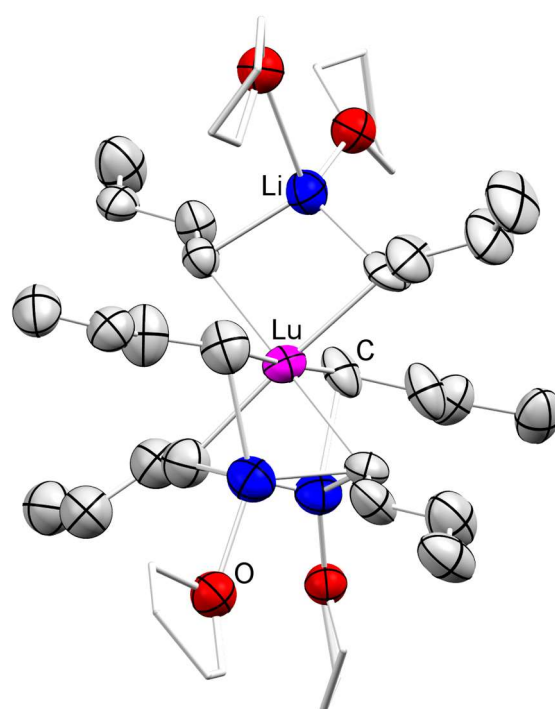
Prof. Dr. Reiner Anwander

2. Berichterstatter:

Prof. Dr. Michael Seitz

Elucidation of Imamoto's Organocerium Reagent

Tassilo Berger



Preface

The following doctoral dissertation consists of a survey on rare-earth-metal alkyls and isolated organoalumoxanes, a summary of the main results, and original scientific papers. The work has been carried out at the Institut für Anorganische Chemie of the Eberhard Karls Universität Tübingen, Germany, over the period from January 2020 to December 2022 under the supervision of Prof. Dr. Reiner Anwänder.

Acknowledgments

First of all, I would like to thank my supervisor Prof. Dr. Reiner Anwander. Thank you for accepting me into your laboratory, providing me with an interesting research topic, and for your scientific insight when problems arose. But most of all thank you for giving me the scientific freedom to pursue topics like methylaluminumoxane, which piqued my interest even though they had little to nothing to do with my primary research topic. And finally, thank you for giving me the great opportunity for a research trip to Polly L. Arnolds group in Berkeley.

Special thanks go to Dr. Cécilia Maichle-Mössmer for measuring and calculating my crystal structures which never was easy with all those temperature-sensitive complexes.

My thanks also go to Dr. Klaus Eichele and Kristina Strohmaier for maintaining the high standard equipment, as well as their help in all aspects regarding NMR spectroscopy. Additionally, I'd like to thank Dr. Markus Kramer for conducting the DOSY NMR experiments, Wolfgang Bock and Mohammad Ghani for performing elemental analyses, and Dr. Jochen Glaser for the ICP measurements.

I further thank Tobias Wolf and especially Elke Niquet for their maintaining the laboratory equipment and their friendly and always helpful nature. Many thanks to Sabine Ehrlich for all her administrative work especially for her helpful and friendly demeanor for any question regarding forms and applications. Additionally, I want to thank the staff of the metal, electronics, and glass workshops for manufacturing and repairing lab equipment.

I also would like to thank my current and former coworkers of the Anwander group. Especially Jakob Lebon my glovebox colleague for the great time working together. Alexandros Mortis for proofreading my first paper and for the helpful answers to a lot of questions I had during the beginning of my work. Further thanks go to everyone else, Dennis Buschmann, Markus Katzenmayer, Felix Kracht, Eric Moinet, Theresa Rieser, Georgios Spiridopoulos, Simon Trzmiel, Yali Yang, Olga Mironova, Jonas Riedmaier, Gernot Zug, Simon Matt, Dr. Dorothea Schädle, Dr. Yucang Liang, Dr. Manfred Manßen, Dr. David Schneider, Dr. Uwe Bayer, Dr. Verena Birkelbach, Dr. Lorenz Bock, Damir Barisic, Denis Burghardt, Dr. Dominic Diether, Dr. Christoph Hollfelder, Dr. Christoph Stuhl and Dr. Lars Hirneise. Thank you for the great discussions, serious and less serious, for the help you gave me, for the great activities outside our work, and for just making our time together actually enjoyable even during a pandemic.

Zu guter Letzt gilt mein unendlicher Dank meiner Familie. Worin sie mich überall unterstützt haben und in welchem Umfang würde jeden Rahmen hier sprengen deswegen einfach nur Danke Walli, Uli und Nora Berger!

Contents

Preface	I
Acknowledgments	II
Contents	III
Abbreviations	IV
Summary	V
Zusammenfassung	VI
Publications and Manuscripts	VII
Personal Contribution	VIII
The Objective of this Thesis	X
A. Imamoto's Organocerium Reagent	1
1 Introduction	2
2 Imamoto's findings on the organocerium compounds	4
3 Studies on Imamoto's Organocerium Reagent.....	7
4 Imamoto's Organocerium Reagent in modern chemistry	12
B. Summary of the Main Results	14
1 Unraveling Imamoto's Organocerium Reagent.....	15
2 Isolation of a MAO species from the reaction of water with AlMe ₃	25
C. Unpublished Results	27
1 Cerium aluminate cluster.....	28
2 Experimental Section.....	31
D. Bibliography	35
E. Publications	40
F. Appendix	223

Abbreviations

Ar	Aryl	Ln	Rare-earth metals (Sc, Y, La – Lu)
Aza crown	1,4,7-Trimethyl-1,4,7-triazacyclononane	MAO	Methylaluminoxane
Bn	Benzyl	Me	Methyl
<i>i</i> Bu	<i>iso</i> -Butyl	Me ₃ TACN	1,4,7-Trimethyl-1,4,7-triazacyclononane
<i>n</i> Bu	<i>n</i> -Butyl	Mes	Mesitylene
<i>t</i> Bu	<i>tert</i> -Butyl	Nacnac	1,3-Diketiminato
COSY	Correlated Spectroscopy	Neosilyl	CH ₂ SiMe ₃
Cp*	C ₅ Me ₅	NMR	Nuclear Magnetic Resonance
Dipp	2,6-Diisopropylphenyl	Ph	Phenyl
do	Donor	<i>i</i> Pr	<i>iso</i> -Propyl
DOSY	Diffusion-Ordered Spectroscopy	r.t.	Ambient temperature
EA	Elemental Analysis	TMEDA	Tetramethylethylenediamine
Et ₂ O	Diethyl ether	THF	Tetrahydrofuran
et al.	<i>et alii</i> or <i>et aliae</i>	vs.	versus
HSQC	Heteronuclear Single Quantum Coherence	VT	Variable Temperature

Summary

In 1984 Tsueno Imamoto published a paper about the binary mixtures CeCl_3/RLi ($\text{R} = n\text{Bu}$, $t\text{Bu}$) and their use in carbon-carbon-bond formation with various carbonyl compounds. The exact structure of these reagents, however, remained a mystery since then.

These mixtures were studied via NMR experiments including ^7Li NMR spectroscopy. Moreover, a procedure was developed to isolate organolithium/lanthanide complexes from these reactions. For example, $\text{Li}_3\text{Ln}(n\text{Bu})_6(\text{thf})_4$ ($\text{Ln} = \text{Sc}$, Y , La , Ce , Lu) and $[\text{Ce}(t\text{Bu})_4][\text{Li}(\text{thf})_4]$ could be accessed and fully characterized. The crucial part of these procedures is a seamless low-temperature syntheses and crystallization sequence, since the products are thermally very unstable.

The working techniques were then applied to isolate the MAO species $[(\text{AlMe}_2)_2\text{O}(\text{thf})]_2$ from the simple reaction of AlMe_3 and water in THF. MAO is the most important co-catalyst in commercial α -olefin polymerization. Although, its structure has remained elusive so far, many model complexes have been synthesized. These complexes, however, require laborious pathways or exotic precursors.

Lastly, the field of organolanthanide complexes was revisited. Using the aza crown (1,4,7-Trimethyl-1,4,7-triazacyclononane = Me_3TACN) the complexes $(\text{Me}_3\text{TACN})\text{Ln}(n\text{Bu})_3$ ($\text{Ln} = \text{La}$, Sm) could be synthesized as the first terminal n -butyl lanthanide complexes, that contain no other metal. Further, the hitherto elusive lanthanum neosilyl complex $[\text{Li}(\text{thf})_4][\text{La}(\text{CH}_2\text{SiMe}_3)_4(\text{thf})]$ was isolated and fully characterized.

Zusammenfassung

Im Jahre 1984 veröffentlichte Tsueno Imamoto eine Arbeit über die binären Gemische CeCl_3/RLi ($\text{R} = n\text{Bu}, t\text{Bu}$) und ihre Verwendung zur Bildung von Kohlenstoff-Kohlenstoff-Bindungen mit verschiedenen Carbonylverbindungen. Die genaue Struktur dieser Reagenzien blieb jedoch seither ein Rätsel.

Mischungen des Typs LnCl_3/RLi ($\text{Ln} = \text{Sc}, \text{Y}, \text{La}, \text{Ce}, \text{Lu}$; $\text{R} = n\text{Bu}, t\text{Bu}$) wurden mittels NMR-Experimenten einschließlich ^7Li -NMR-Spektroskopie untersucht. Dabei wurde ein Verfahren entwickelt, um Organo-Lithium/Lanthanid-Komplexe aus diesen Reaktionen zu isolieren. So konnte zum Beispiel $\text{Li}_3\text{Ln}(n\text{Bu})_6(\text{thf})_4$ ($\text{Ln} = \text{Sc}, \text{Y}, \text{La}, \text{Ce}, \text{Lu}$) und $[\text{Ce}(t\text{Bu})_4][\text{Li}(\text{thf})_4]$ vollständig charakterisiert werden. Das „Herzstück“ dieser Verfahren ist die Verwendung einer ununterbrochenen Kühlkette für die Synthese und Kristallisation, da die Produkte thermisch sehr instabil sind.

Dieselben Arbeitstechniken wurden dann angewandt, um die MAO-Spezies $[(\text{AlMe}_2)_2\text{O}(\text{thf})]_2$ aus der einfachen Reaktion von AlMe_3 und Wasser in THF zu isolieren. MAO ist der wichtigste Co-Katalysator für die kommerzielle α -Olefin Polymerisation. Da seine Struktur bis heute nicht aufgeklärt werden konnte, wurden zum besseren Verständnis bereits viele Modellkomplexe synthetisiert. Die Synthese dieser Komplexe ist jedoch umständlich oder erfordert exotische Ausgangsstoffe.

Schließlich wurde das Gebiet der Organolanthanoid-Komplexe wieder aufgegriffen. Unter Verwendung der Aza-Krone (1,4,7-Trimethyl-1,4,7-triazacyclononan = Me_3TACN) konnten die Komplexe $(\text{Me}_3\text{TACN})\text{Ln}(n\text{Bu})_3$ ($\text{Ln} = \text{La}, \text{Sm}$) als erste terminale n -Butyl-Lanthanoid-Komplexe synthetisiert werden, die kein anderes Metall enthalten. Außerdem wurde der bisher schwer fassbare Lanthan-Neosilyl-Komplex $[\text{Li}(\text{thf})_4][\text{La}(\text{CH}_2\text{SiMe}_3)_4(\text{thf})]$ isoliert und komplett charakterisiert.

Publications and Manuscripts

Publications incorporated into this thesis

- Paper I** CeCl₃/*n*-BuLi: Unraveling Imamoto's Organocerium Reagent
Tassilo Berger, Jakob Lebon, Cécilia Maichle-Mössmer, Reiner Anwander
Angew. Chem. Int. Ed. **2021**, *60*, 15622–15631
<https://doi.org/10.1002/anie.202103889>
<https://doi.org/10.1002/ange.202103889>
- Paper II** Aminolysis of Lithium/Yttrium Bimetallic Alkyls including the Solid-State
Structure of a Europium(II) *n*-Butyl Compound
Tassilo Berger, David Baschnagel, Cécilia Maichle-Mössmer, Reiner
Anwander
Z. Anorg. Allg. Chem. **2022**, e202200274
<https://doi.org/10.1002/zaac.202200274>
- Paper V** Rare-earth-metal trimethylsilylmethyl ate complexes
Alexandros Mortis, Felix Kracht, Tassilo Berger, Jakob Lebon, Cécilia Maichle-
Mössmer, Reiner Anwander
Dalton Transactions, **2023**, *52*, 44–51

Manuscripts incorporated into this thesis

- Paper III** The isolation of a MAO species from the reaction of H₂O with AlMe₃
Tassilo Berger, Markus Kramer, Cécilia Maichle-Mössmer, Reiner Anwander
manuscript
- Paper IV** Me₃TACN induced Monomeric Rare-Earth-Metal Alkyls via low-temperature
Alkylation
Jakob Lebon, Tassilo Berger, Cécilia Maichle-Mössmer, Reiner Anwander
manuscript

Personal Contribution

Paper I:

The synthesis and characterization of $\text{Li}_3\text{CeMe}_6(\text{tmeda})_3$ was performed by Jakob Lebon. All other reactions and analyses described were planned and conducted by myself. Analyses include one-dimensional (^1H , $^7\text{Li}\{^1\text{H}\}$, $^{13}\text{C}\{^1\text{H}\}$, ^{45}Sc) and multi-dimensional (^1H - ^1H COSY, ^1H - ^{13}C HSQC, ^1H - ^{89}Y HSQC) NMR spectroscopic methods. The manuscript was written by me.

Elemental analyses were performed by Wolfgang Bock. The structural analyses by single-crystal X-ray diffraction were performed by Dr. Cécilia Maichle-Mössmer.

Paper II:

All reactions and analyses described were planned by myself and conducted by my lab course student David Baschnagel and myself. Analyses include one-dimensional (^1H , $^{13}\text{C}\{^1\text{H}\}$) and multi-dimensional (^1H - ^1H COSY, ^1H - ^{13}C HSQC) NMR spectroscopic methods. Manuscript writing was also done by me.

Elemental analyses were performed by Wolfgang Bock and Mohammad Ghani. The structural analyses by single-crystal X-ray diffraction were performed by Dr. Cécilia Maichle-Mössmer.

Paper III:

All reactions and analyses described, except the DOSY NMR measurements, were planned and conducted by myself. Analyses include one-dimensional (^1H , $^{13}\text{C}\{^1\text{H}\}$) and multi-dimensional (^1H - ^1H COSY, ^1H - ^{13}C HSQC) NMR spectroscopic methods. Manuscript writing was also done by me.

Elemental analyses were performed by Mohammad Ghani and DOSY NMR measurements by Dr. Markus Kramer. The structural analyses by single-crystal X-ray diffraction were performed by Dr. Cécilia Maichle-Mössmer.

Paper IV:

All reactions and analyses described were planned and conducted by Jakob Lebon and myself. Analyses include one-dimensional (^1H , $^{13}\text{C}\{^1\text{H}\}$) and multi-dimensional (^1H - ^1H COSY, ^1H - ^{13}C HSQC) NMR spectroscopy. Manuscript writing was also done by Jakob Lebon and myself.

Elemental analyses were performed by Wolfgang Bock and Mohammad Ghani. The structural analyses by single-crystal X-ray diffraction were performed by Dr. Cécilia Maichle-Mössmer and Jakob Lebon.

Paper V:

All reactions and analyses described involving $\text{Li}_3\text{Y}(\text{CH}_2\text{SiMe}_3)_6$ were planned and conducted by Alexandros Mortis. Reactions and analysis involving $[\text{Li}(\text{thf})_4][\text{LiSc}_2(\text{CH}_2\text{SiMe}_3)_8]$ were conducted by Felix Kracht. Reactions and analysis involving $[\text{Li}(\text{thf})_4][\text{La}(\text{CH}_2\text{SiMe}_3)_4(\text{thf})]$ were conducted by Jakob Lebon and myself. Analyses include one-dimensional (^1H , ^7Li , $^{13}\text{C}\{^1\text{H}\}$, ^{13}C , ^{29}Si INEPTND, ^{45}Sc), ^1H variable temperature and multi-dimensional (^1H - ^{29}Si HSQC, ^1H - ^{89}Y HSQC NME) spectroscopic methods and DRIFT spectroscopy. The crystal structure and NMR data of $[\text{Li}(\text{thf})_4][\text{LiSc}_2(\text{CH}_2\text{SiMe}_3)_8]$ were obtained by Felix Kracht, crystal structure and NMR data of $[\text{Li}(\text{thf})_4][\text{La}(\text{CH}_2\text{SiMe}_3)_4(\text{thf})]$ were obtained by Jakob Lebon and myself. Manuscript writing was done by Alexandros Mortis except the part about $[\text{Li}(\text{thf})_4][\text{La}(\text{CH}_2\text{SiMe}_3)_4(\text{thf})]$ which was done by myself.

Elemental analyses were performed by Wolfgang Bock and Mohammad Ghani. The structural analyses by single-crystal X-ray diffraction were performed by Dr. Cécilia Maichle-Mössmer.

The Objective of this Thesis

The main emphasis of this thesis is to investigate the Imamoto Reagent $\text{CeCl}_3/n\text{-BuLi}$. A second aspect is to apply the developed cold-chain techniques to the synthesis and isolation of MAO species.

Chapter A gives an overview of Imamoto's organocerium reagent.

Chapter B contains a summary of the main results of this thesis and is divided into two parts:

- Unraveling Imamoto's Organocerium Reagent
- Isolation of a MAO species from the reaction of water with AlMe_3

In **Chapter C** unpublished results, which are not part of a publication or manuscript, are presented. This contains cerium aluminate clusters.

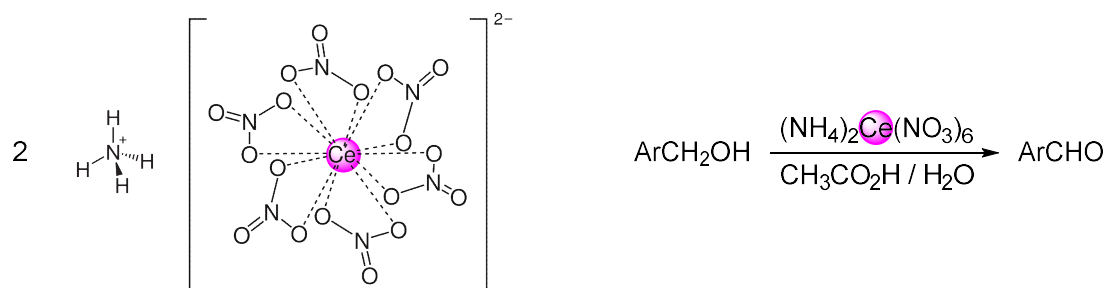
Chapter E is a compilation of publications and manuscripts.

A

**Imamoto's
Organocerium Reagent**

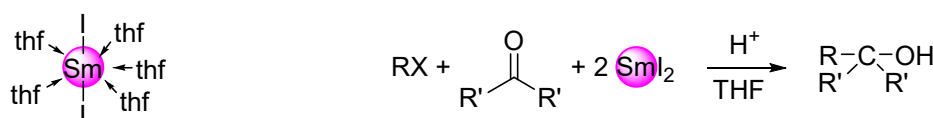
1 Introduction

Four stoichiometric rare-earth-metal reagents are commonly used in organic transformation reactions including natural product synthesis.^{[1],[2],[3],[4]} The first one discovered in 1973 by Ho et al. was CAN or *Ceric Ammonium Nitrate* which is routinely used as an oxidant.^[2a]



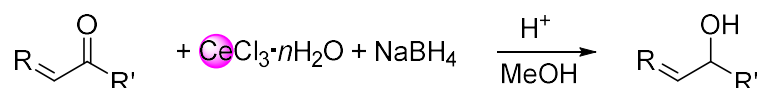
Scheme A 1: Structure of CAN (left) and an exemplary oxidation reaction using CAN (right).

The second reagent features samarium diiodide which was first employed by Namy, Girard, and Kagan in 1977.^[3a] And is often used in Barbier-type reactions.



Scheme A 2: Structure of SmI₂(thf)₅ (left) and an exemplary Barbier reaction using SmI₂ (right).

These two reagents are well understood and fully characterized including their crystal structure.^[5] Shortly after in 1978 the Luche group reported that CeCl₃ in combination with sodium borohydride can be employed as a selective reducing agent only affecting carbonyl groups.^[6]

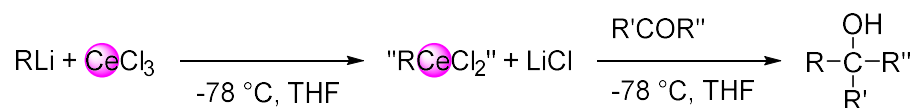


Scheme A 3: An exemplary reducing reaction using the Luche reagent.

The last of the four commonly used rare-earth-metal reagents is Imamoto's organocerium reagent.

Tsuneo Imamoto et al. reported in 1982 their findings, that when CeI₃ was added to lithium alkyls prior to the addition to enolizable ketones excellent yields of the corresponding tertiary

alcohol can be achieved. This was a contrast to employing exclusively the lithium alkyls which led to the recovery of a significant amount of the starting ketone, presumably due to competitive enolization.^[7] In 1984 the Imamoto group followed this up by using a broader range of lithium alkyls, CeCl_3 as an alternative precursor, and most importantly they introduced the formula “ RCeI_2 ”, to describe the basic stoichiometry of the organocerium reagent.^[8] Variations of this formula are used pretty much ever since for organolanthanide reagents similarly prepared.



Scheme A 4: Exemplary ketone transformation reaction using the Imamoto reagent as displayed by Imamoto in 1984.^[9]

This overview will first take a look at the reactivity of these organocerium reagents as reported by the Imamoto group. Then the studies on Imamoto’s organocerium reagent that other groups published so far are surveyed and lastly a perspective is presented how variations of these compounds are used in modern chemistry. This overview will therefore show the importance of these reagents and why a better understanding of them can help improve this field of chemistry.

2 Imamoto's findings on the organocerium compounds

2.1 The difference that the addition of cerium halide makes

The following procedure was reported by the Imamoto group in 1982.^[7] “To an in situ generated slurry of CeI₃ in THF, 1.7 equivalents of *n*-BuLi were added at –65 °C. After 30 minutes 0.5 equivalents of acetophenone were added. The mixture was worked up in an aqueous manner 3 hours later to give 2-phenylhexan-2-ol in 98% yield.”

In contrast, when acetophenone was reacted with only *n*-BuLi, the yield of 2-phenylhexan-2-ol was decreased to 64%. Moreover, the ketone precursor could be recovered in 27%, which they accounted for with a competitive enolization, “probably”.

2.2 The role of the reaction temperature

In the same publication, they also examined the effect of the temperature and the variation of the organolanthanide reagent on acetophenone as the only substrate. The pre-reaction of the rare-earth-metal iodide with the lithium alkyls (*n*-BuLi, *sec*-BuLi, EtLi, MeLi, and PhLi) was performed each time at –65 °C. Afterward the following conditions were applied:

- 30 min at –65 °C
- 15 min at 0 °C
- 15 min at r.t.
- 15 min at 50 °C

The addition of the ketone and subsequent reaction was carried out at the same temperature except for the one at 50 °C, where they let it cool down to ambient temperature and kept it there. Whereas an almost quantitative yield of the nucleophilic addition product was obtained at –65 °C, at 0 °C reductive coupling prevailed and afforded 2,3-dihydroxy-2,3-diphenyl-butane. At ambient temperature, the main product was 1-phenylethanol, which was almost exclusively observed jumping to 50 °C. This was the case for every lithium alkyl that had β-hydrogen atoms (*n*-BuLi, *sec*-BuLi, EtLi), but MeLi and PhLi both underwent nucleophilic addition to the carbonyl group even at ambient temperature exclusively. It's commonly assumed, that this most likely results from the formation of cerium hydride and low-valent cerium complexes via β-hydrogen elimination.^[10]

2.3 Different rare-earth-metals

To assess the effect of the type of rare-earth-metal the Imamoto group used commercially available lanthanoid chlorides ($\text{CeCl}_3(\text{H}_2\text{O})_7$, $\text{LaCl}_3(\text{H}_2\text{O})_7$, $\text{NdCl}_3(\text{H}_2\text{O})_6$, $\text{PrCl}_3(\text{H}_2\text{O})_7$, $\text{SmCl}_3(\text{H}_2\text{O})_6$, $\text{YbCl}_3(\text{H}_2\text{O})_6$,) and dehydrated them in vacuo at 140 °C for 2 hours.^[8] This method was chosen because of experimental convenience rather than applying the methods reported in the literature prior. Those used either ammonium chloride on the lanthanoid oxides at 300 °C to get water free lanthanoid chlorides or thionyl chloride to dehydrate the lanthanoid chloride aqua salts.^[11] In THF at -78 °C, those “dehydrated” salts were reacted with *n*-BuLi before the carbonyl compound was added. 1,3-Diphenyl-2-propanone was employed for each of the rare-earth-metals except ytterbium which was reacted with 3-*t*Bu-cyclohexane-1-on. The yield of the nucleophilic addition products for cerium, lanthanum, neodymium, and ytterbium was excellent surpassing 96%. The yields for praseodymium (85%) and samarium (60%) were significantly lower which was accounted on the incompletely dehydrated salts. In a previous publication, it was already reported that the mixture $\text{SmI}_3/n\text{-BuLi}$ used on acetophenone affords an excellent yield of 98% of the corresponding tertiary alcohol, supporting this assumption.^[7]

According to these findings, every rare-earth-metal could be used for these types of reactions. Considering their prices cerium which is by far the cheapest is the most sensible to use, however. Lanthanum and neodymium could also be considered since those are not outrageously more expensive.

2.4 Especially effective on easily enolizable ketones and α,β -unsaturated carbonyl compounds

The Imamoto group used their organocerium reagent on more than 30 carbonyl compounds.^[1d, 4a, 4b, 7-9, 12] Crucially, all comparisons drawn between the organocerium reagent CeX_3/LiR and the corresponding exclusive lithium alkyl revealed a higher yield of the nucleophilic addition product in case of the organocerium reagent. This ranged from a moderate increase for acetophenone (98 vs. 64%) to significant increases for 1,3-diphenyl-2-propanone (98 vs 33%). In the case of MesCOCH_3 , the yield of the corresponding tertiary alcohol was quite low with 15% for the organocerium reagent but considering that only traces of it were observed using

the lithium alkyl, this was also a success. Overall, the findings show that the easier a ketone is enolizable the more effective is the organocerium reagent over the lithium alkyl.

The organocerium reagent performed also excellent toward α,β -unsaturated carbonyl compounds, whereas the 1,4-addition rather than the 1,2-addition being the major concern. Almost always organocerium reagents engage exclusively in 1,2-addition. When this is not the case the amount of the 1,2-addition product is considerably higher compared to the plain lithium alkyls.

2.5 Imamoto reagent versus Grignard reagent

In follow-up publications, the Imamoto group additionally compared the organocerium reagents not just with the plain lithium alkyl but also with the corresponding Grignard reagent.^[8-9, 12a] It was found that the yield of the nucleophilic addition product is sometimes higher and sometimes lower compared to the lithium alkyl but always considerably lower than the organocerium reagent.

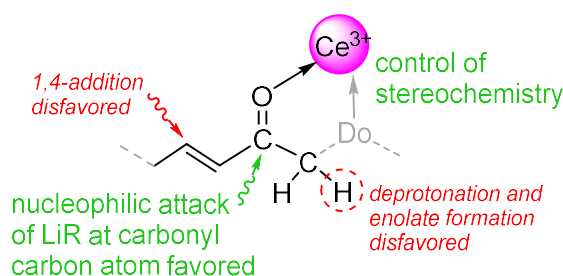
In 1989 however, Imamoto et al. reported their findings that the addition of CeCl_3 to the Grignard reagent prior to adding the carbonyl compound improves the selectivity toward nucleophilic addition considerably.^[12b] For example, in the case of 1,3-diphenyl-2-propanone and $n\text{BuMgBr}$, the yield of the tertiary alcohol could be improved from 18-36% to 98%. These findings were especially exciting since the Grignard reagent of an alkyl is often much easier accessible than the corresponding lithium alkyl. In the same paper, an extensive study with more than 15 carbonyl compounds and 10 Grignard reagents has been conducted. Not all reactions afforded the tertiary alcohol, but many did. For example, treatment of MesCOCH_3 with MeMgBr yielded only traces of the alcohol, while the addition of CeCl_3 improved the yield to 47%.

With these findings, Imamoto had established a type of reagent, which is used in organic synthesis regularly to this day. Naturally, this arose interest in the exact structure of these reagents, but while the structure has remained a mystery, some crucial findings have been reported. These will be summarized in chapter 3.

3 Studies on Imamoto's Organocerium Reagent

3.1 Why does it improve the nucleophilic addition on enolizable ketones?

Two aspects are usually associated with organocerium reagents in comparison with lithium alkyls or Grignard reagents. The first is the milder basicity of cerium alkyls which disfavors deprotonation reactions. The second, which plays a more prominent role, is the strong oxophilicity of the trivalent cerium. This directs the reaction close to the carbonyl group.^[4] The same aspect applies to the Luche reagent. Which selectively reduces carbonyl groups to alcohols.^[6]



Scheme A 5: Visualization of improved nucleophilic additions promoted by cerium(III).^[13]

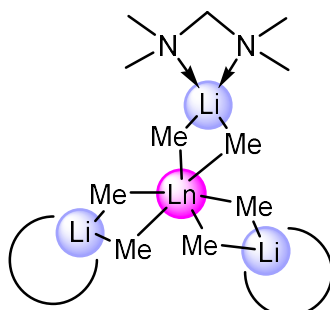
3.2 Studies on the cerium precursor

Evans et al. could show that the method, which the Imamoto group used to dehydrate the commercially available lanthanide chlorides, is insufficient. Heating the salts at 140 °C in vacuo for two hours does not result in the dehydrated salts.^[14] Evans et al. extended the procedure to 150 °C and 0.03 Torr for 12 hours or more to make sure that this method is not a valid procedure to achieve dry lanthanide chlorides. Through Karl Fischer analysis of such treated salts and the reaction with MeLi where methane extrusion was observed they concluded that a significant amount of water remains after the "drying" process. Evans et al. could further crystallize $[\text{Ce}(\mu\text{-Cl})_3(\text{thf})(\text{H}_2\text{O})]_n$ from a THF solution of the treated cerium salt. In a later publication, the same group reported on two yttrium complexes $[\text{YCl}_2(\text{H}_2\text{O})_6]\text{Cl}$ and $\text{Li}_2\text{Y}_8\text{Cl}_{18}\text{O}_4(\text{thf})_{12}$.^[15] The former compound once again shows that the drying process is insufficient, while the latter revealed the complexity of some intermediates that result from the reactions of lithium alkyls with those insufficiently dried salts. The conclusion was that at least one equivalent of water needs to be accounted for when this protocol is used. These findings are in contrast to the report

from Imamoto where they used a stoichiometric amount of *n*-BuLi with the dried salts and about 0.8 equivalents of the ketone for a yield of 98% of the tertiary alcohol.^[8] The most plausible explanation for this is, that the Imamoto group added the lithium alkyl at $-78\text{ }^{\circ}\text{C}$, while the Evans group observed the evolution of methane from MeLi at ambient temperature. This would suggest that the lithium alkyls do not react with the crystal water of those lanthanide salts at low temperatures.

3.3 Isolation of bimetallic lithium lanthanide ate complexes

A better understanding of the reaction products of rare-earth-metal halides and lithium alkyls can be obtained by a look at the publications of Schumann et al. from as early as 1978 might help.^[16] Accordingly, mixtures of $\text{LnCl}_3/\text{MeLi}/\text{Et}_2\text{O}$ and TMEDA (tetramethylethylenediamine) give the heterobimetallic complexes $\text{Li}_3\text{LnMe}_6(\text{tmeda})_3$. Solid-state structures of these complexes for erbium^[16b] and holmium^[16c] have been reported. Similar findings from the Okuda group, as revealed by $\text{Li}_3\text{Sc}_2\text{Me}_9(\text{thf})_2(\text{OEt}_2)_3$ and $\text{Li}_3\text{Ln}_2\text{Me}_9(\text{thf})_3(\text{OEt}_2)_2$ ($\text{Ln} = \text{Y}, \text{Tb}$), underline these results.^[17]



Scheme A 6: Structure of $\text{Li}_3\text{LnMe}_6(\text{tmeda})_3$.

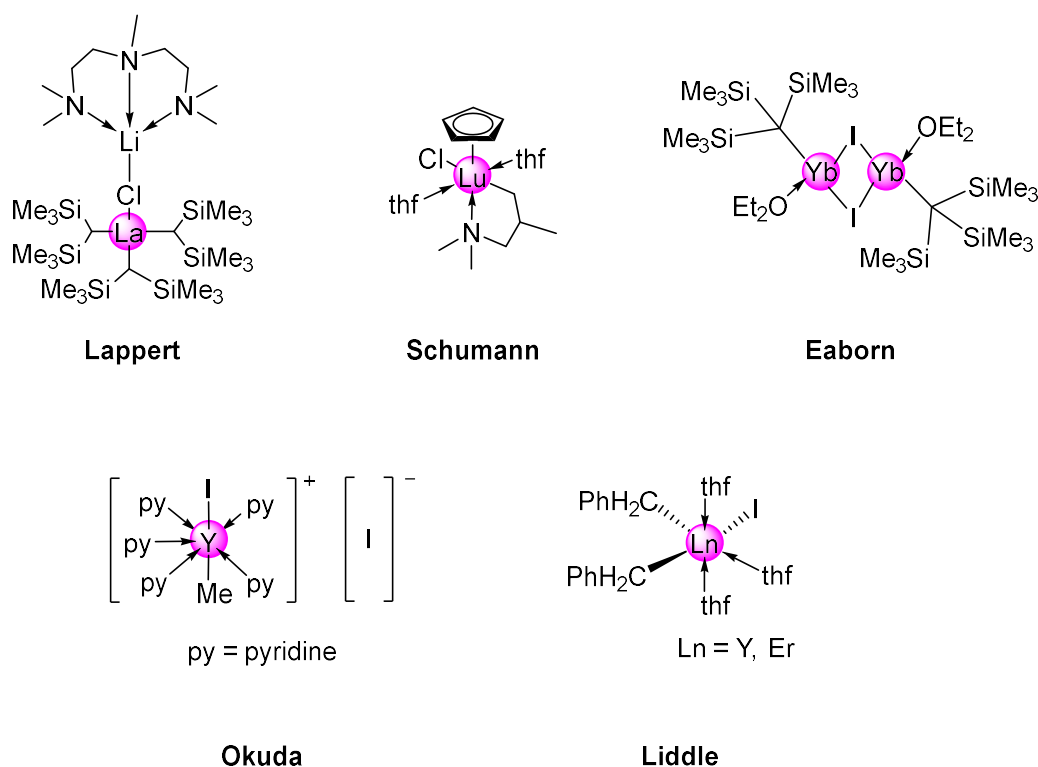
Alkylation reactions of LnCl_3 with *t*-BuLi provided access to solvent-separated ion pairs of $[\text{Li}(\text{do})_x][\text{Ln}(\text{tBu})_4]$ type.^[16c, 18] Complexes $[\text{Li}(\text{tmeda})_2][\text{Lu}(\text{tBu})_4]$ ^[18b] and $[\text{Li}(\text{dme})_2][\text{Er}(\text{tBu})_4]$ ^[18c] (dme = dimethoxyethylene) were structurally characterized.

Finally, saturated trialkyl complexes of the type $\text{Ln}(\text{CH}_2\text{SiMe}_3)_3(\text{thf})_x$ ($x = 2, 3$) could be obtained from the lithium alkyls $\text{LiCH}_2\text{SiMe}_3$, but only for the smaller rare-earth metals (Sc, Y, Sm, Er, Yb, Lu).^[19]

To summarize these findings, depending on the steric demand of the ligands and the size of the rare-earth-metal homoleptic, ate- and solvent-separated complexes have all been reported. Also, if available, neutral donors commonly saturate the coordination sphere of the metals. But so far only a few examples of the mixed alkyl halogenido lanthanide complexes like the proposed “CeCl₂R” have been reported, these are presented in chapter 3.4.

3.4 Mixed alkyl halogenido rare-earth-metal complexes

The first rare-earth metal compound bearing alkyl and halogenido ligands in the absence of a stabilizing ancillary ligand was by the Lappert group in 1988 including an X-ray structure analysis.^[20] The lanthanum ate complex features silylalkyl groups devoid of β-hydrogen atoms, (Scheme A 7). The same applies for complex [YbI(C(SiMe₃)₃)(thf)₂] that was published by Eaborn et. al.^[21] The Schumann group employed an amino-functionalized alkyl for their half-sandwich complex,^[22] while the Liddle group drew on more stable benzyl groups.^[23] Only the separated ion pair yttrium complex [YMeI(thf)₅][BPh₄], that was reported by Okuda et. al. features a “pure” alkyl group.^[17]

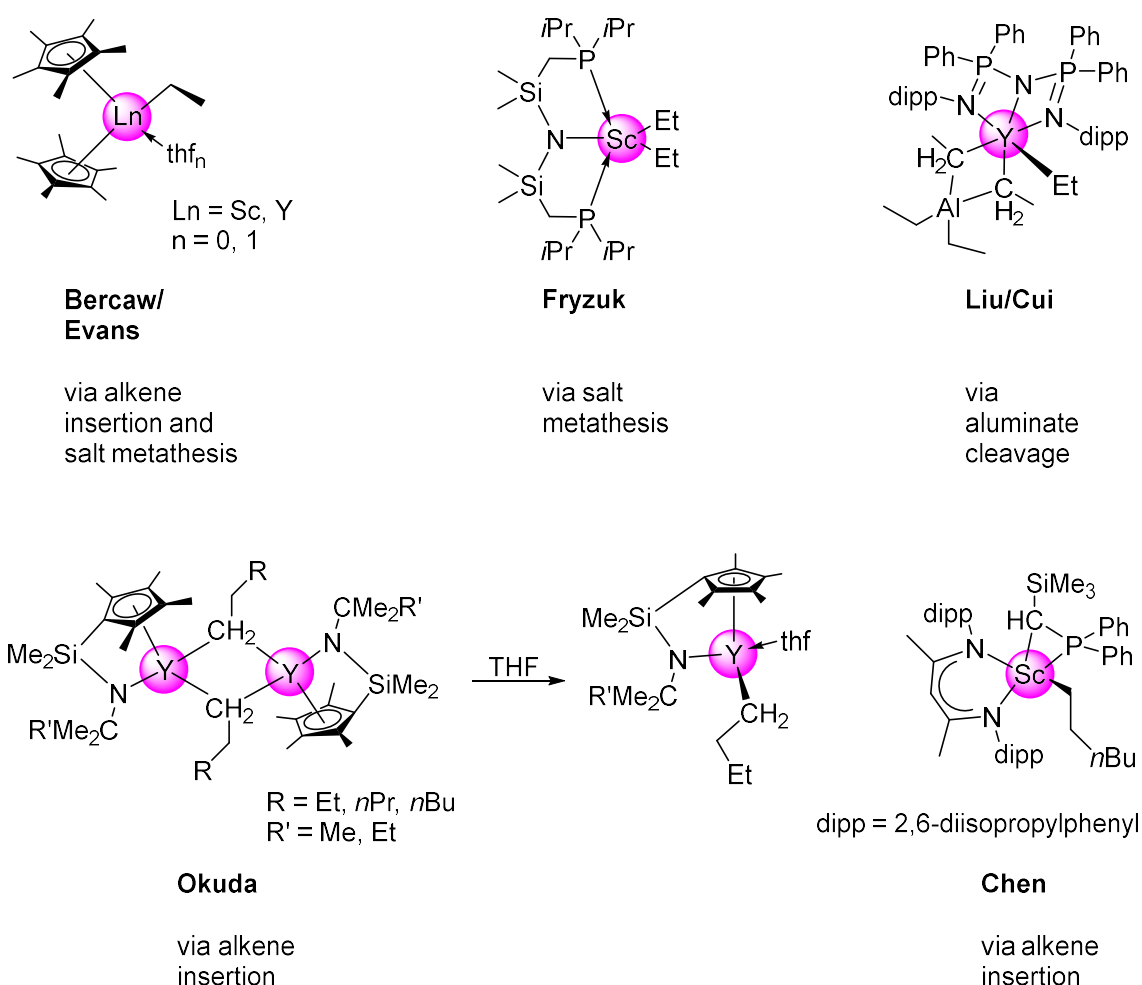


Scheme A 7: Overview of literature known mixed alkyl halogenido complexes.

Since, the Imamoto group focused mostly on the reaction of $\text{CeX}_3/n\text{-BuLi}$ an overview of rare-earth-metal complexes featuring respective alkyls will be given in chapter 3.5.

3.5 Higher alkyl rare-earth-metal complexes

Only a handful of higher alkyl rare-earth-metal complexes have been published so far. "Higher" means that ethyl, propyl, butyl, pentyl, and hexyl groups are coordinated to the rare-earth-metal center (Scheme A 8).

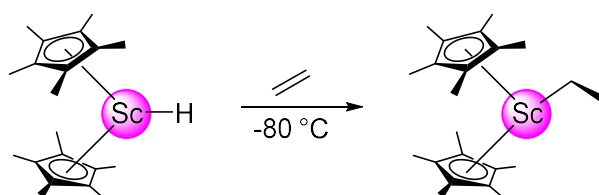


Scheme A 8: Overview of literature known higher alkyl complexes.

This compilation excludes the *t*-butyl groups which have been described in chapter 3.3 and are known to be relatively stable. All other known higher alkyl rare-earth-metal complexes contain at least one stabilizing ancillary ligand. These include Cp* or bulky multidentate ligands. There are three distinct reaction pathways how these complexes could be isolated. Bercaw^[24]

alongside Okuda^[25] and Chen^[26] all used an alkene insertion reaction into a Ln–H bond (Scheme A 8). The group of Liu and Cui could obtain rare-earth-metal ethyl complexes using an aluminate cleavage.^[27] Lastly, the groups of Evans^[28] and Fryzuk^[29] applied a salt metathesis protocol as did the Imamoto group.

It's important to mention that there is a considerable number of rare-earth-metal aluminate complexes, which contain higher alkyl groups, but those are not further discussed in this thesis, since they behave quite different to the Imamoto reagent.



Scheme A 9: Exemplary alkene insertion reaction.

The numerous examples of alkene insertion reactions leading to rare-earth-metal alkyls can also be understood as the back reaction of β -hydrogen elimination. This implies that the reason of the enhanced instability of these higher alkyl rare-earth-metal complexes, is not really the fault of their β -hydrogen atoms.

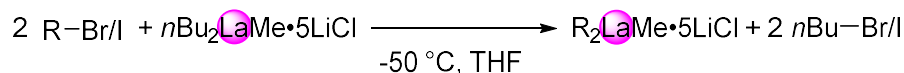
3.5 Incomplete reaction of the cerium precursor at low lithium alkyl loadings

A very significant contribution for helping to understand Imamoto's organocerium reagent was made by Denmark et al. in 1992.^[30] They analyzed the solid residue that remains when reacting CeCl_3 with less than three equivalents of lithium alkyls. As it turned out this is unreacted CeCl_3 clearly indicating that " CeCl_2R " cannot be the main species of the reagent. Confusingly, the best results in ketone transformation are still achieved by a 1:1 ratio of CeCl_3 and lithium alkyl. It was hypothesized that a part of the unreacted CeCl_3 acts as a Lewis acid for carbonyl precoordination, but it could not be proven.

4 Imamoto's Organocerium Reagent in modern chemistry

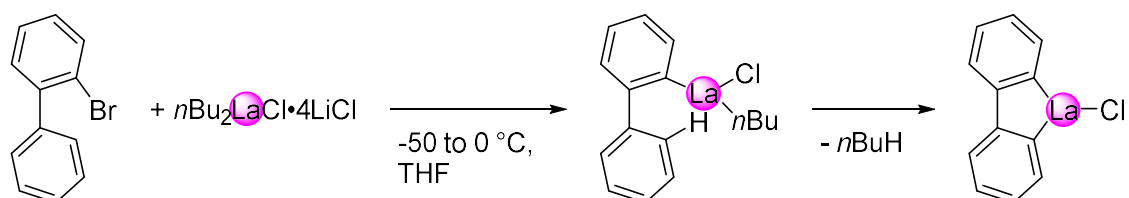
4.1 Halogen-rare-earth-metal exchange

Both Knochel et al. and Didier et al. recently reported that organolanthanide reagents engage in halogen-metal exchange reactions followed by allylations or additions to carbonyls.^[31]



Scheme A 10: Example of a halogen rare-earth-metal exchange reaction.

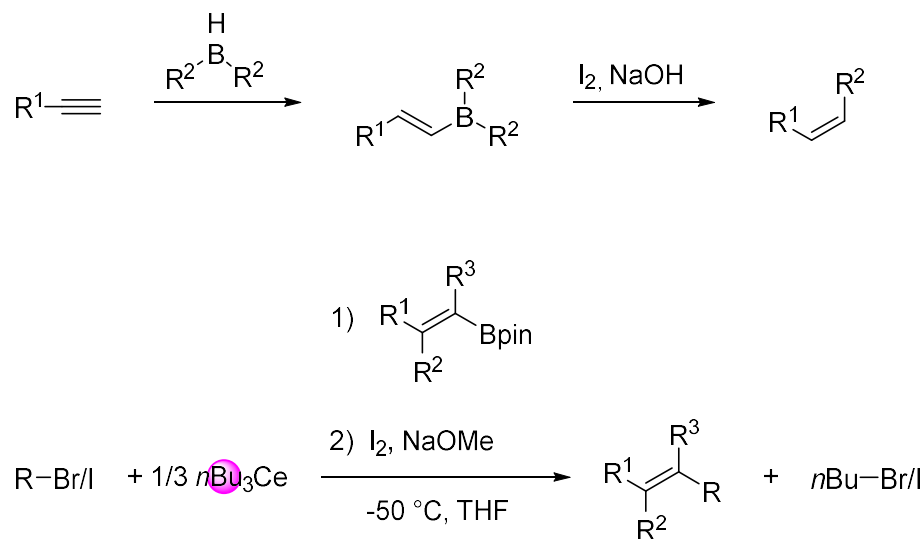
These organolanthanide reagents are prepared in situ and designated as $n\text{Bu}_2\text{LaMe}\cdot 5\text{LiCl}$ and $n\text{Bu}_2\text{SmCl}\cdot 4\text{LiCl}$ or $n\text{Bu}_3\text{Sm}\cdot 5\text{LiCl}$. This method is a great way to extend the range of possible groups that can be nucleophilically added. Since all that is required is a halide group and it only is susceptible to other carbonyl groups. This is one step further than what Imamoto achieved by using Grignard reagents in combination with CeCl_3 . The Knochel group also applied halogen-metal exchange reactions using putative " $n\text{Bu}_2\text{LaCl}\cdot 4\text{LiCl}$ " in 2019. Accordingly, they proposed the first lanthafluorenyl complex and supported this structure by EXAFS and the follow-up chemistry although a solid-state structure could not be obtained.^[31d]



Scheme A 11: Proposed lanthafluorenyl complex.

4.2 Zweifel-type olefination

In 2019 Didier et al. followed up the chemistry developed by Knochel and used such reagents in Zweifel-type olefinations.^[32]



Scheme A 12: General example of the Zweifel olefination (top) and an exemplary reaction using organolanthanide reagents (bottom).

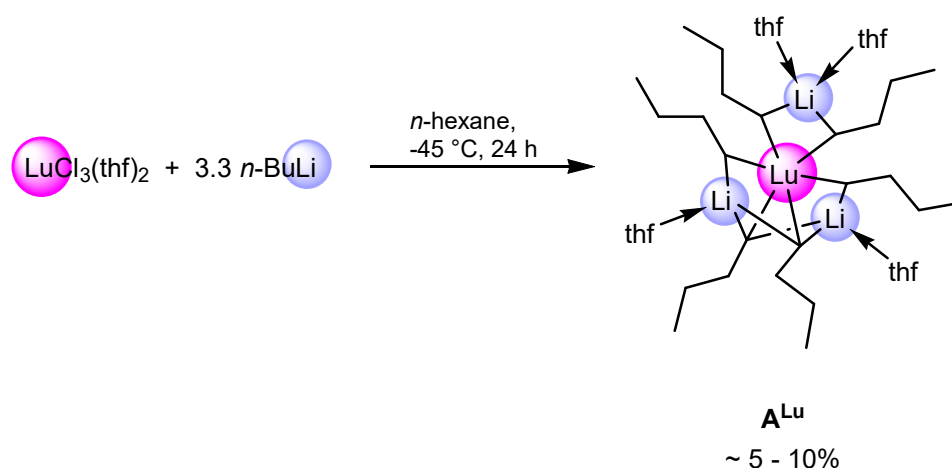
By successfully applying over 50 substrates, they clearly demonstrated the feasibility of this approach, and hence extended, the scope of reactions where organolanthanide complexes can be used, making it a tool every organic chemist should have in their repertoire.

B

Summary of the Main Results

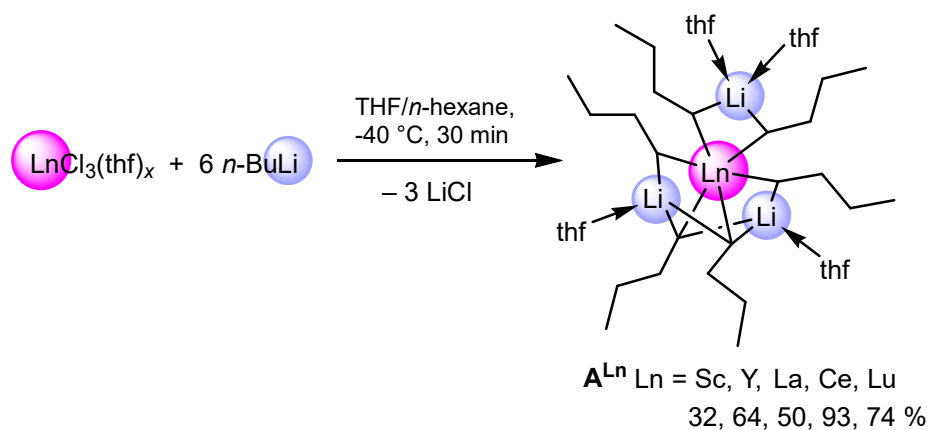
1 Unraveling Imamoto's Organocerium Reagent

Since, a better part of Imamoto's work dealt with the use of cerium halides in combination with *n*-butyllithium, mostly because of their low price,^[1d, 4a, 4b, 7-9, 12, 33] this work was also focused on these two reagents. Because of the thermal lability of the resulting organocerium complexes and the fact that NMR spectroscopy might not provide any useful information, due to the paramagnetism of cerium, lutetium chloride was chosen as another precursor. Diamagnetic lutetium (III) would allow for more comprehensive NMR spectroscopy and its smaller size should generally enhance the stability of alkyl species in comparison to the larger lanthanides. After a lot of trial and error, the first complex could be isolated for the reaction of $\text{LuCl}_3(\text{thf})_2$ with *n*-BuLi. The resulting bimetallic ate complex $\text{Li}_3\text{Lu}(\text{nBu})_6(\text{thf})_4$ (\mathbf{A}^{Lu}) was the breakthrough that led to many more complexes and the respective studies provided great insight into the organocerium reagents used in organic synthesis.



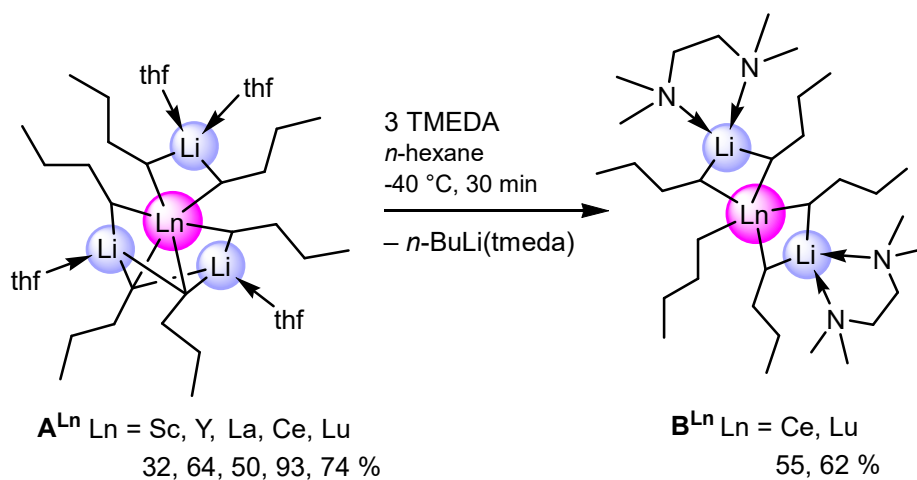
Scheme B 1: Synthesis of bimetallic ate complex $\text{Li}_3\text{Lu}(\text{nBu})_6(\text{thf})_4$ (\mathbf{A}^{Lu}).

The result that six equivalents of *n*-BuLi can react with one lutetium chloride underline the findings of Denmark et al. who observed that a significant amount of unreacted cerium chloride can be recovered at low lithium alkyl loadings.^[30] On closer inspection, the limiting factor of this reaction was in fact the amount of THF introduced to the reaction mixture through the lutetium precursor. Since there are two THF molecules per lutetium in the precursor and four in the product. These findings led to an improved synthesis protocol for complex \mathbf{A}^{Lu} which was also applied to other lanthanides.



Scheme B 2: Improved synthesis protocol for complexes A^{Ln} .

Since crystals of suitable quality for X-ray diffraction could be obtained only for A^{Lu} , a donor exchange, TMEDA for THF, was used on complexes A^{Lu} and A^{Ce} which led to complexes B^{Lu} and B^{Ce} . The fact that these complexes are isostructural and based on the microanalytical data led to the assumption that the cerium complex resulting from the reaction of $\text{CeCl}_3(\text{thf})$ and $n\text{-BuLi}$ should be $\text{Li}_3\text{Ce}(n\text{Bu})_6(\text{thf})_4$ (A^{Ce}).



Scheme B 3: Donor-exchange reaction which led to complexes B^{Ln} .

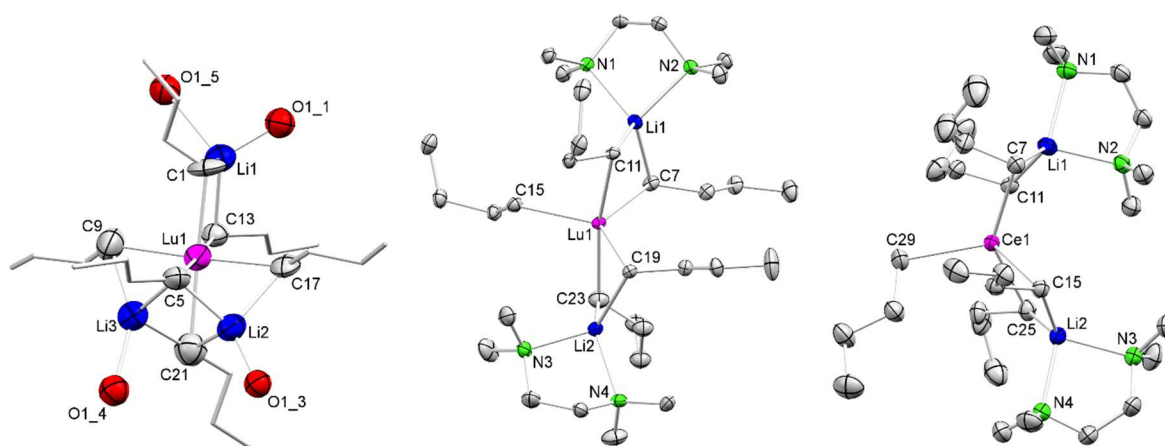


Figure B 1: Crystal structures of $\text{Li}_3\text{Lu}(n\text{-Bu})_6(\text{thf})_4$ (\mathbf{A}^{Lu} , left) $\text{Li}_2\text{Lu}(n\text{-Bu})_5(\text{tmeda})_2$ (\mathbf{B}^{Lu} , middle), and $\text{Li}_2\text{Ce}(n\text{-Bu})_5(\text{tmeda})_2$ (\mathbf{B}^{Ce} , right), with atomic displacement ellipsoids set at 30% probability. Hydrogen atoms, disorders and CH atoms of the THF molecules (\mathbf{A}^{Lu}), and disorders of the *n*-butyl groups (\mathbf{B}^{Lu} , \mathbf{B}^{Ce}) are omitted for clarity.

While the structural motive of complexes \mathbf{A}^{Ln} is very similar to the already known complexes $\text{Li}_3\text{LnMe}_6(\text{tmeda})_3$ ^[16b, 16c], there are a few subtle differences. First, every lithium atom of the methyl complexes connects to two methyl groups. In the *n*-butyl complexes only one lithium atom bridges to two *n*-butyl groups, while the other two bridge to three *n*-butyl groups each. The coordination sphere of the lithium atom that only bridges two *n*-butyl groups is completed by two THF donor molecules, while that of the other two lithium atoms is saturated by one each. When the donor is exchanged to TMEDA there remain only five *n*-butyl ligands bond to the rare-earth-metals, one of which is terminal. And since there are only five *n*-butyl ligands there are only two lithium atoms that bridge to two of the non-terminal *n*-butyl ligands each.

NMR studies on complexes \mathbf{A}^{Ln} and \mathbf{B}^{Ln} revealed surprising solvation behavior. The ^7Li NMR spectra of the paramagnetic cerium complexes, provided great insight into lithium atoms that are close to cerium atoms, because they display considerable chemical shifts. The *n*-butyl complexes \mathbf{A}^{Ce} and \mathbf{B}^{Ce} are compared to the new cerium complexes $\text{Li}_3\text{CeMe}_6(\text{tmeda})_3$ (**C**) and $[\text{Ce}(t\text{Bu})_4][\text{Li}(\text{thf})_4]$ (**D**), which were also characterized in the solid state.

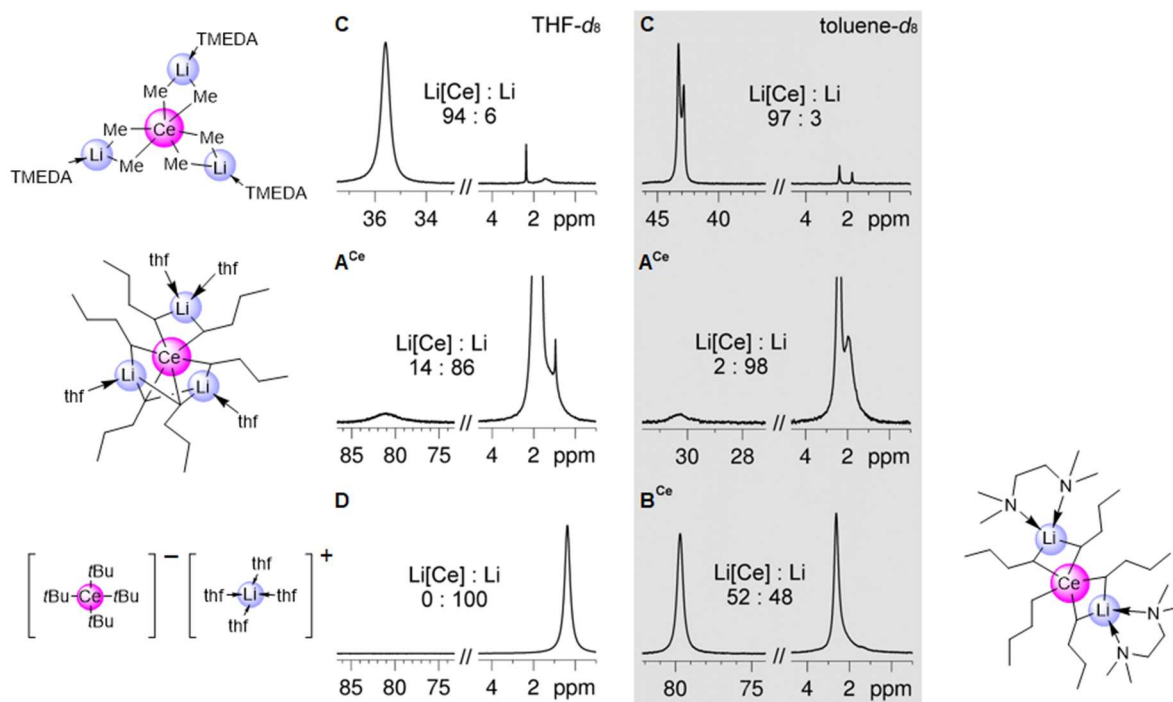


Figure B 2: ^7Li NMR spectra (194.37 MHz, 233 K) of complexes **C**, **D**, **A^{Ce}**, and **B^{Ce}**, recorded in THF- d_8 or toluene- d_8 .

It is evident that all cerium complexes except **D** exhibit a considerably shifted lithium signal. This was expected for complex **D** since it features a separated ion pair with the lithium atom lingering far away from the cerium. Importantly, a non-paramagnetically shifted signal is also observed in every spectrum. This led to the assumption, that the dissolved complexes separate into the corresponding lithium alkyl and a lithium depleted organocerium complex. –

This can also be observed in the proton NMR spectra of the lutetium complex which was used for an extended study with different lithium alkyl loadings.

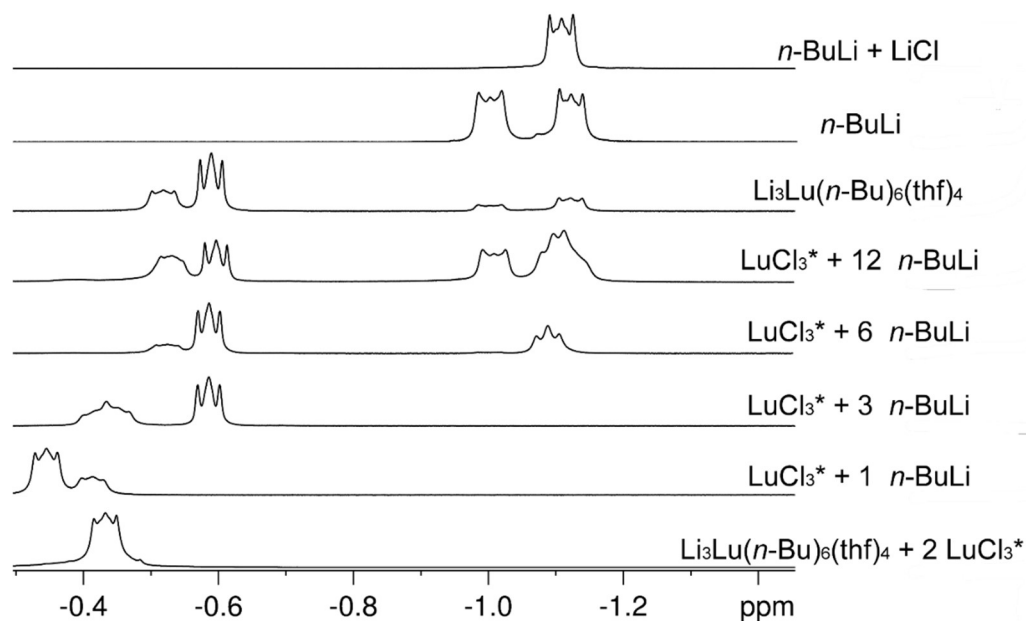


Figure B 3: ¹H NMR spectra (500.13 MHz, THF-*d*₈, 193 K) of LuCl₃(thf)₂ with *x* *n*-BuLi (*x* = 1, 3, 6, 12) compared to A^{Lu}, A^{Lu}+2 LuCl₃(thf)₂, *n*-BuLi, and *n*-BuLi+LiCl.

The quintessence of this study was that only at *n*-BuLi loadings of more than three equivalents, free *n*-BuLi is observed in solution.

Next, ketone transformations using these isolated organolanthanoid complexes have been studied. As a carbonyl compound, 1,3-diphenylpropane-2-one was used, since the Imamoto group used it also extensively and therefore vital information was already accessible. When Li₃Ce(*n*Bu)₆(thf)₄ (A^{Ce}) was reacted with six equivalents of 1,3-diphenylpropane-2-one, the enolized side product Li₄[OC(=CHPh)CH₂Ph]₄(thf)₄ (E) could be isolated and analyzed.

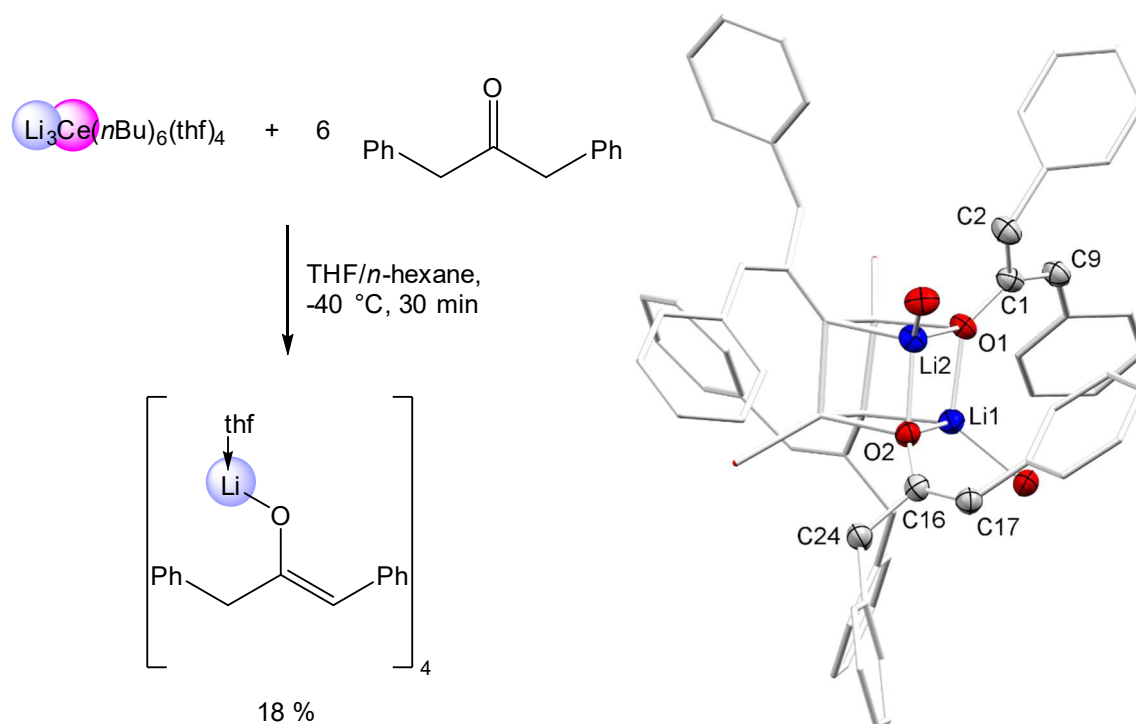
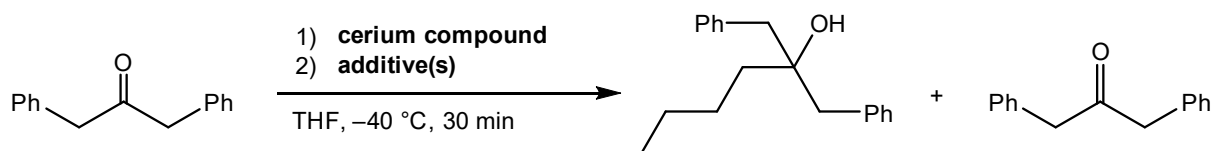


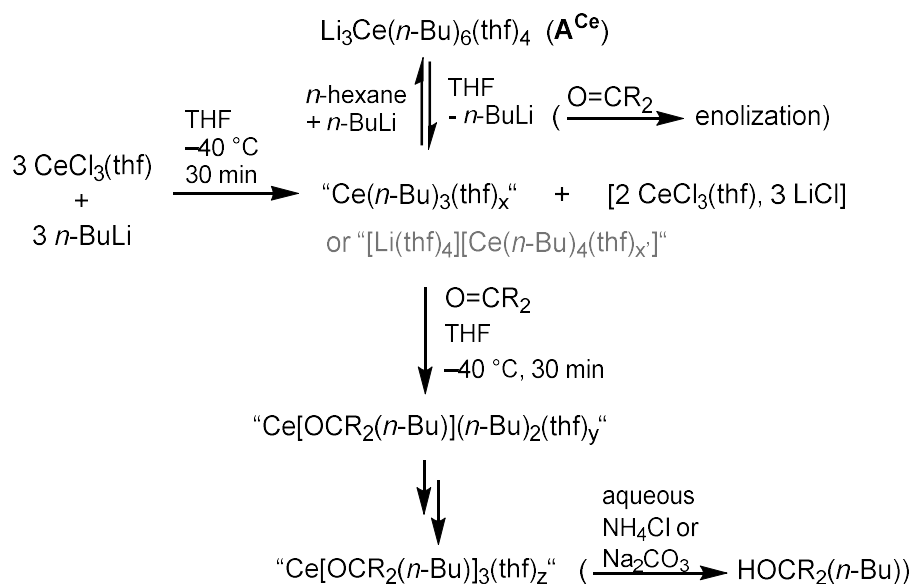
Figure B 4: Synthesis of $\text{Li}_4[\text{OC}(=\text{CHPh})\text{CH}_2\text{Ph}]_4(\text{thf})_4$ (**E**) (left) and solid-state structure of **E** (right).

Table B 1: Summary of the results of the ketone transformation reactions



Entry	Compound	Equiv. ketone	Additives	Isolated yield alcohol [%]	Recovered ketone [%]
1	$\text{CeCl}_3(\text{thf})$	0.77	1 <i>n</i> -BuLi	99	0
2	$\text{CeCl}_3(\text{thf})$	6	6 <i>n</i> -BuLi	77	20
3	\mathbf{A}^{Ce}	6	-	70	13
4	\mathbf{A}^{Ce}	1	-	88	3
5	\mathbf{A}^{Ce}	6	3 LiCl	74	16
6	\mathbf{A}^{Ce}	6	5 $\text{CeCl}_3(\text{thf})$	89	8

The results from the isolation of complex **E** in 18% yield and the amount of recovered ketone from entry 3 in Table 1 agree with each other. This provides proof that enolization is the competing side reaction in these types of reactions. It is also shown that the isolated complexes show similar reactivity to the in situ generated organocerium reagents albeit the yield of isolated tertiary alcohol is a bit lower in the case of the isolated complexes.

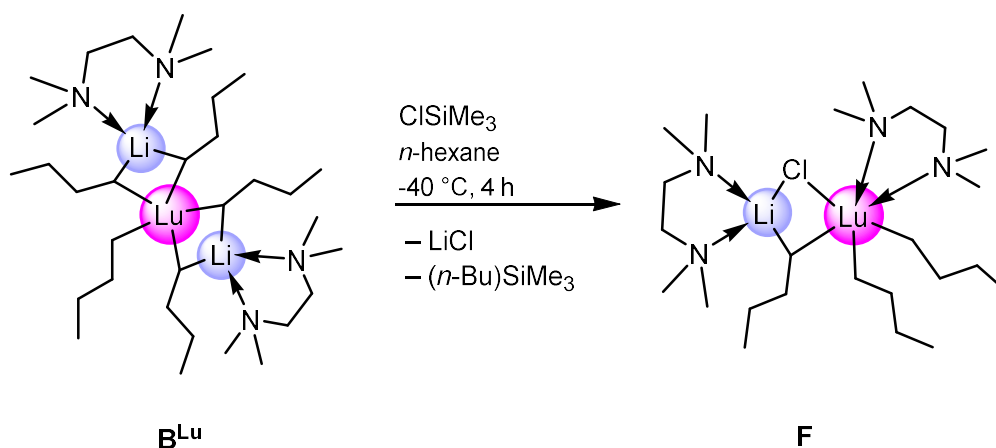


Scheme B 4: Overview of Imamoto's organocerium complex.

The significant findings about Imamoto's organocerium reagent can be summarized as follows. When cerium halides CeX_3 ($\text{X} = \text{Cl}, \text{I}$) are treated with $n\text{-BuLi}$ at least three equivalents of $n\text{-BuLi}$ react with one cerium precursor since the monoalkylated species " $n\text{-BuCeX}_2$ " is most likely considerably better soluble than the cerium halide CeX_3 and therefore it reacts faster with the remaining $n\text{-BuLi}$ in solution, before the cerium halides CeX_3 even have the chance. This is proven by the recovered non-reacted cerium precursor CeX_3 . When more than three equivalents of $n\text{-BuLi}$ are used a bimetallic lithium cerium ate complex is formed that separates into $n\text{-BuLi}$ and an organocerium complex in solution. When the mixture is crystallized from an $n\text{-hexane}$ solution only the bimetallic ate complexes are isolated indicating ligand scrambling at lower lithium alkyl loadings.

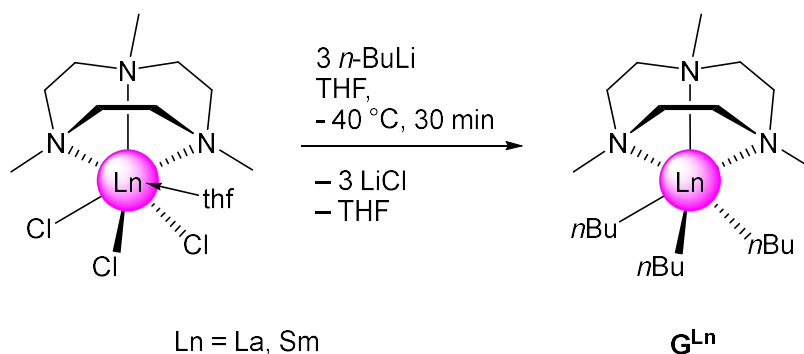
Another goal was to see if non-ate complexes can also be isolated. The first route followed was the depletion of lithium from the isolated complexes **B^{Ln}**. Trimethylsilyl chloride was used as a chlorination agent in the hope that the separated lithium alkyl in the solution would be more reactive toward it than the organolanthanide fragment. This turned out to be the case. When **B^{Lu}** was reacted with trimethylsilyl chloride the "monolithium" complex $\text{Lu}(n\text{Bu})_3(\text{LiCl})(\text{tmeda})_2$

(F) could be obtained. Compound F features only three *n*-butyl ligands but the incorporation of LiCl could not be avoided.



Scheme B 5: Synthesis of lithium-depleted complex F.

The second route exploited the use of the aza-crown 1,4,7-trimethyl-1,4,7-triazacyclononane (Me_3TACN). As was shown previously it can stabilize and monomerize pre-formed amorphous $[\text{ScMe}_3]_n$.^[34] Treatment of the rare-earth-metal halides with this aza-crown in THF afforded the adduct $(\text{Me}_3\text{TACN})\text{LnCl}_3(\text{thf})_x$ ($x = 0,1$). These can then be reacted with lithium alkyls to form the corresponding tri-alkylated lanthanide species. $(\text{Me}_3\text{TACN})\text{La}(n\text{Bu})_3$ (G^{La}) was synthesized according to this procedure.



Scheme B 6: Synthesis of complex G^{Ln}.

Since no crystals suitable for an X-ray analysis could be obtained for the lanthanum species the samarium congener G^{Sm} was also synthesized. The crystals of the samarium complex $(\text{Me}_3\text{TACN})\text{Sm}(n\text{Bu})_3$ (G^{Sm}) were at least good enough to prove its existence and connectivity in the solid state. This once again shows the intrinsic problem associated with *n*-butyl complexes, since the *n*-butyl ligand features extreme flexible conformational flexibility leading

to crystals which are often heavily intertwined. Furthermore, the instability of these complexes in solution even at low temperatures certainly doesn't help. But since a connectivity structure could be obtained for the samarium complex and the NMR spectra of the lanthanum derivative were conclusive, it can be assumed that complexes $(\text{Me}_3\text{TACN})\text{Ln}(n\text{Bu})_3$ display a very similar structure.

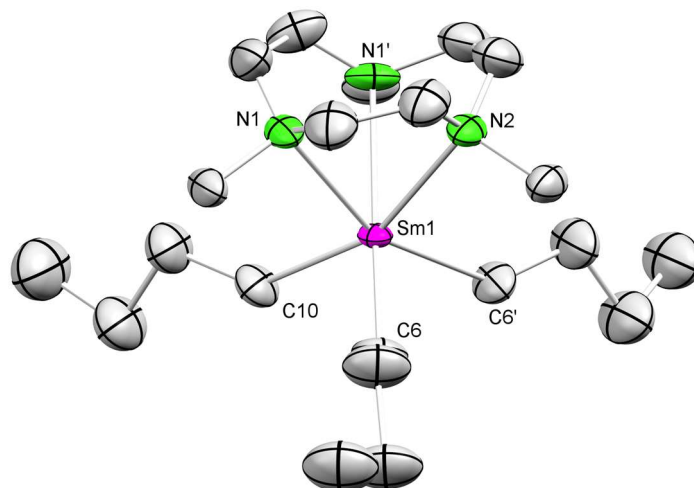
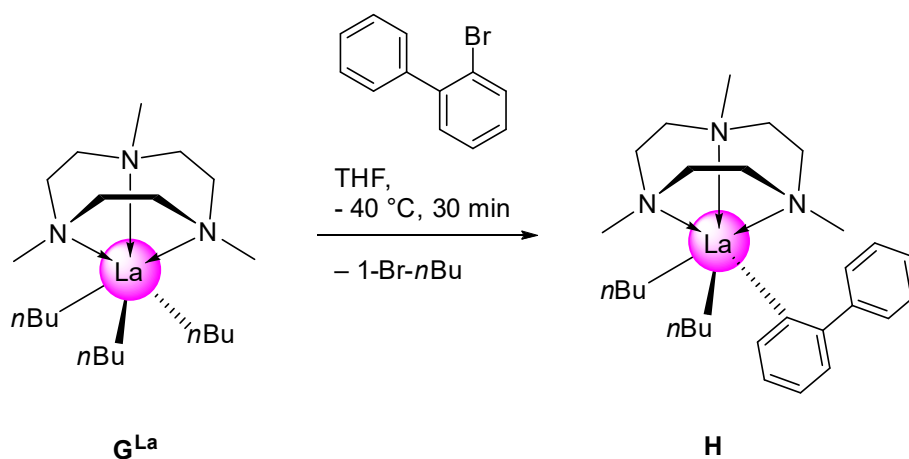


Figure B 5: Connectivity of complex G^{Sm} .

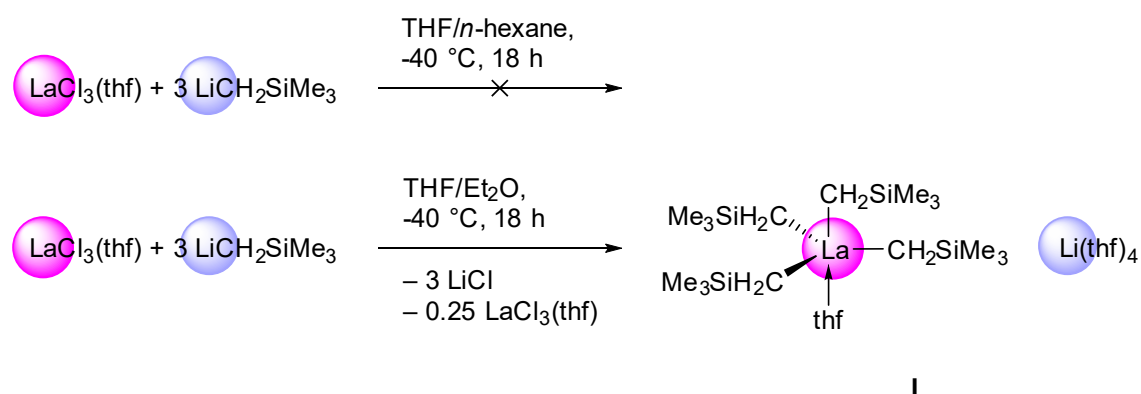
The lanthanum complex was also further reacted with 2-bromo-biphenyl in the hope to isolate a lanthafluorenyl complex as was proposed by the Knochel group.^[31d] However, only complex **H** could be obtained through this method rendering the lanthafluorenyl complex elusive.



Scheme B 7: Synthesis of complex **H**.

Finally, the knowledge of seamless low-temperature organolanthanide synthesis was used to isolate a long-time elusive lanthanum neosilyl complex. The Hessen group used an in situ

generated version of a lanthanum neosilyl complex (via $\text{LaCl}_3/3 \text{LiCH}_2\text{SiMe}_3$) as a precursor once, but no solid-state structure has been reported so far.^[19b] It has been assumed, that lanthanum should also form a complex of the type $\text{La}(\text{CH}_2\text{SiMe}_3)_3(\text{thf})_x$, just like the analogs of the smaller rare-earth metals.^[19] But as it turns out this is not the case. Much like the *t*-butyl cerium complex $[\text{Ce}(t\text{Bu})_4][\text{Li}(\text{thf})_4]$ **D**, the lanthanum neosilyl complex form a solvent-separated ion pair, $[\text{La}(\text{CH}_2\text{SiMe}_3)_4(\text{thf})][\text{Li}(\text{thf})_4]$ (**I**). Seemingly because the neosilyl ligand is sterically a bit less demanding than the *t*-butyl ligand there is some additional space at the rare-earth-metal center which is occupied by a THF molecule.



Scheme B 8: Synthesis of complex I.

The preferred formation of ate complex I was also revealed from reactions of $\text{LaCl}_3(\text{thf})$ with 2.5 and 4 equivalents of $\text{LiCH}_2\text{SiMe}_3$.

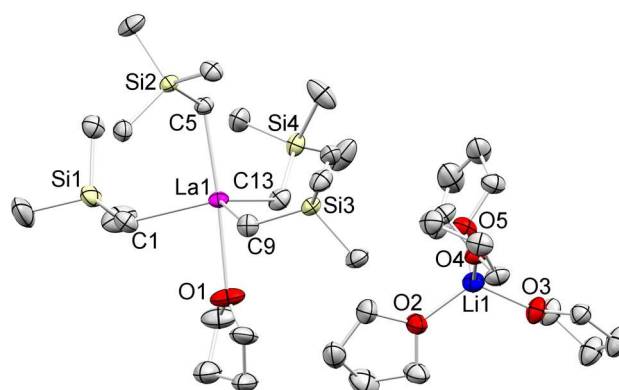
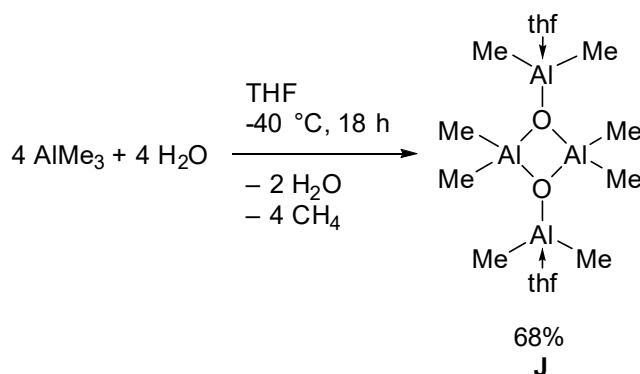


Figure B 6: Crystal structure of $[\text{La}(\text{CH}_2\text{SiMe}_3)_4(\text{thf})][\text{Li}(\text{thf})_4]$ (I**) with atomic displacement ellipsoids set at 50% probability. Hydrogen atoms and disorders of the thf groups are omitted for clarity.**

2 Isolation of a MAO species from the reaction of water with AlMe_3

The seamless cold-chain techniques were also used in the much-studied but still riddled with mystery field of methylalumoxanes.^[35]

Following our low-temperature procedures, a trimethylaluminum-solution in THF was treated with stoichiometric amounts of water strongly diluted in THF. After stirring overnight, the solvents were removed under reduced pressure, still at a low temperature, which took almost two days. This procedure resulted in crystalline $[(\text{Me}_2\text{Al})_2\text{O}(\text{thf})]_2$ (**J**).



Scheme B 9: Synthesis of MAO complex **J**.

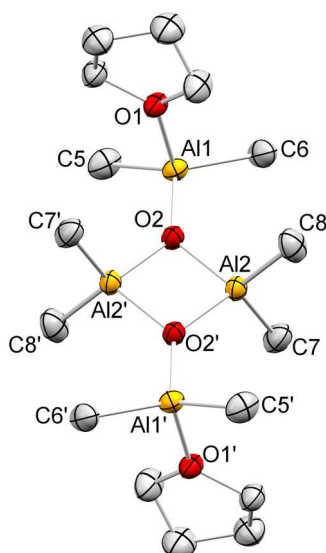
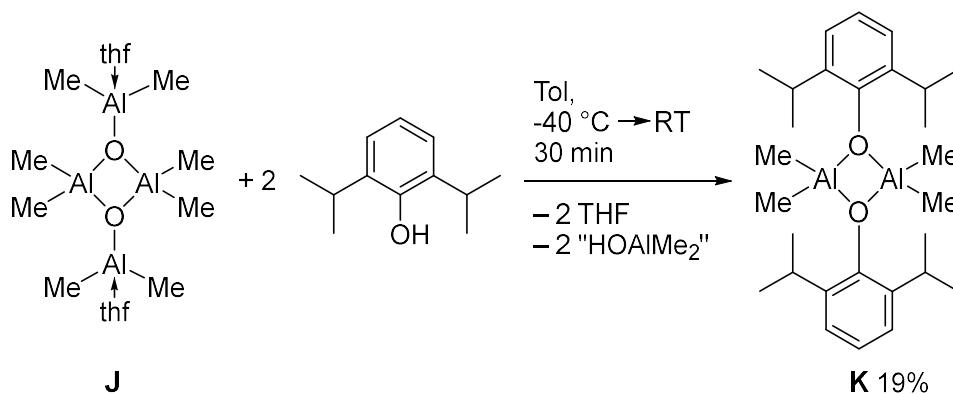


Figure B 7: Crystal structure of $[(\text{AlMe}_2\text{O})(\text{thf})]_2$ (**J**) with atomic displacement ellipsoids set at 50% probability. Hydrogen atoms are omitted for clarity.

NMR studies on this complex including DOSY experiments revealed that in solution the tetraaluminum complex separates most likely into $(\text{AlMe}_2)_2\text{O}(\text{thf})_2$. Moreover, the THF molecules can be separated from the complex via the addition of trimethylaluminum. The complex was also reacted with 2,6-diisopropylphenol to give $(\text{Me}_2\text{AlO-2,6-diisopropylphenyl})_2$ (**K**), (Scheme B 10).



Scheme B 10: Synthesis of MAO complex K.

Due to the low yield of **K** and the other products, which all show chemically similar shifts in the ^1H NMR, the determination of the side products was not possible and therefore the mechanism, to form this unexpected complex also remains unclear.

Finally, first attempts at α -olefin polymerization using $[(\text{Me}_2\text{Al})_2\text{O}(\text{thf})_2]$ (**J**) as a cocatalyst in combination with additional trimethylaluminum showed promising results.

C

Unpublished Results

1 Cerium aluminate cluster

Introduction

When assessing suitable conditions and cerium precursors for reactions with lithium alkyls, the cerium half-sandwich aluminate $\text{Cp}^*\text{Ce}(\text{AlMe}_4)_2$ was employed in salt-metathesis protocols.

Results and Discussion

The two cluster complexes $[\text{Cp}^*_9\text{Ce}_9(\text{AlMe}_4)_4(\text{Me})_6(n\text{-Bu})_3(\text{CH}_2)_3\text{Li}]_2$ (**UP1**) and $\text{Cp}^*_{10}\text{Ce}_{10}(\text{AlMe}_4)_5(\text{Me})_9(n\text{-Bu})_1(\text{CH}_2)_3$ (**UP2**) could be obtained using almost the same reaction conditions, (Scheme C 1).

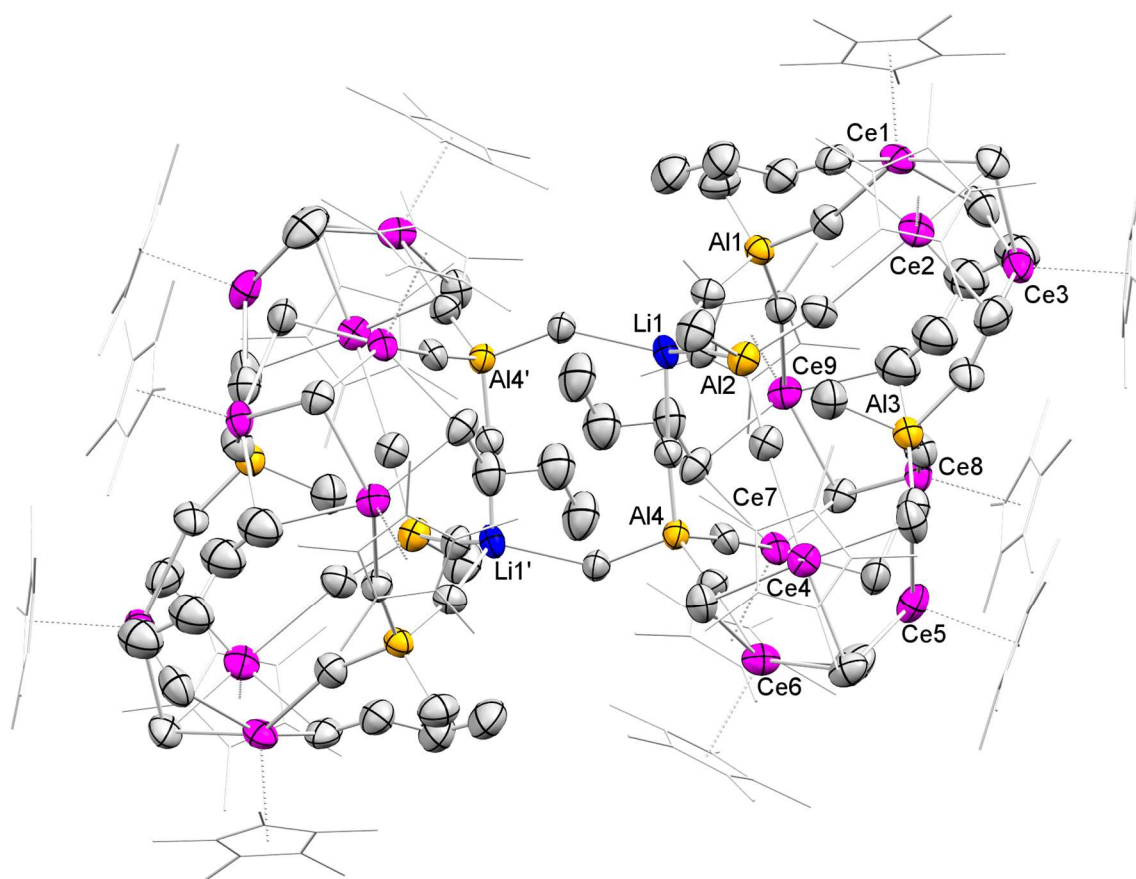


Figure C 1: Crystal structure of $[\text{Cp}^*_9\text{Ce}_9(\text{AlMe}_4)_4(\text{Me})_6(n\text{-Bu})_3(\text{CH}_2)_3\text{Li}]_2$ (**UP1**) with atomic displacement ellipsoids set at 50% probability. Hydrogen atoms and disorders of the Cp^* ligands are omitted for clarity. Cp^* ligands are displayed as sticks for clarity.

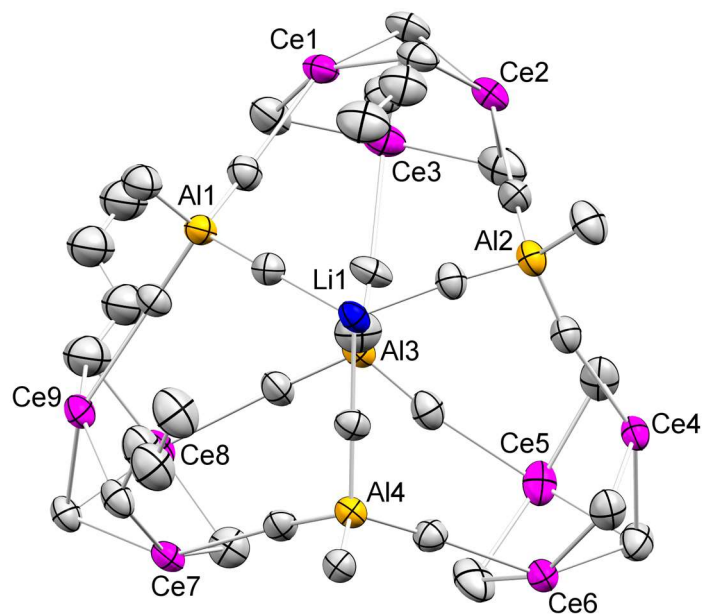


Figure C 2: Asymmetric unit of $[\text{Cp}^*_9\text{Ce}_9(\text{AlMe}_4)_4(\text{Me})_6(n\text{-Bu})_3(\text{CH}_2)_3\text{Li}]_2$ (**UP1**) with atomic displacement ellipsoids set at 50% probability. Hydrogen atoms and Cp* ligands are omitted for clarity. Every cerium atom is also bound to one Cp* ligand.

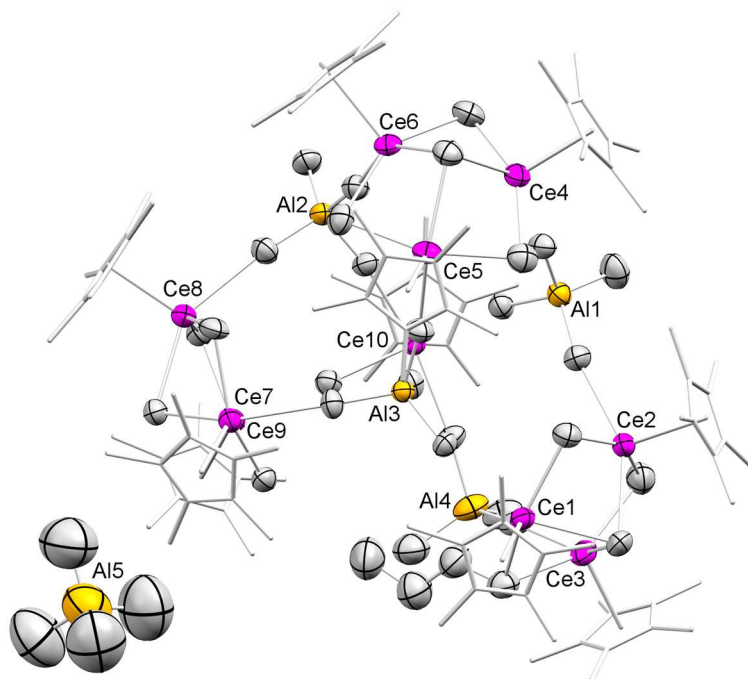
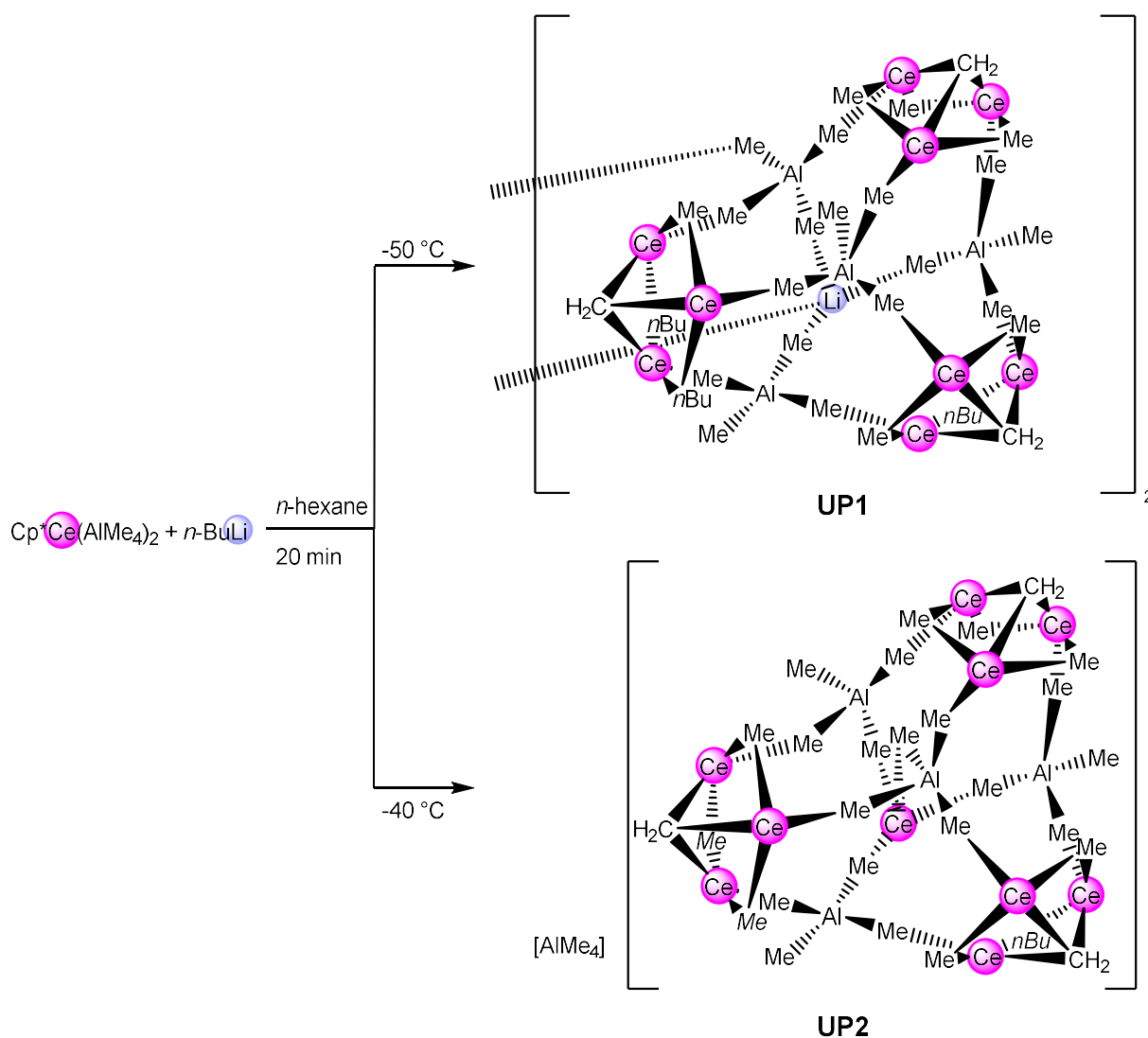


Figure C 3: Crystal structure of $\text{Cp}^*_{10}\text{Ce}_{10}(\text{AlMe}_4)_5(\text{Me})_9(n\text{-Bu})_1(\text{CH}_2)_3$ (**UP2**) with atomic displacement ellipsoids set at 50% probability. Hydrogen atoms and disordered Cp* ligands are omitted for clarity. Cp* ligands are also displayed as sticks for clarity.

It is certainly interesting that the introduction of so few *n*-butyl ligands, six in the case for **UP1** and only one for **UP2** in what seems to be arbitrarily chosen positions, results in the formation of these cluster species. Because these thermally labile complexes are not reproducibly formed but rather randomly (e.g. X-ray analyses), future work will focus on the use of differently-sized diamagnetic rare-earth-metal centers.



Scheme C 1: Syntheses of cerium complexes UP1 and UP2.

2 Experimental Section

General procedure

All manipulations were performed under an inert atmosphere (Ar) using either glovebox (MBraun UNILab^{pro}; <0.1 ppm O₂, <0.1 ppm H₂O) or standard Schlenk techniques with oven-dried glassware. The solvents were purified with Grubbs columns (MBraun SPS, solvent purification system) and stored in a glovebox. Anhydrous cerium(III) chloride (99.9%) was purchased from *abcr* and activated by Soxhlet extraction with THF giving CeCl₃(thf). *n*-Butyllithium (*n*-BuLi) (2.5 M solution in hexanes) was purchased from *Sigma Aldrich* and used as received. THF-*d*₈ was purchased from *Sigma Aldrich*, degassed, dried over NaK alloy for 24 h, filtered, and stored inside a glovebox. NMR spectra of moisture-sensitive compounds were recorded by using J. Young valve NMR tubes on a Bruker AVII+500 (¹H: 500.13 MHz). ¹H NMR shifts are referenced to a solvent resonance and reported in parts per million (ppm) relative to tetramethylsilane.^[36] Analysis of NMR spectra was performed with TopSpin 3.6.1 [Academic License].^[37] Crystals for X-ray crystallography were handpicked in a glovebox, coated with Parabar 10312, pump-oil, or perfluorinated oil, and stored on microscope slides. X-ray data were collected on a Bruker APEX II DUO diffractometer equipped with an I μ S microfocus sealed tube and QUAZAR optics for MoK α ($\lambda = 0.71073$ Å) and CuK α ($\lambda = 1.54184$ Å) radiation. The data collection strategy was determined using COSMO^[38] employing ω -scans. Raw data were processed using APEX^[39] and SAINT,^[40] corrections for absorption effects were applied using SADABS.^[41] The structures were solved by direct methods and refined against all data by full-matrix least-squares methods on F² using SHELXTL^[42] and ShelXL.^[43] Disorder models were calculated using DSR, a program for refining structures in ShelXL.^[44] All graphics were produced employing Mercury 4.2.0^[45] and POV-Ray.^[46]

[Cp*₉Ce₉(AlMe₄)₄(Me)₆(*n*-Bu)₃(CH₂)₃Li]₂ (UP1). Cp*Ce(AlMe₄)₂ (42.0 mg, 0.09 mmol) was dissolved in *n*-hexane (1 mL) and cooled to -50 °C, before a precooled solution of *n*-BuLi in hexanes (0.09 mmol, 1 equiv.) was added dropwise. After 20 min the yellow solution was filtered and concentrated in vacuo to give yellow crystals of [Cp*₉Ce₉(AlMe₄)₄(Me)₆(*n*-Bu)₃(CH₂)₃Li]₂, suitable for X-ray diffraction, in a low yield. Due to the paramagnetism of cerium, the NMR spectra were inconclusive (see Figure C 4 - C 6).

Cp*₁₀Ce₁₀(AlMe₄)₅(Me)₉(*n*-Bu)₁(CH₂)₃ (UP2). Cp*Ce(AlMe₄)₂ (50.0 mg, 0.11 mmol) was dissolved in *n*-hexane (2 mL) and cooled to -40 °C, before a precooled solution of *n*-BuLi in hexanes (0.11 mmol, 1 equiv.) was added dropwise. After 20 min the yellow solution was filtered and concentrated in vacuo to give yellow crystals of Cp*₁₀Ce₁₀(AlMe₄)₅(Me)₉(*n*-Bu)₁(CH₂)₃ (UP2), suitable for X-ray diffraction, in a low yield. Due to the paramagnetism of cerium, the NMR spectra were inconclusive (see Figure C 7).

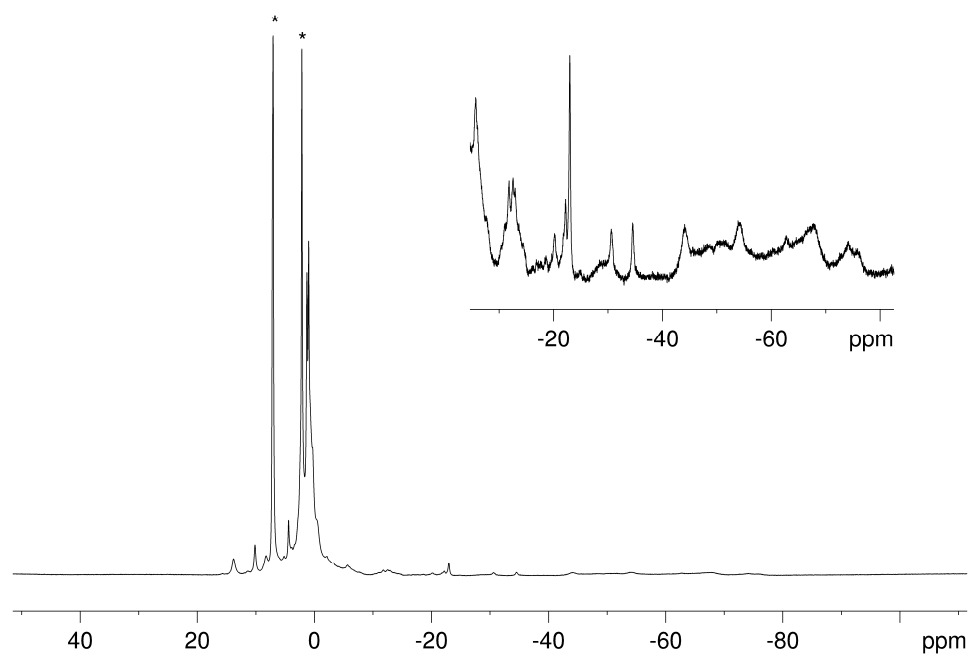


Figure C 4: ^1H NMR spectrum of $[\text{Cp}^*_9\text{Ce}_9(\text{AlMe}_4)_4(\text{Me})_6(\text{n-Bu})_3(\text{CH}_2)_3\text{Li}]_2$ (UP1) (500.13 MHz, THF- d_8 , 233 K) solvent residual signals are marked with *.

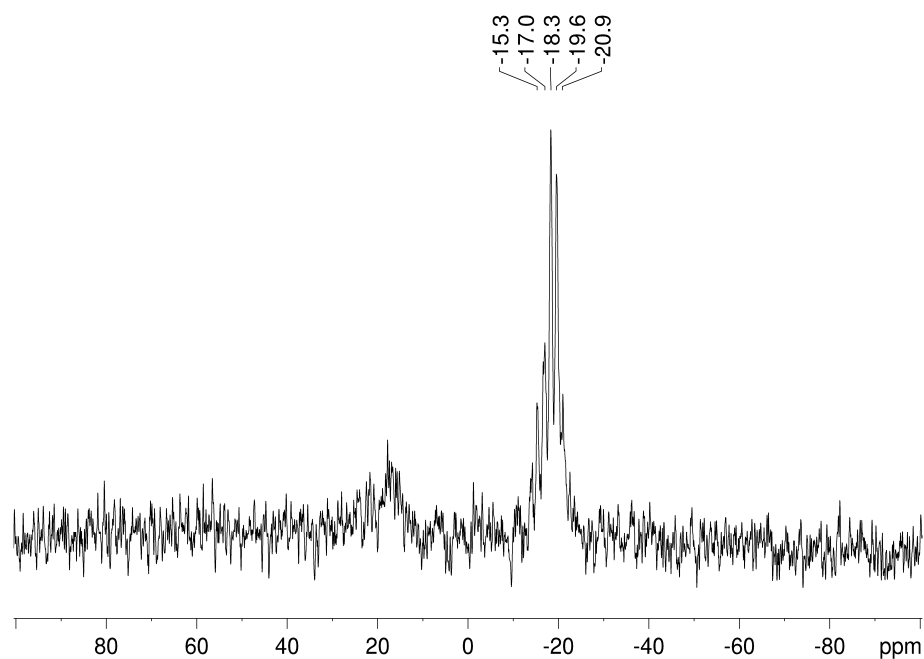


Figure C 5: ^7Li NMR spectrum of $[\text{Cp}^*_9\text{Ce}_9(\text{AlMe}_4)_4(\text{Me})_6(\text{n-Bu})_3(\text{CH}_2)_3\text{Li}]_2$ (UP1) (194.37 MHz, THF- d_8 , 233 K).

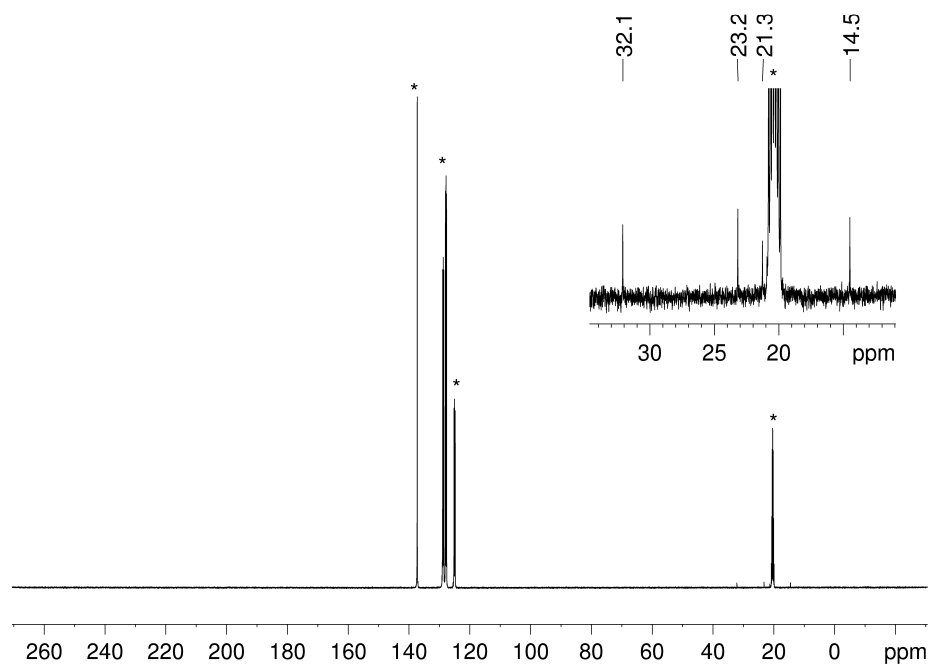


Figure C 6: ^{13}C NMR spectrum of $[\text{Cp}^*_9\text{Ce}_9(\text{AlMe}_4)_4(\text{Me})_6(n\text{-Bu})_3(\text{CH}_2)_3\text{Li}]_2$ (UP1) (125.76 MHz, THF- d_8 , 233 K) solvent residual signals are marked with *.

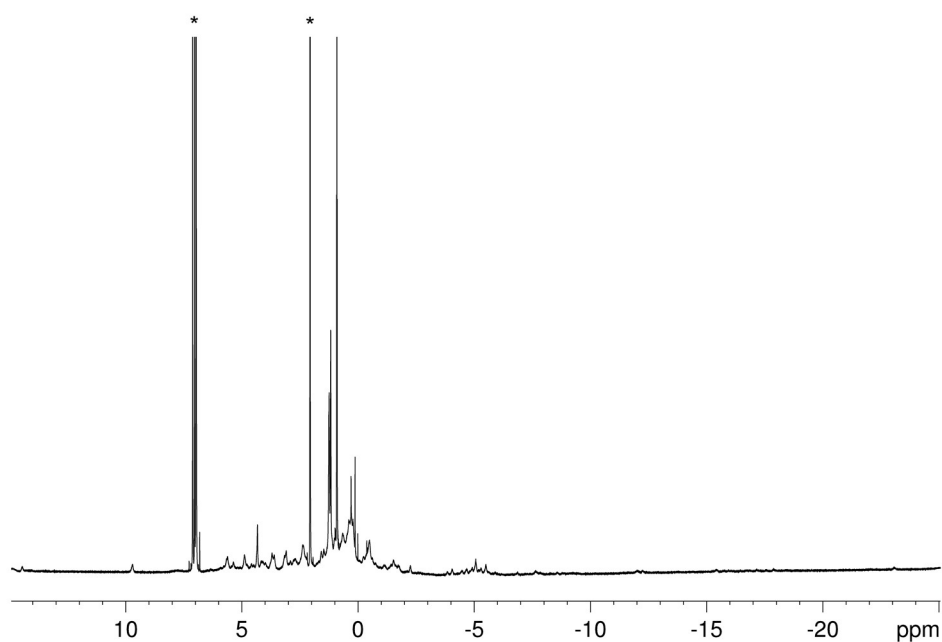


Figure C 7: ^1H NMR spectrum of $\text{Cp}^*_{10}\text{Ce}_{10}(\text{AlMe}_4)_5(\text{Me})_9(n\text{-Bu})_1(\text{CH}_2)_3$ (UP2) (500.13 MHz, THF- d_8 , 233 K) solvent residual signals are marked with *.

Table C 1: X-ray crystallographic parameters for complex **UP1**, **UP2**, and **UP3**

Compound	[Cp* ₉ Ce ₉ (AlMe ₄) ₄ (Me) ₆ (<i>n</i> -Bu) ₃ (CH ₂) ₃ Li] ₂	Cp* ₁₀ Ce ₁₀ (AlMe ₄) ₅ (Me) ₉ (<i>n</i> -Bu) ₁ (CH ₂) ₃
Sample code	UP1	UP2
Sample	TB093	TB125
Empirical formula	C ₁₂₇ H ₂₃₄ Al ₄ Ce ₉ Li	C ₁₃₆ H ₂₅₂ Al ₅ Ce ₁₀
Formula weight	3137.07	3423.46
Temperature [K]	150(2)	173(2)
Crystal system	Triclinic	Triclinic
Space group	P-1	P-1
a [Å]	20.483(3)	18.6901(14)
b [Å]	22.933(3)	19.5822(16)
c [Å]	23.466(4)	26.854(2)
α [°]	96.586(2)	98.587(2)
β [°]	110.423(2)	103.033(2)
γ [°]	115.212(2)	94.682(2)
Volume [Å ³]	8884(2)	9399.8(13)
Z	2	2
ρ _{calc} [g/cm ³]	1.173	1.210
μ [mm ⁻¹]	2.306	2.423
F(000)	3146	3426
Crystal size [mm ³]	0.201 x 0.153 x 0.094	0.141 x 0.115 x 0.024
Radiation	MoK _α (λ = 0.71073)	MoK _α (λ = 0.71073)
Temperature [K]	150	173
Θ range for data collection [°]	0.974 to 23.256	1.210 to 21.966
Index ranges	-22 ≤ h ≤ 22, -25 ≤ k ≤ 25, -26 ≤ l ≤ 26	-19 ≤ h ≤ 19, -20 ≤ k ≤ 20, -28 ≤ l ≤ 28
Reflections collected	138827	117197
Independent reflections	25494 [R _{int} = 0.0805]	22953 [R _{int} = 0.1033]
Data/restraints/parameters	25494 / 28050 / 2111	22953 / 6197 / 1683
Goodness-of-fit on F ² [^a]	1.020	1.022
Final R indexes [I ≥ 2σ(I)] ^[b] [^c]	R ₁ = 0.0558, wR ₂ = 0.1420	R ₁ = 0.0582, wR ₂ = 0.1450
Final R indexes [all data]	R ₁ = 0.0979, wR ₂ = 0.1703	R ₁ = 0.1102, wR ₂ = 0.1715
Largest diff. peak/hole [e Å ⁻³]	2.713 / -0.900	1.552 / -1.111

^[a]GOF = $[\sum w(F_0^2 - F_c^2)^2 / (n_0 - n_p)]^{1/2}$. ^[b]R₁ = $\Sigma(|F_0| - |F_c|) / \Sigma|F_0|$, F₀ > 4σ(F₀). ^[c]wR₂ = $\{\Sigma[w(F_0^2 - F_c^2)^2] / \Sigma[w(F_0^2)^2]\}^{1/2}$.

D

Bibliography

- [1] a) H. B. Kagan, J. L. Namy, *Tetrahedron* **1986**, *42*, 6573-6614; b) B. M. Trost, I. Fleming, *T. Imamoto in Comprehensive organic synthesis*, Eds., Pergamon, Oxford, **1991**, Chapter 1.8; c) G. A. Molander, *Chem. Rev.* **1992**, *92*, 29-68; d) T. Imamoto, *Lanthanides in organic synthesis*, Academic Press, London, **1994**.
- [2] a) H. Tse-Lok, *Synthesis* **1973**, *1973*, 347-354; b) V. Nair, J. Mathew, J. Prabhakaran, *Chem. Soc. Rev.* **1997**, *26*, 127-132; c) A. K. Das, *Coord. Chem. Rev.* **2001**, *213*, 307-325; d) V. Nair, L. Balagopal, R. Rajan, J. Mathew, *Acc. Chem. Res.* **2004**, *37*, 21-30; e) V. Nair, A. Deepthi, *Tetrahedron* **2009**, *65*, 10745-10755; f) V. Sridharan, J. C. Menéndez, *Chem. Rev.* **2010**, *110*, 3805-3849.
- [3] a) J. L. Namy, P. Grirad, H. B. Kagan, *Nou. J. Chim.* **1977**, *1*, 5-7; b) H. B. Kagan, *J. Alloys Compd.* **2006**, *408-412*, 421-426; c) K. C. Nicolaou, S. P. Ellery, J. S. Chen, *Angew. Chem. Int. Ed.* **2009**, *48*, 7140-7165; d) M. Szostak, D. J. Procter, *Angew. Chem. Int. Ed.* **2012**, *51*, 9238-9256; e) M. Szostak, N. J. Fazakerley, D. Parmar, D. J. Procter, *Chem. Rev.* **2014**, *114*, 5959-6039; f) X. Just-Baringo, D. J. Procter, *Acc. Chem. Res.* **2015**, *48*, 1263-1275; g) Á. Péter, D. J. Procter, *CHIMIA* **2020**, *74*, 18-22; h) R. S. Miller, J. M. Sealy, M. Shabangi, M. L. Kuhlman, J. R. Fuchs, R. A. Flowers, *J. Am. Chem. Soc.* **2000**, *122*, 7718-7722; i) E. Prasad, R. A. Flowers, *J. Am. Chem. Soc.* **2002**, *124*, 6895-6899; j) P. R. Chopade, E. Prasad, R. A. Flowers, *J. Am. Chem. Soc.* **2004**, *126*, 44-45; k) J. A. Teprovich Jr., M. N. Balili, T. Pintauer, R. A. Flowers II, *Angew. Chem. Int. Ed.* **2007**, *46*, 8160-8163; l) R. A. Flowers II, *Synlett* **2008**, *2008*, 1427-1439; m) K. A. Choquette, D. V. Sadasivam, R. A. Flowers, *J. Am. Chem. Soc.* **2010**, *132*, 17396-17398; n) D. V. Sadasivam, J. A. Teprovich, D. J. Procter, R. A. Flowers, *Org. Lett.* **2010**, *12*, 4140-4143; o) T. V. Chciuk, W. R. Anderson, R. A. Flowers, *J. Am. Chem. Soc.* **2016**, *138*, 8738-8741; p) S. Maity, R. A. Flowers, *J. Am. Chem. Soc.* **2019**, *141*, 3207-3216.
- [4] a) T. Imamoto, *Pure Appl. Chem.* **1990**, *62*, 747-752; b) T. Imamoto, *Organocerium Reagents, Vol. 1*, Chiba University, Japan, **1992**; c) H.-J. Liu, K.-S. Shia, X. Shang, B.-Y. Zhu, *Tetrahedron* **1999**, *55*, 3803-3830; d) G. Bartoli, E. Marcantoni, M. Marcolini, L. Sambri, *Chem. Rev.* **2010**, *110*, 6104-6143; e) T.-L. Ho, in *Fieser and Fieser's Reagents for Organic Synthesis*, **2017**.
- [5] a) T. A. Beineke, J. Delgaudio, *Inorg. Chem.* **1968**, *7*, 715-721; b) W. J. Evans, T. S. Gummertsheimer, J. W. Ziller, *J. Am. Chem. Soc.* **1995**, *117*, 8999-9002.
- [6] a) J.-L. Luche, L. Rodriguez-Hahn, P. Crabbé, *J. Chem. Soc., Chem. Commun.* **1978**, 601-602; b) J. L. Luche, *J. Am. Chem. Soc.* **1978**, *100*, 2226-2227; c) A. L. Gemal, J. L. Luche, *J. Am. Chem. Soc.* **1981**, *103*, 5454-5459.
- [7] T. Imamoto, T. Kusumoto, M. Yokoyama, *J. Chem. Soc., Chem. Commun.* **1982**, 1042-1044.
- [8] T. Imamoto, T. Kusumoto, Y. Tawarayama, Y. Sugiura, T. Mita, Y. Hatanaka, M. Yokoyama, *J. Org. Chem.* **1984**, *49*, 3904-3912.
- [9] T. Imamoto, Y. Sugiura, N. Takiyama, *Tetrahedron Lett.* **1984**, *25*, 4233-4236.

- [10] a) T. Imamoto, T. Kusumoto, Y. Hatanaka, M. Yokoyama, *Tetrahedron Lett.* **1982**, *23*, 1353-1356; b) W. J. Evans, J. H. Meadows, A. L. Wayda, W. E. Hunter, J. L. Atwood, *J. Am. Chem. Soc.* **1982**, *104*, 2008-2014; c) W. J. Evans, J. H. Meadows, A. L. Wayda, W. E. Hunter, J. L. Atwood, *J. Am. Chem. Soc.* **1982**, *104*, 2015-2017.
- [11] a) J. M. Birmingham, G. Wilkinson, *J. Am. Chem. Soc.* **1956**, *78*, 42; b) J. B. Reed, B. S. Hopkins, L. F. Andrieth, *Inorg. Synth.* **1961**, *1*, 28.
- [12] a) T. Imamoto, Y. Sugiura, *J. Organomet. Chem.* **1985**, *285*, C21-C23; b) T. Imamoto, N. Takiyama, K. Nakamura, T. Hatajima, Y. Kamiya, *J. Am. Chem. Soc.* **1989**, *111*, 4392-4398.
- [13] T. Berger, J. Lebon, C. Maichle-Mössmer, R. Anwender, *Angew. Chem. Int. Ed.* **2021**, *60*, 15622-15631.
- [14] W. J. Evans, J. D. Feldman, J. W. Ziller, *J. Am. Chem. Soc.* **1996**, *118*, 4581-4584.
- [15] W. J. Evans, M. A. Ansari, J. D. Feldman, R. J. Doedens, J. W. Ziller, *J. Organomet. Chem.* **1997**, *545-546*, 157-162.
- [16] a) H. Schumann, J. Müller, *Angew. Chem. Int. Ed. Engl.* **1978**, *17*, 276-276; b) H. Schumann, J. Pickardt, N. Bruncks, *Angew. Chem. Int. Ed. Engl.* **1981**, *20*, 120-121; c) H. Schumann, J. Müller, N. Bruncks, H. Lauke, J. Pickardt, H. Schwarz, K. Eckart, *Organometallics* **1984**, *3*, 69-74.
- [17] M. U. Kramer, D. Robert, S. Arndt, P. M. Zeimentz, T. P. Spaniol, A. Yahia, L. Maron, O. Eisenstein, J. Okuda, *Inorg. Chem.* **2008**, *47*, 9265-9278.
- [18] a) A. L. Wayda, W. J. Evans, *J. Am. Chem. Soc.* **1978**, *100*, 7119-7121; b) H. Schumann, W. Genthe, E. Hahn, J. Pickardt, H. Schwarz, K. Eckart, *J. Organomet. Chem.* **1986**, *306*, 215-225; c) W. Noh, G. S. Girolami, *Polyhedron* **2007**, *26*, 3865-3870.
- [19] a) M. F. Lappert, R. Pearce, *J. Chem. Soc., Chem. Commun.* **1973**, 126-126; b) S. Bambirra, M. W. Bouwkamp, A. Meetsma, B. Hessen, *J. Am. Chem. Soc.* **2004**, *126*, 9182-9183; c) H. Schumann, D. M. M. Freckmann, S. Dechert, *Z. Anorg. Allg. Chem.* **2002**, *628*, 2422-2426.
- [20] J. L. Atwood, M. F. Lappert, R. G. Smith, H. Zhang, *J. Chem. Soc., Chem. Commun.* **1988**, 1308-1309.
- [21] C. Eaborn, P. B. Hitchcock, K. Izod, J. D. Smith, *J. Am. Chem. Soc.* **1994**, *116*, 12071-12072.
- [22] H. Schumann, J. A. Meese-Marktscheffel, A. Dietrich, J. Pickardt, *J. Organomet. Chem.* **1992**, *433*, 241-252.
- [23] D. P. Mills, A. J. Wooles, J. McMaster, W. Lewis, A. J. Blake, S. T. Liddle, *Organometallics* **2009**, *28*, 6771-6776.
- [24] P. J. Shapiro, W. P. Schaefer, J. A. Labinger, J. E. Bercaw, W. D. Cotter, *J. Am. Chem. Soc.* **1994**, *116*, 4623-4640.

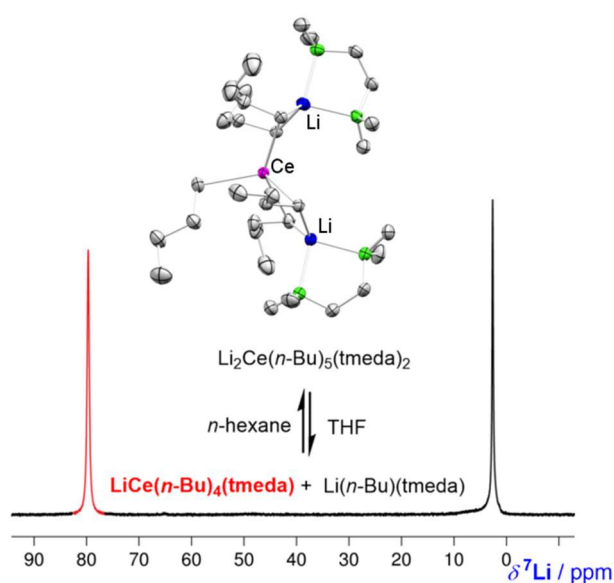
- [25] P. Voth, S. Arndt, T. P. Spaniol, J. Okuda, L. J. Ackerman, M. L. H. Green, *Organometallics* **2003**, *22*, 65-76.
- [26] W. Mao, L. Xiang, C. Alvarez Lamsfus, L. Maron, X. Leng, Y. Chen, *J. Am. Chem. Soc.* **2017**, *139*, 1081-1084.
- [27] W. Rong, M. Wang, S. Li, J. Cheng, D. Liu, D. Cui, *Organometallics* **2018**, *37*, 971-978.
- [28] M. R. MacDonald, R. R. Langeslay, J. W. Ziller, W. J. Evans, *J. Am. Chem. Soc.* **2015**, *137*, 14716-14725.
- [29] M. D. Fryzuk, G. Giesbrecht, S. J. Rettig, *Organometallics* **1996**, *15*, 3329-3336.
- [30] S. E. Denmark, J. P. Edwards, O. Nicaise, *J. Org. Chem.* **1993**, *58*, 569-578.
- [31] a) A. Music, D. Didier, *Synlett* **2019**, *30*, 1843-1849; b) A. D. Benischke, L. Anthore-Dalion, G. Berionni, P. Knochel, *Angew. Chem. Int. Ed.* **2017**, *56*, 16390-16394; c) L. Anthore-Dalion, A. D. Benischke, B. Wei, G. Berionni, P. Knochel, *Angew. Chem. Int. Ed.* **2019**, *58*, 4046-4050; d) B. Wei, D. Zhang, Y.-H. Chen, A. Lei, P. Knochel, *Angew. Chem. Int. Ed.* **2019**, *58*, 15631-15635.
- [32] A. Music, C. Hoarau, N. Hilgert, F. Zischka, D. Didier, *Angew. Chem. Int. Ed.* **2019**, *58*, 1188-1192.
- [33] a) H. Li, *Synlett* **2012**, *23*, 1407-1408; b) T. L. Rathman, J. A. Schwindeman, *Organic Process Research & Development* **2014**, *18*, 1192-1210.
- [34] D. Barisic, D. Diether, C. Maichle-Mössmer, R. Anwander, *J. Am. Chem. Soc.* **2019**, *141*, 13931-13940.
- [35] a) M. Bochmann, *Organometallics* **2010**, *29*, 4711-4740; b) A. Joshi, H. S. Zijlstra, E. Liles, C. Concepcion, M. Linnolahti, J. S. McIndoe, *Chem. Sci.* **2021**, *12*, 546-551; c) S. Pasykiewicz, *Polyhedron* **1990**, *9*, 429-453; d) J.-N. Pédeutour, K. Radhakrishnan, H. Cramail, A. Deffieux, *Macromol. Rapid Commun.* **2001**, *22*, 1095-1123; e) S. S. Reddy, S. Sivaram, *Prog. Polym. Sci.* **1995**, *20*, 309-367; f) J. R. Severn, J. C. Chadwick, *Wiley-VCH, Weinheim* **2008**, *1*, 95-138; g) H. S. Zijlstra, M. C. A. Stuart, S. Harder, *Macromolecules* **2015**, *48*, 5116-5119; h) E. Zurek, T. Ziegler, *Prog. Polym. Sci.* **2004**, *29*, 107-148; i) E. Y.-X. Chen, T. J. Marks, *Chem. Rev.* **2000**, *100*, 1391-1434; j) H. W. Roesky, M. G. Walawalkar, R. Murugavel, *Acc. Chem. Res.* **2001**, *34*, 201-211; k) L. Resconi, S. Bossi, L. Abis, *Macromolecules* **1990**, *23*, 4489-4491; l) H. S. Zijlstra, S. Harder, *Eur. J. Inorg. Chem.* **2015**, 19-43.
- [36] G. R. Fulmer, A. J. M. Miller, N. H. Sherden, H. E. Gottlieb, A. Nudelman, B. M. Stoltz, J. E. Bercaw, K. I. Goldberg, *Organometallics* **2010**, *29*, 2176-2179.
- [37] *TopSpin v. 3.6.1, Bruker AXS Inc., Madison, WI* **2018**.
- [38] *COSMO v. 1.61, Bruker AXS Inc., Madison, WI* **2012**.
- [39] *APEX 3 v. 2017.3-0, Bruker AXS Inc., Madison, WI* **2017**.

-
- [40] *SAINT v. 8.38A, Bruker AXS Inc., Madison, WI* **2017**.
- [41] L. Krause, R. Herbst-Irmer, G. M. Sheldrick, D. Stalke, *J. Appl. Crystallogr.* **2015**, *48*, 3-10.
- [42] G. Sheldrick, *Acta Crystallogr. Sect. C.* **2015**, *71*, 3-8.
- [43] C. B. Hübschle, G. M. Sheldrick, B. Dittrich, *J. Appl. Crystallogr.* **2011**, *44*, 1281-1284.
- [44] D. Kratzert, J. J. Holstein, I. Krossing, *J. Appl. Crystallogr.* **2015**, *48*, 933-938.
- [45] C. F. Macrae, P. R. Edgington, P. McCabe, E. Pidcock, G. P. Shields, R. Taylor, M. Towler, J. van de Streek, *J. Appl. Crystallogr.* **2006**, *39*, 453-457.
- [46] *POV-Ray v.3.6, Persistence of Vision Pty. Ltd., POV-Ray Williamstown, Victoria, Australia*, <http://www.povray.org> **2004**.

E

Publications

CeCl₃/*n*-BuLi: Unraveling Imamoto's Organocerium Reagent



<https://doi.org/10.1002/anie.202103889>
<https://doi.org/10.1002/ange.202103889>
reprinted with permission from
Angew. Chem. Int. Ed. **2021**, *60*, 15622 – 15631
Angew. Chem. **2021**, *133*, 15750 – 15760

VIP Structure Elucidation Very Important Paper

CeCl₃/*n*-BuLi: Unraveling Imamoto's Organocerium Reagent

Tassilo Berger, Jakob Lebon, Cécilia Maichle-Mössmer, and Reiner Anwander*

Dedicated to Professor Karl W. Törnroos on the occasion of his 65th birthday

Abstract: CeCl₃(thf) reacts at low temperatures with MeLi, *t*-BuLi, and *n*-BuLi to isolable organocerium complexes. Solvent-dependent extensive *n*-BuLi dissociation is revealed by ⁷Li NMR spectroscopy, suggesting “Ce(*n*-Bu)₃(thf)_{*x*}” or solvent-separated ion pairs like “[Li(thf)₄][Ce(*n*-Bu)₄(thf)₃]⁺” as the dominant species of the Imamoto reagent. The stability of complexes Li₃Ln(*n*-Bu)₆(thf)₄ increases markedly with decreasing Ln^{III} size. Closer inspection of the solution behavior of crystalline Li₃Lu(*n*-Bu)₆(thf)₄ and mixtures of LuCl₃(thf)₃/*n*-BuLi in THF indicates occurring *n*-BuLi dissociation only at molar ratios of <1:3. *n*-BuLi-depleted complex LiLu(*n*-Bu)₃Cl(tmeda)₂ was obtained by treatment of Li₂Lu(*n*-Bu)₅(tmeda)₂ with ClSiMe₃, at the expense of LiCl incorporation. Imamoto's ketone/tertiary alcohol transformation was examined with 1,3-diphenylpropan-2-one, affording 99% of alcohol.

Introduction

The redox reagents Ceric Ammonium Nitrate (CAN = (NH₄)₂Ce(NO₃)₆) and SmI₂(thf)₂ as well as the binary alkylating agents CeCl₃/LiR (R = alkyl like CH₃ or *n*-C₄H₉) constitute the most commonly employed rare-earth-metal reagents in organic transformations (including natural product synthesis).^[1–4] The cause of reactivity of the redox-active compounds is well understood,^[2–3] and their crystal structures were revealed by X-ray diffraction (XRD) analyses.^[5,6] In the solid state, CAN exhibits a three-dimensional network of 12-coordinate hexanitratocerate anions and ammonium cations interconnected by hydrogen bonding.^[5] On the other hand, samarium diiodide crystallizes as a monomeric pentasolvate, SmI₂(thf)₅, from THF solution.^[6] Due to the extreme air and moisture sensitivity and combined thermal instability, a detailed structural investigation of organocerium reagents has remained elusive.

In 1984, Tsuneo Imamoto et al. described the use of binary mixtures CeI₃/RLi (R = Me, Et, *n*-Bu, *sec*Bu, Ph) and

How to cite: *Angew. Chem. Int. Ed.* **2021**, *60*, 15622–15631
International Edition: doi.org/10.1002/anie.202103889
German Edition: doi.org/10.1002/ange.202103889

CeCl₃/RLi (R = *n*-Bu, *t*Bu) as effective reagents for regioselective carbon–carbon-bond forming with various carbonyl compounds.^[7] The best results were obtained when employing equimolar mixtures at –78 °C to –65 °C. Like for the Luche reagent (CeCl₃(H₂O)₇/NaBH₄),^[8] cerium was launched as the least expensive rare-earth metal while a greater part of transformations was performed with *n*-BuLi as an easy-to-handle (as well as the cheapest) organolithium derivative.^[9] Figure 1 depicts characteristic features of the nucleophilic addition of such organocerium reagents to carbonyl compounds, including smooth and selective 1,2-addition in case of α,β-unsaturated or easily enolizable substrate molecules,^[7] functional group tolerance^[10] as well as diastereocontrol via chelate coordination.^[11]

The much improved selectivity compared to organolithium or Grignard reagents was assigned to a changed basicity of the organocerium reagent and enhanced hardness of the carbonyl carbon atom.^[4] The latter originates from the strong oxophilicity of the trivalent cerium. Although Imamoto's seminal organocerium reagents embarked on a new and prosperous branch of organolanthanide chemistry, very few studies exist that target the structural elucidation of such bimetallic mixtures.^[12] In sharp contrast, heterobimetallic main-group organometallic reagents have been given much greater attention, and entitled modern ate chemistry.^[13]

Imamoto-type rare-earth-metal reagents, more recently employed for halogen-rare-earth-metal exchange reactions^[14] or Zweifel olefinations,^[15] are as a rule generated in situ and have been designated “*n*-Bu₂LaCl·4LiCl”,^[16] “*n*-Bu₃Sm·5LiCl”,^[17] or simply “*n*-Bu₃Ce”.^[15] The formulas were derived from X-ray absorption fine structure (EXAFS) studies^[18] or Raman spectroscopy.^[15] Previous enlightening studies on the CeCl₃/RLi binary system focused mainly on the composition and activation of the cerous chloride precursor^[12,19–20] as well as the effect/effectiveness of reagent stoichiometry.^[21] It was revealed that the generally applied thermal activation of the commercially available heptahydrate CeCl₃(H₂O)₇ not only generates a material of composition [CeCl₃(H₂O)]_{*n*}^[12c] but also benefits from sonication.^[20]

[*] T. Berger, J. Lebon, Dr. C. Maichle-Mössmer, Prof. Dr. R. Anwander
Institut für Anorganische Chemie
Eberhard Karls Universität Tübingen
Auf der Morgenstelle 18, 72076 Tübingen (Germany)
E-mail: reiner.anwander@uni-tuebingen.de

Supporting information and the ORCID identification number(s) for the author(s) of this article can be found under:
https://doi.org/10.1002/anie.202103889.

© 2021 The Authors. Angewandte Chemie International Edition published by Wiley-VCH GmbH. This is an open access article under the terms of the Creative Commons Attribution License, which permits use, distribution and reproduction in any medium, provided the original work is properly cited.

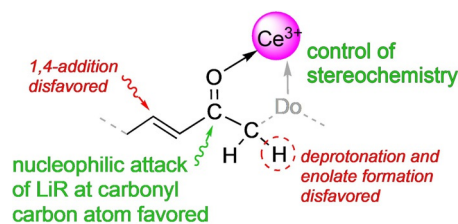


Figure 1. Ce^{III}–carbonyl coordination directs highly selective nucleophilic addition reactions of binary CeX₃/RLi (X = halogenido; R = alkyl).

Importantly, organocerium addition to hydrazones was found most effective and selective for a 1:1 stoichiometry of $\text{CeCl}_3/\text{MeLi}$, but the active reagent formed at different stoichiometries was proposed to be a trimethylcerium species (supported by unreacted CeCl_3).^[21] Although this latter investigation “precluded firm conclusions”, the results “do point out the fallacy of ascribing reagent composition on the basis of mixing stoichiometry especially at low loadings of alkyl lithium”.^[21]

Herein we describe the successful isolation and structural characterization of rare-earth-metal *n*-butyl complexes formed in $\text{LnCl}_3/n\text{-BuLi}$ systems devoid of ancillary ligands. NMR spectroscopic studies involving the ^7Li nucleus provide valuable insights into the solution behavior of such binary mixtures, pointing to the true organocerium species of the Imamoto reagent.

Results and Discussion

Synthesis and Solid-State Structure of the Organocerium Derivatives $\text{Li}_3\text{Ce}(\text{CH}_3)_6(\text{tmeda})_3$ and $[\text{Li}(\text{thf})_4][\text{Ce}(\text{t-Bu})_4]$. For assessing the CeCl_3/LiR salt-metathesis protocol we initially probed the methyl derivative, since this would rule out $\beta\text{-H}$ elimination as a potential decomposition pathway. Complexes of the type $\text{Li}_3\text{LnMe}_6(\text{tmeda})_3$ featuring the entire lanthanide series except for promethium and europium were accessed by Schumann et al. as early as 1978, via mixtures $\text{LnCl}_3/\text{LiMe}/\text{OEt}_2/\text{TMEDA}$ (TMEDA = tetramethylethylenediamine).^[22] Solid-state structures applying XRD analysis were described for the rare-earth metals erbium^[22b] and holmium.^[22c] Moreover, both the stabilizing effect of chelating tmeda, teeda (= tetraethylethylenediamine), and dme (= dimethoxyethylene) coligands and the enhanced instability of derivatives of the “lighter” and larger-sized rare-earth metals have been emphasized.^[23] This is in accord with more recent findings by Okuda et al. on the stability of $\text{Li}_3\text{LnMe}_6(\text{thf})_x$ (isolable for Ln smaller than Eu), which form the pentametallic ate complexes $\text{Li}_3\text{Sc}_2\text{Me}_9(\text{thf})_2(\text{OEt}_2)_3$ and $\text{Li}_3\text{Ln}_2\text{Me}_9(\text{thf})_3(\text{OEt}_2)_2$ (Ln = Y, Tb), when crystallized from diethyl ether solutions.^[24] Such a Ln^{III}-size dependency on thermal stability is commonly observed in rare-earth-metal alkyl chemistry^[25] and showcased for derivatives $\text{Ln}(\text{CH}_2\text{SiMe}_3)_3(\text{thf})_x$,^[26] $[\text{Li}(\text{dme})_3][\text{Ln}(\text{t-Bu})_4]$ (see below),^[27] and solvent-free $[\text{LnMe}_3]_n$.^[28] Since the cerium derivative $\text{Li}_3\text{Ce}(\text{CH}_3)_6(\text{tmeda})_3$ (**1**) was only mentioned briefly as an impure product ($\delta_{\text{CH}_3} = -6.4$ ppm),^[22–23] we re-visited its synthesis applying a slightly modified version of the Schumann protocol. Accordingly, cerous methyl complex **1** could be synthesized at -10°C in good yield (83%), and was obtained in analytically pure, single-crystalline form. The solid-state structure of complex **1** turned out to be isostructural to the derivatives of the considerably smaller-sized erbium and holmium (Figure 2).^[22]

The ^1H NMR spectrum revealed the methyl signal at $\delta = -4.08$ ppm, reflecting a significant paramagnetic shift induced by Ce^{III} (Supporting Information, Figure S4). As expected, the Ce–C distance of 2.6795(19) Å in **1** is considerably longer than those in the holmium (2.563(18) Å)^[22b] and erbium congeners (2.57(2) Å).^[22c] For further comparison, the Ce–C distances in 6-coordinate $\text{Ce}(\text{CH}_2\text{Ph})_3(\text{thf})_3$ and $\text{Ce}(\text{AlMe}_4)_3$

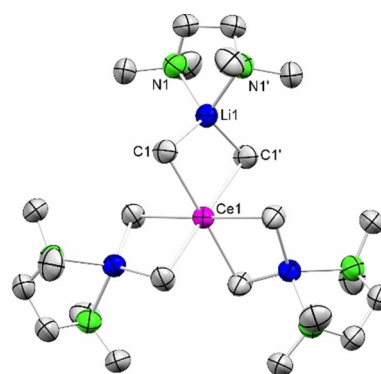


Figure 2. Crystal structure of $\text{Li}_3\text{Ce}(\text{CH}_3)_6(\text{tmeda})_3$ (**1**).^[59] Atomic displacement ellipsoids set at 50% probability. Hydrogen atoms omitted for clarity. Selected interatomic distances [Å] and angles [°]: Ce1–C1 2.6795(19), Li1–C1 2.205(3), Li1–N1 2.106(3); C1–Ce1–C1' 88.05(9).

fall in the range 2.600(2)–2.614(2) Å^[29] and 2.620(7)–2.646(8) Å,^[30] respectively, while those in formally 3-coordinate complexes $\text{Ce}[\text{CH}(\text{SiMe}_3)_2]_3$ and $\text{Ce}[\text{C}(\text{SiHMe}_2)_3]_3$ were detected at 2.475(7) Å^[31] and 2.651(2)/2.659(2)/2.672(2) Å, respectively.^[32]

Homoleptic anionic *tert*-butyl complexes were previously reported for $[\text{Li}(\text{thf})_x][\text{Ln}(\text{t-Bu})_4]$ (Ln = Sm, Er: $x = 4$; Y: $x = 3$),^[27a] $[\text{Li}(\text{OEt}_2)_4][\text{Er}(\text{t-Bu})_4]$,^[22c] $[\text{Li}(\text{tmeda})_2][\text{Ln}(\text{t-Bu})_4]$ (Ln = Tb, Lu),^[22c,27b] and $[\text{Li}(\text{dme})_3][\text{Ln}(\text{t-Bu})_4]$ (Ln = Tb, Er).^[27c] Crystal structures were obtained for $[\text{Li}(\text{tmeda})_2][\text{Lu}(\text{t-Bu})_4]$ ^[27b] and $[\text{Li}(\text{dme})_3][\text{Er}(\text{t-Bu})_4]$,^[27c] whereas the enhanced thermal instability of derivatives of the “lighter” rare-earth metals was pointed out. In order to test our low-temperature set-up for organocerium derivatives prone to $\beta\text{-H}$ elimination,^[33] we targeted the anionic fragment $[\text{Ce}(\text{t-Bu})_4]$. Although the mixture $\text{CeCl}_3(\text{thf})/\text{t-BuLi}/\text{THF}$ gave access to complex $[\text{Li}(\text{thf})_4][\text{Ce}(\text{t-Bu})_4]$ (**2**) at -40°C , single crystals could be obtained only from very concentrated, oily residues, not allowing for decent elemental analysis (^1H NMR spectrum: $\delta_{\text{t-Bu}} = 2.39$ ppm, Figure S7). Notwithstanding an XRD analysis revealed a 4-coordinate cerium center (Figure 3), being isostructural to the previously reported erbium^[27c] and lutetium derivatives.^[27b] The Ce–C distances range from 2.501(11) to 2.544(11) Å and are considerably shorter than those in 6-coordinate **1** (2.6795(19) Å), but match those of $[\text{Li}(\text{tmeda})_2][\text{Lu}(\text{t-Bu})_4]$ (2.32(2)–2.43-

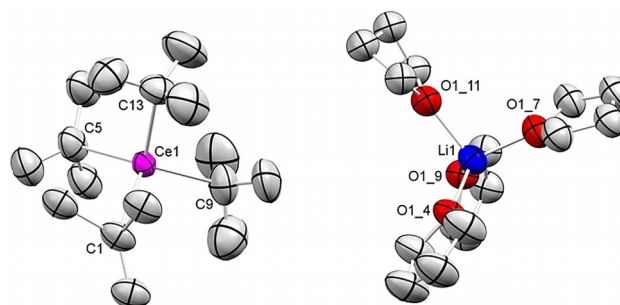
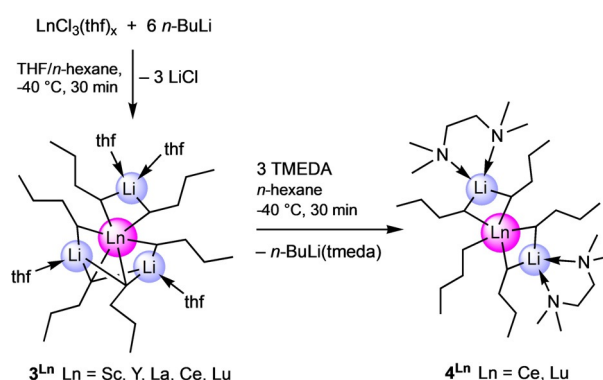


Figure 3. Crystal structure of $[\text{Li}(\text{thf})_4][\text{Ce}(\text{t-Bu})_4]$ (**2**).^[59] Atomic displacement ellipsoids set at 30% probability. Hydrogen atoms omitted for clarity. Selected interatomic distances [Å] and angles [°]: Ce1–C1 2.524(9), Ce1–C5 2.513(8), Ce1–C9 2.50(2), Ce1–C13 2.54(2); C–Ce1–C (range) 105.9(10)–111.8(8).

(2 Å)^[27b] and [Li(dme)₃][Er(*t*-Bu)₄] (2.352(6)–2.395(6) Å)^[27c] when taking into account the Ln^{III} ion size.

Synthesis and Solid-State Structures of *n*-Butyl Derivatives Li₃Ln(*n*-Bu)₆(thf)₄ and Li₂Ln(*n*-Bu)₅(tmeda)₂. Having proven the tamable thermal instability of organocerium complexes **1** and **2** we next tackled the feasibility of the respective *n*-butyl derivatives. Initially, we attempted to isolate a crystalline cerium-containing compound from reactions of cerium chloride (thf adduct) with various amounts of *n*-butyllithium in tetrahydrofuran at low temperatures (−40 °C). Not quite unexpectedly, these endeavors proved to be unsuccessful in the first place. Having in mind the presumably enhanced stability of derivatives of the smaller-sized rare-earth metals and to better follow the metathesis reactions via NMR spectroscopy we quickly began to focus on lutetium. Indeed, at complex Li₃Lu(*n*-Bu)₆(thf)₄ (**3^{Lu}**, Figure 4) could be isolated from the reaction of LuCl₃(thf)₂ with 3.3 equivalents of *n*-BuLi in *n*-hexane. However, in order to accomplish complex **3^{Lu}** six equivalents of *n*-BuLi must have reacted and associated per LuCl₃(thf)₂. It is also notable that four thf molecules have been accommodated in the complex despite the presence of only two in the lutetium chloride precursor. Therefore, THF appeared to be the limiting factor for this reaction. Optimization of the reaction conditions gave the so far best results when anhydrous rare-earth-metal chlorides LnCl₃(thf)_x (Ln = Sc, Y, La, Ce and Lu; covering the entire Ln^{III} size range) were suspended in a mixture of *n*-hexane and THF and cooled to −40 °C prior to the addition of *n*-BuLi. Removal of the volatiles after 30 minutes under reduced pressure, extracting the remaining solid with *n*-hexane, and concentrating the obtained solution gave crystalline Li₃Ln(*n*-Bu)₆(thf)₄ (**3^{Ln}**, Scheme 1).

Despite our best efforts, we could obtain crystals suitable for XRD analysis only for the lutetium derivative **3^{Lu}**. The



Scheme 1. Synthesis of *n*-butyl complexes **3^{Ln}** and **4^{Ln}**.

crystalline material formed for the other “larger” rare-earth-metal centers displayed only very poor diffraction behavior. Complex **3^{Lu}** features a lutetium center surrounded by six *n*-butyl ligands, which show distinct linkages to the lithium atoms. Two hydrocarbyl ligands are unsymmetrically bridged by one alkali metal, while the two remaining lithium atoms are unsymmetrically linked to three *n*-butyl ligands each. The coordination sphere of the three lithium atoms is completed by four THF molecules.

The Lu–C distances range from 2.44(2) to 2.58(3) Å, matching those in Li₃Lu(CH₃)₆(dme)₃ (2.48(4)–2.57(4) Å)^[23a] Lu(AlMe₄)₃ (2.455(2)–2.471(2) Å)^[34] and Lu(GaMe₄)₃ (2.465(2)–2.493(2) Å)^[35] All complexes **3^{Ln}** were characterized by NMR spectroscopy and elemental analysis. A ⁴⁵Sc NMR experiment for **3^{Sc}** showed a broad signal pattern with a main peak centered at +502 ppm, clearly indicating σ-bonded alkyl species in solution (Figure S17)^[36–37] For comparison, the ⁴⁵Sc chemical shift of ScMe₃(thf)_x was detected at +601.7 ppm.^[36] Similarly, the ¹H-⁸⁹Y HSQC NMR

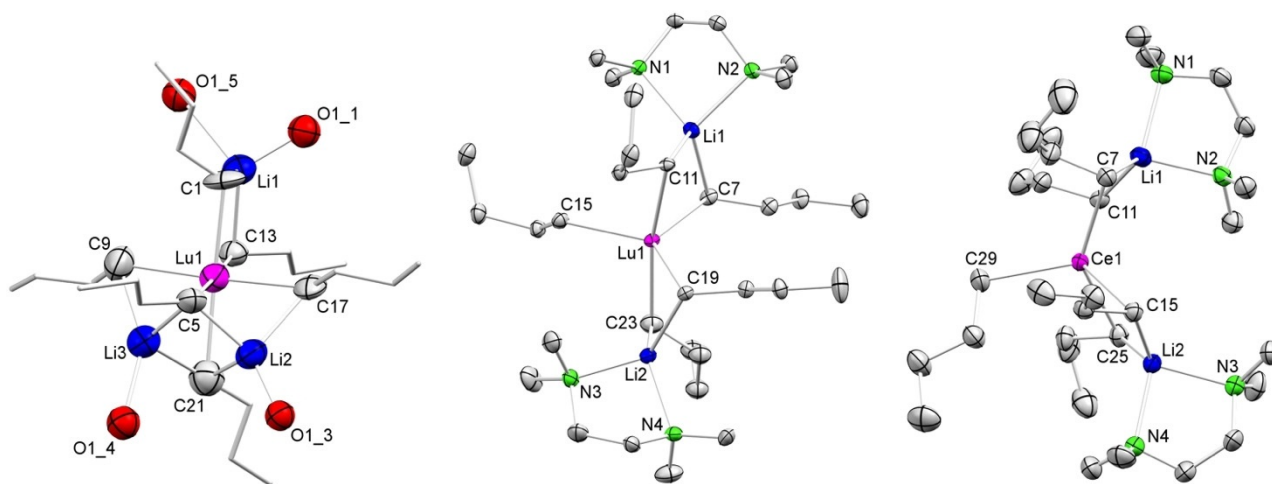


Figure 4. Crystal structures of Li₃Lu(*n*-Bu)₆(thf)₄ (**3^{Lu}**, left) Li₂Lu(*n*-Bu)₅(tmeda)₂ (**4^{Lu}**, middle), and Li₂Ce(*n*-Bu)₅(tmeda)₂ (**4^{Ce}**, right)^[59] with atomic displacement ellipsoids set at 30% probability. Hydrogen atoms, disorders and CH atoms of the THF molecules (**3^{Lu}**), and disorders of the *n*-butyl groups (**4^{Lu}**, **4^{Ce}**) are omitted for clarity. Selected interatomic distances [Å] and angles [°] for **3^{Lu}**: Lu1–C1 2.553(17), Lu1–C5 2.559(18), Lu1–C9 2.46(2), Lu1–C13 2.550(19), Lu1–C17 2.44(2), Lu1–C21 2.58(3), Li1–C1 2.1555(3), Li1–C13 2.3324(3), Li2–C5 2.1928(3), Li2–C17 2.4854(3), Li2–C21 2.4623(3), Li3–C5 2.1307(3), Li3–C9 2.5339(4), Li3–C21 2.3886(3); C1–Lu1–C21 176.68(1), C5–Lu1–C13 177.55(1), C9–Lu1–C17 176.32(1), C1–Lu1–C5 88.63(1). **4^{Lu}**: Lu1–C7 2.468(2), Lu1–C11 2.5293(18), Lu1–C15 2.3797(19), Lu1–C19 2.4620(18), Lu1–C23 2.522(2), Li1–C7 2.217(4), Li1–C11 2.195(4), Li2–C19 2.224(4), Li2–C23 2.191(4); C7–Li1–C11 108.74(1), C19–Li2–C23 105.61(1). **4^{Ce}**: Ce1–C7 2.657(3), Ce1–C11 2.700(5), Ce1–C15 2.674(3), Ce1–C25 2.664(4), Ce1–C29 2.549(3), Li1–C7 2.185(6), Li1–C11 2.222(8), Li2–C15 2.183(6), Li2–C25 2.205(6); C7–Li1–C11 112.1(3), C15–Li2–C25 114.3(3).

spectrum of 3^Y revealed one low-field-shifted ^{89}Y resonance at +771 ppm (Figure S22), in accordance with a single organoyttrium species in solution ($Y(CH_2SiMe_3)_3(thf)_2$: $\delta(^{89}Y) = 882.7$ ppm).^[38] To further corroborate a similar composition of complexes 3^{Ln} , we probed the stabilizing effect of TMEDA for the metal centers cerium and lutetium. Much to our delight, addition of stoichiometric amounts of three equivalents TMEDA prior to the crystallization of the reaction mixtures containing complexes 3^{Ln} afforded complexes $Li_2Ln(n-Bu)_5(tmeda)_2$ (4^{Ln}) ($Ln = Ce$ and Lu , Figure 4).

Surprisingly, besides the expected thf/tmeda donor ligand exchange, displacement of one $n-BuLi(tmeda)$ entity took place. Consequently, the rare-earth-metal centers in isostructural complexes 4^{Ce} and 4^{Lu} feature only five n -butyl ligands. One of these n -butyl ligands is terminal while of the remaining ones two are bridged by a lithium atom each, which are stabilized by one tmeda donor each. Such $n-BuLi(tmeda)$ displacement is in contrast to the Schumann methyl variants $Li_3Ln(CH_3)_6(tmeda)_3$, including complex **1**. A plausible explanation for this is the increased steric bulk/basicity of the n -butyl versus methyl ligands. Complexes 4^{Ce} and 4^{Lu} exhibit distinct $Ln-C$ distances for the terminal and bridging n -butyl ligands (Ce : 2.549(3) Å and 2.657(3)–2.700(5) Å; Lu : 2.3797(19) Å and 2.4620(18)–2.5293(18) Å). Overall, only very limited structural data are available on rare-earth-metal n -butyl complexes likely due to the propensity for β -H elimination. Cyclopentadienyl-supported derivatives include constrained-geometry complexes $[(\eta^5:\eta^1-C_5Me_4SiMe_2NtBu)Y(\mu-n-Bu)]_2$ ($Y-C$: 2.542(2)/2.544(2) Å) and terminal $(\eta^5:\eta^1-C_5Me_4SiMe_2NtBu)Y(n-Bu)(dme)$ ($Y-C$: 2.435(5) Å)^[39] as well as metallocenes $[(C_5H_4Me)_2Ln(n-Bu)]_2$ ($Ln = Y$: 2.551(8)/2.556(11)/2.587(13) Å, Dy : 2.536(18)/2.591(18) Å).^[40] Because cerium and lutetium form the same type of complex for 4^{Ln} , and based on other analytical data, monolanthanide derivatives of general formula $Li_3Ln(n-Bu)_6(thf)_4$ are also proposed for the remaining complexes 3^{Ln} .

At this point we were once more challenged by the question why these reactions would lead to the isolation of ate complexes $Li_3Ln(n-Bu)_6(thf)_4$ rather than the envisaged “ $Ln(n-Bu)_xCl_{3-x}(thf)_y$ ” ($x = 1-3$). When starting from $LnCl_3(thf)_x$, which is very poorly soluble in THF, the simplest explanation would be that treatment of Lewis-acidic rare-earth-metal chloride species with increasing amounts of the strong nucleophile $n-BuLi$ enhances its solubility, and is therefore more likely to react faster in consecutive reactions with $n-BuLi$. The formation of isolable ate complexes $Li_3Ln(n-Bu)_6(thf)_4$ is further driven by the relatively small size of the n -butyl ligand and by switching the solvent from coordinating (THF) to non-coordinating (n -hexane). Predominant ate complexation was also observed for Schumann’s methyl complexes $Li_3LnMe_6(thf)_x$ ^[22] or diisopropylamido derivatives $LiLn(NiPr_2)_4(thf)_x$.^[41] Crucially, independent of the applied $LuCl_3(thf)_x/n-BuLi$ stoichiometry, complex 3^{Lu} could be crystallized as the exclusive Lu^{III} -containing species, upon separation of the solution from unreacted rare-earth-metal halide, its evaporation to dryness, and extraction of the residue with n -hexane (XRD unit-cell check and 1H NMR spectroscopy indicated repeatedly formation of 3^{Lu}). This

finding suggested that the typical reaction (preformation) conditions for a lutetium-derived Imamoto reagent, $LuCl_3/n-BuLi/THF/-78^\circ C/30$ min should form $Li_3Lu(n-Bu)_6(thf)_x$ as the dominant initial lutetium species in solution. Since any persisting equilibria in solution would impact the reactivity of the Imamoto alkylation reagent we next took a closer look at the solution behavior of bimetallic $Li_3Ln(n-Bu)_6(thf)_4$ and the binary system $LnCl_3(thf)_x/n-BuLi$ ($Ln = Ce, Lu$).

Solution Behavior of n -Butyl Complexes 3^{Ln} and 4^{Ln} Probed by NMR spectroscopy. All crystallized n -butyl complexes are stable when stored as solids at $-40^\circ C$. However, when dissolved in any solvent, complexes 3^{La} , 3^{Ce} and 4^{Ce} had fully decomposed after 24 h. In contrast, but not unexpectedly, the complexes of the smaller-sized rare-earth metals are stable in solution at $-40^\circ C$ for up to one week. Warming complexes 3^{Ln} and 4^{Ln} to ambient temperature, decomposition was perceived visually within one hour (in both solution and solid state). To further determine the thermal stability of our complexes, variable-temperature (VT) NMR spectra were measured (Figures S18, S23, S26, S36 and S42). Amazingly, β -H elimination and 1-butene formation was observed only from $+30^\circ C$ onwards, being considerably more pronounced for 3^{La} and 3^{Ce} than for the respective complexes of the smaller-sized rare-earth metals. Because the heating was performed in 10 degree increments starting at $-40^\circ C$ and held at each temperature for 15 minutes before measurement, it can be concluded that these complexes are relatively stable for a short amount of time even at ambient temperature.^[33]

Crucially, both the 1H and 7Li NMR spectra of complexes 3^{Ln} and 4^{Ln} revealed that in solution a considerable portion of $n-BuLi$ gets displaced from the rare-earth-metal center. The degree of dissociation is highly dependent on the solvent and the rare-earth metal. In general, $n-BuLi$ dissociation is more pronounced in THF than in toluene. Ate complexes 3^{Ln} of the smaller-sized rare-earth metals yttrium, lutetium, and scandium are quite stable in toluene solution displaying minor $n-BuLi$ dissociation of ca. 1%, 4%, and 8% respectively (Figures S14/S19/S37). On the other hand, $n-BuLi$ dissociation prevails for 3^{Ce} and 3^{La} (ca. 90%). Interestingly, the presence of tmeda as a donor ligand in complexes 4^{Ln} can either counteract or enforce $n-BuLi$ separation ($3^{Ce}/4^{Ce}$: > 98%/46% versus $3^{Lu}/4^{Lu}$: 4%/20%). For the organocerium(III) complexes, $n-BuLi$ ate complexation is easily detectable by paramagnetically shifted 7Li resonances. Figure 5 depicts the 7Li NMR spectra of complexes **1**, **2**, 3^{Ce} , and 4^{Ce} both in $[D_8]THF$ and $[D_8]toluene$, clearly revealing a) the great stability of the hexamethylate complex **1**, b) the persistence of ion-separated *tert*-butyl complex **2** also in solution, and c) the beneficial effect of tmeda (versus thf) donor ligands for intramolecular ate-complex stabilization. The 7Li NMR spectrum of 4^{Ce} suggests a clean separation into $[LiCe(n-Bu)_4(tmeda)]$ and $n-BuLi$ (signal ratio 1:1).

These findings have important implications for the composition of the “active” $n-BuLi$ -derived Imamoto reagent. When used as a 1:1 mixture of $CeCl_3(thf)$ and $n-BuLi$ in THF at temperatures of $-35^\circ C$, the formation of ate complex $Li_3Ce(n-Bu)_6(thf)_4$ (3^{Ce}) seems highly disfavored. This can be concluded from the 7Li NMR spectrum of 3^{Ce} , which does indicate only a small portion of lithium and paramagnetic

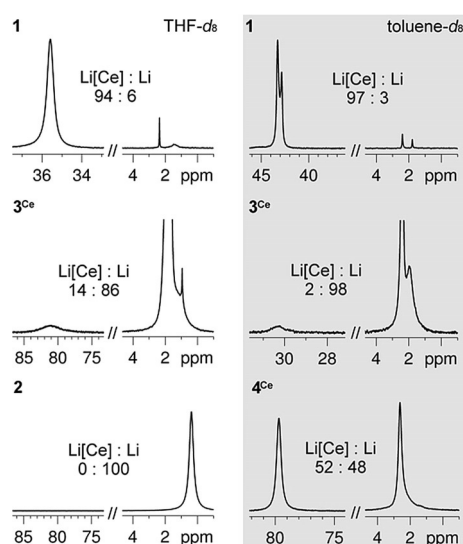


Figure 5. ^7Li NMR spectra (194.37 MHz, 233 K) of complexes **1**, **2**, **3^{Ce}**, and **4^{Ce}**, recorded in $[\text{D}_8]\text{THF}$ or $[\text{D}_8]\text{toluene}$.

cerium(III) in close proximity ($\delta_{\text{Li}} = 81.5$ ppm). An equimolar mixture of $\text{CeCl}_3(\text{thf})$ and $n\text{-BuLi}$ formed in situ in $[\text{D}_8]\text{THF}$ at -45°C did not reveal any paramagnetically shifted ^7Li NMR resonance (Figure S33). The latter seems to appear only at ratios $< 1:3$. For comparison, the intramolecular ate complex $\text{LiCe}[\text{N}(\text{SiHMe}_2)_2]_4(\text{thf})$ (in $\text{C}_6\text{D}_6/1,2\text{-difluorobenzene}$)^[42] and *tmeda*-adduct **4^{Ce}** (in $[\text{D}_8]\text{THF}$) display ^7Li chemical shifts of 84.4 and 81.3 ppm. The ^1H NMR spectrum in $[\text{D}_8]\text{THF}$ of **3^{La}** featuring the similarly sized lanthanum center lends further support to this assumption, as the *n*-butyl resonances appear in an approximate 1:1 ratio (Figure S24). Moreover, 1:1 mixtures of $\text{CeCl}_3(\text{thf})$ and $n\text{-BuLi}$, obtained in THF at -45°C contain a substantial amount (40–50%) of unreacted $\text{CeCl}_3(\text{thf})$ upon preformation for 30 minutes. Incomplete transmetalation in CeCl_3/RLi mixtures has been pointed out previously at various occasions.^[12a,21] Therefore, unlike the smaller rare-earth metals, which favor intramolecular ate complexation even in solution, the organocerium species prevailing under Imamoto conditions are most likely “ $\text{Ce}(n\text{-Bu})_3(\text{thf})_x$ ” or solvent-separated ion pairs like “[$\text{Ce}(n\text{-Bu})_4(\text{thf})_y$][$\text{Li}(\text{thf})_4$]”, similar to *tert*-butyl complex **2**. The

formation of heteroleptic species “ $\text{Ce}(n\text{-Bu})_x\text{Cl}_y(\text{thf})_z$ ” ($x = 1, 2$; $x + y = 3$) seems very unlikely due to the persistence of ligand redistribution forming homoleptic complexes and/or the favorable occurrence of $\beta\text{-H}$ elimination. Non-ate mixed hydrocarbyl/halide Ln^{III} complexes have been structurally authenticated for phenyl and benzyl derivatives but have remained elusive for alkyl ligands capable of $\beta\text{-H}$ elimination. Representative examples include $(\text{C}_6\text{H}_5)_2\text{GdCl}_2(\text{THF})_4$,^[43] $\text{Ln}(\text{CH}_2\text{Ph})_2\text{I}(\text{thf})_3$ ($\text{Ln} = \text{Y}, \text{Er}$),^[44] and ion-separated $[\text{YMeI}(\text{py})_5][\text{I}]$.^[24]

The dissociation behavior was further investigated in a series of NMR experiments (Figure 6), comparing complex **3^{Lu}** to the reactions of $\text{LuCl}_3(\text{thf})_2$ with various amounts of $n\text{-BuLi}$, and $n\text{-BuLi}$ itself. The ^1H NMR spectrum of crystalline ate complex $\text{Li}_3\text{Lu}(n\text{-Bu})_6(\text{thf})_4$ (**3^{Lu}**) shows two signal sets for metal-bonded CH_2 groups (Figure 6, trace III/left). The $\text{Lu}-\text{CH}_2$ moieties resonate at about -0.5 ppm, and hence are significantly shifted to lower field compared to the characteristic pattern of $n\text{-BuLi}$ at -1.0 to -1.5 ppm (cf. trace II/left).^[45–46] The two signal sets are clearly indicative of $n\text{-BuLi}$ dissociation in THF solution (Imamoto conditions). As in case of $n\text{-BuLi}$, the two distinct signals for the lutetium-bonded $n\text{-Bu}$ ligands might represent lutetium complexes of distinct aggregation “ $\text{Li}_x\text{Lu}(n\text{-Bu})_{3+x}(\text{thf})_y$ ” ($x = 0–3$). The dissociation of $n\text{-BuLi}$ in **3^{Lu}** is also corroborated by the ^7Li NMR spectrum (trace III/right) showing the characteristic pattern of $n\text{-BuLi}$ ^[47–48] and a very broad signal at 0 ppm, indicative of $\text{Lu}-n\text{-Bu}-\text{Li}$ moieties and rapid $n\text{-BuLi}$ exchange. Interestingly, when examining in situ formed solutions of $\text{LuCl}_3(\text{thf})_2/n\text{-BuLi}$ (traces IV–VII), free $n\text{-BuLi}$ was observed only when more than three equivalents of $n\text{-BuLi}$ were used per lutetium. This is supported by the respective ^7Li NMR spectra, which also suggest the formation of free LiCl in case of < 3 equivalents of $n\text{-BuLi}$. For better comparison the ^1H and ^7Li spectra of $n\text{-BuLi}-\text{LiCl}$ mixtures are shown (trace I). Moreover, addition of $\text{LuCl}_3(\text{thf})_2$ to ate complex $\text{Li}_3\text{Lu}(n\text{-Bu})_6(\text{thf})_4$ (**3^{Lu}**) results in complete consumption of free $n\text{-BuLi}$ and formation of LiCl (trace VIII). This implies that dissociated $n\text{-BuLi}$ engages in “normal” ligand exchange with added $\text{LuCl}_3(\text{thf})_2$. However, when the solvent is removed the in situ formed complexes scramble to the complex **3^{Lu}**, LuCl_3 and LiCl (upon crystallization from *n*-hexane).

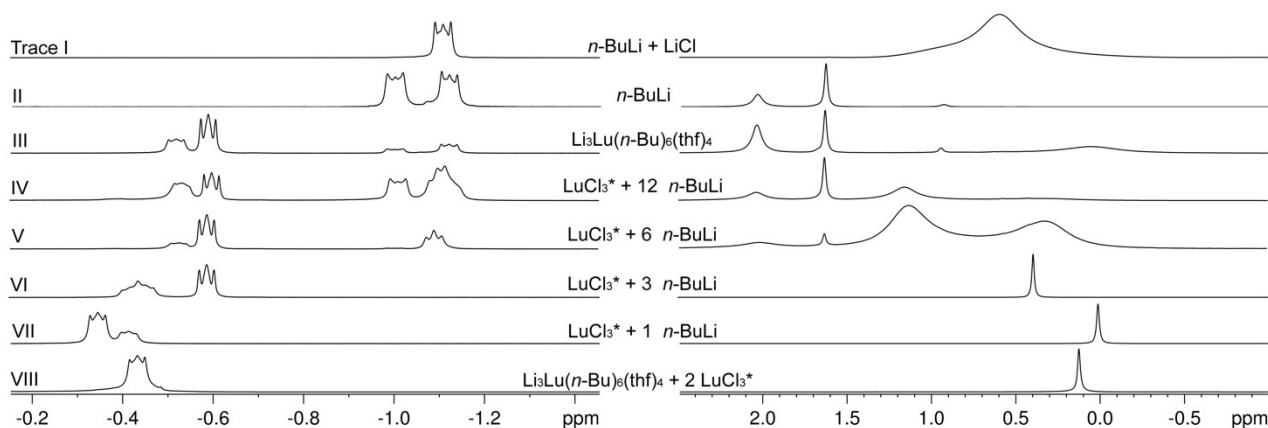
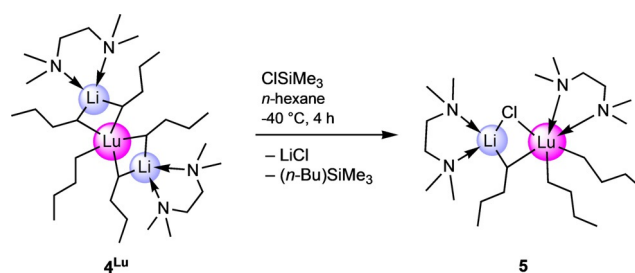


Figure 6. ^1H NMR (500.13 MHz, $[\text{D}_8]\text{THF}$, 193 K) (left) and ^7Li NMR spectra (194.37 MHz, $[\text{D}_8]\text{THF}$, 193 K) (right) of $\text{LuCl}_3(\text{thf})_2$ with x $n\text{-BuLi}$ ($x = 1, 3, 6, 12$) compared to **3^{Lu}**, **3^{Lu}** + $2 \text{LuCl}_3(\text{thf})_2$, $n\text{-BuLi}$, and $n\text{-BuLi} + \text{LiCl}$.

Based on these observations, we can hypothesize about the following scenario. The initial intermediate/transient product of the $\text{LuCl}_3(\text{thf})_2/x \text{ } n\text{-BuLi}$ reaction is certainly “ $\text{Lu}(n\text{-Bu})\text{Cl}_2$ ”. However, as soon as this heteroleptic complex is formed, its better solubility in THF (compared to LuCl_3) will imply a more rapid reaction (compared to LuCl_3) with the remaining $n\text{-BuLi}$ in solution. Thus, ate complexes of the type “ $\text{Li}_x\text{Lu}(n\text{-Bu})_{3+x}(\text{thf})_y$ ”, and ultimately but not exclusively $\text{Li}_3\text{Lu}(n\text{-Bu})_6(\text{thf})_4$ ($\mathbf{3}^{\text{Lu}}$), represent the dominant rare-earth-metal species in solution. As revealed by NMR spectroscopies, $\mathbf{3}^{\text{Lu}}$ is labile in solution and engages in a dissociation equilibrium with $n\text{-BuLi}$; the displaced $n\text{-BuLi}$ should react further with LuCl_3 . Therefore, likely reaction products depending on the $\text{LuCl}_3(\text{thf})_2/n\text{-BuLi}$ ratio are “ $\text{Lu}(n\text{-Bu})_3$ ” and “ $\text{Li}_x\text{Lu}(n\text{-Bu})_{3+x}(\text{thf})_y$ ” with $x \leq 2$ for a ratio of 1:3 and smaller, and species “ $\text{Lu}(n\text{-Bu})_3$ ” and “ $\text{Li}_x\text{Lu}(n\text{-Bu})_{3+x}(\text{thf})_y$ ” with x ranging from 1 to 3, for a ratio of larger than 1:3. A shortage of THF solvent via extraction of the reaction products into $n\text{-hexane}$ leads to ate complex $\text{Li}_3\text{Lu}(n\text{-Bu})_6(\text{thf})_4$ ($\mathbf{3}^{\text{Lu}}$) as the only isolable (crystalline) species. Performing the reactions for longer time periods under otherwise identical conditions resulted in extensive decomposition.

Solution Behavior of n -Butyl Complexes $\mathbf{3}^{\text{Ln}}$ and $\mathbf{4}^{\text{Ln}}$ Probed by Derivatization Reactions. The preferred dissociation of $n\text{-BuLi}$ from ate complexes $\text{Li}_3\text{Ln}(n\text{-Bu})_6(\text{thf})_4$ ($\mathbf{3}^{\text{Ln}}$) of the larger-sized rare-earth metals was further revealed by the reaction of crystalline $\mathbf{3}^{\text{Ce}}$ with $\text{LuCl}_3(\text{thf})_2$ in THF, affording $\mathbf{3}^{\text{Lu}}$ in low crystalline yields of 23% (XRD unit-cell check). Interestingly, the dissociated $n\text{-BuLi}$ seems to exert a stabilizing effect on the organocerium species, since the solution turned brown rather quickly, upon addition of $\text{LuCl}_3(\text{thf})_2$. In order to enforce the formation of $n\text{-BuLi}$ -depleted “ $\text{Ln}(n\text{-Bu})_3$ ” we searched for reactions which would possibly convert any dissociated $n\text{-BuLi}$ selectively and ideally into products not affecting the isolation of putative “ $\text{Ln}(n\text{-Bu})_3$ ”. Luckily, such a reaction path could be observed for the treatment of $\mathbf{4}^{\text{Lu}}$ with trimethylsilyl chloride. The reaction was slow at -40°C , but it produced a minor amount of crystalline $\text{LiLu}(n\text{-Bu})_3\text{Cl}(\text{tmeda})_2$ ($\mathbf{5}$, Scheme 2, Figure 7). On various other occasions, when trying to precipitate LiCl or extract “ $\text{Ln}(n\text{-Bu})_3$ ” from the LiCl -containing residue, only progressive decomposition could be observed. Again, depending on the size of the rare-earth-metal center, complete decomposition took place in a few minutes (“ $\text{Ce}(n\text{-Bu})_3$ ”) or several hours (“ $\text{Y}(n\text{-Bu})_3$ ”). This behavior clearly shows the stabilizing effect of LiCl in these reactions making THF an ideal solvent.

In the solid state, the lutetium atom of complex $\mathbf{5}$ adopts a distorted octahedral coordination geometry, involving three n -butyl ligands, one chlorido ligand and a chelating tmeda molecule. The chlorido and one n -butyl ligand bridge to the lithium atom forming a four-membered ring. The coordination of the lithium atom is completed by the second tmeda molecule. Noteworthy, in the course of this reaction one tmeda ligand was transferred from lithium to lutetium. Striking are the distinct $\text{Lu}-\text{C}$ distances of the terminal n -butyl ligands of 2.367(3) and 2.421(3) Å. While the shorter distance approximately matches the terminal one of complex



Scheme 2. Reactivity of lutetium complex $\mathbf{4}^{\text{Lu}}$ with ClSiMe_3 : “lithium depletion”.

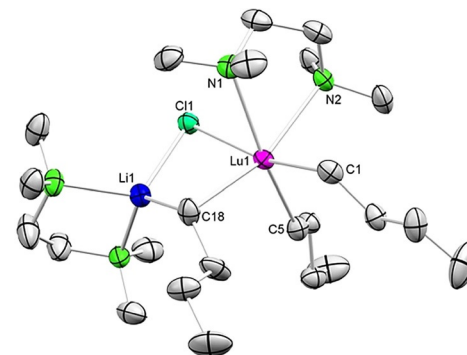
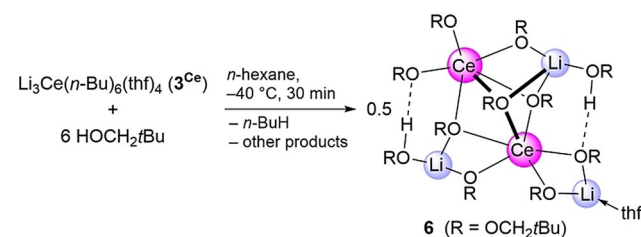


Figure 7. Crystal structure of $\text{LiLu}(n\text{-Bu})_3\text{Cl}(\text{tmeda})_2$ ($\mathbf{5}$) with atomic displacement ellipsoids set at 50% probability.^[59] Hydrogen atoms and disorders of the n -butyl groups are omitted for clarity. Selected interatomic distances [Å] and angles [°] for $\mathbf{5}$: $\text{Lu1}-\text{C1}$ 2.421(3), $\text{Lu1}-\text{C5}$ 2.367(3), $\text{Lu1}-\text{C18}$ 2.447(3), $\text{Lu1}-\text{Cl1}$ 2.7191(9), $\text{Lu1}-\text{N1}$ 2.635(3), $\text{Lu1}-\text{N2}$ 2.540(2), $\text{Li1}-\text{C18}$ 2.287(6), $\text{Li1}-\text{Cl1}$ 2.308(5); $\text{C18}-\text{Lu1}-\text{Cl1}$ 89.26(9), $\text{C18}-\text{Li1}-\text{Cl1}$ 104.6(2).

$\mathbf{4}^{\text{Lu}}$ (2.3797(19) Å), the longer distance is almost as long as that of the bridging n -Bu ligand (2.447(3) Å). This might indicate a *trans* influence of the weakly coordinated chlorido ligand. In accordance with the crystal structure, the ^1H NMR spectrum of $\mathbf{5}$ displays two distinct signal sets for the n -butyl ligands in a 2:1 ratio (Figure S48).

Unsurprisingly, the n -butyl ligands of complexes $\mathbf{3}^{\text{Ln}}$ get easily protonated in the presence of alcoholic substrates. As an example, treatment of $\text{Li}_3\text{Ce}(n\text{-Bu})_6(\text{thf})_4$ ($\mathbf{3}^{\text{Ce}}$) with six equiv of neopentanol resulted in the crystallization of the heterobimetallic cluster $\text{Li}_3\text{Ce}_2(\mu_3\text{-OCH}_2t\text{Bu})_3(\mu_2\text{-OCH}_2t\text{Bu})_4(\text{OCH}_2t\text{Bu})_2(\text{HOCH}_2t\text{Bu})_2(\text{thf})$ ($\mathbf{6}$, Scheme 3, Figure S1). On the basis of the crystal structure and $\text{Ce}-\text{O}$ distances, the connectivity of $\mathbf{6}$ can be assigned as $\text{Li}_3\text{Ce}_2(\mu_3\text{-OCH}_2t\text{Bu})_3(\mu_2\text{-OCH}_2t\text{Bu})_4(\text{OCH}_2t\text{Bu})_2(\text{HOCH}_2t\text{Bu})_2(\text{thf})$. The μ_2 -bridging neopentoxo ligands involve one lithium and cerium each, the μ_3 -bridging ones connect two cerium atoms with one lithium, and the terminal ones are coordinated to one cerium center (Ce1). The

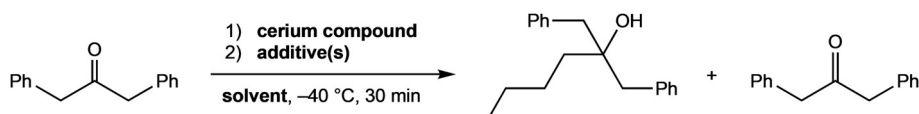


Scheme 3. Alcoholysis of cerium complex $\mathbf{3}^{\text{Ce}}$ with neopentanol.

coordination sphere of the lithium atoms is saturated with one thf and two alcohol donor molecules. The alcohol donors of **6** engage in hydrogen bonding with one terminal (O3) and one μ_2 -bridging neopentoxo ligand (O10). Due to the distinct coordination modes, the Ce–O distances span a wide range of 2.196(2) to 2.608(2) Å, but match those of other cerous alkoxides.^[49] Overall, the solid-state structure of **6** features a completely asymmetric complex with all five metal centers displaying different coordination environments. A similar structure was reported for the yttrium neopentoxide $\text{Li}_3\text{Y}_2(\mu_3\text{-OCH}_2\text{tBu})(\mu_3\text{-HOCH}_2\text{tBu})(\mu_2\text{-OCH}_2\text{tBu})_3(\text{OCH}_2\text{tBu})_3\text{-}(\text{HOCH}_2\text{tBu})_2$.^[50] The formation and structural characterization of Li_3Ce_2 complex **6** clearly reflects lithium depletion compared to the Li_3Ce precursor **3^{Ce}**, and pictures the intricacy of **3^{Ce}** in solution. Complex **6** shows intricate solution behavior itself as evidenced by at least six signals in the ⁷Li NMR spectrum, including paramagnetically shifted ones (Figure S52).

Reactivity of *n*-Butyl Complexes **3^{Ln} toward an Enolizable Ketone.** In this study, 1,3-diphenylpropan-2-one was employed as a test molecule (Table 1), since its selective conversion into the respective tertiary alcohol has been already shown in the original work by Imamoto.^[7] Back then the following protocols were applied: [Ce , I_2 , THF, 0 °C (CeI_3 formed in situ)/*n*-BuLi (1 equiv), –65 °C, 30 min/ketone, –65 °C, 3 h] and [CeCl_3] (later determined as [$\text{CeCl}_3\text{-}(\text{H}_2\text{O})_n$], *n*-BuLi (1 equiv), THF, –78 °C, 1 h/ketone, –65 °C, 3 h], yielding the alcohol in 98% and 96%, respectively.

Table 1: Overview of the ketone reduction.



Entry ^[a]	Compound	Equiv ketone	Solvent	Additives	Yield alcohol [%]	Recovered ketone [%]
1	$\text{CeCl}_3(\text{thf})$	0.77	THF	1 <i>n</i> -BuLi	99	0
2	$\text{CeCl}_3(\text{thf})$	6	THF	6 <i>n</i> -BuLi	77	20
3	3^{Ce}	6	THF	–	70	13
4	3^{Ce}	1	THF	–	88	3
5	3^{Ce}	6	Et_2O	–	54 ^[b]	46 ^[b]
6	3^{Ce}	3	Et_2O	–	78	15
7	3^{Ce}	1	Et_2O	–	89	10
8	3^{Ce}	6	toluene	–	76	11
9	3^{Ce}	6	THF	3 LiCl	74	16
10	3^{Ce}	6	THF	5 $\text{CeCl}_3(\text{thf})$	89	8
11	3^{Ce}	6	THF	5 “Ce turbo chloride” to ketone	80	14
12	3^{Ce}	6	THF	5 “Ce turbo chloride” after ketone	90	1
13	3^{Ce}	6	THF	5 $\text{Sc}(\text{OTf})_3$ after ketone	62 ^[b]	38 ^[b]
14	3^{Ce}	6	THF	5 AlCl_3 after ketone	79	21
15	3^{Ce}	6	THF	3 TMEDA	73	16
16	3^{Lu}	6	THF	–	74	23
17	3^{Lu}	6	THF	3 TMEDA	44	56
18	3^Y	6	THF	–	75	12
19 ^[c]	3^{Lu}	6	THF	–	62	38
20	–	1	THF	1 <i>n</i> -BuLi	50	50

[a] 0 °C. [b] Ratios determined by NMR spectroscopy. [c] Ambient temperature.

In our hands, the slightly modified version [$\text{CeCl}_3(\text{thf})$, *n*-BuLi (1 equivalent), THF, –35 °C, 30 min/ketone, –35 °C, 30 min] gave 99% of alcohol (entry 1), clearly documenting the efficiency of the Imamoto transformation. The importance of using CeCl_3 /*n*-BuLi in a 1:1 stoichiometry is revealed by the reactivity of crystalline or in situ formed complex **3^{Ce}** (entries 2 and 3). The yield of alcohol was significantly decreased at the expense of ketone enolization caused by dissociated *n*-BuLi (for the exclusive reaction behavior of *n*-BuLi, see entry 20). Conducting the reaction in diethyl ether also gave the best results when $\text{CeCl}_3(\text{thf})$ /*n*-BuLi was used in a 1:1 stoichiometry (entries 5–7). Surprisingly, complex **3^{Ce}** performed similarly in THF and toluene (entry 8).

To comprehend why the alcohol yield is lower in case of **3^{Ce}** than for $\text{CeCl}_3(\text{thf})$ /*n*-BuLi (ratio 1:1, entries 3 and 4 versus 1), various additives were tested. While the addition of LiCl did not affect the reaction outcome (entry 9), additional $\text{CeCl}_3(\text{thf})$ did markedly increase the alcohol yield (entry 10). This effect was even significantly enhanced if “cerium turbo chloride” was added to the organocerium compound subsequently to the ketone (entry 12). “Cerium turbo chloride” is the combination of CeCl_3 with two equivalents of LiCl and completely soluble in THF. It was prepared according to the method reported by the Knochel group.^[51] As revealed by NMR spectroscopy in case of lutetium (Figure 6, trace VIII), dissociated *n*-BuLi will react with added LnCl_3 along with ligand scrambling and provide for the further supply of cerium-bonded *n*-butyl. Therefore the limited performance of complex **3^{Ce}** with 6 equivalents of ketone results from progressing *n*-BuLi dissociation and its changed (reduced/non-selective) reactivity toward the ketone. For ate complexes **3^{Ln}** of the smaller-sized yttrium and lutetium, which are more stable in solution, the mediocre performance in the 6-equivalent reaction might be attributable to the formation of sterically demanding alkoxy ligands in putative “ $\text{Li}_3\text{Ln}[\text{OC}(\text{CH}_2\text{Ph})_2\text{n-Bu}]_6$ ”. Overall, any effect of the rare-earth-metal size is not apparent since ate complexes **3^Y** and **3^{Lu}** showed a performance very similar to that of the cerium congener **3^{Ce}** (entries 16 and 18). The importance of performing the transformation in the presence of rare-earth-metal chlorides was also revealed when employing scandium triflate $\text{Sc}(\text{OTf})_3$ or AlCl_3 as Lewis acids instead of additional CeCl_3 (entry 13 and 14). Both reactions led to decreased alcohol yields and increased ketone recovery (via enolization). This and the distinct outcome of the ketone transformation when changing the order of ketone and “cerium turbo chloride” (en-

tries 11 and 12) suggest an intramolecular ketone activation/alkylation scenario akin to a four-membered transition state (1,2-addition), rather than the participation of several metal complexes (Figure 8, A and B). Moreover, favorable ketone coordination/adduct formation^[52–53] and alkoxide formation^[54] have been shown previously.

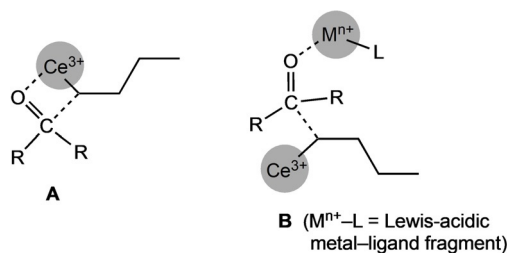


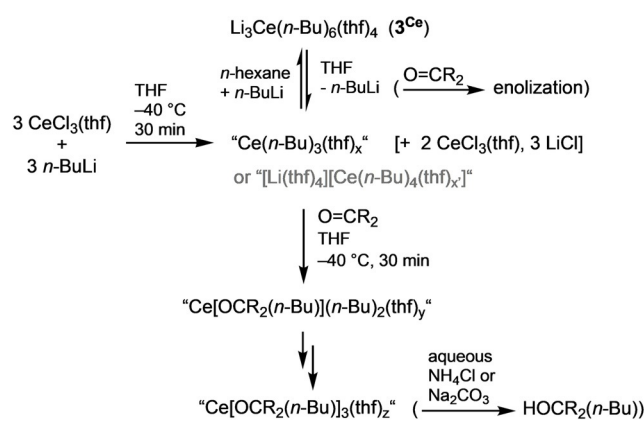
Figure 8. Proposed “intramolecular” reaction involving a four-membered transition state of the ketone reduction (A) rather than a multi-molecular reaction path like B.

The impact of TMEDA was examined for in situ formed **4^{Ce}** and **4^{Lu}** (entries 15 and 17), indicating a pronounced *n*-BuLi(tmeda) dissociation only in case of the lutetium reaction. Finally, performing the ketone transformation with **3^{Lu}** at ambient temperature resulted not unexpectedly in a significant drop of alcohol formation, but also documents the relative Ln^{III}-size-dependent stability of the complexes at ambient temperature for a short time.

Finally, the isolation and crystallization of lithium alkoxide co-products gave further insights into the Imamoto alkylation scenario. Prolonging the reaction time of the “incomplete” transformation of six equivalents of 1,3-diphenylpropan-2-one with **3^{Ce}** (Table 1, entry 3) to three weeks led to the crystallization of the enolization product lithium 1,3-diphenylprop-1-en-2-ate $\text{Li}_4[\text{OC}(=\text{CHPh})\text{CH}_2\text{Ph}]_4(\text{thf})_4$ (**7**, Figure S2). The dissociated, significantly more stable *n*-BuLi (compared to **3^{Ce}**) acts as a base, deprotonating unreacted ketone at the α -position of the carbonyl moiety. This competitive reaction path reflects the main part of the recovered ketone, as listed in Table 1, since aqueous work-up will involve keto–enol tautomerism. Complex **7** features a common structural motif in lithium alkoxide complexes^[55–56] with the lithium and alkoxy oxygen atoms occupying alternating positions of a cube. The lithium atoms are saturated with one THF molecule each.

Preliminary tests with $\text{CeCl}_3(\text{thf})/n\text{-BuLi}$ mixtures in the molar ratio 1:3 and acetone as the substrate led to the crystallization of the lithium alkoxide $\text{Li}_8[\text{OCMe}_2(n\text{-Bu})]_6\text{Cl}_2(\text{thf})_6$ (**8**, Figure S3). The incorporation of LiCl into the cluster core unambiguously documents that it is an integral part of the reagent solution. This is also revealed by the ⁷Li NMR spectra depicted in Figure 6 (right, traces VI–VIII). Dissolved LiCl might also associate with the organocerium species (as detected for complex **5**) thus exerting a stabilizing effect.

Proposed Formation and Reactivity of the Imamoto Organocerium Reagent (Scheme 4). Equimolar amounts of CeCl_3 and *n*-BuLi, when combined in THF at low temperatures (−40 °C), afford the cerous *n*-butyl complex “ $\text{Ce}(n\text{-Bu})_3(\text{thf})_x$ ” or solvent-separated ion pairs like “[$\text{Ce}(n\text{-Bu})_4(\text{thf})_y$][$\text{Li}(\text{thf})_4$],” as suggested by a) ¹H and ⁷Li NMR spec-



Scheme 4. The Imamoto organocerium reagent in action.

troscopies and b) considerable amounts of unreacted cerium chloride. In particular, ⁷Li NMR spectroscopy indicates complete transmetalation (complete consumption of *n*-BuLi) and the absence of adjacent cerium and lithium centers.

Unfortunately, single-crystalline products were not accessible. The formation of such species is further corroborated by the solution behavior of pre-isolated crystalline ate complex $\text{Li}_3\text{Ce}(n\text{-Bu})_6(\text{thf})_4$ (**3^{Ce}**), displaying extensive *n*-BuLi dissociation in THF solution. Note that the product obtained from the reaction of $\text{CeCl}_3 \cdot 2\text{LiCl}$ (cerium turbo chloride) with three equivalents of *n*-BuLi in THF at −30 °C was previously analyzed as “*n*-Bu₃Ce” by Raman spectroscopy (absence of significant CeCl_3 and *n*-BuLi Raman lines).^[15] Activation of the carbonylic substrate and its transformation (here reduction to the alkoxy moiety) takes place at the same cerium center, and can proceed three times. Such 1,2-addition reactions have been proven for yttrium methyls $[\text{YMe}_3]_n$,^[57] $[\text{YMe}_2(\text{thf})_5][\text{BPh}_4]$, and $[\text{YMe}(\text{thf})_6][\text{BPh}_4]_2$,^[24] as well as neosilyls $[\text{Y}(\text{CH}_2\text{SiMe}_3)_2(\text{thf})_4][\text{A}]$ (A = BPh_4 , $\text{Al}(\text{CH}_2\text{SiMe}_3)_4$) and $[\text{Y}(\text{CH}_2\text{SiMe}_3)(\text{thf})_5][\text{BPh}_4]_2$ ^[58] employing fluorenone and benzophenone. Aqueous work-up will lead to the alcoholic product and a recyclable inorganic cerium compound.

Conclusion

Seamless low-temperature synthesis and crystallization techniques give access to isolable organocerium complexes $\text{Li}_3\text{Ce}(\text{CH}_3)_6(\text{tmeda})_3$, $[\text{Li}(\text{thf})_4][\text{Ce}(t\text{-Bu})_4]$, $\text{Li}_3\text{Ce}(n\text{-Bu})_6(\text{thf})_4$, and $\text{Li}_2\text{Ce}(n\text{-Bu})_5(\text{tmeda})_2$. ¹H/⁷Li NMR spectroscopic studies on in situ formed solutions of equimolar mixtures of $\text{CeCl}_3(\text{thf})$ and *n*-BuLi in THF at −35 °C suggest non-isolable “ $\text{Ce}(n\text{-Bu})_3(\text{thf})_x$ ” or solvent-separated ion pairs like “[$\text{Li}(\text{thf})_4$][$\text{Ce}(n\text{-Bu})_4(\text{thf})_y$],” as effective organocerium species in respective Imamoto-type alkylation reactions of carbonylic substrates. This hypothesis is corroborated by the solution behavior of ate complex $\text{Li}_3\text{Ce}(n\text{-Bu})_6(\text{thf})_4$, which displays extensive displacement of *n*-BuLi. As revealed for the benchmark substrate molecule 1,3-diphenylpropan-2-one, the prevailing dissociation of *n*-BuLi results in decreased regioselectivity of the ketone/alcohol transformation. In contrast, ate complexes of the type $\text{Li}_3\text{Ce}(\text{CH}_3)_6(\text{thf})_x$ could

be likely species in methyllithium derived Imamoto-type reagents as revealed by the high stability of $\text{Li}_3\text{Ce}(\text{CH}_3)_6(\text{tmeda})_3$ in THF solution. Not unsurprisingly, the effective composition of such CeCl_3/RLi reagents is highly dependent on the rare-earth metal, the hydrocarbyl group, and the solvent. Finally, the presence of THF-soluble co-product LiCl in situ formed reagents is proposed to adopt an active role by exerting a stabilizing effect on the organocerium species. Compound $\text{LiLu}(n\text{-Bu})_3\text{Cl}(\text{tmeda})_2$ features a structural snapshot of the likely involvement of LiCl in the soluble part of Imamoto-type transformations.

It is a fact that a large number of organometallics-promoted organic transformations (including the in situ formation of the multi-component organometallic reagent) is routinely performed at low temperatures (-78 – 0°C). It can be safely assumed that the application of state-of-the-art cold-chain techniques will continue to promote a better understanding of the reagent's formation, composition, and effectiveness, ultimately leading to both optimized reagents and conditions for substrate conversion.

Acknowledgements

We thank Dr. Klaus Eichele for his help with the NMR measurements. Open access funding enabled and organized by Projekt DEAL.

Conflict of interest

The authors declare no conflict of interest.

Keywords: ^7Li NMR spectroscopy · carbonyl alkylation · cerium · lithium · *n*-butyl

- [1] a) H. B. Kagan, J. L. Namy, *Tetrahedron* **1986**, *42*, 6573–6614; b) B. M. Trost, I. Fleming, T. Imamoto in *Comprehensive organic synthesis*, Pergamon, Oxford, **1991**, Chapter 1.8; c) G. A. Molander, *Chem. Rev.* **1992**, *92*, 29–68; d) T. Imamoto, *Lanthanides in organic synthesis*, Academic Press, London, **1994**.
- [2] a) H. Tse-Lok, *Synthesis* **1973**, *1973*, 347–354; b) V. Nair, J. Mathew, J. Prabhakaran, *Chem. Soc. Rev.* **1997**, *26*, 127–132; c) A. K. Das, *Coord. Chem. Rev.* **2001**, *213*, 307–325; d) V. Nair, L. Balagopal, R. Rajan, J. Mathew, *Acc. Chem. Res.* **2004**, *37*, 21–30; e) V. Nair, A. Deepthi, *Tetrahedron* **2009**, *65*, 10745–10755; f) V. Sridharan, J. C. Menéndez, *Chem. Rev.* **2010**, *110*, 3805–3849.
- [3] a) J. L. Namy, P. Grirad, H. B. Kagan, *Nou. J. Chim.* **1977**, *1*, 5–7; b) H. B. Kagan, *J. Alloys Compd.* **2006**, *408–412*, 421–426; c) K. C. Nicolaou, S. P. Ellery, J. S. Chen, *Angew. Chem. Int. Ed.* **2009**, *48*, 7140–7165; *Angew. Chem.* **2009**, *121*, 7276–7301; d) M. Szostak, D. J. Procter, *Angew. Chem. Int. Ed.* **2012**, *51*, 9238–9256; *Angew. Chem.* **2012**, *124*, 9372–9390; e) M. Szostak, N. J. Fazakerley, D. Parmar, D. J. Procter, *Chem. Rev.* **2014**, *114*, 5959–6039; f) X. Just-Baringo, D. J. Procter, *Acc. Chem. Res.* **2015**, *48*, 1263–1275; g) Á. Péter, D. J. Procter, *Chimia* **2020**, *74*, 18–22; h) R. S. Miller, J. M. Sealy, M. Shabangi, M. L. Kuhlman, J. R. Fuchs, R. A. Flowers, *J. Am. Chem. Soc.* **2000**, *122*, 7718–7722; i) E. Prasad, R. A. Flowers, *J. Am. Chem. Soc.* **2002**, *124*, 6895–6899; j) P. R. Chopade, E. Prasad, R. A. Flowers, *J. Am. Chem. Soc.* **2004**, *126*, 44–45; k) J. A. Teprovich, Jr., M. N. Bailii, T. Pintauer, R. A. Flowers II, *Angew. Chem. Int. Ed.* **2007**, *46*, 8160–8163; *Angew. Chem.* **2007**, *119*, 8308–8311; l) R. A. Flowers II, *Synlett* **2008**, *2008*, 1427–1439; m) K. A. Choquette, D. V. Sadasivam, R. A. Flowers, *J. Am. Chem. Soc.* **2010**, *132*, 17396–17398; n) D. V. Sadasivam, J. A. Teprovich, D. J. Procter, R. A. Flowers, *Org. Lett.* **2010**, *12*, 4140–4143; o) T. V. Chciuk, W. R. Anderson, R. A. Flowers, *J. Am. Chem. Soc.* **2016**, *138*, 8738–8741; p) S. Maity, R. A. Flowers, *J. Am. Chem. Soc.* **2019**, *141*, 3207–3216.
- [4] a) T. Imamoto, *Pure Appl. Chem.* **1990**, *62*, 747–752; b) T. Imamoto, *Organocerium Reagents, Vol. 1*, Chiba University, Japan, **1992**; c) H.-J. Liu, K.-S. Shia, X. Shang, B.-Y. Zhu, *Tetrahedron* **1999**, *55*, 3803–3830; d) G. Bartoli, E. Marcantoni, M. Marcolini, L. Sambri, *Chem. Rev.* **2010**, *110*, 6104–6143; e) T.-L. Ho, in *Fieser and Fieser's Reagents for Organic Synthesis*, Wiley&Sons Inc, New York, **2017**.
- [5] T. A. Beineke, J. Delgaudio, *Inorg. Chem.* **1968**, *7*, 715–721.
- [6] W. J. Evans, T. S. Gummshheimer, J. W. Ziller, *J. Am. Chem. Soc.* **1995**, *117*, 8999–9002.
- [7] a) T. Imamoto, T. Kusumoto, M. Yokoyama, *J. Chem. Soc. Chem. Commun.* **1982**, 1042–1044; b) T. Imamoto, T. Kusumoto, Y. Tawarayama, Y. Sugiura, T. Mita, Y. Hatanaka, M. Yokoyama, *J. Org. Chem.* **1984**, *49*, 3904–3912; c) T. Imamoto, Y. Sugiura, *J. Organomet. Chem.* **1985**, *285*, C21–C23; d) T. Imamoto, Y. Sugiura, N. Takiyama, *Tetrahedron Lett.* **1984**, *25*, 4233–4236; e) T. Imamoto, N. Takiyama, K. Nakamura, T. Hatajima, Y. Kamiya, *J. Am. Chem. Soc.* **1989**, *111*, 4392–4398.
- [8] a) J. L. Luche, *J. Am. Chem. Soc.* **1978**, *100*, 2226–2227; b) J.-L. Luche, L. Rodriguez-Hahn, P. Crabbé, *J. Chem. Soc. Chem. Commun.* **1978**, 601–602; c) A. L. Gemal, J. L. Luche, *J. Am. Chem. Soc.* **1981**, *103*, 5454–5459.
- [9] a) H. Li, *Synlett* **2012**, *23*, 1407–1408; b) T. L. Rathman, J. A. Schwindeman, *Org. Process Res. Dev.* **2014**, *18*, 1192–1210.
- [10] For examples, see: a) T. Sato, R. Kato, K. Gokyu, T. Fujisawa, *Tetrahedron Lett.* **1988**, *29*, 3955–3958; b) G. Bartoli, E. Marcantoni, L. Sambri, M. Tamburini, *Angew. Chem. Int. Ed. Engl.* **1995**, *34*, 2046–2048; *Angew. Chem.* **1995**, *107*, 2163–2164.
- [11] For examples, see: a) H. Fujioka, M. Fuji, Y. Okaichi, T. Yoshida, H. Annoura, Y. Kita, Y. Tamura, *Chem. Pharm. Bull.* **1989**, *37*, 602–605; b) C. Alcaraz, U. Groth, *Angew. Chem. Int. Ed. Engl.* **1997**, *36*, 2480–2482; *Angew. Chem.* **1997**, *109*, 2590–2592.
- [12] a) A. Shakoob, K. Jacob, K.-H. Thiele, *Z. Anorg. Allg. Chem.* **1985**, *521*, 57–60; b) K. Jacob, K.-H. Thiele, *Z. Anorg. Allg. Chem.* **1986**, *536*, 147–152; c) W. J. Evans, J. D. Feldman, J. W. Ziller, *J. Am. Chem. Soc.* **1996**, *118*, 4581–4584; d) W. J. Evans, M. A. Ansari, J. D. Feldman, R. J. Doedens, J. W. Ziller, *J. Organomet. Chem.* **1997**, *545–546*, 157–162; e) D. A. Conlon, D. Kumke, C. Moeder, M. Hardiman, G. Hutson, L. Sailer, *Adv. Synth. Catal.* **2004**, *346*, 1307–1315; f) J. E. Kim, D. S. Weinberger, P. J. Carroll, E. J. Schelter, *Organometallics* **2014**, *33*, 5948–5951; g) J. E. Kim, A. V. Zabula, P. J. Carroll, E. J. Schelter, *Organometallics* **2016**, *35*, 2086–2091.
- [13] a) R. E. Mulvey, *Organometallics* **2006**, *25*, 1060–1075; b) R. E. Mulvey, F. Mongin, M. Uchiyama, Y. Kondo, *Angew. Chem. Int. Ed.* **2007**, *46*, 3802–3824; *Angew. Chem.* **2007**, *119*, 3876–3899; c) R. E. Mulvey, *Acc. Chem. Res.* **2009**, *42*, 743–755; d) T. X. Gentner, R. E. Mulvey, *Angew. Chem. Int. Ed.* **2021**, *60*, 9247–9262; *Angew. Chem.* **2021**, *133*, 9331–9348.
- [14] A. Music, D. Didier, *Synlett* **2019**, *30*, 1843–1849.
- [15] A. Music, C. Hoarau, N. Hilgert, F. Zischka, D. Didier, *Angew. Chem. Int. Ed.* **2019**, *58*, 1188–1192; *Angew. Chem.* **2019**, *131*, 1200–1204.
- [16] A. D. Benischke, L. Anthore-Dalio, G. Berionni, P. Knochel, *Angew. Chem. Int. Ed.* **2017**, *56*, 16390–16394; *Angew. Chem.* **2017**, *129*, 16608–16612.

- [17] L. Anthore-Dalio, A. D. Benischke, B. Wei, G. Berionni, P. Knochel, *Angew. Chem. Int. Ed.* **2019**, *58*, 4046–4050; *Angew. Chem.* **2019**, *131*, 4086–4090.
- [18] B. Wei, D. Zhang, Y.-H. Chen, A. Lei, P. Knochel, *Angew. Chem. Int. Ed.* **2019**, *58*, 15631–15635; *Angew. Chem.* **2019**, *131*, 15777–15782.
- [19] V. Dimitrov, K. Kostova, M. Genov, *Tetrahedron Lett.* **1996**, *37*, 6787–6790.
- [20] a) N. Greeves, L. Lyford, *Tetrahedron Lett.* **1992**, *33*, 4759–4760; b) N. Greeves, L. Lyford, J. E. Pease, *Tetrahedron Lett.* **1994**, *35*, 285–288.
- [21] S. E. Denmark, J. P. Edwards, O. Nicaise, *J. Org. Chem.* **1993**, *58*, 569–578.
- [22] a) H. Schumann, J. Müller, *Angew. Chem. Int. Ed. Engl.* **1978**, *17*, 276; *Angew. Chem.* **1978**, *90*, 307; b) H. Schumann, J. Pickardt, N. Bruncks, *Angew. Chem. Int. Ed. Engl.* **1981**, *20*, 120–121; *Angew. Chem.* **1981**, *93*, 127–128; c) H. Schumann, J. Mueller, N. Bruncks, H. Lauke, J. Pickardt, H. Schwarz, K. Eckart, *Organometallics* **1984**, *3*, 69–74.
- [23] a) H. Schumann, H. Lauke, E. Hahn, J. Pickardt, *J. Organomet. Chem.* **1984**, *263*, 29–35; b) H. Schumann, *J. Less-Common Met.* **1985**, *112*, 327–341.
- [24] M. U. Kramer, D. Robert, S. Arndt, P. M. Zeimentz, T. P. Spaniol, A. Yahia, L. Maron, O. Eisenstein, J. Okuda, *Inorg. Chem.* **2008**, *47*, 9265–9278.
- [25] M. Zimmermann, R. Anwander, *Chem. Rev.* **2010**, *110*, 6194–6259.
- [26] a) M. F. Lappert, R. Pearce, *J. Chem. Soc. Chem. Commun.* **1973**, 126; b) S. Bambirra, M. W. Bouwkamp, A. Meetsma, B. Hessen, *J. Am. Chem. Soc.* **2004**, *126*, 9182–9183; c) H. Schumann, D. M. M. Freckmann, S. Dechert, *Z. Anorg. Allg. Chem.* **2002**, *628*, 2422–2426.
- [27] a) A. L. Wayda, W. J. Evans, *J. Am. Chem. Soc.* **1978**, *100*, 7119–7121; b) H. Schumann, W. Genthe, E. Hahn, J. Pickardt, H. Schwarz, K. Eckart, *J. Organomet. Chem.* **1986**, *306*, 215–225; c) W. Noh, G. S. Girolami, *Polyhedron* **2007**, *26*, 3865–3870.
- [28] a) H. M. Dietrich, G. Raudaschl-Sieber, R. Anwander, *Angew. Chem. Int. Ed.* **2005**, *44*, 5303–5306; *Angew. Chem.* **2005**, *117*, 5437–5440; b) L. C. H. Gerber, E. Le Roux, K. W. Törnroos, R. Anwander, *Chem. Eur. J.* **2008**, *14*, 9555–9564.
- [29] A. J. Woolees, D. P. Mills, W. Lewis, A. J. Blake, S. T. Liddle, *Dalton Trans.* **2010**, *39*, 500–510.
- [30] G. Occhipinti, C. Meermann, H. M. Dietrich, R. Litlabø, F. Auras, K. W. Törnroos, C. Maichle-Mössmer, V. R. Jensen, R. Anwander, *J. Am. Chem. Soc.* **2011**, *133*, 6323–6337.
- [31] A. G. Avent, C. F. Caro, P. B. Hitchcock, M. F. Lappert, Z. Li, X.-H. Wei, *Dalton Trans.* **2004**, 1567–1577.
- [32] A. Pindwal, S. Patnaik, W. C. Everett, A. Ellern, T. L. Windus, A. D. Sadow, *Angew. Chem. Int. Ed.* **2017**, *56*, 628–631; *Angew. Chem.* **2017**, *129*, 643–646.
- [33] W. J. Evans, J. H. Meadows, A. L. Wayda, W. E. Hunter, J. L. Atwood, *J. Am. Chem. Soc.* **1982**, *104*, 2015–2017.
- [34] M. Zimmermann, N. Å. Frøystein, A. Fischbach, P. Sirsch, H. M. Dietrich, K. W. Törnroos, E. Herdtweck, R. Anwander, *Chem. Eur. J.* **2007**, *13*, 8784–8800.
- [35] M. Zimmermann, R. Litlabø, K. W. Törnroos, R. Anwander, *Organometallics* **2009**, *28*, 6646–6649.
- [36] D. Barisic, D. Diether, C. Maichle-Mössmer, R. Anwander, *J. Am. Chem. Soc.* **2019**, *141*, 13931–13940.
- [37] A. Mortis, D. Barisic, K. Eichele, C. Maichle-Mössmer, R. Anwander, *Dalton Trans.* **2020**, *49*, 7829–7841.
- [38] B. R. Elvidge, S. Arndt, P. M. Zeimentz, T. P. Spaniol, J. Okuda, *Inorg. Chem.* **2005**, *44*, 6777–6788.
- [39] P. Voth, S. Arndt, T. P. Spaniol, J. Okuda, L. J. Ackerman, M. L. H. Green, *Organometallics* **2003**, *22*, 65–76.
- [40] R. Grindell, B. M. Day, F.-S. Guo, T. Pugh, R. A. Layfield, *Chem. Commun.* **2017**, *53*, 9990–9993.
- [41] T. Spallek, O. Heß, M. Meermann-Zimmermann, C. Meermann, M. G. Klimpel, F. Estler, D. Schneider, W. Scherer, M. Tafipolsky, K. W. Törnroos, C. Maichle-Mössmer, P. Sirsch, R. Anwander, *Dalton Trans.* **2016**, *45*, 13750–13765.
- [42] U. Bayer, L. Bock, C. Maichle-Mössmer, R. Anwander, *Eur. J. Inorg. Chem.* **2020**, 101–106.
- [43] G. Lin, Z. Jin, Y. Zhang, W. Chen, *J. Organomet. Chem.* **1990**, *396*, 307–313.
- [44] D. P. Mills, A. J. Woolees, J. McMaster, W. Lewis, A. J. Blake, S. T. Liddle, *Organometallics* **2009**, *28*, 6771–6776.
- [45] J. F. McGarrity, C. A. Ogle, *J. Am. Chem. Soc.* **1985**, *107*, 1805–1810.
- [46] O. Tai, R. Hopson, P. G. Williard, *Org. Lett.* **2017**, *19*, 3966–3969.
- [47] a) G. Fraenkel, A. M. Fraenkel, M. J. Geckle, F. Schloss, *J. Am. Chem. Soc.* **1979**, *101*, 4745–4747; b) D. Reed, D. Barr, R. E. Mulvey, R. Snaith, *J. Chem. Soc. Dalton Trans.* **1986**, 557–564; c) A. C. Jones, A. W. Sanders, M. J. Bevan, H. J. Reich, *J. Am. Chem. Soc.* **2007**, *129*, 3492–3493.
- [48] a) G. Fraenkel, M. Henrichs, M. Hewitt, B. M. Su, *J. Am. Chem. Soc.* **1984**, *106*, 255–256; b) B. Qu, D. B. Collum, *J. Am. Chem. Soc.* **2006**, *128*, 9355–9360; c) G. Barozzino-Consiglio, M. Rouen, H. Oulyadi, A. Harrison-Marchand, J. Maddaluno, *Dalton Trans.* **2014**, *43*, 14219–14228.
- [49] T. J. Boyle, L. J. Tribby, S. D. Bunge, *Eur. J. Inorg. Chem.* **2006**, 4553–4563.
- [50] T. J. Boyle, M. L. Neville, J. M. Sears, R. Cramer, *ChemistrySelect* **2016**, *1*, 473–481.
- [51] A. Krasovskiy, F. Kopp, P. Knochel, *Angew. Chem. Int. Ed.* **2006**, *45*, 497–500; *Angew. Chem.* **2006**, *118*, 511–515.
- [52] H. J. Heeres, M. Maters, J. H. Teuben, G. Helgesson, S. Jagner, *Organometallics* **1992**, *11*, 350–356.
- [53] A. R. Crozier, K. W. Törnroos, C. Maichle-Mössmer, R. Anwander, *Eur. J. Inorg. Chem.* **2013**, 409–414.
- [54] U. Bayer, R. Anwander, *Dalton Trans.* **2020**, *49*, 17472–17493.
- [55] E. Weiss, *Angew. Chem. Int. Ed. Engl.* **1993**, *32*, 1501–1523; *Angew. Chem.* **1993**, *105*, 1565–1587.
- [56] For recent examples of lithium enolates, see: a) K. J. Kolonko, D. J. Wherritt, H. J. Reich, *J. Am. Chem. Soc.* **2011**, *133*, 16774–16777; b) J. Guang, Q. P. Liu, R. Hopson, P. G. Williard, *J. Am. Chem. Soc.* **2015**, *137*, 7347–7356; c) J. Jermaks, E. H. Tallmadge, I. Keresztes, D. B. Collum, *J. Am. Chem. Soc.* **2018**, *140*, 3077–3090.
- [57] H. M. Dietrich, C. Meermann, K. W. Törnroos, R. Anwander, *Organometallics* **2006**, *25*, 4316–4321.
- [58] Y. Nakajima, J. Okuda, *Organometallics* **2007**, *26*, 1270–1278.
- [59] Deposition Numbers 2069609 (1), 2069616 (2), 2069613 (3^{LM}), 2069615 (4^{CE}), 2069610 (4^{LM}), 2069611 (5), 2069612 (6), 2069617 (7), and 2069614 (8) contain the supplementary crystallographic data for this paper. These data are provided free of charge by the joint Cambridge Crystallographic Data Centre and Fachinformationszentrum Karlsruhe Access Structures service www.ccdc.cam.ac.uk/structures.

Manuscript received: March 18, 2021
Accepted manuscript online: April 27, 2021
Version of record online: June 8, 2021

Supporting Information

CeCl₃/*n*-BuLi: Unraveling Imamoto's Organocerium Reagent

*Tassilo Berger, Jakob Lebon, Cäcilia Maichle-Mössmer, and Reiner Anwander**

anie_202103889_sm_miscellaneous_information.pdf
anie_202103889_sm_cif.zip

Table of Contents

Experimental Section.....	S6
General Considerations.	S6
[Li ₃ CeMe ₆ (tmeda) ₃] (1).	S6
[Li(thf) ₄][Ce(<i>t</i> -Bu) ₄] (2).	S7
General Procedure for the Synthesis of Li ₃ Ln(<i>n</i> -Bu) ₆ (thf) ₄ (3 ^{Ln} , Ln = Sc, Y, La, Ce, Lu).	S7
Li ₃ Sc(<i>n</i> -Bu) ₆ (thf) ₄ (3 ^{Sc}).	S7
Li ₃ Y(<i>n</i> -Bu) ₆ (thf) ₄ (3 ^Y).	S8
Li ₃ La(<i>n</i> -Bu) ₆ (thf) ₄ (3 ^{La}).	S8
Li ₃ Ce(<i>n</i> -Bu) ₆ (thf) ₄ (3 ^{Ce}).	S8
Li ₃ Lu(<i>n</i> -Bu) ₆ (thf) ₄ (3 ^{Lu}).	S8
Equimolar reaction of CeCl ₃ (thf) with <i>n</i> -BuLi.	S8
Synthesis of 3 ^{Lu} for XRD analysis.	S9
Synthesis of 3 ^{Lu} from “lutetium turbo chloride”	S9
Synthesis of 3 ^{Lu} from 3 ^{Ce}	S9
General Procedure for the Synthesis of Li ₂ Ln(<i>n</i> -Bu) ₅ (tmeda) ₂ (4 ^{Ln} , Ln = Ce, Lu).	S9
Li ₂ Ce(<i>n</i> -Bu) ₅ (tmeda) ₂ (4 ^{Ce}).	S9
Li ₂ Lu(<i>n</i> -Bu) ₅ (tmeda) ₂ (4 ^{Lu}).	S9
LiLu(<i>n</i> -Bu) ₃ Cl(tmeda) ₂ (5).	S10
Synthesis of Li ₃ Ce ₂ (ONep) ₉ (HONep) ₂ (thf) (6).	S10
Synthesis of Li ₄ [OC(=CHPh)(CH ₂ Ph)] ₄ (thf) ₄ (7).	S10
Synthesis of Li ₈ [OCMe ₂ (<i>n</i> -Bu)] ₆ Cl ₂ (thf) ₆ (8).	S11
NMR-scale reactions of LuCl ₃ (thf) ₂ with x <i>n</i> -BuLi (x = 1, 3, 6, 12).	S11
NMR-scale reactions of <i>n</i> -BuLi with 1,3-diphenylpropan-2-one.	S11
Ketone/alcohol transformations employing 1,3-diphenylpropan-2-one.	S11
Ketone/alcohol transformations employing 1,3-diphenylpropan-2-one.	S12
CeCl ₃ and 6 <i>n</i> -BuLi and ketone (Table 1, entry 2).	S12
Li ₃ Ce(<i>n</i> -Bu) ₆ (thf) ₄ (3 ^{Ce}) and ketone/THF (Table 1, entries 3 and 4).	S12
Li ₃ Ce(<i>n</i> -Bu) ₆ (thf) ₄ (3 ^{Ce}) and ketone/OEt ₂ (Table 1, entries 5, 6, and 7).	S12

Li ₃ Ce(<i>n</i> -Bu) ₆ (thf) ₄ (3^{Ce}) and ketone/toluene (Table 1, entry 8).....	S13
Li ₃ Ce(<i>n</i> -Bu) ₆ (thf) ₄ (3^{Ce}) and ketone/THF/LiCl (Table 1, entry 9).	S13
Li ₃ Ce(<i>n</i> -Bu) ₆ (thf) ₄ (3^{Ce}) and ketone/THF/CeCl ₃ (thf) (Table 1, entry 10).	S13
Li ₃ Ce(<i>n</i> -Bu) ₆ (thf) ₄ (3^{Ce}) and ketone/THF/”cerium turbo chloride” (Table 1, entry 11).	S13
Li ₃ Ce(<i>n</i> -Bu) ₆ (thf) ₄ (3^{Ce}) and ketone/THF, then ”cerium turbo chloride” (Table 1, entry 12).....	S14
Li ₃ Ce(<i>n</i> -Bu) ₆ (thf) ₄ (3^{Ce}) and ketone/THF, then Sc(OTf) ₃ (Table 1, entry 13).	S14
Li ₃ Ce(<i>n</i> -Bu) ₆ (thf) ₄ (3^{Ce}) and ketone/THF, then AlCl ₃ (Table 1, entry 14).....	S14
Li ₃ Ce(<i>n</i> -Bu) ₆ (thf) ₄ (3^{Ce}) and ketone/THF/TMEDA (Table 1, entry 15).	S14
Li ₃ Lu(<i>n</i> -Bu) ₆ (thf) ₄ (3^{Lu}) and ketone/THF (Table 1, entry 16).....	S15
Li ₃ Lu(<i>n</i> -Bu) ₆ (thf) ₄ (3^{Lu}) and ketone/THF/TMEDA (Table 1, entry 17).	S15
Li ₃ Y(<i>n</i> -Bu) ₆ (thf) ₄ (3^Y) and ketone/THF (Table 1, entry 18).	S15
Li ₃ Y(<i>n</i> -Bu) ₆ (thf) ₄ (3^Y) and ketone/THF @ ambient temperature (Table 1, entry 19).....	S15
<i>n</i> -BuLi and ketone/THF (Table 1, entry 20).	S16
X-Ray Crystallography.....	S16
Table S1. X-ray crystallographic parameters for complexes 1 , 2 , and 3^{Lu}	S17
Table S2. X-ray crystallographic parameters for complexes 4^{Ce} , 4^{Lu} , and 5	S18
Table S3. X-ray crystallographic parameters for complexes 6 , 7 , and 8	S19
Figure S1. Crystal structure of Li ₃ Ce ₂ (ONep) ₉ (HONep) ₂ (thf) (6)	S20
Figure S2. Crystal structure of Li ₄ [OC(=CHPh)(CH ₂ Ph)] ₄ (thf) ₄ (7).....	S21
Figure S3. Crystal structure of Li ₈ [OCMe ₂ (<i>n</i> -Bu)] ₆ Cl ₂ (thf) ₆ (8).....	S21
NMR Spectra	S22
Figure S4. ¹ H NMR spectrum of Li ₃ CeMe ₆ (tmeda) ₃ (1).....	S22
Figure S5. ⁷ Li NMR spectrum of Li ₃ CeMe ₆ (tmeda) ₃ (1)	S22
Figure S6. ⁷ Li NMR spectrum of Li ₃ CeMe ₆ (tmeda) ₃ (1)	S23
Figure S7. ¹ H NMR spectrum of [Li(thf) ₄][Ce(<i>t</i> -Bu) ₄] (2).....	S23
Figure S8. ⁷ Li NMR spectrum of [Li(thf) ₄][Ce(<i>t</i> -Bu) ₄] (2)	S24
Figure S9. ⁷ Li NMR spectrum of <i>n</i> -BuLi	S24
Figure S10. ⁷ Li NMR spectrum of <i>n</i> -BuLi + 1 equiv. of THF	S25
Figure S11. ⁷ Li NMR spectrum of <i>n</i> -BuLi	S25
Figure S12. ⁷ Li NMR spectrum of <i>n</i> -BuLi + 1 equiv. of TMEDA	S26

Figure S13. ^7Li NMR spectrum of $n\text{-BuLi}$ + 1 equiv. of TMEDA	S26
Figure S14. ^1H NMR spectrum of $\text{Li}_3\text{Sc}(n\text{-Bu})_6(\text{thf})_4$ ($\mathbf{3}^{\text{Sc}}$).....	S27
Figure S15. $^{13}\text{C}\{^1\text{H}\}$ NMR spectrum of $\text{Li}_3\text{Sc}(n\text{-Bu})_6(\text{thf})_4$ ($\mathbf{3}^{\text{Sc}}$).....	S27
Figure S16. ^7Li NMR spectrum of $\text{Li}_3\text{Sc}(n\text{-Bu})_6(\text{thf})_4$ ($\mathbf{3}^{\text{Sc}}$)	S28
Figure S17. ^{45}Sc NMR spectrum of $\text{Li}_3\text{Sc}(n\text{-Bu})_6(\text{thf})_4$ ($\mathbf{3}^{\text{Sc}}$)	S28
Figure S18. VT ^1H NMR spectra of $\text{Li}_3\text{Sc}(n\text{-Bu})_6(\text{thf})_4$ ($\mathbf{3}^{\text{Sc}}$).....	S29
Figure S19. ^1H NMR spectrum of $\text{Li}_3\text{Y}(n\text{-Bu})_6(\text{thf})_4$ ($\mathbf{3}^{\text{Y}}$).....	S29
Figure S20. $^{13}\text{C}\{^1\text{H}\}$ NMR spectrum of $\text{Li}_3\text{Y}(n\text{-Bu})_6(\text{thf})_4$ ($\mathbf{3}^{\text{Y}}$).....	S30
Figure S21. ^7Li NMR spectrum of $\text{Li}_3\text{Y}(n\text{-Bu})_6(\text{thf})_4$ ($\mathbf{3}^{\text{Y}}$).....	S30
Figure S22. ^1H - ^{89}Y HSQC NMR spectrum of $\text{Li}_3\text{Y}(n\text{-Bu})_6(\text{thf})_4$ ($\mathbf{3}^{\text{Y}}$)	S31
Figure S23. VT ^1H NMR spectra of $\text{Li}_3\text{Y}(n\text{-Bu})_6(\text{thf})_4$ ($\mathbf{3}^{\text{Y}}$).....	S31
Figure S24. ^1H NMR spectrum of $\text{Li}_3\text{La}(n\text{-Bu})_6(\text{thf})_4$ ($\mathbf{3}^{\text{La}}$)	S32
Figure S25. ^7Li NMR spectrum of $\text{Li}_3\text{La}(n\text{-Bu})_6(\text{thf})_4$ ($\mathbf{3}^{\text{La}}$).....	S32
Figure S26. VT ^1H NMR spectra of $\text{Li}_3\text{La}(n\text{-Bu})_6(\text{thf})_4$ ($\mathbf{3}^{\text{La}}$)	S33
Figure S27. Wide ^1H NMR spectrum of $\text{Li}_3\text{Ce}(n\text{-Bu})_6(\text{thf})_4$ ($\mathbf{3}^{\text{Ce}}$)	S33
Figure S28. Narrow ^1H NMR spectrum of $\text{Li}_3\text{Ce}(n\text{-Bu})_6(\text{thf})_4$ ($\mathbf{3}^{\text{Ce}}$).....	S34
Figure S29. ^1H NMR spectrum of $\text{Li}_3\text{Ce}(n\text{-Bu})_6(\text{thf})_4$ ($\mathbf{3}^{\text{Ce}}$).....	S34
Figure S30. ^7Li NMR spectrum of $\text{Li}_3\text{Ce}(n\text{-Bu})_6(\text{thf})_4$ ($\mathbf{3}^{\text{Ce}}$)	S35
Figure S31. ^7Li NMR spectrum of $\text{Li}_3\text{Ce}(n\text{-Bu})_6(\text{thf})_4$ ($\mathbf{3}^{\text{Ce}}$)	S35
Figure S32. ^1H NMR spectrum of $\text{CeCl}_3(\text{thf})$ + 1 equiv. of $n\text{-BuLi}$	S36
Figure S33. ^7Li NMR spectrum of $\text{CeCl}_3(\text{thf})$ + 1 equiv. of $n\text{-BuLi}$	S36
Figure S34. ^1H NMR spectrum of $\text{CeCl}_3(\text{thf})$ + 3 equivs. of $n\text{-BuLi}$	S37
Figure S35. ^7Li NMR spectrum of $\text{CeCl}_3(\text{thf})$ + 3 equivs. of $n\text{-BuLi}$	S37
Figure S36. VT ^1H NMR spectra of $\text{Li}_3\text{Ce}(n\text{-Bu})_6(\text{thf})_4$ ($\mathbf{3}^{\text{Ce}}$).....	S38
Figure S37. ^1H NMR spectrum of $\text{Li}_3\text{Lu}(n\text{-Bu})_6(\text{thf})_4$ ($\mathbf{3}^{\text{Lu}}$).....	S38
Figure S38. ^1H NMR spectrum of $\text{Li}_3\text{Lu}(n\text{-Bu})_6(\text{thf})_4$ ($\mathbf{3}^{\text{Lu}}$).....	S39
Figure S39. $^{13}\text{C}\{^1\text{H}\}$ NMR spectrum of $\text{Li}_3\text{Lu}(n\text{-Bu})_6(\text{thf})_4$ ($\mathbf{3}^{\text{Lu}}$).....	S39
Figure S40. ^7Li NMR spectrum of $\text{Li}_3\text{Lu}(n\text{-Bu})_6(\text{thf})_4$ ($\mathbf{3}^{\text{Lu}}$)	S40
Figure S41. ^7Li NMR spectrum of $\text{Li}_3\text{Lu}(n\text{-Bu})_6(\text{thf})_4$ ($\mathbf{3}^{\text{Lu}}$)	S40
Figure S42. VT ^1H NMR spectra of $\text{Li}_3\text{Lu}(n\text{-Bu})_6(\text{thf})_4$ ($\mathbf{3}^{\text{Lu}}$).....	S41

Figure S43. ^1H NMR spectrum of $\text{Li}_2\text{Ce}(n\text{-Bu})_5(\text{tmeda})_2$ (4^{Ce}).....	S41
Figure S44. ^7Li NMR spectrum of $\text{Li}_2\text{Ce}(n\text{-Bu})_5(\text{tmeda})_2$ (4^{Ce}).....	S42
Figure S45. ^1H NMR spectrum of $\text{Li}_2\text{Lu}(n\text{-Bu})_5(\text{tmeda})_2$ (4^{Lu})	S42
Figure S46. $^{13}\text{C}\{^1\text{H}\}$ NMR spectrum of $\text{Li}_2\text{Lu}(n\text{-Bu})_5(\text{tmeda})_2$ (4^{Lu})	S43
Figure S47. ^7Li NMR spectrum of $\text{Li}_2\text{Lu}(n\text{-Bu})_5(\text{tmeda})_2$ (4^{Lu}).....	S43
Figure S48. ^1H NMR spectrum of $\text{LiLu}(n\text{-Bu})_3\text{Cl}(\text{tmeda})_2$ (5).....	S44
Figure S49. $^{13}\text{C}\{^1\text{H}\}$ NMR spectrum of $\text{LiLu}(n\text{-Bu})_3\text{Cl}(\text{tmeda})_2$ (5).....	S44
Figure S50. ^7Li NMR spectrum of $\text{LiLu}(n\text{-Bu})_3\text{Cl}(\text{tmeda})_2$ (5)	S45
Figure S51. ^1H NMR spectrum of $\text{Li}_3\text{Ce}_2(\text{ONep})_9(\text{HONep})_2(\text{thf})$ (6).....	S45
Figure S52. ^7Li NMR spectrum of $\text{Li}_3\text{Ce}_2(\text{ONep})_9(\text{HONep})_2(\text{thf})$ (6)	S46
Figure S53. ^1H NMR spectrum of $\text{Li}_4[\text{OC}(=\text{CHPh})(\text{CH}_2\text{Ph})]_4(\text{thf})_4$ (7)	S46
Figure S54. $^{13}\text{C}\{^1\text{H}\}$ NMR spectrum of $\text{Li}_4[\text{OC}(=\text{CHPh})(\text{CH}_2\text{Ph})]_4(\text{thf})_4$ (7)	S47
Figure S55. ^7Li NMR spectrum of $\text{Li}_4[\text{OC}(=\text{CHPh})(\text{CH}_2\text{Ph})]_4(\text{thf})_4$ (7).....	S47
Figure S56. ^1H NMR spectrum of $\text{Li}_8[\text{OCMe}_2(n\text{-Bu})]_6\text{Cl}_2(\text{thf})_6$ (8)	S48
Figure S57. ^7Li NMR spectrum of $\text{Li}_8[\text{OCMe}_2(n\text{-Bu})]_6\text{Cl}_2(\text{thf})_6$ (8).....	S48
Figure S58. ^1H NMR spectrum of the reaction of 1,3-diphenylpropan-2-one and $n\text{-BuLi}$	S49
Figure S59. ^7Li NMR spectrum of the reaction of 1,3-diphenylpropan-2-one with $n\text{-BuLi}$	S49
Figure S60. ^1H NMR spectrum of 1,3-diphenylpropan-2-one	S50
Figure S61. ^1H NMR spectrum of 1,3-diphenyl-2-butylpropan-2-ol	S50
Figure S62. ^1H NMR spectrum of a mixture of 1,3-diphenylpropan-2-one and 1,3-diphenyl-2-butylpropan-2-ol from the reaction of $\text{Li}_3\text{Ce}(n\text{-Bu})_6(\text{thf})_4$ (3^{Ce}) with six equiv. of 1,3-diphenylpropan-2-one	S51
References	S51

Experimental Section

General Considerations. *Caution!* The organocerium compounds are highly pyrophoric and react violently when exposed to air and/or moisture. All manipulations were performed under an inert atmosphere (Ar) using either glovebox (MBraun UNIlab^{pro}; <0.1 ppm O₂, <0.1 ppm H₂O) or standard Schlenk techniques with oven-dried glassware. The solvents were purified with Grubbs columns (MBraun SPS, solvent purification system) and stored in a glovebox. Anhydrous cerium(III) chloride (99.9%), anhydrous lanthanum(III) chloride (99.9%), anhydrous yttrium(III) chloride (99.9%), anhydrous scandium(III) chloride (99.9%), and anhydrous lutetium(III) chloride (99.9%), were purchased from *abc*r and activated by Soxhlet extraction with THF giving CeCl₃(thf), LaCl₃(thf), YCl₃(thf)₂, ScCl₃(thf)₃, and LuCl₃(thf)₂. A 0.26 M CeCl₃·2 LiCl THF solution (“Ce turbo chloride”) was prepared according to literature.¹ *n*-Butyllithium (*n*-BuLi) (2.5 M solution in hexanes) and 1,3-diphenyl-2-propanon (99%) were purchased from *Sigma Aldrich* and used as received. TMEDA (98%), scandium(III)-trifluoromethanesulfonate Sc(OTf)₃ (97%), anhydrous aluminum chloride (99%), and anhydrous lithium chloride (98%) were purchased from *abc*r and used as received. Benzene-*d*₆, toluene-*d*₈, and THF-*d*₈ were purchased from *Sigma Aldrich*, degassed, dried over NaK alloy for 24 h, filtered and stored inside a glovebox. NMR spectra of moisture-sensitive compounds were recorded by using J. Young valve NMR tubes on either a Bruker AVII+400 (¹H: 400.13 MHz), a Bruker AVIIIHD (¹H: 300.13 MHz), or a Bruker AVII+500 (¹H: 500.13 MHz). ¹H NMR shifts are referenced to a solvent resonance and reported in parts per million (ppm) relative to tetramethylsilane.² Analysis of NMR spectra was performed with TopSpin 3.6.1 [Academic License].³ Multiplicities of signals are given as s (singlet), bs (broad singlet), d (doublet) and dd (doublet of doublets). Coupling constants (J) are given in Hz. Signals were assigned via 2D NMR experiments. Infrared spectra were recorded on a *ThermoFisher* Scientific NICOLET 6700 FTIR ($\tilde{\nu}$ = 4000 – 400 cm⁻¹) spectrometer using a DRIFTS chamber with dry KBr/sample mixtures and KBr windows. Elemental analysis (C, H, N) was performed on an *Elementar vario MICRO cube*. Crystals for X-ray crystallography were handpicked in a glovebox, coated with Parabar 10312, pump-oil, or perfluorinated oil, and stored on microscope slides. X-ray data were collected on a Bruker APEX II DUO diffractometer equipped with an I μ S microfocus sealed tube and QUAZAR optics for MoK α (λ = 0.71073 Å) and CuK α (λ = 1.54184 Å) radiation. The data collection strategy was determined using COSMO⁴ employing ω -scans. Raw data were processed using APEX⁵ and SAINT,⁶ corrections for absorption effects were applied using SADABS.⁷ The structures were solved by direct methods and refined against all data by full-matrix least-squares methods on F² using SHELXTL⁸ and ShelXle.⁹ Disorder models were calculated using DSR, a program for refining structures in ShelXI.¹⁰ All graphics were produced employing Mercury 4.2.0¹¹ and POV-Ray.¹²

[Li₃CeMe₆(tmeda)₃] (1). A slightly modified procedure from that published by Schumann and coworkers¹³ was used to obtain cerous compound **1**. CeCl₃ (303.0 mg, 1.23 mmol) was suspended in

THF (10 mL), cooled to $-10\text{ }^{\circ}\text{C}$, and TMEDA (714.3 mg, 6.25 mmol, 5 equiv.) added dropwise. After stirring for 30 min, MeLi (243.9 mg, 11.06 mmol, 9 equiv.) was added, which turned the suspension instantly into a yellowish/greenish solution. After 18 h, the solvent was removed in vacuo and the remaining solid extracted with cold Et₂O. The ethereal solution was concentrated under reduced pressure and stored at $-40\text{ }^{\circ}\text{C}$, yielding yellow crystals of **1** (83%) suitable for XRD analysis. ¹H NMR (500.13 MHz, 223 K, THF-*d*₈): $\delta = 6.47$ (bs, 36 H, CH₃ tmeda), 5.82 (bs, 12 H, CH₂ tmeda), -4.08 (bs, 18 H, Ce-CH₃) ppm. ⁷Li NMR, (194.37 MHz, 223 K, THF-*d*₈): $\delta = 43.3$ and 42.8 (*Li*₃CeMe₆(tmeda)₃, 97%), 2.4 and 1.8 (MeLi(tmeda), 3%) ppm. IR (KBr, cm⁻¹) $\nu = 2981$ (m), 2952 (m), 2833 (m), 2789 (m), 2749 (w), 1464 (m), 1356 (w), 1291(m), 1255 (w), 1157 (m), 1038 (m), 1021 (w), 948 (m), 790 (w) 475 (s), 445 (s). Anal. (%) Calcd. for C₂₄H₆₆CeLi₃N₆ (599.77 g mol⁻¹): C 48.06, H 11.09, N 14.01; found: C 47.48, H 10.70, N 13.87. The analysis is slightly off because of a small LiCl impurity.

[Li(thf)₄][Ce(*t*-Bu)₄] (2). CeCl₃(thf) (63.7 mg, 0.20 mmol) was suspended in THF (0.5 mL) and cooled to $-40\text{ }^{\circ}\text{C}$. Then, *t*-BuLi (51.2 mg, 0.80 mmol) dissolved in *n*-hexane was added dropwise. After stirring the suspension for 30 min, it was filtered and the solvent removed in vacuo to give a red powder of [Ce(*t*-Bu)₄][Li(thf)₄] \cdot *x*LiCl in approximate 65% yield. Crystals of **2** suitable for XRD analysis were obtained from a highly concentrated Et₂O solution. Note: The oily consistency of the crystallization process is not a suitable method for purification. Amount of LiCl was determined via elemental analysis. ¹H NMR, (300.13 MHz, 299 K, THF-*d*₈): $\delta = 3.62$ (m, 16 H, thf) 2.39 (bs, 36 H, *t*-Bu), 1.78 ppm (m, 16 H, thf). ⁷Li NMR, (116.64 MHz, 299 K, THF-*d*₈): $\delta = 0.4$ (bs, *Li*(thf)₄) ppm. Anal. (%) calcd. for C₃₂H₆₈CeLiO₄ (663.95 gmol⁻¹): C 57.89 49.92, H 10.32 8.90; found: C 49.65, H 7.66. The deviation between theoretical and experimental microanalytical data derives from LiCl incorporation, e.g., the presence of 2.5 LiCl per molecule would correspond to C 49.92, H 8.90.

General Procedure for the Synthesis of Li₃Ln(*n*-Bu)₆(thf)₄ (3Ln, Ln = Sc, Y, La, Ce, Lu). LnCl₃(thf)_{*x*} (0.2 mmol) was suspended in *n*-hexane (1 mL) and THF (0.4 mL), and *n*-BuLi (2.5 M in hexanes, 480.0 μ L, 1.2 mmol) was added dropwise at $-40\text{ }^{\circ}\text{C}$. The mixture was stirred for 30 min at $-40\text{ }^{\circ}\text{C}$, then filtered, and the solvent evaporated in vacuo at $-40\text{ }^{\circ}\text{C}$. The residue was extracted with cold *n*-hexane (~ 8 mL) and the extract filtered again. The solution was slowly concentrated under reduced pressure at $-40\text{ }^{\circ}\text{C}$ and stored at $-40\text{ }^{\circ}\text{C}$ for crystallization giving **3**^{Ln}. Notes: Complexes **3**^{Ln} of the larger Ln (Ce and La) are better soluble in *n*-hexane than the complexes of the smaller Ln (Y, Lu, and Sc), but the latter are more stable. For example, **3**^{Lu} is stable in a *n*-hexane solution for months, whereas **3**^{Ce} had fully decomposed after about three days (at $-40\text{ }^{\circ}\text{C}$). Solvent-free crystals however were stable for all complexes (at $-40\text{ }^{\circ}\text{C}$) except for **3**^{La} which could only be obtained as an oil and had decomposed after a week. The ¹H and ⁷Li NMR spectra indicated partial cleavage of *n*-BuLi, dependent on the Ln(III) size and the solvent.

Li₃Sc(*n*-Bu)₆(thf)₄ (3^{Sc}). Colorless solid, yield: 44.7 mg (0.06 mmol, 32%). ¹H NMR (500.13 MHz, 233 K, toluene-*d*₈): $\delta = 3.65$ (m, 16 H, thf), 2.09 (m, 12 H, CH₂-2-butyl), 1.84 (m, 12 H, CH₂-3-butyl), 1.36

(m, 34 H, CH_3 -4-butyl and thf), 0.33 ppm (m, 12 H, CH_2 -1-butyl). $^{13}C\{^1H\}$ NMR (125.76 MHz, 233 K, toluene- d_8): δ = 68.1 (s, thf), 34.0 (s, CH_2 -2-butyl), 32.8 (s, CH_2 -3-butyl), 29.9 (s, CH_2 -1-butyl), 25.3 (s, thf), 14.6 ppm (s, CH_3 -4-butyl). 7Li NMR (194.37 MHz, 233 K, toluene- d_8): δ = 2.3 (free $n-BuLi(thf)$, ~8%), 1.2 ppm ($Li_3Sc(n-Bu)_6(thf)_4$, ~92%). ^{45}Sc NMR (121.49 MHz, 233 K, toluene- d_8): δ = 502 ppm (s, lwhh = 11787 Hz).

$Li_3Y(n-Bu)_6(thf)_4$ (3^Y). Colorless solid, yield: 93.7 mg (0.13 mmol, 64%). 1H NMR (500.13 MHz, 233 K, toluene- d_8): δ = 3.59 (m, 16 H, thf), 2.01 (m, 12 H, CH_2 -2-butyl), 1.80 (m, 12 H, CH_2 -3-butyl), 1.31 (m, 34 H, CH_3 -4-butyl and thf), 0.05 ppm (m, 12 H, CH_2 -1-butyl). $^{13}C\{^1H\}$ NMR (125.76 MHz, 233 K, toluene- d_8): δ = 68.1 (s, thf), 33.3 (s, CH_2 -2-butyl), 33.1 (s, CH_2 -3-butyl), 29.2 (s, CH_2 -1-butyl), 25.3 (s, thf), 14.5 ppm (s, CH_3 -4-butyl). 7Li NMR (194.37 MHz, 233 K, toluene- d_8): δ = 2.3 (free $n-BuLi(thf)$, ~1%), 1.6 ppm ($Li_3Y(n-Bu)_6(thf)_4$, ~99%). ^{89}Y (from 1H - ^{89}Y HSQC) NMR (24.52 MHz, 233 K, toluene- d_8): δ = 771 ppm (s, lwhh = 143 Hz). Anal. (%) Calcd. for $C_{40}H_{86}Li_3YO_4$ (740.85 $g\ mol^{-1}$): C 64.85, H 11.70; found: C 64.74, H 12.51.

$Li_3La(n-Bu)_6(thf)_4$ (3^{La}). Colorless solid/oil, yield: ~50% yield (no complete removal of THF at -40 °C). Because most of the $n-BuLi$ is cleaved off in solution, not all signals could be assigned with complete accuracy in the 1H NMR spectrum. 1H NMR (500.13 MHz, 233 K, toluene- d_8): δ = 3.67 (m, thf), 1.86 (m, CH_2 -2-butyl, CH_2 -3-butyl, and $n-BuLi$), 1.29 (m, CH_2 -4-butyl, and thf), 0.91 (t, $n-BuLi$), 0.00 (bs, CH_2 -1-butyl), -0.53 ppm (m, $n-BuLi$). 7Li NMR (194.37 MHz, 233 K, toluene- d_8): δ = 2.3, 2.1 and 1.70 ($n-BuLi(thf)$).

$Li_3Ce(n-Bu)_6(thf)_4$ (3^{Ce}). Yellow solid, yield: 146.8 mg (0.19 mmol, 93%). Due to the paramagnetism of Ce(III) the 1H NMR spectrum was not conclusive (see Figure S25–S27). 7Li NMR (194.37 MHz, 233 K, toluene- d_8): δ = 30.2 ($Li[Ce]$, ~2%), 2.4, 2.0 ppm (free $n-BuLi(thf)$, ~98%). Elemental analysis calcd. (%) for $C_{40}H_{86}Li_3CeO_4$ (792.06 $g\ mol^{-1}$): C 61.12, H 10.26; found: C 61.34, H 10.50.

$Li_3Lu(n-Bu)_6(thf)_4$ (3^{Lu}). Colorless solid, yield: 121.9 mg (0.14 mmol, 74%). 1H NMR (500.13 MHz, 233 K, toluene- d_8): δ = 3.59 (m, 16 H, thf), 2.01 (m, 12 H, CH_2 -2-butyl), 1.79 (m, 12 H, CH_2 -3-butyl), 1.30 (m, 34 H, CH_3 -4-butyl, and thf), 0.14 ppm (m, 12 H, CH_2 -1-butyl). $^{13}C\{^1H\}$ NMR (125.76 MHz, 233 K, toluene- d_8): δ = 68.4 (s, thf), 33.9 (s, CH_2 -2-butyl), 33.6 (s, CH_2 -3-butyl), 33.0 (s, CH_2 -1-butyl), 25.5 (s, thf), 14.8 ppm (s, CH_3 -4-butyl). 7Li NMR (194.37 MHz, 233 K, toluene- d_8): δ = 2.3 (free $n-BuLi(thf)$, ~4%), 1.9 ppm ($Li_3Lu(n-Bu)_6(thf)_4$, ~96%). Anal. (%) Calcd. for $C_{40}H_{86}Li_3LuO_4$ (826.87 $g\ mol^{-1}$): C 58.10, H 10.48; found: C 57.93, H 10.50.

Equimolar reaction of $CeCl_3(thf)$ with $n-BuLi$. $CeCl_3(thf)$ (100.0 mg, 0.31 mmol) was suspended in THF and cooled to -40 °C. Then, $n-BuLi$ (2.5 M in hexanes, 125.6 μL , 0.31 mmol, one equiv.) was added and the mixture stirred for 30 min. After allowing time for settling of the insoluble parts, the supernatant was carefully removed. The residue was evaporated in vacuo to leave ~44 mg (44%) of unconsumed $CeCl_3(thf)$.

Synthesis of 3^{Lu} for XRD analysis. $\text{LuCl}_3(\text{thf})_2$ (72.5 mg, 0.18 mmol) was suspended in *n*-hexane (2 mL) and *n*-BuLi (2.5 M in hexanes, 240.0 μL , 0.6 mmol, 3.33 equiv.) was added dropwise at -45°C . Stirring the mixture for 24 h at -45°C caused the formation of an oily white precipitate. After filtration the solution was concentrated (under reduced pressure) and stored at -40°C to give colorless crystals suitable for XRD analysis in low yields ($\sim 5\text{-}10\%$).

Synthesis of 3^{Lu} from “lutetium turbo chloride”. $\text{LuCl}_3(\text{thf})_2$ (83.4 mg, 0.2 mmol) and LiCl (17.0 mg, 0.4 mmol) were stirred together in THF (5 mL). Complete dissolution of the mixed metal chloride was observed after 30 min. The solution was cooled to -40°C and *n*-BuLi (2.5 M in hexanes, 480.0 μL , 1.2 mmol) was added dropwise. The mixture was stirred for 30 min at -40°C and then filtered. The solvent of the filtrate was evaporated in vacuo at -40°C , extracted with cold *n*-hexane (~ 8 mL), and the extract filtered again. The obtained solution was slowly concentrated under reduced pressure at -40°C and stored at -40°C for crystallization. The obtained colorless crystals were identified as 3^{Lu} ($\sim 70\%$) via XRD unit-cell check and ^1H NMR spectroscopy.

Synthesis of 3^{Lu} from 3^{Ce} . To a suspension of $\text{LuCl}_3(\text{thf})_2$ (56.4 mg, 0.14 mmol) in THF (0.4 mL) and *n*-hexane (1 mL), compound 3^{Ce} (106.5 mg, 0.14 mmol) dissolved in *n*-hexane (3 mL) was added at -40°C . After stirring for 18 h at -40°C the brown mixture was filtered and concentrated to give 3^{Lu} (26.3 mg, 0.03 mmol, 23%) as colorless crystals (characterized by XRD unit-cell check).

General Procedure for the Synthesis of $\text{Li}_2\text{Ln}(\textit{n}\text{-Bu})_5(\text{tmeda})_2$ (4^{Ln} , Ln = Ce, Lu). $\text{LnCl}_3(\text{thf})_x$ (0.2 mmol) was suspended in *n*-hexane (1 mL) and THF (0.4 mL) and *n*-BuLi (2.5 M in hexanes, 480.0 μL , 1.2 mmol, six equiv.) were added dropwise at -40°C . The mixture was stirred for 30 min at -40°C . After filtration the solvent was evaporated in vacuo at -40°C , the obtained residue extracted with cold *n*-hexane (~ 8 mL) and the extract filtered again. Cold TMEDA (90.5 μL , 0.6 mmol, three equiv.) was added to the solution before it was slowly concentrated under reduced pressure at -40°C until the onset of crystallization. Storage at -40°C yielded single-crystalline 4^{Ln} .

$\text{Li}_2\text{Ce}(\textit{n}\text{-Bu})_5(\text{tmeda})_2$ (4^{Ce}). 73.2 mg (0.11 mmol, 55%). Due to the paramagnetism of Ce(III) the ^1H NMR spectrum was not conclusive (see Figure S41). ^7Li NMR (194.37 MHz, 233 K, toluene- d_8): $\delta = 79.7$ (*Li*[Ce], $\sim 54\%$), 2.6 ppm (free *n*-BuLi(tmeda), $\sim 46\%$). Anal. (%) Calcd. for $\text{C}_{32}\text{H}_{77}\text{Li}_2\text{CeN}_4$ (671.97 g mol $^{-1}$): C 57.54, H 11.02, N 8.39; found: C 58.78, H 12.59, N 8.63. The deviation between theoretical and experimental microanalytical data derives from decomposition of 4^{Ce} at ambient temperature (change from crystalline to oily consistency).

$\text{Li}_2\text{Lu}(\textit{n}\text{-Bu})_5(\text{tmeda})_2$ (4^{Lu}). Colorless solid, yield: 87.8 mg (0.12 mmol, 62%). ^1H NMR (500.13 MHz, 233 K, toluene- d_8): $\delta = 2.06$ (bs, 24 H, tmeda- CH_3), 1.98 (m, 10 H, CH_2 -2-butyl), 1.86 (m, 10 H, CH_2 -3-butyl), 1.64 (bs, 8 H, tmeda- CH_2), 1.37 (t, 15 H, CH_3 -4-butyl), 0.05 ppm (m, 10 H, CH_2 -1-butyl). $^{13}\text{C}\{^1\text{H}\}$ NMR (125.76 MHz, 233 K, toluene- d_8): $\delta = 56.3$ (s, tmeda- CH_2), 45.8 (s, tmeda- CH_3), 41.8 (s, CH_2 -1-butyl), 32.8 (s, CH_2 -3-butyl), 32.0 (s, CH_2 -2-butyl), 14.8 ppm (s, CH_3 -4-butyl). ^7Li NMR (194.37

MHz, 233 K, toluene-*d*₈): δ = 2.5 (free *n*-BuLi(tmeda), ~20%), 1.8 ppm (*Li*₂Lu(*n*-Bu)₅(tmeda)₂, ~80%). Anal. (%) Calcd. for C₃₂H₇₇Li₂LuN₄ (706.82 gmol⁻¹): C 54.69, H 10.47, N 7.97; found: C 53.73, H 11.32, N 8.58. The deviation between theoretical and experimental microanalytical data derives from decomposition of **4^{Lu}** at ambient temperature (change from crystalline to oily consistency).

LiLu(*n*-Bu)₃Cl(tmeda)₂ (5). Li₂Lu(*n*-Bu)₅(tmeda)₂ (**4^{Lu}**) (87.8 mg, 0.12 mmol) was dissolved in *n*-hexane (4 mL) at -40 °C and ClSiMe₃ (76.3 μ L, 0.60 mmol, five equiv.) was added. After stirring for 4 h the mixture was filtered and the volatiles were removed in vacuo at -40 °C. The crude product was redissolved in *n*-hexane, and after filtration and concentration under reduced pressure at -40 °C, compound **5** was obtained as colorless crystals, suitable for XRD analysis, albeit in a low yield. ¹H NMR (500.13 MHz, 233 K, THF-*d*₈): δ = 2.32 (s, 8 H, tmeda-CH₂), 2.17 (s, 24 H, tmeda-CH₃), 1.64 (m, 6 H, CH₂-2-butyl), 1.25 (m, 4 H, CH₂-3-butyl), 1.19 (m, 2 H, CH₂-3-Li-butyl), 0.84 (m, 9 H, CH₂-4-butyl), -0.39 (m, 4 H, CH₂-1-butyl), -0.54 ppm (m, 2 H, CH₂-1-Li-butyl). ¹³C {¹H} NMR (125.76 MHz, 233 K, THF-*d*₈): δ = 58.0 (s, tmeda-CH₂), 52.8 (s, CH₂-1-Li-butyl), 49.8 (s, CH₂-1-butyl), 45.5 (s, tmeda-CH₃), 34.2 (s, CH₂-2-Li-butyl) 33.1 (s, CH₂-2-butyl), 32.8 (s, CH₂-3-Li-butyl), 31.6 (s, CH₂-3-butyl), 14.4 (s, CH₃-4-Li-butyl) 14.0 ppm (s, CH₃-4-butyl). ⁷Li NMR (194.37 MHz, 233 K, THF-*d*₈): δ = 0.28 ppm. The small amount of product was not sufficient for microanalysis (NMR study was prioritized).

Synthesis of Li₃Ce₂(ONep)₉(HONep)₂(thf) (6). Li₃Ce(*n*-Bu)₆(thf)₄ (**3^{Ce}**) (133.8 mg, 0.20 mmol) was dissolved in *n*-hexane (4 mL) at -40 °C and solution of neopentanol (105.8 mg, 1.20 mmol, six equiv.) in *n*-hexane was added. After stirring for 30 min the mixture was concentrated under reduced pressure at -40 °C and filtered. The obtained solution was stored at -40 °C to afford **6** as colorless crystals, suitable for XRD analysis, albeit in a low yield. ¹H NMR (300.13 MHz, 299 K, benzene-*d*₆): δ = 8.23 (bs, 2 H, OH), 3.76 (bs, 22 H, CH₂), 3.62 (bs, 4 H, thf), 1.04 (bs, 4 H, thf), 0.55 ppm (bs, 99 H, CH₃). ⁷Li NMR (116.64 MHz, 299 K, benzene-*d*₆): δ = 91.76, 65.11, 57.55, 30.67, 26.28, 23.75, 22.83, 13.09, 10.80, 3.76, 2.59, 1.85, 0.80 ppm. Anal. (%) Calcd. for C₅₉H₁₃₁Ce₂Li₃O₁₂ (1333.69 gmol⁻¹): C 53.13, H 9.90; found: C 51.76, H 11.90. The elemental analysis is slightly off, because of some remaining solvent.

Li₄[OC(=CHPh)(CH₂Ph)]₄(thf)₄ (7). CeCl₃(thf) (63.7 mg, 0.2 mmol) was suspended in THF (0.4 mL), *n*-hexane (1 mL) and cooled to -40 °C. Then *n*-BuLi (2.5 M in hexanes, 480.0 μ L, 1.2 mmol, six equiv.) was added dropwise. After 30 min of stirring at -40 °C cold 1,3-diphenylpropan-2-one (252.3 mg, 1.2 mmol, six equiv.) was added to the yellow solution, which instantly decolorized to slightly yellow. The mixture was stirred for another 30 min at -40 °C. Then it was filtered, concentrated under reduced pressure, and stored at -40 °C for three weeks, which produced heavily intertwined colorless crystals. The yellow supernatant was removed and the crystals were recrystallized several times from a *n*-hexane/THF mixture affording colorless crystals of **7**. Yield: 69.3 mg, 0.05 mmol, 18% (after crystals had been removed for XRD analysis). ¹H NMR (300.13 MHz, 299 K, THF-*d*₈; numbering scheme, see Figures S51 and S52): δ = 7.58 (m, 2 H, CH-aromatic 5&9), 7.31 (m, 2 H, CH-aromatic 11&15), 7.19 (m, 2 H, CH-aromatic 12&14), 7.10 (m, 1 H, CH-aromatic 13), 7.00 (m, 2 H, CH-aromatic 6&8), 6.66

(m, 1 H, CH-aromatic 7), 4.75 (s, 1 H, CH 1), 3.61 (m, 4 H, THF), 3.38 (s, 2 H, CH₂ 3), 1.76 ppm (m, 4 H, THF). ¹³C{¹H} NMR (75.47 MHz, 299 K, THF-*d*₈): δ = 167.6 (s, C 2), 143.1 (s, C 10), 142.1 (s, C 4), 129.0 (s, C 11&15), 127.5 (s, C 12&14), 127.1 (s, C 6&8), 124.9 (s, C 13), 124.8 (s, C 5&9), 119.9 (s, C 7), 96.1 (s, C 1), 67.2 (s, THF), 49.1 (s, C 3), 25.4 ppm (s, THF). ⁷Li NMR (116.64 MHz, 299 K, THF-*d*₈): δ = 0.14 ppm.

Synthesis of Li₈[OCMe₂(*n*-Bu)]₆Cl₂(thf)₆ (8**).** CeCl₃(thf) (63.7 mg, 0.2 mmol) was suspended in THF (2 mL) and cooled to -40 °C. Then *n*-BuLi (2.5 M in hexanes, 240.0 μL, 0.6 mmol, three equiv.) was added dropwise. After 30 min of stirring at -40 °C, cold acetone (44.4 μL, 0.6 mmol, three equiv.) was added to the yellow solution which decolorized immediately. The mixture was stirred for another 30 min at -40 °C before it was filtered and stored at -40 °C for two weeks to yield colorless crystals of **8** in a low yield.

NMR-scale reactions of LuCl₃(thf)₂ with *x* *n*-BuLi (*x* = 1, 3, 6, 12). In a J.-Young valved NMR tube LuCl₃(thf)₂ was suspended in THF-*d*₈ and cooled down to -40 °C. Then *x* (1, 3, 6, 12) equivalents of *n*-BuLi were added. After 30 min at -40 °C, during which the NMR tube was regularly shaken ¹H and ⁷Li NMR spectra were measured at -80 °C.

NMR-scale reactions of *n*-BuLi with 1,3-diphenylpropan-2-one. In a J.-Young valved NMR tube 1,3-diphenylpropan-2-one (21.0 mg, 0.1 mmol) was dissolved in THF-*d*₈ and *n*-BuLi (2.5 M in hexanes, 40.0 μL, 0.1 mmol, one equiv.) was added, upon which the solution turned deep red immediately. After 30 min during which time the NMR tube was regularly shaken ¹H and ⁷Li NMR spectra were measured (see Figures S56 and S57). The NMR spectra appear intricate, but clearly show that both the Li₄[OC(=CHPh)(CH₂Ph)]₄(thf)₄ and the lithium salt of 1,3-diphenyl-2-butylpropan-2-ol are produced alongside of further unknown side products. The NMR spectra did not change after 18 h.

Ketone/alcohol transformations employing 1,3-diphenylpropan-2-one. A detailed reaction is described as a typical example (Table 1, entry 1). For the other reactions, see the supporting information. The ketone reduction with an equimolar amount of CeCl₃ and *n*-BuLi was adapted from the original work by the Imamoto group in 1984.⁷ A suspension of CeCl₃(thf) (414.2 mg, 1.3 mmol) in THF (5 mL) was cooled to -35 °C. Then *n*-BuLi (2.5 M in hexanes, 520.0 μL, 1.3 mmol, one equiv.) was added dropwise. After 30 min of stirring at -35 °C a pre-cooled solution of 1,3-diphenylpropan-2-one (210.3 mg, 1.0 mmol, 0.77 equiv.) dissolved in THF (5 mL) was added and the mixture stirred for another 30 min at -35 °C. The mixture was then quenched with a saturated aqueous solution of sodium carbonate, and the aqueous layer was extracted three times with diethyl ether. The combined organic layers were dried over anhydrous sodium sulfate and the volatiles were removed in vacuo giving 1,3-diphenyl-2-butylpropan-2-ol as a colorless oil. Yield: 266.8 mg (0.99 mmol, 99%). ¹H NMR (400.11 MHz, 299 K, benzene-*d*₆): δ = 7.18-7.03 (m, 12 H, phenyl), 2.65 (s, 4 H, 1,3-CH₂-propan), 1.33-1.06 (m, 6 H, CH₂-1-butyl, CH₂-2-butyl, and CH₂-3-butyl), 0.81 ppm (t, 3 H, CH₃-4-butyl).

Ketone/alcohol transformations employing 1,3-diphenylpropan-2-one. For incomplete reactions, the ketone/alcohol ratio was determined via the CH₂ groups of the propane part of the molecules in the ¹H NMR spectra: for 1,3-diphenylpropan-2-one, one singlet at 3.33 ppm; for 1,3-diphenyl-2-butylpropan-2-ol, one singlet at 2.65 ppm. Due to equal number of protons, comparison of the integrals of these two signals will indicate the molar ratio of the ketone and alcohol. Weighting of the ratio with the molecular weight of the ketone and alcohol lead to the yield according to the formula shown below.

$$\text{alcohol [mmol]} = \frac{\text{yield of alcohol + ketone [mg]}}{\text{alcohol}[M] + \left(\frac{\text{ketone[mol \%]}}{\text{alcohol [mol \%]}}\right) \times \text{ketone}[M]}$$

CeCl₃ and 6 *n*-BuLi and ketone (Table 1, entry 2). A suspension of CeCl₃(thf) (63.7mg, 0.2 mmol) in THF (2 mL) was cooled to -40 °C before *n*-BuLi (2.5 M in hexanes, 480.0 μL, 1.2 mmol, six equiv.) was added dropwise. After 30 min of stirring at -40 °C a pre-cooled solution of 1,3-diphenylpropan-2-one (252.3 mg, 1.2 mmol, six equiv.) dissolved in THF (2 mL) was added and the mixture stirred for another 30 min at -40 °C. The mixture was then quenched with a saturated aqueous solution of sodium carbonate, and the aqueous layer was extracted three times with diethyl ether. The combined organic layers were dried over anhydrous sodium sulfate and the volatiles were removed in vacuo giving 1,3-diphenyl-2-butylpropan-2-ol as a colorless oil. Yield: 246.9 mg (0.92 mmol, 77%); amount of recovered ketone: 50.5 mg (0.24 mmol, 20%).

Li₃Ce(*n*-Bu)₆(thf)₄ (3^{Ce}) and ketone/THF (Table 1, entries 3 and 4). A chilled solution of 3^{Ce} (158.4 mg, 0.2 mmol) in *n*-hexane (2 mL, -40 °C) was added dropwise to a pre-cooled solution of 1,3-diphenylpropan-2-one (252.3 mg/1.2 mmol/six equiv. or 42.1 mg/0.2 mmol/one equiv.) dissolved in THF (2 mL) and stirred for 30 min at -40 °C. The mixture was then quenched with a saturated aqueous solution of sodium carbonate, and the aqueous layer was extracted three times with diethyl ether. The combined organic layers were dried over anhydrous sodium sulfate and the volatiles were removed in vacuo giving 1,3-diphenyl-2-butylpropan-2-ol as a colorless oil. Yield for six equivs. of ketone: 226.1 mg (0.84 mmol, 70%); amount of recovered ketone: 33.7 mg (0.16 mmol, 13%). Yield for one equiv. of ketone: 47.2 mg (0.18 mmol, 88%); amount of recovered ketone 1.2 mg (0.01 mmol, 3%).

Li₃Ce(*n*-Bu)₆(thf)₄ (3^{Ce}) and ketone/OEt₂ (Table 1, entries 5, 6, and 7). A chilled solution of 3^{Ce} (158.4 mg, 0.2 mmol) in *n*-hexane (2 mL, -40 °C) was added dropwise to a pre-cooled solution of 1,3-diphenylpropan-2-one (252.3 mg/1.2 mmol/six equiv. or 126.2 mg/0.6 mmol/three equiv. or 42.1 mg/0.2 mmol/one equiv.) dissolved in Et₂O (2 mL) and stirred for 30 min at -40 °C. The mixture was then quenched with a saturated aqueous solution of sodium carbonate, and the aqueous layer was extracted three times with diethyl ether. The combined organic layers were dried over anhydrous sodium sulfate

and the volatiles were removed in vacuo giving 1,3-diphenyl-2-butylpropan-2-ol as a colorless oil. Yield for six equiv. of ketone: could not be determined gravimetrically because the volatiles were not removed completely, so only the NMR ratio of the alcohol and ketone are stated here: alcohol 54%, ketone 46%. Yield for three equivs. of ketone: 125.8 mg (0.47 mmol, 78%); amount of recovered ketone: 19.3 mg (0.09 mmol, 15%). Yield for one equiv. of ketone: 47.9 mg (0.18 mmol, 89%); amount of recovered ketone: 4.1 mg (0.02 mmol, 10%).

Li₃Ce(*n*-Bu)₆(thf)₄ (3^{Ce}) and ketone/toluene (Table 1, entry 8). A chilled solution of 3^{Ce} (158.4 mg, 0.2 mmol) in *n*-hexane (2 mL, -40 °C) was added dropwise to a pre-cooled solution of 1,3-diphenylpropan-2-one (252.3 mg, 1.2 mmol, six equiv.) dissolved in toluene (2 mL) and stirred for 30 min at -40 °C. The mixture was then quenched with a saturated aqueous solution of sodium carbonate, and the aqueous layer was extracted three times with diethyl ether. The combined organic layers were dried over anhydrous sodium sulfate and the volatiles were removed in vacuo giving 1,3-diphenyl-2-butylpropan-2-ol as a colorless oil. Yield: 243.7 mg (0.91 mmol, 76%); amount of recovered ketone: 28.5 mg (0.14 mmol, 11%).

Li₃Ce(*n*-Bu)₆(thf)₄ (3^{Ce}) and ketone/THF/LiCl (Table 1, entry 9). A chilled solution of 3^{Ce} (158.4 mg, 0.2 mmol) in *n*-hexane (2 mL, -40 °C) was added dropwise to a pre-cooled mixture of 1,3-diphenylpropan-2-one (252.3 mg, 1.2 mmol, six equiv.) and LiCl (25.4 mg, 0.6 mmol, three equiv.) dissolved in THF (2 mL), and stirred for 30 min at -40 °C. The mixture was then quenched with a saturated aqueous solution of sodium carbonate, and the aqueous layer was extracted three times with diethyl ether. The combined organic layers were dried over anhydrous sodium sulfate and the volatiles were removed in vacuo giving 1,3-diphenyl-2-butylpropan-2-ol as a colorless oil. Yield: 238.9 mg (0.89 mmol, 74%); amount of recovered ketone: 40.3 mg (0.19 mmol, 16%).

Li₃Ce(*n*-Bu)₆(thf)₄ (3^{Ce}) and ketone/THF/CeCl₃(thf) (Table 1, entry 10). A chilled solution of 3^{Ce} (158.4 mg, 0.2 mmol) in *n*-hexane (2 mL, -40 °C) was added dropwise to a pre-cooled mixture of 1,3-diphenylpropan-2-one (252.3 mg, 1.2 mmol, six equiv.) and CeCl₃(thf) (318.6 mg, 1.0 mmol, five equiv.) suspended in THF (5 mL), and stirred for 30 min at -40 °C. The mixture was then quenched with a saturated aqueous solution of sodium carbonate, and the aqueous layer was extracted three times with diethyl ether. The combined organic layers were dried over anhydrous sodium sulfate and the volatiles were removed in vacuo giving 1,3-diphenyl-2-butylpropan-2-ol as a colorless oil. Yield: 285.3 mg, (1.06 mmol, 89%), amount of recovered ketone: 20.8 mg (0.10 mmol, 8%).

Li₃Ce(*n*-Bu)₆(thf)₄ (3^{Ce}) and ketone/THF/“cerium turbo chloride” (Table 1, entry 11). A chilled solution of 3^{Ce} (158.4 mg, 0.2 mmol) in *n*-hexane (2 mL, -40 °C) was added dropwise to a pre-cooled mixture of 1,3-diphenylpropan-2-one (252.3 mg, 1.2 mmol, six equiv.) and “cerium turbo chloride” (1.0 mmol, five equiv.) dissolved in THF (5 mL) and stirred for 30 min at -40 °C. The mixture was then quenched with a saturated aqueous solution of sodium carbonate, and the aqueous layer was extracted three times with diethyl ether. The combined organic layers were dried over anhydrous sodium sulfate

and the volatiles were removed in vacuo giving 1,3-diphenyl-2-butylpropan-2-ol as a colorless oil. Yield: 258.6 mg (0.96 mmol, 80%); amount of recovered ketone: 36.0 mg (0.17 mmol, 14%).

Li₃Ce(*n*-Bu)₆(thf)₄ (3^{Ce}) and ketone/THF, then "cerium turbo chloride" (Table 1, entry 12). A chilled solution of 3^{Ce} (158.4 mg, 0.2 mmol) in *n*-hexane (2 mL, -40 °C) was added dropwise to a pre-cooled mixture of 1,3-diphenylpropan-2-one (252.3 mg, 1.2 mmol, six equiv.) dissolved in THF (3 mL). After stirring for 5 min at -40 °C an equally cold solution of "cerium turbo chloride" (1.0 mmol, five equiv.) was added. The mixture was then stirred for another 30 min at -40 °C before it was quenched with a saturated aqueous solution of sodium carbonate, and the aqueous layer was extracted three times with diethyl ether. The combined organic layers were dried over anhydrous sodium sulfate and the volatiles were removed in vacuo giving 1,3-diphenyl-2-butylpropan-2-ol as a colorless oil. Yield: 292.2 mg (1.08 mmol, 90%); amount of recovered ketone: 2.3 mg (0.01 mmol, 1%).

Li₃Ce(*n*-Bu)₆(thf)₄ (3^{Ce}) and ketone/THF, then Sc(OTf)₃ (Table 1, entry 13). A chilled solution of 3^{Ce} (158.4 mg, 0.2 mmol) in *n*-hexane (2 mL, -40 °C) was added dropwise to a pre-cooled mixture of 1,3-diphenylpropan-2-one (252.3 mg, 1.2 mmol, six equiv.) dissolved in THF (3 mL). After stirring for five min at -40 °C an equally cold solution of scandium(III) triflate (1.0 mmol, five equiv.) in THF (2 mL) was added. The mixture was then stirred for another 30 min at -40 °C before it was quenched with a saturated aqueous solution of sodium carbonate, and the aqueous layer was extracted three times with diethyl ether. The combined organic layers were dried over anhydrous sodium sulfate and the volatiles were removed in vacuo giving 1,3-diphenyl-2-butylpropan-2-ol as a colorless oil. The yield could not be determined gravimetrically because the lithium triflate could not be removed completely by this work-up procedure; so only the NMR ratios of the alcohol and ketone are stated here: alcohol 62%, ketone 38%.

Li₃Ce(*n*-Bu)₆(thf)₄ (3^{Ce}) and ketone/THF, then AlCl₃ (Table 1, entry 14). A chilled solution of 3^{Ce} (158.4 mg, 0.2 mmol) in *n*-hexane (2 mL, -40 °C) was added dropwise to a pre-cooled mixture of 1,3-diphenylpropan-2-one (252.3 mg, 1.2 mmol, six equiv.) dissolved in THF (3 mL). After stirring for five min at -40 °C an equally cold solution of AlCl₃ (1.0 mmol, five equiv.) in THF (2 mL) was added. The mixture was then stirred for another 30 min at -40 °C before it was quenched with a saturated aqueous solution of sodium carbonate, and the aqueous layer was extracted three times with diethyl ether. The combined organic layers were dried over anhydrous sodium sulfate and the volatiles were removed in vacuo giving 1,3-diphenyl-2-butylpropan-2-ol as a colorless oil. Yield: 254.2 mg (0.95 mmol, 79%); amount of recovered ketone: 52.8 mg (0.25 mmol, 21%).

Li₃Ce(*n*-Bu)₆(thf)₄ (3^{Ce}) and ketone/THF/TMEDA (Table 1, entry 15). A chilled solution of 3^{Ce} (158.4 mg, 0.2 mmol) in *n*-hexane (2 mL, -40 °C) was added dropwise to a pre-cooled mixture of 1,3-diphenylpropan-2-one (252.3 mg, 1.2 mmol, six equiv.) and TMEDA (90.5 μL, 0.6 mmol, three equiv.) dissolved in THF (5 mL), and stirred for 30 min at -40 °C. The mixture was then quenched with a saturated aqueous solution of sodium carbonate, and the aqueous layer was extracted three times with

diethyl ether. The combined organic layers were dried over anhydrous sodium sulfate and the volatiles were removed in vacuo giving 1,3-diphenyl-2-butylpropan-2-ol as a colorless oil. Yield: 235.1 mg (0.88 mmol, 73%); amount of recovered ketone: 40.2 mg (0.19 mmol, 16%).

Li₃Lu(*n*-Bu)₆(thf)₄ (3^{Lu}) and ketone/THF (Table 1, entry 16). A chilled solution of 3^{Lu} (100.6 mg, 0.12 mmol) in *n*-hexane (2 mL, -40 °C) was added dropwise to a pre-cooled solution of 1,3-diphenylpropan-2-one (153.4 mg, 0.73 mmol, six equiv.) dissolved in THF (2 mL) and stirred for 30 min at -40 °C. The mixture was then quenched with a saturated aqueous solution of sodium carbonate, and the aqueous layer was extracted three times with diethyl ether. The combined organic layers were dried over anhydrous sodium sulfate and the volatiles were removed in vacuo giving 1,3-diphenyl-2-butylpropan-2-ol as a colorless oil. Yield: 145.4 mg (0.54 mmol, 74%); amount of recovered ketone: 34.6 mg (0.16 mmol, 23%).

Li₃Lu(*n*-Bu)₆(thf)₄ (3^{Lu}) and ketone/THF/TMEDA (Table 1, entry 17). A chilled solution of 3^{Lu} (165.4 mg, 0.2 mmol) in *n*-hexane (2 mL, -40 °C) was added dropwise to a pre-cooled solution of 1,3-diphenylpropan-2-one (252.3 mg, 1.2 mmol, six equiv.) and TMEDA (90.5 μL, 0.6 mmol, three equiv.) dissolved in THF (5 mL) and stirred for 30 min at -40 °C. The mixture was then quenched with a saturated aqueous solution of sodium carbonate, and the aqueous layer was extracted three times with diethyl ether. The combined organic layers were dried over anhydrous sodium sulfate and the volatiles were removed in vacuo giving 1,3-diphenyl-2-butylpropan-2-ol as a colorless oil. Yield: 141.7 mg (0.53 mmol, 44%); amount of recovered ketone: 141.6 mg (0.67 mmol, 56%).

Li₃Y(*n*-Bu)₆(thf)₄ (3^Y) and ketone/THF (Table 1, entry 18). A chilled solution of 3^Y (93.7 mg, 0.13 mmol) in *n*-hexane (2 mL, -40 °C) was added dropwise to a pre-cooled solution of 1,3-diphenylpropan-2-one (160.9 mg, 0.73 mmol, six equiv.) dissolved in THF (2 mL) and stirred for 30 min at -40 °C. The mixture was then quenched with a saturated aqueous solution of sodium carbonate, and the aqueous layer was extracted three times with diethyl ether. The combined organic layers were dried over anhydrous sodium sulfate and the volatiles were removed in vacuo giving 1,3-diphenyl-2-butylpropan-2-ol as a colorless oil. Yield: 155.7 mg (0.58 mmol, 75%); amount of recovered ketone: 19.4 mg (0.09 mmol, 12%).

Li₃Y(*n*-Bu)₆(thf)₄ (3^Y) and ketone/THF @ ambient temperature (Table 1, entry 19). A chilled solution of 3^Y (38.1 mg, 0.05 mmol) in *n*-hexane (2 mL, -40 °C) was added dropwise to a solution of 1,3-diphenylpropan-2-one (65.3 mg, 0.31 mmol, six equiv.) dissolved in THF (2 mL) and stirred for 30 min at ambient temperature. The mixture was then quenched with a saturated aqueous solution of sodium carbonate, and the aqueous layer was extracted three times with diethyl ether. The combined organic layers were dried over anhydrous sodium sulfate and the volatiles were removed in vacuo giving 1,3-diphenyl-2-butylpropan-2-ol as a colorless oil. Yield: 51.6 mg (0.19 mmol, 62%); amount of recovered ketone: 24.7 mg (0.12 mmol, 38%).

***n*-BuLi and ketone/THF (Table 1, entry 20).** To a chilled solution of 1,3-diphenylpropan-2-one (420.5 mg, 2.0 mmol) dissolved in THF (5 mL, -40 °C) *n*-BuLi (2.5 M in hexanes, 800.0 µL, 2.0 mmol, one equiv.) was added dropwise and stirred for 30 min at -40 °C. The mixture was then quenched with a saturated aqueous solution of sodium carbonate, and the aqueous layer was extracted three times with diethyl ether. The combined organic layers were dried over anhydrous sodium sulfate and the volatiles were removed under reduced pressure giving 1,3-diphenyl-2-butylpropan-2-ol as a colorless oil. Yield: 268.1 mg (1.00 mmol, 50%); amount of recovered ketone: 209.2 mg (0.99 mmol, 50%).

X-Ray Crystallography

All crystals are extremely sensitive toward oxygen and moisture. The preparation for XRD analysis must be carried out under seamless cooling. The behavior at low temperatures was also very different, which causes the different measuring temperatures for the complexes in Tables S1, S2, and S3 below. For compound **2** a very small slot between 200 and 220 K had to be used for a successful preparation and measuring of the crystal. For most of the compounds disorder was observed and restraints have to be used for most of them.

Table S1. X-ray crystallographic parameters for complexes 1, 2, and 3^{Lu}

Compound	Li ₃ CeMe ₆ (tmeda) ₃	[Li(thf) ₄][Ce(tBu) ₄]	Li ₃ Lu(<i>n</i> -Bu) ₆ (thf) ₄
Sample code	1	2	3^{Lu}
CCDC	2069609	2069616	2069613
Empirical formula	C ₂₄ H ₆₆ CeLi ₃ N ₆	C ₃₂ H ₆₈ CeLiO ₄	C ₄₀ H ₈₆ Li ₃ LuO ₄
Formula weight	599.77	663.92	826.87
Temperature [K]	150(2)	220(2)	173(2)
Crystal system	Trigonal	Monoclinic	Monoclinic
Space group	R-3c	Pc	P2 ₁
a [Å]	16.4893(12)	11.0681(16)	12.6114(17)
b [Å]	16.4893(12)	9.7385(14)	14.251(2)
c [Å]	26.526(3)	18.666(3)	12.9534(17)
α [°]	90.00	90.00	90.00
β [°]	90.00	89.994(3)	91.914(3)
γ [°]	120	90.00	90.00
Volume [Å ³]	6246.0(11)	2012.0(5)	2326.8(5)
Z	6	2	2
ρ _{calc} [g/cm ³]	0.957	1.096	1.180
μ [mm ⁻¹]	1.109	1.157	2.153
F(000)	1914	706	876
Crystal size [mm ³]	0.298 × 0.242 × 0.195	0.457 × 0.448 × 0.274	0.528 × 0.381 × 0.278
Radiation	MoK _α (λ = 0.71073)	MoK _α (λ = 0.71073)	MoK _α (λ = 0.71073)
Temperature [K]	150	220	173
Θ range for data collection [°]	3.379 to 29.559	1.091 to 25.682	1.573 to 24.749
Index ranges	-22 ≤ h ≤ 15, -22 ≤ k ≤ 22, -35 ≤ l ≤ 35	-13 ≤ h ≤ 13, -11 ≤ k ≤ 11, -22 ≤ l ≤ 22	-14 ≤ h ≤ 14, -16 ≤ k ≤ 16, -15 ≤ l ≤ 15
Reflections collected	11031	40711	56503
Independent reflections	1930 [R _{int} = 0.0308]	7636 [R _{int} = 0.0319]	7964 [R _{int} = 0.0937]
Data/restraints/parameters	1930 / 123 / 97	7636 / 1847 / 536	7964 / 2167 / 629
Goodness-of-fit on F ² [a]	1.030	1.028	1.034
Final R indexes [I > 2σ(I)] ^[b] [c]	R ₁ = 0.0203, wR ₂ = 0.0489	R ₁ = 0.0299, wR ₂ = 0.0649	R ₁ = 0.0601, wR ₂ = 0.1532
Final R indexes [all data]	R ₁ = 0.0363, wR ₂ = 0.0582	R ₁ = 0.0414, wR ₂ = 0.0713	R ₁ = 0.0930, wR ₂ = 0.1869
Largest diff. peak/hole [e Å ⁻³]	0.318 / -0.153	0.564 / -0.164	1.504 / -1.240

^[a]GOF = $[\sum w(F_o^2 - F_c^2)^2 / (n_o - n_p)]^{1/2}$. ^[b]R₁ = $\Sigma(|F_o| - |F_c|) / \Sigma|F_o|$, F₀ > 4σ(F₀). ^[c]wR₂ = $\{\Sigma[w(F_o^2 - F_c^2)^2] / \Sigma[w(F_o^2)^2]\}^{1/2}$.

Table S2. X-ray crystallographic parameters for complexes 4^{Ce}, 4^{Lu}, and 5

Compound	Li ₂ Ce(<i>n</i> -Bu) ₅ (tmeda) ₂	Li ₂ Lu(<i>n</i> -Bu) ₅ (tmeda) ₂	LiLu(<i>n</i> -Bu) ₅ Cl(tmeda) ₂
Sample code	4 ^{Ce}	4 ^{Lu}	5
CCDC	2069615	2069610	2069611
Empirical formula	C ₃₂ H ₇₇ CeLi ₂ N ₄	C ₃₂ H ₇₇ Li ₂ LuN ₄	C ₂₄ H ₅₉ ClLiLuN ₄
Formula weight	671.97	706.82	621.11
Temperature [K]	150(2)	100(2)	100(2)
Crystal system	Monoclinic	Monoclinic	Monoclinic
Space group	P2 ₁ /n	P2 ₁ /c	P2 ₁ /n
a [Å]	12.9223(12)	21.2812(6)	14.962(4)
b [Å]	21.4375(19)	9.9334(3)	14.748(3)
c [Å]	14.6340(13)	20.0178(6)	16.608(3)
α [°]	90.00	90.00	90.00
β [°]	91.063(2)	110.6500(10)	116.449(4)
γ [°]	90.00	90.00	90.00
Volume [Å ³]	4053.2(6)	3959.8(2)	3281.1(12)
Z	4	4	4
ρ _{calc} [g/cm ³]	1.101	1.186	1.257
μ [mm ⁻¹]	1.145	2.515	3.105
F(000)	1444	1496	1288
Crystal size [mm ³]	0.365 × 0.289 × 0.056	0.373 × 0.196 × 0.191	0.345 × 0.123 × 0.113
Radiation	MoK _α (λ = 0.71073)	MoK _α (λ = 0.71073)	MoK _α (λ = 0.71073)
Temperature [K]	150	100	100
θ range for data collection [°]	1.685 to 27.910	2.045 to 31.655	1.945 to 31.565
Index ranges	-17 ≤ h ≤ 17, -28 ≤ k ≤ 28, -19 ≤ l ≤ 19	-29 ≤ h ≤ 31, -14 ≤ k ≤ 14, -27 ≤ l ≤ 29	-21 ≤ h ≤ 21, -21 ≤ k ≤ 21, -23 ≤ l ≤ 24
Reflections collected	62172	88118	73017
Independent reflections	9673 [R _{int} = 0.0549]	13298 [R _{int} = 0.0332]	10452 [R _{int} = 0.0865]
Data/restraints/parameters	9673 / 195 / 458	13298 / 116 / 447	10452 / 0 / 323
Goodness-of-fit on F ² [a]	1.025	1.042	1.018
Final R indexes [I ≥ 2σ(I)] ^[b] [c]	R ₁ = 0.0387, wR ₂ = 0.0760	R ₁ = 0.0252, wR ₂ = 0.0588	R ₁ = 0.0344, wR ₂ = 0.0657
Final R indexes [all data]	R ₁ = 0.0584, wR ₂ = 0.0845	R ₁ = 0.0322, wR ₂ = 0.0617	R ₁ = 0.0593, wR ₂ = 0.0727
Largest diff. peak/hole [e Å ⁻³]	1.496 / -1.014	2.127 / -0.830	2.165 / -0.977

^[a]GOF = [Σw(F_o² - F_c²)² / (n_o - n_p)]^{1/2}. ^[b]R₁ = Σ(|F_o| - |F_c|) / Σ|F_o|, F_o > 4σ(F_o). ^[c]wR₂ = {Σ[w(F_o² - F_c²)² / Σ[w(F_o²)²]}^{1/2}.

Table S3. X-ray crystallographic parameters for complexes 6, 7, and 8

Compound	Li ₃ Ce ₂ (ONep) ₉ (HONep) ₂ (thf)	Li ₄ [OC(=CHPh)(CH ₂ Ph)] ₄ (thf) ₄	Li ₈ [OCMe ₂ (<i>n</i> -Bu)] ₆ Cl ₂ (thf) ₆
Sample code	6	7	8
CCDC	2069612	2069617	2069614
Empirical formula	C ₅₉ H ₁₃₁ Ce ₂ Li ₃ O ₁₂	C ₈₄ H ₁₀₀ Li ₄ O ₁₀	C ₆₆ H ₁₃₈ Cl ₂ Li ₈ O ₁₂
Formula weight	1333.69	1297.39	1250.18
Temperature [K]	100(2)	100(2)	173(2)
Crystal system	Monoclinic	Tetragonal	Triclinic
Space group	P2 ₁ /c	I4 ₁ /a	P-1
a [Å]	12.0469(12)	17.7858(11)	11.6640(4)
b [Å]	22.287(2)	17.7858(11)	14.1661(5)
c [Å]	27.095(3)	50.026(5)	14.2938(5)
α [°]	90.00	90.00	62.4460(10)
β [°]	93.595(2)	90.00	73.8420(10)
γ [°]	90.00	90.00	74.2460(10)
Volume [Å ³]	7260.4(12)	15825(2)	1982.74(12)
Z	4	8	1
ρ _{calc} [g/cm ³]	1.218	1.089	1.047
μ [mm ⁻¹]	1.287	0.069	0.132
F(000)	2816	5568	688
Crystal size [mm ³]	0.224 x 0.174 x 0.050	0.251 x 0.227 x 0.218	0.429 x 0.135 x 0.134
Radiation	MoK _α (λ = 0.71073)	MoK _α (λ = 0.71073)	MoK _α (λ = 0.71073)
Temperature [K]	100	100	173
θ range for data collection [°]	1.506 to 29.159	1.215 to 25.309	1.633 to 25.082
Index ranges	-15 ≤ h ≤ 16, -30 ≤ k ≤ 30, -36 ≤ l ≤ 37	-14 ≤ h ≤ 21, -20 ≤ k ≤ 20, -60 ≤ l ≤ 60	-13 ≤ h ≤ 13, -16 ≤ k ≤ 16, -17 ≤ l ≤ 17
Reflections collected	82404	50086	44374
Independent reflections	19554 [R(int) = 0.0655]	7224 [R _{int} = 0.0717]	7033 [R _{int} = 0.0472]
Data/restraints/parameters	19554 / 1075 / 843	7224 / 150 / 466	7033 / 36 / 406
Goodness-of-fit on F ² [a]	1.034	1.021	1.038
Final R indexes [I ≥ 2σ(I)] ^[b] [c]	R ₁ = 0.0415, wR ₂ = 0.0870	R ₁ = 0.0565, wR ₂ = 0.1450	R ₁ = 0.0532, wR ₂ = 0.1384
Final R indexes [all data]	R ₁ = 0.0652, wR ₂ = 0.0998	R ₁ = 0.0927, wR ₂ = 0.1682	R ₁ = 0.0698, wR ₂ = 0.1532
Largest diff. peak/hole [e Å ⁻³]	1.701 / -0.657	0.334 / -0.372	0.983 / -0.367

^[a]GOF = $[\sum w(F_o^2 - F_c^2)^2 / (n_o - n_p)]^{1/2}$. ^[b]R₁ = $\Sigma(|F_o| - |F_c|) / \Sigma|F_o|$, F_o > 4σ(F_o). ^[c]wR₂ = $\{\Sigma[w(F_o^2 - F_c^2)^2] / \Sigma[w(F_o^2)^2]\}^{1/2}$.

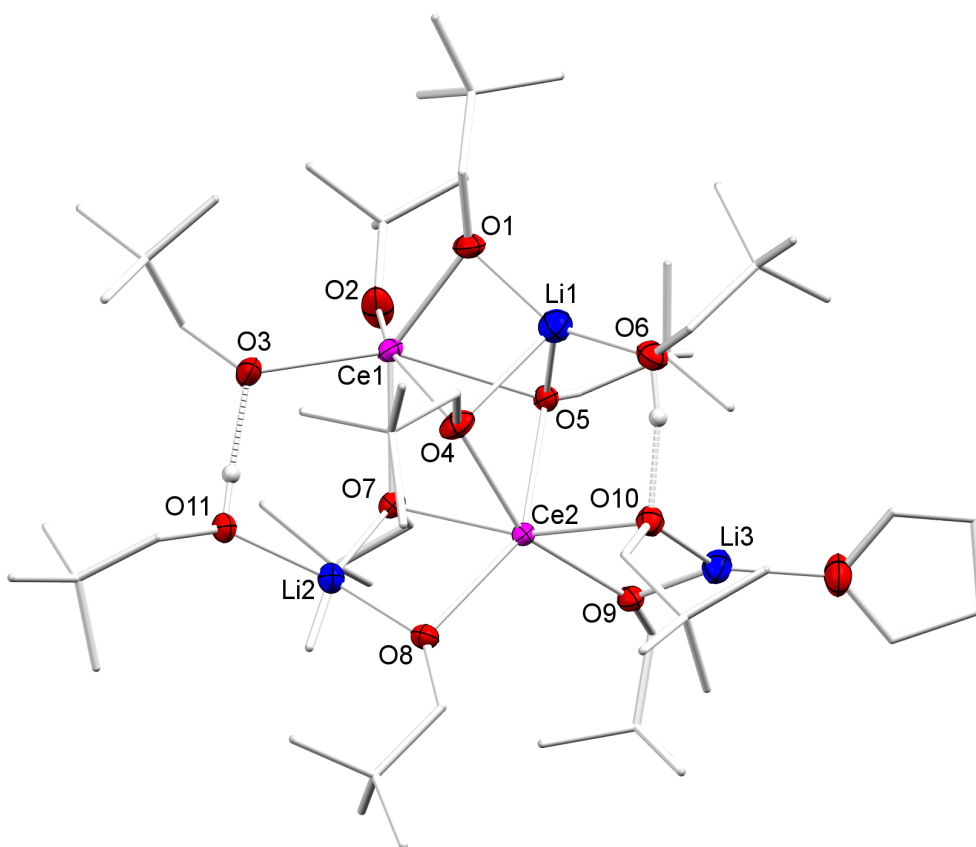


Figure S1. Crystal structure of $\text{Li}_3\text{Ce}_2(\text{OCH}_2t\text{Bu})_9(\text{HOCH}_2t\text{Bu})_2(\text{thf})$ (**6**) with atomic displacement ellipsoids set at 50% probability. Hydrogen atoms except those engaging in hydrogen bridges are omitted for clarity. The neopentoxy and thf carbon atoms are shown in a ball-and-stick representation. Selected interatomic distances [\AA] for **6**: Ce1–O1 2.327(2), Ce1–O2 2.196(2), Ce1–O3 2.337(2), Ce1–O4 2.585(2), Ce1–O5 2.608(2), Ce1–O7 2.496(2), Ce2–O4 2.393(2), Ce2–O5 2.421(2), Ce2–O7 2.472(2), Ce2–O8 2.354(2), Ce2–O9 2.320(2), Ce2–O10 2.447(2).

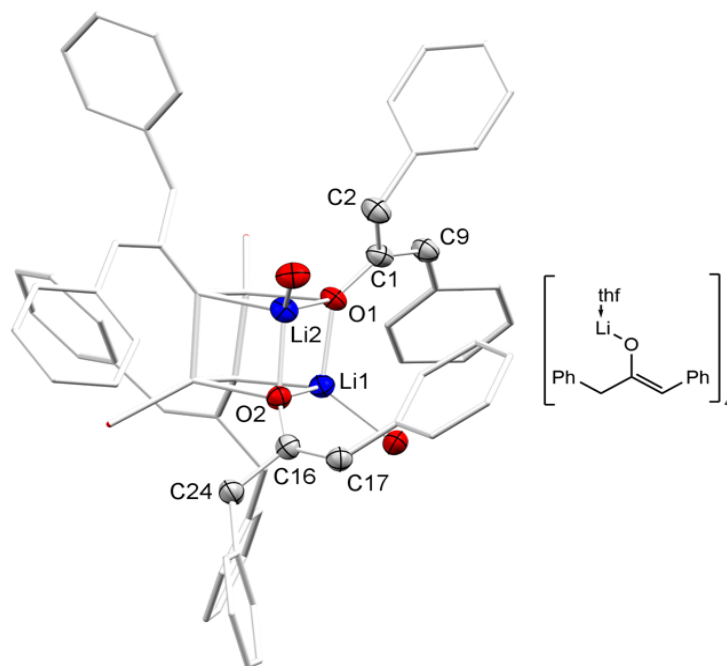


Figure S2. Crystal structure of $\text{Li}_4[\text{OC}(=\text{CHPh})\text{CH}_2\text{Ph}]_4(\text{thf})_4$ (**7**) with atomic displacement ellipsoids set at 50% probability. Hydrogen atoms, part of the THF molecules, and lattice THF are omitted for clarity. The second part of the complex is created by symmetry. Selected interatomic distances [Å] and angles [°] for **7**: Li1–O1 1.934(4), Li1–O2 1.991(4), Li2–O1 2.028(4), Li2–O2 1.931(4), Li1–O2' 2.036(4), O1–Li2' 1.985(4), C1–C2 1.528(3), C1–C9 1.349(3), C16–C17 1.352(3), C16–C24 1.521(3), O1–Li1–O2 94.25(15), Li1–O1–Li2 84.56(15).

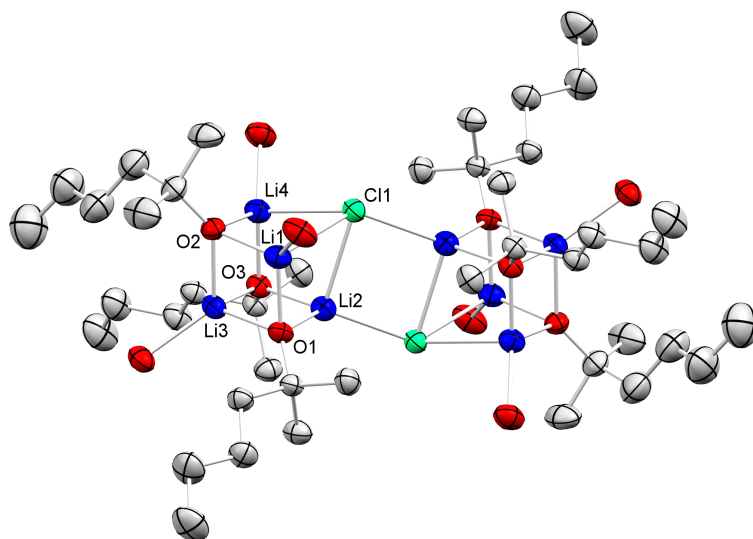


Figure S3. Crystal structure of $\text{Li}_8[\text{OCMe}_2(n\text{-Bu})]_6\text{Cl}_2(\text{thf})_6$ (**8**) with atomic displacement ellipsoids set at 50% probability. Hydrogen atoms and THF carbon atoms are omitted for clarity. Selected interatomic distances [Å] and angles [°] for **8**: Li1–O1 1.892(4), Li1–O2 1.932(4), Li1–Cl1 2.533(4), Li2–O1 1.926(4), Li2–O3 1.932(4), Li2–Cl1 2.517(4), Li2–Cl1' 2.517(4), Li3–O1 1.974(4), Li3–O2 1.962(4), Li3–O3 1.957(4), Li4–O2 1.941(4), Li4–O3 1.893(4), Li4–Cl1 2.516(4), Li1–O1–Li2 92.59(16), Li1–O1–Li3 83.67(16), Li2–O1–Li3 83.24(16), Cl1–Li4–O2 96.05(1), O2–Li4–O3 97.68(1), Cl1–Li4–O3 99.82(1), O1–Li3–O2 94.84(1), O1–Li3–O3 95.37(1), O2–Li3–O3 94.89(1), Li1–Cl1–Li2 66.27(1), Li1–Cl1–Li4 66.73(1), Li2–Cl1–Li4 66.44(1), Cl1–Li2–Cl1' 98.06(1), Li2–Cl1–Li2' 81.94(1).

NMR Spectra

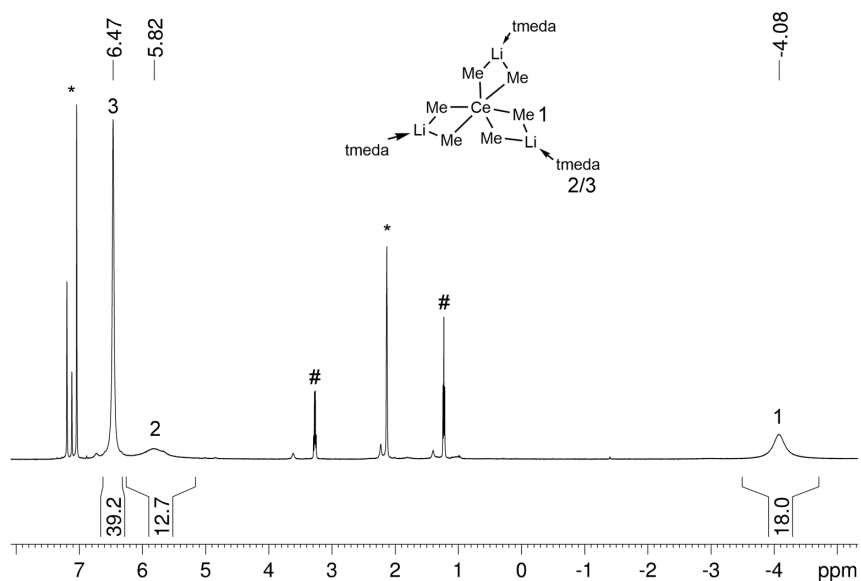


Figure S4. ^1H NMR spectrum of $\text{Li}_3\text{CeMe}_6(\text{tmeda})_3$ (**1**) (500.13 MHz, toluene- d_8 , 233 K) solvent residual signals are marked with *. The signals of non-coordinated TMEDA are marked with #.

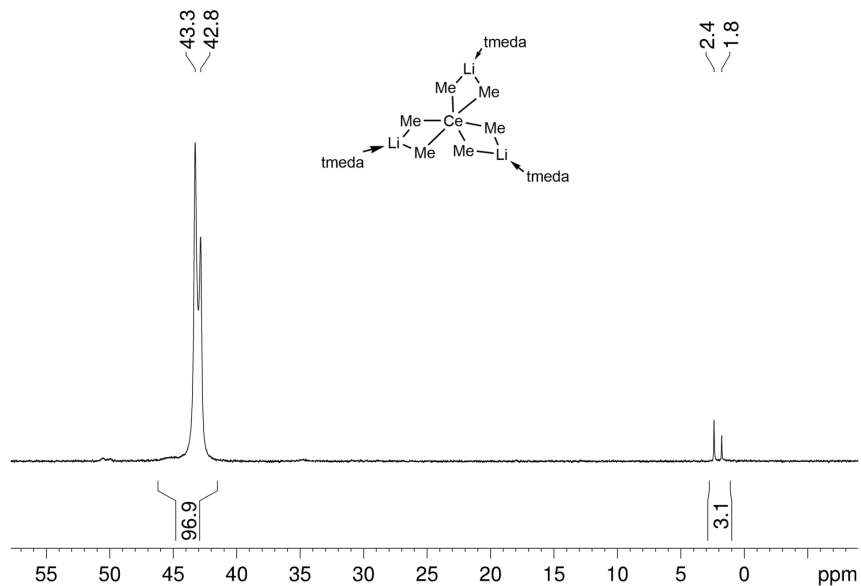


Figure S5. ^7Li NMR spectrum of $\text{Li}_3\text{CeMe}_6(\text{tmeda})_3$ (**1**) (194.37 MHz, toluene- d_8 , 233 K).

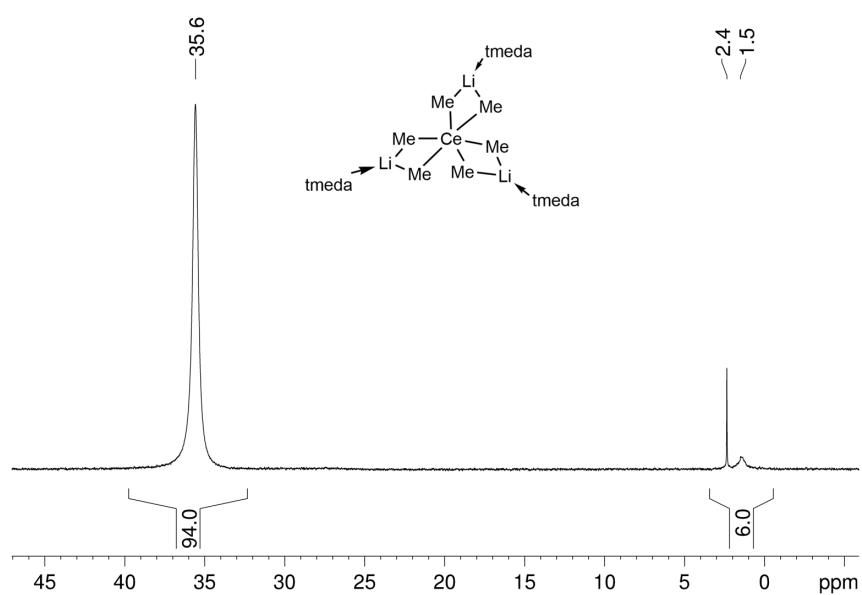


Figure S6. ^7Li NMR spectrum of $\text{Li}_3\text{CeMe}_6(\text{tmeda})_3$ (**1**) (194.37 MHz, $\text{THF-}d_8$, 233 K).

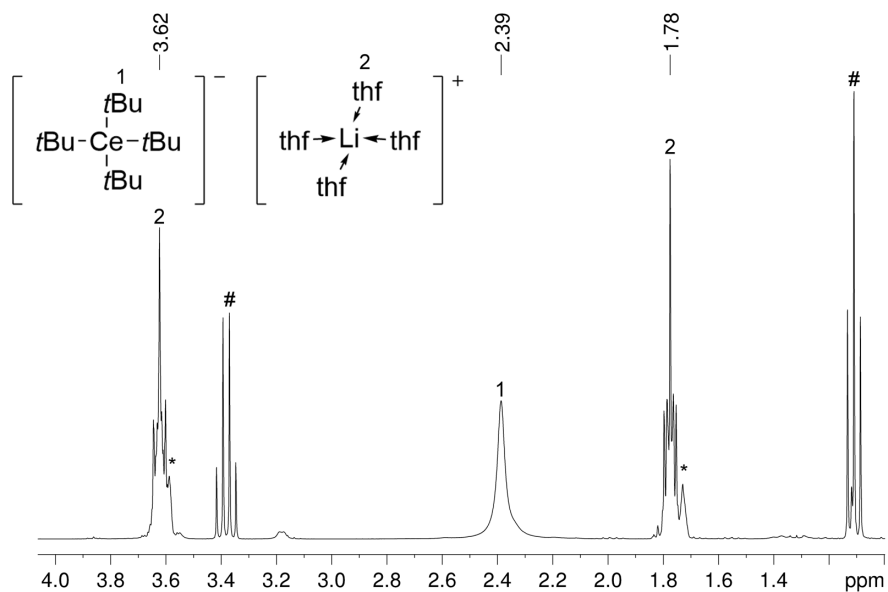


Figure S7. ^1H NMR spectrum of $[\text{Li}(\text{thf})_4][\text{Ce}(t\text{-Bu})_4]$ (**2**) (300.13 MHz, $\text{THF-}d_8$, 299 K). Solvent residual signals are marked with *. Residual Et_2O is marked with #.

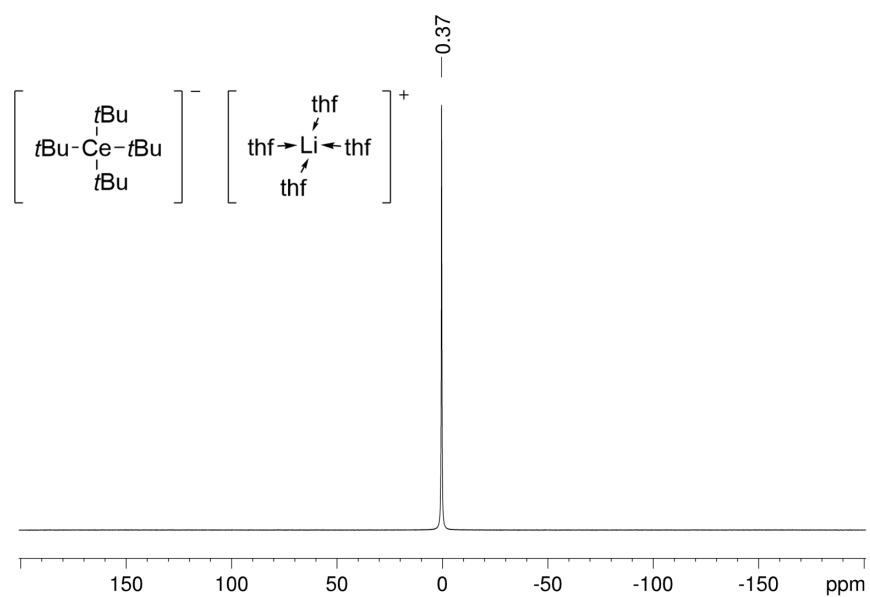


Figure S8. ^7Li NMR spectrum of $[\text{Li}(\text{thf})_4][\text{Ce}(t\text{-Bu})_4]$ (**2**) (116.64 MHz, $\text{THF-}d_8$, 299 K).

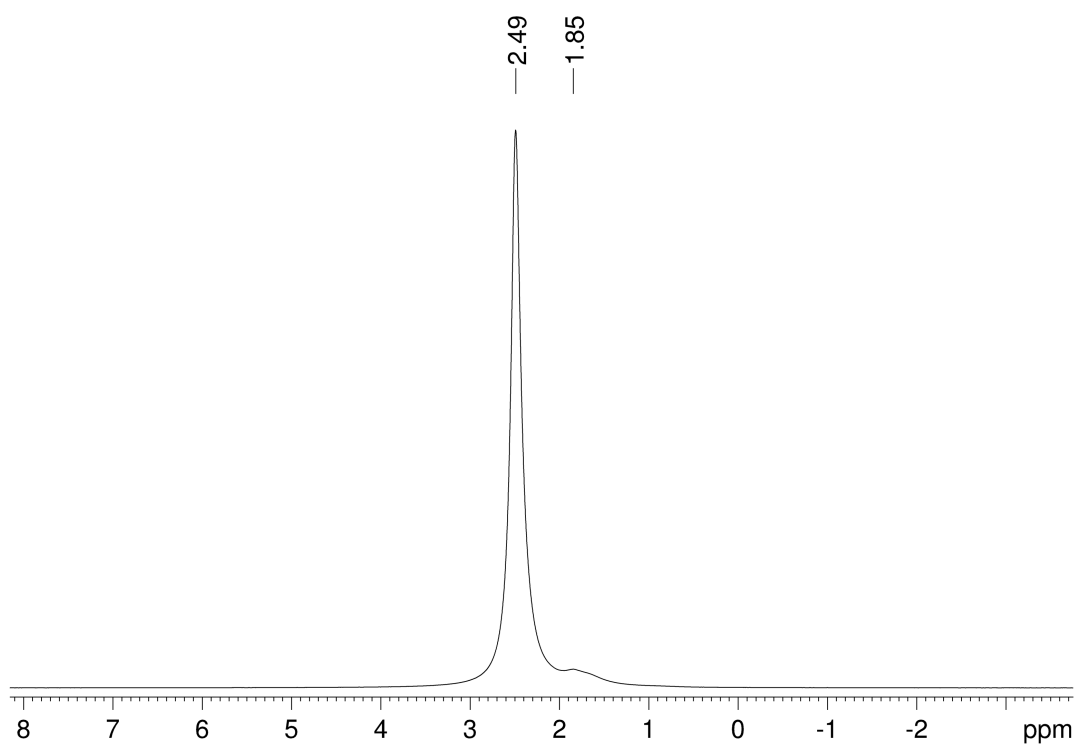


Figure S9. ^7Li NMR spectrum of $n\text{-BuLi}$ (194.37 MHz, $\text{toluene-}d_8$, 233 K).

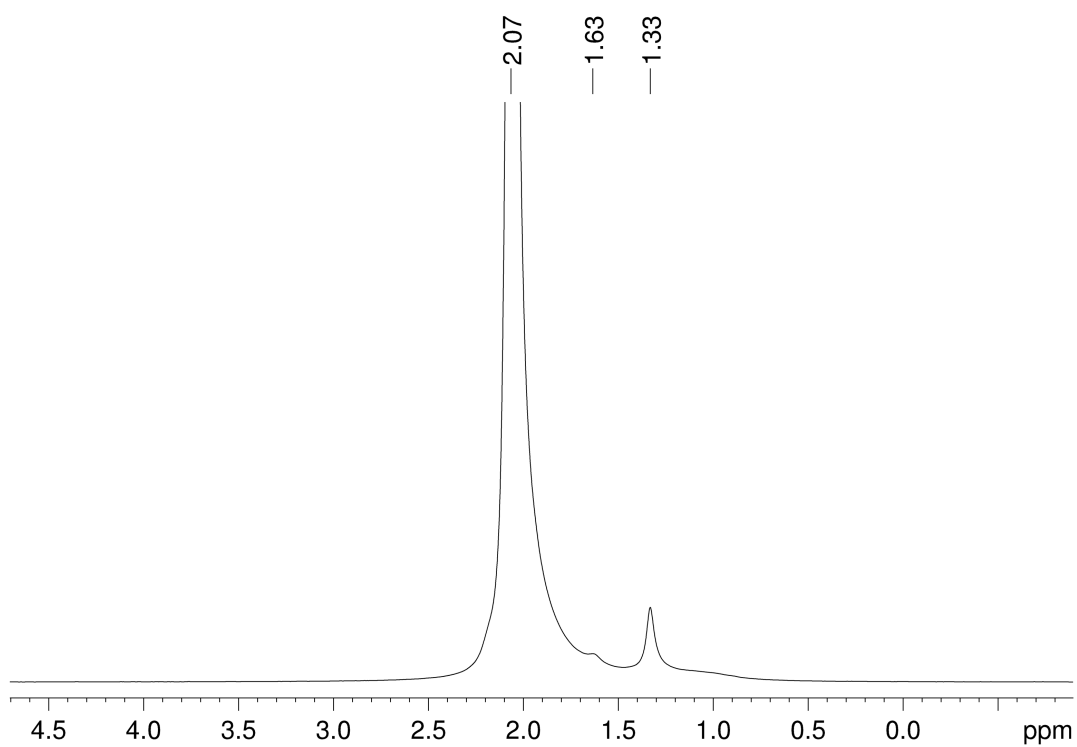


Figure S10. ${}^7\text{Li}$ NMR spectrum of *n*-BuLi + 1 equiv. of THF (194.37 MHz, toluene- d_8 , 233 K).

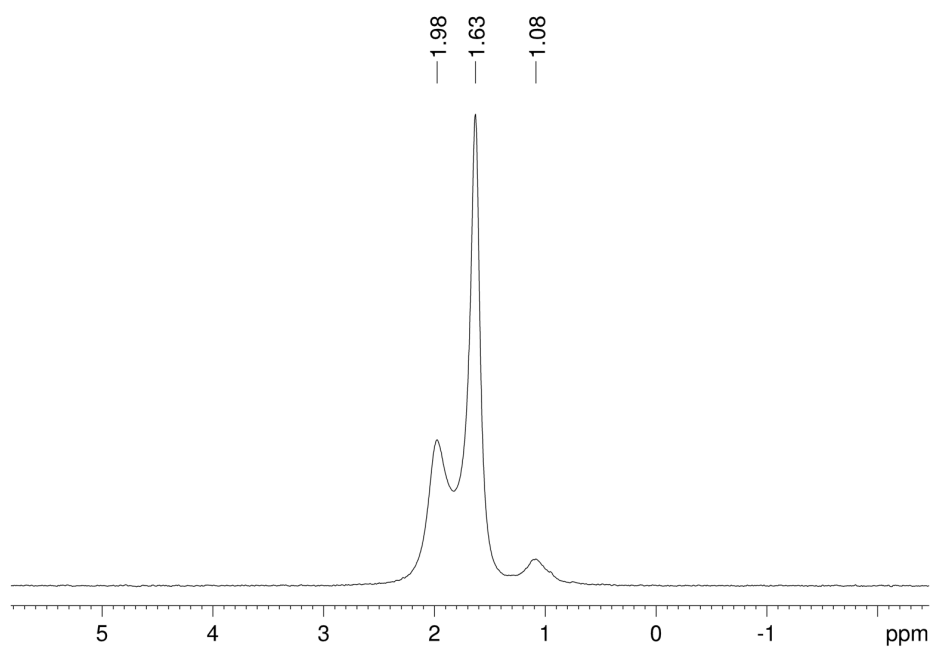


Figure S11. ${}^7\text{Li}$ NMR spectrum of *n*-BuLi (194.37 MHz, THF- d_8 , 233 K).

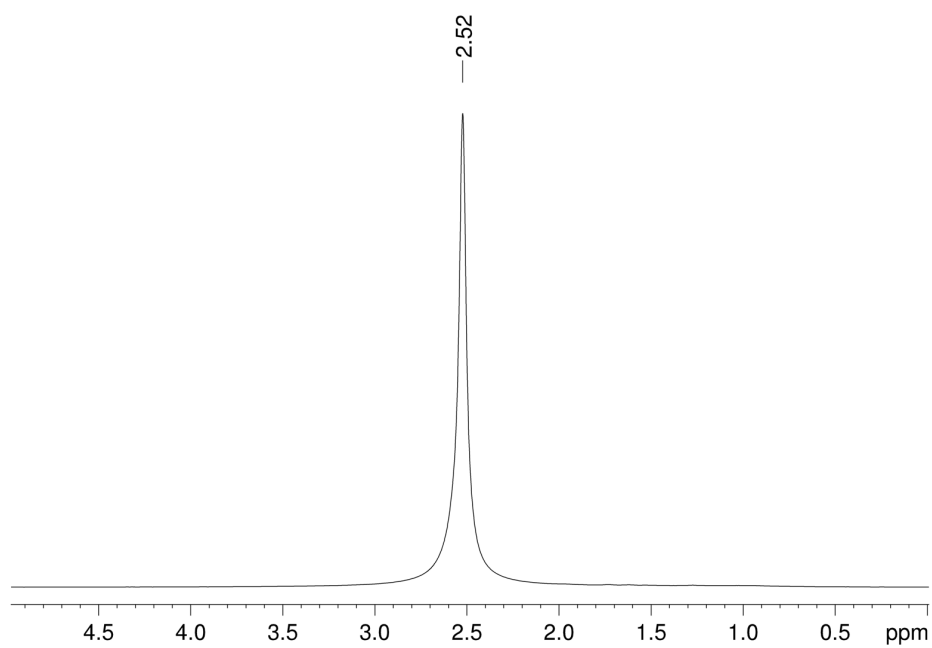


Figure S12. ^7Li NMR spectrum of *n*-BuLi + 1 equiv. of TMEDA (194.37 MHz, toluene- d_8 , 233 K).

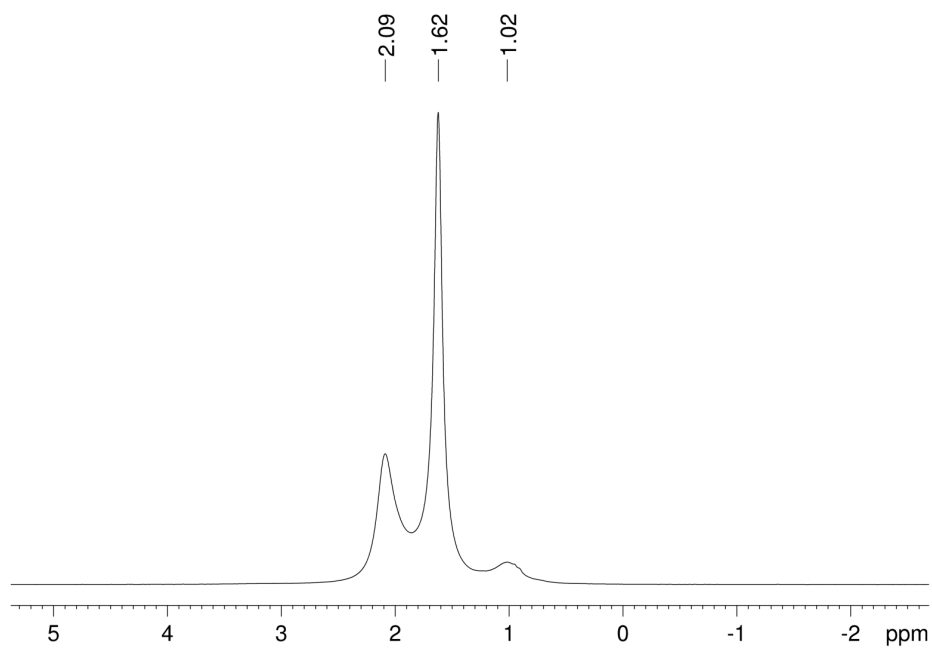


Figure S13. ^7Li NMR spectrum of *n*-BuLi + 1 equiv. of TMEDA (194.37 MHz, THF- d_8 , 233 K).

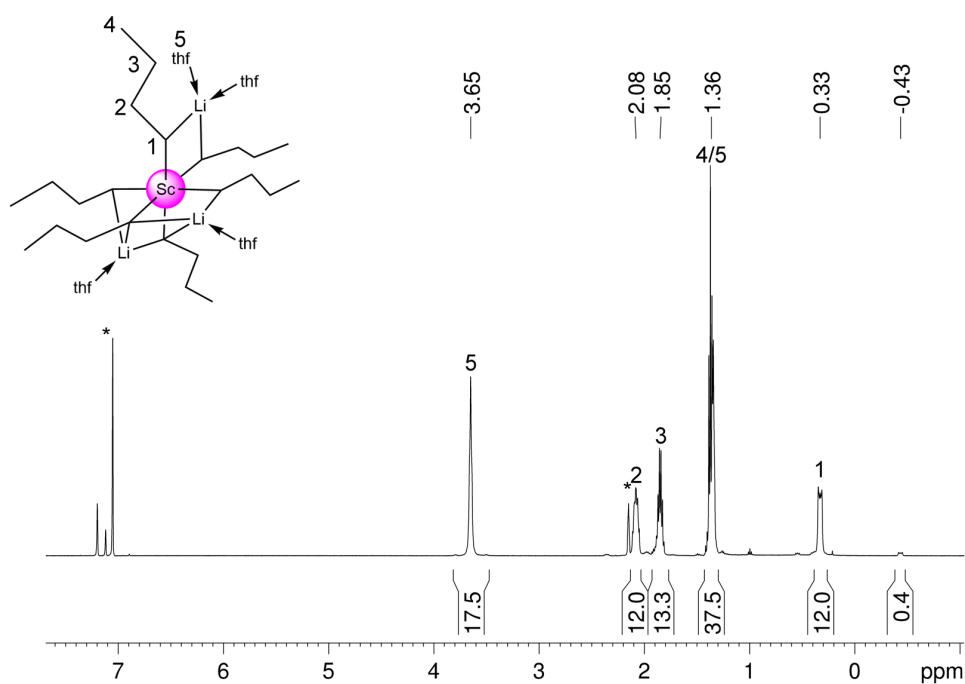


Figure S14. ^1H NMR spectrum of $\text{Li}_3\text{Sc}(\text{n-Bu})_6(\text{thf})_4$ (3^{Sc}) (500.13 MHz, toluene-d_8 , 233 K). Solvent residual signals are marked with *.

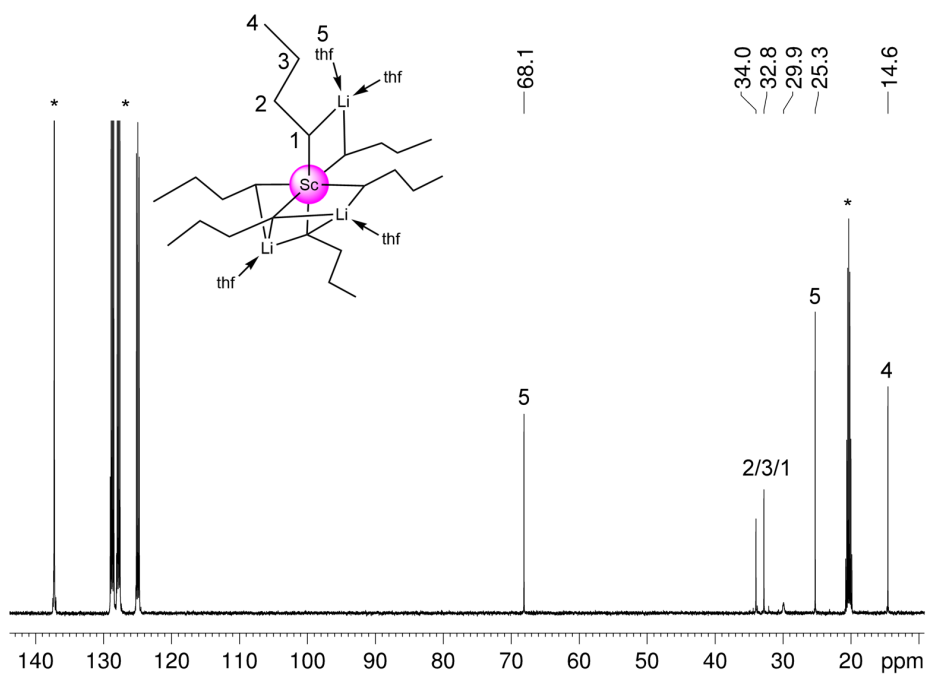


Figure S15. $^{13}\text{C}\{^1\text{H}\}$ NMR spectrum of $\text{Li}_3\text{Sc}(\text{n-Bu})_6(\text{thf})_4$ (3^{Sc}) (125.76 MHz, toluene-d_8 , 233 K). Solvent residual signals are marked with *.

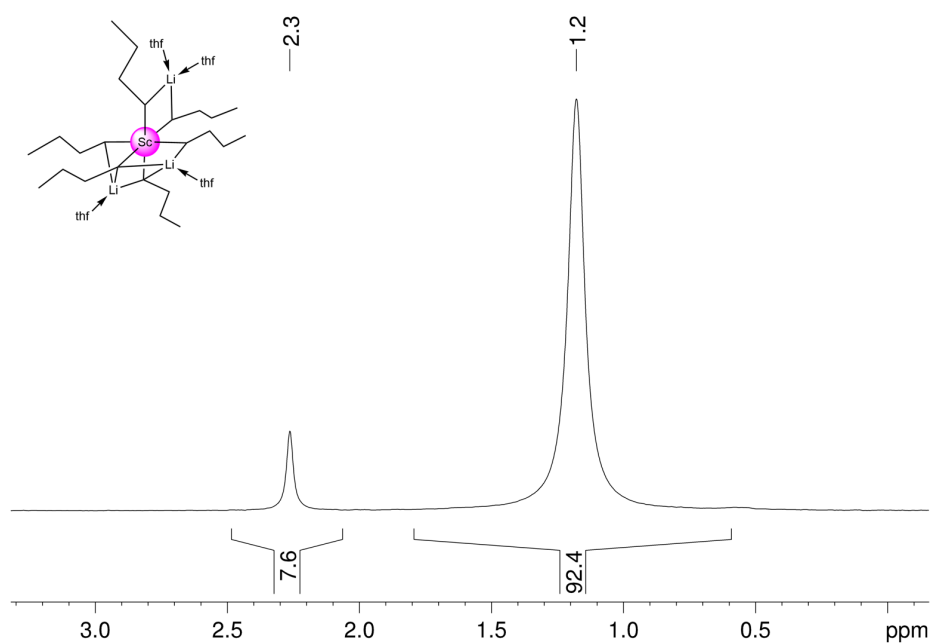


Figure S16. ^7Li NMR spectrum of $\text{Li}_3\text{Sc}(\textit{n}\text{-Bu})_6(\text{thf})_4$ ($\mathbf{3}^{\text{Sc}}$) (194.37 MHz, toluene- d_8 , 233 K), showing free $\textit{n}\text{-BuLi}(\text{thf})$ at 2.3 ppm and the mixed scandium–lithium complex at 1.2 ppm.

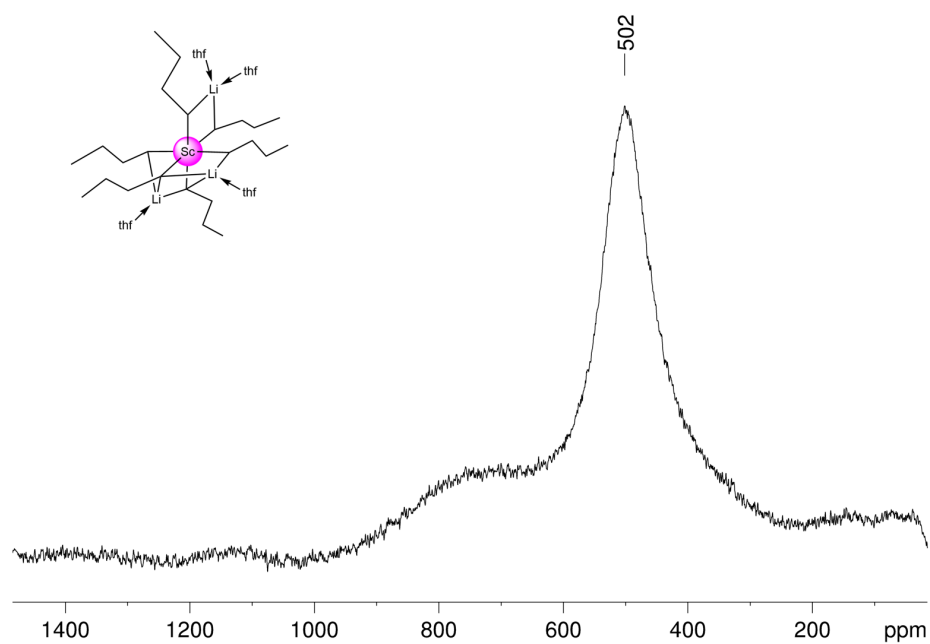


Figure S17. ^{45}Sc NMR spectrum of $\text{Li}_3\text{Sc}(\textit{n}\text{-Bu})_6(\text{thf})_4$ ($\mathbf{3}^{\text{Sc}}$) (121.49 MHz, toluene- d_8 , 233 K), showing a main signal at 502 ppm with a line width at half height of 11787 Hz.

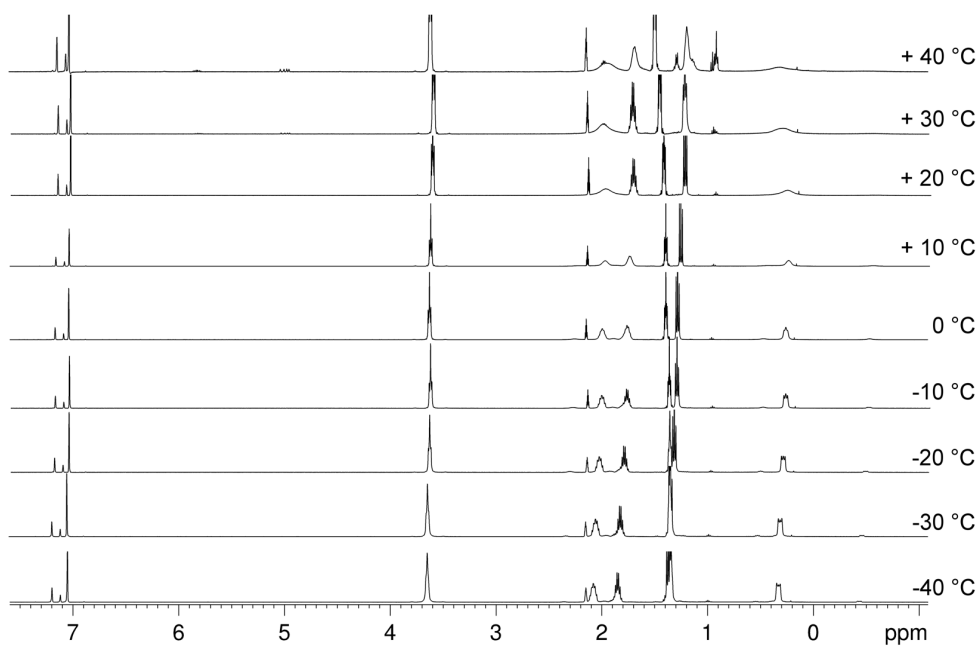


Figure S18. VT ^1H NMR spectra of $\text{Li}_3\text{Sc}(n\text{-Bu})_6(\text{thf})_4$ (3^{Sc}) (500.13 MHz, toluene- d_8 , 233 K-313 K) showing a slight amount of the decomposition product 1-butene at 5.82 and 4.99 ppm at +30 °C and +40 °C.

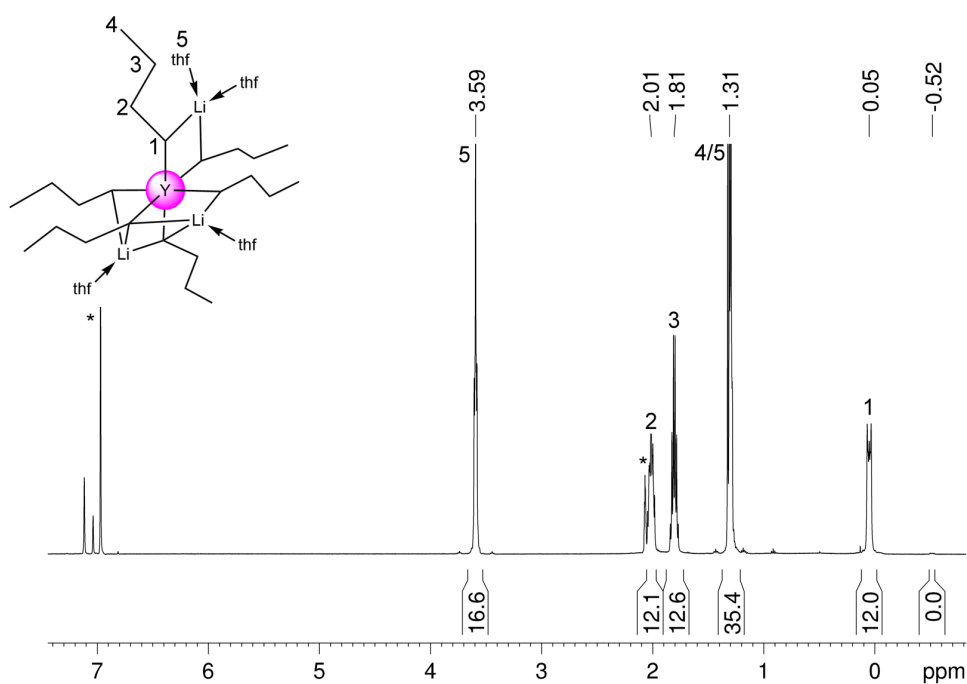


Figure S19. ^1H NMR spectrum of $\text{Li}_3\text{Y}(n\text{-Bu})_6(\text{thf})_4$ (3^{Y}) (500.13 MHz, toluene- d_8 , 233 K). Solvent residual signals are marked with *.

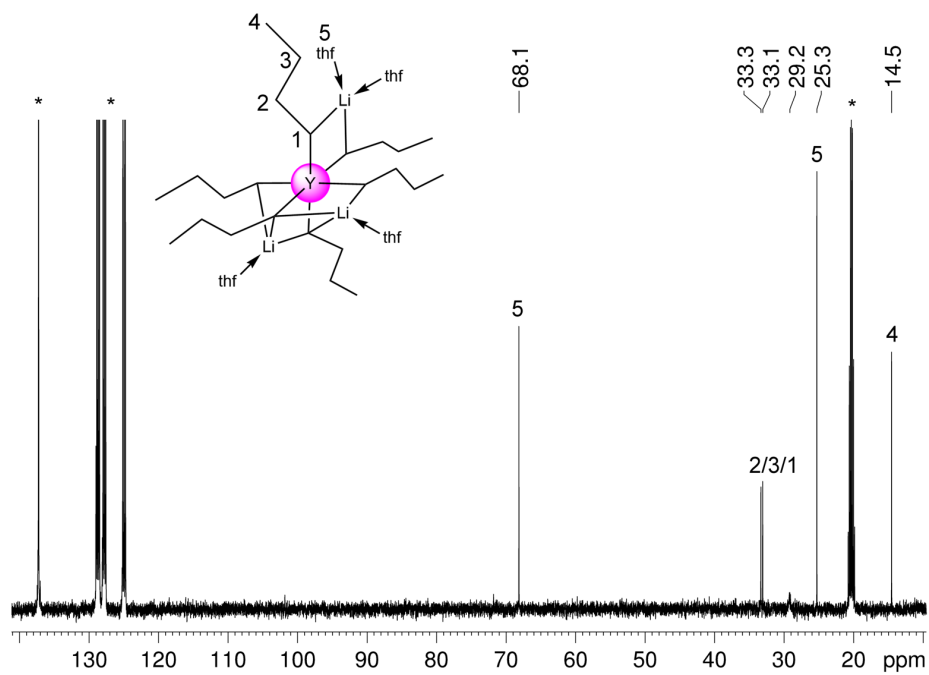


Figure S20. $^{13}\text{C}\{^1\text{H}\}$ NMR spectrum of $\text{Li}_3\text{Y}(\text{n-Bu})_6(\text{thf})_4$ ($\mathbf{3}^{\text{Y}}$) (125.76 MHz, toluene- d_8 , 233 K). Solvent residual signals are marked with *.

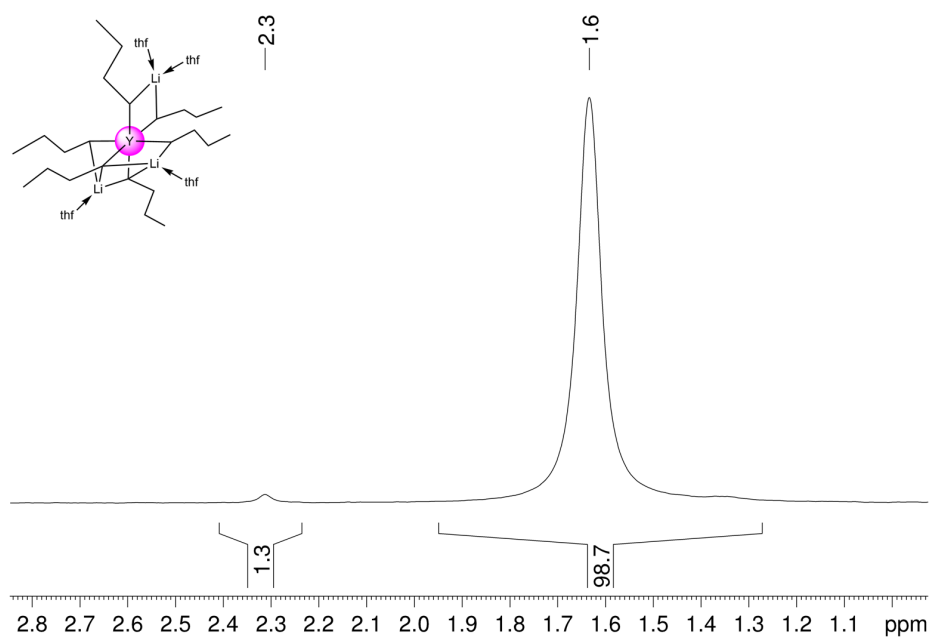


Figure S21. ^7Li NMR spectrum of $\text{Li}_3\text{Y}(\text{n-Bu})_6(\text{thf})_4$ ($\mathbf{3}^{\text{Y}}$) (194.37 MHz, toluene- d_8 , 233 K), showing free $n\text{-BuLi}(\text{thf})$ at 2.3 ppm and the mixed yttrium–lithium complex at 1.6 ppm.

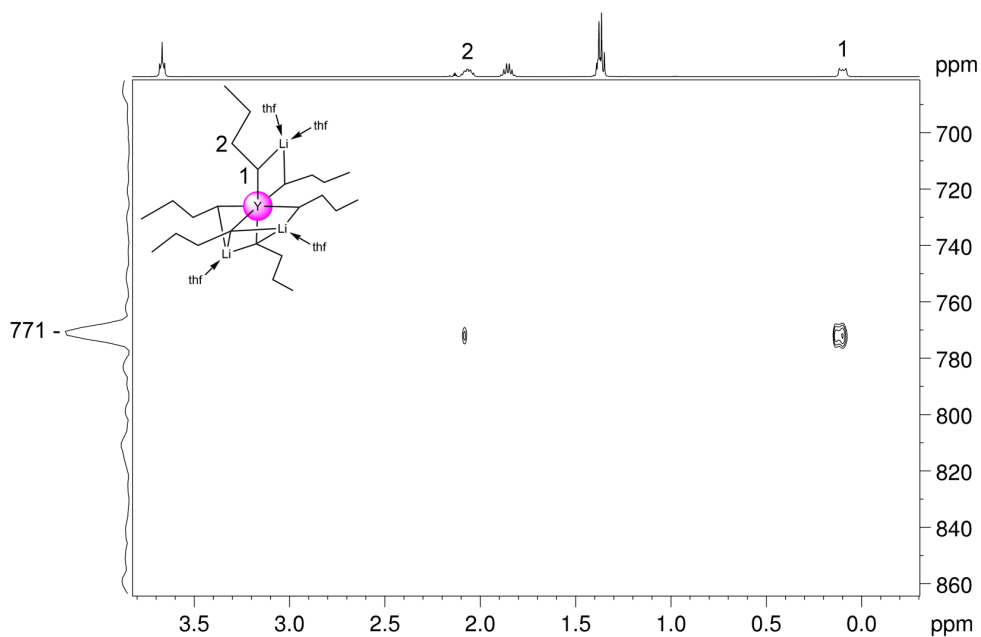


Figure S22. ^1H - ^{89}Y HSQC NMR spectrum of $\text{Li}_3\text{Y}(\text{n-Bu})_6(\text{thf})_4$ (3^{Y}) (500.13/24.51 MHz, toluene- d_8 , 233 K), showing a single yttrium signal at 771 ppm with a line width at half height of 143 Hz.

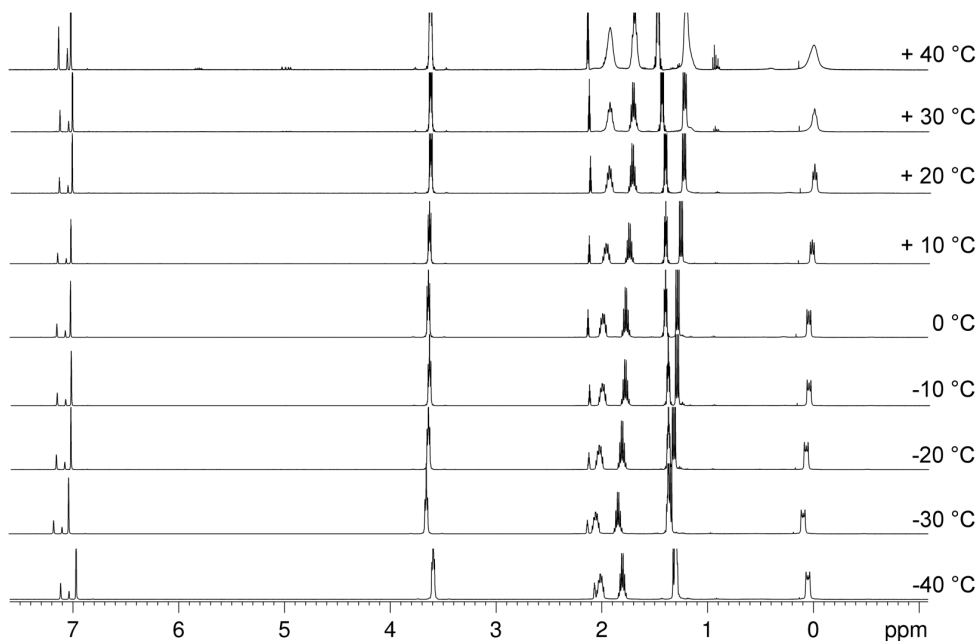


Figure S23. VT ^1H NMR spectra of $\text{Li}_3\text{Y}(\text{n-Bu})_6(\text{thf})_4$ (3^{Y}) (500.13 MHz, toluene- d_8 , 233 K-313 K), showing a slight amount of the decomposition product 1-butene at 5.82 and 4.99 ppm at +30 °C and +40 °C.

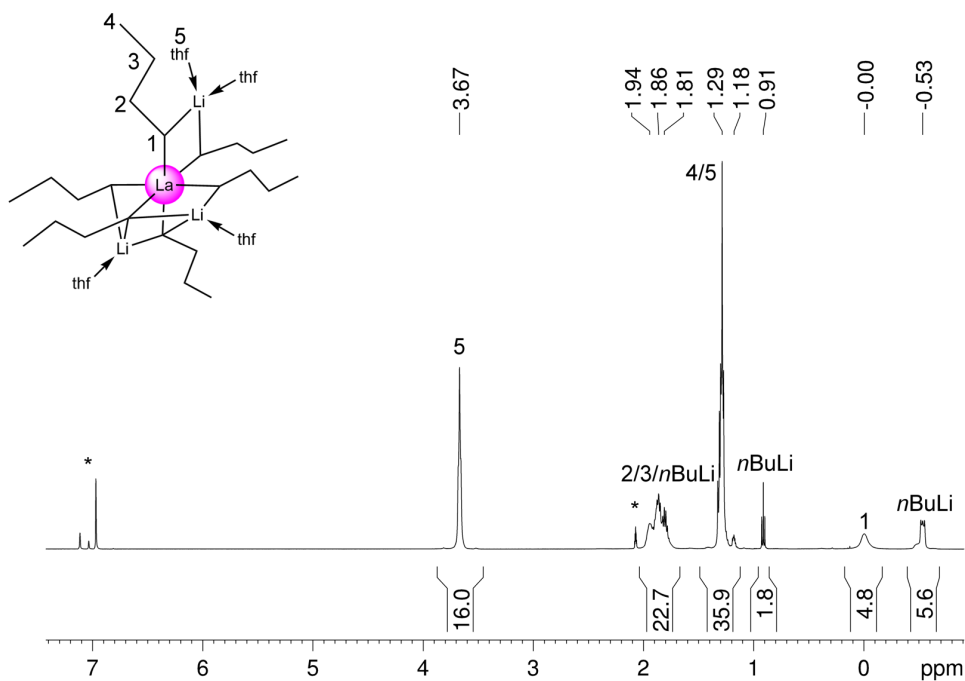


Figure S24. ^1H NMR spectrum of $\text{Li}_3\text{La}(\text{n-Bu})_6(\text{thf})_4$ (3^{La}) (500.13 MHz, $\text{toluene-}d_8$, 233 K). Solvent residual signals are marked with *.

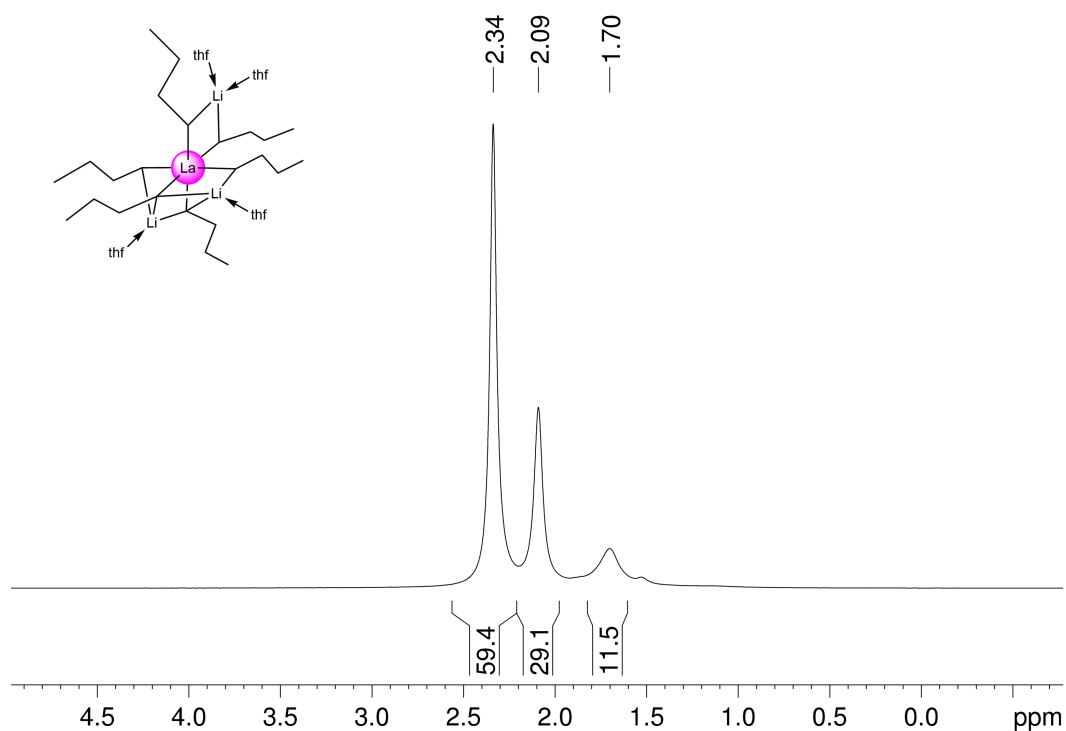


Figure S25. ^7Li NMR spectrum of $\text{Li}_3\text{La}(\text{n-Bu})_6(\text{thf})_4$ (3^{La}) (194.37 MHz, $\text{toluene-}d_8$, 233 K), showing mainly $n\text{-BuLi}(\text{thf})$.

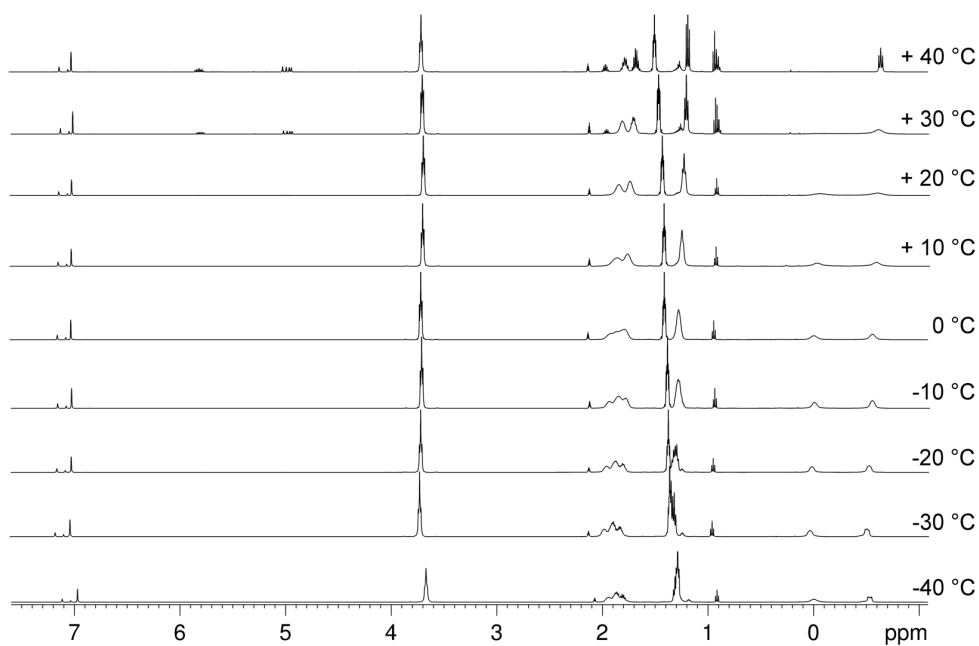


Figure S26. VT ^1H NMR spectra of $\text{Li}_3\text{La}(\textit{n}\text{-Bu})_6(\text{thf})_4$ ($\mathbf{3}^{\text{La}}$) (500.13 MHz, toluene- d_8 , 233 K-313 K), showing a slight amount of the decomposition product of 1-butene at 5.82 and 4.99 ppm at +30 °C and +40 °C.

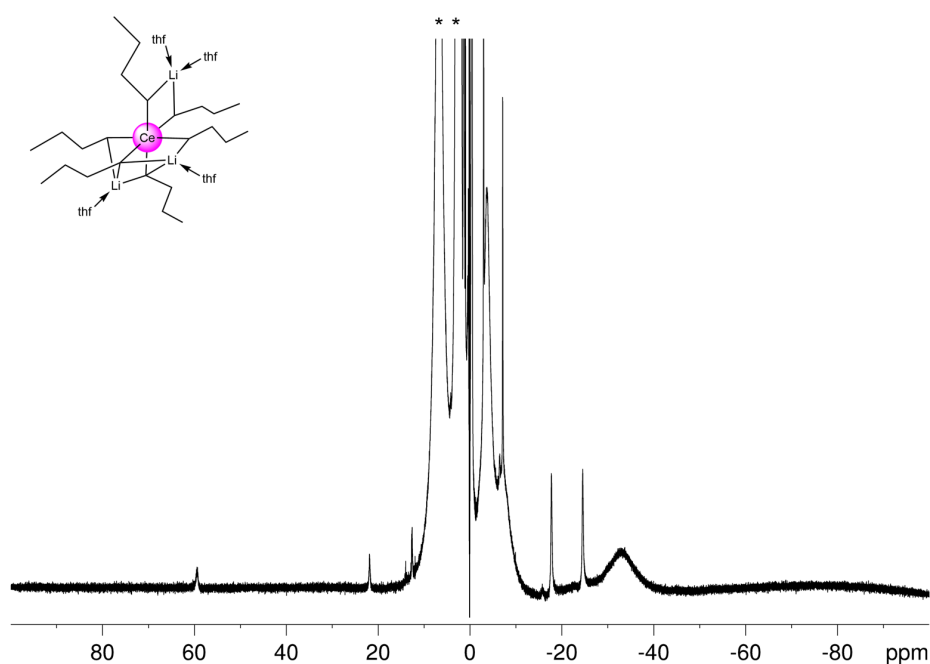


Figure S27. Wide ^1H NMR spectrum of $\text{Li}_3\text{Ce}(\textit{n}\text{-Bu})_6(\text{thf})_4$ ($\mathbf{3}^{\text{Ce}}$) (500.13 MHz, toluene- d_8 , 233 K). Solvent residual signals are marked with *. Except for the sharp $\textit{n}\text{-BuLi}(\text{thf})$ signals, resonance assignment is not conclusive.

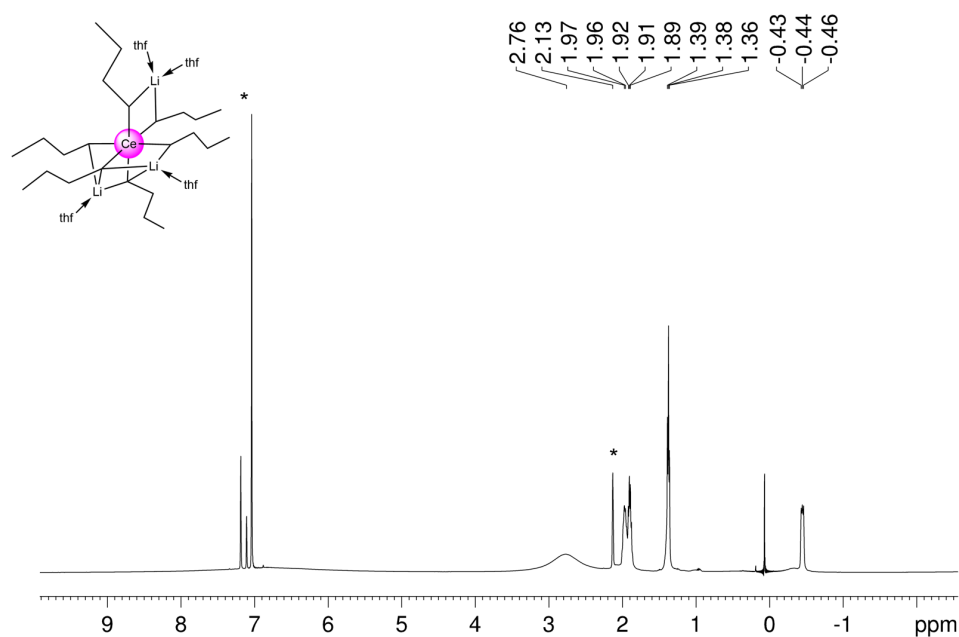


Figure S28. Narrow ^1H NMR spectrum of $\text{Li}_3\text{Ce}(\text{n-Bu})_6(\text{thf})_4$ (3^{Ce}) (500.13 MHz, $\text{toluene-}d_8$, 233 K). Solvent residual signals are marked with *. The sharp signals can all be assigned to free $n\text{-BuLi}$ or $n\text{-BuLi}(\text{thf})$.

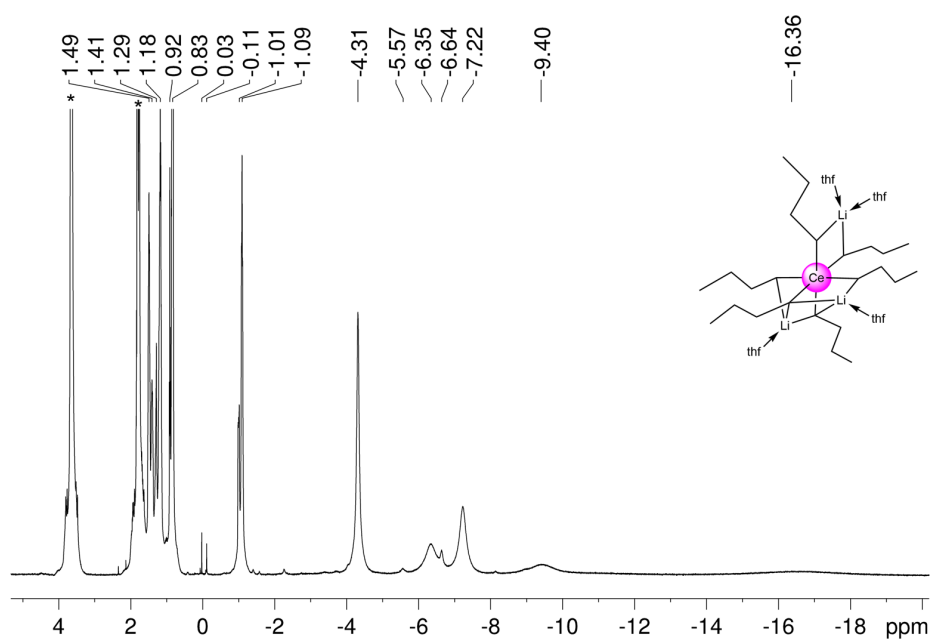


Figure S29. ^1H NMR spectrum of $\text{Li}_3\text{Ce}(\text{n-Bu})_6(\text{thf})_4$ (3^{Ce}) (500.13 MHz, $\text{THF-}d_8$, 233 K). Solvent residual signals are marked with *.

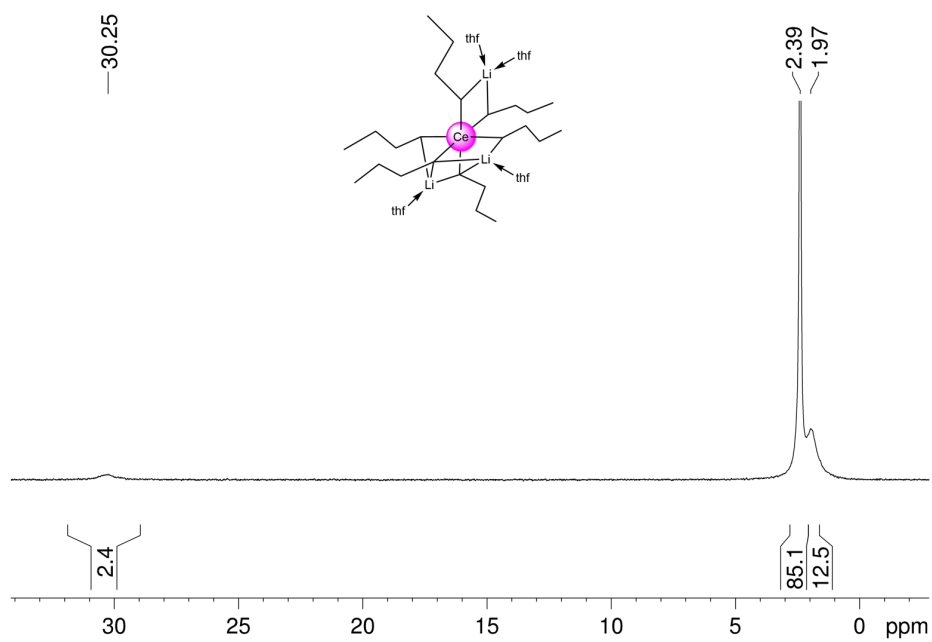


Figure S30. ^7Li NMR spectrum of $\text{Li}_3\text{Ce}(\textit{n}\text{-Bu})_6(\text{thf})_4$ (3^{Ce}) (194.37 MHz, $\text{toluene-}d_8$, 233 K), showing the *n*-BuLi(thf) at 2.4 and 2.0 ppm and a mixed cerium–lithium species at 30.3 ppm.

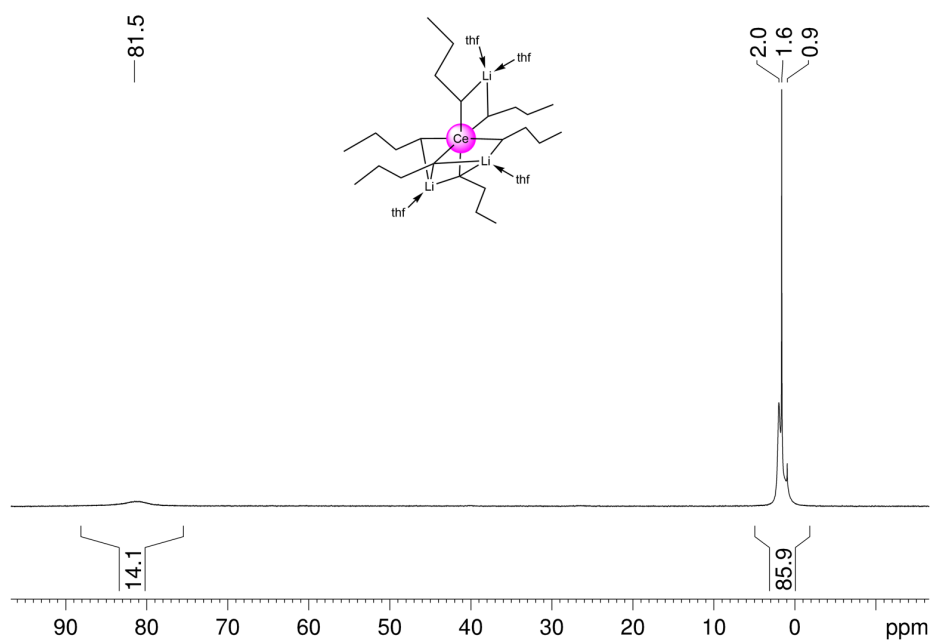


Figure S31. ^7Li NMR spectrum of $\text{Li}_3\text{Ce}(\textit{n}\text{-Bu})_6(\text{thf})_4$ (3^{Ce}) (194.37 MHz, $\text{THF-}d_8$, 233 K), showing the *n*-BuLi(thf) at 2.0, 1.6 and 0.9 ppm and a mixed cerium–lithium species at 81.5 ppm.

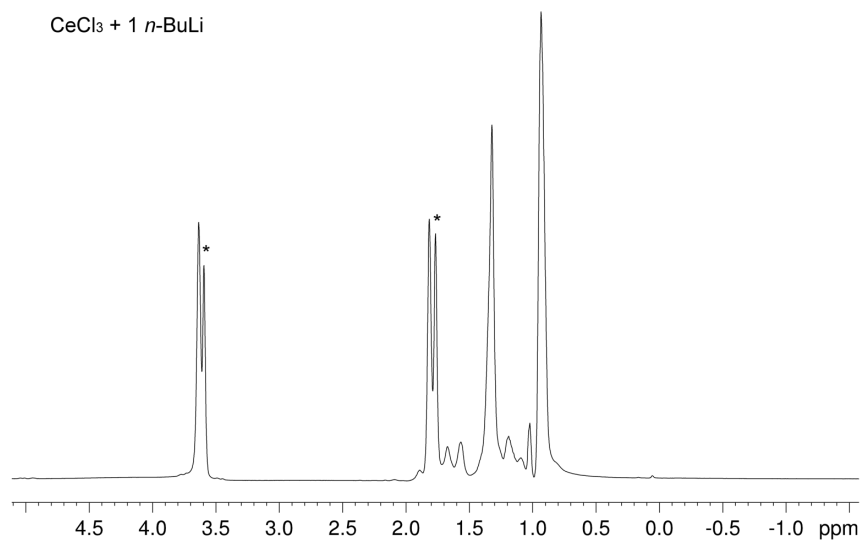


Figure S32. ¹H NMR spectrum of CeCl₃(thf) + 1 equiv. of *n*-BuLi (500.13 MHz, THF-*d*₈, 233 K). Solvent residual signals are marked with *.

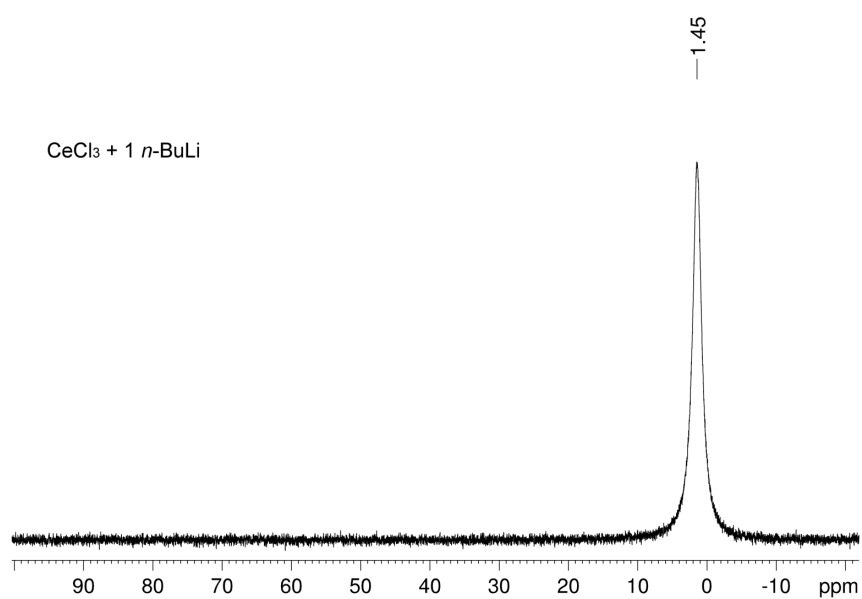


Figure S33. ⁷Li NMR spectrum of CeCl₃(thf) + 1 equiv. of *n*-BuLi (194.37 MHz, THF-*d*₈, 233 K).

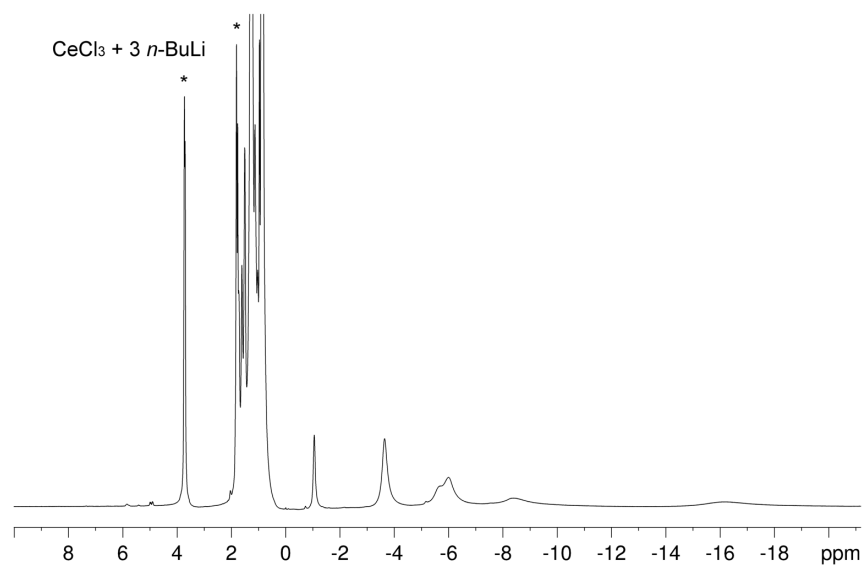


Figure S34. ^1H NMR spectrum of $\text{CeCl}_3(\text{thf}) + 3$ equivs. of $n\text{-BuLi}$ (500.13 MHz, $\text{THF-}d_8$, 233 K). Solvent residual signals are marked with *.

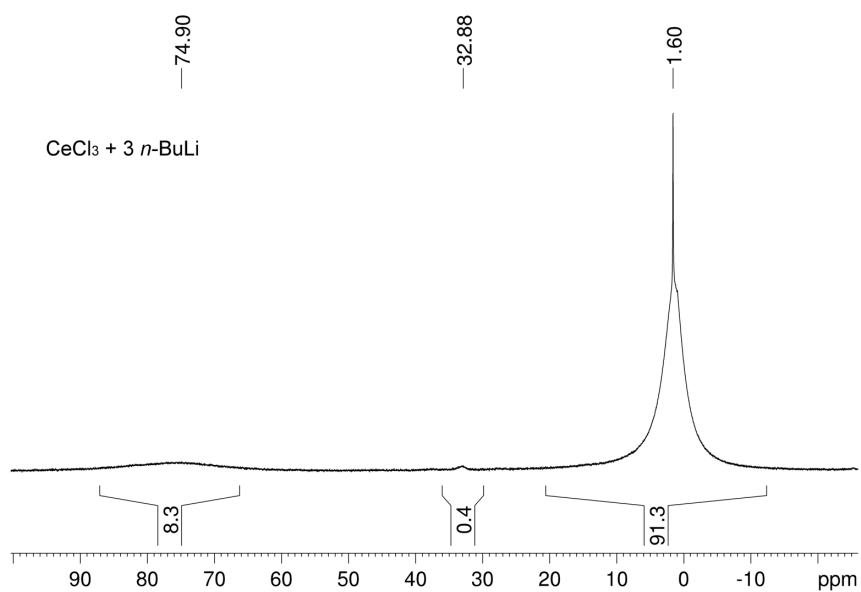


Figure S35. ^7Li NMR spectrum of $\text{CeCl}_3(\text{thf}) + 3$ equivs. of $n\text{-BuLi}$ (194.37 MHz, $\text{THF-}d_8$, 233 K).

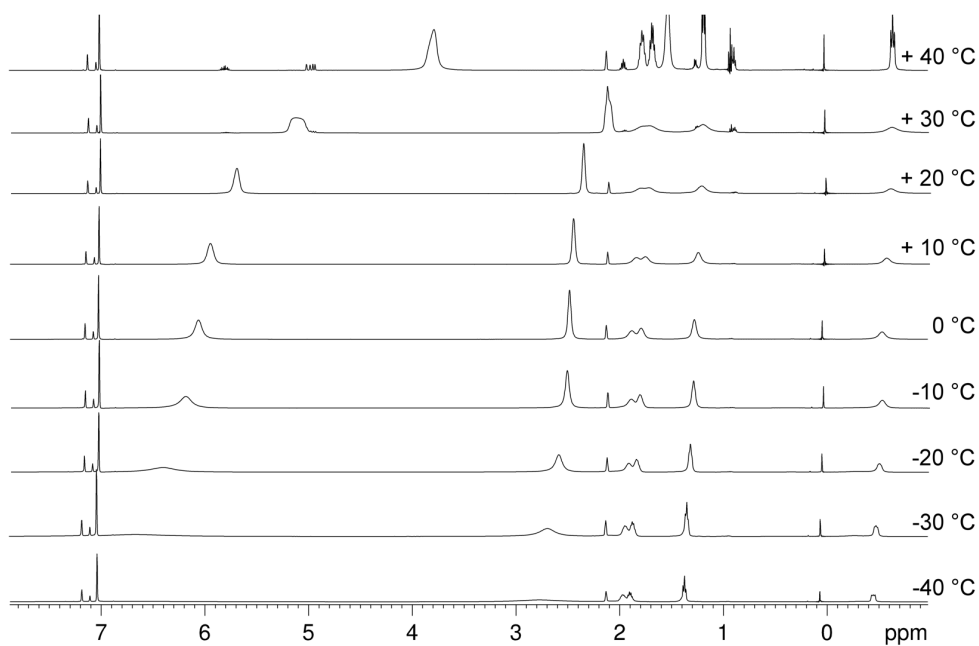


Figure S36. VT ^1H NMR spectra of $\text{Li}_3\text{Ce}(\textit{n}\text{-Bu})_6(\text{thf})_4$ ($\mathbf{3}^{\text{Ce}}$) (500.13 MHz, toluene- d_8 , 233 K-313 K), showing a slight amount of the decomposition product of 1-butene at 5.82 and 4.99 ppm at +30 °C and +40 °C.

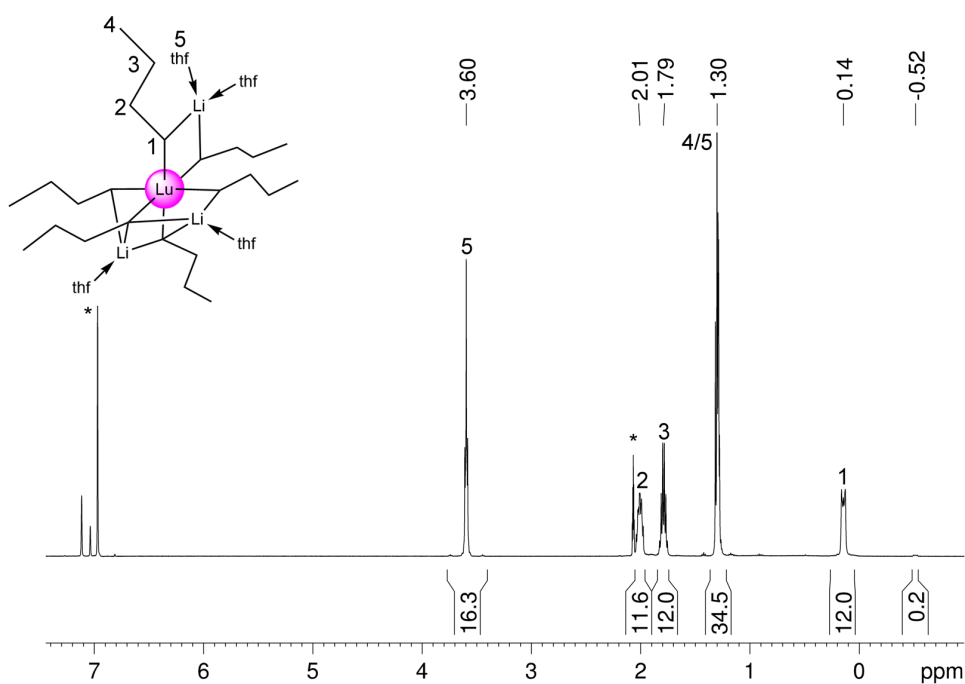


Figure S37. ^1H NMR spectrum of $\text{Li}_3\text{Lu}(\textit{n}\text{-Bu})_6(\text{thf})_4$ ($\mathbf{3}^{\text{Lu}}$) (500.13 MHz, toluene- d_8 , 233 K). Solvent residual signals are marked with *.

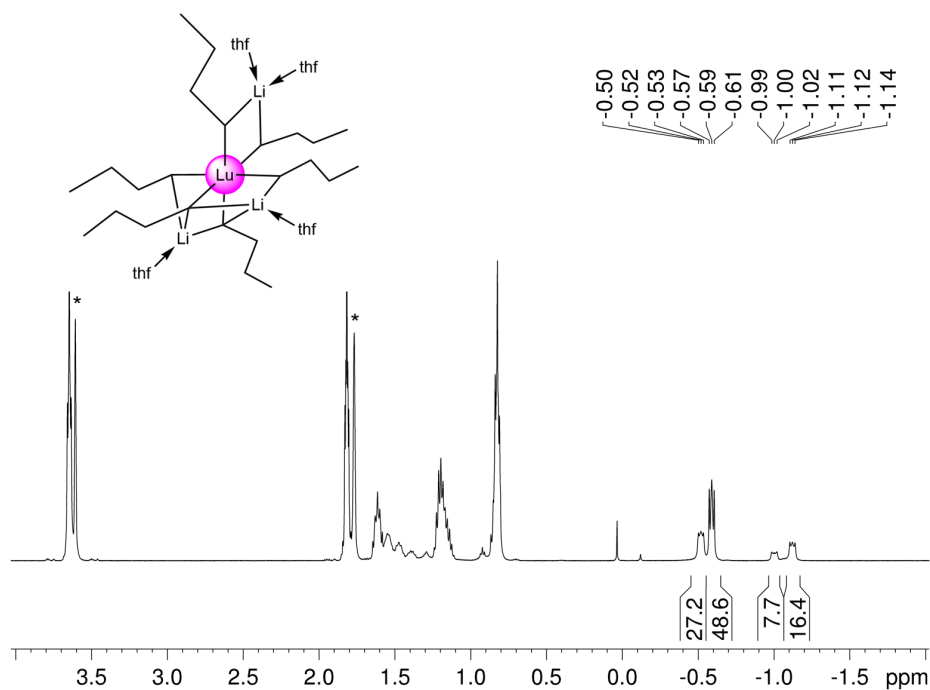


Figure S38. ^1H NMR spectrum of $\text{Li}_3\text{Lu}(n\text{-Bu})_6(\text{thf})_4$ (3^{Lu}) (500.13 MHz, $\text{THF-}d_8$, 193 K). Solvent residual signals are marked with *. The signal set at -0.52 and -0.59 are from the CH_2 groups bonded to the lutetium and the signals at -1.00 and -1.12 are from dissociated $n\text{-BuLi}(\text{thf})$.

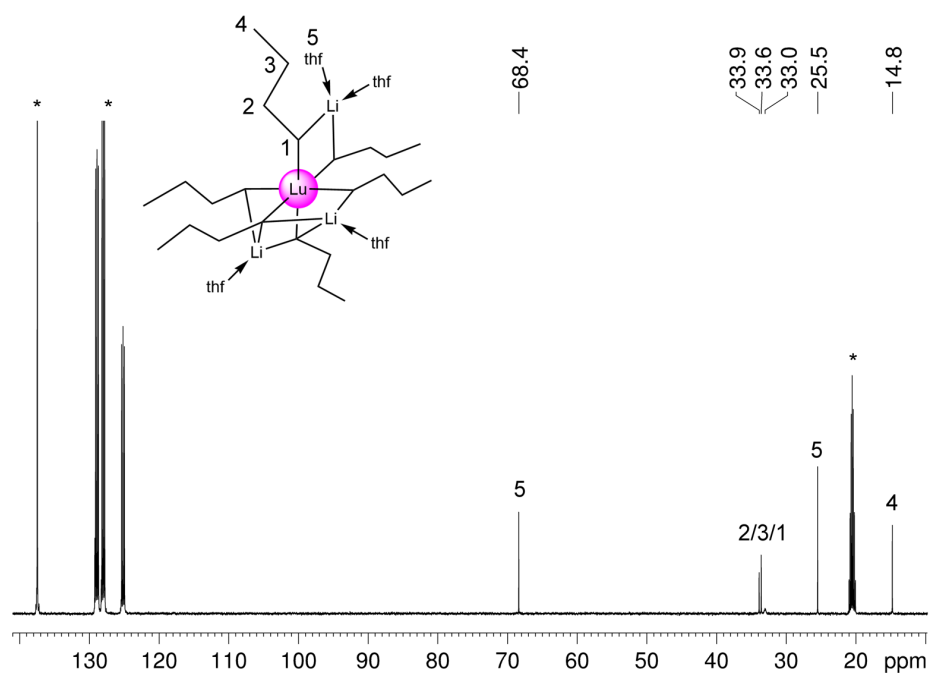


Figure S39. $^{13}\text{C}\{^1\text{H}\}$ NMR spectrum of $\text{Li}_3\text{Lu}(n\text{-Bu})_6(\text{thf})_4$ (3^{Lu}) (125.76 MHz, $\text{toluene-}d_8$, 233 K). Solvent residual signals are marked with *.

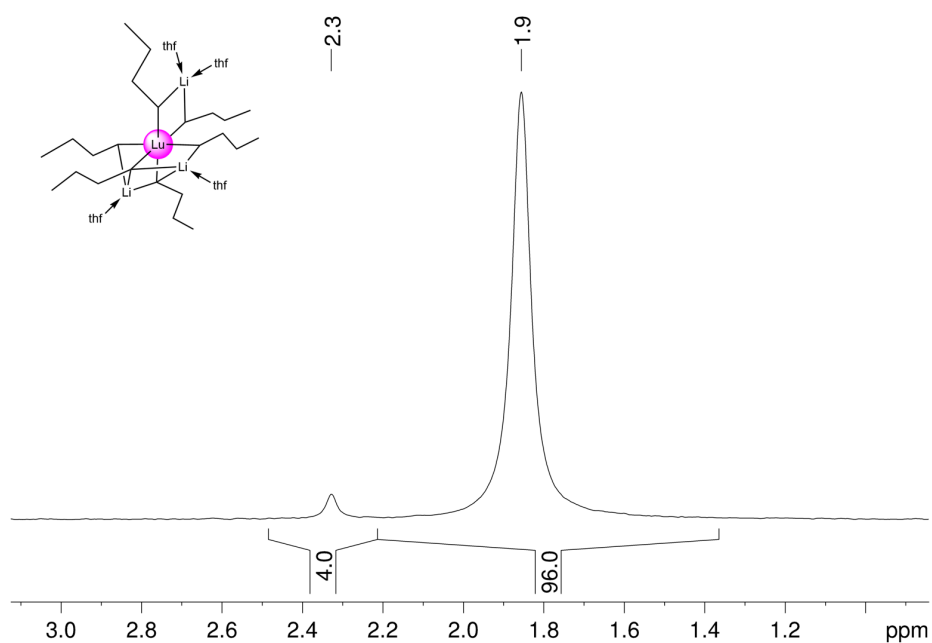


Figure S40. ^7Li NMR spectrum of $\text{Li}_3\text{Lu}(\text{n-Bu})_6(\text{thf})_4$ (3^{Lu}) (194.37 MHz, $\text{toluene-}d_8$, 233 K), showing free $\text{n-BuLi}(\text{thf})$ at 2.3 ppm and the mixed lutetium–lithium complex at 1.9 ppm.

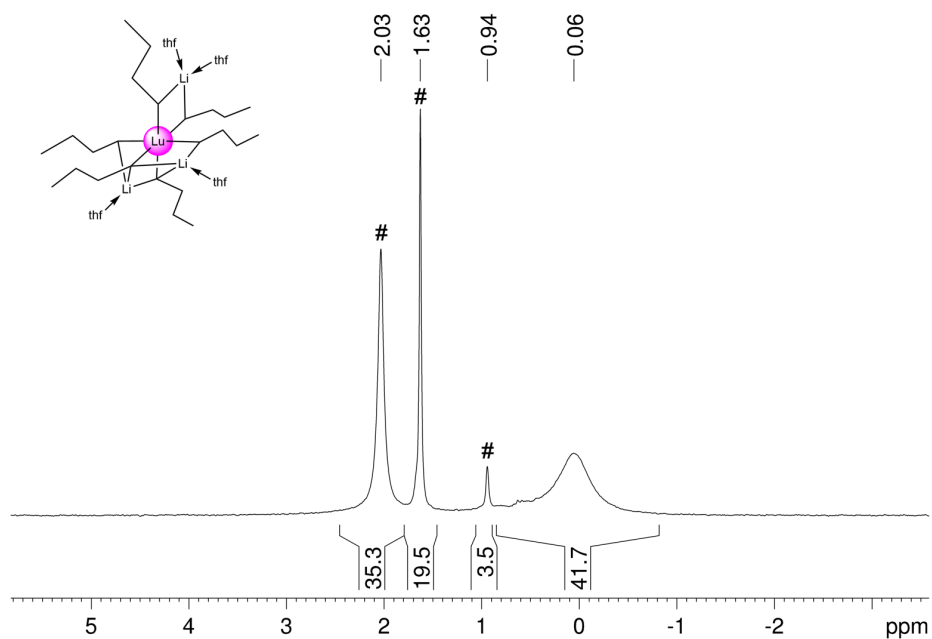


Figure S41. ^7Li NMR spectrum of $\text{Li}_3\text{Lu}(\text{n-Bu})_6(\text{thf})_4$ (3^{Lu}) (194.37 MHz, $\text{THF-}d_8$, 193 K). Dissociated $\text{n-BuLi}(\text{thf})$ is marked with #.

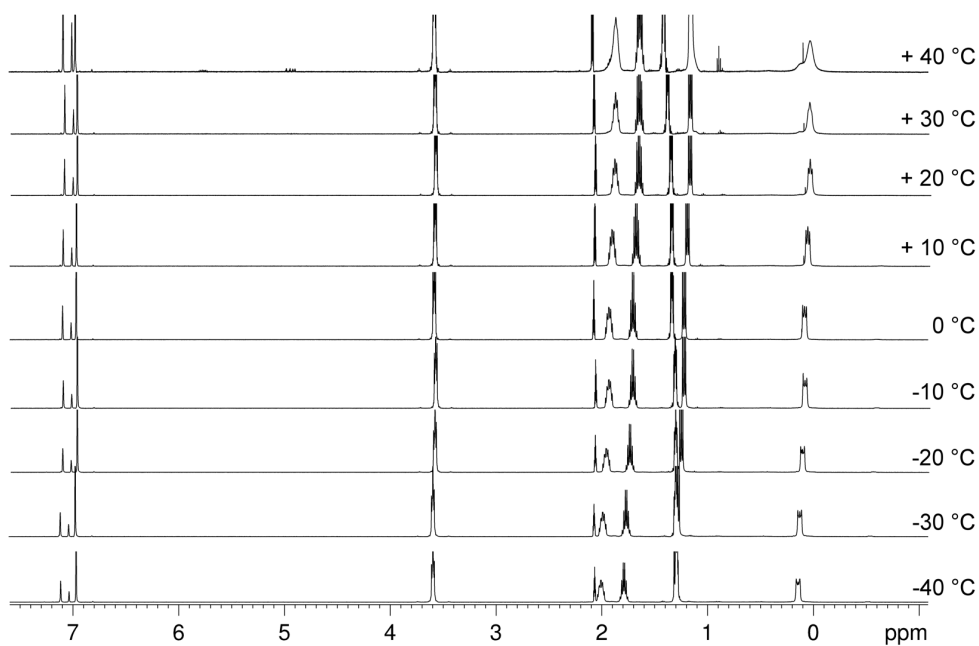


Figure S42. VT ^1H NMR spectra of $\text{Li}_3\text{Lu}(\text{n-Bu})_6(\text{thf})_4$ (3^{Lu}) (500.13 MHz, toluene- d_8 , 233 K-313 K), showing a slight amount of the decomposition product 1-butene at 5.82 and 4.99 ppm at +30 °C and +40 °C.

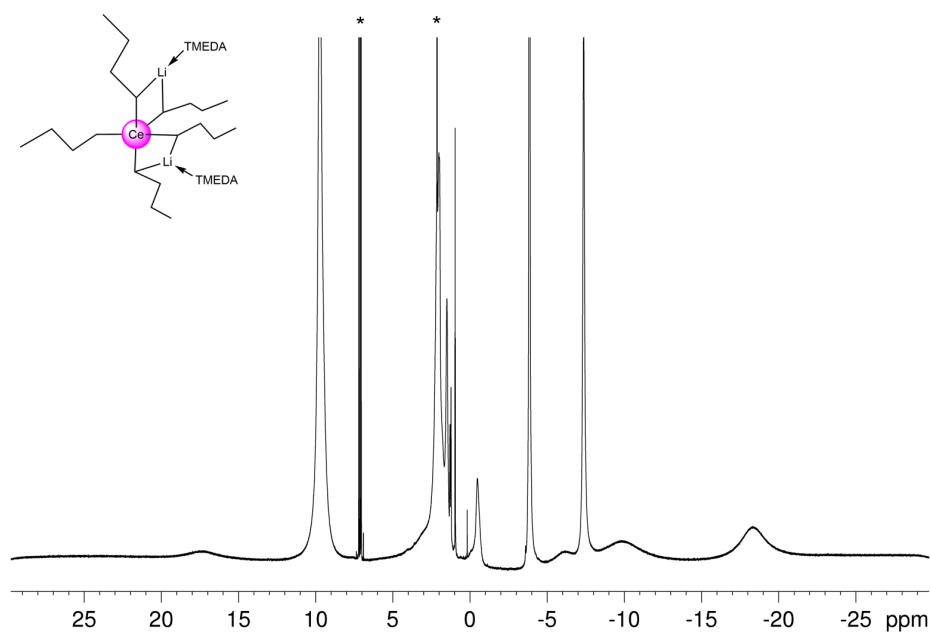


Figure S43. ^1H NMR spectrum of $\text{Li}_2\text{Ce}(\text{n-Bu})_5(\text{tmeda})_2$ (4^{Ce}) (500.13 MHz, toluene- d_8 , 233 K). Solvent residual signals are marked with *. Except for the sharp $\text{n-BuLi}(\text{tmeda})$ signals, resonance assignment is not conclusive.

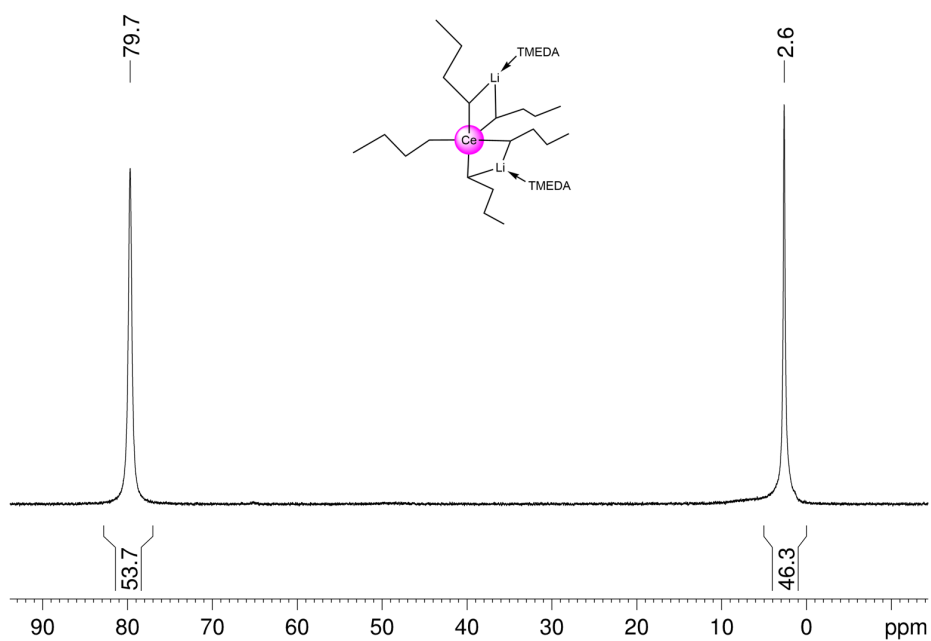


Figure S44. ^7Li NMR spectrum of $\text{Li}_2\text{Ce}(n\text{-Bu})_5(\text{tmeda})_2$ (4^{Ce}) (194.37 MHz, toluene- d_8 , 233 K), showing the $n\text{-BuLi}(\text{tmeda})$ 2.6 ppm and a mixed cerium–lithium species at 79.7 ppm.

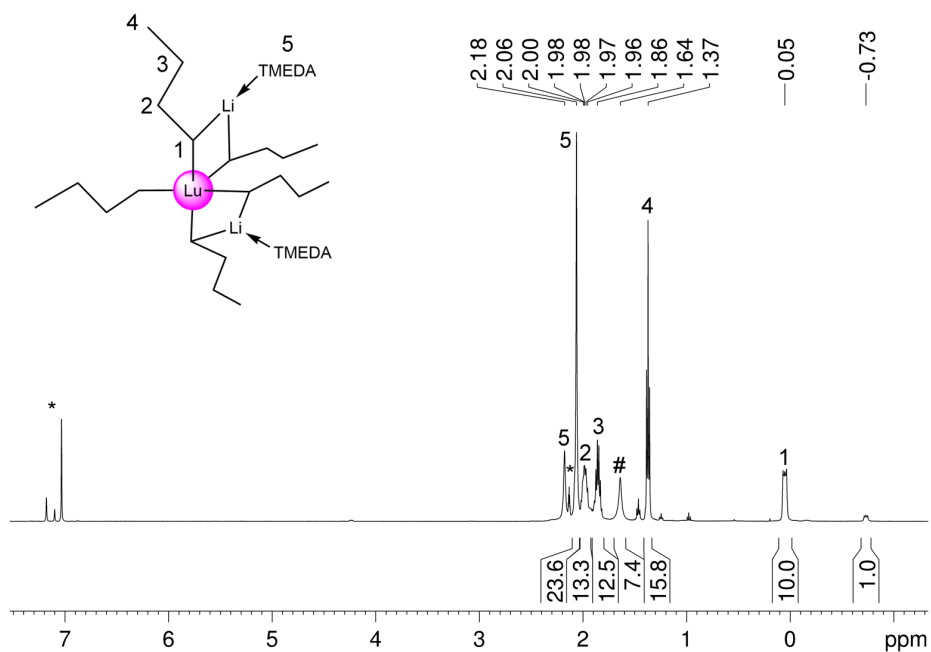


Figure S45. ^1H NMR spectrum of $\text{Li}_2\text{Lu}(n\text{-Bu})_5(\text{tmeda})_2$ (4^{Lu}) (500.13 MHz, toluene- d_8 , 233 K). Solvent residual signals are marked with *. An unknown impurity is marked with #.

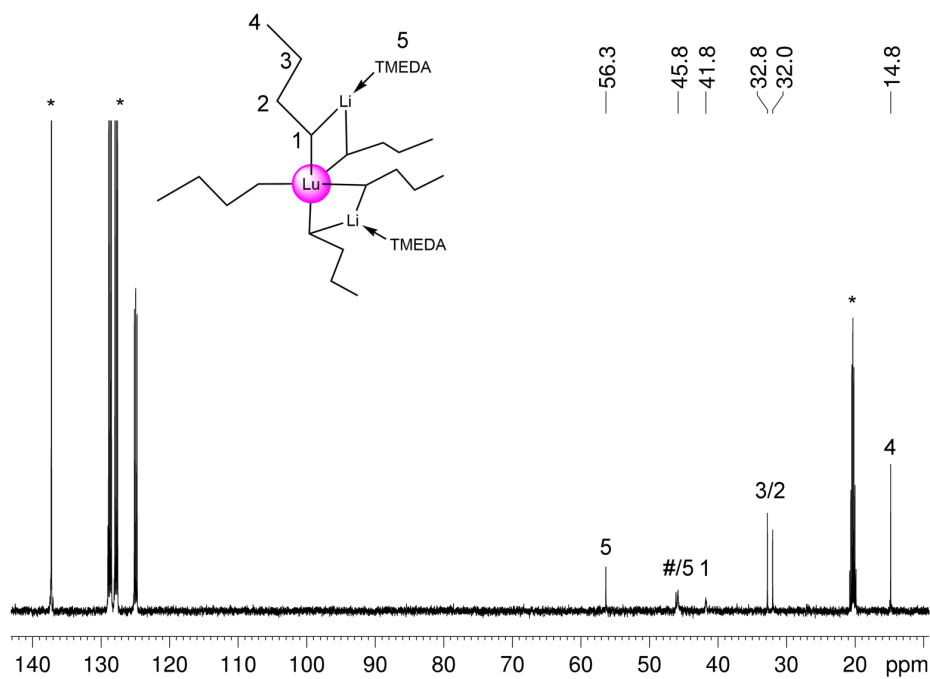


Figure S46. $^{13}\text{C}\{^1\text{H}\}$ NMR spectrum of $\text{Li}_2\text{Lu}(\textit{n}\text{-Bu})_5(\textit{tmeda})_2$ (4^{Lu}) (125.76 MHz, toluene- d_8 , 233 K). Solvent residual signals are marked with *. An unknown impurity is marked with #.

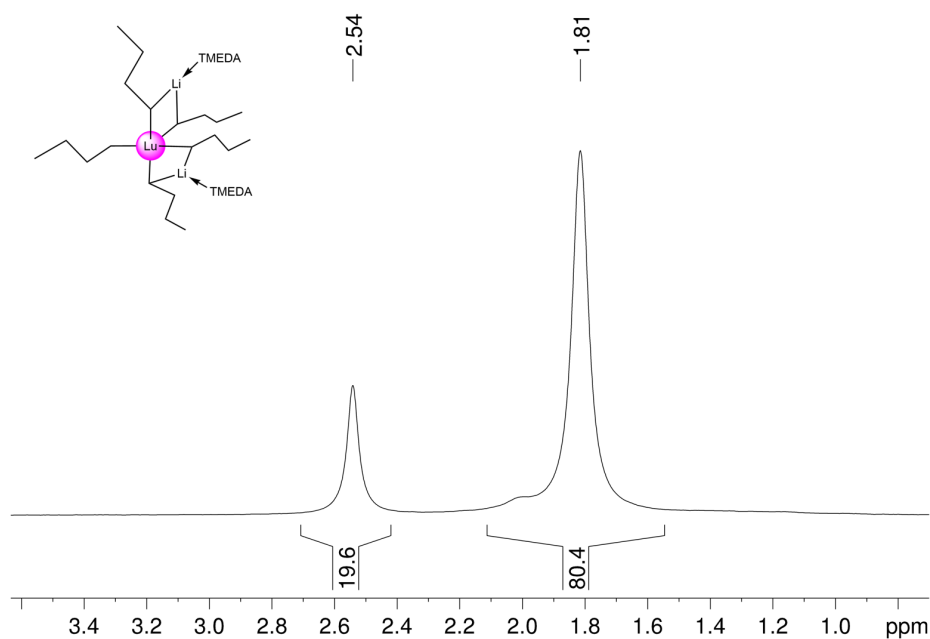


Figure S47. ^7Li NMR spectrum of $\text{Li}_2\text{Lu}(\textit{n}\text{-Bu})_5(\textit{tmeda})_2$ (4^{Lu}) (194.37 MHz, toluene- d_8 , 233 K), showing the $\textit{n}\text{-BuLi}(\textit{tmeda})$ at 2.5 ppm and a mixed lutetium–lithium species at 1.8 ppm.

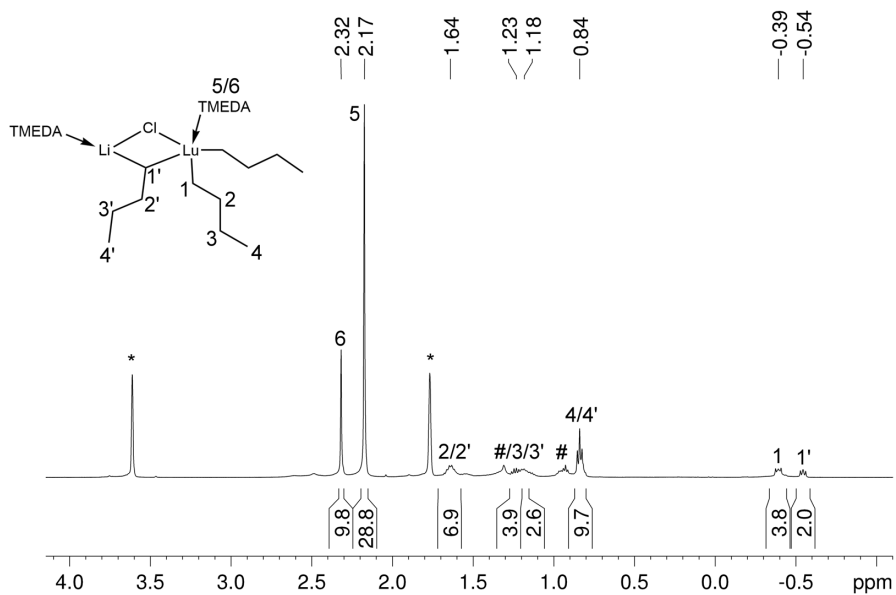


Figure S48. ^1H NMR spectrum of $\text{LiLu}(n\text{-Bu})_3\text{Cl}(\text{tmeda})_2$ (**5**) (500.13 MHz, $\text{THF-}d_8$, 233 K). Solvent residual signals are marked with *. Unknown impurities are marked with #.

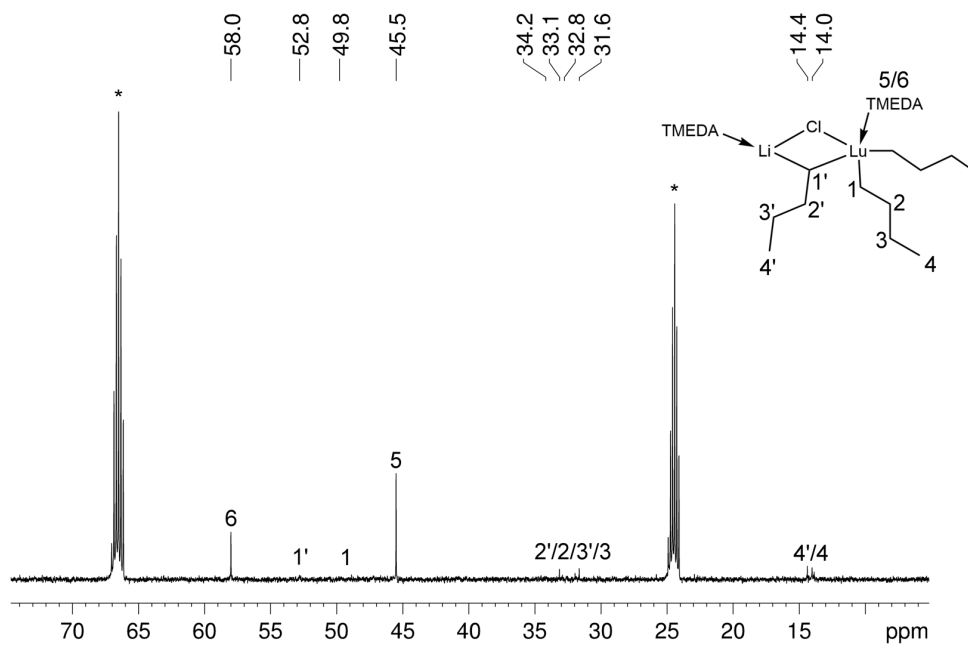


Figure S49. $^{13}\text{C}\{^1\text{H}\}$ NMR spectrum of $\text{LiLu}(n\text{-Bu})_3\text{Cl}(\text{tmeda})_2$ (**5**) (125.76 MHz, $\text{THF-}d_8$, 233 K). Solvent residual signals are marked with *.

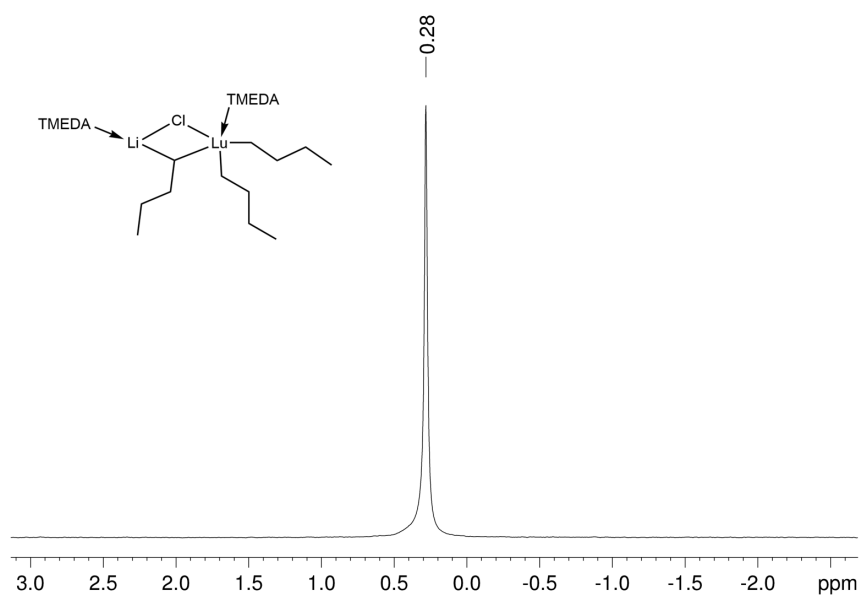


Figure S50. ^7Li NMR spectrum of $\text{LiLu}(n\text{-Bu})_3\text{Cl}(\text{tmeda})_2$ (**5**) (194.37 MHz, $\text{THF-}d_8$, 233 K).

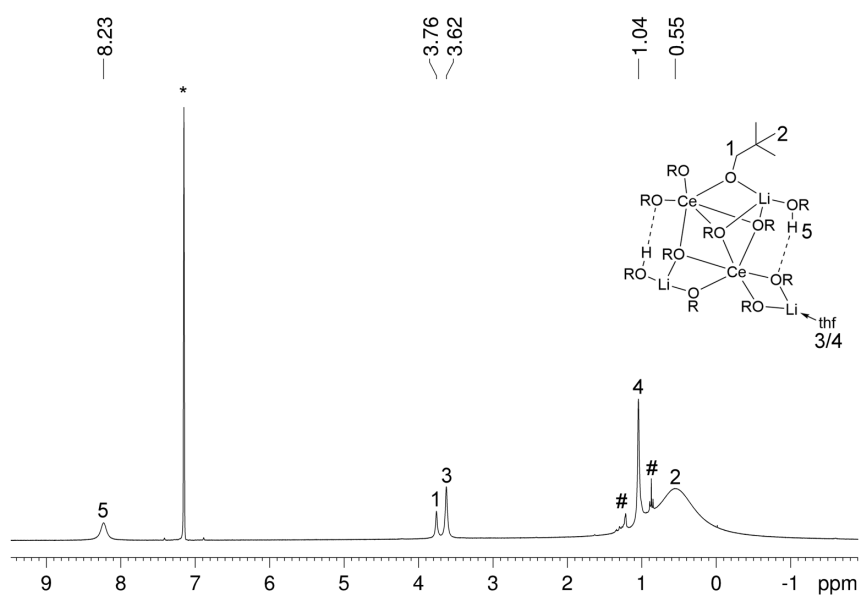


Figure S51. ^1H NMR spectrum of $\text{Li}_3\text{Ce}_2(\text{ONep})_9(\text{HONep})_2(\text{thf})$ (**6**) (300.13 MHz, $\text{benzene-}d_6$, 299 K). The solvent residual signal is marked with *. Residual *n*-hexane is marked with #.

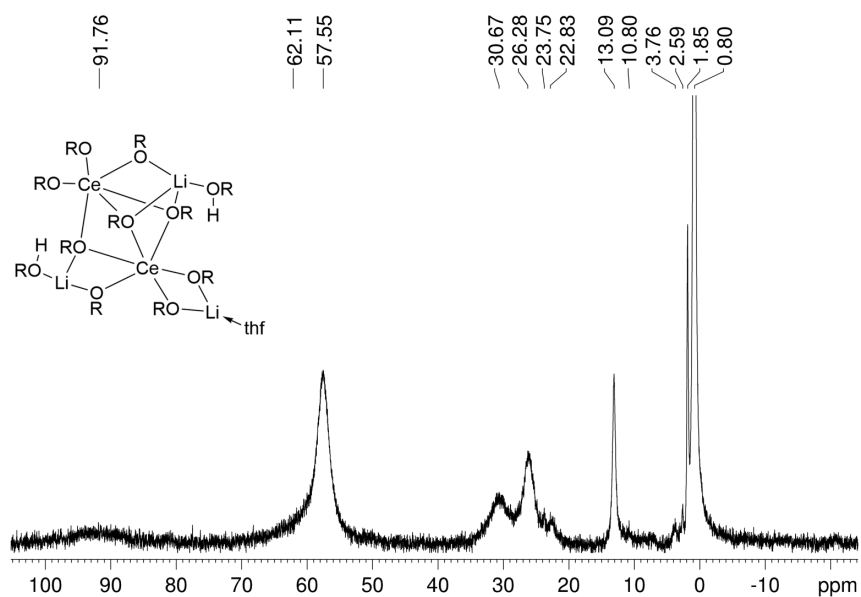


Figure S52. ^7Li NMR spectrum of $\text{Li}_3\text{Ce}_2(\text{ONep})_9(\text{HONep})_2(\text{thf})$ (**6**) (116.64 MHz, benzene- d_6 , 299 K).

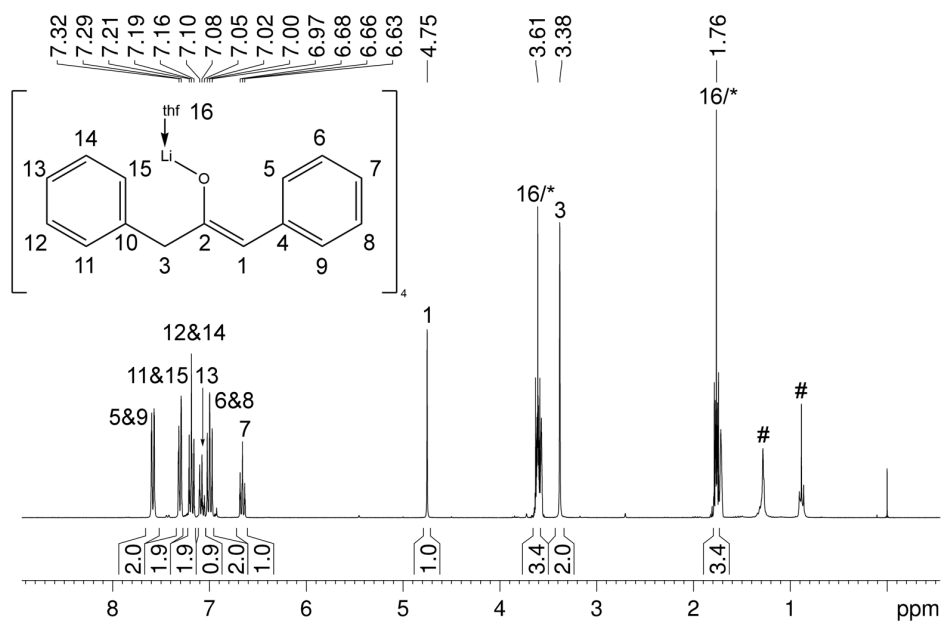


Figure S53. ^1H NMR spectrum of $\text{Li}_4[\text{OC}(=\text{CHPh})(\text{CH}_2\text{Ph})]_4(\text{thf})_4$ (**7**) (300.13 MHz, THF- d_8 , 299 K). Solvent residual signals are marked with *. Residual *n*-hexane is marked with #.

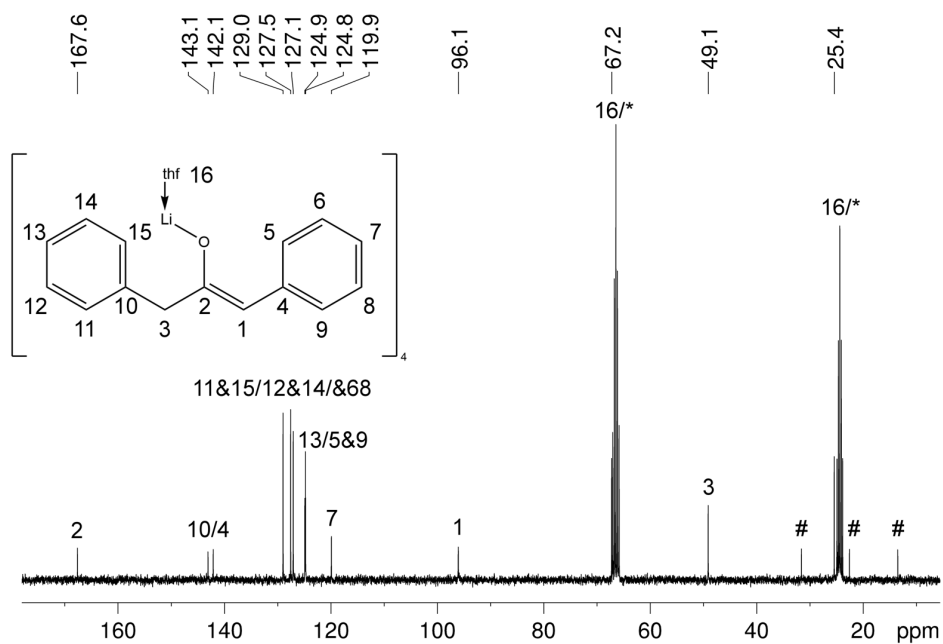


Figure S54. $^{13}\text{C}\{^1\text{H}\}$ NMR spectrum of $\text{Li}_4[\text{OC}(=\text{CHPh})(\text{CH}_2\text{Ph})_4(\text{thf})_4$ (7) (75.47 MHz, $\text{THF-}d_8$, 299 K). Solvent residual signals are marked with *. Residual *n*-hexane is marked with #.

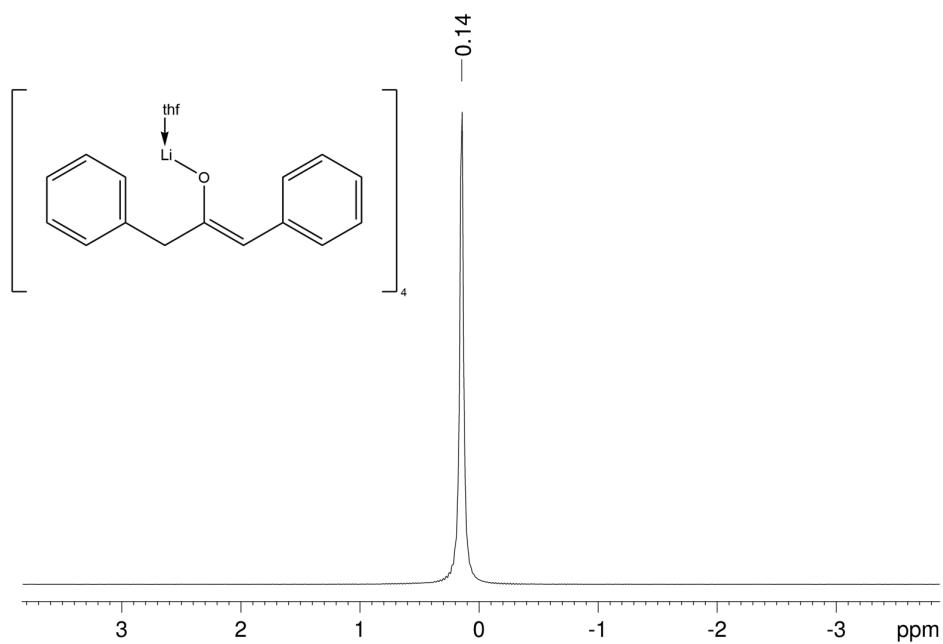


Figure S55. ^7Li NMR spectrum of $\text{Li}_4[\text{OC}(=\text{CHPh})(\text{CH}_2\text{Ph})_4(\text{thf})_4$ (7) (116.64 MHz, $\text{THF-}d_8$, 299 K).

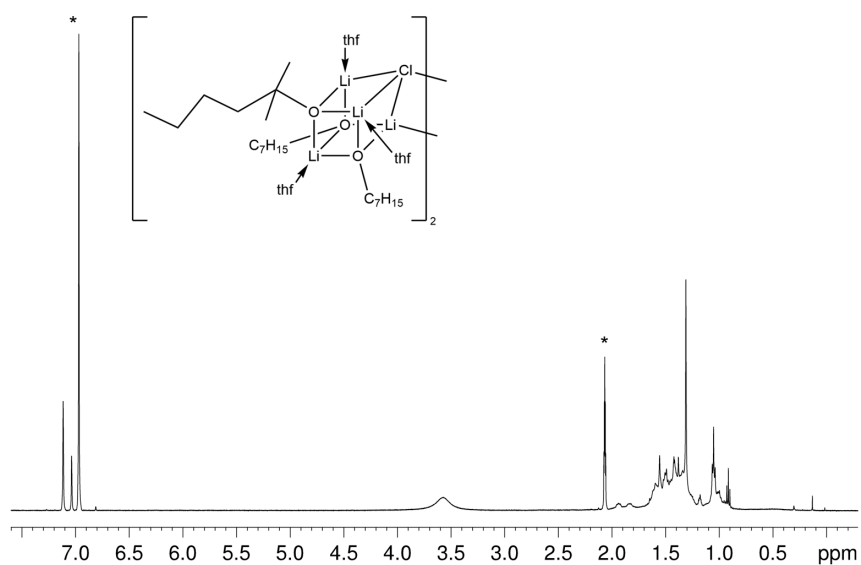


Figure S56. ^1H NMR spectrum of $\text{Li}_8[\text{OCMe}_2(n\text{-Bu})]_6\text{Cl}_2(\text{thf})_6$ (**8**) (500.13 MHz, toluene- d_8 , 233 K). Solvent residual signals are marked with *.

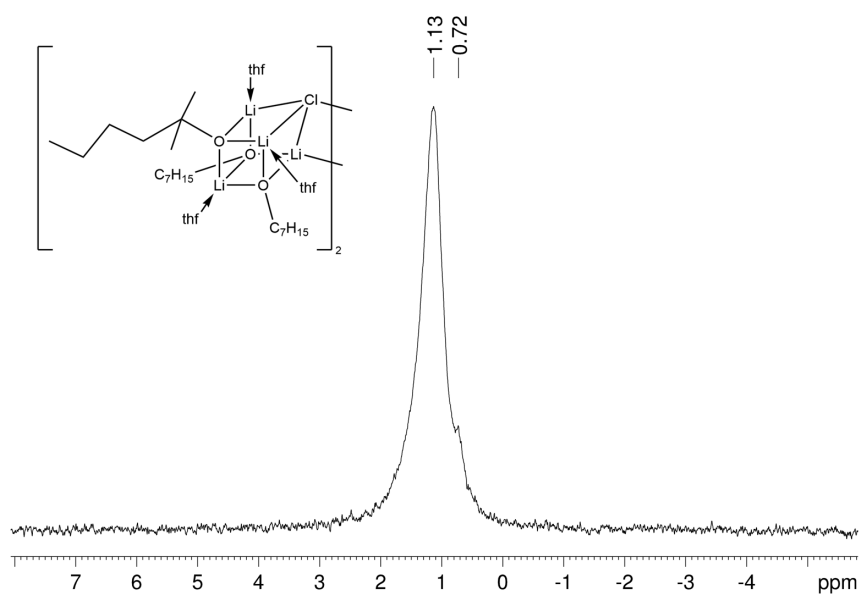


Figure S57. ^7Li NMR spectrum of $\text{Li}_8[\text{OCMe}_2(n\text{-Bu})]_6\text{Cl}_2(\text{thf})_6$ (**8**) (194.37 MHz, toluene- d_8 , 233 K).

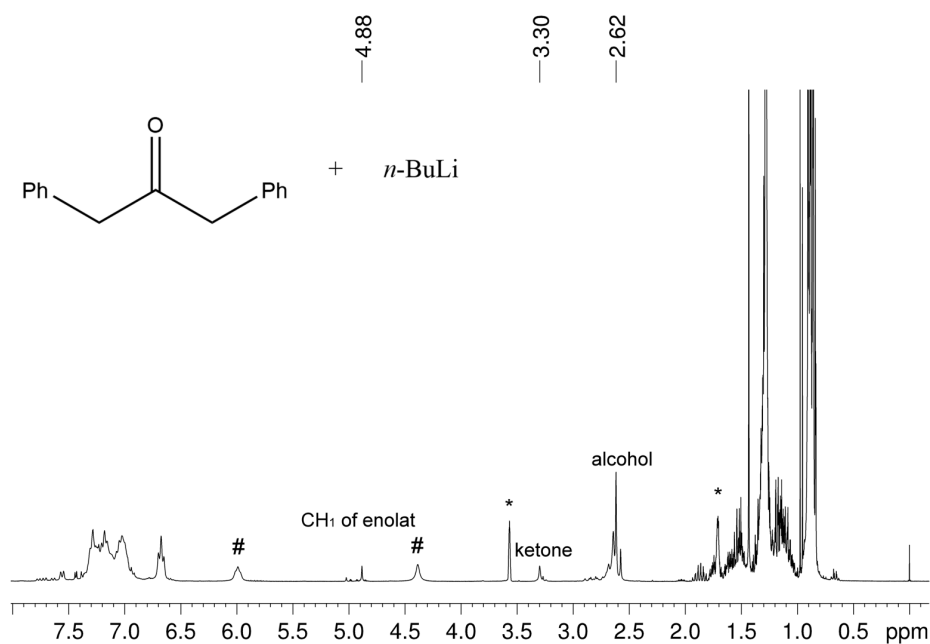


Figure S58. ¹H NMR spectrum of the reaction of 1,3-diphenylpropan-2-one and *n*-BuLi (300.13 MHz, THF-*d*₈, 299 K). Solvent residual signals are marked with *. An unknown impurity is marked with #.

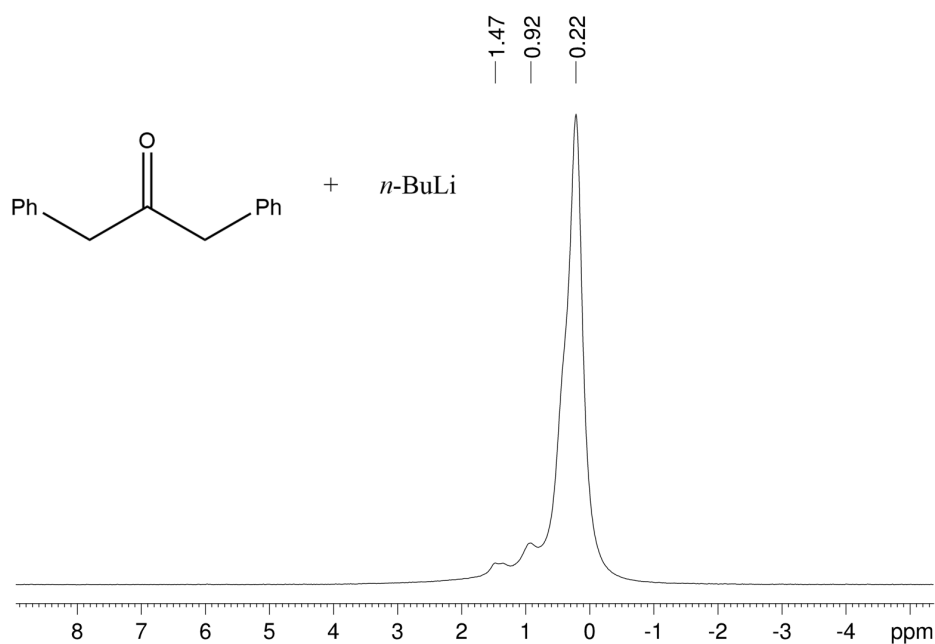


Figure S59. ⁷Li NMR spectrum of the reaction of 1,3-diphenylpropan-2-one with *n*-BuLi (116.64 MHz, THF-*d*₈, 299 K).

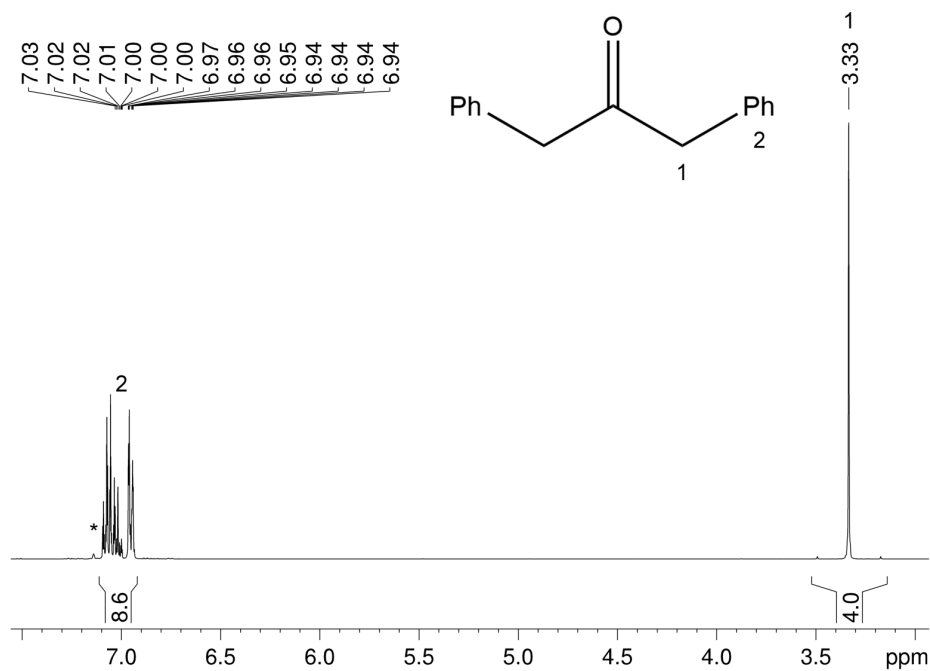


Figure S60. ^1H NMR spectrum of 1,3-diphenylpropan-2-one (400.11 MHz, benzene- d_6 , 299 K). The solvent residual signal is marked with *.

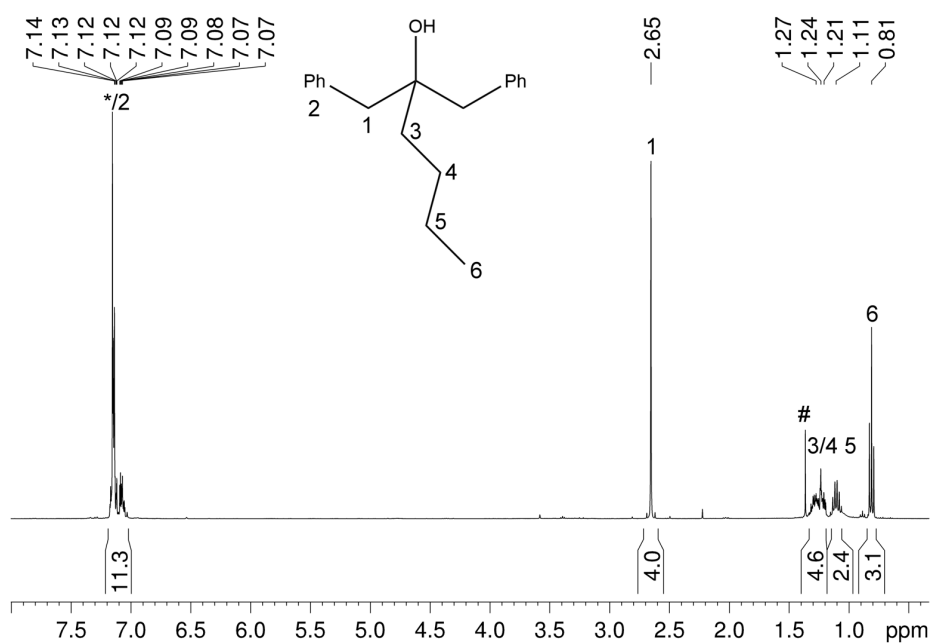


Figure S61. ^1H NMR spectrum of 1,3-diphenyl-2-butylpropan-2-ol (400.11 MHz, benzene- d_6 , 299 K). The solvent residual signal is marked with *. Residual acetone impurity is marked with #.

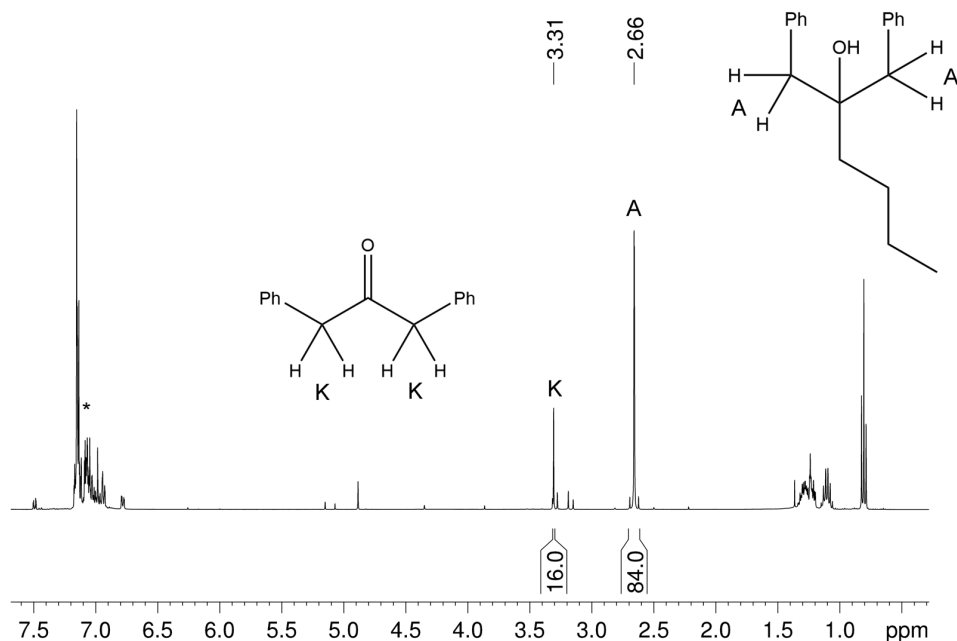
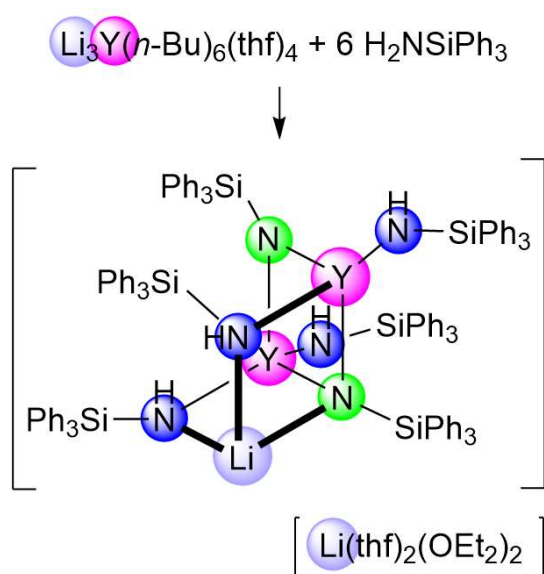


Figure S62. ¹H NMR spectrum of a mixture of 1,3-diphenylpropan-2-one and 1,3-diphenyl-2-butylpropan-2-ol from the reaction of Li₃Ce(*n*-Bu)₆(thf)₄ (**3**^{Ce}) with six equiv. of 1,3-diphenylpropan-2-one (400.11 MHz, benzene-*d*₆, 299 K). The solvent residual signal is marked with *.

References

1. A. Krasovskiy, F. Kopp, P. Knochel, *Angew. Chem. Int. Ed.* **2006**, *45*, 497-500; *Angew. Chem.* **2006**, *118*, 511-515.
2. G. R. Fulmer, A. J. M. Miller, N. H. Sherden, H. E. Gottlieb, A. Nudelman, B. M. Stoltz, J. E. Bercaw, K. I. Goldberg, *Organometallics* **2010**, *29*, 2176-2179.
3. TopSpin v. 3.6.1, Bruker AXS Inc., Madison, WI. 2018.
4. COSMO v. 1.61, Bruker AXS Inc., Madison, WI., 2012.
5. APEX 3 v. 2017.3-0, Bruker AXS Inc., Madison, WI. 2017.
6. SAINT v. 8.38A, Bruker AXS Inc., Madison, WI. 2017.
7. L. Krause, R. Herbst-Irmer, G. M. Sheldrick, D. Stalke, *J. Appl. Crystallogr.* **2015**, *48*, 3-10.
8. G. Sheldrick, *Acta Crystallogr. Sect. C* **2015**, *71*, 3-8.
9. C. B. Hubschle, G. M. Sheldrick, B. Dittrich, *J. Appl. Crystallogr.* **2011**, *44*, 1281-1284.
10. D. Kratzert, J. J. Holstein, I. Krossing, *J. Appl. Crystallogr.* **2015**, *48*, 933-938.
11. C. F. Macrae, P. R. Edgington, P. McCabe, E. Pidcock, G. P. Shields, R. Taylor, M. Towler, J. van de Streek, *J. Appl. Crystallogr.* **2006**, *39*, 453-457.
12. POV-Ray v.3.6, Persistence of Vision Pty. Ltd., POV-Ray Williamstown, Victoria, Australia. <http://www.povray.org>, 2004.
13. H. Schumann, J. Mueller, N. Bruncks, H. Lauke, J. Pickardt, H. Schwarz, K. Eckart, *Organometallics* **1984**, *3*, 69-74.

Aminolysis of Lithium/Yttrium Bimetallic Alkyls including the Solid-State Structure of a Europium(II) *n*-Butyl Compound



<https://doi.org/10.1002/zaac.202200274>
reprinted with permission from
Z. Anorg. Allg. Chem. **2022**, e202200274

DOI: 10.1002/zaac.202200274

Aminolysis of Lithium/Yttrium Bimetallic Alkyls including the Solid-State Structure of a Europium(II) *n*-Butyl Compound

Tassilo Berger,^[a] David Baschnagel,^[a] Cécilia Maichle-Mössmer,^[a] and Reiner Anwander*^[a]Dedicated to Professor Sjoerd Harder on the occasion of his 60th birthday

Using previously established salt-metathesis procedures at low temperature, heterobimetallic ate complexes $\text{Li}_6\text{Eu}^{\text{II}}(n\text{-Bu})_8(\text{thf})_6$ and $\text{Li}_3\text{Y}^{\text{III}}(i\text{-Bu})_6(\text{thf})_4$ could be synthesized and their solid-state structures analyzed by X-ray diffraction. Recently described complex $\text{Li}_3\text{Y}(n\text{-Bu})_6(\text{thf})_4$ was probed as a precursor in protonolyses with various amines, revealing distinct reaction path-

ways. Identified products comprise homoleptic amide $\text{Y}^{\text{III}}[\text{HNC}_6\text{H}_3(\text{mes})_2\text{-}2,6]_3$ ($\text{mes} = \text{C}_6\text{H}_2\text{Me}_3\text{-}2,4,6$), heteroleptic C–H bond activated $\text{Li}_3\text{Y}(n\text{-Bu})_2[\text{N}(\text{SiMe}_2\text{CH}_2)(\text{C}_6\text{H}_3\text{-Me}_2\text{-}3,5)]_2(\text{thf})_5$, and mixed amido/imido complex $[\text{LiY}_2(\text{HNSiPh}_3)_4(\text{NSiPh}_3)_2][\text{Li}(\text{thf})_2(\text{OEt})_2]$.

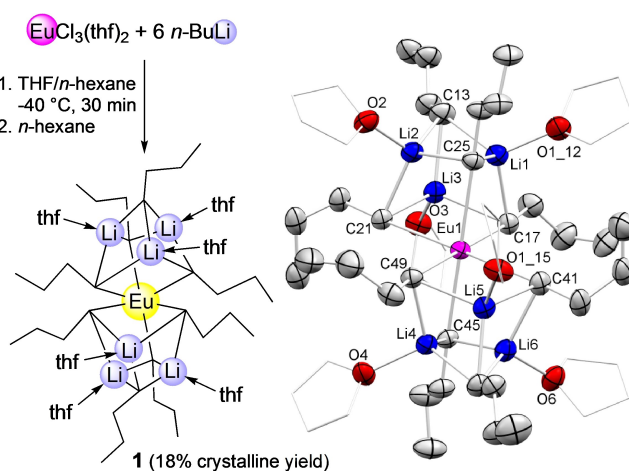
Introduction

Lithium/rare-earth metal (Ln) bimetallic alkyls have emerged as prime reagents for carbon-carbon bond forming reactions on easily enolizable ketones, ever since the original report by Imamoto in 1982.^[1] Because of the thermal instability of Imamoto-type reagents, the targeted organic transformations are routinely conducted at low temperatures (-78°C).^[2] It is also for this reason that the structural elucidation of such heterobimetallic alkyls has proven elusive,^[3] in particular for derivatives with higher alkyl moieties like *n*-butyl.^[4] Recently our group could isolate the ate complexes $[\text{Li}(\text{thf})_4][\text{Ce}(t\text{-Bu})_4]$, $\text{Li}_3\text{Ln}(n\text{-Bu})_6(\text{thf})_4$ ($\text{Ln} = \text{Sc}, \text{Y}, \text{La}, \text{Ce}, \text{Lu}$), and $\text{Li}_2\text{Ln}(n\text{-Bu})_5(\text{tmeda})_2$ ($\text{Ln} = \text{Ce}, \text{Lu}$) by applying seamless low-temperature syntheses and crystallization techniques.^[5] Initial studies on the reactivity of these complexes (in addition to applications in organic transformations) resulted in the lithium depleted complex $\text{LiLu}(n\text{-Bu})_3\text{Cl}(\text{tmeda})_2$ (via reaction of $\text{Li}_2\text{Lu}(n\text{-Bu})_5(\text{tmeda})_2$ with ClSiMe_3) and the neopentolate complex $\text{Li}_3\text{Ce}_2(\text{OCH}_2t\text{Bu})_3(\text{HOCH}_2t\text{Bu})_2(\text{thf})$ (via alcoholysis of $\text{Li}_3\text{Ce}(n\text{-Bu})_6(\text{thf})_4$).^[5] Herein, we report the synthesis of the first europium(II) *n*-butyl complex, the first rare-earth-metal *i*-butyl

complex, and the reactivity of $\text{Li}_3\text{Y}(n\text{-Bu})_6(\text{thf})_4$ toward various primary amines.

Results and Discussion

Synthesis and Solid-State Structure of Europium(II) Alkyl Compound $\text{Li}_6\text{Eu}(n\text{-Bu})_8(\text{thf})_6$. Applying the protocol recently reported for the synthesis of $\text{Li}_3\text{Ln}(n\text{-Bu})_6(\text{thf})_4$ ($\text{Ln} = \text{Sc}, \text{Y}, \text{La}, \text{Ce}, \text{Lu}$), colorless $\text{EuCl}_3(\text{thf})_2$ and *n*-BuLi afforded yellow divalent complex $\text{Li}_6\text{Eu}(n\text{-Bu})_8(\text{thf})_6$ (Scheme 1). The inherent reduction of



Scheme 1. Synthesis of divalent $\text{Li}_6\text{Eu}(n\text{-Bu})_8(\text{thf})_6$ (**1**) and its crystal structure, with atomic displacement ellipsoids set at 50% probability. Hydrogen atoms and disorders of the *n*-butyl groups are omitted for clarity. The carbon atoms of the THF molecules are represented by a wireframe model for the sake of clarity. Only one out of three molecules of **1** in the asymmetric unit is displayed. Selected interatomic distances [Å] for **1**: Eu1–C17 2.78(2), Eu1–C21 2.75(2), Eu1–C25 2.75(2), Eu1–C41 2.81(2), Eu1–C45 2.75(2), Eu1–C49 2.76(2).

[a] T. Berger, D. Baschnagel, Dr. C. Maichle-Mössmer, Prof. Dr. R. Anwander
Institut für Anorganische Chemie
Eberhard Karls Universität Tübingen
Auf der Morgenstelle 18, 72076 Tübingen
E-mail: reiner.anwander@uni-tuebingen.de

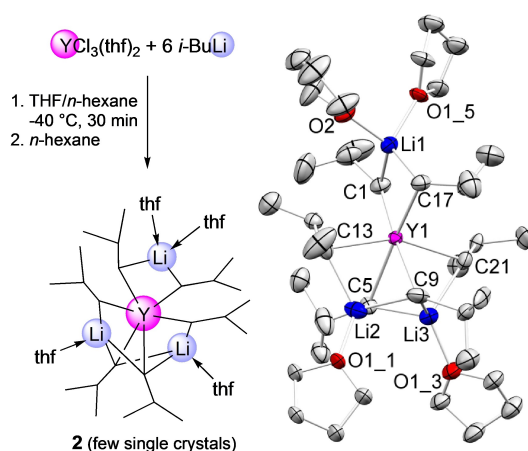
Supporting information for this article is available on the WWW under <https://doi.org/10.1002/zaac.202200274>

© 2022 The Authors. Zeitschrift für anorganische und allgemeine Chemie published by Wiley-VCH GmbH. This is an open access article under the terms of the Creative Commons Attribution Non-Commercial NoDerivs License, which permits use and distribution in any medium, provided the original work is properly cited, the use is non-commercial and no modifications or adaptations are made.

the Eu(III) center in the presence of strongly nucleophilic alkyls is unsurprising and crucial for the nonexistence of Eu(III) alkyl complexes.^[4] An early example features the instant reduction of EuCl_3 by methyl lithium, however, an organoeuropium compound could not be isolated from this reaction.^[6] In a similar vein, trivalent amides like $\text{Eu}[\text{N}(\text{SiHMe}_2)_3](\text{thf})_2$ are reduced by AlR_3 ($\text{R} = \text{Me}, \text{Et}$) to yield the divalent tetraalkylaluminates $[\text{Eu}(\text{AlR}_2)_2]_n$.^[7]

The X-ray diffraction (XRD) analysis of **1** revealed an europium(II) center coordinated by six *n*-butyl ligands. The σ -bonded CH_2 methylene moieties are further interacting with two lithium atoms each, resulting in μ_2 -bonded alkyls. Each three of the lithium atoms are arranged in a trigonal plane which is capped by another peripheral *n*-butyl ligand. The coordination sphere of the lithium atoms is completed by one THF molecule each. To the best of our knowledge, this is the first example of a divalent rare-earth-metal complex bearing *n*-butyl ligands. The $\text{Eu(II)}-\text{C}$ distances average 2.77 Å, and hence are in the range of those detected in heterobimetallic $[\text{Eu(II)}(\text{AlEt}_2)_2]_n$ (2.71(2) to 2.95(5) Å).^[7] Other σ -bonded europium(II) alkyls comprise agostic $\text{Eu}[\text{C}(\text{SiMe}_3)_2]$ ($\text{Eu}-\text{C}$ 2.605(6) and 2.612(7) Å)^[8] and the terphenyl derivative $\text{Eu}(\text{C}_6\text{H}_3\text{Ph}_2-2,6)_2(\text{thf})_2$ ($\text{Eu}-\text{C}$ 2.606(4) and 2.623(4) Å).^[9]

Synthesis and Solid-State Structure of Yttrium(III) Alkyl Compound $\text{Li}_3\text{Y}(\textit{i}\text{-Bu})_6(\text{thf})_4$. Although the protocol shown in Scheme 1 gave previously yttrium complex $\text{Li}_3\text{Y}(\textit{n}\text{-Bu})_6(\text{thf})_4$, crystals suitable for XRD analysis could only be obtained for the lutetium derivative. It was found that “larger” rare-earth-metal centers generated crystals with very poor diffraction behavior.^[5] In an effort to access a crystalline Li/Y derivative we switched from the *n*-butyl to the *i*-butyl ligand. Using the same reaction conditions (Scheme 2), $\text{YCl}_3(\text{thf})_2$ and six equivalents of *i*-BuLi gave a product showing intricate NMR spectra, but generating also a small amount of single-crystalline yttrium *i*-butyl complex $\text{Li}_3\text{Y}(\textit{i}\text{-Bu})_6(\text{thf})_4$ (**2**). Complex **2** is isostructural with the lutetium



Scheme 2. Synthesis of $\text{Li}_3\text{Y}(\textit{i}\text{-Bu})_6(\text{thf})_4$ (**2**) and its crystal structure, with atomic displacement ellipsoids set at 50% probability. Hydrogen atoms and disorders of the *i*-butyl groups, as well as the THF molecules, are omitted for clarity. Selected interatomic distances [Å] for **2**: Y1–C1 2.517(6), Y1–C5 2.7609(2), Y1–C9 2.7212(2), Y1–C13 2.506(5), Y1–C17 2.557(5), Y1–C21 2.546(5).

n-butyl complex $\text{Li}_3\text{Lu}(\textit{n}\text{-Bu})_6(\text{thf})_4$. Because of the larger ionic radius of yttrium(III) compared to lutetium, the $\text{Ln}-\text{C}$ distances are longer in compound **2** (2.506(5)–2.7609(2) Å versus (2.44(2)–2.58(3) Å). A closer examination of the $\text{Y}-\text{C}(\text{CH}_2)$ distances revealed that the triply bridging *n*-butyl ligands ($\text{Y}/2\text{Li}$) display considerably longer distances (2.7212(2) and 2.7609(2) Å) than the remaining four doubly bridging ones (2.506(5) to 2.557(5) Å). For comparison, the $\text{Y}-\text{C}$ distances in 6-coordinate $\text{Y}(\text{AlMe}_2)_3$ range from 2.505(6) to 2.514(8) Å^[10] while those in yttrium neosilyl complex $\text{Y}(\text{CH}_2\text{SiMe}_3)_3(\text{thf})_2$ range from 2.416 to 2.436 Å.^[11]

Furthermore, the solution behavior of compound **2** seems to be very similar to the *n*-butyl complexes in the sense that *i*-BuLi gets partly displaced, resulting in complex NMR spectra like the ^7Li NMR spectrum shown in Figure 1.

Reactivity of Yttrium(III) Alkyl Compound $\text{Li}_3\text{Y}(\textit{i}\text{-Bu})_6(\text{thf})_4$ toward Amines. We had previously shown that ate complexes of the type $\text{Li}_3\text{Ln}(\textit{n}\text{-Bu})_6(\text{thf})_4$ readily engage in neopentanol-mediated alcoholysis affording single-crystalline $\text{Li}_3\text{Ce}_2(\text{OCH}_2\text{tBu})_9(\text{HOCH}_2\textit{t}\text{-Bu})_2(\text{thf})$.^[5] To broaden the scope of such protonolysis reactions, we envisaged aminolysis and hence the conversion of less Brønsted-acidic substrate molecules. Of particular interest was the use of primary amines H_2NR , which might lead to imide complexes,^[12] when reacted with ate complexes $\text{Li}_3\text{Ln}(\textit{n}\text{-Bu})_6(\text{thf})_4$. It seemed plausible that the primary amine would initially form a rare-earth-metal amide complex $[\text{Ln}(\text{NHR})_3]$ via rapid protonolysis of three *n*-butyl ligands (liberating *n*-butane). Subsequently, the presence of extra “built-in” or (in solution) displaced *n*-BuLi might promote the second deprotonation and hence imide formation ($[\text{LiLn}(\text{NR})_2]$). It has been shown previously, that external bases like LiR or LiNR_2 can accomplish the ultimate deprotonation of a $[\text{Ln}-\text{NHR}]$ moiety, leading to metal-capping or bridging imido functionalities.^[13] More precisely, depending on the ratio $[\text{Yb}(\text{NHAr}^{\text{Pr}})_4\text{Na}(\text{thf})]/\textit{n}\text{-BuLi}$, Xie’s group could either access the mixed amido-imido-ytterbium complex $[\text{Yb}_2(\text{NHAr}^{\text{Pr}})_2(\text{NAr}^{\text{Pr}})_4\text{Li}_2\text{Na}_2(\text{thf})_4]$ or imide complex $[\text{Yb}_2(\text{NAr}^{\text{Pr}})_6\text{Li}_4\text{Na}_2(\text{thf})_4]$ ($\text{Ar}^{\text{Pr}} = \text{C}_6\text{H}_3\textit{i}\text{Pr}_2-2,6$).^[13c]

The aminolysis reactions were examined with yttrium complex $\text{Li}_3\text{Y}(\textit{n}\text{-Bu})_6(\text{thf})_4$, being accessible in decent yield^[5] and bearing the ^{89}Y nucleus as a favorable spectroscopic probe. In

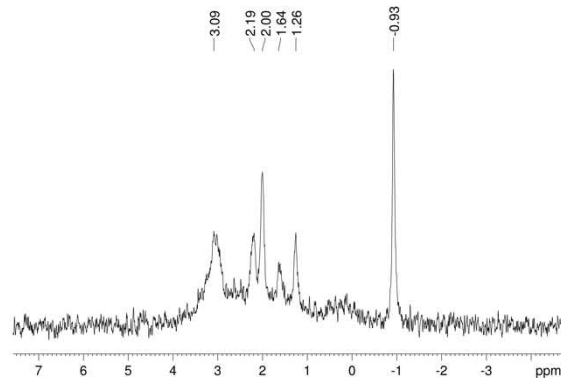
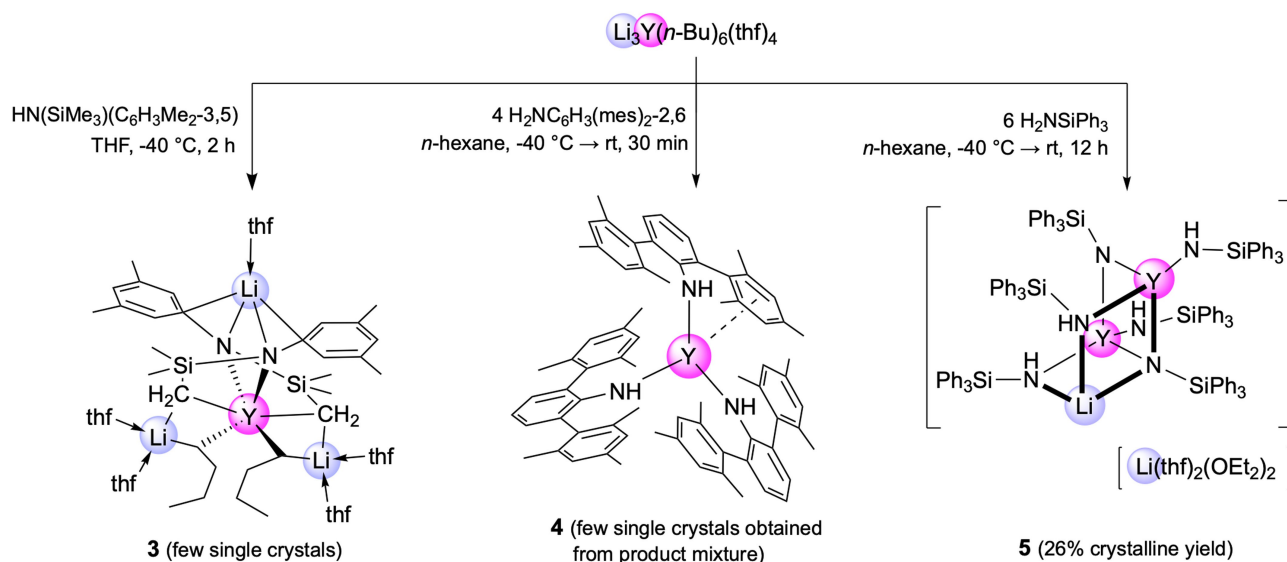


Figure 1. ^7Li NMR spectrum of complex **2** in toluene- d_8 at 298 K.

order to probe the general feasibility of aminolysis, we set out with the bulky secondary amine $\text{HN}(\text{SiMe}_3)(\text{C}_6\text{H}_3\text{Me}_2-3,5)$. Conducting an equimolar reaction led to the isolation of a small amount of single-crystalline $\text{Li}_3\text{Y}(\text{n-Bu})_2[\text{N}(\text{SiMe}_2\text{CH}_2)(\text{C}_6\text{H}_3\text{Me}_2-3,5)]_2(\text{thf})_5$ (**3**) (Scheme 3, Figure 2). Surprisingly, two amido ligands were incorporated into one $\text{Li}_3\text{Y}(\text{n-Bu})_6(\text{thf})_4$ molecule, despite the addition of only one equivalent of amine. Apparently, two *n*-butyl ligands afforded the deprotonation of the amine as envisaged, but two more *n*-butyl moieties

engaged into C–H-bond activation with the SiMe_3 substituents. The solid-state structure of **4** displays a six-coordinate yttrium center, bonded to two $\text{CH}_2(\text{n-butyl})$, two $\text{CH}_2(\text{silyl})$, and two amido nitrogen atoms. Two lithium atoms bridge the $\text{CH}_2(\text{n-butyl})$ and $\text{CH}_2(\text{silyl})$ groups, thus participating in two four-membered heterometallacycles. The coordination sphere of these lithium atoms is completed by two THF molecules each. The third lithium atom is 5-coordinated, bridging the two amido nitrogen atoms as well as the two *ipso*-carbon atoms of



Scheme 3. Synthesis of complexes **3**, **4**, and **5** from $\text{Li}_3\text{Y}(\text{n-Bu})_6(\text{thf})_4$ and various amines, using distinct reaction conditions.

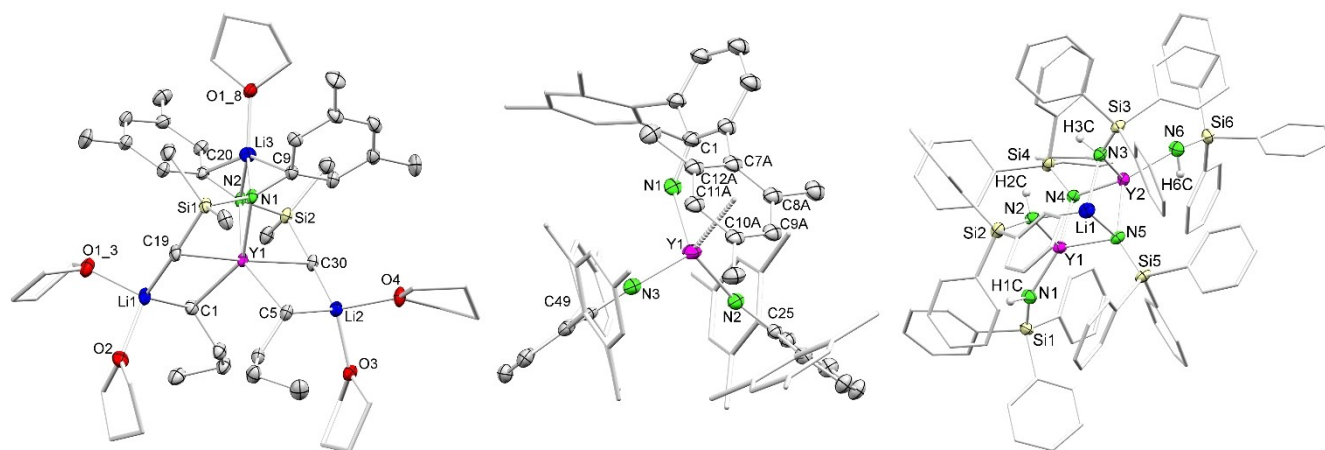


Figure 2. Left: crystal structure of $\text{Li}_3\text{Y}(\text{n-Bu})_2[\text{N}(\text{SiMe}_2\text{CH}_2)(\text{C}_6\text{H}_3\text{Me}_2-3,5)]_2(\text{thf})_5$ (**3**) with atomic displacement ellipsoids set at 30% probability. Hydrogen atoms, disorders of the *n*-Bu groups, and THF molecules are omitted for clarity. The THF carbon atoms are represented by a wireframe model for the sake of clarity. The unit cell contains two molecules of **3** and two lattice THF molecules. Selected interatomic distances [Å] and angles [°] for **3**: Y1–C1 2.512(5), Y1–C5 2.528(5), Y1–C19 2.632(5), Y1–C30 2.656(5), Y1–N1 2.414(4), Y1–N2 2.435(4), C19–Y1–C30 176.94(15), C1–Y1–N1 149.45(14). Middle: crystal structure of $[\text{Y}(\text{HNC}_6\text{H}_3(\text{mes})_2-2,6)_3]$ (**4**) with atomic displacement ellipsoids set at 30% probability. Hydrogen atoms and disorders of the amido ligands are omitted for clarity. Selected interatomic distances [Å] for **4**: Y1–N1 2.158(10), Y1–N2 2.218(3), Y1–N3 2.222(3), average Y1–(C7A–C12A) 2.735. Right: crystal structure of $[\text{Li}_2\text{Y}(\text{HNSiPh}_3)_4(\text{NSiPh}_3)_2][\text{Li}(\text{thf})_2(\text{OEt}_2)_2]$ (**5**) with atomic displacement ellipsoids set at 50% probability. The cationic fragment, hydrogen atoms, and disorders of the THF groups and one lattice Et_2O molecule are omitted for clarity. The carbon atoms of the phenyl rings are represented by a wireframe model for the sake of clarity. Selected interatomic distances [Å] for **5**: Y1–N1 2.252(3), Y1–N2 2.273(3), Y1–N4 2.165(3), Y1–N5 2.276(3), Y2–N3 2.295(3), Y2–N4 2.205(3), Y2–N5 2.233(3), Y2–N6 2.255(4).

the phenyl rings, while a THF molecule adds to the coordination sphere. The Y–CH₂(*n*-butyl) distances of 2.512(5) and 2.528(5) Å match those of the doubly bridging CH₂(*isobutyl*) in complex 2. The Y–CH₂(silyl) distances of 2.632(5) and 2.656(5) Å are comparatively longer than those of similar known Y–N–Si–CH₂ four-membered ring structures.^[14] This can be explained by the increased coordination of the yttrium center in 3 (CN=6) but also the formation of two fused 4-membered rings via bridging lithium atoms. The C–H-bond activation of Si–CH₃ groups however, is well known.^[14] The Y–N distances of 2.414(4) and Y1–N2 2.435(4) Å are in the range of 6-coordinate yttrium anilide complexes with Y–N–Li linkages (cf., 2.443(4) Å in [(NO)^{MeO}Li(thf)]₃ with linked aryloxy/anilido ligands).^[15] Unfortunately, complex 3 is thermally very unstable and the yield was extremely low. Only a few small crystals could be obtained upon several crystallization attempts, which, however, proved the feasibility of the aminolysis reactions envisaged.

Aiming at a putative yttrium imide complex, we first employed bulky 2,6-dimesitylaniline as a primary amine. While the treatment of Li₃Y(*n*-Bu)₆(thf)₄ with one to three equivalents of amine did not yield any isolable yttrium-containing product, the 4-equivalent reaction gave homoleptic complex Y-[HNC₆H₃(mes)₂-2,6]₃ (4). All these transformations have in common the formation of the respective lithium anilide as indicated by NMR spectroscopy. While complex 4 is easily accessible and could be an interesting precursor (e.g., for subsequent deprotonation reactions), the separation from the lithium salt side product so far proved unsuccessful. Neither fractional crystallization nor sublimation (decomposition occurred at around 90 °C/10^{−3} mbar) was effective for the purification of 4. The ⁸⁹Y NMR chemical shift of complex 4 was detected at 425.0 ppm (¹H–⁸⁹Y HSQC, 298 K, C₆D₆), considerably shifted to higher field compared to the 570.0 ppm of homoleptic Y[N(SiMe₃)₂]₃ (296 K, CDCl₃).^[16] An XRD analysis of complex 4 revealed a monomeric molecular structure featuring an η⁶-arene interaction of one of the ortho mesityl substituents. Interestingly, the adjacent nitrogen (N1) seems to form a closer contact to the yttrium center (2.158(10) than those of the other anilido ligands (2.218(3) and 2.222(3) Å). For comparison, complex [Y(μ-NHC₆H₃/Pr₂-2,6)(NHC₆H₃/Pr₂-2,6)]₂ also shows such η⁶-arene interactions, but to the adjacent yttrium center each.^[17] The Y–N distances are similar to those of the terminal amido ligands in NaY(NiPr₂)₂(μ-NiPr₂-2,6)₂(thf)₂ (2.228(2) and 2.230(2) Å), with a formally 4-coordinate yttrium center.^[18] The structure of 4 is fluxional in solution since only one signal set was observed in the ¹H NMR spectrum for the mesityl moieties.

Finally, ate complex Li₃Y(*n*-Bu)₆(thf)₄ was treated with six equivalents of the primary silylamine H₂NSiPh₃ to afford the mixed amido/imido complex [LiY₂(HNSiPh₃)₄(NSiPh₃)₂][Li(thf)₂(OEt)₂] (5). The anionic part of the molecular structure of 5 features a cuboid core with one corner cut off. The “cube corners” are occupied by two yttrium, one lithium, and four nitrogen atoms. There are two distinct imido coordination modes, one imido moiety bridging the two yttrium atoms (Y–N–Y) and the other connecting additionally to the lithium atom (Y₂–N–Li). The two amido nitrogen atoms participating in the core structure form metal-amido-metal linkages (Y–N–Li)

exclusively. Both yttrium centers are 4-coordinated and bear one additional terminal amido ligand each. In agreement with the solid-state structure, the ¹H–⁸⁹Y HSQC NMR spectrum of complex 5 revealed a single signal for both yttrium centers at 652.8 ppm (298 K, C₆D₆). Previously, ⁸⁹Y NMR chemical shifts of heteroleptic imide complexes were detected in the range of 216.5 to 467.8 ppm.^[19] The core lithium atom is only bonded to three nitrogen atoms, while the lithium counter ion is coordinated to two THF and two diethyl ether molecules. The terminal Y–N(amido) distances are slightly shorter than the bridging ones (2.252(3) and 2.255(4) Å versus 2.273(3) and 2.295(3) Å). These distances are in the range of other 4-coordinate yttrium amide complexes.^[18,20] Not unexpectedly, the Y–N(imido) distances are different reflecting the μ₂ (Y–N4: 2.165(3) and 2.205(3) Å) and μ₃ imido sites (Y–N5: 2.276(3) and 2.233(3) Å). Overall, the Y–N(imido) distances are in the range of literature known complexes ([Cp*Y(μ₂-NC₆H₃(CF₃)₂-3,5)(thf)₂]₂: 2.222(4)–2.304(4) Å).^[19e]

Conclusions

Applying seamless low-temperature syntheses and crystallization techniques we could structurally authenticate complex Li₆Eu(*n*-Bu)₈(thf)₆ featuring the first lanthanide(III) complex with *n*-butyl ligands. Using the same methodology the molecular structure of the first rare-earth-metal isobutyl complex Li₃Y(*i*-Bu)₆(thf)₄ could be identified, being isostructural to the *n*-butyl complex Li₃Lu(*n*-Bu)₆(thf)₄. Although aminolysis reactions of the *n*-butyl compound Li₃Y(*n*-Bu)₆(thf)₄ proved hard to control, crystallographic analyses provided valuable insights into the reactivity of such ate complexes. The reaction with secondary amine HN(SiMe₃)(C₆H₃Me₂-3,5) afforded protonolysis but also indicated the propensity of the trimethylsilyl moieties to engage in C–H-bond activation forming metallacycles as evidenced for Li₃Y(*n*-Bu)₂[N(SiMe₂CH₂)(C₆H₃-Me₂-3,5)]₂(thf)₅. Treatment of Li₃Y(*n*-Bu)₆(thf)₄ with primary amines, 2,6-dimesitylaniline and triphenylsilylamine, revealed distinct reaction pathways. In the former case, homoleptic complex Y[HNC₆H₃(mes)₂-2,6]₃ seems the preferred product defying further deprotonation, most likely due to steric restraints. Imide formation, however, is viable in the latter case as proven for the isolation of mixed imido/amido complex [LiY₂(HNSiPh₃)₄(NSiPh₃)₂][Li(thf)₂(OEt)₂]. Though ate complexes of the type Li₃Ln(*n*-Bu)₆(thf)₄ can give access to rare-earth-metal imides, the intricacy of the involved protonolysis reactions is evident. For example, not fully displaced *n*-butyl ligands might engage in undesired reaction pathways and/or lead to thermally unstable products. Moreover, displaced “*n*-BuLi” can result in unwanted side reactions (inseparable co-products) as well as the incorporation of lithium into the rare-earth-metal containing product.

Experimental Section

General procedures

All manipulations were performed under an argon atmosphere using either glovebox (MBraun UNILab^{pro}; <0.1 ppm O₂, <0.1 ppm H₂O) or standard Schlenk techniques with oven-dried glassware. The solvents were purified with Grubbs-type columns (MBraun SPS, solvent purification system) and stored in a glovebox. Anhydrous europium(III) chloride (99.9%) and anhydrous yttrium(III) chloride (99.9%), were purchased from *abcr* and activated by Soxhlet extraction with THF giving EuCl₃(thf)₂ and YCl₃(thf)₂, respectively. *n*-Butyllithium (*n*-BuLi) (2.5 M solution in hexanes), *iso*-butyllithium (*i*-BuLi) (1.7 M solution in heptane), HN(SiMe₃)(C₆H₃Me₂-3,5), H₂NC₆H₃(C₆H₂Me₃-2,4,6)₂-2,6 (=H₂NC₆H₃(mes)₂-2,6), and H₂NSiPh₃ were purchased from *Sigma Aldrich* and used as received. Benzene-*d*₆, toluene-*d*₈, and THF-*d*₈ were purchased from *Sigma Aldrich*, degassed, dried over NaK alloy for 24 h, filtered, and stored inside a glovebox. NMR spectra of moisture-sensitive compounds were recorded by using J. Young-valved NMR tubes on either a Bruker AVII + 400 (1H: 400.13 MHz), or a Bruker AVIIHD (1H: 300.13 MHz), or a Bruker AVII + 500 (1H: 500.13 MHz). 1H NMR shifts are referenced to a solvent resonance and reported in parts per million (ppm) relative to tetramethylsilane.^[22] Analysis of the NMR spectra was performed with TopSpin 3.6.1 [Academic License].^[23] Multiplicities of signals are given as s (singlet), bs (broad singlet), d (doublet), and dd (doublet of doublets). Coupling constants (J) are given in Hz. Signals were assigned via 2D NMR experiments. Elemental analysis (C, H, N) was performed on an *Elementar vario MICRO cube*. Crystals suitable for XRD analysis were grown by standard techniques from solutions using *n*-hexane (1, 2), *n*-hexane/toluene (3, 4) and diethyl ether for 5 at -40 °C. Single crystals were handpicked in a glovebox, coated with Parabar 10312 (previously known as Paratone N, Hampton Research/performance vacuum oil, Edwards) or perfluorinated oil, and stored on microscope slides and fixed on a microloop. It is essential to keep the compounds (1, 2, 3) at low temperature from crystallization up to mounting the crystals on the diffractometer, including data collection. Compound 3 co-crystallized with THF, the relatively high vapor pressure of which allowed its diffusion out of the crystal lattice. This is likely the reason for the bad quality of the diffraction data. X-ray data were collected on a Bruker APEX II DUO diffractometer equipped with an μ S microfocus sealed tube and QUAZAR optics for MoK α (λ = 0.71073 Å) and CuK α (λ = 1.54184 Å) radiation. The data collection strategy was determined using COSMO^[24] employing ω -scans. Raw data were processed using APEX^[25] and SAINT,^[26] corrections for absorption effects were applied using SADABS.^[27] The structures were solved by direct methods and refined against all data by full-matrix least-squares methods on F² using SHELXTL^[28] and ShelXle.^[29] Disorder models were calculated using DSR, a program for refining structures in ShelXl.^[30] All graphics were produced employing Mercury 4.2.0^[31] and POV-Ray.^[32]

Li₃Eu(*n*-Bu)₆(thf)₆ (1). EuCl₃(thf)₂ (80.3 mg, 0.2 mmol) was suspended in a mixture of *n*-hexane (1 mL) and THF (0.4 mL), and *n*-BuLi (2.5 M in hexanes, 480.0 μ L, 1.2 mmol) was added dropwise at -40 °C. The mixture was stirred for 30 min at -40 °C, then filtered, and the solvent evaporated in vacuo at -40 °C. The residue was extracted with cold *n*-hexane (~8 mL) and the extract was filtered again. The solution was slowly concentrated under reduced pressure at -40 °C and stored at -40 °C for crystallization giving compound 1 in 18% yield. NMR spectra were not attempted because of the paramagnetism of europium(II). Due to the temperature sensitivity, meaningful microanalytical data could not be obtained.

Li₃Y(*i*-Bu)₆(thf)₄ (2). YCl₃(thf)₂ (69.3 mg, 0.2 mmol) was suspended in a mixture of *n*-hexane (1 mL) and THF (0.4 mL), and *i*-BuLi (1.7 M in heptane, 700.0 μ L, 1.2 mmol) was added dropwise at -40 °C. The mixture was stirred for 30 min at -40 °C, then filtered, and the solvent evaporated in vacuo at -40 °C. The residue was extracted with cold *n*-hexane (~8 mL) and the extract was filtered again. The solution was slowly concentrated under reduced pressure at -40 °C and stored at -40 °C for crystallization affording 2 in low yield. Due to their complexity, the NMR spectra were inconclusive and could not be assigned. Partial separation of *i*-BuLi from the complex in solution was indicated. The raw NMR spectra are displayed in the supporting information. Due to the temperature sensitivity, meaningful microanalytical data could not be obtained.

Li₃Y(*n*-Bu)₂[N(SiMe₂CH₂)(C₆H₃Me₂-3,5)]₂(thf)₅ (3). Li₃Y(*n*-Bu)₆(thf)₄ (44.3 mg, 0.06 mmol) was dissolved in THF (2 mL) at -40 °C. Then HN(SiMe₃)(C₆H₃Me₂-3,5) (11.6 mg, 0.06 mmol) dissolved and pre-cooled in THF was added dropwise. After 2 h the solvent was removed in vacuo. The crude product was extracted with *n*-hexane, filtered, and concentrated in vacuo to give 3 as colorless crystals in very low yield. Due to the extremely low (crystalline) yield, NMR spectroscopic studies could not be conducted. Moreover, the pronounced thermal instability of the product impeded any further analyses.

Y[HNC₆H₃(mes)₂-2,6]₃ (4). Li₃Y(*n*-Bu)₆(thf)₄ (16.7 mg, 0.02 mmol) was dissolved in *n*-hexane (2 mL) at -40 °C. Then H₂NC₆H₃(mes)₂-2,6 (29.7 mg, 0.09 mmol, 4 equiv) dissolved and pre-cooled in *n*-hexane was added dropwise. The mixture was then allowed to warm to ambient temperature. After 30 min the mixture was concentrated in vacuo to give 4 as green crystals in low yield. 1H NMR (500.13 MHz, 298 K, C₆D₆): δ = 6.81 (s, 4 H, CH₃-Mes), 6.81 (s, 12 H, aryl-*H*-Mes), 6.68 (s, 9 H, phenyl *H*), 3.71 (s, 3 H, NH), 2.19 (s, 36 H, CH₃-Mes), 1.97 ppm (s, 18 H, CH₃-Mes). 13C NMR (125.76 MHz, 298 K, C₆D₆): δ = 153.4 (tertiary C), 140.0 (tertiary C), 137.9 (tertiary C), 137.2 (tertiary C), 129.8 (aryl-C-Mes), 129.6 (phenyl C), 126.8 (tertiary C), 115.2 (phenyl C), 21.0 (CH₃-Mes), 20.6 ppm (CH₃-Mes). 89Y NMR (24.5 MHz, 298 K, C₆D₆): δ = 425.0 ppm. Since the product could not be separated from the side product LiHNC₆H₃(mes)₂-2,6 in a reproducible way, the best obtained microanalytical data are given: elemental analysis calcd (%) for C₇₂H₇₈N₃Y: C 80.49, H 7.32, N 3.91; found: C 79.37, H 7.54, N 3.56.

[LiY₂(HNSiPh₃)₄(NSiPh₃)₂][Li(thf)₂(OEt₂)₂] (5). Li₃Y(*n*-Bu)₆(thf)₄ (69.5 mg, 0.09 mmol) was dissolved in *n*-hexane (2 mL) at -40 °C. Then, H₂NSiPh₃ (155.0 mg, 0.56 mmol) dissolved and pre-cooled in *n*-hexane was added dropwise. After 12 h the solvent was removed in vacuo. The crude product was extracted with Et₂O, filtered, and concentrated in vacuo to give [LiY₂(HNSiPh₃)₄(NSiPh₃)₂][Li(thf)₂(OEt₂)₂] as colorless crystals in 26% yield. 1H NMR (500.13 MHz, 298 K, C₆D₆): δ = 0.74 ppm (s, 4 H, NH). 7Li NMR (194.4 MHz, 298 K, C₆D₆): δ = 1.58, 0.72 ppm. 89Y NMR (24.5 MHz, 298 K, C₆D₆): δ = 652.8 ppm. Due to issues of signal overlap, the phenyl resonances could not be assigned. The THF and Et₂O signals overlap with Et₂O solvent impurities. elemental analysis calcd (%) for C₁₂₈H₁₄₀N₆Li₂O₅Si₆Y₂: C 69.79, H 6.41, N 3.82; found: C 73.86, H 6.92, N 3.93. Although these results are outside the range viewed as establishing analytical purity, they are provided to illustrate the best values obtained to date.

Acknowledgements

Open Access funding enabled and organized by Projekt DEAL.

Conflict of Interest

The authors declare no conflict of interest.

Data Availability Statement

The data that support the findings of this study are available in the supplementary material of this article.

Keywords: Amide · Butyl · Europium · Lithium · Yttrium

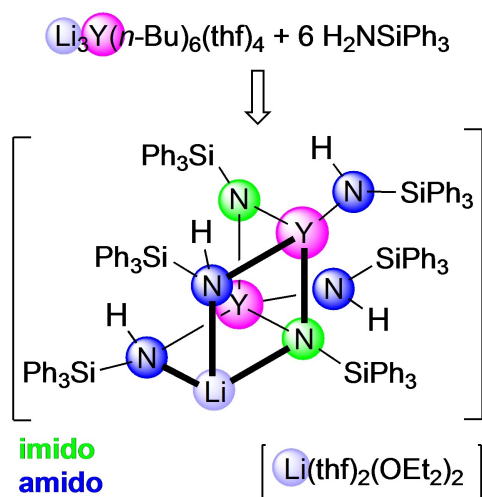
- [1] a) T. Imamoto, T. Kusumoto, Y. Hatanaka, M. Yokoyama, *Tetrahedron Lett.* **1982**, 23, 1353–1356; b) B. M. Trost, I. Fleming, *T. Imamoto in Comprehensive organic synthesis*, Eds., Pergamon, Oxford, **1991**, Chapter 1.8.
- [2] a) T. Imamoto, T. Kusumoto, M. Yokoyama, *J. Chem. Soc. Chem. Commun.* **1982**, 1042–1044; b) T. Imamoto, T. Kusumoto, Y. Tawarayama, Y. Sugiura, T. Mita, Y. Hatanaka, M. Yokoyama, *J. Org. Chem.* **1984**, 49, 3904–3912; c) T. Imamoto, Y. Sugiura, *J. Organomet. Chem.* **1985**, 285, C21–C23; d) T. Imamoto, Y. Sugiura, N. Takiyama, *Tetrahedron Lett.* **1984**, 25, 4233–4236; e) T. Imamoto, N. Takiyama, K. Nakamura, T. Hatajima, Y. Kamiya, *J. Am. Chem. Soc.* **1989**, 111, 4392–4398.
- [3] a) W. J. Evans, J. D. Feldman, J. W. Ziller, *J. Am. Chem. Soc.* **1996**, 118, 4581–4584; b) W. J. Evans, M. A. Ansari, J. D. Feldman, R. J. Doedens, J. W. Ziller, *J. Organomet. Chem.* **1997**, 545–546, 157–162; c) V. Dimitrov, K. Kostova, M. Genov, *Tetrahedron Lett.* **1996**, 37, 6787–6790; d) N. Greeves, L. Lyford, *Tetrahedron Lett.* **1992**, 33, 4759–4760; e) N. Greeves, L. Lyford, J. E. Pease, *Tetrahedron Lett.* **1994**, 35, 285–288.
- [4] M. Zimmermann, R. Anwender, *Chem. Rev.* **2010**, 110, 6194–6259.
- [5] T. Berger, J. Lebon, C. Maichle-Mössmer, R. Anwender, *Angew. Chem. Int. Ed.* **2021**, 60, 15622–15631; *Angew. Chem.* **2021**, 133, 15750–15760.
- [6] H. Schumann, J. Mueller, N. Bruncks, H. Lauke, J. Pickardt, H. Schwarz, K. Eckart, *Organometallics* **1984**, 3, 69–74.
- [7] G. Occhipinti, C. Meermann, H. M. Dietrich, R. Litlabø, F. Auras, K. W. Törnroos, C. Maichle-Mössmer, V. R. Jensen, R. Anwender, *J. Am. Chem. Soc.* **2011**, 133, 6323–6337.
- [8] C. Eaborn, P. B. Hitchcock, K. Izod, Z.-R. Lu, J. D. Smith, *Organometallics* **1996**, 15, 4783–4790.
- [9] G. Heckmann, M. Niemeyer, *J. Am. Chem. Soc.* **2000**, 122, 4227–4228.
- [10] W. J. Evans, R. Anwender, J. W. Ziller, *Organometallics* **1995**, 14, 1107–1109.
- [11] W. J. Evans, J. C. Brady, J. W. Ziller, *J. Am. Chem. Soc.* **2001**, 123, 7711–7712.
- [12] D. Schädle, R. Anwender, *Chem. Soc. Rev.* **2019**, 48, 5752–5805.
- [13] For examples, see: a) W. J. Evans, M. A. Ansari, J. W. Ziller, S. I. Khan, *Inorg. Chem.* **1996**, 35, 5435–5444; b) J. C. Gordon, G. R. Giesbrecht, D. L. Clark, P. J. Hay, D. W. Keogh, R. Poli, B. L. Scott, J. G. Watkin, *Organometallics* **2002**, 21, 4726–4734; c) H.-S. Chan, H.-W. Li, Z. Xie, *Chem. Commun.* **2002**, 652–653; d) L. A. Solola, A. V. Zabula, W. L. Dorfner, B. C. Manor, P. J. Carroll, E. J. Schelter, *J. Am. Chem. Soc.* **2016**, 138, 6928–6931.
- [14] For examples, see: a) M. Karl, K. Harms, G. Seybert, W. Massa, S. Fau, G. Frenking, K. Dehnicke, *Z. Anorg. Allg. Chem.* **1999**, 625, 2055–2063; b) M. Niemeyer, *Inorg. Chem.* **2006**, 45, 9085–9095; c) F. Ortu, M. Gregson, A. J. Wooles, D. P. Mills, S. T. Liddle, *Organometallics* **2017**, 36, 4584–4590; d) R. Thim, C. Maichle-Mössmer, R. Anwender, *Organometallics* **2018**, 37, 2563–2570.
- [15] J. Qiu, M. Lu, Y. Yao, Y. Zhang, Y. Wang, Q. Shen, *Dalton Trans.* **2013**, 42, 10179–10189.
- [16] R. E. White, T. P. Hanusa, *Organometallics* **2006**, 25, 5621–5630.
- [17] W. J. Evans, M. A. Ansari, J. W. Ziller, S. I. Khan, *Inorg. Chem.* **1996**, 35, 5435–5444.
- [18] T. Spallek, O. Heß, M. Meermann-Zimmermann, C. Meermann, M. G. Klimpel, F. Estler, D. Schneider, W. Scherer, M. Tafipolsky, K. W. Törnroos, C. Maichle-Mössmer, P. Sirsch, R. Anwender, *Dalton Trans.* **2016**, 45, 13750–13765.
- [19] a) D. Schädle, C. Schädle, K. W. Törnroos, R. Anwender, *Organometallics* **2012**, 31, 5101–5107; b) C. Schädle, D. Schädle, K. Eichele, R. Anwender, *Angew. Chem. Int. Ed.* **2013**, 52, 13238–13242; *Angew. Chem.* **2013**, 125, 13480–13484; c) D. Schädle, C. Maichle-Mössmer, C. Schädle, R. Anwender, *Chem. Eur. J.* **2015**, 21, 662–670; d) D. Schädle, C. Schädle, D. Schneider, C. Maichle-Mössmer, R. Anwender, *Organometallics* **2015**, 34, 4994–5008; e) R. Thim, H. M. Dietrich, M. Bonath, C. Maichle-Mössmer, R. Anwender, *Organometallics* **2018**, 37, 2769–2777.
- [20] B. Liu, D. Cui, J. Ma, X. Chen, X. Jing, *Chem. Eur. J.* **2007**, 13, 834–845.
- [21] For examples, see: a) D. Cui, M. Nishiura, Z. Hou, *Angew. Chem. Int. Ed.* **2005**, 44, 959–962; *Angew. Chem.* **2005**, 117, 981–984.
- [22] G. R. Fulmer, A. J. M. Miller, N. H. Sherden, H. E. Gottlieb, A. Nudelman, B. M. Stoltz, J. E. Bercaw, K. I. Goldberg, *Organometallics* **2010**, 29, 2176–2179.
- [23] *TopSpin v. 3.6.1, Bruker AXS Inc., Madison, WI 2018.*
- [24] *COSMO v. 1.61, Bruker AXS Inc., Madison, WI 2012.*
- [25] *APEX 3 v. 2017.3-0, Bruker AXS Inc., Madison, WI 2017.*
- [26] *SAINT v. 8.38 A, Bruker AXS Inc., Madison, WI 2017.*
- [27] L. Krause, R. Herbst-Irmer, G. M. Sheldrick, D. Stalke, *J. Appl. Crystallogr.* **2015**, 48, 3–10.
- [28] G. Sheldrick, *Acta Crystallogr. Sect. C.* **2015**, 71, 3–8.
- [29] C. B. Hübschle, G. M. Sheldrick, B. Dittrich, *J. Appl. Crystallogr.* **2011**, 44, 1281–1284.
- [30] D. Kratzert, J. J. Holstein, I. Krossing, *J. Appl. Crystallogr.* **2015**, 48, 933–938.
- [31] C. F. Macrae, P. R. Edgington, P. McCabe, E. Pidcock, G. P. Shields, R. Taylor, M. Towler, J. van de Streek, *J. Appl. Crystallogr.* **2006**, 39, 453–457.
- [32] *POV-Ray v.3.6, Persistence of Vision Pty. Ltd., POV-Ray Williams-town, Victoria, Australia, http://www.povray.org 2004.*

Manuscript received: August 11, 2022

Revised manuscript received: September 12, 2022

Accepted manuscript online: September 19, 2022

RESEARCH ARTICLE



T. Berger, D. Baschnagel, Dr. C.
Maichle-Mössmer, Prof. Dr. R.
Anwander*

1 – 7

Aminolysis of Lithium/Yttrium Bi-
metallic Alkyls including the
Solid-State Structure of a
Europium(II) *n*-Butyl Compound



Zeitschrift für anorganische und allgemeine Chemie

Supporting Information

Aminolysis of Lithium/Yttrium Bimetallic Alkyls including the Solid-State Structure of a Europium(II) *n*-Butyl Compound

Tassilo Berger, David Baschnagel, Cäcilia Maichle-Mössmer, and Reiner Anwander*

Aminolysis of Lithium/Yttrium Bimetallic Alkyls including the Solid-State Structure of a Europium(II) *n*-Butyl Compound

Tassilo Berger, David Baschnagel, Cécilia Maichle-Mössmer, and Reiner Anwander*^[a]

Table of contents

¹ H NMR spectrum of Li ₃ Y(<i>i</i> -Bu) ₆ (thf) ₄ (2)	S2
⁷ Li NMR spectrum of Li ₃ Y(<i>i</i> -Bu) ₆ (thf) ₄ (2)	S2
¹ H NMR spectrum of Y[HNC ₆ H ₃ (mes) _{2-2,6}] ₃ (4)	S3
¹³ C NMR spectrum of Y[HNC ₆ H ₃ (mes) _{2-2,6}] ₃ (4)	S3
¹ H– ⁸⁹ Y HSQC NMR spectrum of Y[HNC ₆ H ₃ (mes) _{2-2,6}] ₃ (4)	S4
¹ H NMR spectrum of [LiY ₂ (HNSiPh ₃) ₄ (NSiPh ₃) ₂][Li(thf) ₂ (OEt ₂) ₂] (5)	S4
⁷ Li NMR spectrum of [LiY ₂ (HNSiPh ₃) ₄ (NSiPh ₃) ₂][Li(thf) ₂ (OEt ₂) ₂] (5)	S5
¹ H– ⁸⁹ Y HSQC NMR spectrum of [LiY ₂ (HNSiPh ₃) ₄ (NSiPh ₃) ₂][Li(thf) ₂ (OEt ₂) ₂] (5)	S5
X-ray crystallographic parameters for complex 1 , 2 and 3	S6
X-ray crystallographic parameters for complex 4 and 5	S7
Crystal structure of Li ₆ Eu(<i>n</i> -Bu) ₈ (thf) ₆ (1)	S8
Crystal structure of Li ₃ Y(<i>i</i> -Bu) ₆ (thf) ₄ (2)	S9
Crystal structure of Li ₃ Y(<i>n</i> -Bu) ₂ [N(SiMe ₂ CH ₂)C ₆ H ₃ -Me ₂ -3,5] ₂ (thf) ₅ (3)	S11
Crystal structure of Y[HNC ₆ H ₃ (mes) _{2-2,6}] ₃ (4)	S10
Crystal structure of [LiY ₂ (HNSiPh ₃) ₄ (NSiPh ₃) ₂][Li(thf) ₂ (OEt ₂) ₂] (5)	S12

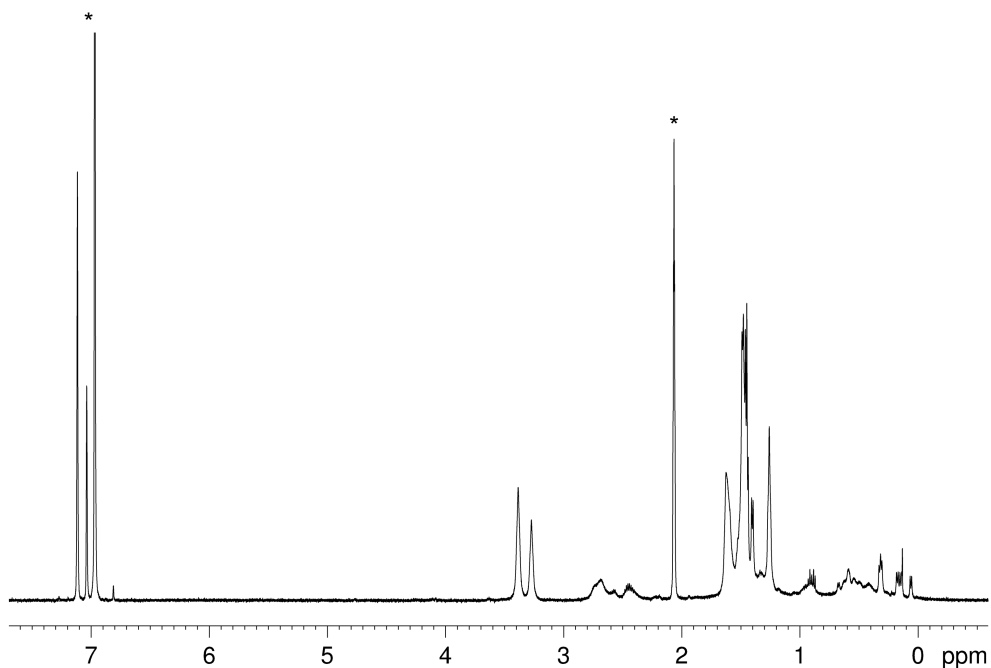


Figure S1. ^1H NMR spectrum of $\text{Li}_3\text{Y}(\textit{i}\text{-Bu})_6(\text{thf})_4$ (**2**) (500.13 MHz, $\text{toluene-}d_8$, 233 K) solvent signals are marked with*. Because of the complexity resulting from the dissociation of complex **2** in solution an assignment of the signals was not possible.

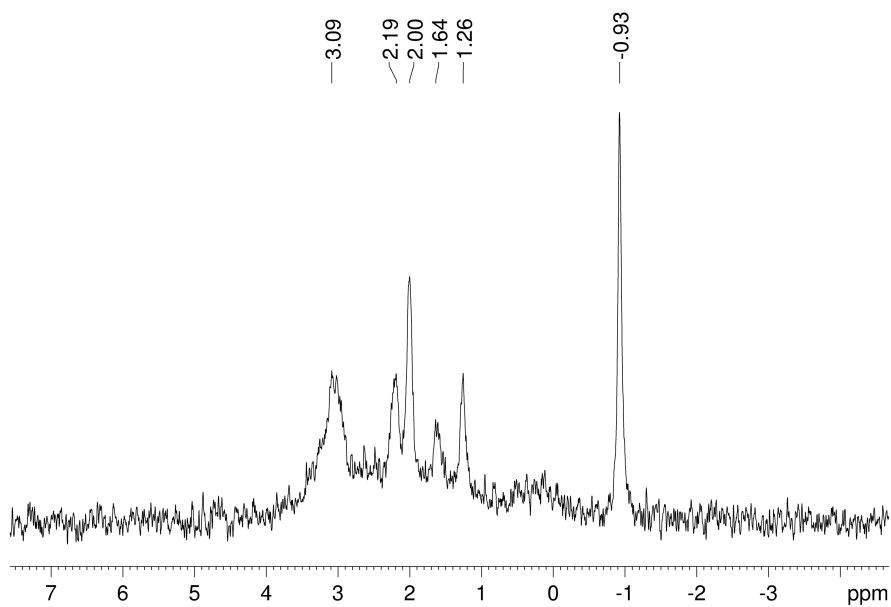


Figure S2. ^7Li NMR spectrum of $\text{Li}_3\text{Y}(\textit{i}\text{-Bu})_6(\text{thf})_4$ (**2**) (194.4 MHz, $\text{toluene-}d_8$, 233 K). Because of the complexity resulting from the dissociation of complex **2** in solution an assignment of the signals was not possible.

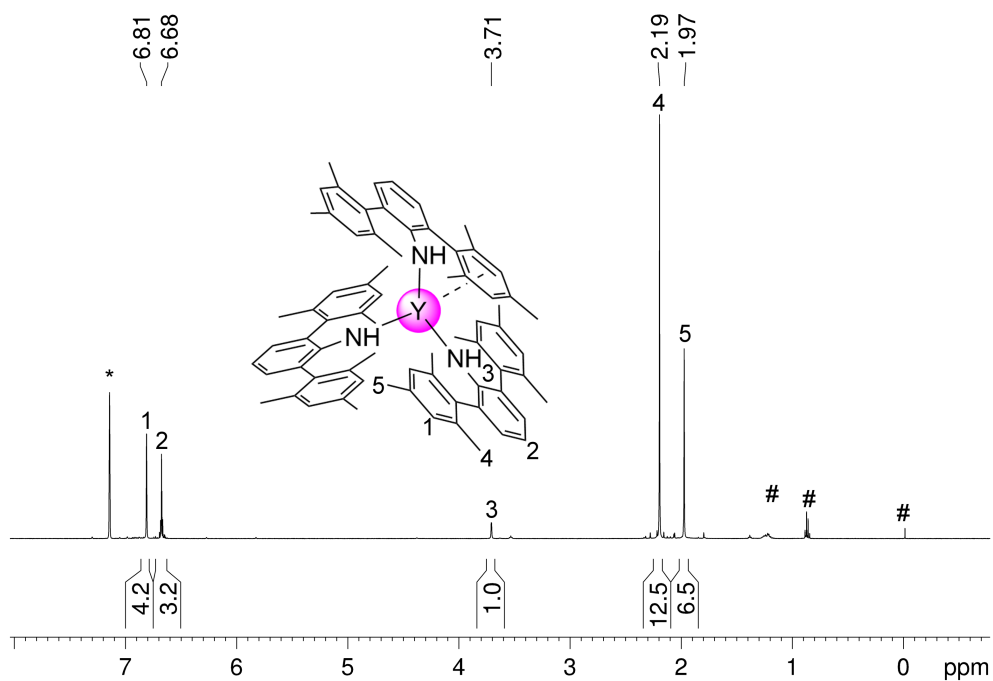


Figure S3. ¹H NMR spectrum of Y[HNC₆H₃(mes)₂-2,6]₃ (**4**) (500.13 MHz, C₆D₆, 298 K) solvent signals are marked with*. TMS and *n*-hexane impurities are marked with #.

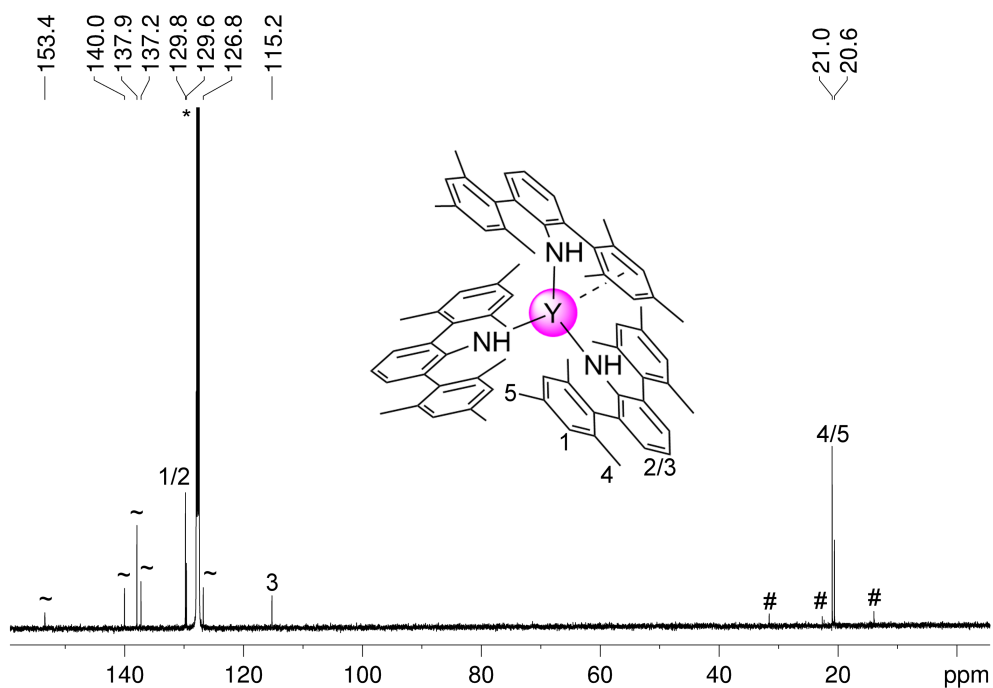


Figure S4. ¹³C NMR spectrum of Y[HNC₆H₃(mes)₂-2,6]₃ (**4**) (125.76 MHz, C₆D₆, 298 K) solvent signals are marked with*. TMS and *n*-hexane impurities are marked with #. The tertiary carbons are marked with ~.

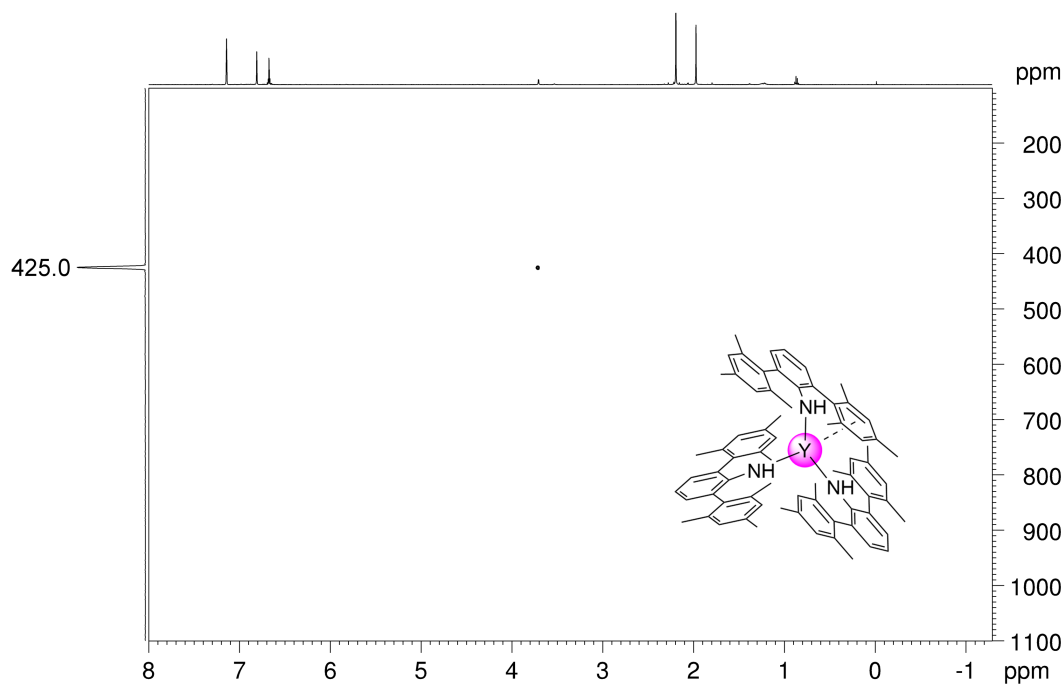


Figure S5. ^1H - ^{89}Y HSQC NMR spectrum of $\text{Y}[\text{HNC}_6\text{H}_3(\text{mes})_2-2,6]_3$ (**4**) (24.5 MHz, C_6D_6 , 298 K).

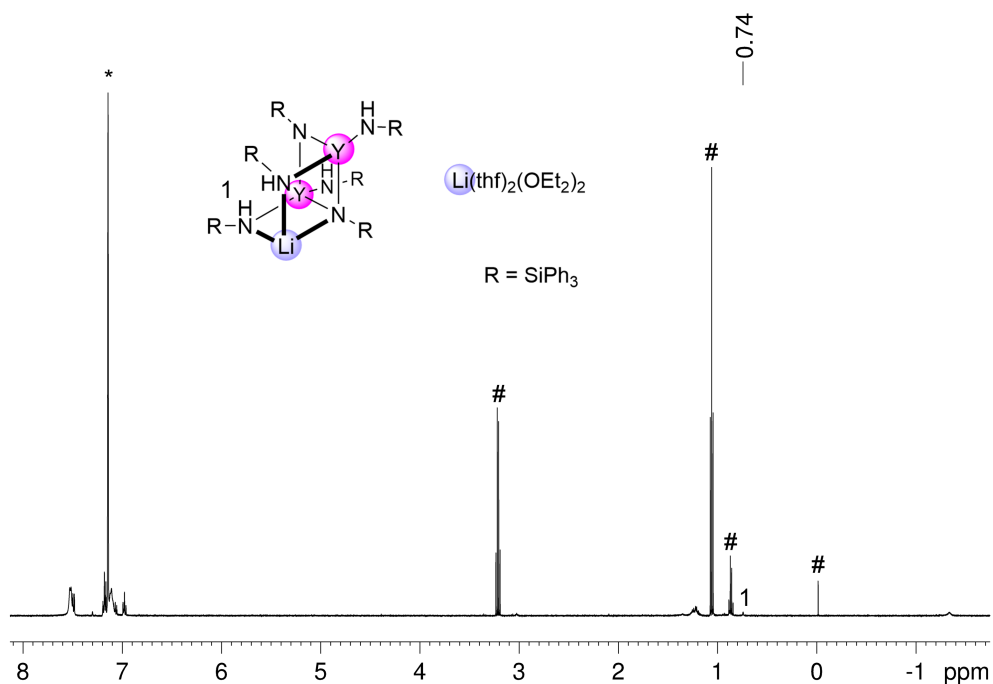


Figure S6. ^1H NMR spectrum of $[\text{LiY}_2(\text{HNSiPh}_3)_4(\text{NSiPh}_3)_2][\text{Li}(\text{thf})_2(\text{OEt})_2]$ (**5**) (500.13 MHz, C_6D_6 , 298 K), solvent signals are marked with*. TMS, Et_2O and n -hexane impurities are marked with #. The Phenyl signals could not be assigned due to sheer amount of them and the Et_2O and THF signals overlap with the impurities.

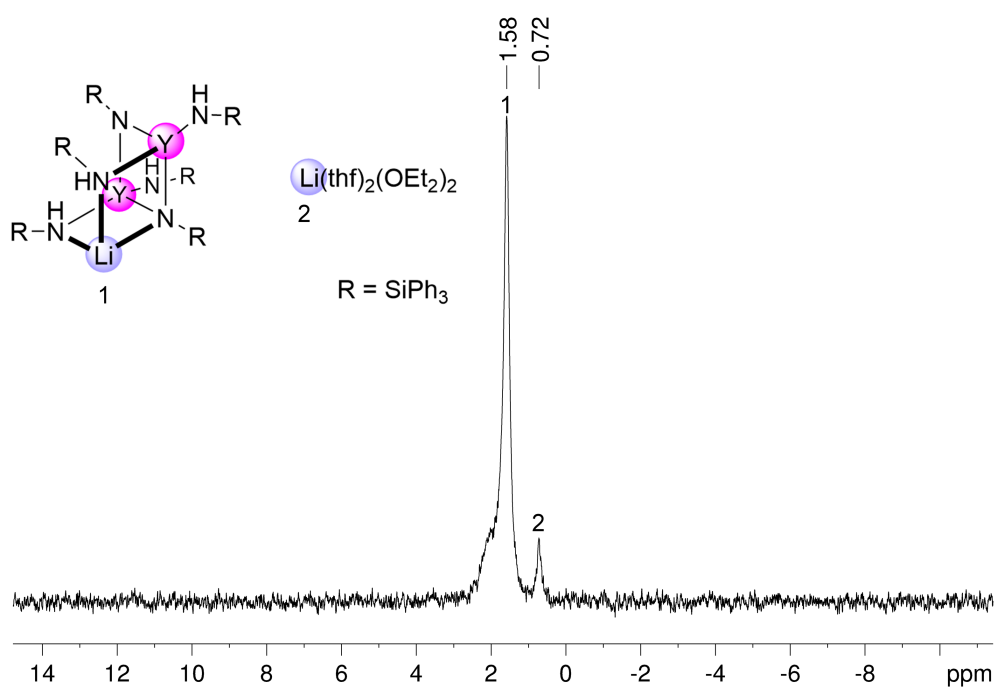


Figure S7. ^7Li NMR spectrum of $[\text{LiY}_2(\text{HNSiPh}_3)_4(\text{NSiPh}_3)_2][\text{Li}(\text{thf})_2(\text{OEt})_2]$ (**5**) (194.4 MHz, C_6D_6 , 298 K).

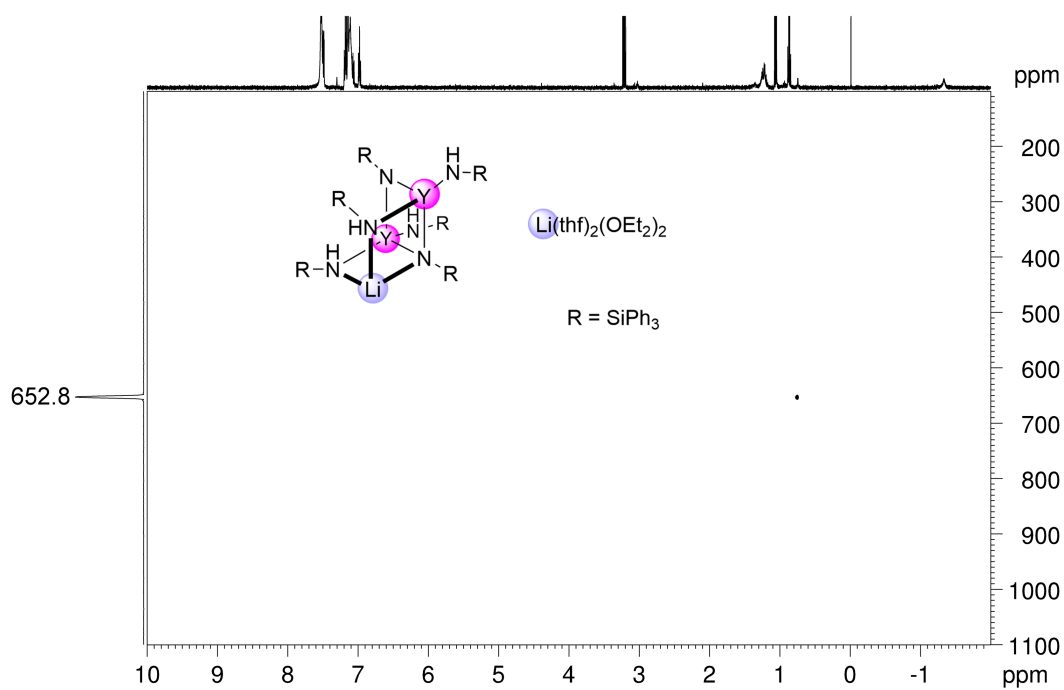


Figure S8. ^1H - ^{89}Y HSQC NMR spectrum of $[\text{LiY}_2(\text{HNSiPh}_3)_4(\text{NSiPh}_3)_2][\text{Li}(\text{thf})_2(\text{OEt})_2]$ (**5**) (24.5 MHz, C_6D_6 , 298 K).

Table S1. X-ray crystallographic parameters for complex **1**, **2**, and **3**

Compound	$\text{Li}_6\text{Eu}(n\text{-Bu})_8(\text{thf})_6$	$\text{Li}_3\text{Y}(i\text{-Bu})_6(\text{thf})_4$	$\text{Li}_3\text{Y}(n\text{-Bu})_2\text{-}[\text{N}(\text{SiMe}_2\text{CH}_2)(\text{C}_6\text{H}_3\text{Me}_2\text{-}3,5)_2(\text{thf})_5]$
Sample code	1	2	3 ^[d]
CCDC	2195051	2195049	2195052
Empirical formula	$\text{C}_{56}\text{H}_{120}\text{EuLi}_6\text{O}_6$	$\text{C}_{40}\text{H}_{86}\text{Li}_3\text{O}_4\text{Y}$	$\text{C}_{54}\text{H}_{100}\text{Li}_3\text{N}_2\text{O}_6\text{Si}_2\text{Y}$
Formula weight	1083.11	740.81	1039.26
Temperature [K]	173(2)	100(2)	100(2)
Crystal system	Orthorhombic	Monoclinic	Triclinic
Space group	$\text{P}2_12_12_1$	$\text{P}2_1/\text{c}$	$\text{P}\bar{1}$
a [Å]	19.285(3)	10.7528(8)	13.793(12)
b [Å]	19.682(3)	23.6118(17)	18.375(16)
c [Å]	50.621(7)	18.0205(13)	24.41(2)
α [°]	90	90	88.649(15)
β [°]	90	96.394(2)	78.038(13)
γ [°]	90	90	87.643(13)
Volume [Å ³]	19214(5)	4546.8(6)	6047(9)
Z	12	4	4
ρ_{calc} [g/cm ³]	1.123	1.082	1.141
μ [mm ⁻¹]	1.020	1.315	1.048
F(000)	7020	1624	2248
Crystal size [mm ³]	0.255 x 0.132 x 0.119	0.275 x 0.147 x 0.114	0.328 x 0.120 x 0.064
Radiation	$\text{MoK}\alpha$ ($\lambda = 0.71073$)	$\text{MoK}\alpha$ ($\lambda = 0.71073$)	$\text{MoK}\alpha$ ($\lambda = 0.71073$)
Θ range for data collection [°]	2.917 to 27.421	1.427 to 24.781	1.109 to 26.609
Index ranges	$-24 \leq h \leq 24, -25 \leq k \leq 25, -65 \leq l \leq 65$	$-12 \leq h \leq 12, -27 \leq k \leq 27, -21 \leq l \leq 21$	$-17 \leq h \leq 17, -22 \leq k \leq 23, -30 \leq l \leq 30$
Reflections collected	207130	54346	164715
Independent reflections	43631 [$R_{\text{int}} = 0.1191$]	7787 [$R_{\text{int}} = 0.0766$]	24983 [$R_{\text{int}} = 0.2040$]
Data/restraints/parameters	43631 / 11315 / 2683	7787 / 840 / 703	24983 / 2481 / 1458
Goodness-of-fit ^[a]	0.992	1.158	1.021
Final R indexes [$ I \geq 2\sigma(I)$] ^{[b][c]}	$R_1 = 0.0553, wR_2 = 0.1146$	$R_1 = 0.0667, wR_2 = 0.1490$	$R_1 = 0.0719, wR_2 = 0.1628$
Final R indexes [all data]	$R_1 = 0.1550, wR_2 = 0.1572$	$R_1 = 0.0896, wR_2 = 0.1579$	$R_1 = 0.1459, wR_2 = 0.1994$
Largest diff. peak/hole [e Å ⁻³]	1.281 / -0.892	0.524 / -0.477	0.814 / -0.893

^[a]GOF = $[\sum w(F_o^2 - F_c^2)^2 / (n_o - n_p)]^{1/2}$. ^[b] $R_1 = \sum(|F_o| - |F_c|) / \sum|F_o|, F_o > 4\sigma(F_o)$. ^[c] $wR_2 = \{\sum[w(F_o^2 - F_c^2)^2] / \sum[w(F_o^2)^2]\}^{1/2}$.

^[d] Bad crystal quality.

Table S2. X-ray crystallographic parameters for complex **4** and **5**

Compound	Y[HNC ₆ H ₃ (mes) ₂ -2,6] ₃	[LiY ₂ (HNSiPh ₃) ₄ (NSiPh ₃) ₂][Li(thf) ₂ (OEt ₂) ₂]
Sample code	4	5
CCDC	2195050	2195053
Empirical formula	C ₇₂ H ₇₈ N ₃ Y	C ₁₂₈ H ₁₄₀ Li ₂ N ₆ O ₅ Si ₆ Y ₂
Formula weight	1074.28	2202.69
Temperature [K]	100(2)	100(2)
Crystal system	Monoclinic	Monoclinic
Space group	C2/c	P2 ₁ /c
a [Å]	37.869(2)	20.038(10)
b [Å]	19.7238(11)	13.595(7)
c [Å]	16.3752(10)	42.38(2)
α [°]	90	90
β [°]	94.466(2)	94.459(6)
γ [°]	90	90
Volume [Å ³]	12193.8(13)	11511(10)
Z	8	4
ρ _{calc} [g/cm ³]	1.170	1.271
μ [mm ⁻¹]	1.000	1.123
F(000)	4560	4632
Crystal size [mm ³]	0.522 x 0.209 x 0.150	0.392 x 0.226 x 0.177
Radiation	MoK _α (λ = 0.71073)	MoK _α (λ = 0.71073)
θ range for data collection [°]	1.676 to 25.054	2.082 to 26.489
Index ranges	-45 ≤ h ≤ 44, -23 ≤ k ≤ 23, -19 ≤ l ≤ 19	-23 ≤ h ≤ 25, -17 ≤ k ≤ 17, -53 ≤ l ≤ 50
Reflections collected	83526	192138
Independent reflections	10791 [R _{int} = 0.0649]	23744 [R _{int} = 0.0991]
Data/restraints/parameters	10791 / 1228 / 933	23744 / 1248 / 1518
Goodness-of-fit ^[a]	1.026	1.024
Final R indexes [I ≥ 2σ(I)] ^{[b][c]}	R ₁ = 0.0581, wR ₂ = 0.1382	R ₁ = 0.0620, wR ₂ = 0.1591
Final R indexes [all data]	R ₁ = 0.0937, wR ₂ = 0.1599	R ₁ = 0.0962, wR ₂ = 0.1786
Largest diff. peak/hole [e Å ⁻³]	1.080 / -1.385	1.356 / -0.878

^[a]GOF = $[\sum w(F_o^2 - F_c^2)^2 / (n_o - n_p)]^{1/2}$. ^[b]R₁ = $\Sigma(|F_o| - |F_c|) / \Sigma|F_o|$, F_o > 4σ(F_o). ^[c]wR₂ = $\{\Sigma[w(F_o^2 - F_c^2)^2] / \Sigma[w(F_o^2)^2]\}^{1/2}$

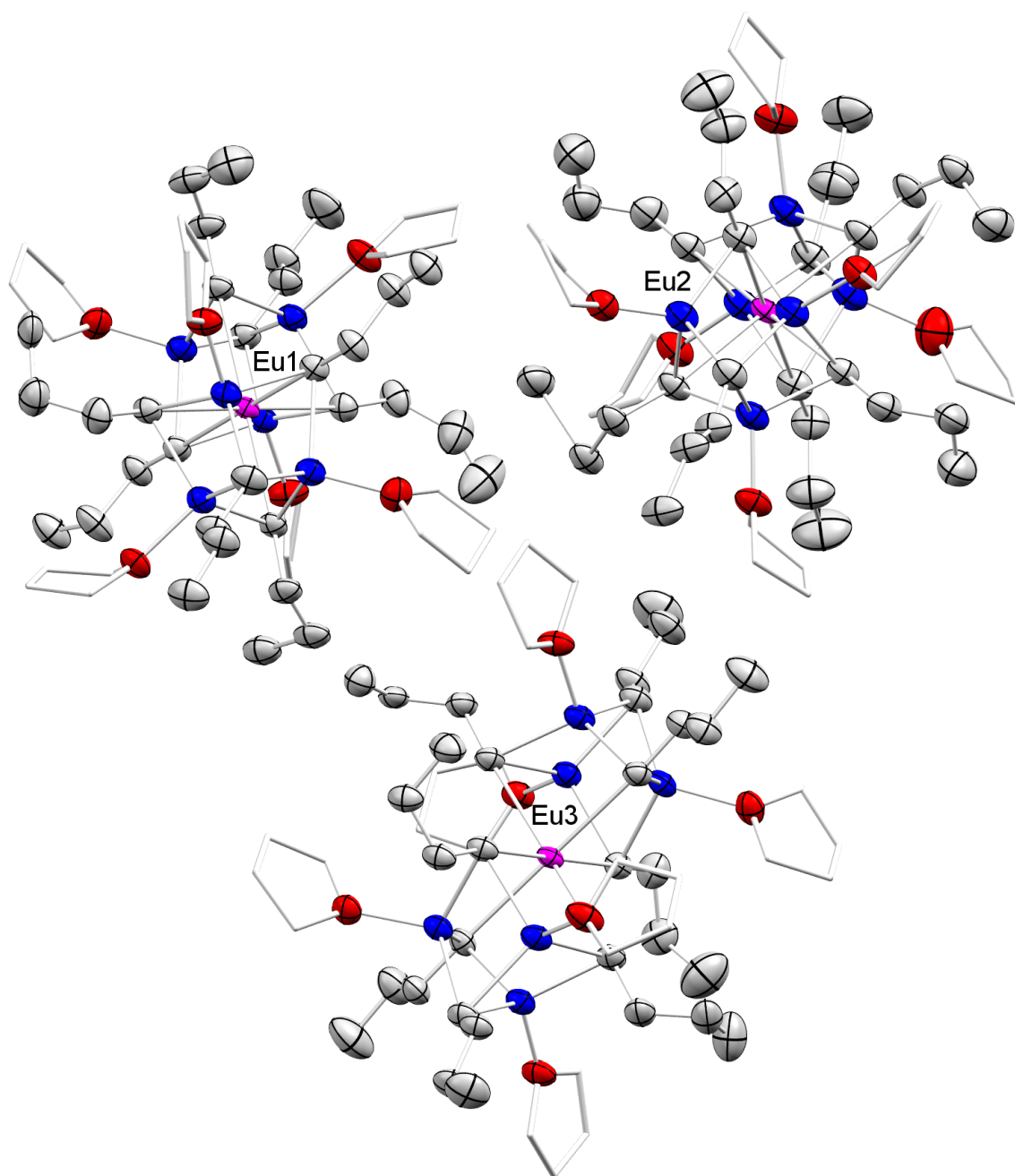


Figure S9. Crystal structure of $\text{Li}_6\text{Eu}(\textit{n}\text{-Bu})_6(\text{thf})_6$ (**1**) with atomic displacement ellipsoids set at 50% probability. Hydrogen atoms and disorders of the *n*-butyl groups are omitted for clarity. The carbon atoms of the THF molecules are represented by a wireframe model. Selected interatomic distances [Å] for **1**: range Eu–C 2.74(2) to 2.81(2), Li–C 2.12(4)–2.61(4), Li–O 1.78(4)–2.11(5).

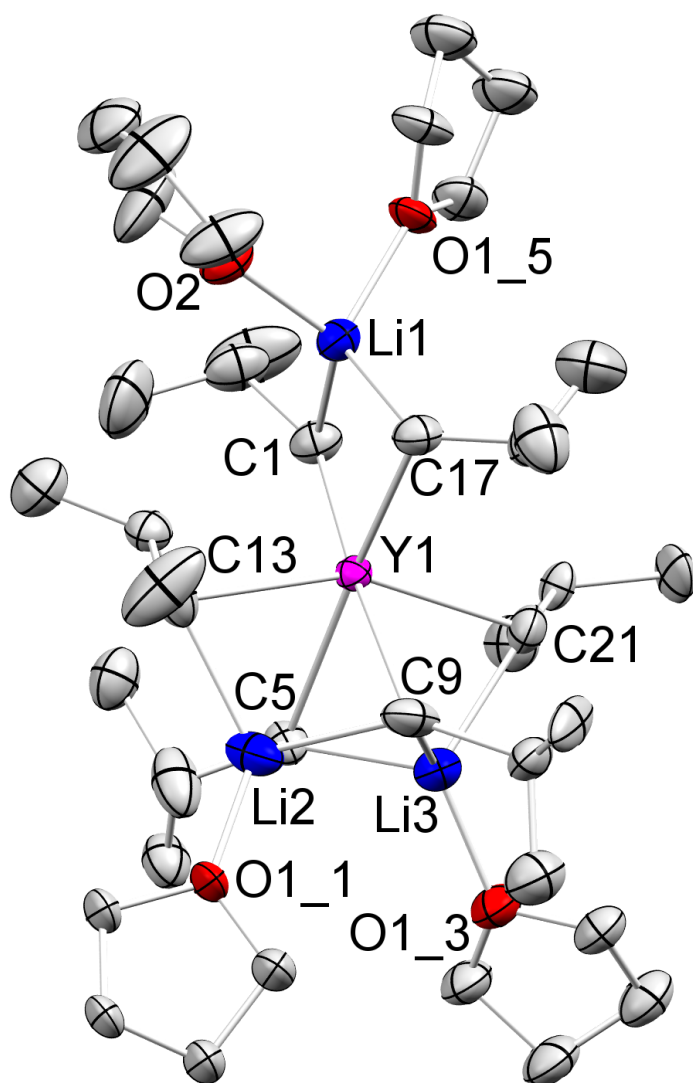


Figure S10. Crystal structure of $\text{Li}_3\text{Y}(\textit{i}\text{-Bu})_6(\text{thf})_4$ (**2**), with atomic displacement ellipsoids set at 50% probability. Hydrogen atoms and disorders of the isobutyl groups, as well as the THF molecules, are omitted for clarity. Selected interatomic distances [Å] for **2**: Y1–C1 2.517(6), Y1–C5 2.7609(2), Y1–C9 2.7212(2), Y1–C13 2.506(5), Y1–C17 2.557(5), Y1–C21 2.546(5), Li–C 2.233(11)–2.338(12), Li–O 1.933(13)–2.039(16).

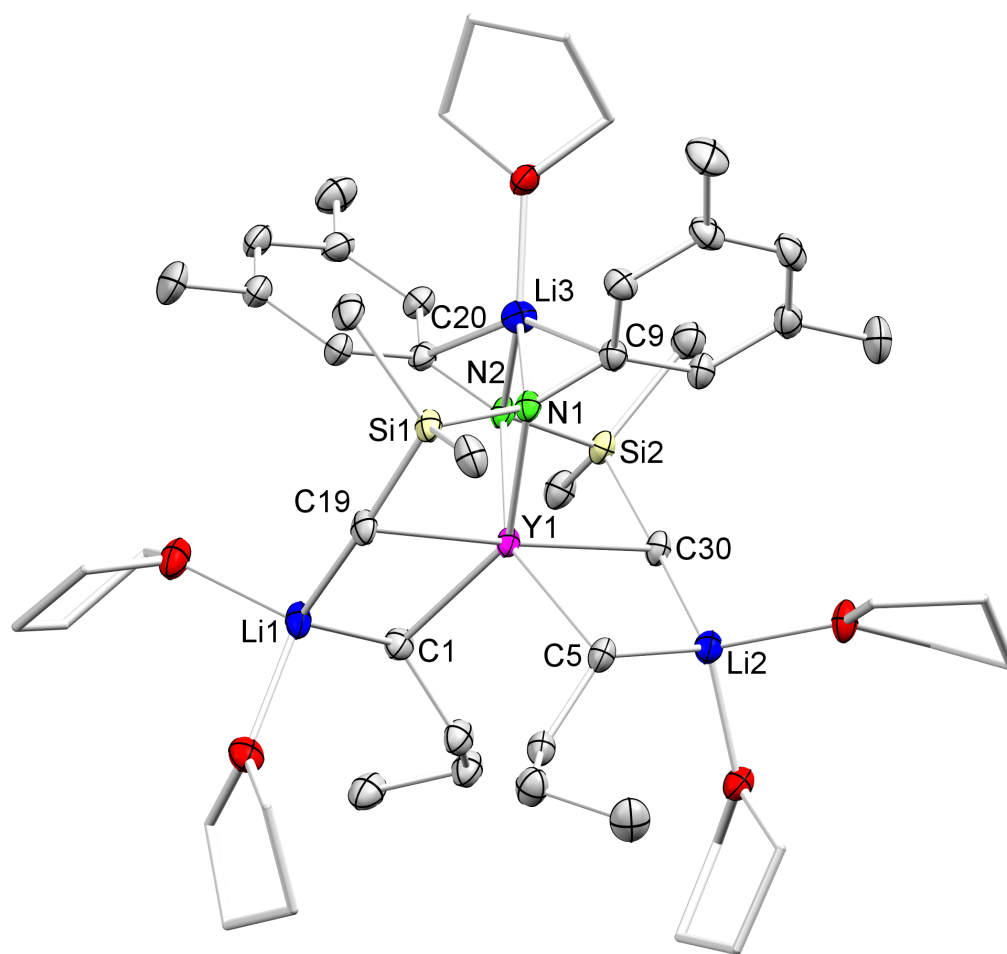


Figure S11. Crystal structure of $\text{Li}_3\text{Y}(\textit{n}\text{-Bu})_2(\text{N}(\text{SiMe}_2\text{CH}_2)\text{C}_6\text{H}_3\text{-Me}_2\text{-3,5})_2(\text{thf})_5$ (**3**) with atomic displacement ellipsoids set at 30% probability. Hydrogen atoms, disorders of the *n*-Bu groups, and THF molecules are omitted for clarity. The THF carbon atoms are represented by a wireframe model. The asymmetric unit contains two molecules of **3** and two lattice THF molecules. Selected interatomic distances [Å] and angles [°] for **3**: Y1–C1 2.512(5), Y1–C5 2.528(5), Y1–C19 2.632(5), Y1–C30 2.656(5), Y1–N1 2.414(4), N1–C9 1.394(5), N2–C20 1.398(6), Li3–C9 2.431(9), Li3–C20 2.427(9), Li3–N1 2.056(9), Li3–N2 2.033(9), Li–C 2.187(9)–2.431(9), Li–O 1.870(19)–2.032(9), Y1–N2 2.435(4), C19–Y1–C30 176.94(15), C1–Y1–N1 149.45(14), Y1–N1–C9 129.2(3), Y1–N1–Si1 100.18(16), Y1–N2–C20 129.1(3), Y1–N2–Si2 99.64(16).

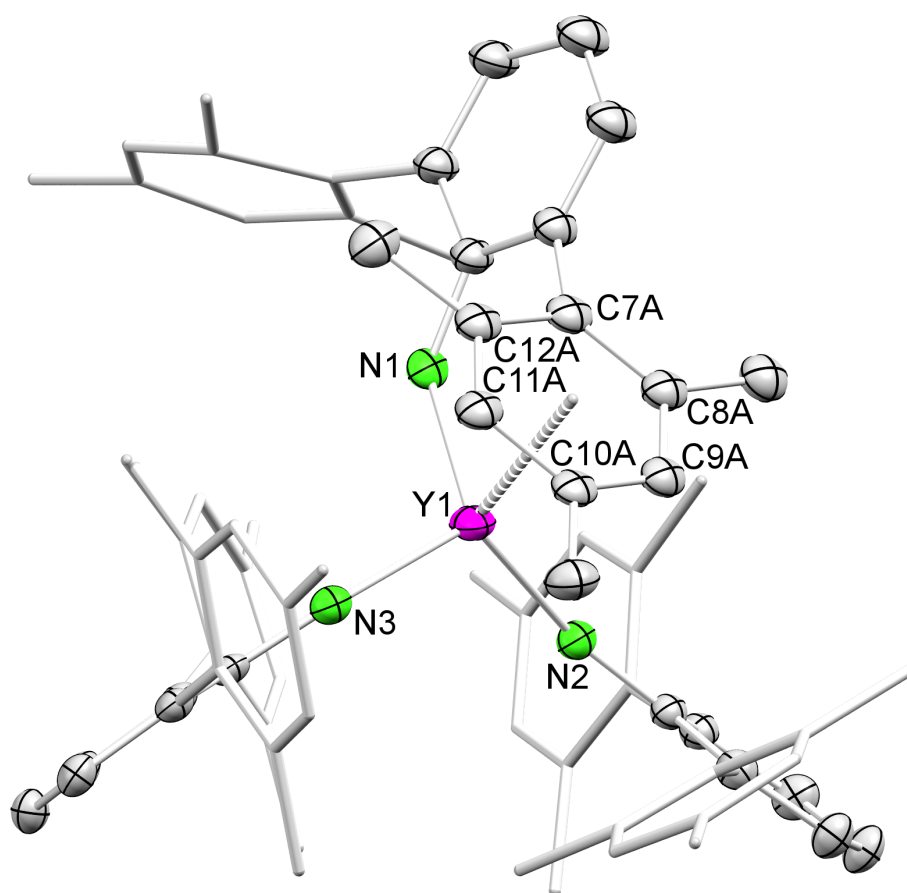


Figure S12. Crystal structure of $\text{Y}[\text{HNC}_6\text{H}_3(\text{mes})_{2-2,6}]_3$ (**4**) with atomic displacement ellipsoids set at 30% probability. Hydrogen atoms and disorders of the amid ligands are omitted for clarity. Selected interatomic distances [Å] and angles [°] for **4**: Y1–N1 2.158(10), Y1–N2 2.218(3), Y1–N3 2.222(3), mean Y1–(C7A–C12A) 2.735(3), Y1–N1–C1 132.8(6), Y1–N2–C25 156.9(3), Y1–N3–C49 147.9(3).

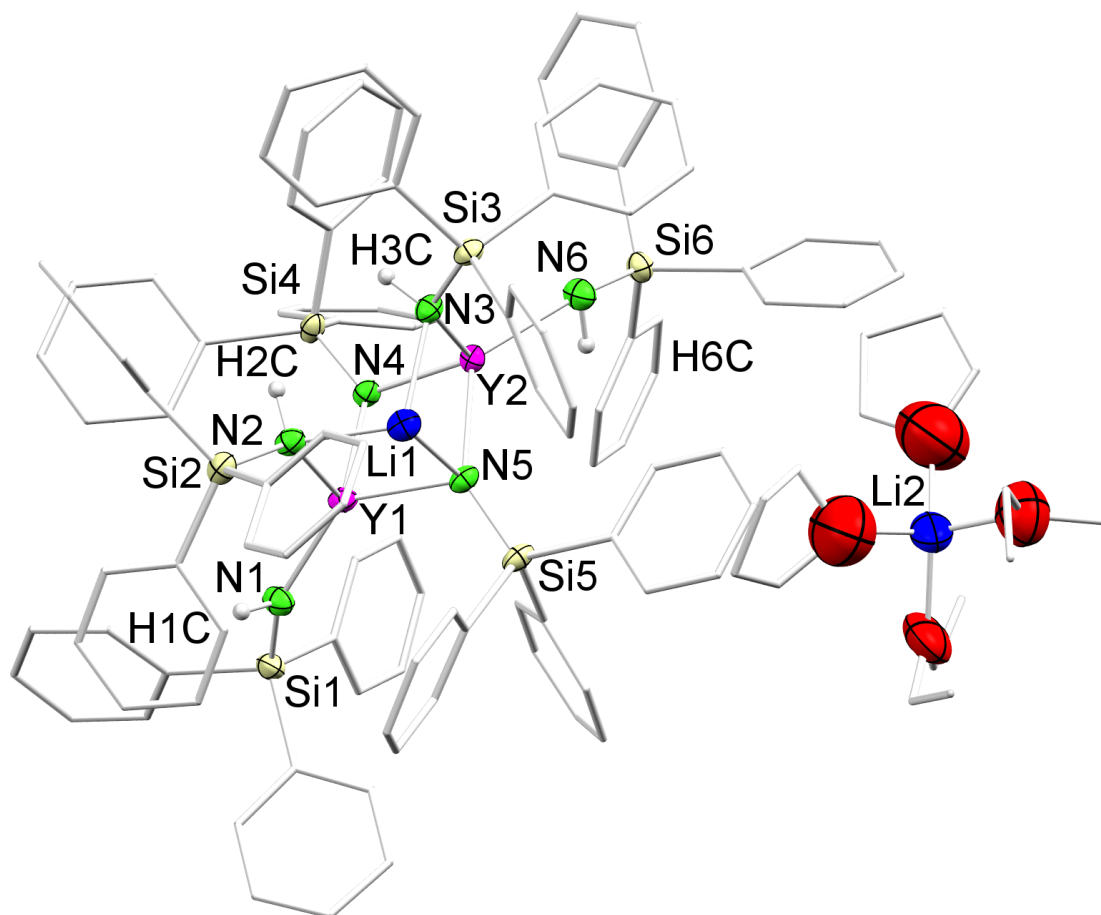


Figure S13. Crystal structure of $[\text{LiY}_2(\text{HNSiPh}_3)_4(\text{NSiPh}_3)_2][\text{Li}(\text{thf})_2(\text{OEt}_2)_2]$ (**5**) with atomic displacement ellipsoids set at 50% probability. Hydrogen atoms and disorders of the THF groups and one lattice Et_2O molecule are omitted for clarity. The carbon atoms of the THF and Et_2O molecules, as well as of the phenyl rings are represented by a wireframe model. Selected interatomic distances [Å] and angles [°] for **5**: Y1–N1 2.252(3), Y1–N2 2.273(3), Y1–N4 2.165(3), Y1–N5 2.276(3), Y2–N3 2.295(3), Y2–N4 2.205(3), Y2–N5 2.233(3), Y2–N6 2.255(4), Li1–N2 2.065(8), Li1–N3 2.086(8), Li1–N5 2.130(8), Y1–N4–Y2 97.48(12), Y1–N5–Y2 93.51(11), Y1–N1–Si1 149.1(2), Y1–N2–Si2 134.43(19), Y1–N4–Si4 134.67(18), Y1–N5–Si5 117.57(17), Y2–N3–Si3 134.82(18), Y2–N4–Si4 121.01(17), Y2–N5–Si5 142.23(19), Y2–N6–Si6 149.8(2).

**The isolation of a MAO
species from the reaction of
H₂O with AlMe₃**

manuscript

The isolation of a MAO species from the reaction of H₂O with AlMe₃

*Tassilo Berger, Căcilia Maichle-Mössmer, Markus Kramer, and Reiner Anwander**

Abstract:

At low temperature using THF as solvent AlMe₃ reacts with H₂O to the isolable MAO species [(Me₂Al)₂O(thf)]₂. NMR studies reveal that the dimer separates in solution into two (Me₂Al)O(thf)₂ molecules. [(Me₂Al)₂O(thf)]₂ reacts with 2,6-Diisopropylphenol to (Me₂AlOAlMe-2,6-diisopropylphenol)₂. Using Cp₂ZrMe₂ as catalyst [(Me₂Al)₂O(thf)]₂ together with 10 equivalents of AlMe₃ can be used in propylene polymerization.

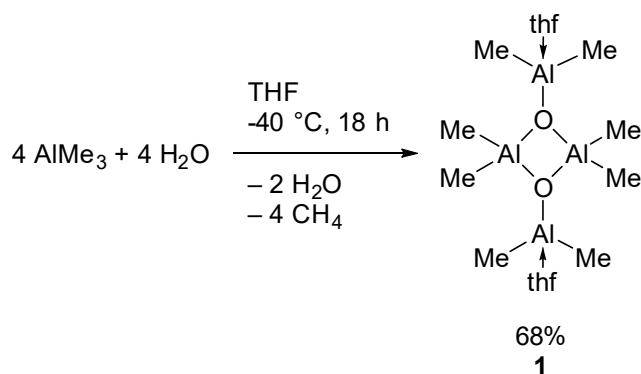
Introduction:

When Kaminsky et al. reported their findings that trimethylaluminum in combination with water is highly active as a cocatalyst in olefin polymerization in 1980, they struck gold like there are just a few examples in the history of modern chemistry.¹ Methylalumoxanes or MAO as it is called now is one of the most used cocatalysts, especially in ethylene polymerization which in turn is one of the most important polymers in our modern society.² This unsurprisingly motivated many chemists to study MAO in all of its aspects, and while its role in polymerization is well documented³, its structure and exact mechanism regarding polymerization still remain a black box. There are many great reviews for MAO both very specialized in one field⁴ and more broad ones⁵ to which we want to redirect the readers if they want to learn more. We want to focus us in this work on the methods that different groups used to isolate alkylalumoxanes and more specifically methylalumoxanes. In the beginning, we need to mention the two MAO anions that Atwood et al. [Al₇O₆Me₁₆]⁻ and [Me₂AlO•AlMe₃]²⁻₂ were able to isolate.⁶ The Atwood group used potassium superoxide and AlMe₃ to isolate these. Another method used by many groups is the use of sterically more demanding organoaluminium compounds like tri-tert-butylaluminum⁷, trimesitylaluminum⁸, or even substituted mesityl ligands⁹. Another novel approach to stabilize alkylalumoxane structures is the deprotonation of them using bases.¹⁰ To summarize two main approaches are commonly used to isolate alkylalumoxanes the first is to stabilize the aluminum source and the second is to use not water directly but different substances as an oxygen source, or quite commonly a combination of both.

We decided to stabilize AlMe₃ using tetrahydrofuran (THF) as a neutral donor. Herein we want to report the isolation of a well-defined MAO species from the reaction of H₂O with AlMe₃.

Results and Discussion:

We prepared a two-molar solution of H₂O in THF and reacted this with AlMe₃ which was also heavily diluted in THF. It further proved essential to perform this reaction including the whole workup procedure at low temperature (-40 °C). After one night we removed the volatiles in vacuo. This took almost two days including the co-evaporation with *n*-pentane. When the resulting oil couldn't be concentrated any further it was no longer soluble in *n*-pentane or *n*-hexane. At this point, we carefully washed it with *n*-pentane a few times. The resulting oil crystallized completely overnight at -40 °C (For a picture see Figure S1 in the supporting information). The fact that these crystals have a melting point very close to -40 °C made it pretty difficult, but with our cooling setup for mounting crystals, we were able to analyze them via x-ray diffraction. The result was that we have synthesized [(Me₂Al)₂O(thf)]₂ (**1**)(scheme 1).



Scheme 1: Synthesis of MAO species **1**.

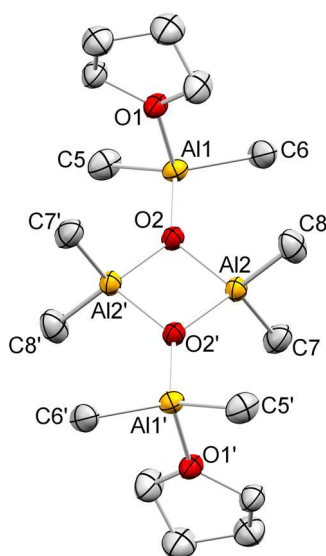
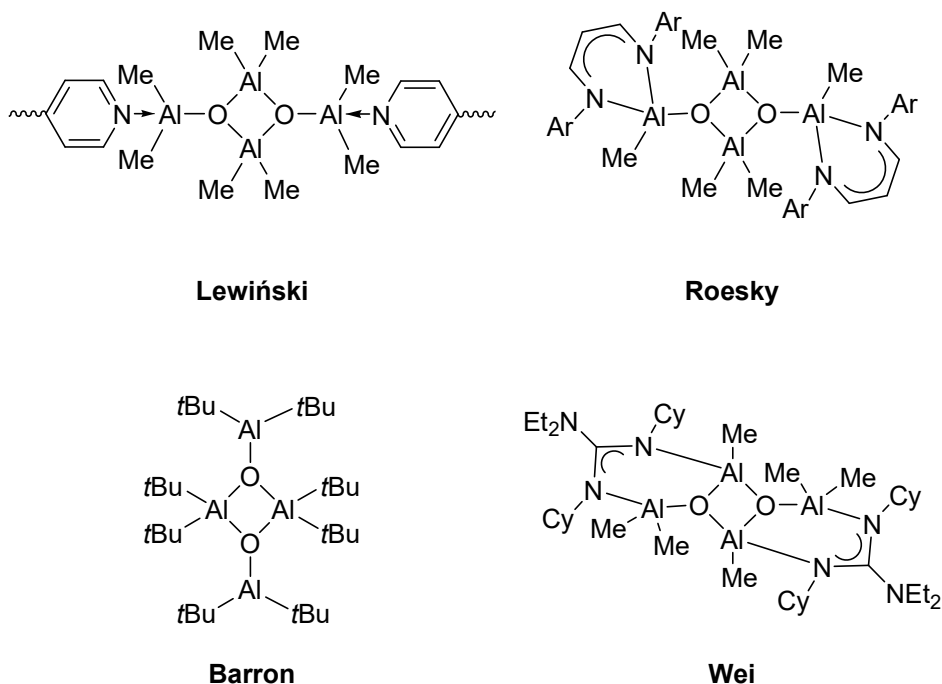


Figure 1: Crystal structure of $[(\text{AlMe}_2)_2\text{O}(\text{thf})]_2$ (**1**) with atomic displacement ellipsoids set at 50% probability. Hydrogen atoms are omitted for clarity. Selected interatomic distances [Å] and angles [°] for **1**: O1–Al1 1.9027(13), Al1–O2 1.7561(13), O2–Al2 1.8239(13), O2–Al2' 1.8235(13), Al1–C5 1.956(2), Al1–C6 1.955(2), Al2–C7 1.964(2), Al2–C8 1.962(2), Al2–O2–Al2' 93.91(6), O2–Al2–O2' 86.09(6).

1 consists of 4 AlMe_2 subunits two of which are terminal and the other two bridging. The coordination sphere of the terminal AlMe_2 units is saturated with one THF molecule each. The bridging AlMe_2 units form an Al–O–Al–O four-membered ring.

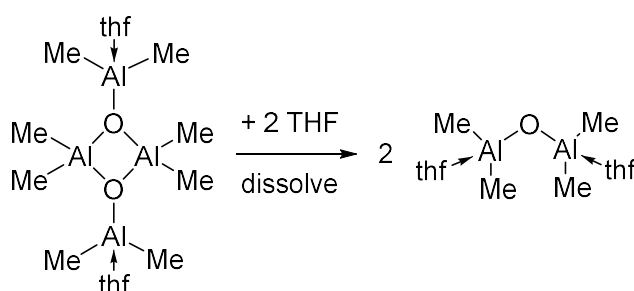
This structure when not stabilized with THF is well described as the elusive product from the reaction of the simplest MAO aggregate $(\text{MeAlO})_2$ with AlMe_3 .^{5a} Lewiński et al. were able to isolate this structure in a polymeric form linked by bis(pyridyl)ethane.¹¹ They however used phthalic acid with AlMe_3 instead of water. The Roesky group could also synthesize a similar structure where one methyl group of the terminal AlMe_2 subunits was substituted by a bulky nacnac ligand.¹² They used a nacnac methyl aluminum hydroxide and AlMe_3 as precursors. The organoaluminum hydroxide was prepared using water however under extreme conditions. They reacted nacnac methyl aluminum chloride with KOH, H_2O , and KH in liquid ammonia.¹³ In this multistep reaction the Roesky group never used water and AlMe_3 in the same step. We want to also mention the $[(t\text{-Bu}_2\text{Al})_2\text{O}]_2$ structure from Barron and coworkers. They used $\text{Al}(t\text{-Bu})_3$ and water containing salt as precursors.⁷ The interatomic distances and angles of these structures compared to **1** are almost identical. Lastly, the group of Wei used AlMe_3 and then water on a guanidinatoaluminium complex to get an MAO containing guanidinato complex.¹⁴



Scheme 2: Similar structures to $[(\text{Me}_2\text{Al})_2\text{O}(\text{thf})]_2$ (**1**).

Unintuitively we needed to use one equivalent of water per AlMe_3 despite only 0.5 equivalents reacting with the AlMe_3 . When using less we could only isolate the THF adduct $\text{AlMe}_3(\text{thf})$. Which was no longer observed when using one equivalent of water. And perplexingly product **1** does not react any further with additional H_2O . This, however, is of course only true at low temperatures. When warmed up additional release of methane can be observed. However, no product can be isolated from this. In fact, when the addition of water is too fast or the solution is not diluted enough the formation of a second MAO species can be observed via NMR spectroscopy. This species sadly remains an oil and cannot be crystallized (see figure **S7** in the supporting information).

When we measured the NMR spectra we were once again surprised by this compound. We could only observe one signal for the methyl groups both in the ^1H and the ^{13}C NMR spectrum. The integral in the ^1H NMR spectrum further showed that there are 4 THF molecules per molecule in solution instead of two. The crystals that we dissolved remained quite sticky so it can be assumed that a bit of THF cannot be removed in vacuo. The fact that only one methyl signal can be observed, however, remains. We then tried to vary the temperature while measuring the NMR spectra. Yet despite measuring in a range from -80 to $+100$ °C we could not separate the methyl signals (see figure **S8** in the supporting information). An assumption we came up with was that in solution the dimer $[(\text{Me}_2\text{Al})_2\text{O}(\text{thf})]_2$ separates into two $(\text{Me}_2\text{Al})\text{O}(\text{thf})_2$ molecules and we only have identical, terminal, THF stabilized AlMe_2 units (Scheme **3**).

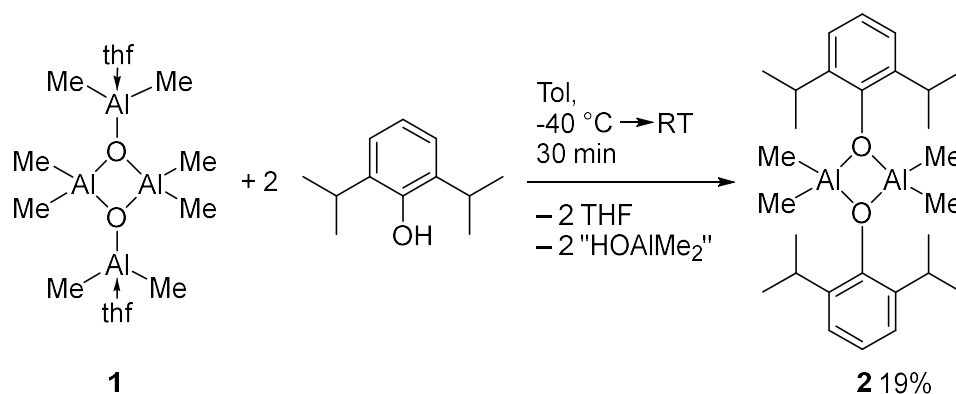


Scheme 3: Supposed separation of **1** in solution.

To support this assumption, we measured a DOSY experiment of this complex and compared the D values to that of the solvent toluene- d_8 . The result was a hydrodynamic radius of 3.82 Å. While not exactly fitting with the theoretical values of $(\text{Me}_2\text{Al})\text{O}(\text{thf})_2$ (mean radius of 4.85 Å), it shows us that the species in solution is considerably smaller than $[(\text{Me}_2\text{Al})_2\text{O}(\text{thf})]_2$ (mean radius of 5.30 Å) should be (for full details of the DOSY experiment see the supporting information).

As mentioned before we had to carefully maintain a cold chain during the whole synthesis of **1**. Yet we also mentioned that we measured NMR spectra in the range of -80 to $+100$ °C and did not observe any reaction or decomposition. So once $[(\text{Me}_2\text{Al})_2\text{O}(\text{thf})]_2$ is built and separated from any additional water it is remarkably stable. This however is only the case for **1** in solution. When we take -40 °C cold crystallin **1** and let it warm up to ambient temperature. We first see that the crystals melt, then a slow extrusion of gas is observed and after about an hour the substance solidified like glass completely clear, almost indistinguishable from the glass vial. When force is used with a sharp object it even cracks and breaks like glass albeit easier. The substance is completely insoluble in toluene or THF but reacts strongly with water under the formation of aluminum oxide. When we took some of the substance while the gas extrusion is observed and tried to dissolve it in THF- d_8 , some of it was still soluble. In the proton NMR spectrum of this, we could observe methane and a new signal in the methyldene region (see figure S10 in the supporting information). The product could not be analyzed further.

Next, we wanted to see if we can see two different methyl signals if we react **1** with an alcohol we choose 2,6-Diisopropylphenol. The x-ray structure of the resulting crystals revealed that we have synthesized $(\text{Me}_2\text{AlO}-2,6\text{-diisopropylphenyl})_2$. (**2**) This was quite puzzling since that meant that the formal side product would be Dimethylaluminum hydroxide (scheme 4). Which we couldn't observe when we repeated the reaction in deuterated toluene and measured the reaction mixture (figure SXX in the supporting information). Due to the low yield of **2** and the many side products, which all show similar chemical shifts in the $^1\text{H-NMR}$ it was not possible to determine the reaction mechanism.



Scheme 4: Reaction of **1** with 2,6-Diisopropylphenol.

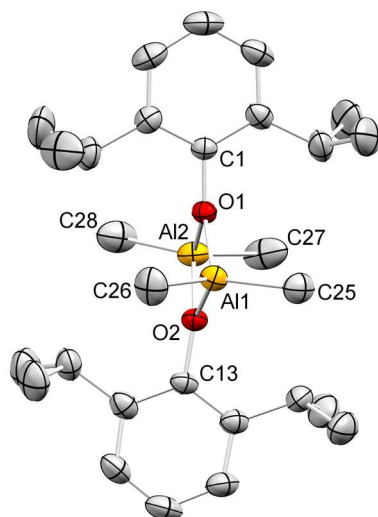


Figure 2: Crystal structure of $(\text{Me}_2\text{AlO-2,6-diisopropylphenyl})_2$ (**2**) with atomic displacement ellipsoids set at 50% probability. Hydrogen atoms are omitted for clarity. Selected interatomic distances [Å] and angles [°] for **2**: C1–O1 1.4066(15), O1–Al1 1.8585(10), O1–Al2 1.8580(10), O2–Al1 1.8622(10), O2–Al2 1.8623(10), O2–C13 1.4094(15), Al1–C25 1.9425(17), Al1–C26 1.9427(17), Al2–C27 1.9394(18), Al2–C28 1.9348(19), Al1–O1–Al2 100.07, Al1–O2–Al2 99.78(5), O1–Al1–O2 79.78(4), O1–Al2–O2 79.79(4).

Compared to **1** the aluminum oxygen distances are slightly elongated but the aluminum methyl distances are slightly shortened.

In the proton NMR spectrum of **2**, we can also see a second product. Which turned out to be the main product rather than a side product for this reaction (figure S14 in the supporting information). The signals with their integrals would fit $(\text{Me}_2\text{AlOAlMe-2,6-diisopropylphenol})_2$ (or the monomeric form), which we expected in the first place. This substance, however, remains an oil under our conditions (see S13 in the supporting information).

The fact that we can remove the THF from **1** motivated us to try this with different chemicals. The first attempt was using trimethylsilyl iodide. The results for this however remain inconclusive. It seems, that trimethylsilyl iodide also reacts with the MAO species, not just the THF. The second attempt was to use an excess of AlMe_3 . Much like it is used in commercial MAO. The result was only a single signal for all methyl groups in the proton NMR spectrum (see S9 in the supporting information). We located the signal at -0.39 ppm right in the middle of the signals for AlMe_3 (-0.36) and that of **1** (-0.52). And we didn't see a signal where we would expect for the $\text{AlMe}_3(\text{thf})$ adduct (-1.02). When we tried to crystallize the product, however, we could only crystallize $\text{AlMe}_3(\text{thf})$. This shows a few things. First, in solution, there is a fast-changing equilibrium where the THF is located. Second, it is favored that the THF is located on AlMe_3 instead of the MAO species at a lower temperature. And lastly, the MAO species is still stable without the THF donor molecules since we didn't observe any decomposition.

The last thing we wanted to check for $[(\text{Me}_2\text{Al})_2\text{O}(\text{thf})]_2$ (**1**) is if it is usable as a cocatalyst in polymerization. We decided on propylene as the monomer and zirconocenedimethyl as the catalyst in toluene. For just **1** with Cp_2ZrMe_2 , we didn't observe any polymer. When we used **1** and 10 equivalents of AlMe_3 however, we could observe the formation of a polymer, but just a tiny amount. We repeated the same reaction without adding any monomer to see how much polymer we actually got. The activity is extremely low with just 2.2 [$\text{kg}_{\text{PP}} \text{mol}_{\text{Zr}}^{-1} \text{h}^{-1}$]. To see if this can be right we repeated the reaction again this time with commercially available MAO. The result with an activity of 17.8 [$\text{kg}_{\text{PP}} \text{mol}_{\text{Zr}}^{-1} \text{h}^{-1}$] was slightly higher but still pretty low. Studies

using different monomers and catalysts are currently underway, as are further studies regarding the reactivity of our isolated MAO species.

Conclusion

Seamless low-temperature working techniques gave access to the isolable MAO species, $[(\text{Me}_2\text{Al})_2\text{O}(\text{thf})]_2$, from the reaction of water with AlMe_3 . THF had to be used as the solvent to lower the reactivity of AlMe_3 . NMR studies revealed that this dimer separates in solution into two $(\text{Me}_2\text{Al})\text{O}(\text{thf})_2$ molecules. Protonolysis reaction with the alcohol 2,6-Diisopropylphenol showed unexpected reactivity with the formation of $(\text{Me}_2\text{AlO}-2,6\text{-diisopropylphenyl})_2$. And first attempts at polymerization using $[(\text{Me}_2\text{Al})_2\text{O}(\text{thf})]_2$ as a cocatalyst together with additional AlMe_3 are promising. With using just water, AlMe_3 , and THF, $[(\text{Me}_2\text{Al})_2\text{O}(\text{thf})]_2$ is an extremely cheap, easily reproducible, and straightforward method to a well-defined MAO species. The already unexpected reactivity in protonolysis reactions and the fact that it is usable in polymerization, $[(\text{Me}_2\text{Al})_2\text{O}(\text{thf})]_2$ will no doubt help us deepen our understanding of the vast and still largely unexplored field that are the Methylaluminoxanes.

- (a) Sinn, H.; Kaminsky, W.; Vollmer, H.-J.; Woldt, R., "Living Polymers" on Polymerization with Extremely Productive Ziegler Catalysts. *Angew. Chem. Int. Ed. Engl.* **1980**, *19*, 390-392; (b) Kaminsky, W., The discovery of metallocene catalysts and their present state of the art. *J. Polym. Sci., Part A: Polym. Chem.* **2004**, *42*, 3911-3921; (c) Kaminsky, W., Discovery of Methylaluminoxane as Cocatalyst for Olefin Polymerization. *Macromolecules* **2012**, *45*, 3289-3297; (d) Kaminsky, W.; Sinn, H., Methylaluminoxane: Key Component for New Polymerization Catalysts. In *Polyolefins: 50 years after Ziegler and Natta II: Polyolefins by Metallocenes and Other Single-Site Catalysts*, Kaminsky, W., Ed. Springer Berlin Heidelberg: Berlin, Heidelberg, 2013; pp 1-28.
- Plastics the Facts 2014/2015. **2015**.
- (a) Brintzinger, H. H.; Fischer, D.; Mühlaupt, R.; Rieger, B.; Waymouth, R. M., Stereospecific Olefin Polymerization with Chiral Metallocene Catalysts. *Angew. Chem. Int. Ed. Engl.* **1995**, *34*, 1143-1170; (b) Angermund, K.; Fink, G.; Jensen, V. R.; Kleinschmidt, R., Toward Quantitative Prediction of Stereospecificity of Metallocene-Based Catalysts for α -Olefin Polymerization. *Chem. Rev.* **2000**, *100*, 1457-1470; (c) Bochmann, M., Kinetic and mechanistic aspects of metallocene polymerisation catalysts. *J. Organomet. Chem.* **2004**, *689*, 3982-3998.
- (a) Pasykiewicz, S., Alumoxanes: Synthesis, structures, complexes and reactions. *Polyhedron* **1990**, *9*, 429-453; (b) Resconi, L.; Bossi, S.; Abis, L., Study on the role of methylalumoxane in homogeneous olefin polymerization. *Macromolecules* **1990**, *23*, 4489-4491; (c) Reddy, S. S.; Sivaram, S., Homogeneous metallocene-methylaluminoxane catalyst systems for ethylene polymerization. *Prog. Polym. Sci.* **1995**, *20*, 309-367; (d) Pédeutour, J.-N.; Radhakrishnan, K.; Cramail, H.; Deffieux, A., Reactivity of Metallocene Catalysts for Olefin Polymerization: Influence of Activator Nature and Structure. *Macromol. Rapid Commun.* **2001**, *22*, 1095-1123; (e) Zurek, E.; Ziegler, T., Theoretical studies of the structure and function of MAO (methylaluminoxane). *Prog. Polym. Sci.* **2004**, *29*, 107-148; (f) Severn, J. R.; Chadwick, J. C., Tailor-made polymers. *Wiley-VCH, Weinheim* **2008**, *1*, 95-138; (g) Zijlstra, H. S.; Stuart, M. C. A.; Harder, S., Structural Investigation of Methylalumoxane Using Transmission Electron Microscopy. *Macromolecules* **2015**, *48*, 5116-5119; (h) Joshi, A.; Zijlstra, H. S.; Liles, E.; Concepcion, C.; Linnolahti, M.; McIndoe, J. S., Real-time analysis of methylalumoxane formation. *Chemical Science* **2021**, *12*, 546-551.
- (a) Zijlstra, H. S.; Harder, S., Methylalumoxane – History, Production, Properties, and Applications. *Eur. J. Inorg. Chem.* **2015**, *2015*, 19-43; (b) Chen, E. Y.-X.; Marks, T. J., Cocatalysts for Metal-Catalyzed Olefin Polymerization: Activators, Activation Processes, and Structure–Activity Relationships. *Chem. Rev.* **2000**, *100*, 1391-1434; (c) Roesky, H. W.; Walawalkar, M. G.; Murugavel, R., Is Water a Friend or Foe in Organometallic Chemistry? The Case of Group 13 Organometallic Compounds†. *Acc. Chem. Res.* **2001**, *34*, 201-211; (d) Bochmann, M., The Chemistry of Catalyst Activation: The Case of Group 4 Polymerization Catalysts. *Organometallics* **2010**, *29*, 4711-4740.
- (a) Atwood, J. L.; Hrcir, D. C.; Priester, R. D.; Rogers, R. D., Decomposition of high-oxygen content organoaluminum compounds. The formation and structure of the $[Al_7O_6Me_6]^-$ anion. *Organometallics* **1983**, *2*, 985-989; (b) Atwood, J. L.; Zaworotko, M. J., The formation and structure of the novel aluminoxane anion $[Me_2AlO \cdot AlMe_3]^{2-}$. *J. Chem. Soc., Chem. Commun.* **1983**, 302-303.
- Mason, M. R.; Smith, J. M.; Bott, S. G.; Barron, A. R., Hydrolysis of tri-tert-butylaluminum: the first structural characterization of alkylalumoxanes $[(R_2Al)_2O]_n$ and $(RAlO)_n$. *J. Am. Chem. Soc.* **1993**, *115*, 4971-4984.
- Storre, J.; Klemp, A.; Roesky, H. W.; Schmidt, H.-G.; Noltemeyer, M.; Fleischer, R.; Stalke, D., Hydrolysis of Trimesitylgallium and Trimesitylaluminum: Structures Along a Reaction Pathway. *J. Am. Chem. Soc.* **1996**, *118*, 1380-1386.
- Wehmschulte, R. J.; Power, P. P., A New Synthetic Route to Organoalumoxanes $(RAlO)_n$: Synthesis of $(Mes^*AlO)_4$ ($Mes^* = -C_6H_2-2,4,6-t-Bu_3$) and Its Reactions with AlR_3 ($R = Me$ or Et). *J. Am. Chem. Soc.* **1997**, *119*, 8387-8388.
- Storre, J.; Schnitter, C.; Roesky, H. W.; Schmidt, H.-G.; Noltemeyer, M.; Fleischer, R.; Stalke, D., A Novel Approach for the Stabilization and Structural Characterization of Group 13 Organometallic Hydroxides: The Way to Well Defined Crystalline Methylalumoxanes. *J. Am. Chem. Soc.* **1997**, *119*, 7505-7513.

11. Lewiński, J.; Bury, W.; Justyniak, I.; Lipkowski, J., Efficient Route to Tetramethylalumoxane and Carboxylate Alumoxanes through the Alkylation of Phthalic Acid. *Angew. Chem. Int. Ed.* **2006**, *45*, 2872-2875.
12. Yang, Y.; Zhu, H.; Roesky, H. W.; Yang, Z.; Tan, G.; Li, H.; John, M.; Herbst-Irmer, R., Trinuclear Alumoxanes with an Acyclic Al-O-Al-O-Al Core and Studies of Their Reactivity. *Chemistry – A European Journal* **2010**, *16*, 12530-12533.
13. Bai, G.; Singh, S.; Roesky, H. W.; Noltemeyer, M.; Schmidt, H.-G., Mononuclear Aluminum Hydroxide for the Design of Well-Defined Homogeneous Catalysts. *J. Am. Chem. Soc.* **2005**, *127*, 3449-3455.
14. Han, H.-F.; Guo, Z.-Q.; Zhang, S.-F.; Li, J.; Wei, X.-H., Guanidinatoaluminum complexes: synthesis, crystal structures and reactivities. *RSC Advances* **2016**, *6*, 101437-101446.

Table of Contents

Experimental section	3
General Considerations.	3
[(AlMe ₂) ₂ O(thf)] ₂ (1).	5
(Me ₂ AlO-2,6-diisopropylphenyl) ₂ (2).	5
Propylene polymerization with commercially available MAO and [(AlMe₂)₂O(thf)]₂ (1).	5
Figure S1: Picture of a vial with crystallin [(AlMe ₂) ₂ O(thf)] ₂ (1).	6
Table S1. X-ray crystallographic parameters for complexes 1 and 2	7
[(AlMe ₂) ₂ O(thf)] ₂	7
(Me ₂ AlO-2,6-diisopropylphenyl) ₂	7
Figure S2. Crystal structure of [(AlMe ₂) ₂ O(thf)] ₂ (1).	8
Figure S3. Crystal structure of (Me ₂ AlO-2,6-diisopropylphenyl) ₂ (2).	8
Figure S4. ¹ H NMR spectrum of [(AlMe ₂) ₂ O(thf)] ₂ (1).	9
Figure S5. ¹³ C NMR spectrum of [(AlMe ₂) ₂ O(thf)] ₂ (1).	9
Figure S6. ²⁷ Al NMR spectrum of [(AlMe ₂) ₂ O(thf)] ₂ (1).	10
Figure S7. ¹ H NMR spectrum of [(AlMe ₂) ₂ O(thf)] ₂ (1) (bottom) and from a reaction where H ₂ O was added quicker to AlMe ₃ (top)	10
Figure S8. ¹ H NMR spectrum of [(AlMe ₂) ₂ O(thf)] ₂ (1) with unknown MAO species at -80 °C (bottom), 26 °C (middle) and 100 °C (top)	11
Figure S9. ¹ H NMR spectrum of [(AlMe ₂) ₂ O(thf)] ₂ (1) (bottom), 1 + 10 AlMe ₃ (second from bottom), AlMe ₃ in toluene (third from bottom) and AlMe ₃ in THF (top)	11
Figure S10. ¹ H NMR spectrum of [(AlMe ₂) ₂ O(thf)] ₂ (1) (bottom) and of 1 that partly decomposed (top)	12
Figure S11. ¹ H NMR spectrum of (Me ₂ AlO-2,6-diisopropylphenyl) ₂	12
Figure S12. ¹³ C NMR spectrum of (Me ₂ AlO-2,6-diisopropylphenyl) ₂ (2).	13
Figure S13. ¹ H NMR spectrum of likely (Me ₂ AlOAlMe-2,6-diisopropylphenol) ₂	13
Figure S14. ¹ H NMR spectrum of the reaction mixture of 1 with 2 equiv. 2,6-Diisopropylphenol.	14
DOES experiment of [(AlMe ₂) ₂ O(thf)] ₂ (1)	15
References	17

Experimental section

General Considerations. **Caution!** Trimethylaluminum and the Methylaluminoxane (MAO) compounds reported in this paper are highly pyrophoric and react violently when exposed to air and/or moisture. All manipulations were performed under an inert atmosphere (Ar) using either glovebox (MBraun UNIlab^{pro}; <0.1 ppm O₂, <0.1 ppm H₂O) or standard Schlenk techniques with oven-dried glassware. All reactions, if not stated otherwise, were done in the cold well or precooled copper blocks in that glovebox, at usually -40 °C. This includes every reaction step, including the removal of solvents in vacuo. All solvents and other instruments used were also precooled. The solvents were purified with Grubbs columns (MBraun SPS, solvent purification system) and stored in a glovebox. THF and Et₂O were further dried using molecular sieves. Trimethylaluminum (98%) was purchased from abcr and used as received. Cp₂ZrCl₂ (98%), Trimethylsilyl iodide (97%), MAO (10w% in toluene), and 2,6-Diisopropylphenol (97%) were purchased from Sigma-Aldrich and used as received. Methyl lithium (1.6 M in Et₂O) was purchased from Sigma-Aldrich and dried in vacuo before it was stored in a glovebox. A 2 M H₂O solution in THF was prepared from double distilled, degassed water, and dried, degassed THF. A lecture bottle of propene (Propen 2.3, 15.8g, 8.9 l) was purchased from Westfalen and used as received. Cp₂ZrMe₂ was prepared from Cp₂ZrCl₂ and methyl lithium. Benzene-*d*₆, toluene-*d*₈, and THF-*d*₈ were purchased from *Sigma Aldrich*, degassed, dried over molecular sieve for at least 24 h, filtered, and stored inside a glovebox. NMR spectra of moisture-sensitive compounds were recorded by using J. Young valve NMR tubes on either a Bruker AVII+400 (¹H: 400.13 MHz), a Bruker AVIIIHD (¹H: 300.13 MHz), or a Bruker AVII+500 (¹H: 500.13 MHz). ¹H NMR shifts are referenced to a solvent resonance and reported in parts per million (ppm) relative to tetramethylsilane.^[1] Analysis of NMR spectra was performed with TopSpin 3.6.1 [Academic License].^[2] Multiplicities of signals are given as s (singlet), bs (broad singlet), d (doublet), t (triplet), and sep(septet). Signals were assigned via 2D NMR experiments.

All pulse gradient spin echo NMR measurements were performed on an Avance III HD spectrometer (Bruker) operating at 700.29 MHz for ¹H, using a TCI prodigy cryoprobe head equipped with a z-gradient unit. The gradient was calibrated using “doped water” (1% H₂O in D₂O with traces of CuSO₄), assuming a diffusion coefficient of $1.91 \times 10^{-5} \text{ cm}^2 \text{ s}^{-1}$ for HDO. The diffusion measurements used a modified bipolar gradient pulse pair-stimulated echo sequence incorporating a longitudinal eddy current delay (BPP-LED). The gradient pulse length (δ) and the diffusion time (Δ) were kept at fixed values while the gradient strength was gradually increased. Typical values for δ and Δ were 0.8 and 70 ms, respectively. A longitudinal eddy current delay (T_e) of 5 ms was used. Sine-shaped gradient pulses were linearly varied between 1 and 52 G cm⁻¹ (2–98%) in 32 steps, and at each step 16 scans were acquired. Four measurements per sample were performed at a constant sample temperature of $298 \pm 0.1 \text{ K}$ (Bruker Variable Temperature Unit BCU II). The data were analyzed with the T₁/T₂ relaxation module of

Topspin 4.1.3. The signal areas were plotted against the gradient strength and the best fit was calculated using the Stejskal–Tanner equation

$$I_g = I_0 \exp [-4\pi^2\gamma^2\delta^2G^2 (\Delta - \delta/3)]$$

(with D being the diffusion coefficient in $\text{cm}^2 \text{s}^{-1}$, γ the gyromagnetic ratio in Hz/G , G the gradient strength in G cm^{-1} , δ the gradient length in ms , Δ the interval between gradient pulses (diffusion time) in ms , I_g the signal area, and I_0 the signal intensity at $G = 0\%$). Mean values for each sample are reported.^[3]

Elemental analysis (C, H, N) was performed on an *Elementar vario MICRO cube*. Crystals for X-ray crystallography were handpicked in a glovebox, coated with Parabar 10312, pump-oil, or perfluorinated oil, and stored on microscope slides. X-ray data were collected on a Bruker APEX II DUO diffractometer equipped with an I μ S microfocus sealed tube and QUAZAR optics for MoK_α ($\lambda = 0.71073 \text{ \AA}$) and CuK_α ($\lambda = 1.54184 \text{ \AA}$) radiation. The data collection strategy was determined using COSMO^[4] employing ω -scans. Raw data were processed using APEX^[5] and SAINT,^[6] corrections for absorption effects were applied using SADABS.^[7] The structures were solved by direct methods and refined against all data by full-matrix least-squares methods on F^2 using SHELXTL^[8] and ShelXle.^[9] Disorder models were calculated using DSR, a program for refining structures in ShelXl.^[10] All graphics were produced employing Mercury 4.2.0^[11] and POV-Ray.^[12]

[(AlMe₂)₂O(thf)]₂ (1). Trimethylaluminum (AlMe₃) (360.4 mg, 2.0 mmol) was dissolved in THF (5 mL) and cooled to -40 °C. Then, H₂O (2 M in THF, 1.0 mL, 2.0 mmol, 1 equiv.) was further diluted with THF (5 mL) and also precooled to -40 °C. The H₂O/THF solution was slowly (5 min) added dropwise to the stirring TMA/THF solution. After stirring the reaction mixture for 18 hours, the solvent was removed in vacuo. This took about two days until the product was dry, including multiple coevaporations with *n*-pentane. Giving [(AlMe₂)₂O(thf)]₂ as colorless crystals, with 1 equiv. THF (calculated from the ¹H NMR) as colorless oil in between them which cannot be removed, in 68% yield. Crystals of **1** suitable for XRD analysis were removed from the reaction mixture before it was completely dried. ¹H NMR, (500.13 MHz, 299 K, toluene-*d*₈): δ = 3.42 (s, 16 H, THF), 1.10 (s, 16 H, THF), -0.53 ppm (s, 24 H, Al-CH₃). ¹³C NMR, (125.76 MHz, 299 K, toluene-*d*₈): δ = 70.3 (s, THF), 25.0 (s, THF), -8.7 ppm (s, Al-CH₃). ²⁷Al NMR, (130.32 MHz, 299 K, toluene-*d*₈): δ = 185.1 ppm (bs, Al-CH₃). Anal. (%) calcd. for C₂₄H₅₆Al₄O₆ (548.63 gmol⁻¹): C 52.54, H 10.29; found: C 43.16, H 9.24. The deviation between theoretical and experimental microanalytical data derives from the fast decomposition of [(AlMe₂)₂O(thf)]₂(THF)₂ at ambient temperature in the dried state. For example, the second sample of [(AlMe₂)₂O(thf)]₂(THF)₂ measured 10 min after the first resulted in microanalytical values of C 32.78 H 7.35.

(Me₂AlO-2,6-diisopropylphenyl)₂ (2). [(AlMe₂)₂O(thf)]₂(THF)₂ (47.4 mg, 0.09 mmol) was dissolved in cold toluene, before 2,6-Diisopropylphenol (0.18 mmol, 2 equiv.) dissolved in toluene was added dropwise. The reaction mixture was stirred for 30 min, during which it was allowed to warm up to ambient temperature. The solvent was then removed in vacuo. To give as colorless crystals of (Me₂AlO-2,6-diisopropylphenyl)₂ in about 19% yield (another product, most likely (Me₂AlOAlMe-2,6-diisopropylphenyl)₂, could be observed in the ¹H NMR spectra, see S12). Crystals of **1** suitable for XRD analysis were removed from the reaction mixture before it was completely dried. ¹H NMR, (500.13 MHz, 299 K, toluene-*d*₈): δ = 6.99 (d, 2 H, phenyl), 6.98 (bs, 1H, phenyl), 3.73 (sep, 2 H, CH₁-isopropyl), 1.24 (d, 12 H, CH₃-isopropyl), -0.38 ppm (s, 6 H, Al-CH₃). ¹³C NMR, (125.76 MHz, 299 K, toluene-*d*₈): δ = 144.2 (s, phenyl tertiary), 141.1 (s, phenyl tertiary), 125.7 (s, phenyl), 125.4 (s, phenyl), 26.8 (s, CH₁-isopropyl), 25.5 (s, CH₃-isopropyl), -8.0 ppm (s, Al-CH₃).

Propylene polymerization with commercially available MAO and [(AlMe₂)₂O(thf)]₂ (1). Cp₂ZrMe₂ (5.0 mg, 0.02 mmol) was stirred with commercially available MAO (10w%) (200 mg, ~0.02 mmol, ~1 equiv) for 30 minutes at -40 °C. The mixture was then moved to a polymerization reactor and allowed to warm up to ambient temperature. The reactor was then pressurized with propylene to about 2 bar before the gas flow was stopped again. The reaction mixture was stirred at 600 rpm for 30 minutes, before it was quenched with methanol+0.01 w% 2,6-ditertbutyl-4-methylphenole. The polymer was dried in vacuo and afterward in an oven at 60 °C.

The same steps were repeated without propylene addition to calculate the exact polymer weight.

This reaction was repeated using $[(\text{AlMe}_2)_2\text{O}(\text{thf})]_2(\text{THF})_2$ (11.0 mg, 0.02 mmol) and AlMe_3 (14.4 mg, 0.20 mmol, 10 equiv.) instead of commercial MAO.

Commercial MAO polymer yield: 177.7 mg \rightarrow activity of 17.8 $[\text{kg}_{\text{PP}} \text{mol}_{\text{Zr}}^{-1} \text{h}^{-1}]$

$[(\text{AlMe}_2)_2\text{O}(\text{thf})]_2(\text{THF})_2 + 10 \text{ AlMe}_3$ polymer yield: 21.5 mg \rightarrow activity of 2.2 $[\text{kg}_{\text{PP}} \text{mol}_{\text{Zr}}^{-1} \text{h}^{-1}]$



Figure S1: Picture of a vial with crystallin $[(\text{AlMe}_2)_2\text{O}(\text{thf})]_2$ (**1**).

Table S1. X-ray crystallographic parameters for complexes **1** and **2**.

Compound	[(AlMe ₂) ₂ O(thf)] ₂	(Me ₂ AlO-2,6-diisopropylphenyl) ₂
Sample code	1	2
CCDC	XXX	XXX
Empirical formula	C ₁₆ H ₄₀ Al ₄ O ₄	C ₂₈ H ₄₆ Al ₂ O ₂
Formula weight	404.40	468.61
Temperature [K]	100(2)	100(2)
Crystal system	Monoclinic	Monoclinic
Space group	P2 ₁ /n	P2 ₁ /c
a [Å]	8.7185(4)	17.9344(10)
b [Å]	14.7641(7)	9.5257(6)
c [Å]	9.6569(5)	17.2987(9)
α [°]	90	90
β [°]	95.456(2)	93.3400(10)
γ [°]	90	90
Volume [Å ³]	1237.41(10)	2950.3(3)
Z	2	4
ρ _{calc} [g/cm ³]	1.085	1.055
μ [mm ⁻¹]	0.203	0.118
F(000)	440	1024
Crystal size [mm ³]	0.512 x 0.352 x 0.228	0.451 x 0.364 x 0.238
Radiation	MoK _α (λ = 0.71073)	MoK _α (λ = 0.71073)
Temperature [K]	100	100
Θ range for data collection [°]	2.528 to 26.357	2.275 to 27.737
Index ranges	-10 ≤ h ≤ 10, -18 ≤ k ≤ 18, -12 ≤ l ≤ 11	-22 ≤ h ≤ 23, -12 ≤ k ≤ 12, -22 ≤ l ≤ 22
Reflections collected	15993	44098
Independent reflections	2511 [R _{int} = 0.0485]	6934 [R _{int} = 0.0444]
Data/restraints/parameters	2511 / 0 / 113	6934 / 0 / 302
Goodness-of-fit on F ^{2[a]}	1.067	1.036
Final R indexes [I ≥ 2σ (I)] ^{[b][c]}	R ₁ = 0.0391, wR ₂ = 0.0937	R ₁ = 0.0433, wR ₂ = 0.1094
Final R indexes [all data]	R ₁ = 0.0570, wR ₂ = 0.1028	R ₁ = 0.0610, wR ₂ = 0.1214
Largest diff. peak/hole [e Å ⁻³]	0.468 / -0.180	0.236 / -0.178

^[a]GOF = $[\sum w(F_0^2 - F_c^2)^2 / (n_0 - n_p)]^{1/2}$. ^[b]R₁ = $\Sigma(|F_0| - |F_c|) / \Sigma|F_0|$, F₀ > 4σ(F₀). ^[c]wR₂ = $\{\Sigma[w(F_0^2 - F_c^2)^2] / \Sigma[w(F_0^2)^2]\}^{1/2}$.

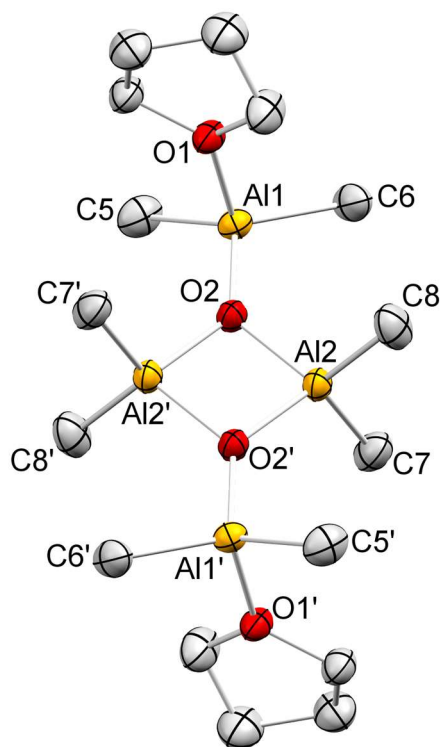


Figure S2. Crystal structure of $[(\text{AlMe}_2)_2\text{O}(\text{thf})]_2$ (**1**) with atomic displacement ellipsoids set at 50% probability. Hydrogen atoms are omitted for clarity. Selected interatomic distances [\AA] and angles [$^\circ$] for **1**: O1–Al1 1.9027(13), Al1–O2 1.7561(13), O2–Al2 1.8239(13), O2–Al2' 1.8235(13), Al1–C5 1.956(2), Al1–C6 1.955(2), Al2–C7 1.964(2), Al2–C8 1.962(2), Al2–O2–Al2' 93.91(6), O2–Al2–O2' 86.09(6).

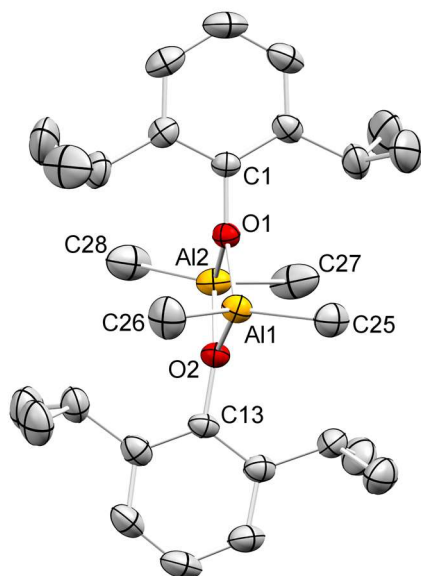


Figure S3. Crystal structure of $(\text{Me}_2\text{AlO-2,6-diisopropylphenyl})_2$ (**2**) with atomic displacement ellipsoids set at 50% probability. Hydrogen atoms are omitted for clarity. Selected interatomic distances [\AA] and angles [$^\circ$] for **2**: C1–O1 1.4066(15), O1–Al1 1.8585(10), O1–Al2 1.8580(10), O2–Al1 1.8622(10), O2–Al2 1.8623(10), O2–C13 1.4094(15), Al1–C25 1.9425(17), Al1–C26 1.9427(17), Al2–C27 1.9394(18), Al2–C28 1.9348(19), Al1–O1–Al2 100.07, Al1–O2–Al2 99.78(5), O1–Al1–O2 79.78(4), O1–Al2–O2 79.79(4).

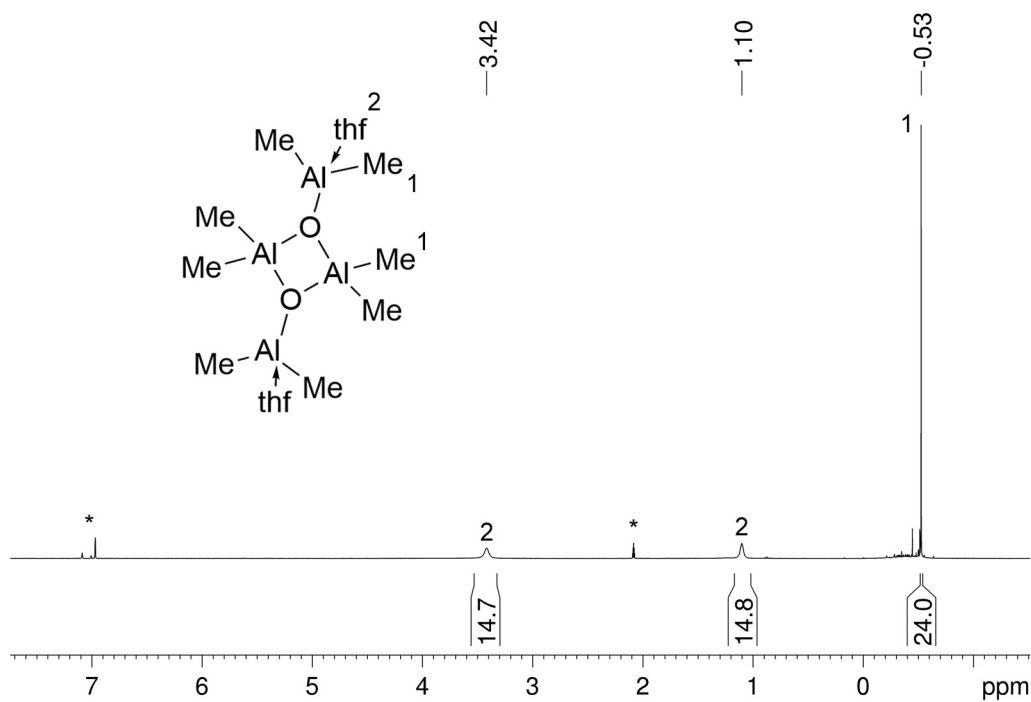


Figure S4. ^1H NMR spectrum of $[(\text{AlMe}_2)_2\text{O}(\text{thf})]_2$ (1) (500.13 MHz, toluene- d_8 , 299 K) solvent residual signals are marked with *.

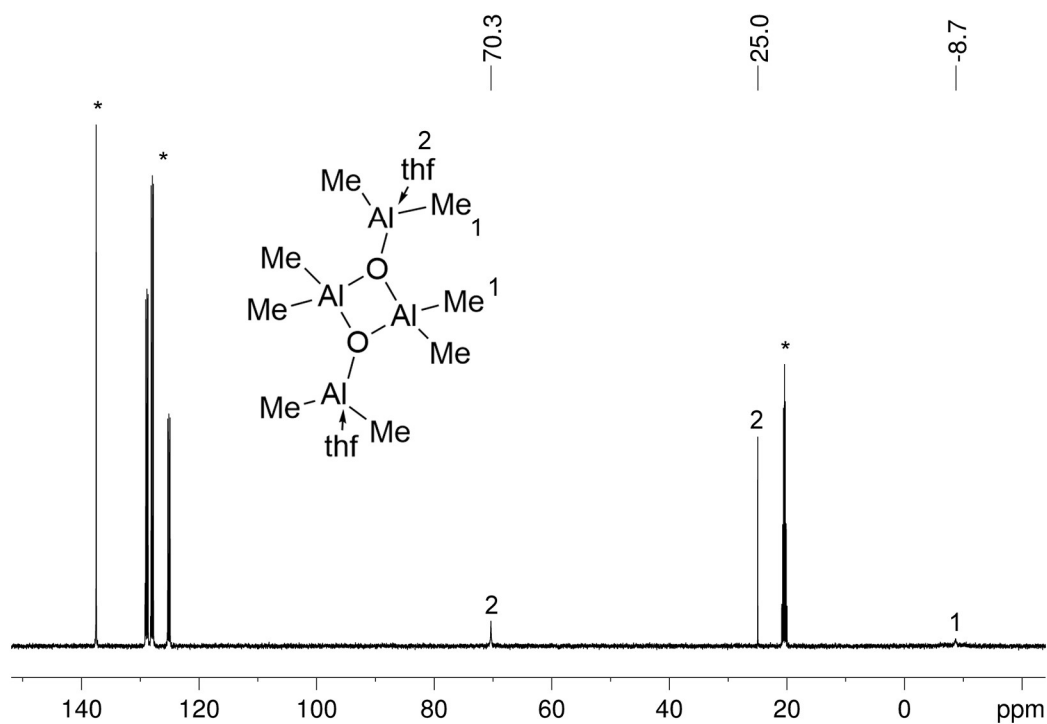


Figure S5. ^{13}C NMR spectrum of $[(\text{AlMe}_2)_2\text{O}(\text{thf})]_2$ (1) (125.76 MHz, toluene- d_8 , 299 K) solvent residual signals are marked with *.

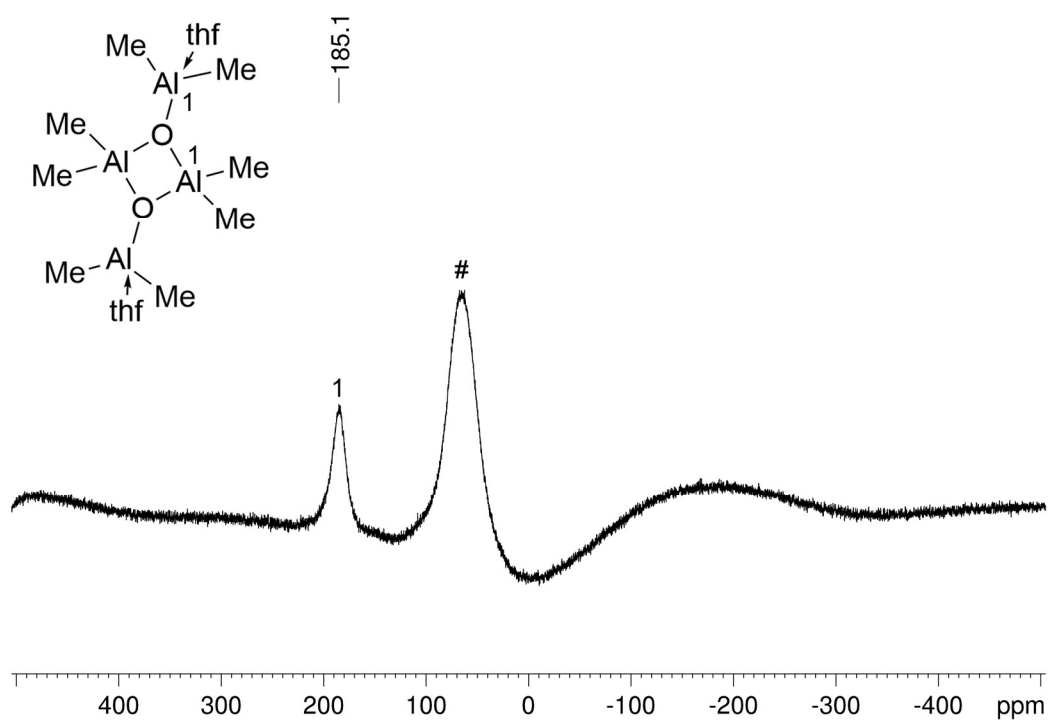


Figure S6. ^{27}Al NMR spectrum of $[(AlMe_2)_2O(thf)]_2$ (**1**) (130.32 MHz, toluene- d_8 , 299 K). A prob head signal is marked with #.

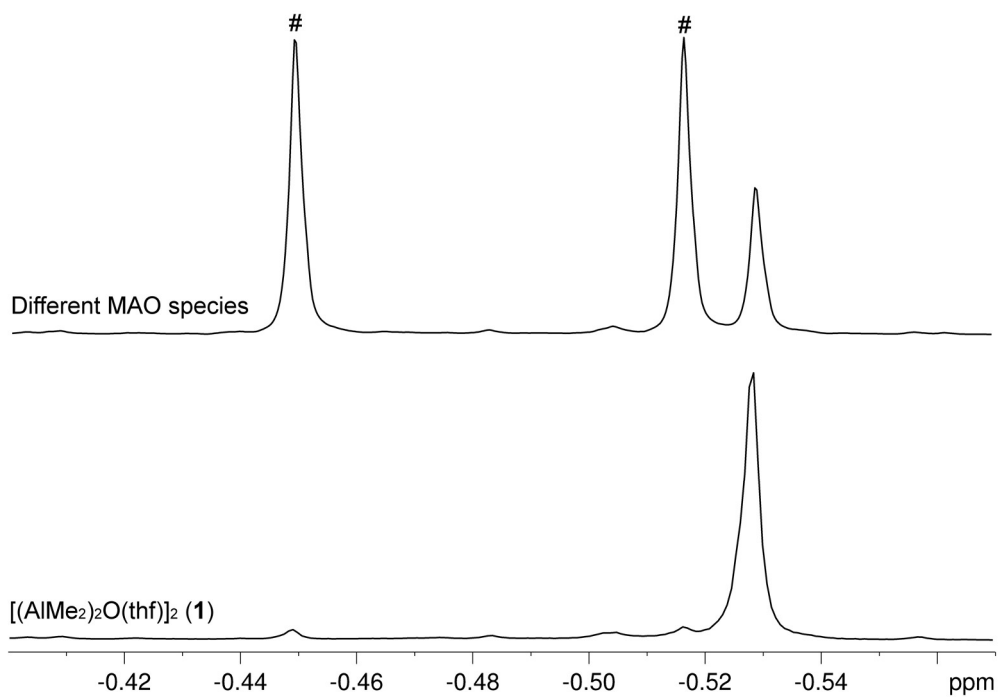


Figure S7. 1H NMR spectrum of $[(AlMe_2)_2O(thf)]_2$ (**1**) (bottom) and from a reaction where H_2O was added quicker to $AlMe_3$ (top) (500.13 MHz, toluene- d_8 , 299 K). The two methyl signals from an unknown MAO species are marked with #.

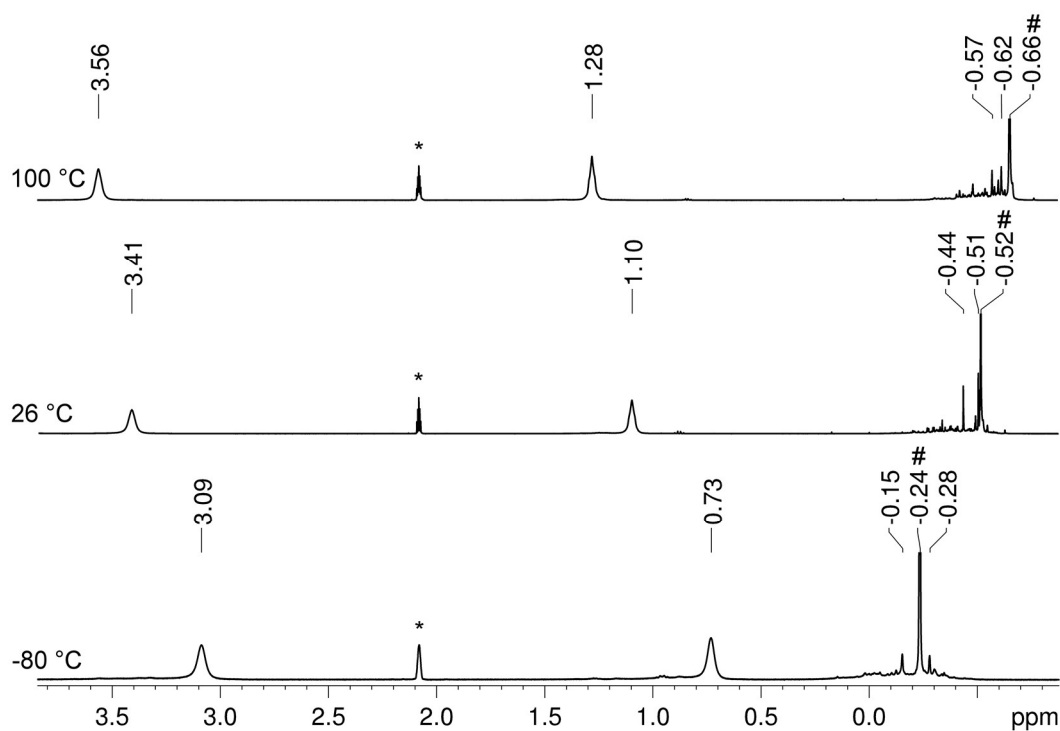


Figure S8. ^1H NMR spectrum of $[(\text{AlMe}_2)_2\text{O}(\text{thf})]_2$ (**1**) with unknown MAO species at $-80\text{ }^\circ\text{C}$ (bottom), $26\text{ }^\circ\text{C}$ (middle) and $100\text{ }^\circ\text{C}$ (top) (500.13 MHz, toluene- d_8) solvent residual signals are marked with *. Methyl signals from **1** are marked with #.

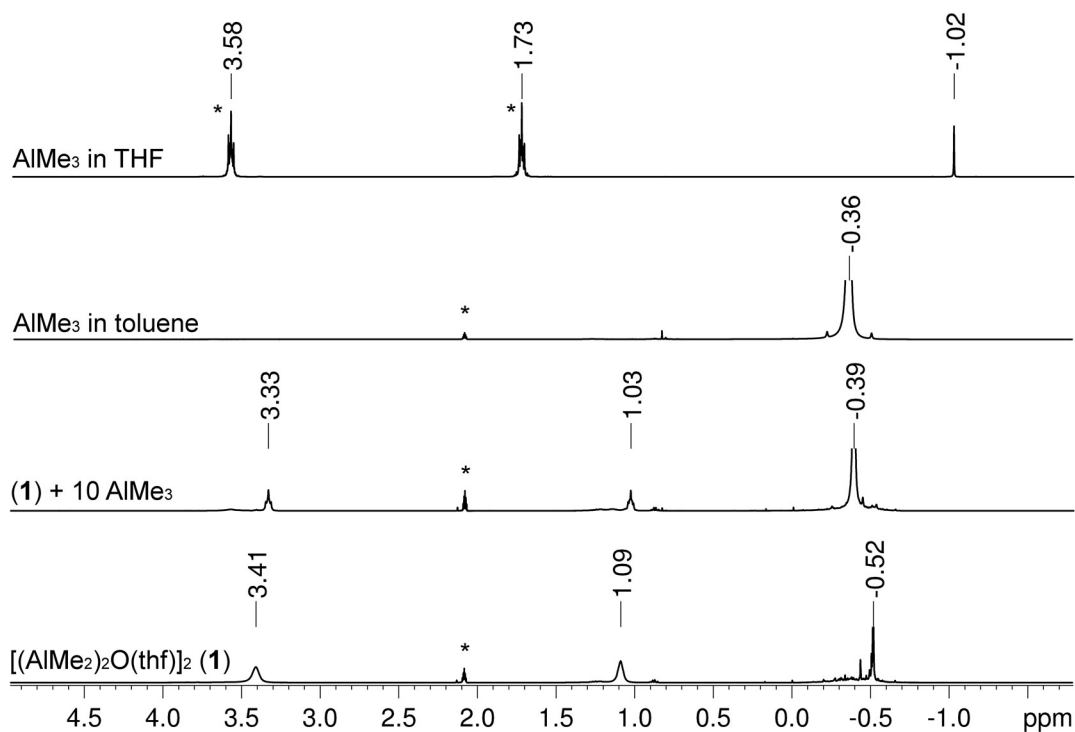


Figure S9. ^1H NMR spectrum of $[(\text{AlMe}_2)_2\text{O}(\text{thf})]_2$ (**1**) (bottom), **1** + 10 AlMe_3 (second from bottom), AlMe_3 in toluene (third from bottom) and AlMe_3 in THF (top) (500.13 MHz, toluene- d_8 (THF- d_8 for top), 299 K) solvent residual signals are marked with *.

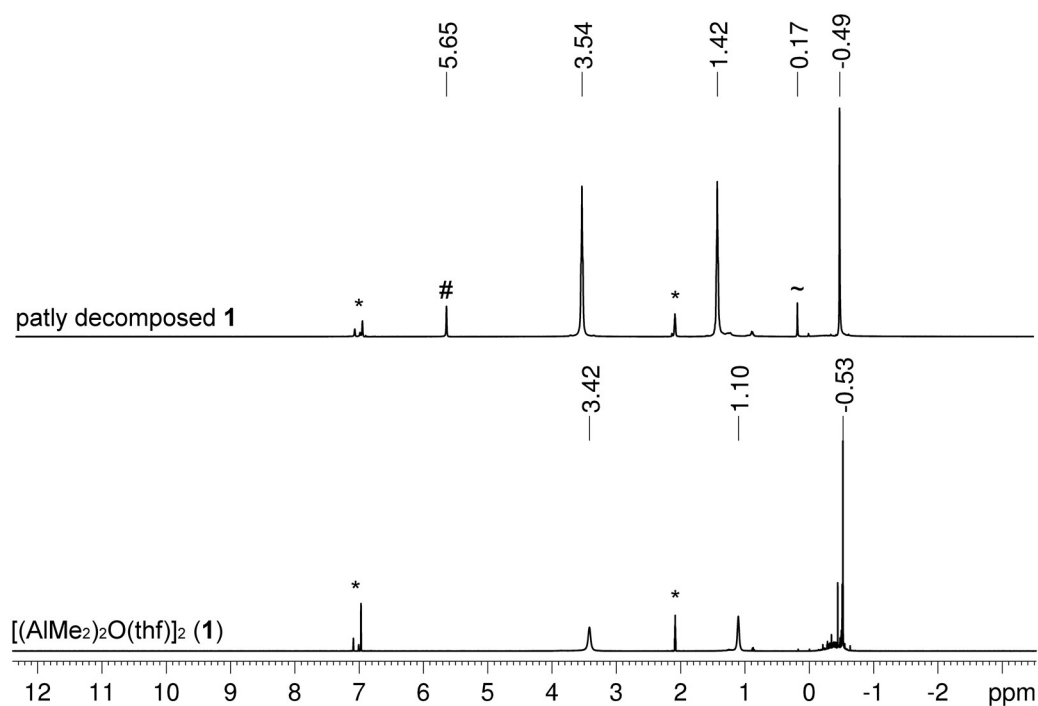


Figure S10. ¹H NMR spectrum of [(AlMe₂)₂O(thf)]₂ (**1**) (bottom) and of **1** that partly decomposed (top) (500.13 MHz, toluene-*d*₈, 299 K) solvent residual signals are marked with *. Methane is marked with ~ and a new signal in the alkylidene region is marked with #. The decomposition only happens at ambient temperature in the dried state.

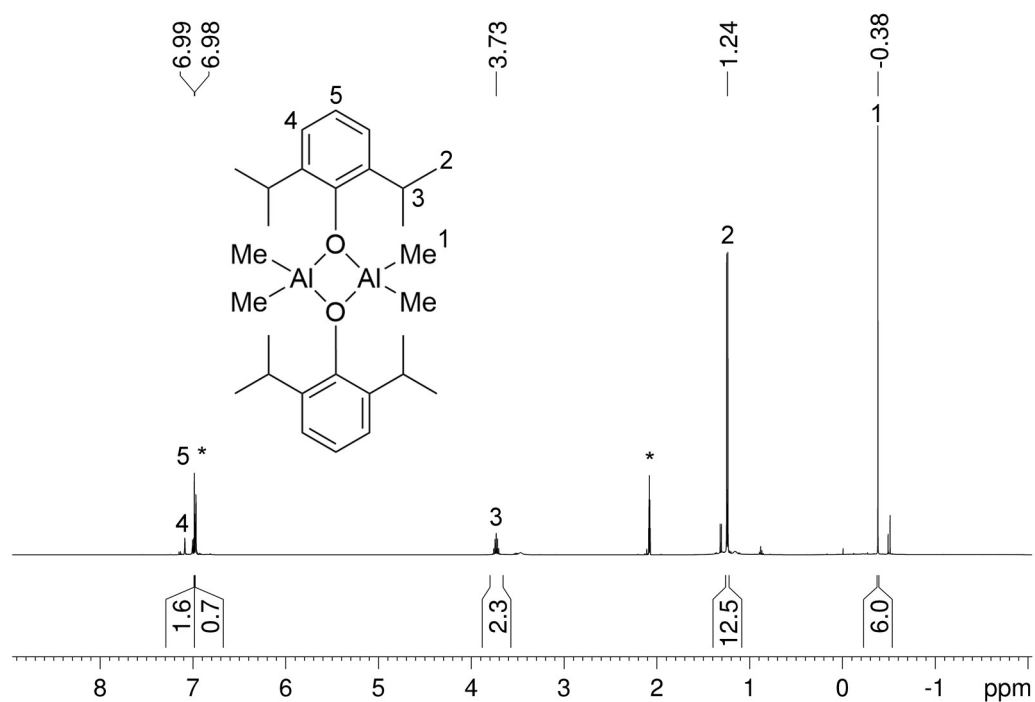


Figure S11. ¹H NMR spectrum of (Me₂AlO-2,6-diisopropylphenyl)₂ (500.13 MHz, toluene-*d*₈, 299 K) solvent residual signals are marked with *.

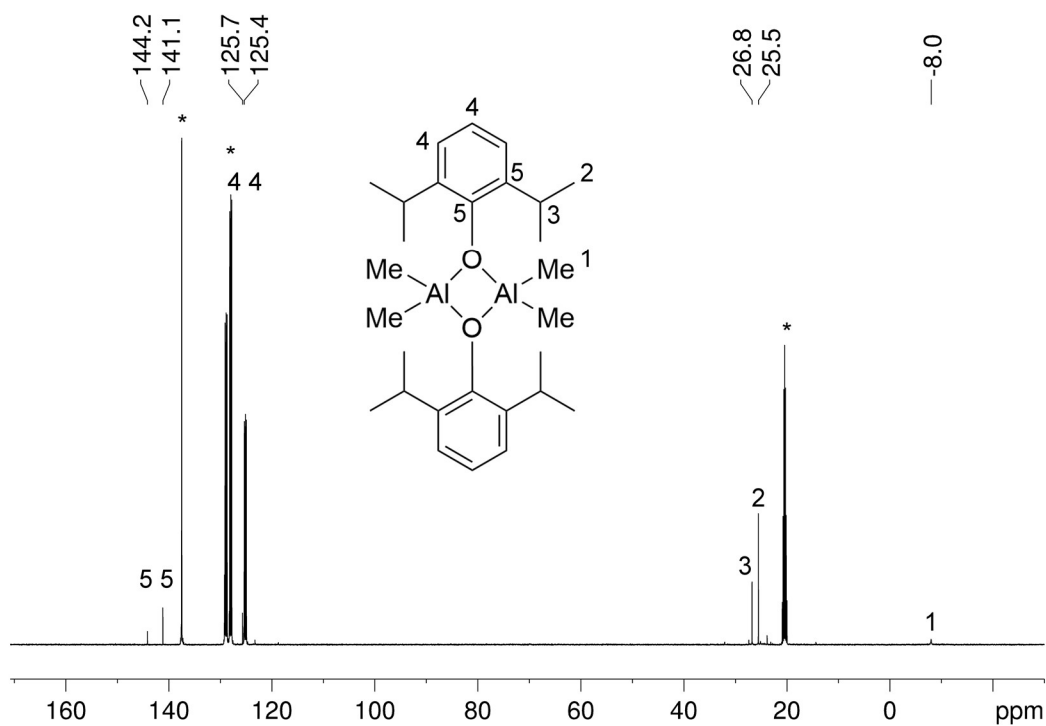


Figure S12. ¹³C NMR spectrum of (Me₂AlO-2,6-diisopropylphenyl)₂ (**2**) (125.76 MHz, toluene-d₈, 299 K) solvent residual signals are marked with *.

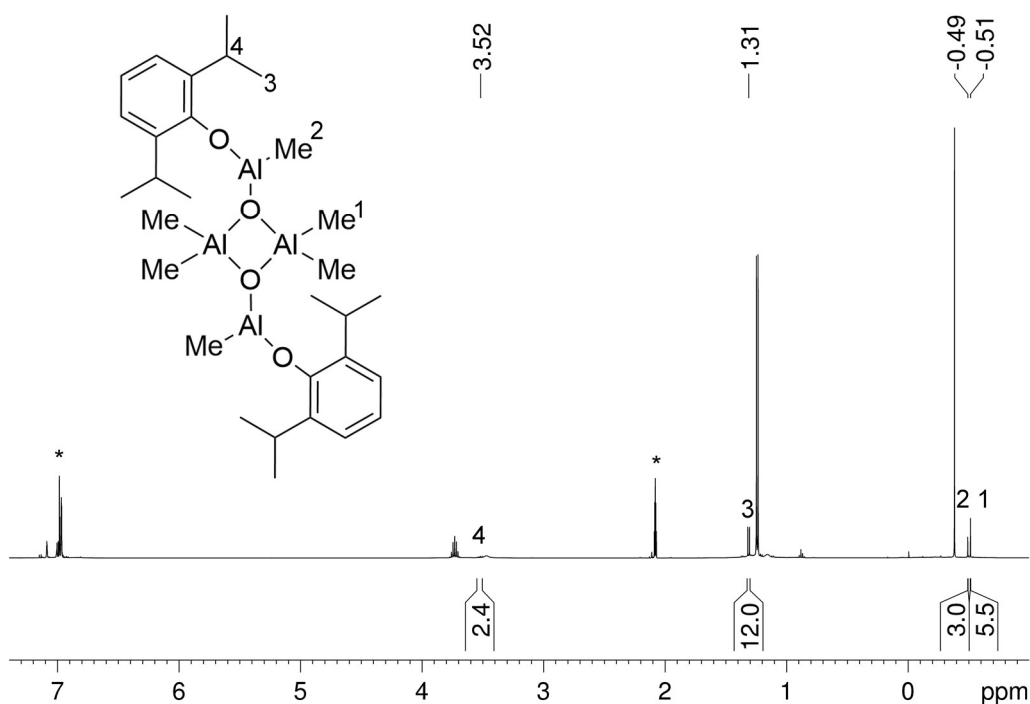


Figure S13. ¹H NMR spectrum of likely (Me₂AlOAlMe-2,6-diisopropylphenol)₂ (500.13 MHz, toluene-d₈, 299 K) solvent residual signals are marked with *.

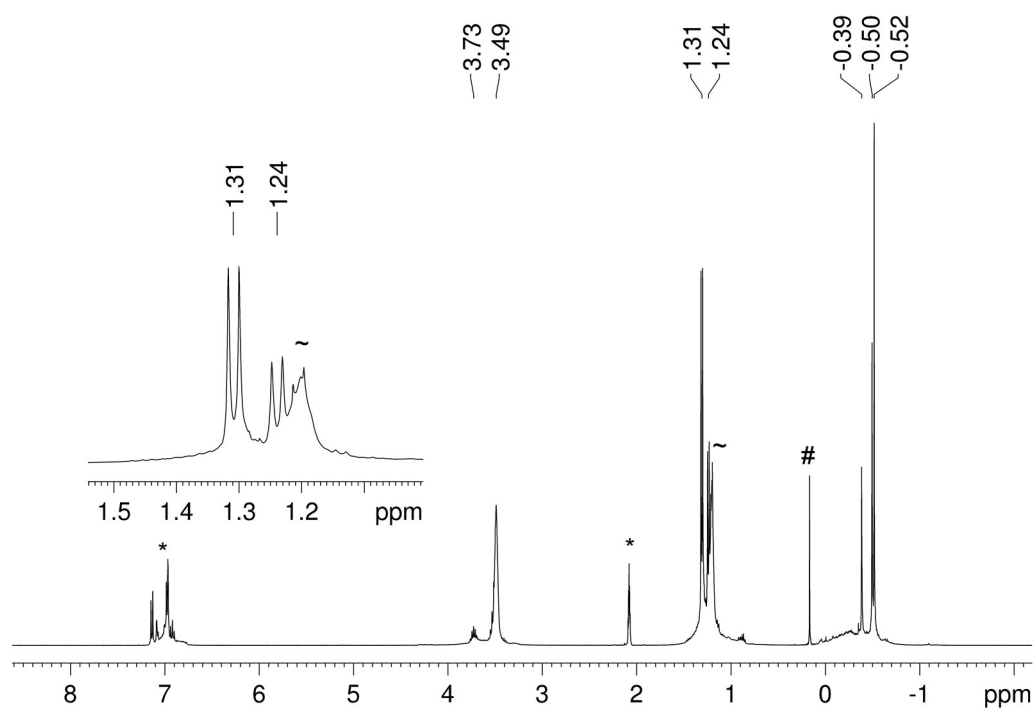


Figure S14. ^1H NMR spectrum of the reaction mixture of **1** with 2 equiv. 2,6-Diisopropylphenol (400.11 MHz, toluene- d_8 , 299 K) solvent residual signals are marked with *. Methane is marked with # and an unknown side product is marked with ~.

DOES experiment of $[(\text{AlMe}_2)_2\text{O}(\text{thf})_2]$ (**1**)

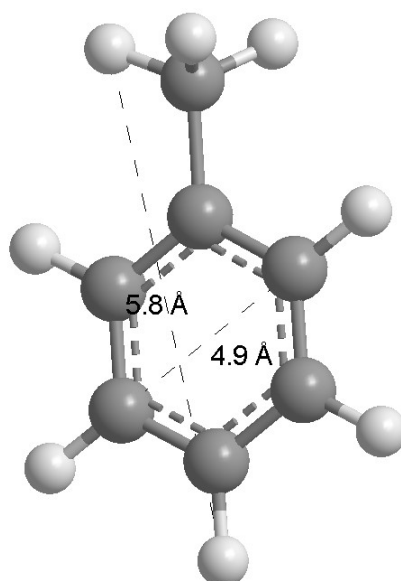


Figure S 15: Chem3D structure of toluene- d_8 .

The following mean radius from the Chem3D optimized structure (**S15**) were used.

Substance	Radius (r)
Toluene- d_8	2.7 Å

The following D-constants were set via the ^1H detected PGSE experiments

Signal	Proton	D-constant
6.9 – 7.2 ppm	Toluene- d_8 (aromatic)	$2.24 \cdot 10^{-9} \text{ m}^2/\text{s}$
-0.47 ppm	O–Al–(CH ₃) ₂ (1)	$1.58 \cdot 10^{-9} \text{ m}^2/\text{s}$

With the Stokes-Einstein correlation $D = \frac{k_B \cdot T}{6\pi \cdot \eta \cdot r_H}$, the solvent radius and the correlating D-constant the viscosity of the sample could be estimated.

$$\eta(\text{sample}) = \frac{k_B \cdot T}{6\pi \cdot D \cdot r_H} = 3,61 \cdot 10^{-4} \text{ Pa s}$$

With this we get a hydrodynamic radius for $[(\text{AlMe}_2)_2\text{O}(\text{thf})_2]$ (**1**) of:

$$r_H = \frac{k_B \cdot T}{6\pi \cdot \eta(\text{sample}) \cdot D(\mathbf{1})} = 3,82 \text{ Å}$$

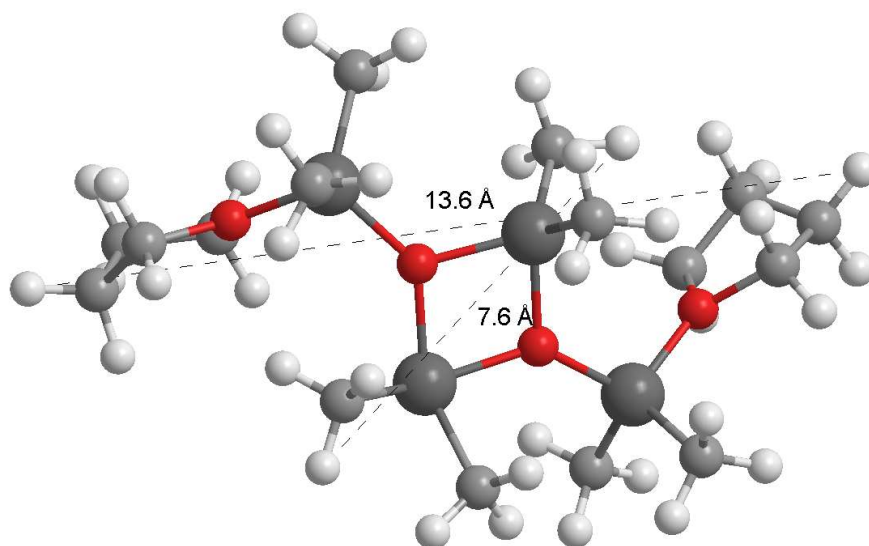


Figure S 16: Chem3D structure of $[(\text{AlMe}_2)_2\text{O}(\text{thf})]_2$ (1).

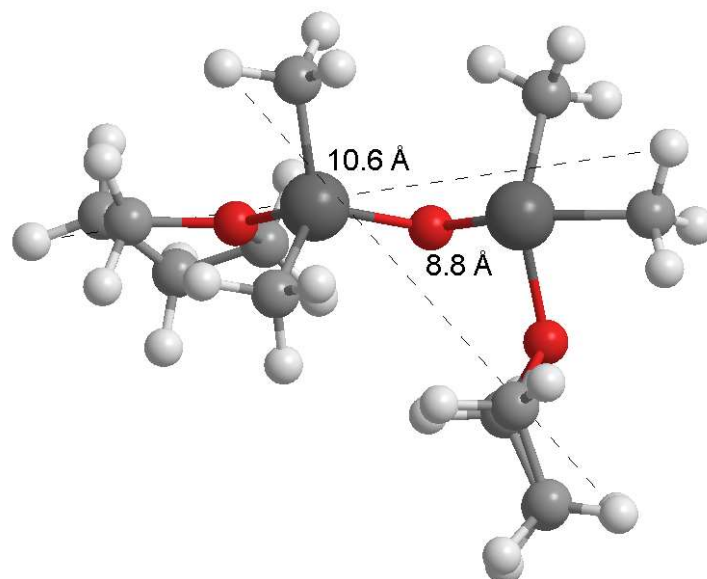


Figure S 17: Chem3D structure the monomer $(\text{AlMe}_2)_2\text{O}(\text{thf})_2$.

References

1. G. R. Fulmer, A. J. M. Miller, N. H. Sherden, H. E. Gottlieb, A. Nudelman, B. M. Stoltz, J. E. Bercaw, K. I. Goldberg, *Organometallics* **2010**, *29*, 2176-2179.
2. TopSpin v. 3.6.1, Bruker AXS Inc., Madison, WI. 2018.
3. L. Bock, X. Tran, Y. Liang, M. Kramer, C. Maichle-Mössmer, R. Anwander, *Organometallics* **2020**, *39*, 1046-1058.
4. COSMO v. 1.61, Bruker AXS Inc., Madison, WI, 2012.
5. APEX 3 v. 2017.3-0, Bruker AXS Inc., Madison, WI. 2017.
6. SAINT v. 8.38A, Bruker AXS Inc., Madison, WI. 2017.
7. L. Krause, R. Herbst-Irmer, G. M. Sheldrick, D. Stalke, *J. Appl. Crystallogr.* **2015**, *48*, 3-10.
8. G. Sheldrick, *Acta Crystallogr. Sect. C* **2015**, *71*, 3-8.
9. C. B. Hubschle, G. M. Sheldrick, B. Dittrich, *J. Appl. Crystallogr.* **2011**, *44*, 1281-1284.
10. D. Kratzert, J. J. Holstein, I. Krossing, *J. Appl. Crystallogr.* **2015**, *48*, 933-938.
11. C. F. Macrae, P. R. Edgington, P. McCabe, E. Pidcock, G. P. Shields, R. Taylor, M. Towler, J. van de Streek, *J. Appl. Crystallogr.* **2006**, *39*, 453-457.
12. POV-Ray v.3.6, Persistence of Vision Pty. Ltd., POV-Ray Williamstown, Victoria, Australia. <http://www.povray.org>, 2004.

**Me₃TACN induced Monomeric
Rare-Earth-Metal Alkyls
via low-temperature Alkylation**

manuscript

Me₃TACN induced Monomeric Rare-Earth-Metal Alkyls via low-temperature Alkylation

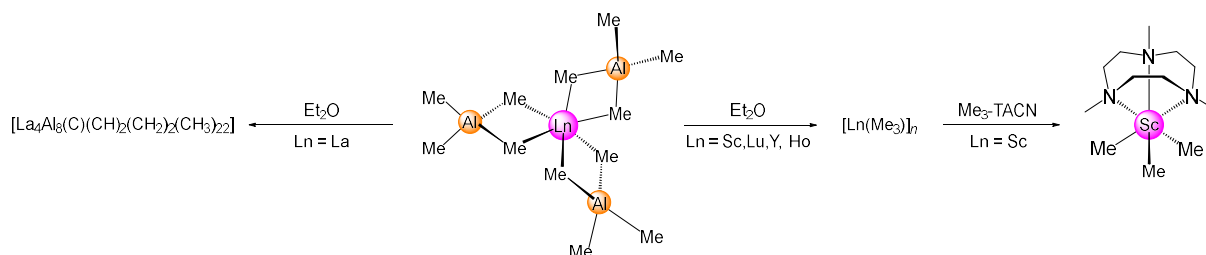
*Jakob Lebon, Tassilo Berger, Cäcilia Maichle-Mössmer, and Reiner Anwander**

Abstract:

Me₃TACN-LnCl₃(thf) was synthesized from the rare-earth-metal chlorides and used as precursor to isolate monomeric alkyls Me₃TACN-LnMe₃(thf) (Ln = La, Ce) and Me₃TACN-Ln(*n*Bu)₃(thf) (Ln = La, Sm). For neodymium monomeric mixed methyl halide lanthanide complexes could be obtained using lower loadings of methyl lithium. The methyl complexes were further reacted with neopentyl alcohol to Me₃TACN-Ln(OCH₂*t*Bu)₃ and the lanthanum *n*-butyl complex was reacted with 2-Bromo-biphenyl to Me₃TACN-La(*n*Bu)₂(2-biphenyl). Solid-state structures of most of these complexes have been obtained and are discussed together with the NMR studies.

Introduction:

While the middle to smaller (Sc, Y-Lu) sized rare-earth-metal tri-methyls are known since 2005, the synthesis of the early rare-earth-metal tri-methyls is an ongoing topic for rare-earth chemists, due to the abundance and lower price of the corresponding precursors. The archetypal tri-methyl complexes [Ln(CH₃)₃] (Ln = Sc, Lu, Y, and Ho) could be achieved in our group via the utilization of donor-induced-aluminate-cleavage with the corresponding tetramethylaluminate complexes [Ln(AlMe₄)₃]^[1-2]. Those transformations are not possible for the larger-sized rare-earth metals, resulting in multiple CH bond activations [La₄Al₃(C)(CH)₂(CH₂)₂(CH₃)₂₂(toluene)]^[3-4] (Scheme 1). Despite several attempts *via* low-temperature cleavage or different donor molecules, the outcome was always too temperature sensitive, thus performing CH bond activations. It is already known that the 1,4,7-Me₃-TACN ligand and related neutral nitrogen ligand systems can stabilize and monomerize pre-formed amorphous [ScMe₃]_{*n*}, and other smaller-sized rare-earth-metal alkyls (Scheme 1). This route is not feasible for the early lanthanides due to the lack of homoleptic alkyl precursors.^[1, 5-7]



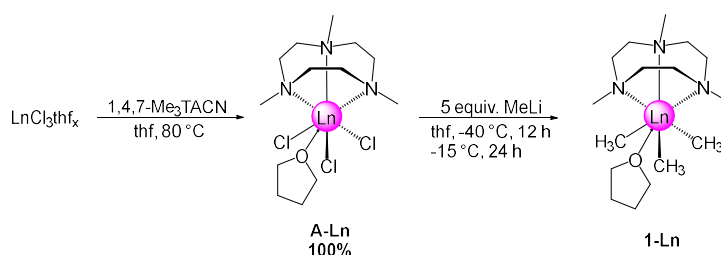
Scheme 1. Known synthesis routes towards homoleptic and donor stabilized rare-earth-metal alkyls.

Other approaches, use the hexamethylate ate-complexes $\text{Li}_3\text{Ln}(\text{Me})_6(\text{do})_x$ as precursors, but always carry the burden of lithium with them^[8-10]. Therefore, the approach in this work was to address this problem *via* a direct synthesis protocol, starting from the Me_3 -TACN stabilized $\text{LnCl}_3\text{thf}_x$, to isolate the hitherto elusive earlier rare-earth-metal methyl complexes.

Results and Discussion:

Jakob Teil:

Utilizing the stabilizing and in particular monomerizing effects of the 1,4,7- Me_3 TACN (Me_3 -TACN) aza-crown, we synthesized the tris methyl complexes for lanthanum and cerium (Scheme 2). While the earlier published $\text{Me}_3\text{TACN-ScMe}_3$ shows considerable stability when the aza-crown is added on to the pure amorphous ScMe_3 , the route via the referring Me_3TACN stabilized rare-earth halide (**A-Ln**) with MeLi bearing a possible repositioning of the aza-crown towards lithium in MeLi or the resulting LiCl , thus destabilizing the alkyl^[1].



Scheme 2. Synthesis route of the $\text{Me}_3\text{TACN-LnMe}_3(\text{thf})$ (**1-Ln**) species via the $\text{Me}_3\text{TACN-LnLnE}_3(\text{thf})$ (**A-Ln**).

This exchange and the intrinsic thermal lability of the resulting $\text{Me}_3\text{TACN-LnMe}_3(\text{thf})$ led to this synthesis protocol, yielding the trialkyl species **1-La** and **1-Ce** (Figure 1). Being the first tris methyl complexes of the earlier rare-earth-metals, no unexpected change in the interatomic distance occurs. Respectively two of the methyl groups are at the same distance to the center and one is slightly elongated, the same happens for the nitrogen-Ln bond. The proton NMR of **1-La** shows a splitting of two signals for the “exo” and “endo” protons of the ethyl bridge and a singlet for the methyl groups on the nitrogen. The methyl groups on the lanthanum are with –

1.08 ppm, stronger shifted to higher fields, compared to the earlier published $\text{Me}_3\text{TACN-ScMe}_3$ with -0.65 ppm^[1].

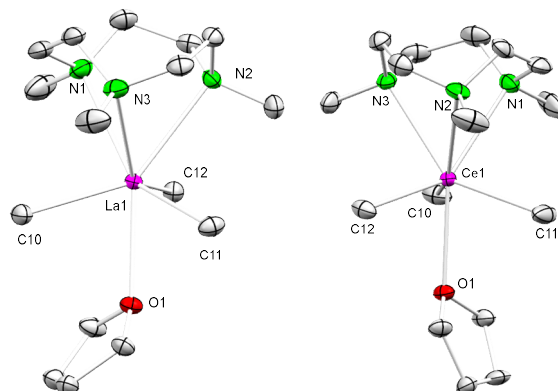


Figure 1. Crystal structure of **1-La** (left) and **1-Ce** (right). All hydrogen atoms have been omitted for clarity. Selected interatomic distances (Å) and angles (°): La(1)-N(2) 2.772(5), La(1)-N(1) 2.795(3), La(1)-N(3) 2.824(3), La(1)-C(10) 2.628(10), La(1)-C(12) 2.699(8), C(11)-La(1) 2.628(3), C(10A)-La(1)-C(11) 118.1(2), C(10)-La(1)-O(1) 76.4(2), C(10)-La(1)-N(1) 87.0(2), O(1)-La(1)-N(1) 142.78(8); C(10)-Ce(1) 2.606(3), C(11)-Ce(1) 2.639(3), C(12)-Ce(1) 2.641(3), N(1)-Ce(1) 2.793(3), N(2)-Ce(1) 2.752(2), N(3)-Ce(1) 2.764(3), O(1)-Ce(1) 2.6835(18), C(10)-Ce(1)-O(1) 75.51(8), C(10)-Ce(1)-N(1) 85.38(12), O(1)-Ce(1)-N(1) 143.82(9).

It is crucial to mention, that commercially available MeLi contains a certain amount of LiCl , therefore it was important for the formation of the Me_3TACN -stabilized tri-methyls, to use 5 equivalents of MeLi . If however, lower equivalents of MeLi are used, utilizing the same route (Scheme 2), we were able to isolate mixed halogen methyl species for Me_3TACN -stabilized neodymium chlorides (Figure 2). The amount of remaining halogen on the rare-earth metal could be attested via elemental analysis and SCXRD. To our surprise, a statistical distribution takes place. Thus, there must be an active chloride/methyl exchange between the different species from $\text{Me}_3\text{TACN-LnMe}_3(\text{thf})$ and $\text{Me}_3\text{TACN-LnCl}_3(\text{thf})$ and their mixed chloride/methyl intermediates.

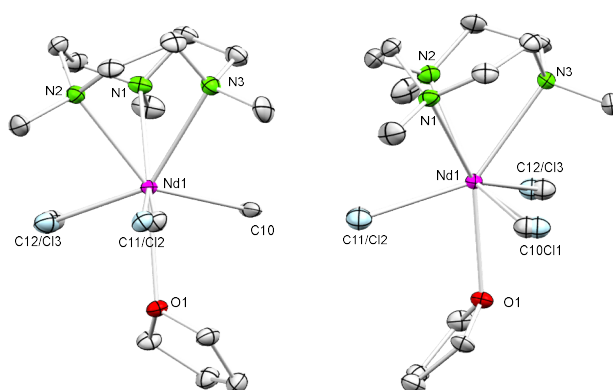
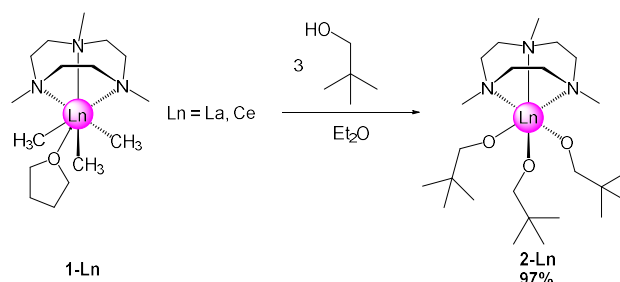


Figure 2. Crystal structure of **1-NdCl_{0.25}** (left) and **1-NdCl_{0.5}** (right). For selected interatomic distances and angles, see SI (Figure S 25 and S 26).

To further investigate the properties of the $\text{Me}_3\text{TACN-LnMe}_3(\text{thf})$, we choose a simple reaction with 3 equivalents of neopentyl alcohol, resulting in the monomeric species **2-La** and **2-Ce** (Scheme 3).



Scheme 3. Reaction of $\text{Me}_3\text{TACN-LnMe}_3(\text{thf})$ with 3 equiv. of HOCH_2tBu , yielding in the lanthanum complex (**2-La**) and the cerium complex (**2-Ce**).

While the complex is well stabilized via alkoxides and the aza-crown, the steric demand is almost too much. Hence, one of the aza-crown nitrogen atoms is not at a bonding distance from the cerium core anymore (N1-Ce1 3.295 Å), while the other two are (N2-Ce1 2.784(7) and N3-Ce1 2.813(6) Å). The same interatomic distance splitting can be shown by the Ce-O , with the two bonds in a shorter range (1.929(5) and 1.947(4) Å) and one extremely elongated Ce-O distance with 2.451(5) Å (Figure 4).

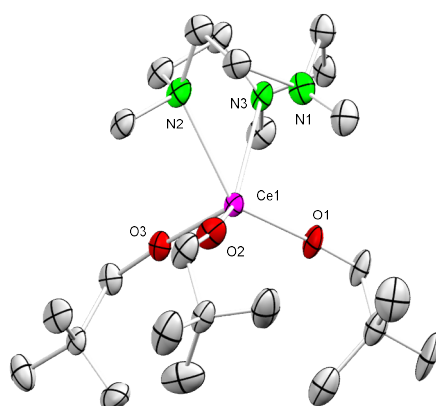


Figure 3. Crystal structure of $\text{Me}_3\text{TACN-Ce}(\text{OCH}_2\text{tBu})_3$ (**2-Ce**). All hydrogen atoms have been omitted for clarity. Selected interatomic distances (Å) and angles ($^\circ$): $\text{N}(1)\text{-Ce}(1)$ 3.295, $\text{N}(2)\text{-Ce}(1)$ 2.784(7), $\text{N}(3)\text{-Ce}(1)$ 2.813(6), $\text{Ce}(1)\text{-O}(2)$ 1.929(5), $\text{Ce}(1)\text{-O}(1)$ 1.947(4), $\text{Ce}(1)\text{-O}(3)$ 2.451(5), $\text{C}(3)\text{-N}(2)\text{-Ce}(1)$ 106(2), $\text{C}(2)\text{-N}(2)\text{-Ce}(1)$ 133.6(14), $\text{O}(2)\text{-Ce}(1)\text{-O}(1)$ 104.4(2), $\text{O}(2)\text{-Ce}(1)\text{-O}(3)$ 107.0(2), $\text{O}(1)\text{-Ce}(1)\text{-O}(3)$ 108.8(2).

Tassilo Teil:

Since we saw that we can isolate monomeric rare-earth methyls. We next wanted to see if this is also possible for other alkyls. The first we tested was *n*-butyl. We reacted $\text{Me}_3\text{TACN-LaCl}_3(\text{thf})$ with three equivalents of *n*-BuLi. The NMR spectra we recorded of this substance fit well but we could not get any crystals that were suitable for x-ray diffraction. We repeated this

reaction with different rare-earth-metal chlorides and had luck with samarium that we could at least get a connectivity (Figure 5).

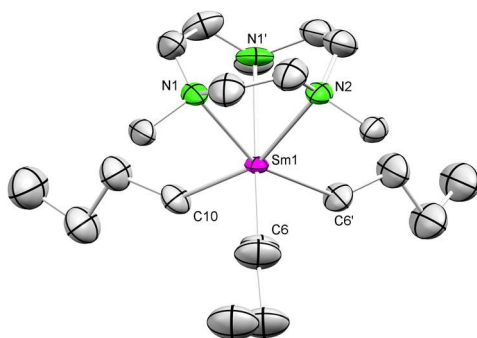
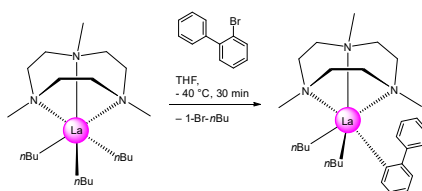


Figure 4. Connectivity of $\text{Me}_3\text{TACN-Sm}(\text{nBu})_3$ (**3**) with ellipsoids set at 30%.

The samarium is bound to three-terminal *n*-butyl ligands and the coordination sphere is completed with the aza-crown. Since the NMR fits it can be assumed that the lanthanum analog is similar. It is noteworthy, that these *n*-butyl complexes are pretty unstable at least similar to the $\text{Li}_3\text{Ln}(\text{nBu})_6(\text{thf})_4$ complexes we reported earlier.^[11] Maybe even more so, after a few hours in solution at $-40\text{ }^\circ\text{C}$ the complexes already decomposed completely. Since we still have such a high reactivity we wanted to test the lanthanum complex on the findings the Knochel group reported recently.^[12] Here they used 2-bromo-biphenyl derivatives and the proposed $\text{nBu}_2\text{LaCl}(\text{LiCl})_4$ to get supposedly lantha-fluorenyl complexes (Scheme 4).



Scheme 4. Reaction of $\text{Me}_3\text{TACN-La}(\text{nBu})_3$ (**4**) with 2-Bromo-biphenyl.

At low temperature, we could however only see the exchange of one *n*-butyl ligand for a biphenyl (Figure 6).

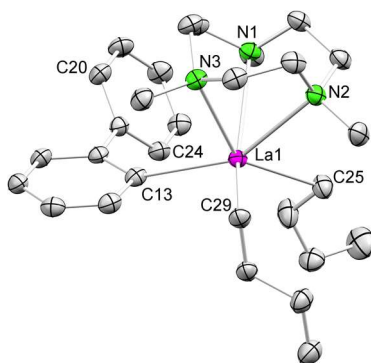


Figure 5. Crystal structure of $\text{Me}_3\text{TACN-La}(\text{nBu})_2(2\text{-biphenyl})$ (**4**) with atomic displacement ellipsoids set at 50% probability. Hydrogen atoms and disorders of one *n*-Bu group are omitted for clarity. Selected interatomic distances [Å] and angles [°] for X:

La1–C25 2.567(3), La1–C29 2.544(2), La1–C13 2.672(2), La1–C24 4.3552(2), La1–C20 5.2256(2), La1–N1 2.7458(19), La1–N2 2.813(2), La1–N3 2.780(2), C29–La1–C25 106.10(9), C13–La1–C29 102.53(8), C13–La1–C25 120.57(8).

One carbon atom (C24) is oriented in the direction of the lanthanum core but is still quite far away with 4.3552(2) Å. We did also warm up the biphenyl complex. It decomposed quite fast into a black solution. During this time, we observed the aromatic region but didn't observe activation of a proton (Figure S11 see SI). We therefore couldn't observe the formation of a lanthan-fluorenyl complex with the aza-crown present.

Conclusion

Using the monomerizing effect of the Me₃-TACN ligand the tri-methyl complexes Me₃TACN-LnMe₃(thf) for lanthanum and cerium could be isolated. For neodymium incomplete methylation was observed and the novel, monomeric, mixed alkyl chloride complex Me₃TACN-NdMe_{2,75/2,5}Cl_{0,25/0,5}(thf) was characterized. The cerium complex was reacted with neopentanol resulting in the complex Me₃TACN-Ce(OCH₂*t*Bu)₃. The Me₃-TACN ligand coordinates in this complex only via two nitrogen atoms, demonstrating its flexibility in chase of too much sterical demand of the other ligands. Furthermore, the stabilizing effects of the Me₃-TACN ligand were studied using the thermodynamically less stable *n*-butyl ligand in comparison to the methyl ligand. A connectivity of Me₃TACN-Sm(*n*Bu)₃ is reported and NMR studies of the lanthanum analog suggest the same structure.

Uncategorized References

- [1] D. Barisic, D. Diether, C. Maichle-Mössmer, R. Anwander, *J. Am. Chem. Soc.* **2019**, *141*, 13931-13940.
- [2] H. M. Dietrich, G. Raudaschl-Sieber, R. Anwander, **2005**, *44*, 5303-5306.
- [3] M. Zimmermann, D. Rauschmaier, K. Eichele, K. W. Törnroos, R. Anwander, *Chem. Commun.* **2010**, *46*, 5346-5348.
- [4] L. C. Gerber, E. Le Roux, K. W. Törnroos, R. Anwander, *Chemistry—A European Journal* **2008**, *14*, 9555-9564.
- [5] S. Ge, A. Meetsma, B. Hessen, *Organometallics* **2008**, *27*, 5339-5346.
- [6] S. Ge, S. Bambirra, A. Meetsma, B. Hessen, *Chem. Commun.* **2006**, 3320-3322.
- [7] C. S. Tredget, S. C. Lawrence, B. D. Ward, R. G. Howe, A. R. Cowley, P. Mountford, *Organometallics* **2005**, *24*, 3136-3148.
- [8] H. Schumann, *Organometallics* **1984**, *3*, 10.1021.
- [9] H. Schumann, J. Pickardt, N. Bruncks, *Angew. Chem. Int. Ed. Engl.* **1981**, *20*, 120-121.
- [10] H. Schumann, J. Müller, *Angew. Chem. Int. Ed. Engl.* **1978**, *17*, 276-276.
- [11] T. Berger, J. Lebon, C. Maichle-Mössmer, R. Anwander, *Angew. Chem. Int. Ed.* **2021**, *60*, 15622-15631.
- [12] B. Wei, D. Zhang, Y.-H. Chen, A. Lei, P. Knochel, *Angew. Chem. Int. Ed.* **2019**, *58*, 15631-15635.

Me₃TACN-LaMe₃(thf) (1-La). Me₃TACN-LaCl₃(thf) (200 mg, 0.41 mmol) was suspended in thf (10 mL) and cooled to -40 °C. Then, a solution of MeLi (35.98 mg, 1.63 mmol, 4 equiv., in thf) was added dropwise. The suspension was stirred for 12 h at -40 °C and additional 24 h at -15 °C. The suspension was filtered and concentrated in vacuo. Crystals of **1-Ce** suitable for XRD analysis were obtained from a highly concentrated thf solution.

¹H NMR, (500.13 MHz, 233 K, thf-*d*₈): δ = 3.61 (s, 4 H, thf), 3.08–3.01 (m, 6 H, CH₂-Me₃TACN), 2.71–2.61 (m, 6 H, CH₂-Me₃TACN), 2.64 (s, 9 H, CH₃-Me₃TACN), 1.77 (s, 4 H, thf), -1.08 (s, 9 H, La(CH₃)₃) ppm.

¹³C NMR of, (125.76 MHz, 233 K, thf-*d*₈): δ = 69.4 (thf), 57.3 (CH₂-Me₃TACN), 47.9 (CH₃-Me₃TACN), 38.7 (La(CH₃)₃), 27.6 (thf) ppm.

Anal. (%) calcd. for C₁₆H₃₈LaN₃O (427.41 gmol⁻¹): C 44.96, H 8.96, N 9.83; found: C 43.93, H 8.29, N 9.99. The deviation between theoretical and experimental microanalytical data derives from the fast decomposition at ambient temperature.

Me₃TACN-CeMe₃(thf) (1-Ce). Me₃TACN-CeCl₃(thf) (200 mg, 0.41 mmol) was suspended in thf (10 mL) and cooled to -40 °C. Then, a solution of MeLi (35.89 mg, 1.63 mmol, 4 equiv., in thf) was added dropwise. The suspension was stirred for 12 h at -40 °C and additional 24 h at -15 °C. The suspension was filtered and concentrated in vacuo. Crystals of **1-Ce** suitable for XRD analysis were obtained from a highly concentrated thf solution.

¹H NMR, (500.13 MHz, 233 K, thf-*d*₈): δ = 9.37 (s, 9 H, La(CH₃)₃), 7.72 (s, 9 H, CH₃-Me₃TACN), 3.56 (s, 4 H, thf), 1.77 (s, 4 H, thf), 0.66 (m, 6 H, CH₂-Me₃TACN), -5.11 (m, 6 H, CH₂-Me₃TACN) ppm.

Anal. (%) calcd. for C₁₆H₃₈CeN₃O (428.62 gmol⁻¹): C 44.84, H 8.94, N 9.80; found: C 44.24, H 8.50, N 9.92.

Me₃TACN-NdMe_{2.5}Cl_{0.5}(thf) (1-NdCl_{0.5}). Me₃TACN-NdCl₃(thf) (200 mg, 0.41 mmol) was suspended in thf (10 mL) and cooled to -40 °C. Then, a solution of MeLi (35.89 mg, 1.63 mmol, 3.5 equiv., in thf) was added dropwise. The suspension was stirred for 12 h at -40 °C and additional 24 h at -15 °C. The suspension was filtered and concentrated in vacuo. Crystals of **1-NdCl_{0.25}** suitable for XRD analysis were obtained from a highly concentrated thf solution.

Anal. (%) calcd. for C₁₆H₃₈NdN₃O (442.74 gmol⁻¹): C 42.08, H 8.31, N 9.49; found: C 41.68, H 8.04, N 10.92.

Me₃TACN-NdMe_{2.75}Cl_{0.25}(thf) (1-NdCl_{0.25}). Me₃TACN-NdCl₃(thf) (200 mg, 0.41 mmol) was suspended in thf (10 mL) and cooled to -40 °C. Then, a solution of MeLi (35.89 mg, 1.63 mmol, 3 equiv., in thf) was added dropwise. The suspension was stirred for 12 h at -40 °C and additional 24 h at

–15 °C. The suspension was filtered and concentrated in vacuo. Crystals of **1-NdCl_{0.25}** suitable for XRD analysis were obtained from a highly concentrated thf solution.

Anal. (%) calcd. for C₁₆H₃₈NdN₃O (438.14 gmol⁻¹): C 43.16, H 8.56, N 9.59; found: C 42.83, H 8.22, N 9.15.

Me₃TACN-La(OCH₂*t*Bu)₃ (**2-La**). Me₃TACN-LaMe₃(thf) (100 mg, 0.23 mmol) was suspended in thf (3 mL) and cooled to –40 °C. Then, a solution of HOCH₂*t*Bu (61.87 mg, 0.70 mmol, 3 equiv., in Et₂O) was added dropwise. The suspension was stirred for 1 h at ambient temperatures. The solution was concentrated in vacuo.

¹H NMR, (400.11 MHz, 298 K, C₆D₆): δ = 3.86 (s, 6 H, OCH₂C(CH₃)₃), 2.46 (s, 9 H, CH₃-Me₃TACN), 2.34–2.26 (m, 6 H, CH₂-Me₃TACN), 1.82–1.74 (m, 6 H, CH₂-Me₃TACN), 1.23 (s, 27 H, OCH₂C(CH₃)₃) ppm.

¹³C NMR of, (100.61 MHz, 298 K, C₆D₆): δ = 81.5 (OCH₂(CH₃)₃), 57.3 (CH₂-Me₃TACN), 45.4 (CH₃-Me₃TACN), 34.9 (OCH₂C(CH₃)₃), 27.1 (OCH₂C(CH₃)₃) ppm.

Anal. (%) calcd. for C₂₄H₅₄LaN₃O₃ (571.62 gmol⁻¹): C 50.43, H 9.52, N 7.35; found: C 50.22, H 9.31, N 7.57. Crystals of **2-La** suitable for XRD analysis were obtained from a highly concentrated Et₂O solution.

With the same reaction conditions Me₃TACN-Ce(OCH₂*t*Bu)₃ (**2-Ce**) was also synthesized. Crystals of **2-Ce** suitable to SCXRD structure obtained from a highly concentrated *n*-hexane solution.

Me₃TACN-La(*n*Bu)₃ (**3-La**). Me₃TACN-LaCl₃(thf) (30.0 mg, 0.06 mmol) was suspended in Et₂O (5 mL) and cooled to –40 °C. Then, *n*-BuLi (0.18 mmol, 3 equiv., 2.5 M in hexanes) was added dropwise. After stirring the suspension for one hour, it was filtered and the solvent removed in vacuo to give white powder of Me₃TACN-La(*n*Bu)₃·*x*LiCl (*x*≤3). The exact yield could not be determined due to the incorporation of LiCl and some minor THF and *n*-BuLi impurities. But it appears to be almost quantitative.

¹H NMR, (500.13 MHz, 233 K, toluene-*d*₈): δ = 2.30 (s, 9 H, CH₃-Me₃TACN), 2.13 (m, 6 H, CH₂-Me₃TACN), 2.04 (m, 6 H (integral overlaps with toluene-*d*₈ signal), CH₂-*n*Bu), 1.94 (m, 6 H, CH₂-*n*Bu), 1.54 (m, 6 H, CH₂-Me₃TACN), 1.39 (t, 9 H, CH₃-*n*Bu), 0.10 ppm (t, 6 H, CH₂-*n*Bu).

¹³C NMR of, (125.76 MHz, 233 K, toluene-*d*₈): δ = 55.4 (CH₂-*n*Bu), 53.8 (CH₂-Me₃TACN), 45.3 (CH₃-Me₃TACN), 32.3 (CH₂-*n*Bu), 31.4 (CH₂-*n*Bu), 15.3 ppm (CH₃-*n*Bu).

Anal. (%) calcd. for C₂₁H₄₈LaN₃ (481.54 gmol⁻¹): C 52.38, H 10.05, N 8.73; found: C 52.07, H 9.77, N 7.34. The deviation between theoretical and experimental microanalytical data derives from the fast

decomposition at ambient temperature. With the same reaction conditions $\text{Me}_3\text{TACN-Sm}(n\text{Bu})_3$ (**3-Sm**) was also synthesized. Crystals of **3-Sm** suitable to get a connectivity in a XRD analysis were obtained from a highly concentrated THF/n-hexane solution.

$\text{Me}_3\text{TACN-La}(n\text{Bu})_2(2\text{-biphenyl})$ (**4**). $\text{Me}_3\text{TACN-LaCl}_3(\text{thf})$ (30.0 mg, 0.06 mmol) was suspended in Et_2O (5 mL) and cooled to $-40\text{ }^\circ\text{C}$. Then, $n\text{-BuLi}$ (0.18 mmol, 3 equiv., 2.5 M in hexanes) was added dropwise. After stirring the suspension for one hour, 2-Br-biphenyl (14.0 mg, 0.06 mmol, 1 equiv.) dissolved in Et_2O was added dropwise. The suspension was further stirred for 30 min, before it was filtered and the solvent removed in vacuo to give white powder of $\text{Me}_3\text{TACN-La}(n\text{Bu})_2(2\text{-biphenyl})\cdot x\text{LiCl}$ ($x \leq 3$). The exact yield could not be determined due to the incorporation of LiCl and some THF impurities. But it appears to be almost quantitative. Crystals of **4** suitable for XRD analysis were obtained from a highly concentrated Et_2O solution. Note: The oily consistency of the crystallization process is not a suitable method for purification.

$^1\text{H NMR}$, (500.13 MHz, 233 K, $\text{THF-}d_8$): $\delta = 7.84$ (d, 1 H, *H*-biphenyl), 7.62 (d, 2 H, *H*-biphenyl), 7.19 (t, 2 H, *H*-biphenyl), 7.08 (d, 1 H, *H*-biphenyl), 7.01 (t, 1 H, *H*-biphenyl), 6.69 (m, 2 H, *H*-biphenyl), 2.86 (m, 3 H, $\text{CH}_2\text{-Me}_3\text{TACN}$), 2.66 (m, 3 H, $\text{CH}_2\text{-Me}_3\text{TACN}$), 2.54, 2.52 (m, 7 H, $\text{CH}_2\text{-Me}_3\text{TACN}$, $\text{CH}_3\text{-Me}_3\text{TACN}$), 2.40 (m, 3 H, $\text{CH}_2\text{-Me}_3\text{TACN}$), 2.21 (s, 4 H, $\text{CH}_3\text{-Me}_3\text{TACN}$), 1.47 (m, 4 H, $\text{CH}_2\text{-}n\text{Bu}$), 1.19 (m, 4 H, $\text{CH}_2\text{-}n\text{Bu}$), 0.82 (m, 6 H, $\text{CH}_3\text{-}n\text{Bu}$), -0.50 ppm (m, 4 H, $\text{CH}_2\text{-}n\text{Bu}$).

$^{13}\text{C NMR}$, (125.76 MHz, 233 K, $\text{THF-}d_8$): $\delta = 152.8$ (*C*-biphenyl), 142.9 (*C*-biphenyl), 129.4 (*C*-biphenyl), 128.6 (*C*-biphenyl), 127.7 (*C*-biphenyl), 127.5 (*C*-biphenyl), 124.2 (*C*-biphenyl), 123.7 (*C*-biphenyl), 122.8 (*C*-biphenyl), 121.9 (*C*-biphenyl), 58.4 ($\text{CH}_2\text{-}n\text{Bu}$), 55.2 ($\text{CH}_2\text{-Me}_3\text{TACN}$), 53.9 ($\text{CH}_2\text{-Me}_3\text{TACN}$), 46.0 ($\text{CH}_3\text{-Me}_3\text{TACN}$), 45.9 ($\text{CH}_3\text{-Me}_3\text{TACN}$), 35.0 ($\text{CH}_2\text{-}n\text{Bu}$), 33.8 ($\text{CH}_2\text{-}n\text{Bu}$), 14.6

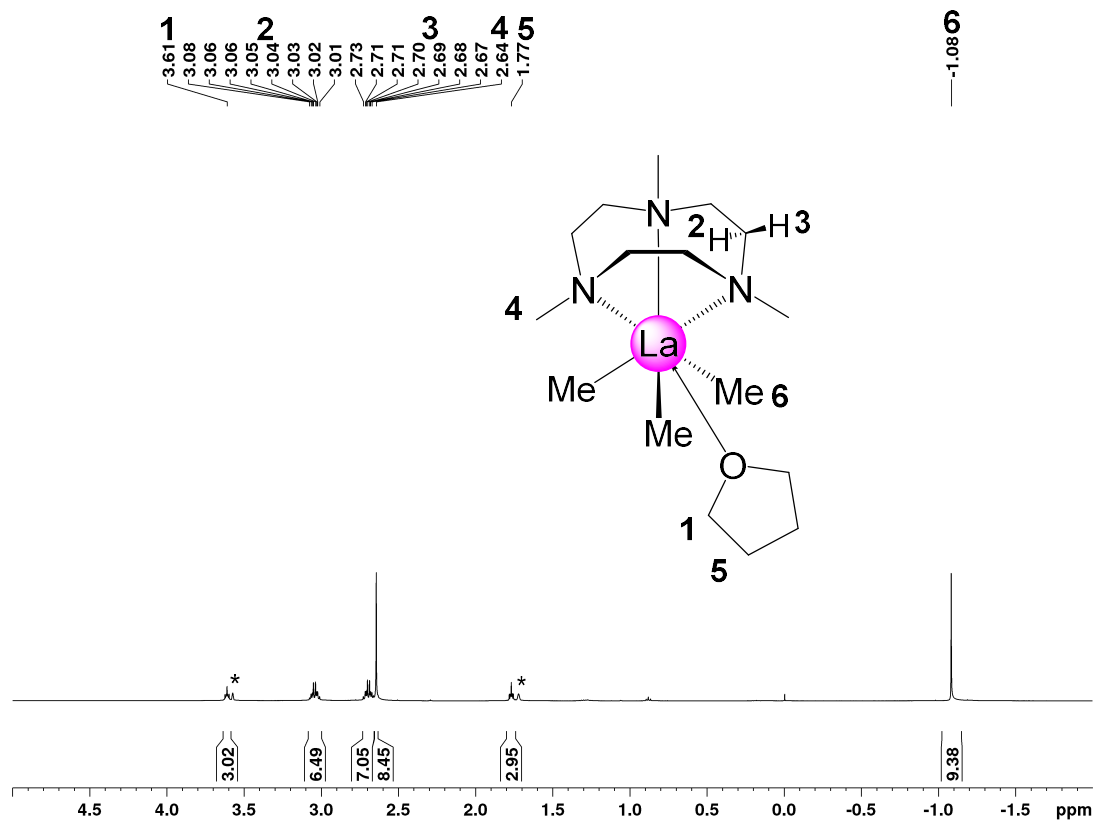


Figure S 1. ¹H NMR spectrum of Me₃TACN-LaMe₃thf (1-La) (500.13 MHz, thf-d₈, 233 K) solvent residual signals are marked with *.

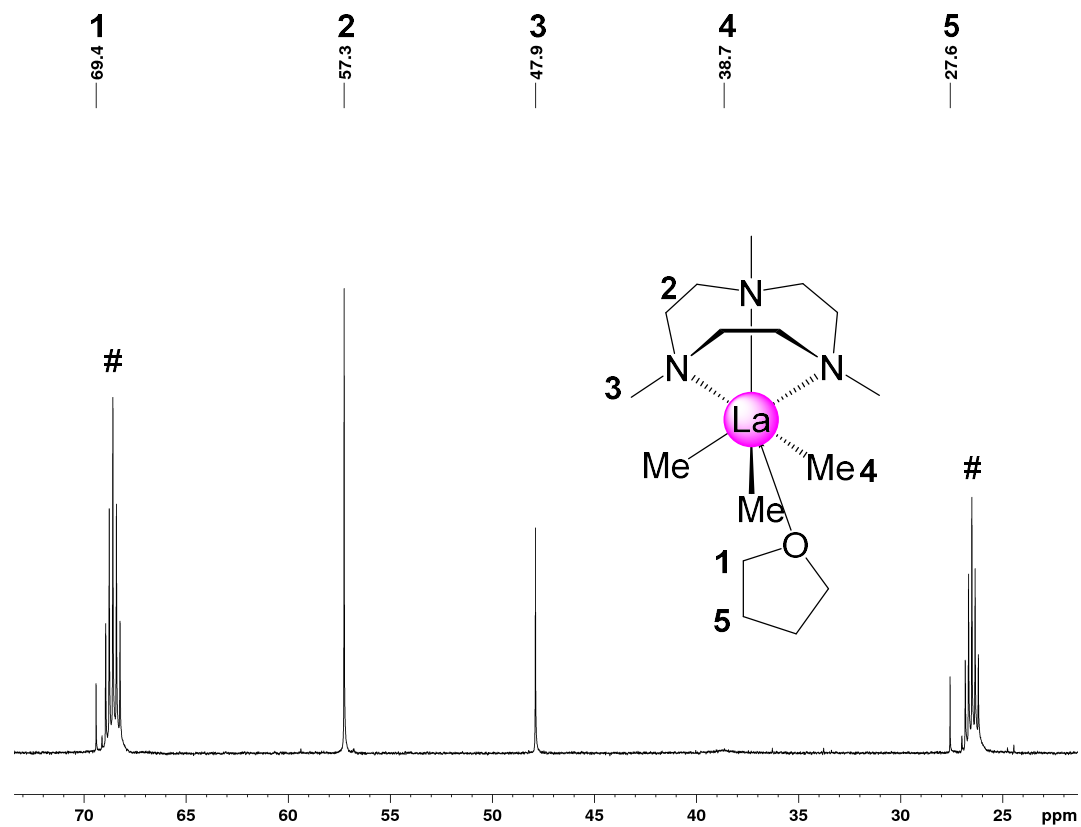


Figure S 2. ¹³C NMR spectrum of Me₃TACN-LaMe₃thf (1-La) (125.76 MHz, thf-d₈, 233 K) solvent residual signals are marked with #.

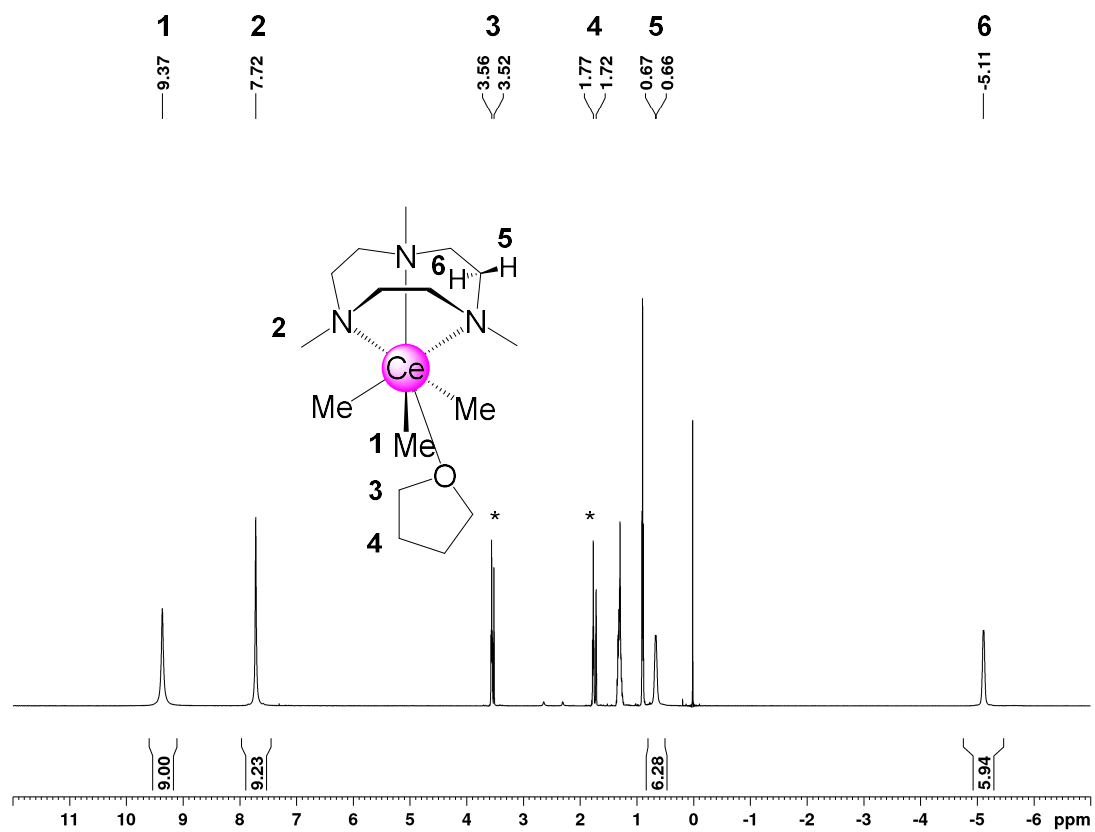


Figure S 3. ^1H NMR spectrum of $\text{Me}_3\text{TACN-CeMe}_3\text{thf}$ (1-Ce) (500.13 MHz, thf-d_8 , 233 K) solvent residual signals are marked with *.

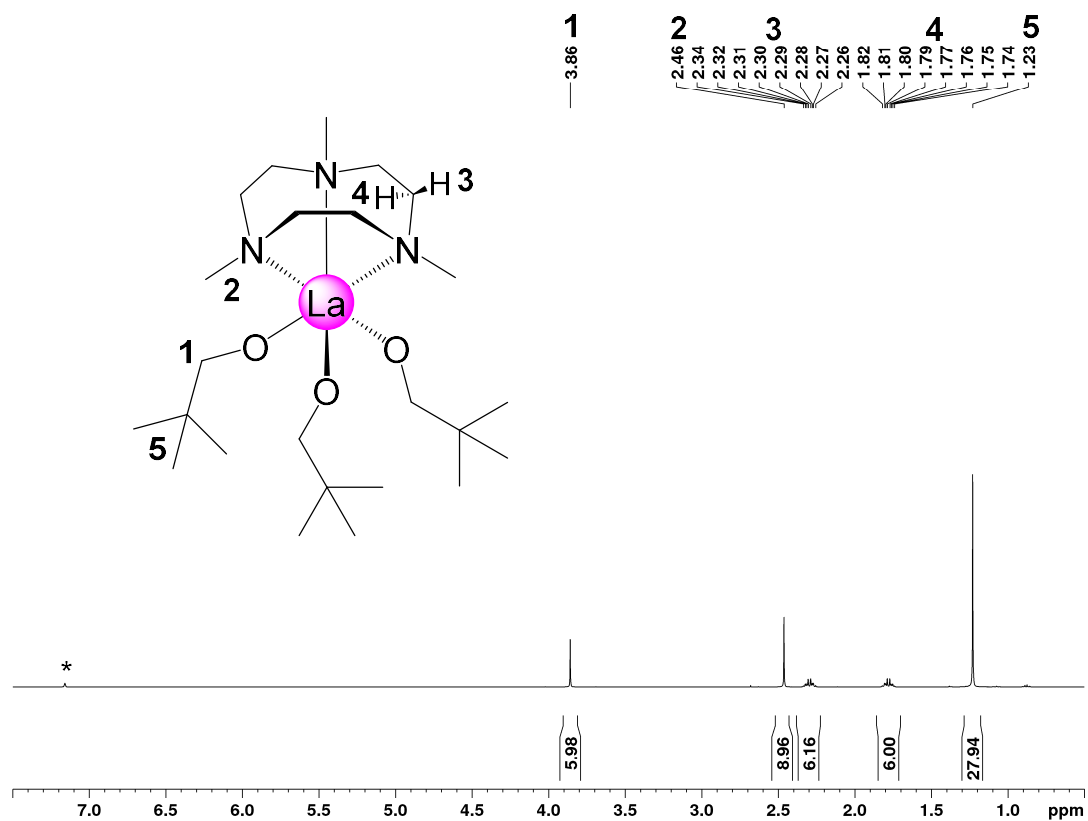


Figure S 4. ^1H NMR spectrum of $\text{Me}_3\text{TACN-La}(\text{OCH}_2\text{tBu})_3$ (2-La) (400.11 MHz, thf-d_8 , 298 K) solvent residual signals are marked with *.

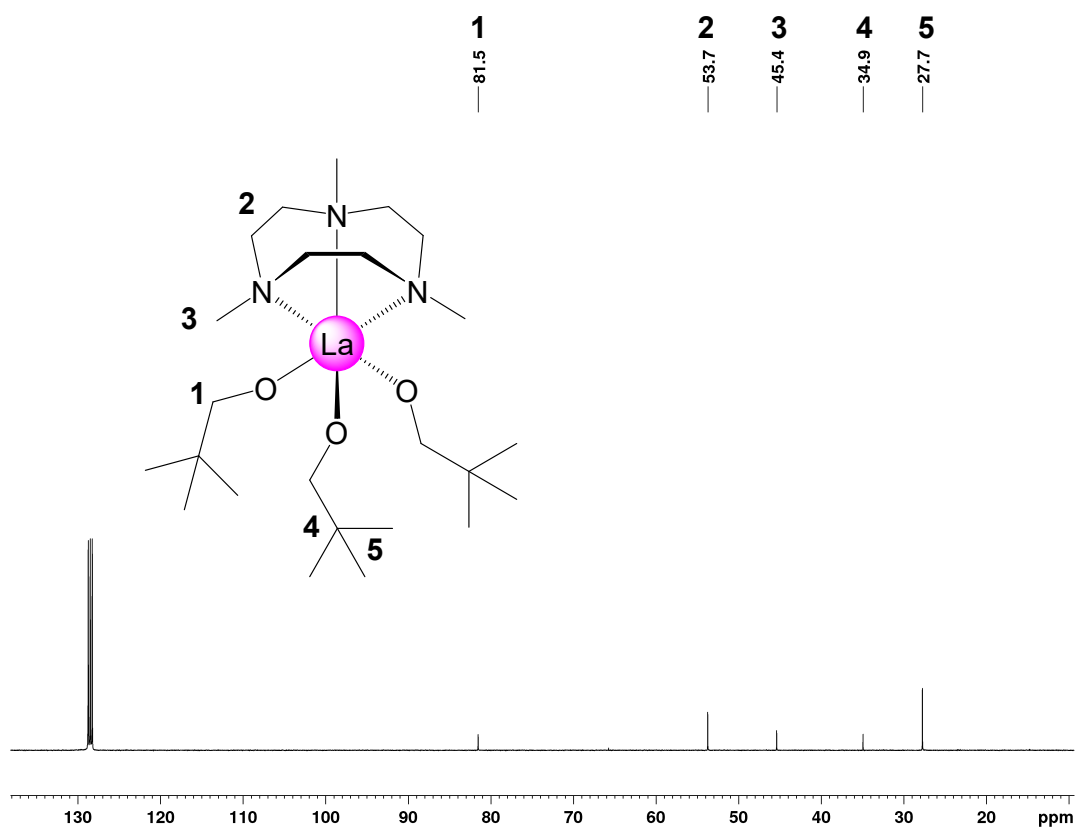


Figure S 5. ^{13}C NMR spectrum of $\text{Me}_3\text{TACN-La}(\text{OCH}_2\text{tBu})_3$ (**3-La**) (100.60 MHz, thf-d_8 , 298 K) solvent residual signals are marked with * impurities with #

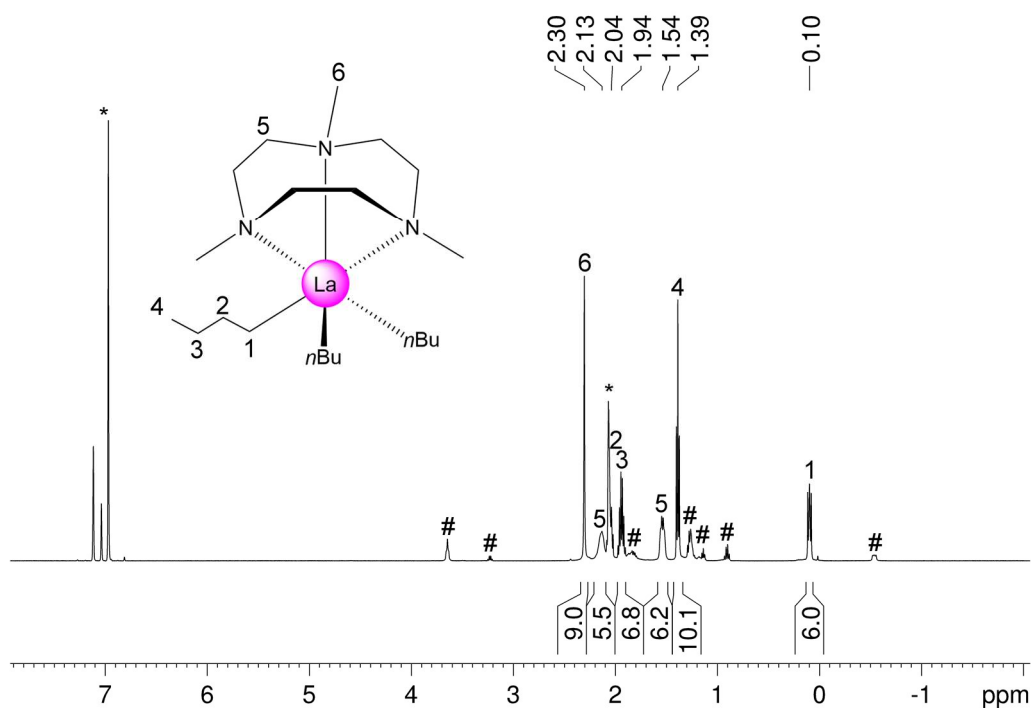


Figure S6. ^1H NMR spectrum of $\text{Me}_3\text{TACN-La}(\text{nBu})_3$ (**3-La**) (500.13 MHz, toluene-d_8 , 233 K) solvent residual signals are marked with *. *n*-BuLi and THF impurities are marked with #.

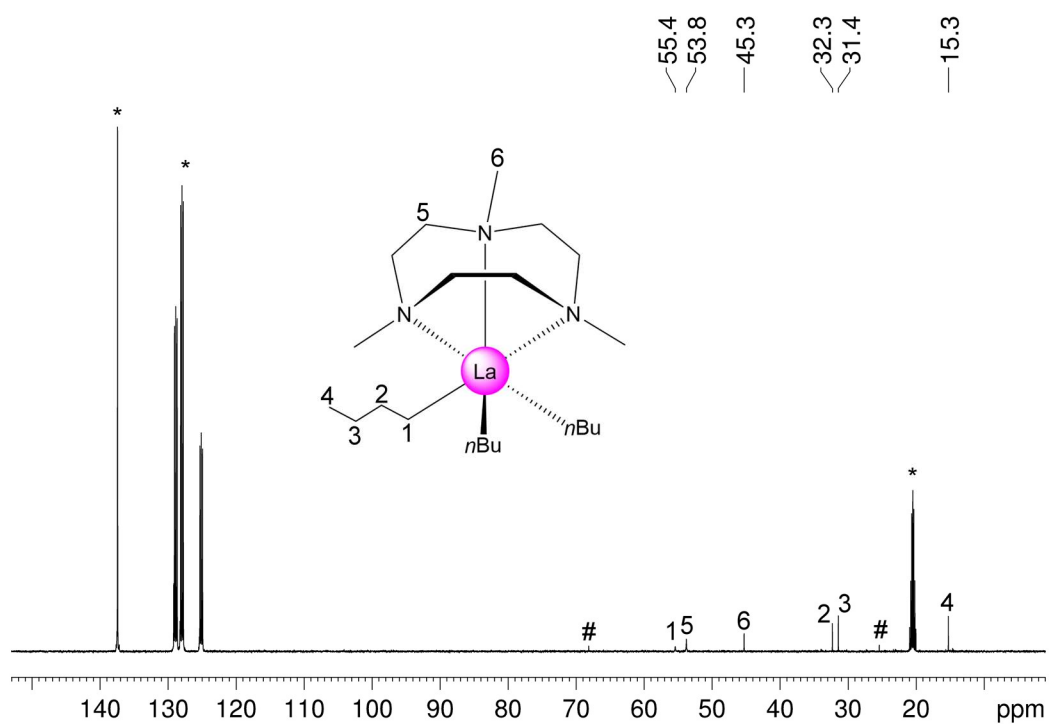


Figure S7. ^{13}C NMR spectrum of $\text{Me}_3\text{TACN-La}(\text{nBu})_3$ (**3-La**) (125.76 MHz, toluene- d_6 , 233 K) solvent residual signals are marked with *. Unknown impurities are marked with #.

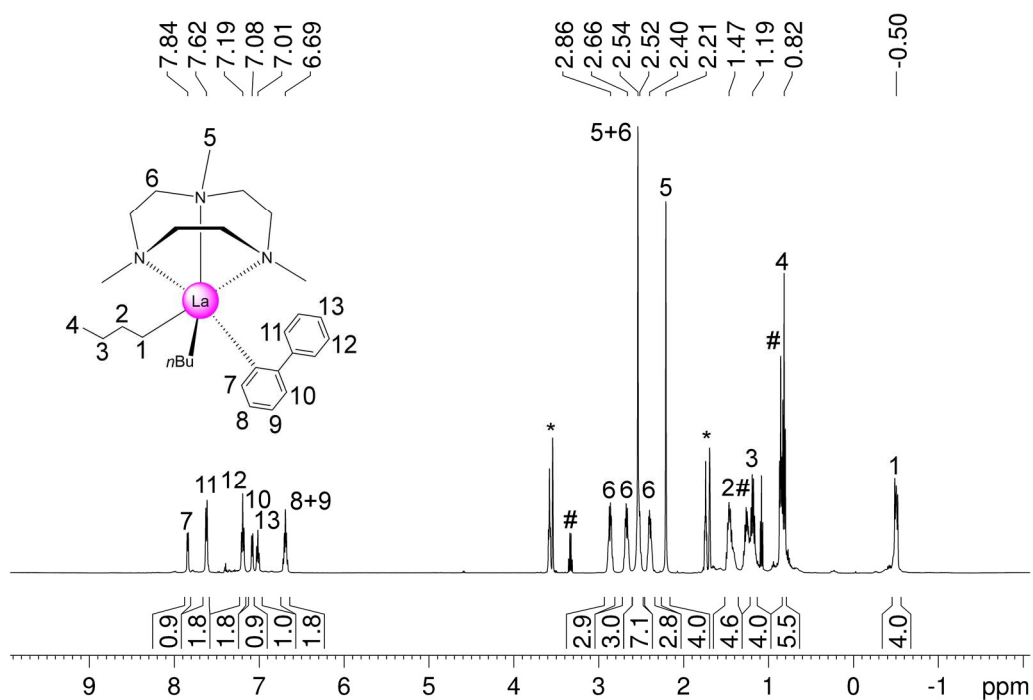


Figure S 8. ^1H NMR spectrum of $\text{Me}_3\text{TACN-La}(\text{nBu})_2(2\text{-biphenyl})$ (**4**) (500.13 MHz, thf-d_6 , 233 K) solvent residual signals are marked with *. Unknown impurities are marked with #.

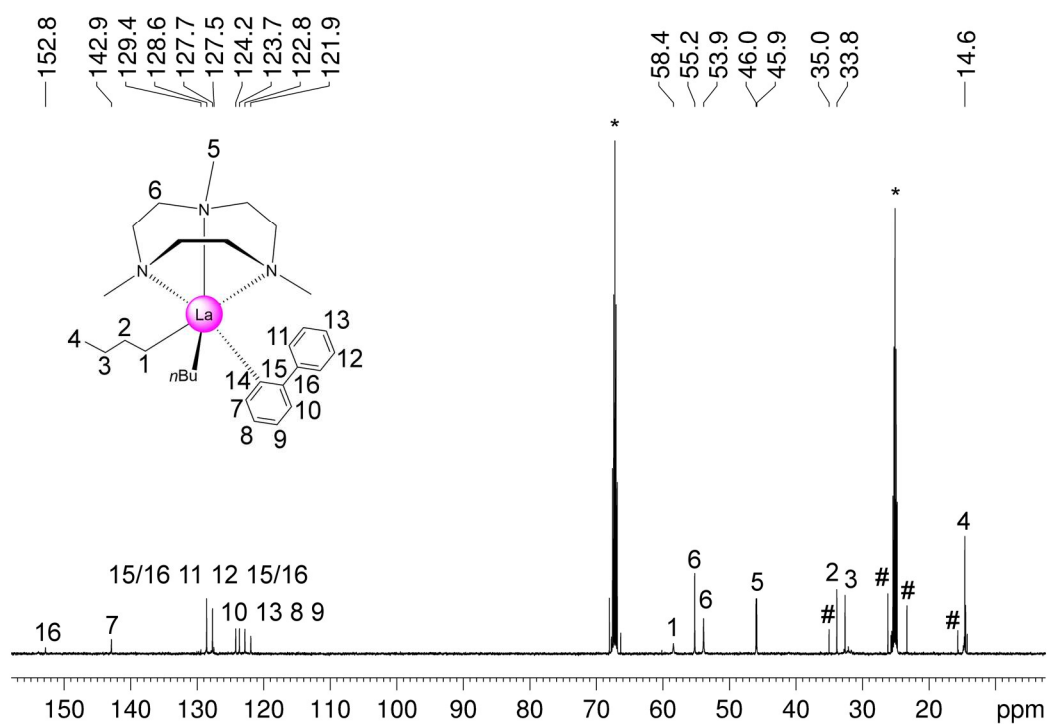


Figure S 9. ^{13}C NMR spectrum of $\text{Me}_3\text{TACN-La}(\text{nBu})_2(2\text{-biphenyl})$ (4) (125.76 MHz, thf-d_8 , 233 K) solvent residual signals are marked with *. Unknown impurities are marked with #.

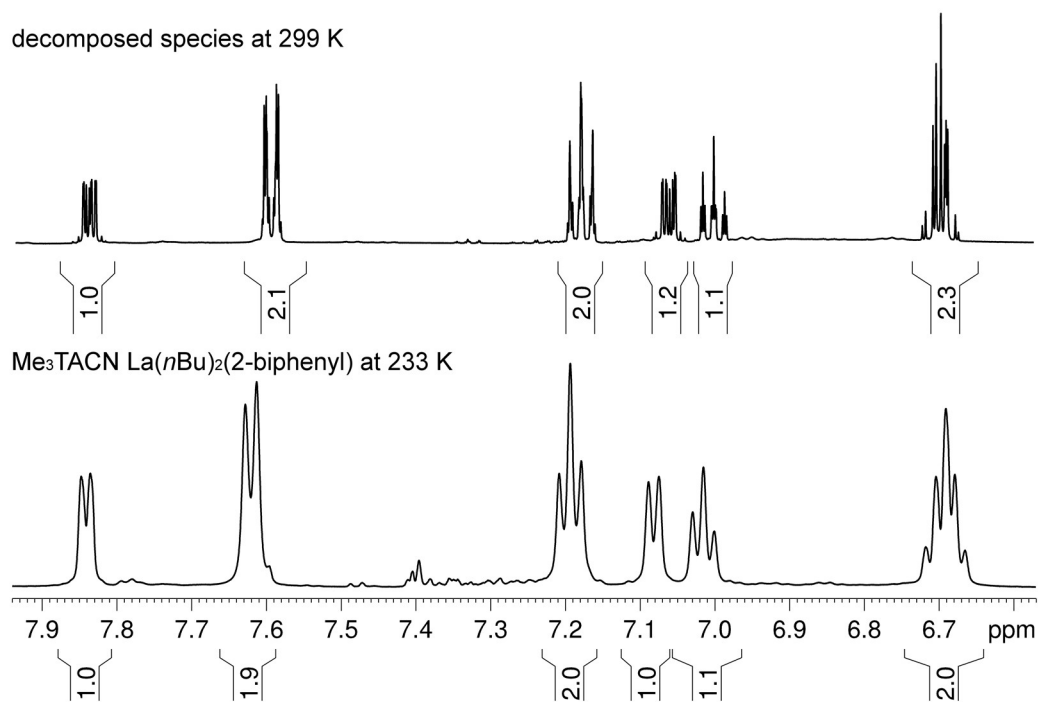


Figure S 10. ^1H NMR spectrum of $\text{Me}_3\text{TACN-La}(\text{nBu})_2(2\text{-biphenyl})$ (4) at 233 K (bottom) and the decomposed species at 299 K (top) (500.13 MHz, thf-d_8 , 233 K / 299 K) only the aromatic region of the biphenyl is displayed.

Table S 1. X-ray crystallographic parameters for complexes **1-La**, **1-Ce**, **1-NdCl_{0.25}**, **1-NdCl_{0.5}**.

Compound	Me ₃ -TACN-LaMe ₃ (thf)	Me ₃ -TACN-CeMe ₃ (thf)	Me ₃ -TACN-NdMe _{2.5} Cl _{0.5} (thf)	Me ₃ -TACN-NdMe _{2.75} Cl _{0.25} (thf)
Sample code	1-La	1-Ce	1-NdCl_{0.25}	1-NdCl_{0.5}
CCDC	XXX	XXX	XXX	XXX
Empirical formula	C ₁₆ H ₃₈ LaN ₃ O	C ₁₆ H ₃₈ CeN ₃ O	C _{15.5} H _{36.5} Cl _{0.5} N ₃ NdO	C _{15.5} H _{36.5} Cl _{0.5} N ₃ NdO
Formula weight	427.40	428.61	442.78	438.14
Temperature [K]	100(2)	100(2)	100(2)	100(2)
Crystal system	monoclinic	monoclinic	monoclinic	monoclinic
Space group	P21/n	P21/n	P21/n	P21/n
a [Å]	9.8618(4)	9.8823(7)	9.9207(7)	9.9252(7)
b [Å]	15.6659(7)	15.5844(10)	15.4639(11)	15.4993(11)
c [Å]	12.9232(5)	12.8472(9)	12.7597(9)	12.7649(9)
α [°]	90	90	90	90
β [°]	90.055(8)	90.1490(10)	90.1930(10)	90.3260(10)
γ [°]	90	90	90	90
Volume [Å ³]	1996.56(14)	1978.6(2)	1957.5(2)	1963.6(2)
Z	4	4	4	4
ρ _{calc} [g/cm ³]	1.422	1.439	1.502	1.482
μ [mm ⁻¹]	2.143	2.304	2.723	2.684
F(000)	880	884	908	900
Crystal size [mm ³]	0.163 x 0.152 x 0.131	0.197 x 0.180 x 0.113	0.286 x 0.183 x 0.157	0.249 x 0.160 x 0.146
Radiation	MoK _α (λ = 0.71073)	MoK _α (λ = 0.71073)	MoK _α (λ = 0.71073)	MoK _α (λ = 0.71073)
θ range for data collection [°]	2.043/30.675	2.054/28.699	2.053/ 29.619	2.437 to 29.572
Index ranges	-14 ≤ h ≤ 14, -22 ≤ k ≤ 22, -18 ≤ l ≤ 18	-13 ≤ h ≤ 13, -21 ≤ k ≤ 21, -17 ≤ l ≤ 17	-13 ≤ h ≤ 13, -21 ≤ k ≤ 21, -17 ≤ l ≤ 17	-13 ≤ h ≤ 13, -21 ≤ k ≤ 21, -17 ≤ l ≤ 17
Reflections collected	34261	35593	46564	23668
Independent reflections	6182 [R(int) = 0.0339]	5095 [R(int) = 0.0547]	5200 [R(int) = 0.0380]	5491 [R(int) = 0.0365]
Data/restraints/parameters	6182 / 750 / 310	5095 / 0 / 216	5200 / 0 / 216	5491 / 30 / 224
Goodness-of-fit on F ^{2[a]}	1.042	1.075	1.031	1.098
Final R indexes [I ≥ 2σ (I)] ^{[b][c]}	R1 = 0.0236, wR2 = 0.0505	R1 = 0.0265, wR2 = 0.0662	R1 = 0.0224, wR2 = 0.0497	R1 = 0.0265, wR2 = 0.0654
Final R indexes [all data]	R1 = 0.0276, wR2 = 0.0523	R1 = 0.0297, wR2 = 0.0681	R1 = 0.0247, wR2 = 0.0507	R1 = 0.0289, wR2 = 0.0668
Largest diff. peak/hole [e Å ⁻³]	1.524 and -0.615	1.123 and -0.646	1.312 and -0.659	1.917 and -0.943

^[a]GOF = $\{\sum w(F_o^2 - F_c^2)^2 / (n_o - n_p)\}^{1/2}$. ^[b]R1 = $\{\sum(|F_o| - |F_c|) / \sum|F_o|\}$, $F_o > 4\sigma(F_o)$. ^[c]wR2 = $\{\sum[w(F_o^2 - F_c^2)^2] / \sum[w(F_o^2)^2]\}^{1/2}$.

Table S 2. Continued X-ray crystallographic parameters for complexes **2**, **3-Ce**, and **4-Sm**.

Compound	Me ₃ -TACN- Ce(OCH ₂ C(CH ₃) ₃) ₃	Me ₃ -TACNSm(<i>n</i> Bu) ₃	Me ₃ TACN- La(<i>n</i> Bu) ₂ (2-biphenyl)
Sample code	2-Ce	3-Sm	4
CCDC	XXX	XXX	XXX
Empirical formula	C ₂₄ H ₅₄ CeN ₃ O ₃	C ₂₁ H ₄₈ SmN ₃	C ₂₉ H ₄₈ LaN ₃
Formula weight	572.82	481.54	577.61
Temperature [K]	100(2)	100(2)	100(2)
Crystal system	orthorhombic		triclinic
Space group	P2 ₁ 2 ₁ 2 ₁		P-1
a [Å]	13.9090(3)		8.6871(3)
b [Å]	11.4509(5)		12.5108(5)
c [Å]	19.2007(12)		13.8744(5)
α [°]	90		92.9220(10)
β [°]	90		96.5950(10)
γ [°]	90		105.3270(10)
Volume [Å ³]	3058.1(2)		1439.43(9)
Z	4		2
ρ _{calc} [g/cm ³]	1.244		1.333
μ [mm ⁻¹]	1.513		1.504
F(000)	1204		600
Crystal size [mm ³]	0.188 x 0.119 x 0.112		0.271 × 0.148 × 0.082
Radiation	MoK _α (λ = 0.71073)	MoK _α (λ = 0.71073)	MoK _α (λ = 0.71073)
θ range for data collection [°]	1.808 to 39.242		2.155 to 28.731
Index ranges	-16 ≤ h ≤ 16, -20 ≤ k ≤ 20, -26 ≤ l ≤ 26		-11 ≤ h ≤ 11, -16 ≤ k ≤ 16, -18 ≤ l ≤ 18
Reflections collected	28384		62633
Independent reflections	9897 [R(int) = 0.0710]		7411 [R _{int} = 0.0560]
Data/restraints/parameters	9897 / 482 / 348		7411 / 0 / 313
Goodness-of-fit on F ² [^a]	1.040		1.065
Final R indexes [I ≥ 2σ(I)] [^b][^c]	R ₁ = 0.0536, wR ₂ = 0.1245		R ₁ = 0.0290, wR ₂ = 0.0653
Final R indexes [all data]	R ₁ = 0.0707, wR ₂ = 0.1372		R ₁ = 0.0335, wR ₂ = 0.0676
Largest diff. peak/hole [e Å ⁻³]	1.793 and -1.637		2.425 / -0.846

^[a]GOF = $[\sum w(F_o^2 - F_c^2)^2 / (n_o - n_p)]^{1/2}$. ^[b]R₁ = $\Sigma(|F_o| - |F_c|) / \Sigma|F_o|$, F_o > 4σ(F_o). ^[c]wR₂ = $\{\Sigma[w(F_o^2 - F_c^2)^2 / \Sigma w(F_o^2)^2]\}^{1/2}$.

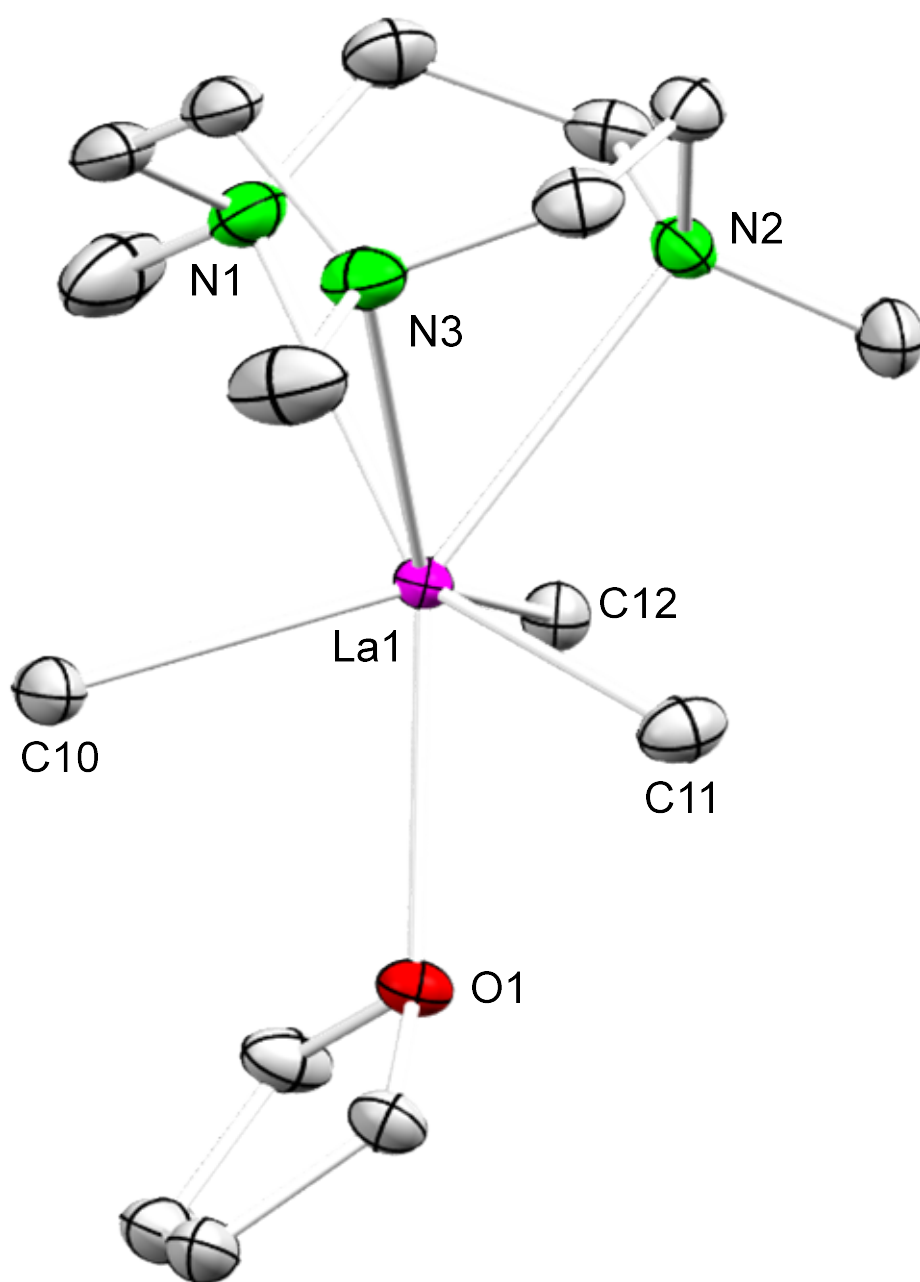


Figure S 11. Crystal structure of **1-La** (ellipsoids set at 50 %). All hydrogen atoms have been omitted for clarity. Selected interatomic distances (Å) and angles (°): La(1)-N(2) 2.772(5), La(1)-N(1) 2.795(3) La(1)-N(3) 2.824(3), La(1)-C(10) 2.628(10) La(1)-C(12) 2.699(8), C(11)-La(1) 2.628(3), C(10A)-La(1)-C(11) 118.1(2), C(10)-La(1)-O(1) 76.4(2), C(10)-La(1)-N(1) 87.0(2), O(1)-La(1)-N(1) 142.78(8).

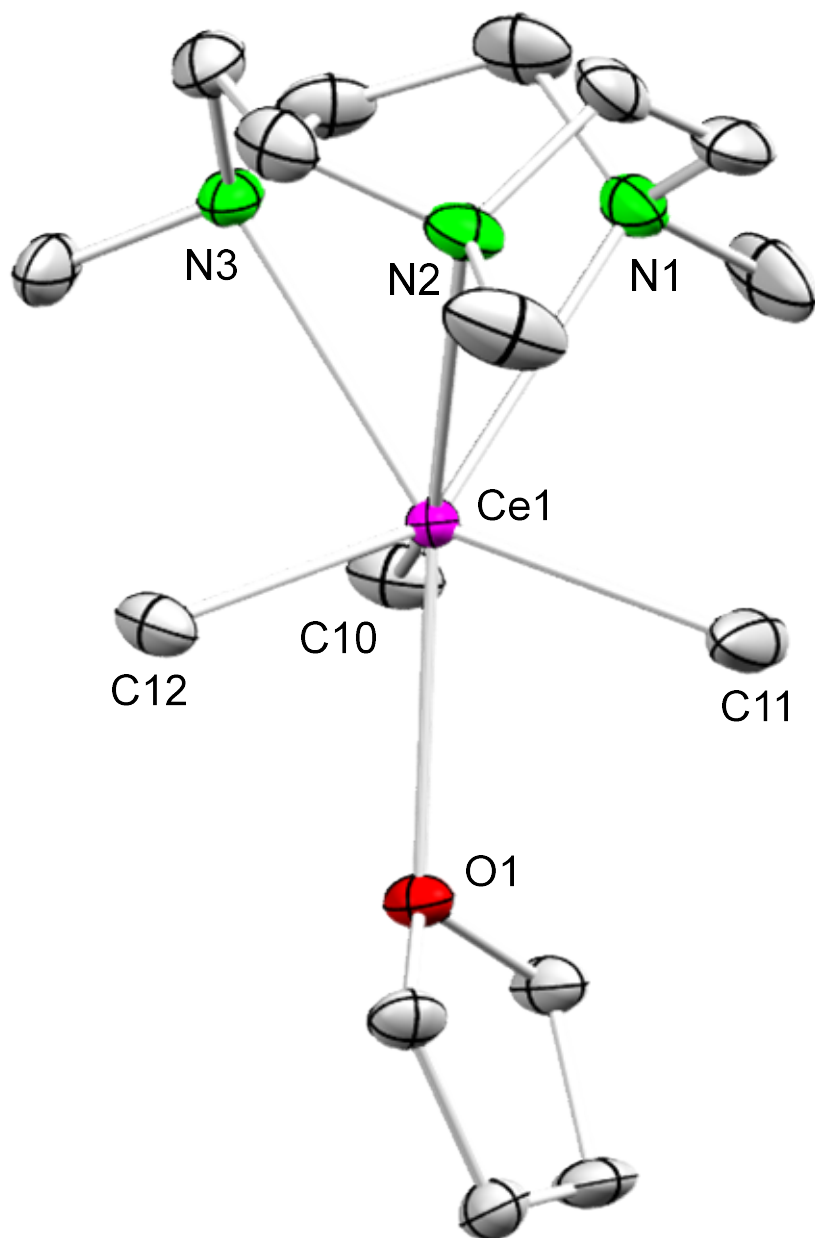


Figure S 12. Crystal structure of **1-Ce** (ellipsoids set at 50 %). All hydrogen atoms have been omitted for clarity. Selected interatomic distances (Å) and angles (°): C(10)-Ce(1) 2.606(3), C(11)-Ce(1) 2.639(3), C(12)-Ce(1) 2.641(3), N(1)-Ce(1) 2.793(3), N(2)-Ce(1) 2.752(2), N(3)-Ce(1) 2.764(3), O(1)-Ce(1) 2.6835(18), C(10)-Ce(1)-O(1) 75.51(8), C(10)-Ce(1)-N(1) 85.38(12), O(1)-Ce(1)-N(1) 143.82(9).

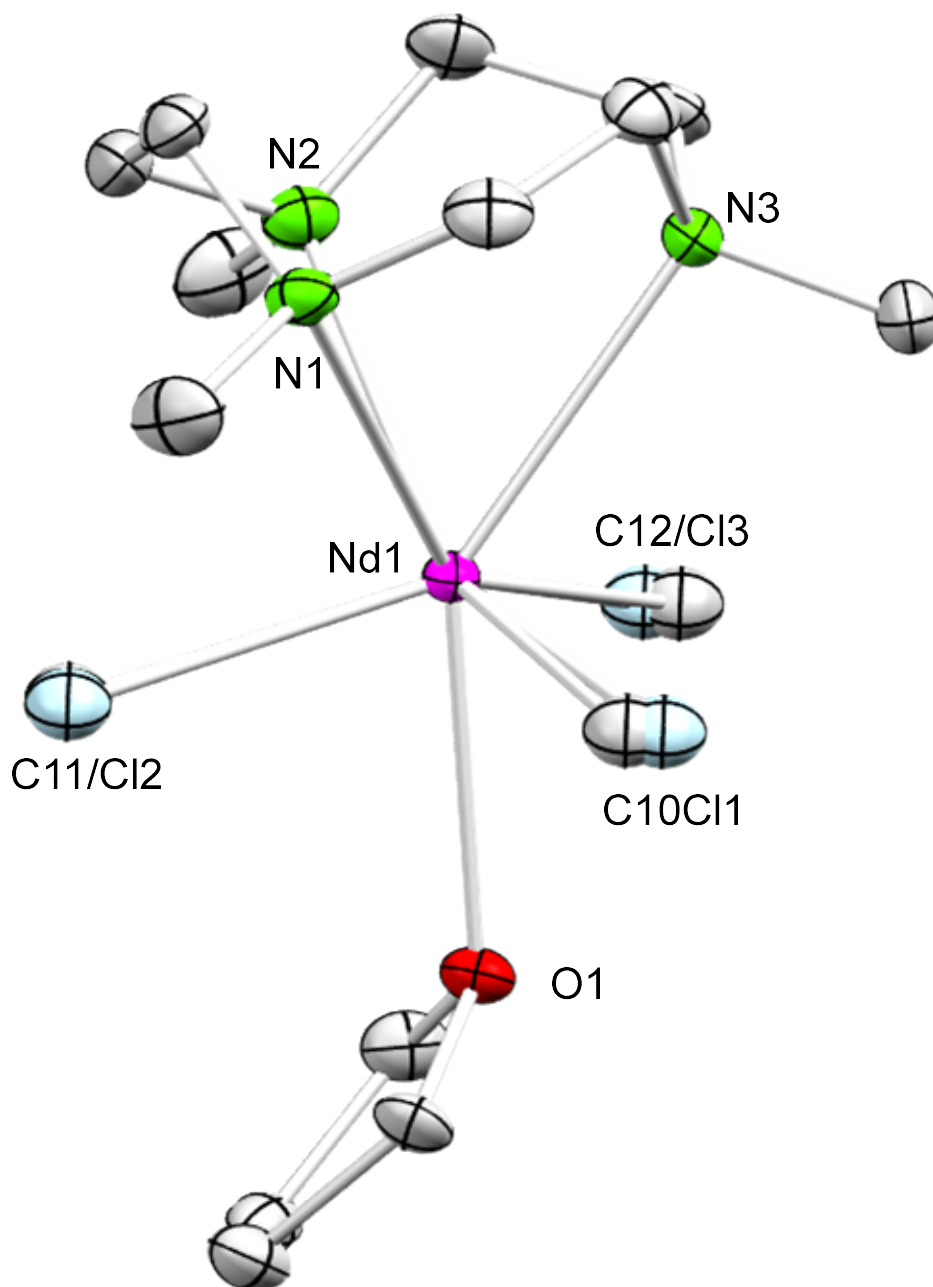


Figure S 13. Crystal structure of **1-NdCl_{0.5}** (ellipsoids set at 50 %). All hydrogen atoms have been omitted for clarity. Selected interatomic distances (Å) and angles (°): N(1)-Nd(1) 2.752(2), N(2)-Nd(1) 2.7242(18), N(3)-Nd(1) 2.716(2), O(2)-Nd(1) 2.6418(13), Nd(1)-C(10) 2.578(10), Nd(1)-C(12) 2.599(4), Nd(1)-Cl(3) 2.601(10), Nd(1)-Cl(2) 2.609(10), Nd(1)-C(11) 2.669(9), Nd(1)-Cl(1) 2.690(9), C(10)-Nd(1)-C(12) 112.5(2), C(10)-Nd(1)-Cl(3) 103.7(3), Cl(2)-Nd(1)-O(2) 74.43(19), C(10)-Nd(1)-N(3) 142.39(19), Cl(3)-Nd(1)-N(3) 87.65(19), O(2)-Nd(1)-N(3) 141.71(6).

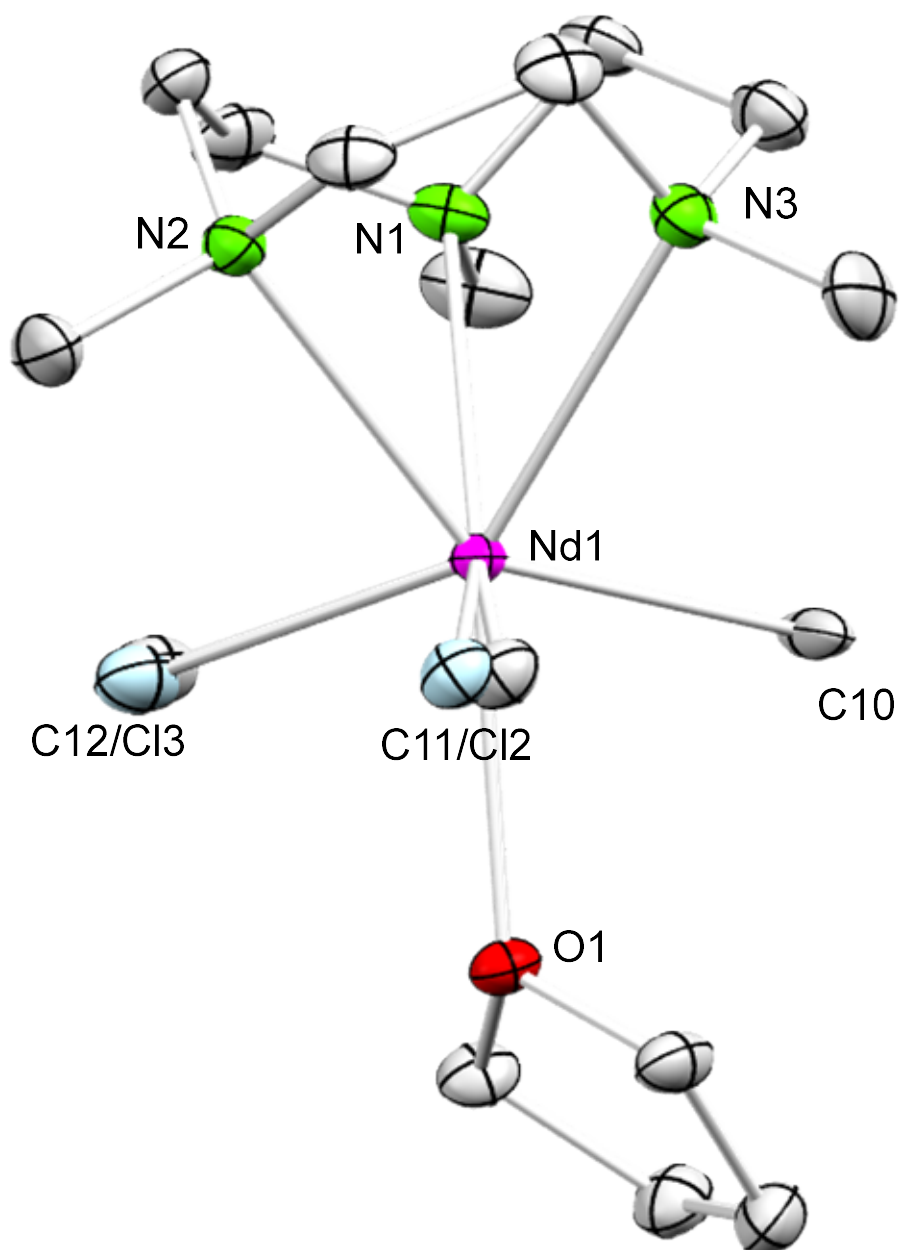


Figure S 14. Crystal structure of **1-NdCl_{0.25}** (ellipsoids set at 50 %). All hydrogen atoms have been omitted for clarity. Selected interatomic distances (Å) and angles (°): C(10)-Nd(1) 2.582(3), Cl(1)-Nd(1) 2.70(2), C(11)-Nd(1) 2.589(13), Cl(2)-Nd(1) 2.64(3), C(12)-Nd(1) 2.60(2), N(1)-Nd(1) 2.729(2), N(2)-Nd(1) 2.756(2), N(3)-Nd(1) 2.721(2), O(3)-Nd(1) 2.6472(17), C(11)-Nd(1)-N(1) 85.2(3) C(12)-Nd(1)-N(1) 85.6(5), Cl(2)-Nd(1)-N(1) 84.7(8), O(3)-Nd(1)-N(1) 141.54(6), Cl(1)-Nd(1)-N(1) 81.0(5), N(3)-Nd(1)-N(1) 64.40(7), C(10)-Nd(1)-N(2) 85.17(9), C(11)-Nd(1)-N(2) 142.7(3), C(12)-Nd(1)-N(2) 82.4(5), Cl(2)-Nd(1)-N(2) 84.4(7), O(3)-Nd(1)-N(2) 143.17(7), Cl(1)-Nd(1)-N(2) 141.3(6), N(3)-Nd(1)-N(2) 64.05(7).

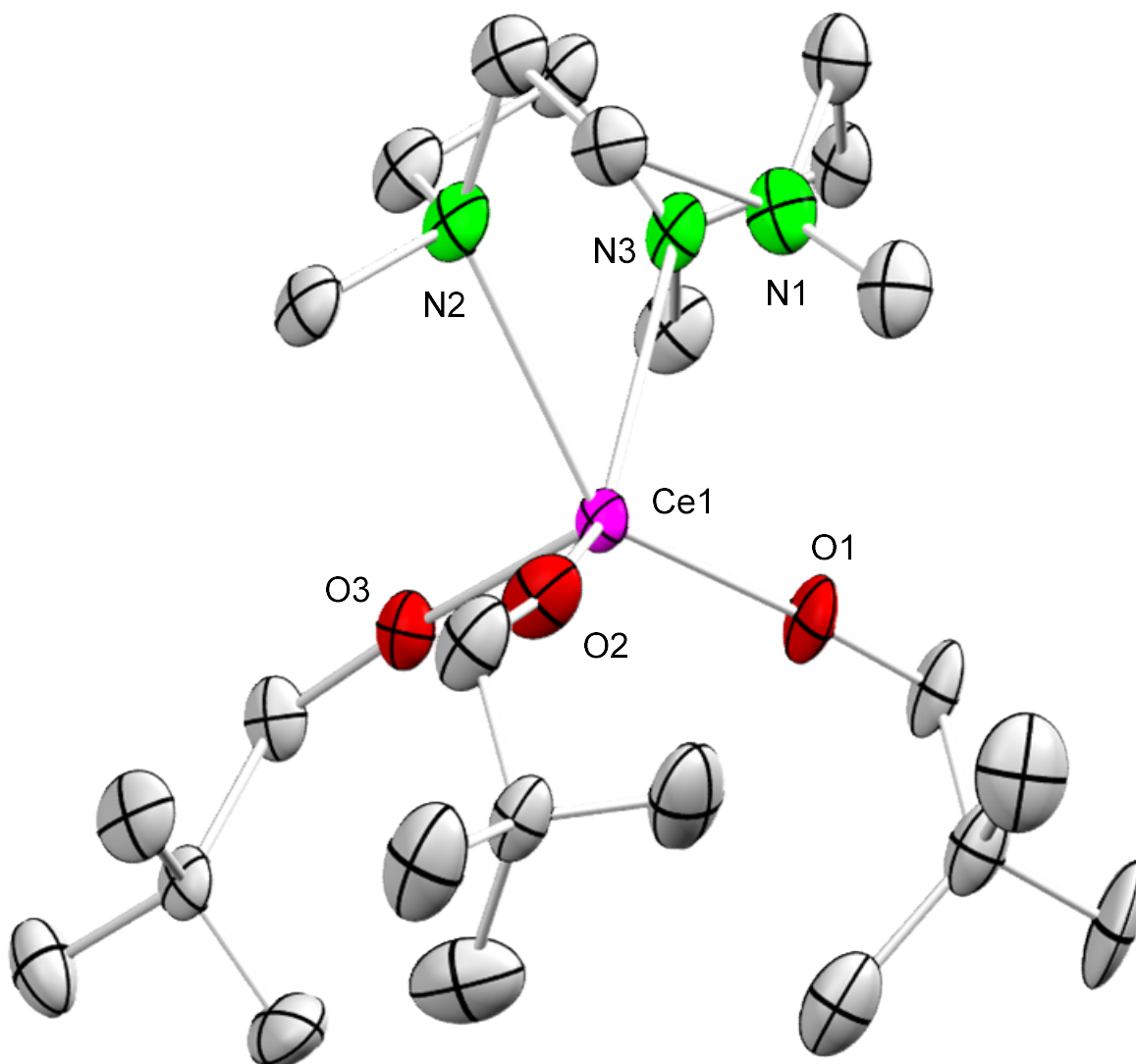


Figure S 15. Crystal structure of **2-Ce** (ellipsoids set at 50 %). All hydrogen atoms have been omitted for clarity. Selected interatomic distances (Å) and angles (°): N(1)-Ce(1) 3.295, N(2)-Ce(1) 2.784(7), N(3)-Ce(1) 2.813(6), Ce(1)-O(2) 1.929(5), Ce(1)-O(1) 1.947(4), Ce(1)-O(3) 2.451(5), C(3)-N(2)-Ce(1) 106(2), C(2)-N(2)-Ce(1) 133.6(14), O(2)-Ce(1)-O(1) 104.4(2), O(2)-Ce(1)-O(3) 107.0(2), O(1)-Ce(1)-O(3) 108.8(2).

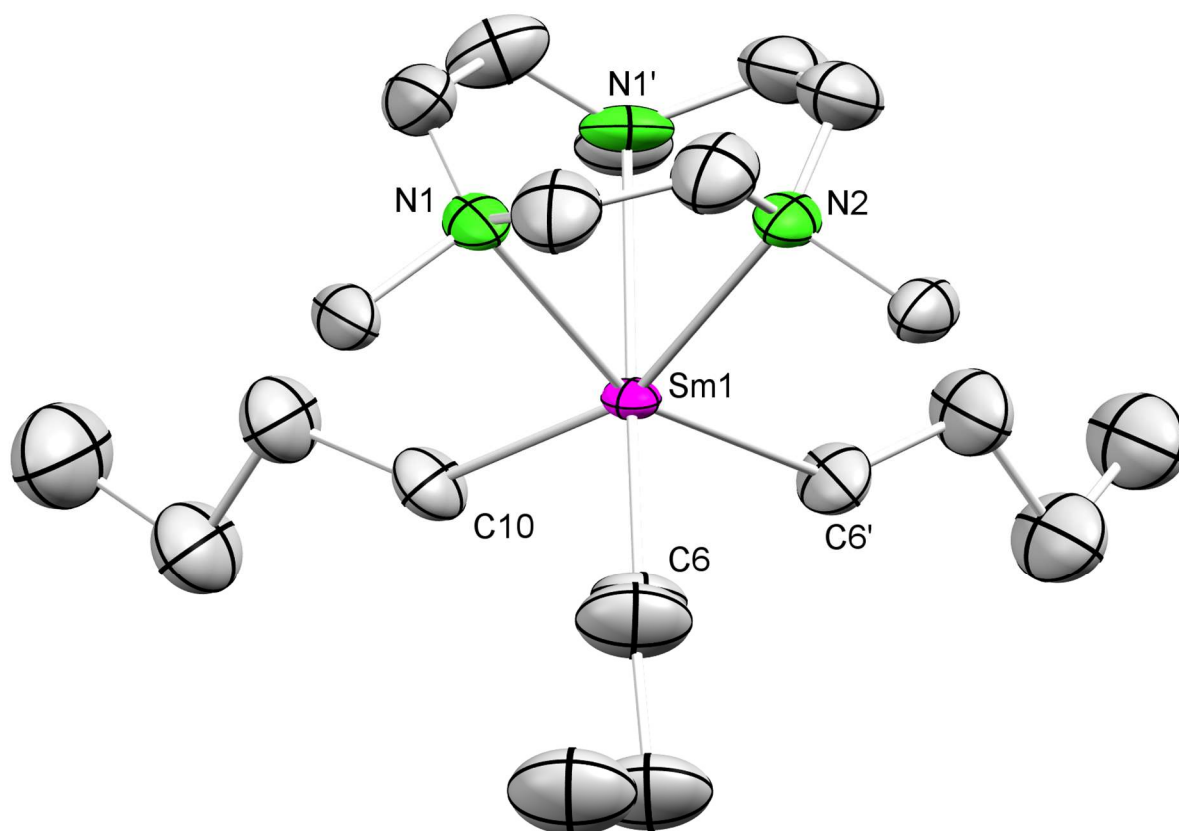


Figure S16. Connectivity of Me₃TACN-Sm(*n*Bu)₃ **3-Sm** with atomic displacement ellipsoids set at 30% probability. Hydrogen atoms and disorders of one *n*Bu group are omitted for clarity.

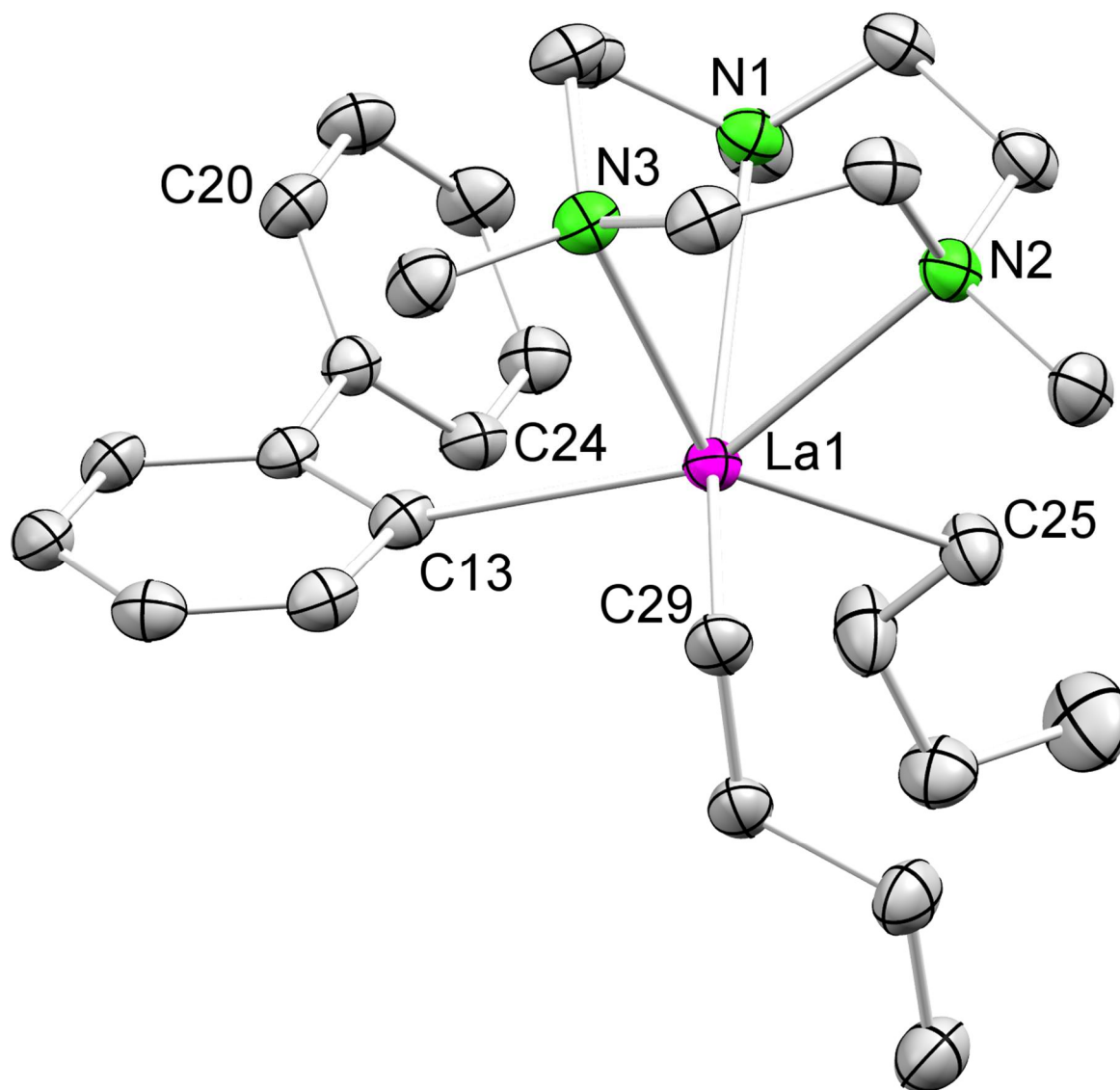


Figure S 17. Crystal structure of $\text{Me}_3\text{TACN-La}(n\text{Bu})_2(2\text{-biphenyl})$ **4** with atomic displacement ellipsoids set at 50% probability. Hydrogen atoms and disorders of one *n*Bu group are omitted for clarity. Selected interatomic distances [Å] and angles [°] for X: La1–C25 2.567(3), La1–C29 2.544(2), La1–C13 2.672(2), La1–C24 4.3552(2), La1–C20 5.2256(2), La1–N1 2.7458(19), La1–N2 2.813(2), La1–N3 2.780(2), C29–La1–C25 106.10(9), C13–La1–C29 102.53(8), C13–La1–C25 120.57(8).

**Rare-earth-metal
trimethylsilylmethyl ate
complexes**

manuscript

PAPER

Cite this: *Dalton Trans.*, 2023, **52**, 44

Rare-earth-metal trimethylsilylmethyl ate complexes†

Alexandros Mortis,¹ Felix Kracht,² Tassilo Berger,³ Jakob Lebon,⁴ Cäcilia Maichle-Mössmer¹ and Reiner Anwander¹*

En route to putative rare-earth-metal alkylidene complex $\text{Li}[\text{Lu}(\text{CH}_2\text{SiMe}_3)_2(\text{CHSiMe}_3)]$, according to Schumann's original protocol, the reaction of YCl_3 with $\text{LiCH}_2\text{SiMe}_3$ in a mixture of diethyl ether and *n*-pentane afforded a neosilyl ate complex of composition $\text{Li}_3\text{Y}(\text{CH}_2\text{SiMe}_3)_6$. Tetrametallic complex $\text{Li}_3\text{Y}(\text{CH}_2\text{SiMe}_3)_6$ shows an unprecedented structural motif in the solid state and was further characterized by heteronuclear $^1\text{H}/^{13}\text{C}/^7\text{Li}/^{29}\text{Si}/^{89}\text{Y}$, as well as VT NMR and DRIFT spectroscopies. Analysis of the thermolysis product *via* heteronuclear NMR spectroscopy and its reactivity towards benzophenone gave strong evidence for an alkylidene formation upon decomposition. Application of a similar protocol for the smallest rare-earth-metal scandium led to the isolation of ate complex $[\text{Li}(\text{thf})_4][\text{LiSc}_2(\text{CH}_2\text{SiMe}_3)_8]$ as the preferred crystallized product. Here, the reaction of adduct $\text{ScCl}_3(\text{thf})_3$ and $\text{LiCH}_2\text{SiMe}_3$ was performed in $\text{Et}_2\text{O}/n$ -hexane, in the absence of additional THF. The reaction of $\text{LaCl}_3(\text{thf})$ with 3 equiv. of $\text{LiCH}_2\text{SiMe}_3$ in THF/ Et_2O at -40°C yielded the ate complex $[\text{Li}(\text{thf})_4][\text{La}(\text{CH}_2\text{SiMe}_3)_4(\text{thf})]$, which is the first of its kind.

Received 27th October 2022,
Accepted 18th November 2022

DOI: 10.1039/d2dt03491c

rsc.li/dalton

Introduction

Trimethylsilylmethyl complexes of the rare-earth metals, $\text{Ln}(\text{CH}_2\text{SiMe}_3)_3(\text{thf})_x$, are routine precursors for the synthesis of homogeneous catalysts as employed *e.g.*, in hydroelementation and polymerization reactions.¹ However, their effective applicability is impeded by thermal instability at ambient temperature, which culminates in the non-availability of derivatives with rare-earth-metal centers of size larger than Sm^{3+} .² The formation of alkylidene derivatives as proposed by Schumann for neutral $[\text{Er}(\text{CH}_2\text{SiMe}_3)(\text{CHSiMe}_3)]$ is assumed to feature a major "prominent" decomposition path.³ On the other hand, ate complexation can effectively stabilize and promote the isolation of metal compounds with highly nucleophilic ligands exclusively. Representative examples with large Ln^{3+} centers, which have been structurally authenticated, include $\text{Li}_3\text{Ce}(\text{CH}_3)_6(\text{tmeda})_3$, $[\text{Li}(\text{thf})_4][\text{Ce}(t\text{-Bu})_4]$, and $\text{Li}_2\text{Ce}(n\text{-Bu})_5(\text{tmeda})$.⁴ The existence of neosilyl ate complexes of type $[\text{Li}(\text{do})_x][\text{Ln}(\text{CH}_2\text{SiMe}_3)_4]$ ($\text{Ln} = \text{Y, Tb, Er, Yb, Lu}$; $\text{do} = \text{thf}$ or OEt_2 , $x = 4$; $\text{do} = \text{tmeda}$, $x = 2$) was already described in the early studies from Lappert and Schumann.^{3,5} Back then, complex $[\text{Li}(\text{Et}_2\text{O})_4][\text{Lu}(\text{CH}_2\text{SiMe}_3)_4]$ was reported to decompose *via* the release of

diethyl ether and SiMe_4 under vacuum, forming putative alkylidene $\text{Li}[\text{Lu}(\text{CH}_2\text{SiMe}_3)_2(\text{CHSiMe}_3)]$. So far, both the ate complex precursors and the proposed alkylidene product have evaded structural characterization. Generally, very few X-ray diffraction (XRD) analyses of rare-earth-metal trimethylsilylmethyl ate complexes are available, with complex $[(\text{Me}_3\text{SiCH}_2)_x(\text{Me}_3\text{CO})_{1-x}\text{Y}(\mu\text{-OCMe}_3)_4][\text{Li}(\text{thf})_4][\text{Y}(\text{CH}_2\text{SiMe}_3)_4]$ most closely resembling $[\text{Li}(\text{do})_x][\text{Ln}(\text{CH}_2\text{SiMe}_3)_4]$.⁶ Preparations of the respective ate complexes of large rare-earth-metal centers were seemingly not attempted, most likely because of the enhanced instability of their $\text{Ln}(\text{CH}_2\text{SiMe}_3)_3(\text{thf})_x$ counterparts.^{1a,2} Furthermore, only three examples of lanthanide complexes with the silylalkylidene ligand $[\text{CHSiMe}_3]^{2-}$ have been reported, however, all of them with stabilizing ancillary ligands.⁷ Since the NMR-active nuclei ^{89}Y ($I = 1/2$)⁸ and ^{45}Sc ($I = 7/2$)⁹ might provide useful complementary probes for assessing ate complexation and any involved decomposition reactions, we thought it worthwhile to revisit such rare-earth-metal neosilyl derivatives.

Results and discussion

Yttrium

Applying Schumann's protocol,^{3,5} we targeted ate complex $[\text{Li}(\text{Et}_2\text{O})_x][\text{Y}(\text{CH}_2\text{SiMe}_3)_4]$ for which the THF pendant already exists.¹⁰ Accordingly, anhydrous YCl_3 was reacted with 4 equiv. of $\text{LiCH}_2\text{SiMe}_3$ in a 1:2 $\text{Et}_2\text{O}/n$ -pentane mixture (Scheme 1). Upon workup, the ^1H NMR spectrum of the crystalline residue

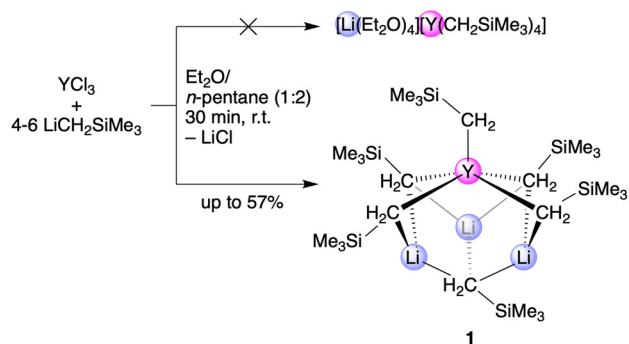
Institut für Anorganische Chemie, Eberhard Karls Universität Tübingen, Auf der Morgenstelle 18, D-72076 Tübingen, Germany.

E-mail: reiner.anwander@uni-tuebingen.de

† Electronic supplementary information (ESI) available. CCDC 2215407–2215409.

For ESI and crystallographic data in CIF or other electronic format see DOI:

<https://doi.org/10.1039/d2dt03491c>



Scheme 1 Envisaged synthesis route towards separated ion-pair $[\text{Li}(\text{Et}_2\text{O})_4][\text{Y}(\text{CH}_2\text{SiMe}_3)_4]$ and actual reaction product $\text{Li}_3\text{Y}(\text{CH}_2\text{SiMe}_3)_6$ (**1**).

1 in C_6D_6 showed only two signals: one very broad singlet at $\delta = -0.73$ ppm for the methylene moiety and one sharp singlet for the protons of the SiMe_3 groups at 0.23 ppm. Apparently, all weakly coordinating diethyl ether molecules got displaced upon exposure of **1** to vacuum (Fig. S1†). This is contrary to the ^1H NMR spectrum of previously characterized complex $[\text{Li}(\text{thf})_4][\text{Y}(\text{CH}_2\text{SiMe}_3)_4]$, which shows a much sharper signal with a resolved doublet for the Y-bound CH_2 -groups and also coordinated THF molecules.¹¹ Since the above-stated ^1H NMR spectrum was not revealing much about the actual structure of compound **1** in solution at ambient temperature, a VT ^1H NMR study was conducted (cf., Fig. S3†). The progression from -80 °C to $+26$ °C revealed several highly dynamic species in solution: at -60 °C the resonance for exclusively Li-bound CH_2 -groups emerged at about -2 ppm (dissociation of $\text{LiCH}_2\text{SiMe}_3$) and disappeared after heating to above 0 °C, likely because of the higher mobility of the individual moieties in the complex. Notably, rapid dissociation and recombination reactions according to the equilibrium $[\text{Li}(\text{thf})_4][\text{Y}(\text{CH}_2\text{SiMe}_3)_4] \rightleftharpoons \text{Y}(\text{CH}_2\text{SiMe}_3)_3(\text{thf})_2 + \text{Li}(\text{CH}_2\text{SiMe}_3)(\text{thf})_x$ have been postulated on the basis of a ^{13}C VT NMR study.⁵ The resonance at about -0.5 ppm attributed to the Y- CH_2 moieties split up into two signals at -80 °C, which converged at -60 °C to one sharp signal with a smaller shoulder, which further converged into the main signal above 0 °C. Above -10 °C this main signal broadened significantly, indicating a high fluxionality of all neosilyl groups in complex **1**. The resonance for the SiMe_3 groups at about 0.5 ppm revealed one main species at 26 °C. At lower temperatures, the methylene signal of separated $\text{LiCH}_2\text{SiMe}_3$ became prominent appearing as a shoulder at -10 °C and being fully separated from the main peak at -30 °C. It can be concluded that yttrium complex **1** shows a multitude of fluxional species in solution, which unambiguously explains the ^1H NMR spectrum at ambient temperature. The ^{89}Y NMR chemical shift of compound **1** was detected at $\delta = 954.5$ ppm (cf. Fig. S6†), which is located in between the tris(alkyl) complex $\text{Y}(\text{CH}_2\text{SiMe}_3)_3(\text{thf})_2$ ($\delta = 882.7$ ppm)¹² and the tetrakis(neosilyl) ate complex $[\text{Li}(\text{thf})_4][\text{Y}(\text{CH}_2\text{SiMe}_3)_4]$ showing a resonance at $\delta = 1151.0$ ppm in aromatic solvents.¹⁰ Since it was shown that the ^{89}Y chemical shift correlates with the

number of Ln-bound alkyl groups,¹³ it is not too far-fetched to assume that dissolved complex **1** should bear multiple alkyl groups and that its actual composition in the solid state should be similar as well.¹⁰ The ^{89}Y and ^7Li NMR spectra recorded at lower temperatures were indicative of the fluxional nature of **1** in solution. While the ^{89}Y spectrum at -40 °C shows an additional peak at a higher field (ca. 800 ppm, Fig. S6†) indicative of an (lithium)alkyl-depleted species, the ^7Li spectra suggest the emergence of the signal attributed to $\text{LiCH}_2\text{SiMe}_3$ (Fig. S4†). Upon crystallization from a saturated toluene/*n*-hexane mixture, a rather unusual structure with the general composition $\text{Li}_3\text{Y}(\text{CH}_2\text{SiMe}_3)_6$ (**1**) (cf. Scheme 1 and Fig. 1) could be elucidated. Consequently, the reaction was repeated with a 1:6 molar ratio of YCl_3 and lithium alkyl, which produced complex **1** reproducibly in yields of up to 57%.

There are many examples in the literature where yttrium is coordinated by six alkyl groups, for example, ate complexes $[\text{Li}(\text{solvent})_x]_3[\text{LnMe}_6]$, $[\{\text{Li}(\text{dme})_3\}\{\text{Y}(\text{CH}_2\text{-X-CH}_2)_6\}]$ with $\text{X} = \text{C}_2\text{H}_4, \text{C}_3\text{H}_6, \text{Si}(\text{CH}_3)_2$ and others.¹⁴ Complex **1** features a donor-free ate complex with three incorporated lithium atoms. The yttrium atom is bonded to five neosilyl ligands adopting a square pyramidal coordination geometry. The sixth alkyl group is peripheral, bridging the lithium atoms exclusively. Only one of the yttrium-bound alkyl groups is terminal. The structural motif is reminiscent of the solid-state structure of hexameric $[\text{LiCH}_2\text{SiMe}_3]_6$, which was found as one of the decomposition products (*vide infra*).¹⁵ The three lithium atoms and the yttrium atom of **1** form a distorted trigonal pyramid (cf. ESI†) with a basal Li_3 isosceles triangle and an apical yttrium atom. The Li1-Li2-Li3 connection is almost rectangular at $89.3(5)^\circ$. The Y-Li distances range between $2.838(10)$ Å and $2.936(11)$ Å. The terminal Y-C distance in **1** amounts to $2.362(6)$ Å, while the bridging ones range from $2.467(7)$ to $2.628(7)$ Å. For comparison, the homoleptic 4-coordinate anionic fragment

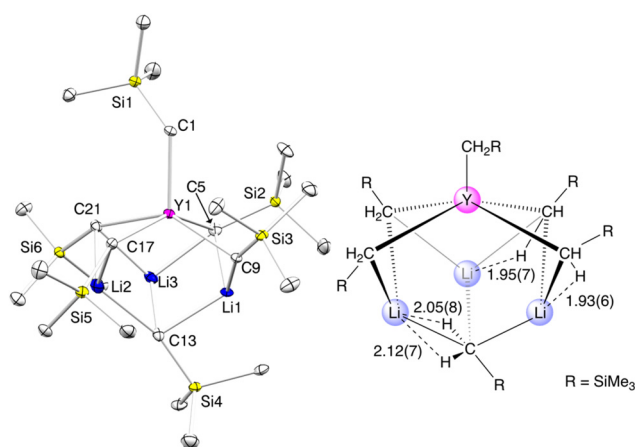


Fig. 1 Left: Crystal structure of one of two independent molecules in the unit cell of $\text{Li}_3\text{Y}(\text{CH}_2\text{SiMe}_3)_6$ (**1**) (ellipsoids set at the 50% probability level). Hydrogen atoms are omitted for clarity. For detailed metric parameters, cf. ESI.† Right: Illustration of secondary $\text{Li}\cdots\text{H}$ interactions with respective distances in Å.

$[\text{Y}(\text{CH}_2\text{SiMe}_3)_4]$ of complex $[(\text{Me}_3\text{SiCH}_2)_x(\text{Me}_3\text{CO})_{1-x}\text{Y}(\mu\text{-OCMe}_3)_4\{\text{Li}(\text{THF})\}_4(\mu_4\text{-Cl})][\text{Y}(\text{CH}_2\text{SiMe}_3)_4]$ shows Y–C distances in a similar range (2.382(8) Å to 2.420(9) Å).⁶ Ion-separated heteroleptic complex $(\text{Me}_3\text{SiCH}_2\text{Y}[(\mu\text{-CH}_2)_2\text{SiMe}_2][(\mu\text{-OCMe}_3)\text{Li}(\text{thf})_2]_2)$, also reported by the Evans group, features a terminal Y–C_{silylalkyl} bond of 2.450(8) Å (CN_Y = 5), and Y–Li distances of 3.044(13) Å and 3.008(12) Å.¹⁶ The Li3–C13 distance of 2.163(13) Å in **1** seems to be slightly shorter than the Li–C distances in $[\text{LiCH}_2\text{SiMe}_3]_6$ which were reported as 2.24 Å on average.¹⁵ The 3-coordinate lithium atoms in **1** form additional Li⋯H interactions, which is illustrated in Fig. 1 (right). Two of the lithium atoms interact with one additional hydrogen atom each, with Li⋯H distances of 1.93(6) Å and 1.95(7) Å. The third lithium atom is close to two additional hydrogen atoms, albeit with slightly longer Li⋯H distances (2.05(8) and 2.12(7)). The latter match the shortest Li⋯H contacts in $[\text{LiCH}_2\text{SiMe}_3]_6$ ranging from 2.014 to 2.218 Å.¹⁷

Reports of solid-state structures with lanthanide trimethylsilylmethyl ate complexation *via* lithium are very scarce. To the best of our knowledge complex **1** is the only example of an ate complex completely devoid of any additional ligands or solvent molecules and only trimethylsilylmethyl ligands. A few examples of these kinds of complexes have been reported, albeit all of them with additional anionic ligands like cyclopentadienyl or aryloxy/alkoxy derivatives.¹⁸ Comparable “oligomeric” structural motifs with CN_{Ln} = 5 are also observed in solvent-donor free alkoxide complexes $\text{Li}_5\text{Sm}(\text{OtBu})_8$ and $\text{Na}_8\text{Y}(\text{OtBu})_{10}(\text{X})$ (X = Cl, OH), respectively.¹⁹ By performing the Schumann protocol with LuCl_3 and either 4 or 6 equiv. of $\text{LiCH}_2\text{SiMe}_3$ under the same conditions (NMR-scale reactions), the only soluble component detectable by ¹H, ⁷Li and ¹³C NMR spectroscopy was $\text{LiCH}_2\text{SiMe}_3$ (ESI, Fig. S20–S22†). Furthermore, the signals in the ¹H and ⁷Li NMR spectra did not change upon addition of additional diethyl ether (*cf.* ESI†). From this, we inferred that there is no access to separated ion-pair $[\text{Li}(\text{Et}_2\text{O})_4][\text{Lu}(\text{CH}_2\text{SiMe}_3)_4]$ or even a complex similar to yttrium ate complex $\text{Li}_3\text{Y}(\text{CH}_2\text{SiMe}_3)_6$ (**1**), under the same reaction conditions.

Scandium

The reaction system $\text{ScCl}_3/6\text{LiCH}_2\text{SiMe}_3$ in $\text{Et}_2\text{O}/n$ -pentane (the same conditions as for yttrium) gave a mixture of $[\text{Li}(\text{solvent})_4][\text{Sc}(\text{CH}_2\text{SiMe}_3)_4]$ (major component) and $\text{Sc}(\text{CH}_2\text{SiMe}_3)_3(\text{solvent})_x$ (minor component), unambiguously identified *via* their respective ⁴⁵Sc NMR chemical shifts (*cf.* Fig. 3, ESI†).^{10,20} Unfortunately, attempts to crystallize a product out of this reaction mixture yielded only $[\text{LiCH}_2\text{SiMe}_3]_6$, identified *via* XRD (unit cell check).¹⁵ The reaction of $\text{ScCl}_3(\text{thf})_3$ with 2.95 $\text{LiCH}_2\text{SiMe}_3$ in *n*-hexane at –40 °C also revealed various products in the ¹H NMR spectrum (*cf.* ESI†). The respective ⁴⁵Sc NMR spectrum was remarkably similar to the aforementioned, showing one resonance at $\delta = 741$ ppm, corresponding to $\text{Sc}(\text{CH}_2\text{SiMe}_3)_3(\text{thf})_2$, and one at $\delta = 919.5$ ppm. The latter signal is in a range similar to the resonance of $[\text{Li}(\text{thf})_4][\text{Sc}(\text{CH}_2\text{SiMe}_3)_4]$ ($\delta = 933.4$ ppm),¹⁰ although it slightly shifted to higher fields and was broader

(*cf.* ESI†). By overlaying both the ¹H and the ⁴⁵Sc NMR spectra (*cf.* ESI†), the similarities between the two reactions became more apparent. The ⁷Li NMR spectrum of **2** shows two signals, one close to $\delta = 0$ ppm (indicative of a separated Li⁺ ion) and also one around $\delta = 2$ ppm in the lithium alkyl region, similar to complex **1** (*cf.* Fig. 2).

Luckily, concentrating an *n*-hexane solution of the $\text{ScCl}_3(\text{thf})_3/2.95\text{LiCH}_2\text{SiMe}_3$ reaction induced the crystallization of compound **2**. XRD analysis of **2** revealed an ate complex of composition $[\text{Li}(\text{thf})_4][\text{LiSc}_2(\text{CH}_2\text{SiMe}_3)_8]$ (**2**) (*cf.*, Scheme 2 and Fig. 2). Repeating the reaction under identical conditions reproducibly gave crystals with the same unit cell. Complex **2** consists of a separated ion-pair featuring the trimetallic anion $[\text{LiSc}_2(\text{CH}_2\text{SiMe}_3)_8]^-$ and $[\text{Li}(\text{thf})_4]^+$ as a “classical” cation. Each scandium atom is bridged by two trimethylsilylmethyl ligands to the central lithium and the remaining two trimethylsilylmethyl ligands bind in a terminal way, which in turn is consistent with the ⁷Li NMR spectrum (*cf.* ESI†). This closely resembles the proposed tetrahedral structure of $[\text{Sc}(\text{CH}_2\text{SiMe}_3)_4]^-$, albeit with a lithium atom which is sandwiched by two of such entities. The structural motif at hand is hitherto unprecedented and best comparable to ate complexes $\text{Li}_3\text{Ln}_2\text{Me}_9(\text{solvent})_5$ (Ln = Sc, Y, Gd–Lu),^{14b} or others like $[\text{Sc}\{\text{CH}(\text{SiMe}_3)_2\}_2\text{ClLi}(\text{thf})_2]_2$ and $[(\text{C}_5\text{Me}_4\text{CH}_2\text{CH}_2\text{NMe}_2)\text{YMe}_2(\text{MeLi})]_2$.^{10,21} The average Sc–C_{bridge} distances are 2.322 Å, while the terminal Sc–C distances are significantly shorter ranging from 2.17(3) to 2.32(3) Å. The central lithium atom is coordinated tetrahedrally by four bridging alkyl ligands. We presume that a lack of a thf donor leads to an incomplete lithium separation and formation of complex **2**. Interestingly, the Sc–Li distances are quite short with about 2.81(2) Å each. The Li2–O distances of the cationic moiety are in the expected range of 1.82(3)–1.94(4) Å. A similar kind of “sandwiched” alkali–metal complex with lanthanum, aryloxy $\{\text{Cs}_2[\text{La}(\text{OAr})_5]\}_n$ (Ar = C₆H₃iPr₂-2,6), has been reported.²²

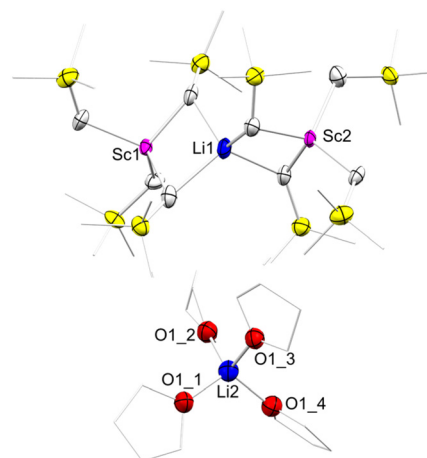


Fig. 2 Crystal structure of $[\text{Li}(\text{thf})_4][\text{LiSc}_2(\text{CH}_2\text{SiMe}_3)_8]$ (**2**) (ellipsoids set at the 50% probability level). Hydrogen atoms and disorders are omitted for clarity. The carbon atoms of THF and the SiMe_3 groups were rendered as wireframes. For detailed metrical parameters, *cf.* ESI†

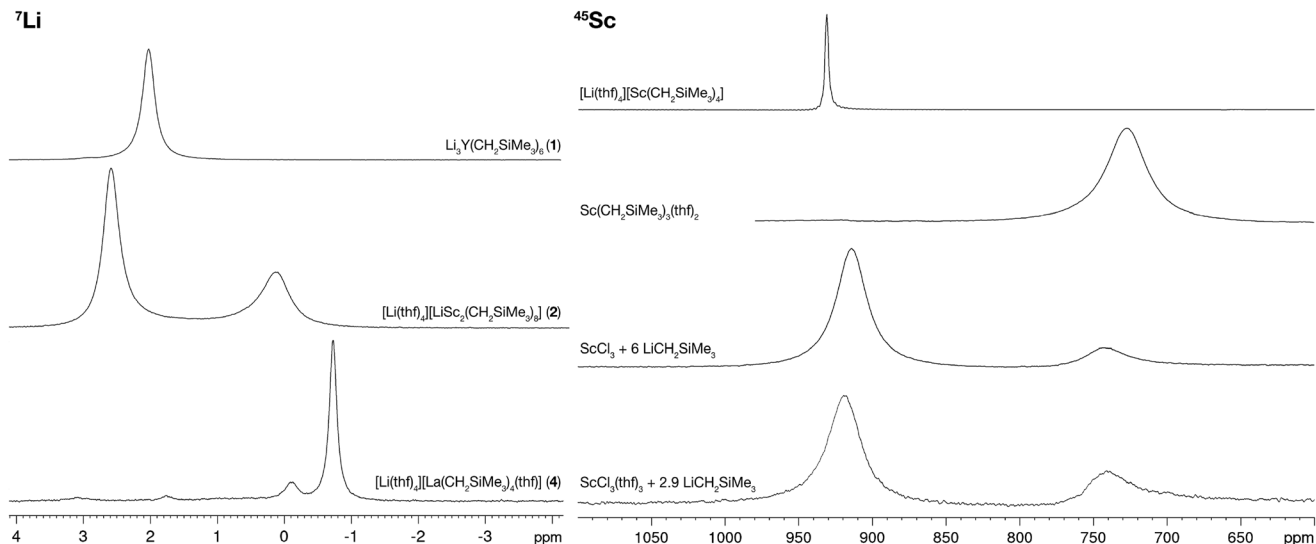
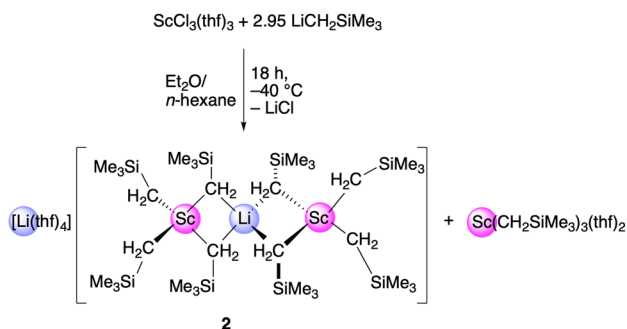


Fig. 3 Left: ^7Li NMR spectra of $\text{Li}_3\text{Y}(\text{CH}_2\text{SiMe}_3)_6$ (**1**), $[\text{Li}(\text{thf})_4][\text{LiSc}_2(\text{CH}_2\text{SiMe}_3)_8]$ (**2**) and $[\text{Li}(\text{thf})_4][\text{La}(\text{CH}_2\text{SiMe}_3)_4(\text{thf})]$ (**3**). Right: ^{45}Sc NMR spectra of pure complexes $[\text{Li}(\text{thf})_4][\text{Sc}(\text{CH}_2\text{SiMe}_3)_4]$ and $\text{Sc}(\text{CH}_2\text{SiMe}_3)_3(\text{thf})_2$ and reaction mixtures of $\text{ScCl}_3/6\text{LiCH}_2\text{SiMe}_3$ and $\text{ScCl}(\text{thf})_3/2.95\text{LiCH}_2\text{SiMe}_3$.

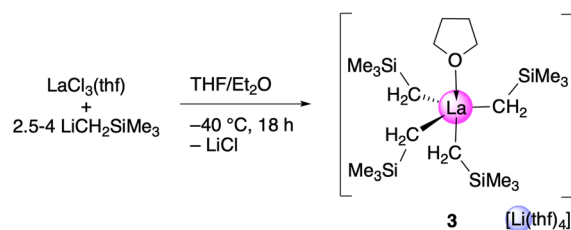


Scheme 2 Reaction of $\text{ScCl}_3(\text{thf})_3$ with 2.95 equivalents of $\text{LiCH}_2\text{SiMe}_3$ towards $[\text{Li}(\text{thf})_4][\text{LiSc}_2(\text{CH}_2\text{SiMe}_3)_8]$ (**2**) and $\text{Sc}(\text{CH}_2\text{SiMe}_3)_3(\text{thf})_2$.

Lanthanum

Neither adducts $\text{Ln}(\text{CH}_2\text{SiMe}_3)_3(\text{thf})_x$ nor ate complexes $[\text{Li}(\text{donor})_x][\text{Ln}(\text{CH}_2\text{SiMe}_3)_4]$ could so far be effectively isolated for rare-earth-metal centers of size larger than Sm^{3+} . Employing our recently established low-temperature syntheses and crystallization techniques, giving access to the alkyl ate complexes $\text{Li}_3\text{Lu}(n\text{-Bu})_6(\text{thf})_4$, $\text{Li}_2\text{Ln}(n\text{-Bu})_5(\text{tmeda})_2$ ($\text{Ln} = \text{Ce}, \text{Lu}$), $[\text{Ce}(t\text{-Bu})_4][\text{Li}(\text{thf})_4]$, $\text{Li}_6\text{Eu}(n\text{-Bu})_8(\text{thf})_6$, and $\text{Li}_3\text{Y}(i\text{-Bu})_6(\text{thf})_4$, the reaction system $\text{LaCl}_3(\text{thf})/3\text{LiCH}_2\text{SiMe}_3$ was investigated similarly.²³ When using a solvent mixture of THF and *n*-hexane, no reaction took place at -40°C . However, switching to a mixture of THF and diethyl ether accomplished a slow reaction which led to the isolation of crystalline $[\text{Li}(\text{thf})_4][\text{La}(\text{CH}_2\text{SiMe}_3)_4(\text{thf})]$ (**3**) (Scheme 3 and Fig. 4).

The ^1H NMR spectrum of **3** shows a sharp CH_2 signal at -0.17 ppm, which is slightly shifted to lower field compared to **1** (-0.73 ppm), but considerably to a higher field in comparison with $\text{LiCH}_2\text{SiMe}_3$ (-2.13 ppm). To probe the feasibility of putative adduct $\text{La}(\text{CH}_2\text{SiMe}_3)_3(\text{thf})_x$, the reaction depicted in



Scheme 3 Reaction of $\text{LaCl}_3(\text{thf})$ with 3 equiv. of $\text{LiCH}_2\text{SiMe}_3$, yielding $[\text{Li}(\text{thf})_4][\text{La}(\text{CH}_2\text{SiMe}_3)_4(\text{thf})]$ (**3**).

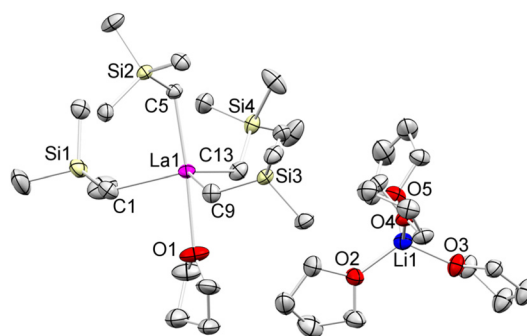


Fig. 4 Crystal structure of $[\text{Li}(\text{thf})_4][\text{La}(\text{CH}_2\text{SiMe}_3)_4(\text{thf})]$ (**3**) (ellipsoids set at the 50% probability level). Hydrogen atoms and disorders are omitted for clarity. For detailed metrical parameters, cf. ESI.†

Scheme 3 was conducted with 2.5 and 4 equivalents of $\text{LiCH}_2\text{SiMe}_3$.^{2a} Unfortunately, only the formation of $[\text{Li}(\text{thf})_4][\text{La}(\text{CH}_2\text{SiMe}_3)_4(\text{thf})]$ (**3**) was observed under these conditions. This seems to be plausible, since the alkylation reaction proceeds relatively slowly, and, in addition to this, LaCl_3 is not as soluble as a proposed mono-, di- or tri-alkylated lanthanum species. Consequently, these species react faster

with dissolved $\text{LiCH}_2\text{SiMe}_3$, leading to the preferred formation of ate complex **3**. A similar scenario has also been proposed for the reaction system $\text{LnCl}_3/\text{LiNiPr}_2$.²⁴

The 5-coordinate lanthanum centre of the anionic entity of ate complex **3** adopts a trigonal bipyramidal coordination geometry with one neosilyl and thf in the apical positions. As routinely observed, the counter ion lithium is stabilized by four THF molecules. This binding motif is very similar to previously reported $[\text{Li}(\text{thf})_4][\text{Ce}(t\text{-Bu})_4]$.⁴ However, since the neosilyl ligand is sterically less demanding than the *tert*-butyl ligand the lanthanum in complex **3** can accommodate one additional THF molecule. The La–C distances range between 2.598(3) Å and 2.614(2) Å. This correlates well with the previously reported complexes $\text{La}[\text{CH}(\text{SiMe}_3)_2]_3(\mu\text{-Cl})\text{Li}(\text{pmdeta})$ ($\text{CN}_{\text{La}} = 4$, La–C: 2.55(2)–2.68(4) Å,²⁵ $\text{La}(\text{AlMe}_4)_3$ ($\text{CN}_{\text{La}} = 7$, La–C: 2.696(3)–2.980(3) Å,²⁶ and $[\text{Li}(\text{thf})_x][\text{XN}_2\text{La}(\text{CH}_2\text{SiMe}_3)_2]$ ($\text{XN}_2 = 4,5$ -bis(2,4,6-triisopropylanilino)-2,7-di-*tert*-butyl-9,9-dimethylxanthene, $\text{CN}_{\text{La}} = 5$, La–C: 2.573(7)–2.613(7) Å).²⁷

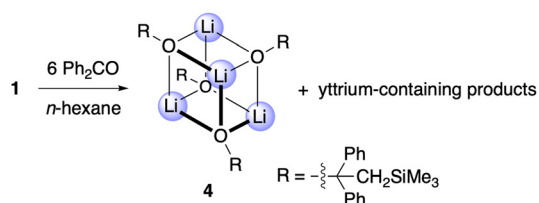
Reactivity of **1**

Recently, our group employed ClSiMe_3 in a “lithium depletion” reaction of $\text{Li}_2\text{Lu}(n\text{-Bu})_5(\text{tmeda})_2$ to yield $\text{Li}(\text{tmeda})\text{Lu}(n\text{-Bu})_3\text{Cl}$.⁴ Accordingly, complex **1** was treated with ClSiMe_3 (first 1 equiv., then up to 5 equiv.) in either toluene or THF. Unfortunately, the only isolable product of the reaction was $[\text{LiCH}_2\text{SiMe}_3]_6$, which could be identified *via* XRD (unit cell check). Moreover, the reaction of **1** with 6 equiv. of benzophenone gave an ill-defined mixture in the ^1H NMR spectrum (*cf.* ESI†) and at least seven signals in the ^7Li NMR spectrum of the raw product (Fig. S18†), of which the main species was later identified to be complex **4** (*vide infra*). However, ^1H - ^{89}Y HSQC NMR spectroscopy revealed one major yttrium species in solution with a chemical shift $\delta(^{89}\text{Y}) = 251$ ppm. Coan *et al.* reported that $\text{Y}_5\text{O}(\text{O}i\text{Pr})_{13}$ shows two resonances at 217.7 and 214.0 ppm; so the assumption of the formation of an yttrium alkoxide species seems to be plausible.²⁸ Crystallization attempts from *n*-hexane, however, only yielded lithium alkoxide $[\text{LiOC}(\text{CH}_2\text{SiMe}_3)(\text{Ph})_2]_4$ (**4**, Scheme 4), the solid-state structure of which was reported recently.²⁹

Thermal decomposition of **1**

Since the ^1H NMR spectra of **1** confirmed a silane elimination (SiMe_4) after a relatively short time (*cf.* Fig. S1†), it was assumed that the complex has a high tendency to decompose in solution rapidly. Being driven by Schumann’s originally pro-

posed alkylidene complex $\text{Li}[\text{Lu}(\text{CH}_2\text{SiMe}_3)_2(\text{CHSiMe}_3)]$, complex **1** was dissolved in benzene and stirred at ambient temperature in an argon atmosphere for seven days. After this period of time the colorless solution turned yellowish-orange and the reaction mixture was evaporated to dryness under reduced pressure (removal of the volatile side product SiMe_4). Again, $\text{LiCH}_2\text{SiMe}_3$ was identified as one of the main decomposition products (resonances in the ^1H NMR spectrum at $\delta = -2.05$ and 0.17 ppm). Other than this, there was one very broad resonance at 0.35 ppm (*cf.* ESI†), which correlated with an yttrium species in an ^1H - ^{89}Y HSQC NMR experiment with a chemical shift of $\delta(^{89}\text{Y}) = 685$ ppm. This low-field chemical shift suggested an yttrium center with several σ -bonded alkyl ligands, which is consistent with literature data (*e.g.*, $[\text{Y}(\text{CH}_2\text{SiMe}_3)_2(\text{thf})_4][\text{BPh}_4]$ shows a resonance at $\delta(^{89}\text{Y}) = 660.2$ ppm (ref. 30)).^{10,13} XRD experiments of colorless crystals obtained from a toluene/*n*-hexane solution revealed the known structural motif of $[\text{LiCH}_2\text{SiMe}_3]_6$, however, in a recently reported different unit cell.¹⁷ As discussed above, this nicely agrees with the fact that the bottom part of the solid-state structure of **1** strongly resembles the hexameric solid-state structure of $[\text{LiCH}_2\text{SiMe}_3]_6$ (*cf.*, Fig. S40†).¹⁵ Separation of the colorless crystals of $[\text{LiCH}_2\text{SiMe}_3]_6$ was not straightforward. Attempts to isolate a series of yttrium-containing crystals by multiple crystallization/filtration cycles failed. However, since an yttrium-containing thermal decomposition product of **1** was supposed to contain a “ $\text{Y}=\text{CHSiMe}_3$ ”-moiety, the existence of such a species was checked *via* the reactivity towards a ketone. Since **1** was already shown to react as a nucleophile with benzophenone (*vide supra*), any putative alkylidene moiety should engage in a Tebbe-like exchange reaction. Consequently, a sample of decomposed **1** was dissolved in toluene/*n*-hexane and stored at -40 °C. Afterwards, any crystallized $\text{LiCH}_2\text{SiMe}_3$ was separated *via* decantation and the remaining solution, containing the presumed yttrium alkylidene complex, was reacted with benzophenone in a sealed J. Young-valved NMR tube. Immediately a color change from yellow to dark blue was observed. The ^1H NMR spectrum showed a weak resonance at δ 6.37 ppm (Fig. S12†), which can be assigned to the respective alkene $\text{Ph}_2\text{C}=\text{CHSiMe}_3$ that was already reported by the Li group.^{7a} The formation of such a small amount of olefination product is consistent with a follow-up study by Schumann on the thermal decomposition of $\text{Lu}(\text{CH}_2\text{SiMe}_3)_3(\text{thf})_2$, favoring γ -H abstraction and concomitant metallacycle formation as the major decomposition pathway.³¹ Regrettably, we could not isolate any yttrium-containing species from this reaction.



Scheme 4 Reactivity of $\text{Li}_3\text{Y}(\text{CH}_2\text{SiMe}_3)_6$ (**1**) towards six equivalents of benzophenone.

Conclusions

The reaction of anhydrous yttrium chloride with four to six equivalents of lithium trimethylsilylmethyl resulted in $\text{Li}_3\text{Y}(\text{CH}_2\text{SiMe}_3)_6$, featuring a hitherto unknown type of yttrium ate complex. The scandium reaction reproducibly produced a mixture of scandium tris(alkyl) and lithium scandium

tetrakis(alkyl) ate complexes as evidenced by ^{45}Sc NMR spectroscopy. Treatment of $\text{ScCl}_3(\text{thf})_3$ with 2.95 $\text{LiCH}_2\text{SiMe}_3$ in the absence of THF gave compound $[\text{Li}(\text{thf})_4][\text{LiSc}_2(\text{CH}_2\text{SiMe}_3)_8]$ with yet another new structural motif. The tetrametallic $\text{Li}[\text{LiSc}_2]$ ate complex displays a ^{45}Sc chemical shift similar to $[\text{Li}(\text{thf})_4][\text{Sc}(\text{CH}_2\text{SiMe}_3)_4]$, albeit shifted to slightly higher fields with a broader resonance, indicative of the less symmetric coordination environment of the scandium atoms. Using the previously established seamless low-temperature synthesis and crystallization techniques the hitherto elusive lanthanum neosilyl complex could be isolated. In stark contrast to the previously reported neosilyl derivatives $\text{Ln}(\text{CH}_2\text{SiMe}_3)_3(\text{thf})_x$, obtained for the smaller lanthanides, the lanthanum reaction afforded ate complex $[\text{Li}(\text{thf})_4][\text{La}(\text{CH}_2\text{SiMe}_3)_4(\text{thf})]$. The reaction of $\text{Li}_3\text{Y}(\text{CH}_2\text{SiMe}_3)_6$ with six equivalents of benzophenone gave the 1,2-addition product only for the lithium alkyl, and an ill-defined mixture with several other species. ^{89}Y NMR spectroscopy suggested the presence of an yttrium alkoxide as a minor metalation product. The thermal decomposition of $\text{Li}_3\text{Y}(\text{CH}_2\text{SiMe}_3)_6$ resulted in a bright orange solution, along with the separation of SiMe_4 and lithium alkyl. Addition of benzophenone to the isolated orange residue led to a resonance in the ^1H NMR spectrum attributable to an olefinic proton, indicative of an yttrium silylalkylidene formation.

Experimental section

General considerations

All manipulations were performed under rigorous exclusion of air and moisture using standard Schlenk, high-vacuum, and glovebox techniques (MBraun MB150B-G-II; <1 ppm O_2 , <1 ppm H_2O , argon atmosphere) except where noted otherwise. The solvents *n*-hexane, *n*-pentane, diethyl ether (Et_2O) and toluene were purified using Grubbs-type columns (MBraun SPS, solvent purification system). C_6D_6 (99.6%, Sigma-Aldrich) and $[\text{D}_8]\text{toluene}$ were dried by letting it stand over a Na/K-alloy for at least 24 h and subsequent filtration. All solvents were stored inside a glovebox. Lithium Trimethylsilylmethyl solution (0.7 M or 10 wt% in *n*-hexane) was purchased from aber GmbH. It was filtered, its solvent was removed *in vacuo* and it was recrystallized from *n*-hexane prior to use. ScCl_3 , YCl_3 and LaCl_3 were purchased from aber GmbH. The THF solvate of LaCl_3 was synthesized by Soxhlet extraction, and ScCl_3 was activated by stirring over THF overnight. NMR spectra of the air and moisture sensitive compounds were recorded by using J. Young-valved NMR tubes at ambient temperature. Solution-state NMR spectra were measured on Bruker AV 400 (^1H , ^{13}C), and Bruker AVII 500 (^7Li , ^{29}Si , ^{45}Sc , ^{89}Y) spectrometers, referenced to internal solvent residual signals and reported relative to tetramethylsilane (^1H , ^{13}C , ^{29}Si), LiCl (^7Li), $\text{Sc}(\text{NO}_3)_3$ (^{45}Sc) and YCl_3 (^{89}Y). Coupling constants are given in Hertz. IR spectra were recorded on a NICOLET 6700 FTIR spectrometer with a DRIFT cell (KBr window). Samples were prepared inside a glovebox by

mixing with the KBr powder. Elemental analyses were performed on an Elementar Vario Micro Cube.

$\text{Li}_3\text{Y}(\text{CH}_2\text{SiMe}_3)_6$ (1)

Anhydrous YCl_3 (138.9 mg, 0.711 mmol) was suspended in 10 mL of a 1:1 $\text{Et}_2\text{O}/n$ -pentane mixture. $\text{LiCH}_2\text{SiMe}_3$ (401.9 mg, 2.845 mmol) dissolved in 5 mL of *n*-pentane was added dropwise at ambient temperature and stirred for 30 min. Afterwards, LiCl was filtered off and the residual solvent was removed *in vacuo*. Then, the residue was redissolved in 5 mL of benzene and the mixture was filtered again. The resulting solution was thoroughly dried under vacuum to yield the product as colorless crystals (256.8 mg, 0.405 mmol, 57%). Crystals suitable for X-ray diffraction analysis were grown from a saturated *n*-hexane/toluene solution. ^1H NMR (500.1 MHz, C_6D_6 , 26 °C): δ 0.23 (s, 54H, SiCH_3), -0.69 (br s, 12H, Y/LiCH_2) ppm. ^{13}C NMR (125 MHz, $[\text{D}_8]\text{toluene}$, 26 °C): δ 3.5 (SiMe_3), -0.4 (Y/Li-CH_2) ppm. ^7Li NMR (116.6 MHz, C_6D_6 , 26 °C): δ 2.0 ppm. ^{29}Si INEPTND NMR (99.4 MHz, $[\text{D}_8]\text{toluene}$, 26 °C): δ -0.4 (br, SiCH_3) ppm. ^{89}Y NMR (from $^{89}\text{Y-}^1\text{H}$ HSQC, 24.5 MHz, $[\text{D}_8]\text{toluene}$, 26 °C): δ 954.5 ppm. DRIFTS ($\tilde{\nu}$): 2948.1 (s), 2889.4 (w), 2840.1 (w), 2797.4 (w), 1429.1 (vw), 1245.5 (s), 848.2 (vs), 819.9 (vs), 725.0 (s), 679.3 (w), 602.9 (vw), 456.5 (w), 426.9 (w), 401.1 (w) cm^{-1} . Elemental analysis (%) calculated for $\text{C}_{24}\text{H}_{66}\text{Li}_3\text{Si}_6\text{Y}$ (633.03): C 45.54, H 10.51, found: C 45.42, H 10.83.

Thermal decomposition of 1

Compound 1 (59.8 mg, 0.094 mmol) was dissolved in benzene and stirred at ambient temperature. A color change from colorless to yellowish-orange was observed. After seven days, the solution was dried under reduced pressure to yield an orange solid. The orange solid was extracted with 3 mL of toluene and with 3 mL of *n*-hexane (no residue remained) and both extracts were stored at -40 °C. From the *n*-hexane extract colorless crystals of $(\text{LiCH}_2\text{SiMe}_3)_6$ were separated and identified *via* X-ray diffraction. ^1H NMR (500.1 MHz, C_6D_6 , 26 °C): δ 0.35 (br), 0.17 (s, $\text{Si}(\text{CH}_3)_3$), -2.05 (Li-CH_2) ppm. ^7Li NMR (194.4 MHz, C_6D_6 , 26 °C): δ 2.5 ($\text{LiCH}_2\text{SiMe}_3$), 3.9 (br) ppm. ^{29}Si DEPT45 (99.4 MHz, C_6D_6 , 26 °C): δ -0.2 (" Y-CHSiMe_3 "), -0.5 ($\text{LiCH}_2\text{SiMe}_3$) ppm. ^{89}Y NMR (from $^{89}\text{Y-}^1\text{H}$ HSQC, 24.5 MHz, C_6D_6 , 26 °C): δ 680.2 ppm.

$[\text{Li}(\text{thf})_4][\text{LiSc}_2(\text{CH}_2\text{SiMe}_3)_8]$ (2)

$\text{ScCl}_3(\text{thf})_3$ (107.7 mg, 0.293 mmol) was suspended in 5 mL of *n*-hexane and pre-cooled to -40 °C. Afterwards, $\text{LiCH}_2\text{SiMe}_3$ (80.0 mg, 0.850 mmol) was dissolved in 5 mL of *n*-hexane at an equally cold temperature and was added. The reaction mixture was stirred at -40 °C for 18 h and afterwards the solvent carefully evaporated at this temperature. During solvent evaporation at -40 °C, the colorless solution froze and overnight the residue transformed into colorless crystals of 2 suitable for X-ray diffraction analysis. Crude yield: 97.6 mg. ^7Li NMR (194 MHz, C_6D_6 , 10 °C): δ 2.6 (Li-CH_2), 0.1 ($\text{Li}(\text{thf})_4^+$) ppm. ^{29}Si NMR (99 MHz, C_6D_6 , 10 °C): δ 0.8, -1.2 ($\text{Sc}(\text{CH}_2\text{SiMe}_3)_3(\text{thf})_2$),

−4.9 ppm. ^{45}Sc NMR (121.5 MHz, C_6D_6 , 10 °C) δ 919.5 ($\text{Sc}(\text{CH}_2\text{SiMe}_3)_4^-$), 741.0 ($\text{Sc}(\text{CH}_2\text{SiMe}_3)_3(\text{thf})_2$) ppm.

[Li(thf)₄][La(CH₂SiMe₃)₄(thf)] (3)

To $\text{LaCl}_3(\text{thf})$ (63.5 mg, 0.200 mmol), THF (0.4 mL) and Et_2O (1 mL) were added and the suspension was cooled to −40 °C. Afterwards, $\text{LiCH}_2\text{SiMe}_3$ (56.5 mg, 0.6 mmol, 3 equiv.) dissolved in Et_2O and precooled to −40 °C was added dropwise. After stirring the suspension for 18 h, it was filtered and the solvent was removed *in vacuo*. The crude product was extracted with cold Et_2O and filtered and the solvent was once again removed *in vacuo* to give a white powder of $[\text{Li}(\text{thf})_4][\text{La}(\text{CH}_2\text{SiMe}_3)_4(\text{thf})]$ (130.0 mg, 0.152 mmol, 76%) (calcd for 3 $\text{LiCH}_2\text{SiMe}_3$). Crystals of 3 suitable for X-ray diffraction analysis were obtained from a highly concentrated Et_2O solution. When employing 2.5 or 4 equiv. of $\text{LiCH}_2\text{SiMe}_3$ the yields were 95% and 87%, respectively. ^1H NMR, (500.13 MHz, $[\text{D}_8]$ toluene, −40 °C): δ = 3.52 (s, 10 H, THF), 3.46 (s, 10 H, THF), 1.73 (s, 10 H, THF), 1.38 (s, 10 H, THF), 0.55 (s, 36 H, $\text{CH}_2\text{Si}(\text{CH}_3)_3$), −0.17 (s, 8 H, $\text{CH}_2\text{Si}(\text{CH}_3)_3$) ppm. ^{13}C NMR, (125.76 MHz, $[\text{D}_8]$ toluene, −40 °C): δ = 68.6 (s, THF), 67.9 (s, THF), 25.8 (s, THF), 25.7 (s, THF), 5.3 ppm (s, $\text{CH}_2\text{Si}(\text{CH}_3)_3$). No signal for the CH_2 groups could be observed. ^7Li NMR, (194.37 MHz, $[\text{D}_8]$ toluene, −40 °C): δ = −0.73 (s, $\text{Li}(\text{thf})_4$) ppm. Anal. (%) calcd for $\text{C}_{36}\text{H}_{84}\text{LaLiO}_5\text{Si}_4$ (855.24): C 50.56, H 9.90; found: C 49.65, H 9.49. The deviation between theoretical and experimental microanalytical data originates from rapid decomposition of $[\text{Li}(\text{thf})_4][\text{La}(\text{CH}_2\text{SiMe}_3)_4(\text{thf})]$ at ambient temperature.

[LiOC(CH₂SiMe₃)(Ph)₂]₄ (4)

At ambient temperature, **1** (24.5 mg, 0.039 mmol) was dissolved in *n*-hexane (2 mL). Afterwards, benzophenone (42.4 mg, 0.232 mmol), dissolved in an equal amount of *n*-hexane, was added. The reaction mixture was stirred for 15 min after which the mixture began to turn to a slight shade of yellow. Afterwards, the reaction mixture was concentrated and stored. Overnight, colorless crystals of **4** suitable for X-ray analysis could be harvested at −40 °C. ^1H NMR (500.1 MHz, C_6D_6 , 26 °C): δ −0.25 (s, 36H, SiCH_3), 1.43 (s, 8H, CH_2), 7.08 (m, 8H, Ar-*H*), 7.12 (t, $^3J_{\text{H-H}} = 7.3$ Hz, 16H, Ar-*H*), 7.24 (d, $^3J_{\text{H-H}} = 7.5$ Hz, 16H, Ar-*H*) ppm. ^{13}C NMR (125.8 MHz, C_6D_6 , 26 °C): δ 0.1 (SiMe_3), 38.5 (CH_2), 79.0 (O-*C*), 126.3 (Ar-*C*), 127.0 (Ar-*C*), 128.7 (Ar-*C*), 154.1 (Ar-*C*_{ipso}) ppm. ^7Li NMR (116.6 MHz, C_6D_6 , 26 °C): δ 0.4 ppm. ^{29}Si DEPT45 NMR (99.4 MHz, $[\text{D}_8]$ toluene, 26 °C): δ −3.8 (br, SiCH_3) ppm. Elemental analysis (%) calculated for $\text{C}_{68}\text{H}_{84}\text{Li}_4\text{O}_4\text{Si}_4$ (1105.52): C 73.88, H 7.55, found: C 74.02, H 7.77.

X-ray crystallography and crystal structure determinations

Crystals of **1** were grown from a saturated *n*-hexane/toluene solution at −40 °C. Crystals of **2** were produced by evaporating a saturated toluene solution at −40 °C. Crystals of **4** were grown from an *n*-hexane solution at −40 °C. Suitable crystals for XRD analyses were selected inside a glovebox and coated with Parabar 10312 (previously known as Paratone N,

Hampton Research) and fixed on a microloop. X-ray data were collected on a Bruker APEX III DUO instrument equipped with an $\text{I}\mu\text{S}$ microfocus sealed tube and QUAZAR optics for $\text{MoK}\alpha$ ($\lambda = 0.71073$ Å) radiation. Data collection was performed using COSMO³² employing ω -scans. Raw data were processed using APEX³³ and SAINT,³⁴ and corrections for absorption effects were applied using SADABS.³⁵ The structures were solved by direct methods and refined against all data by full-matrix least-squares methods on F^2 using SHELXTL³⁶ and SHELXL.³⁷ All graphics were produced employing CSD Mercury 4.1.0.³⁸ Disordered models were calculated using DSR,³⁹ a program included in SHELXL, for refining the disordered models. Further details regarding the refinement and crystallographic data are listed in Table S1 and in the CIF files.† CCDC depositions 2215407–2215409 contain all the supplementary crystallographic data for this paper.†

Conflicts of interest

There are no conflicts to declare.

References

- (a) M. Zimmermann and R. Anwender, *Chem. Rev.*, 2010, **110**, 6194–6259; (b) F. Ortu, *Chem. Rev.*, 2022, **122**, 6040–6116.
- (a) H. Schumann, D. M. M. Freckmann and S. Dechert, *Z. Anorg. Allg. Chem.*, 2002, **628**, 2422–2426; (b) S. Bambirra, M. W. Bouwkamp, A. Meetsma and B. Hessen, *J. Am. Chem. Soc.*, 2004, **126**, 9182–9183.
- H. Schumann and J. Müller, *J. Organomet. Chem.*, 1979, **169**, C1–C4.
- T. Berger, J. Lebon, C. Maichle-Mössmer and R. Anwender, *Angew. Chem., Int. Ed.*, 2021, **60**, 15622–15631.
- J. L. Atwood, W. E. Hunter, R. D. Rogers, J. Holton, J. McMeeking, R. Pearce and M. F. Lappert, *J. Chem. Soc., Chem. Commun.*, 1978, 140–142.
- W. J. Evans, J. L. Shreeve, R. N. R. Broomhall-Dillard and J. W. Ziller, *J. Organomet. Chem.*, 1995, **501**, 7–11.
- (a) S. Li, M. Wang, B. Liu, L. Li, J. Cheng, C. Wu, D. Liu, J. Liu and D. Cui, *Chem. – Eur. J.*, 2014, **20**, 15493–15498; (b) T. Li, G. Zhang, J. Guo, S. Wang, X. Leng and Y. Chen, *Organometallics*, 2016, **35**, 1565–1572; (c) F. Yan, S. Li, L. Li, W. Zhang, D. Cui, M. Wang and Y. Dou, *Eur. J. Inorg. Chem.*, 2019, **2019**, 2277–2283.
- M. Carravetta, M. Concistre, W. Levason, G. Reid and W. Zhang, *Inorg. Chem.*, 2016, **55**, 12890–12896.
- (a) S. A. Bartlett, G. Cibin, A. J. Dent, J. Evans, M. J. Hanton, G. Reid, R. P. Tooze and M. Tromp, *Dalton Trans.*, 2013, **42**, 2213–2223; (b) F. Mazzotta and D. Kunz, *Organometallics*, 2021, **40**, 3003–3011.
- A. Mortis, D. Barisic, K. Eichele, C. Maichle-Mössmer and R. Anwender, *Dalton Trans.*, 2020, **49**, 7829–7841.

- 11 B. Wang, D. Wang, D. Cui, W. Gao, T. Tang, X. Chen and X. Jing, *Organometallics*, 2007, **26**, 3167–3172.
- 12 B. R. Elvidge, S. Arndt, P. M. Zeimentz, T. P. Spaniol and J. Okuda, *Inorg. Chem.*, 2005, **44**, 6777–6788.
- 13 R. E. White and T. P. Hanusa, *Organometallics*, 2006, **25**, 5621–5630.
- 14 (a) R. Fischer, S. Bode, M. Köhler, J. Langer, H. Görls, M. D. Hager, U. S. Schubert and M. Westerhausen, *Organometallics*, 2015, **34**, 23–31; (b) M. U. Kramer, D. Robert, S. Arndt, P. M. Zeimentz, T. P. Spaniol, A. Yahia, L. Maron, O. Eisenstein and J. Okuda, *Inorg. Chem.*, 2008, **47**, 9265–9278; (c) H. Schumann, J. Pickardt and N. Bruncks, *Angew. Chem., Int. Ed. Engl.*, 1981, **20**, 120–121; (d) H. Schumann, J. Mueller, N. Bruncks, H. Lauke, J. Pickardt, H. Schwarz and K. Eckart, *Organometallics*, 1984, **3**, 69–74.
- 15 B. Tecele, A. F. M. Maqsdur Rahman and J. P. Oliver, *J. Organomet. Chem.*, 1986, **317**, 267–275.
- 16 W. J. Evans, T. J. Boyle and J. W. Ziller, *J. Organomet. Chem.*, 1993, **462**, 141–148.
- 17 J. O. Bauer, *Z. Kristallogr. - New Cryst. Struct.*, 2020, **235**, 353–356.
- 18 (a) W. J. Evans, R. Dominguez, K. R. Levan and R. J. Doedens, *Organometallics*, 1985, **4**, 1836–1841; (b) D. L. Clark, J. C. Gordon, J. C. Huffman, J. G. Watkin and B. D. Zwick, *Organometallics*, 1994, **13**, 4266–4270; (c) W. J. Evans, R. N. R. Broomhall-Dillard and J. W. Ziller, *J. Organomet. Chem.*, 1998, **569**, 89–97; (d) A. A. Trifonov, D. M. Lyubov, G. K. Fukin, E. V. Baranov and Y. A. Kurskii, *Organometallics*, 2006, **25**, 3935–3942; (e) B. Shen, L. Ying, J. Chen and Y. Luo, *Inorg. Chim. Acta*, 2008, **361**, 1255–1260; (f) S. Barroso, J. Cui, J. M. Carretas, A. Cruz, I. C. Santos, M. T. Duarte, J. P. Telo, N. Marques and A. M. Martins, *Organometallics*, 2009, **28**, 3449–3458; (g) P. L. Arnold, Z. R. Turner, R. Bellabarba and R. P. Tooze, *J. Am. Chem. Soc.*, 2011, **133**, 11744–11756; (h) X. Tao, W. Gao, H. Huo and Y. Mu, *Organometallics*, 2013, **32**, 1287–1294; (i) A. A. Kissel, T. V. Mahrova, D. M. Lyubov, A. V. Cherkasov, G. K. Fukin, A. A. Trifonov, I. Del Rosal and L. Maron, *Dalton Trans.*, 2015, **44**, 12137–12148; (j) X. Zhu, D. Guo, Y. Zhang, Y. Wei, S. Zhou, M. Xu, S. Wang, Y. Yang and Y. Qi, *Organometallics*, 2020, **39**, 4584–4591.
- 19 (a) H. Schumann, G. Kociok-Köhn, A. Dietrich and F. H. Görlitz, *Z. Naturforsch., B: Chem. Sci.*, 1991, **46**, 896–900; (b) W. J. Evans, M. S. Sollberger and J. W. Ziller, *J. Am. Chem. Soc.*, 1993, **115**, 4120–4127.
- 20 D. Barisic, D. Diether, C. Maichle-Mössmer and R. Anwander, *J. Am. Chem. Soc.*, 2019, **141**, 13931–13940.
- 21 L. N. Jende, C. Maichle-Mössmer, C. Schädle and R. Anwander, *J. Organomet. Chem.*, 2013, **744**, 74–81.
- 22 D. L. Clark, G. B. Deacon, T. Feng, R. V. Hollis, B. L. Scott, B. W. Skelton, J. G. Watkin and A. H. White, *Chem. Commun.*, 1996, 1729–1730.
- 23 T. Berger, D. Baschnagel, C. Maichle-Mössmer and R. Anwander, *Z. Anorg. Allg. Chem.*, 2022, e202200274.
- 24 T. Spallek, O. Heß, M. Meermann-Zimmermann, C. Meermann, M. G. Klimpel, F. Estler, D. Schneider, W. Scherer, M. Tafipolsky, K. W. Törnroos, C. Maichle-Mössmer, P. Sirsch and R. Anwander, *Dalton Trans.*, 2016, **45**, 13750–13765.
- 25 J. L. Atwood, M. F. Lappert, R. G. Smith and H. Zhang, *J. Chem. Soc., Chem. Commun.*, 1988, 1308–1309.
- 26 M. Zimmermann, N. Å. Frøystein, A. Fischbach, P. Sirsch, H. M. Dietrich, K. W. Törnroos, E. Herdtweck and R. Anwander, *Chem. – Eur. J.*, 2007, **13**, 8784–8800.
- 27 K. S. A. Motolko, D. J. H. Emslie and J. F. Britten, *RSC Adv.*, 2017, **7**, 27938–27945.
- 28 P. S. Coan, L. G. Hubert-Pfalzgraf and K. G. Caulton, *Inorg. Chem.*, 1992, **31**, 1262–1267.
- 29 N. Davison, P. G. Waddell, C. Dixon, C. Wills, T. J. Penfold and E. Lu, *Dalton Trans.*, 2022, **51**, 10707–10713.
- 30 S. Arndt and J. Okuda, *Adv. Synth. Catal.*, 2005, **347**, 339–354.
- 31 K. Rufanov, D. M. M. Freckmann, H.-J. Kroth, S. Schutte and H. Schumann, *Z. Naturforsch., B: Chem. Sci.*, 2005, **60**, 533–537.
- 32 COSMO v. 1.61, Bruker AXS Inc., Madison, WI, 2012.
- 33 APEX, 3 V. 2017.3-0, Bruker AXS Inc., Madison, WI, 2017.
- 34 SAINT v. 8.38A, Bruker AXS Inc., Madison, WI, 2017.
- 35 SADABS: L. Krause, R. Herbst-Irmer, G. M. Sheldrick and D. Stalke, *J. Appl. Crystallogr.*, 2015, **48**, 3–10.
- 36 G. M. Sheldrick, SHELXTL, *Acta Crystallogr., Sect. A: Found. Adv.*, 2015, **71**, 3–8; G. M. Sheldrick, Shelxl, *Acta Crystallogr., Sect. C: Struct. Chem.*, 2015, **71**, 3–8.
- 37 SHELXLE: C. B. Hübschle, G. M. Sheldrick and B. Dittrich, ShelXle: a Qt graphical user interface for SHELXL, *J. Appl. Crystallogr.*, 2011, **44**, 1281–1284.
- 38 C. F. Macrae, I. J. Bruno, J. A. Chisholm, P. R. Edgington, P. McCabe, E. Pidcock, L. Rodriguez-Monge, R. Taylor, J. Van de Streek and P. A. Wood, *J. Appl. Crystallogr.*, 2008, **41**, 466–470.
- 39 D. Kratzert, J. J. Holstein and I. Krossing, DSR: enhanced modelling and refinement of disordered structures with SHELXL, *J. Appl. Crystallogr.*, 2015, **48**, 933–938.

Supporting Information

Rare-earth-metal trimethylsilylmethyl ate complexes

Alexandros Mortis, Felix Kracht, Tassilo Berger, Jakob Lebon, Cäcilia Maichle-Mössmer, and Reiner Anwander*

Institut für Anorganische Chemie, Eberhard Karls Universität Tübingen, Auf der Morgenstelle 18, 72076 Tübingen, Germany

*E-mail for R. A.: reiner.anwander@uni-tuebingen.de

Table of Contents

NMR Spectra	S3
X-Ray Crystallography	S23

NMR Spectra

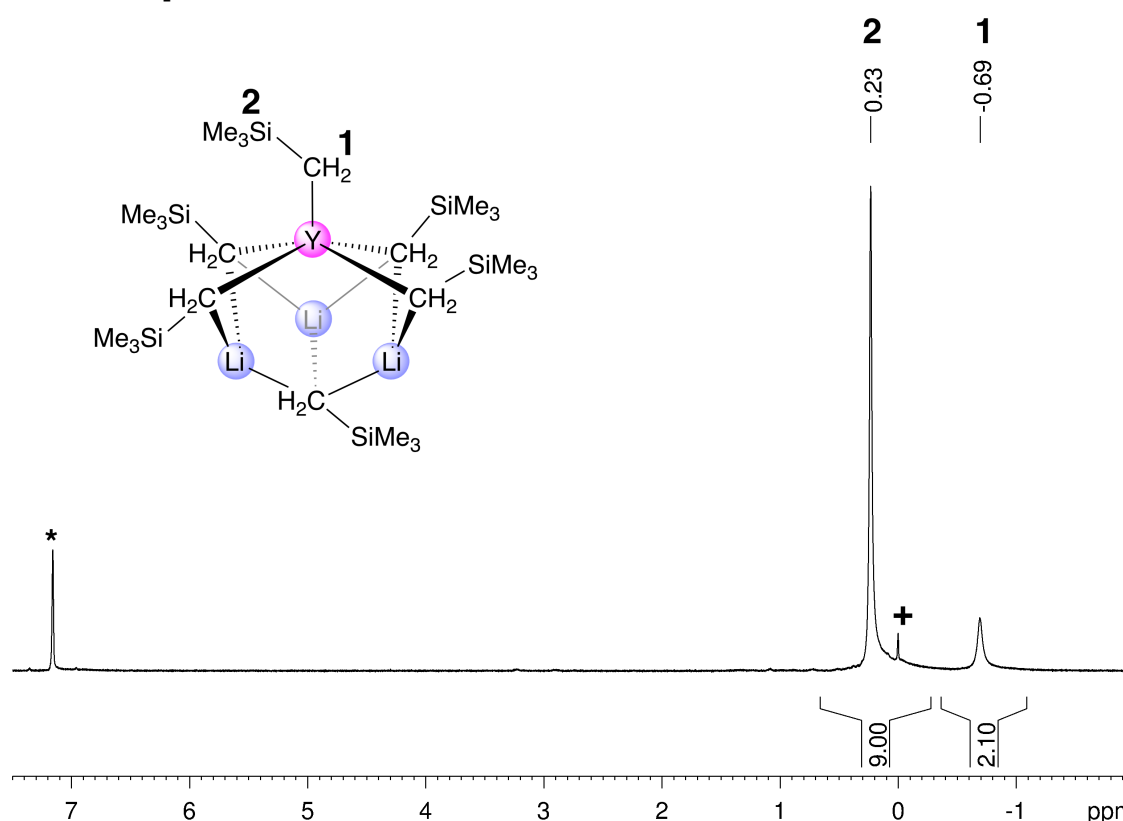


Figure S1. ^1H NMR spectrum (500 MHz) of $\text{Li}_3\text{Y}(\text{CH}_2\text{SiMe}_3)_6$ (**1**) in C_6D_6 at 26 °C. The solvent residual signal is marked with an asterisk, + denotes emerging SiMe_4 as the decomposition product.

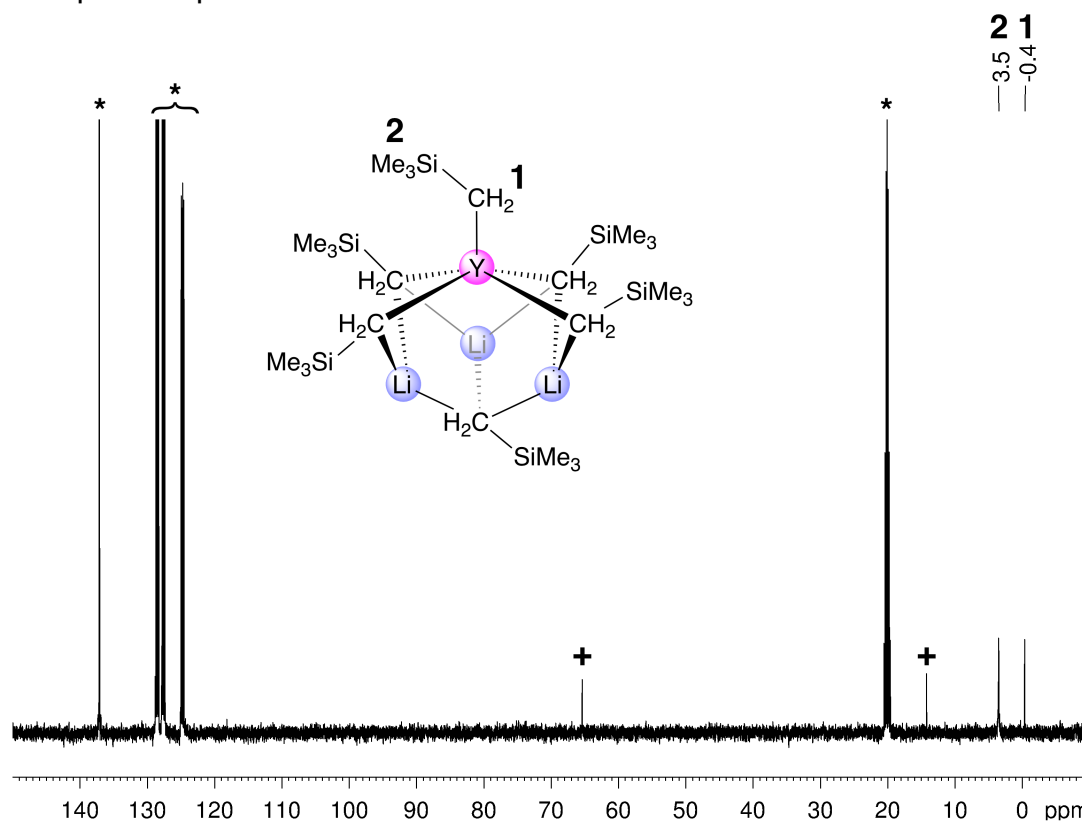


Figure S2. $^{13}\text{C}\{^1\text{H}\}$ NMR spectrum (125 MHz) of $\text{Li}_3\text{Y}(\text{CH}_2\text{SiMe}_3)_6$ (**1**) in $[\text{D}_8]\text{toluene}$ at 26 °C. The solvent residual signals are marked with asterisks, + denotes residual Et_2O .

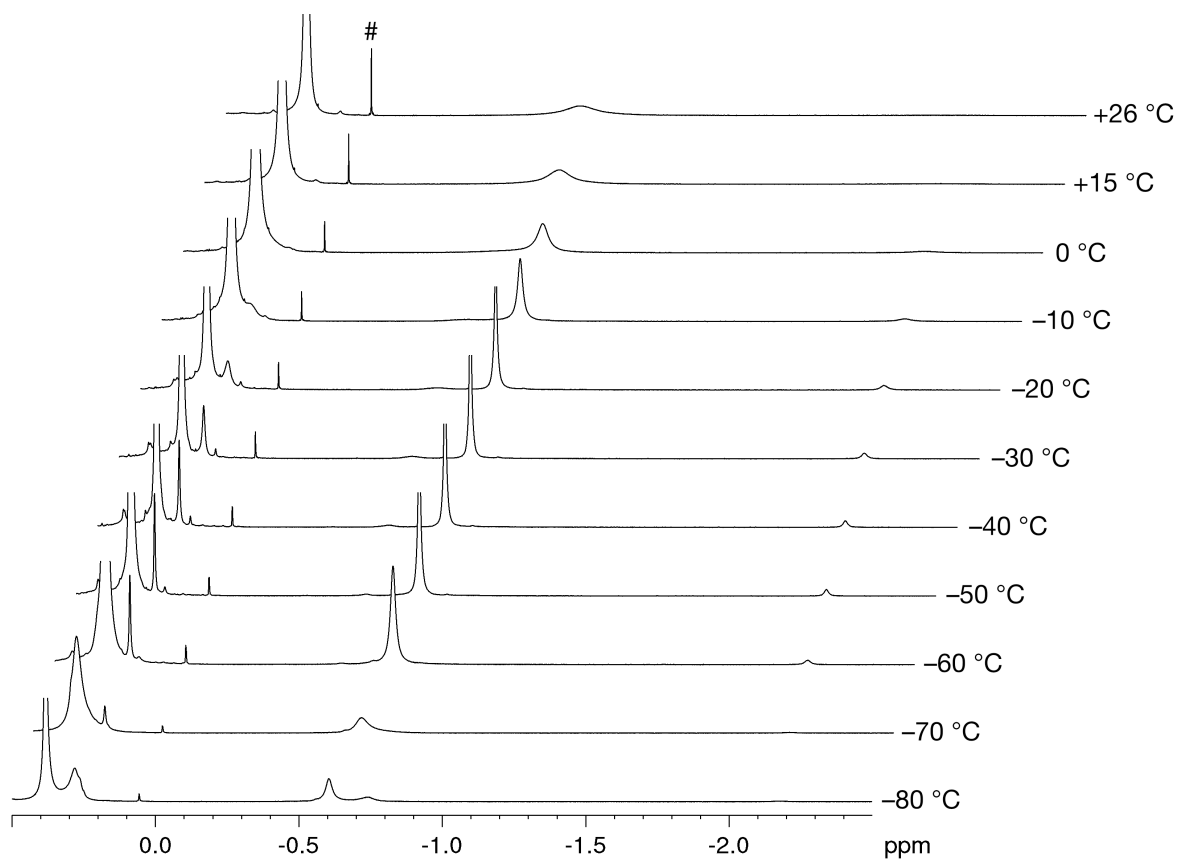


Figure S3. VT ^1H NMR spectrum (500 MHz) of $\text{Li}_3\text{Y}(\text{CH}_2\text{SiMe}_3)_6$ (1) in $[\text{D}_8]\text{toluene}$, # denotes emerging decomposition product SiMe_4 .

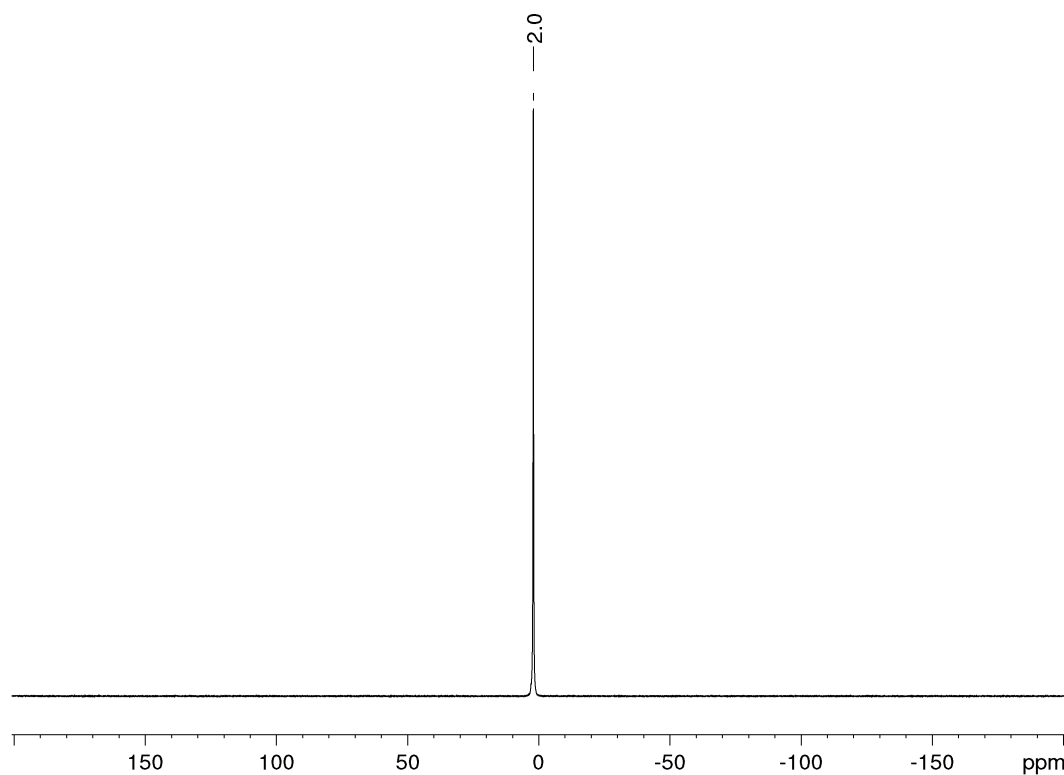


Figure S4. ^7Li NMR spectrum (116 MHz) of $\text{Li}_3\text{Y}(\text{CH}_2\text{SiMe}_3)_6$ (1) in C_6D_6 at 26 °C.

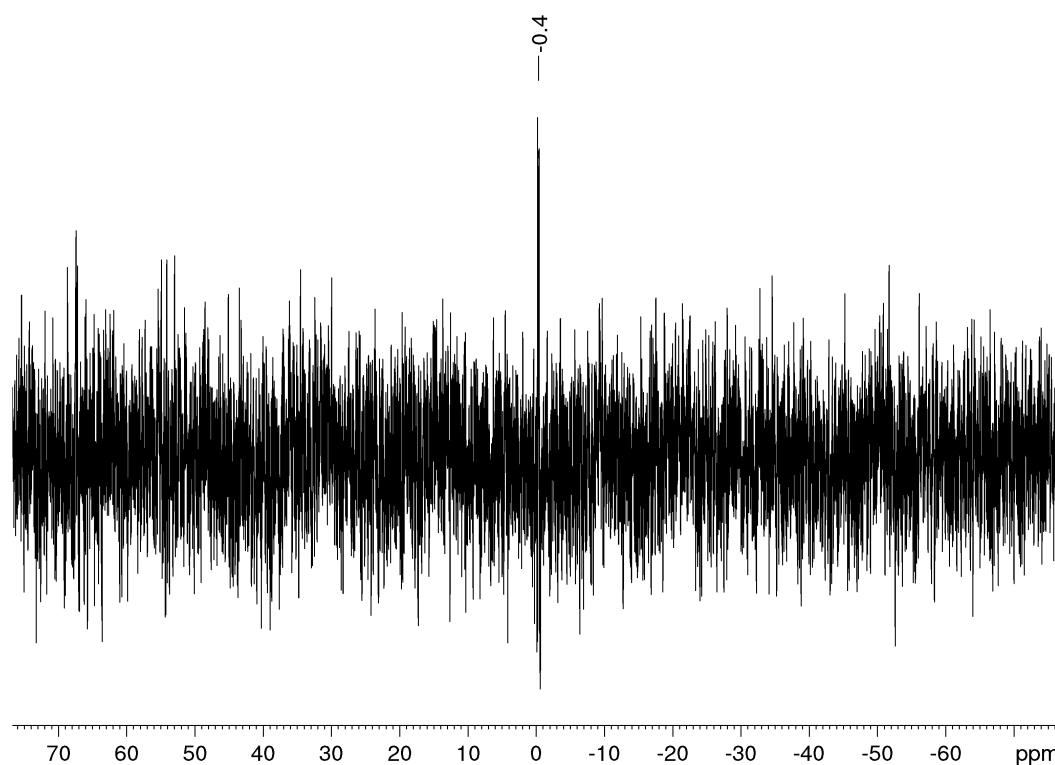


Figure S5. ^{29}Si INEPTND NMR spectrum (99 MHz) of $\text{Li}_3\text{Y}(\text{CH}_2\text{SiMe}_3)_6$ (**1**) in $[\text{D}_8]\text{toluene}$ at 26 °C.

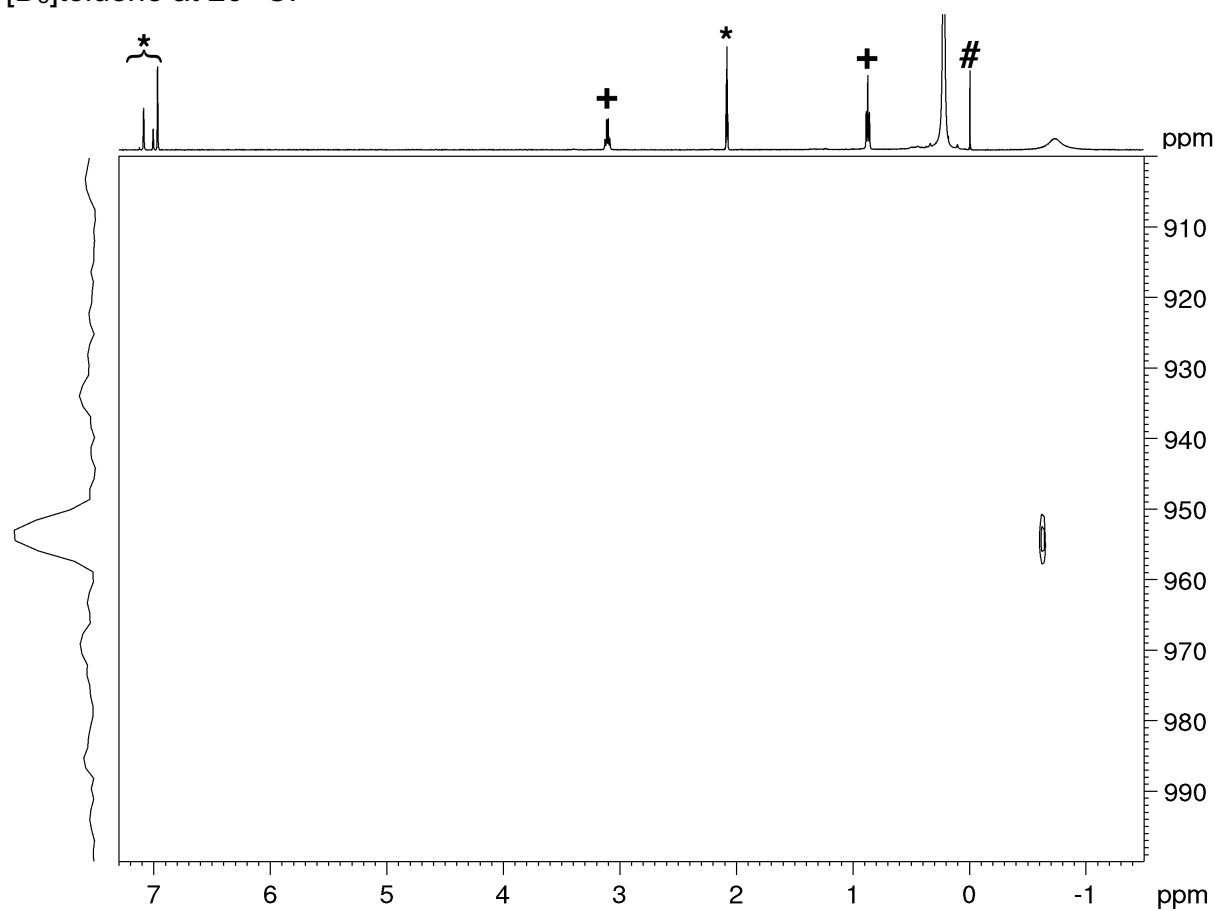


Figure S6. ^1H - ^{89}Y NMR spectrum (25 MHz) of $\text{Li}_3\text{Y}(\text{CH}_2\text{SiMe}_3)_6$ (**1**) in $[\text{D}_8]\text{toluene}$ at 26 °C. The solvent residual signals are marked with asterisks, + denotes residual Et_2O and # decomposition product SiMe_4 .

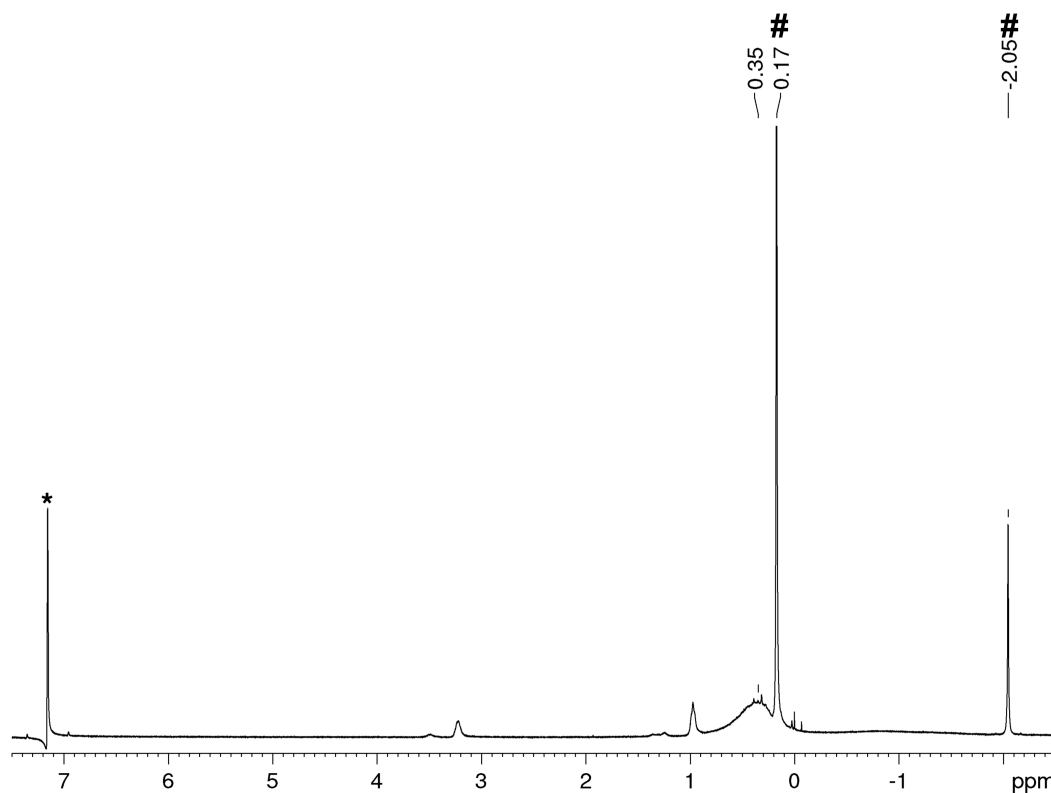


Figure S7. ^1H NMR spectrum (500 MHz) of decomposition products of **1** in C_6D_6 at 26 $^\circ\text{C}$. Solvent residual signal is marked with an asterisk, # denotes $\text{LiCH}_2\text{SiMe}_3$.

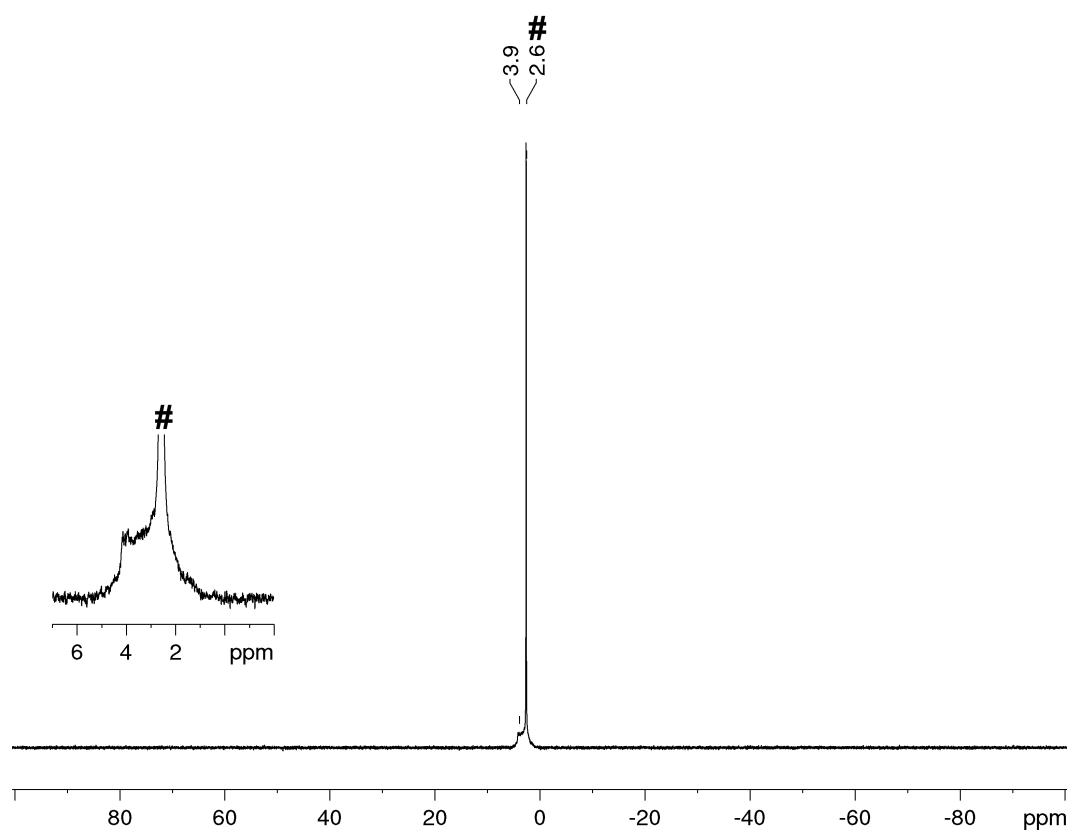


Figure S8. ^7Li NMR spectrum (194 MHz) of decomposition products of **1** in C_6D_6 at 26 $^\circ\text{C}$, # denotes $\text{LiCH}_2\text{SiMe}_3$.

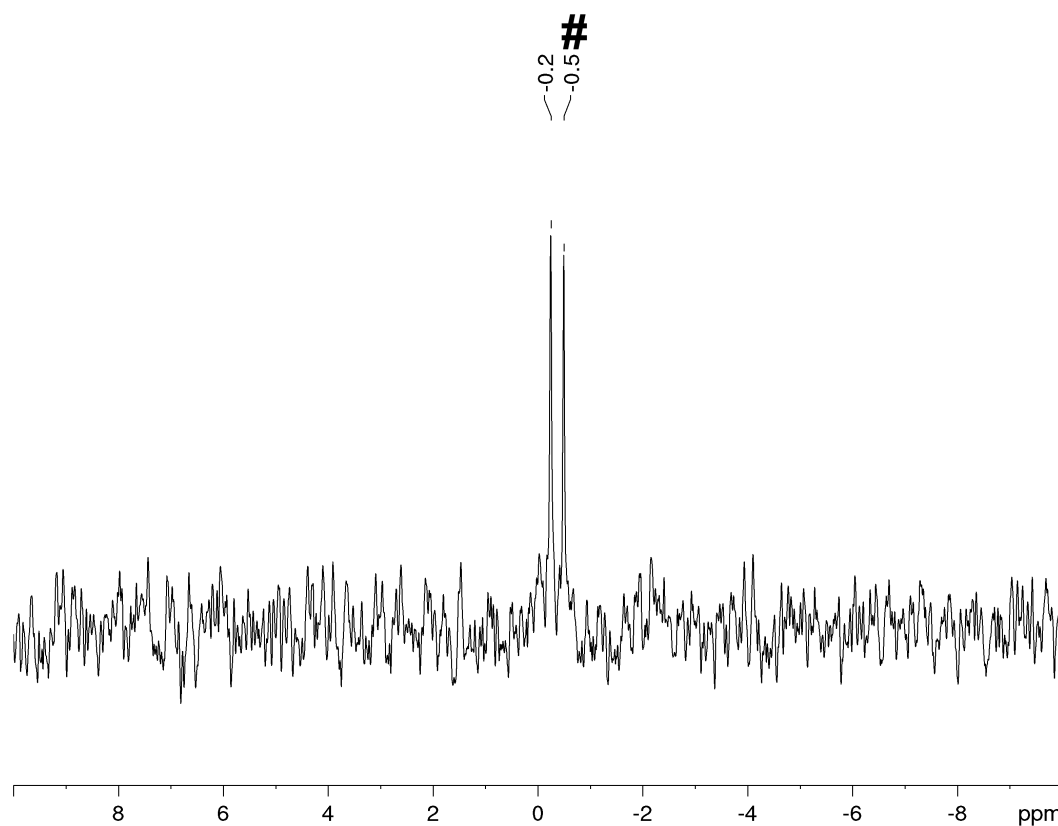


Figure S9. ^{29}Si DEPT45 NMR spectrum (99 MHz) of decomposition products of **1** in C_6D_6 at 26 °C, # denotes $\text{LiCH}_2\text{SiMe}_3$.

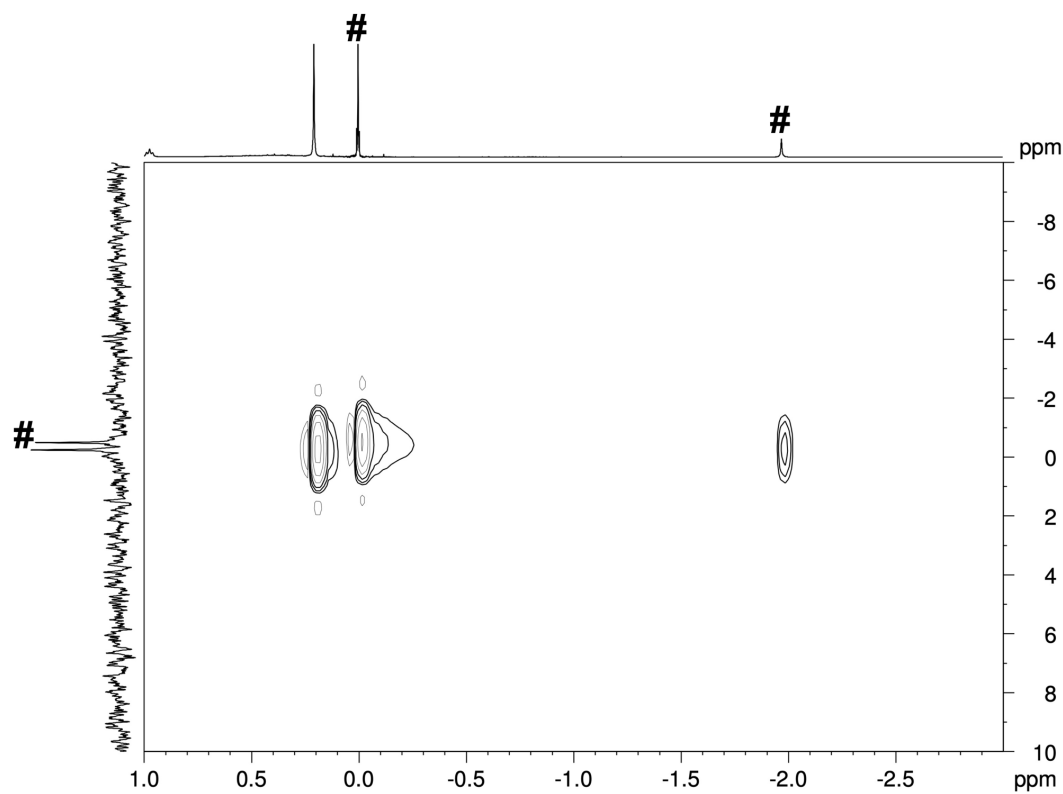


Figure S10. ^1H - ^{29}Si HSQC NMR spectrum (99 MHz) of decomposition products of **1** in C_6D_6 at 26 °C, # denotes $\text{LiCH}_2\text{SiMe}_3$.

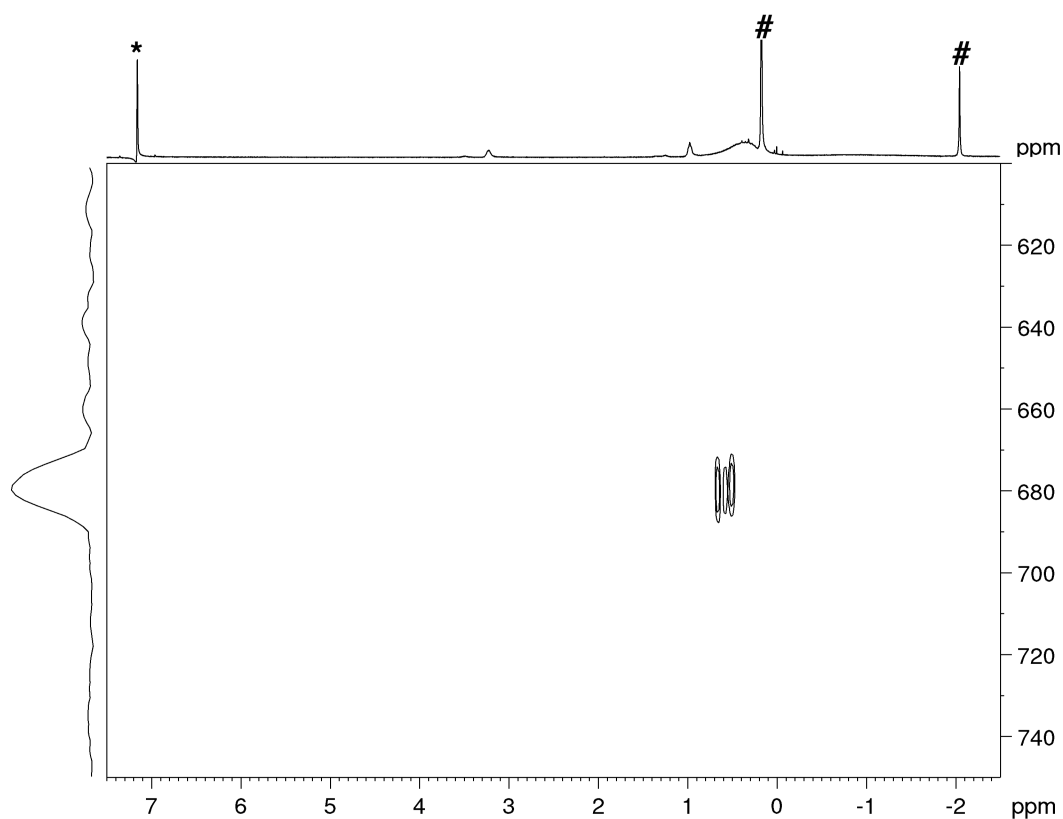


Figure S11. ^1H - ^{89}Y HSQC NMR spectrum (25 MHz) of decomposition products of **1** in C_6D_6 at 26 °C. Solvent residual signal is marked with an asterisk, # denotes $\text{LiCH}_2\text{SiMe}_3$.

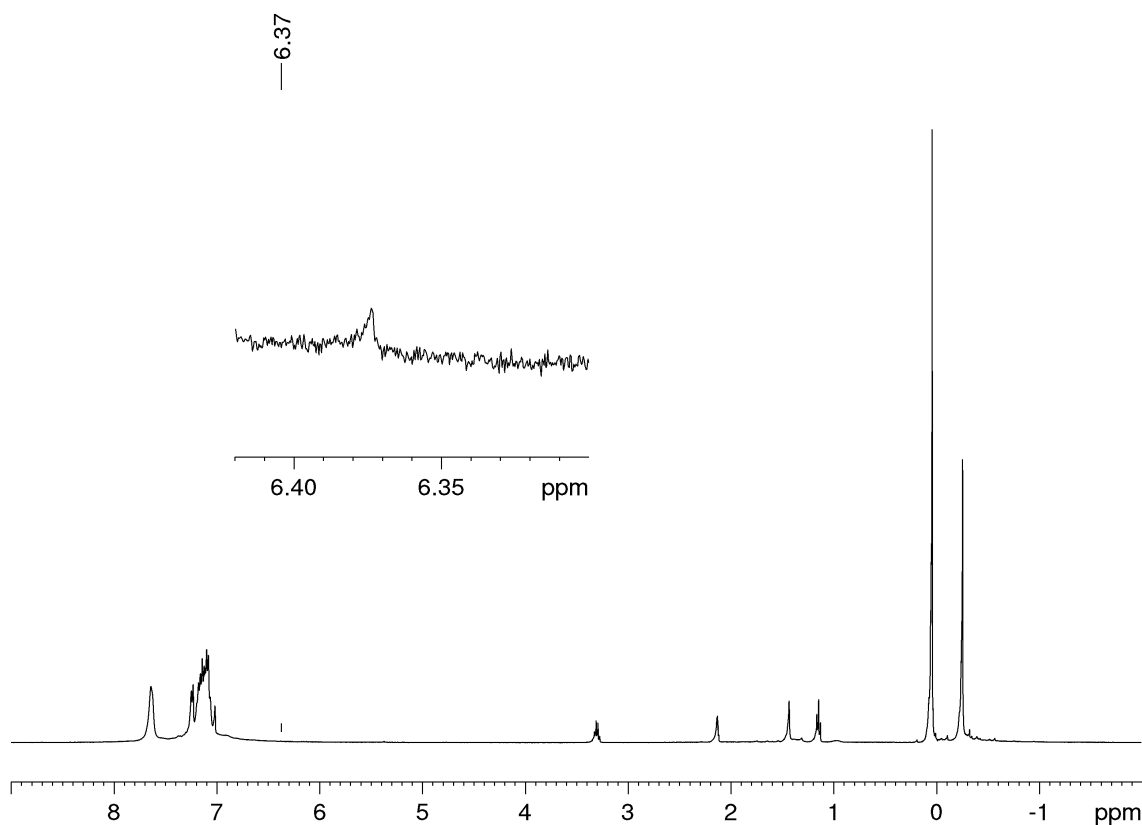


Figure S12. ^1H NMR spectrum (400 MHz) of the reaction of decomposition products of **1** with benzophenone in C_6D_6 at 26 °C.

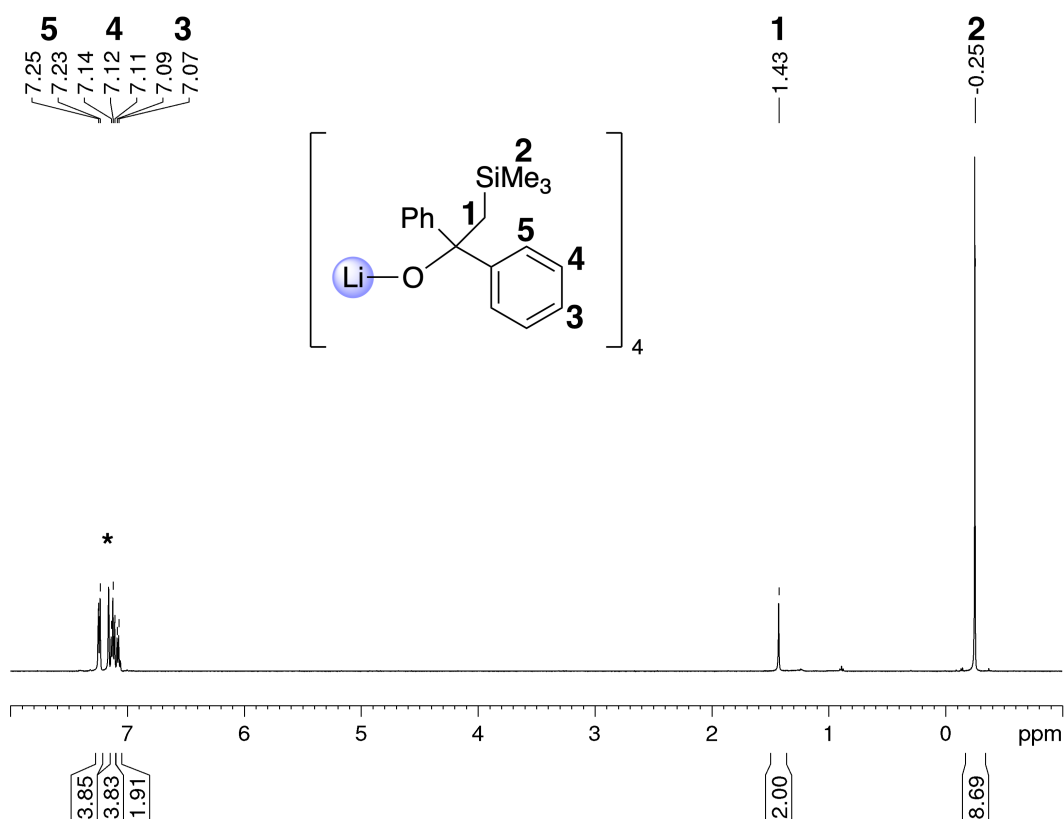


Figure S13. ^1H NMR spectrum (500 MHz) of $[\text{LiOC}(\text{CH}_2\text{SiMe}_3)(\text{Ph})_2]_4$ (**3**) in C_6D_6 at 26 °C, solvent residual signal is marked with an asterisk.

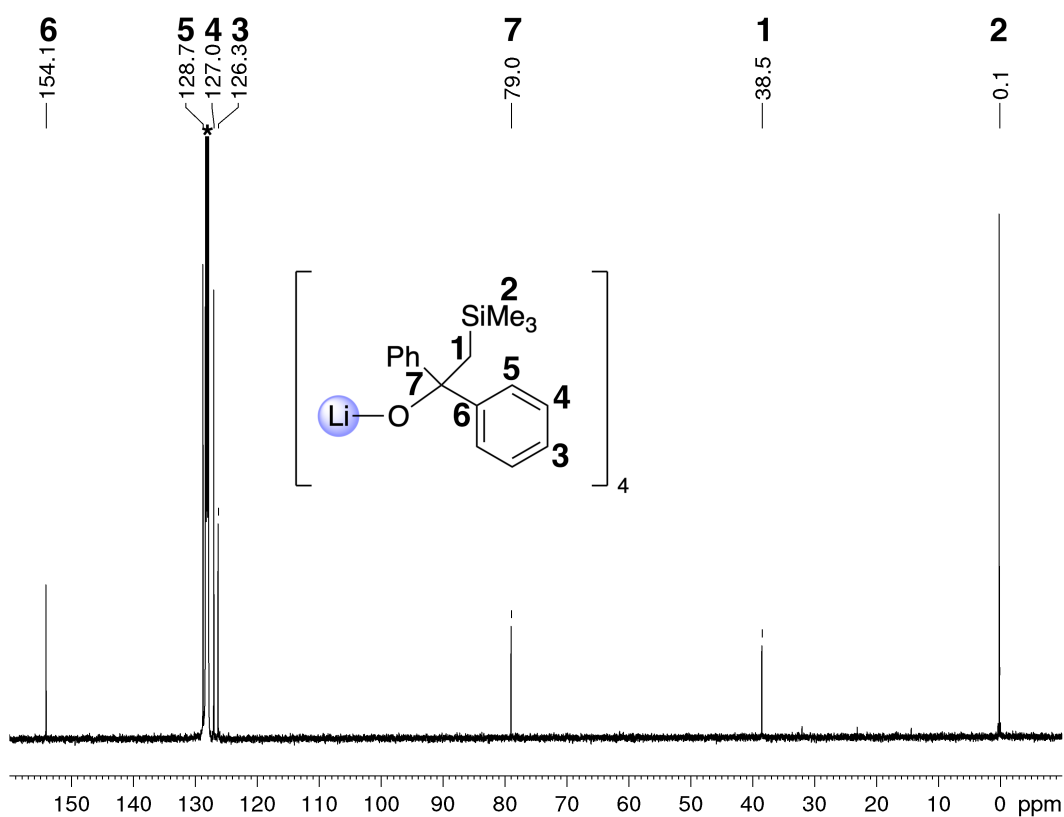


Figure S14. $^{13}\text{C}\{^1\text{H}\}$ NMR spectrum (126 MHz) of $[\text{LiOC}(\text{CH}_2\text{SiMe}_3)(\text{Ph})_2]_4$ (**3**) in C_6D_6 at 26 °C. The solvent residual signals are marked with an asterisk.

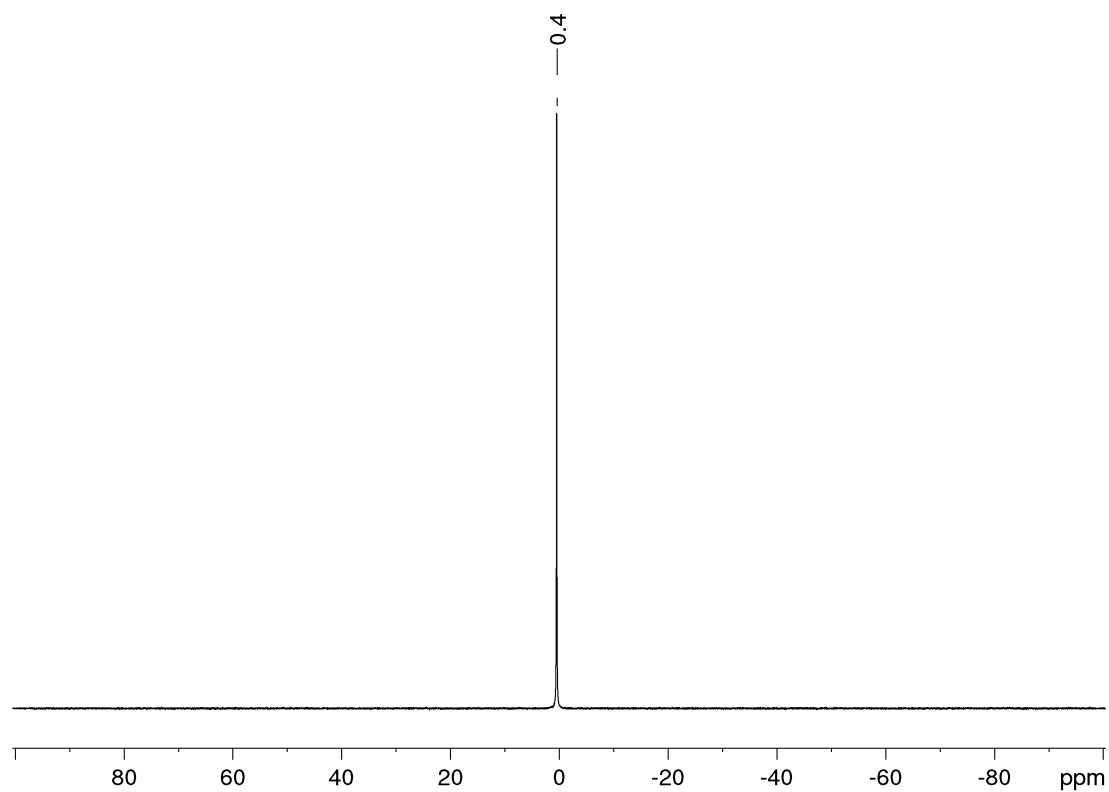


Figure S15. ${}^7\text{Li}$ NMR spectrum (194 MHz) of $[\text{LiOC}(\text{CH}_2\text{SiMe}_3)(\text{Ph})_2]_4$ (**3**) in C_6D_6 at 26 $^\circ\text{C}$.

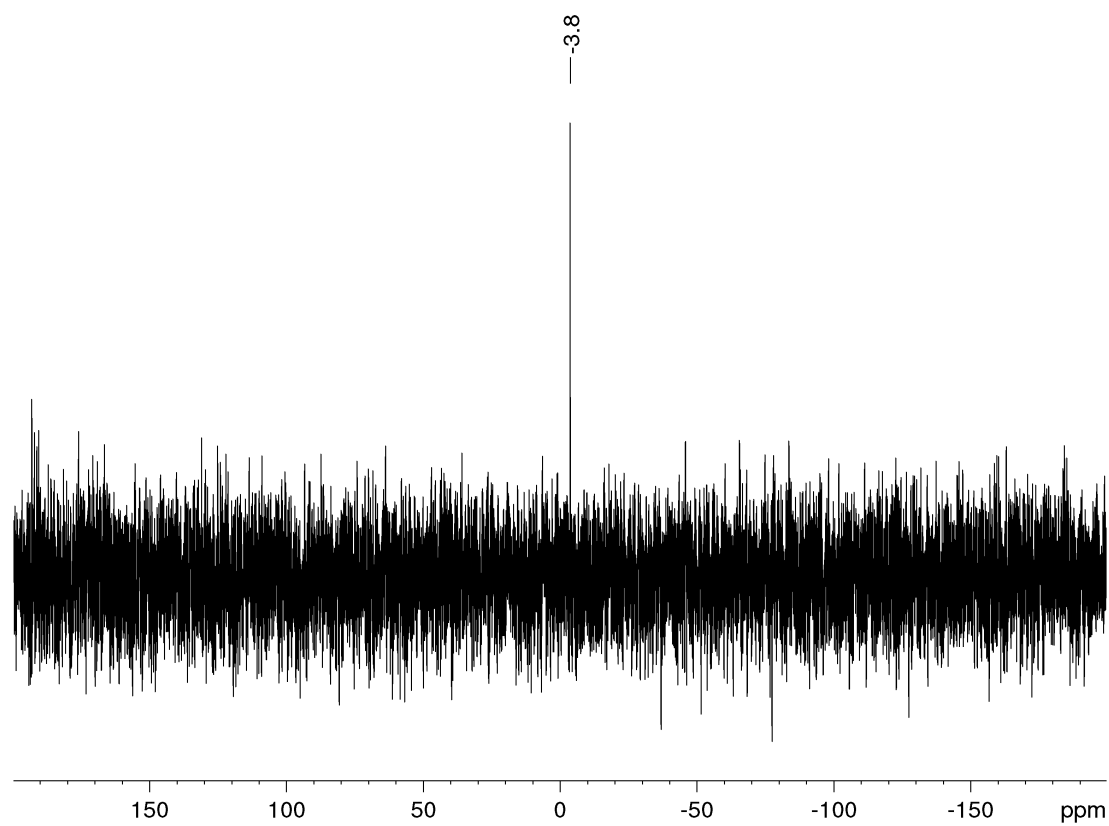


Figure S16. ${}^{29}\text{Si}$ DEPT45 NMR spectrum (99 MHz) of $[\text{LiOC}(\text{CH}_2\text{SiMe}_3)(\text{Ph})_2]_4$ (**3**) in C_6D_6 at 26 $^\circ\text{C}$.

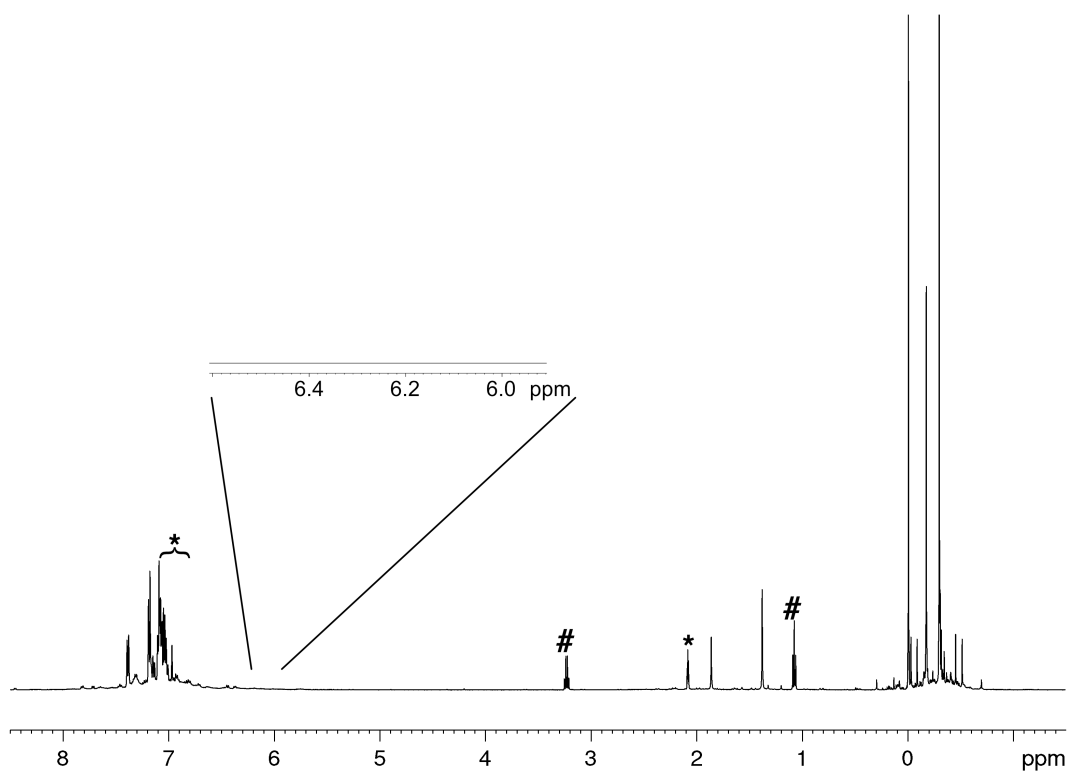


Figure S17. ^1H NMR spectrum (500 MHz) of the reaction of $\text{Li}_3\text{Y}(\text{CH}_2\text{SiMe}_3)_6$ (**1**) with 6 equivs. benzophenone in $[\text{D}_8]\text{toluene}$ at $26\text{ }^\circ\text{C}$, solvent residual signal is marked with asterisks.

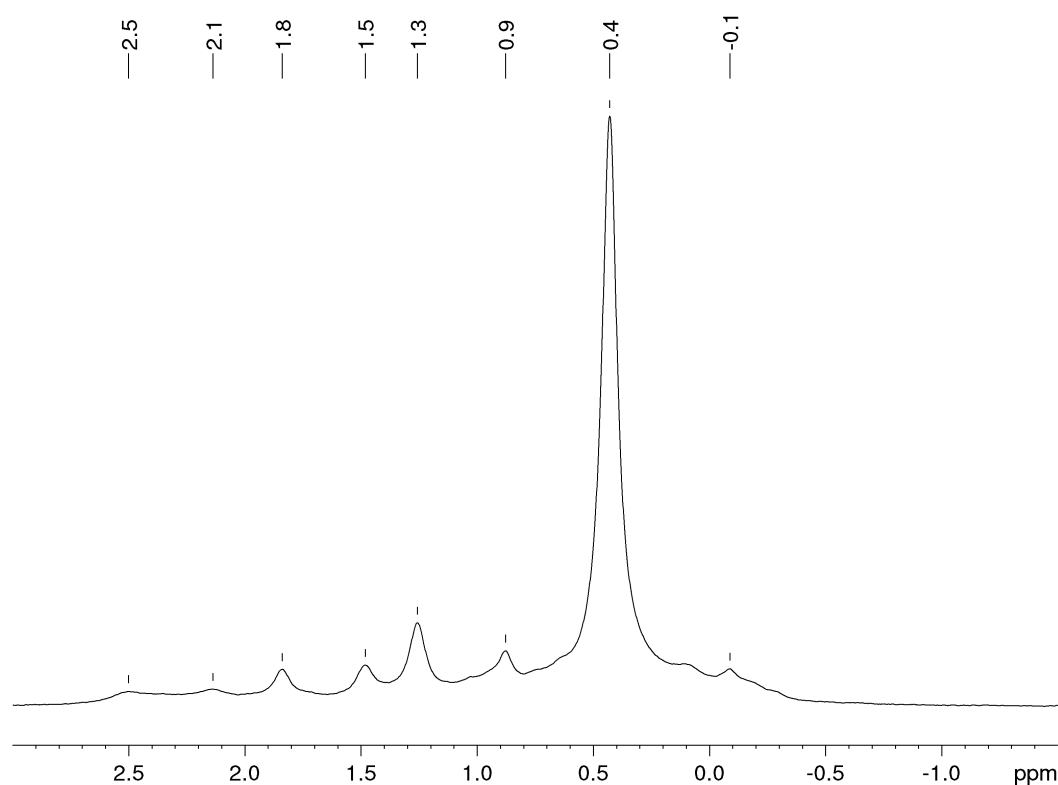


Figure S18. ^7Li NMR spectrum (194 MHz) of the reaction of $\text{Li}_3\text{Y}(\text{CH}_2\text{SiMe}_3)_6$ (**1**) with 6 equivs. benzophenone in $[\text{D}_8]\text{toluene}$ at $26\text{ }^\circ\text{C}$. The main peak at 0.4 ppm corresponds to $[\text{LiOC}(\text{CH}_2\text{SiMe}_3)(\text{Ph})_2]_4$ (**3**).

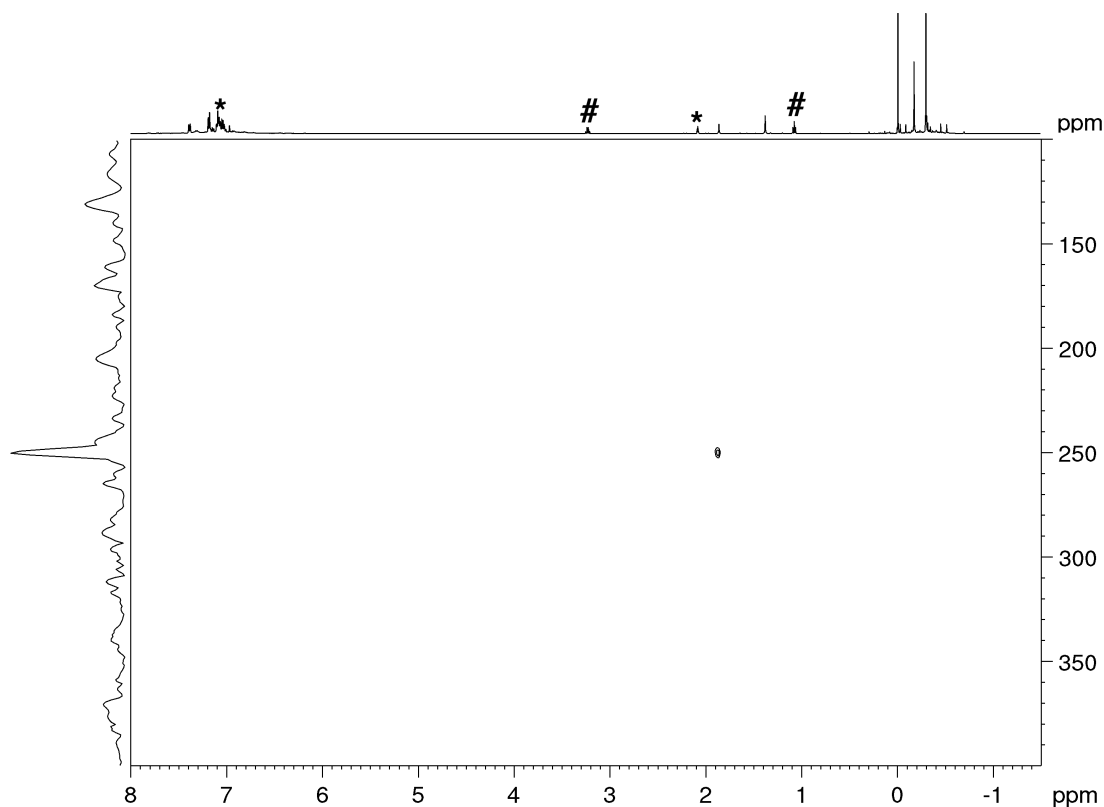


Figure S19. ^1H - ^{89}Y HSQC NMR spectrum (25 MHz) of the reaction of $\text{Li}_3\text{Y}(\text{CH}_2\text{SiMe}_3)_6$ (**1**) with 6 equivs. benzophenone in $[\text{D}_8]\text{toluene}$ at 26 °C, solvent residual signal is marked with asterisks.

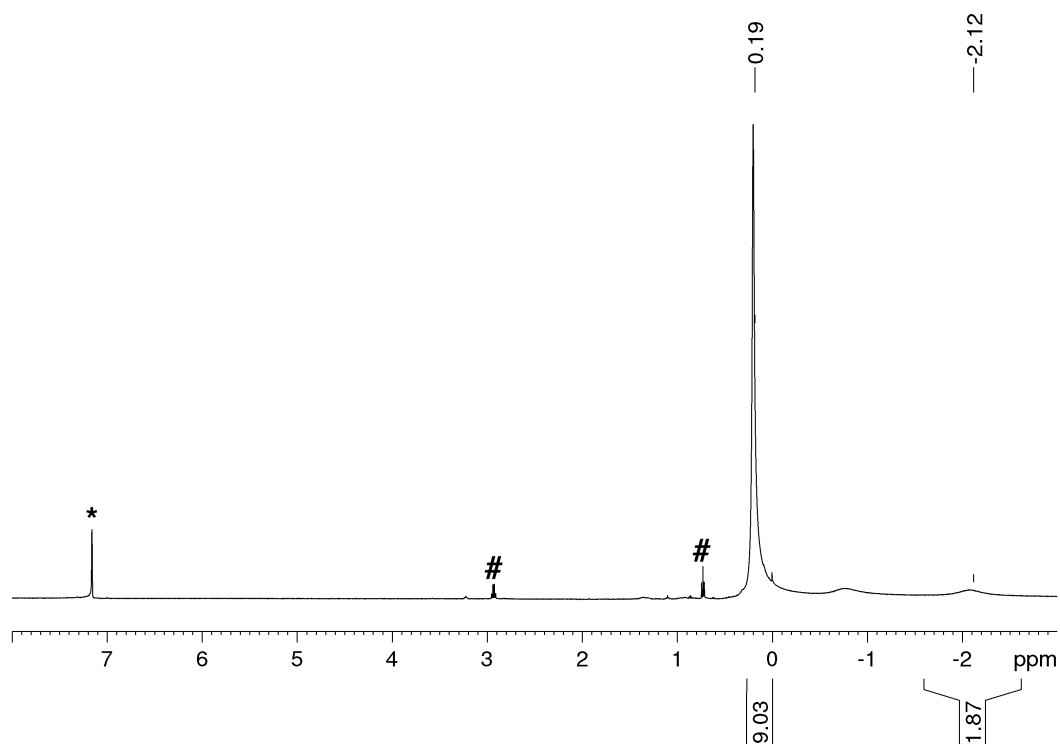


Figure S20. ^1H NMR spectrum (500 MHz) of the reaction of LuCl_3 with 4 equivs. of $\text{LiCH}_2\text{SiMe}_3$ after workup in C_6D_6 at 26 °C. Solvent residual signal is marked with an asterisk, diethyl ether with #.

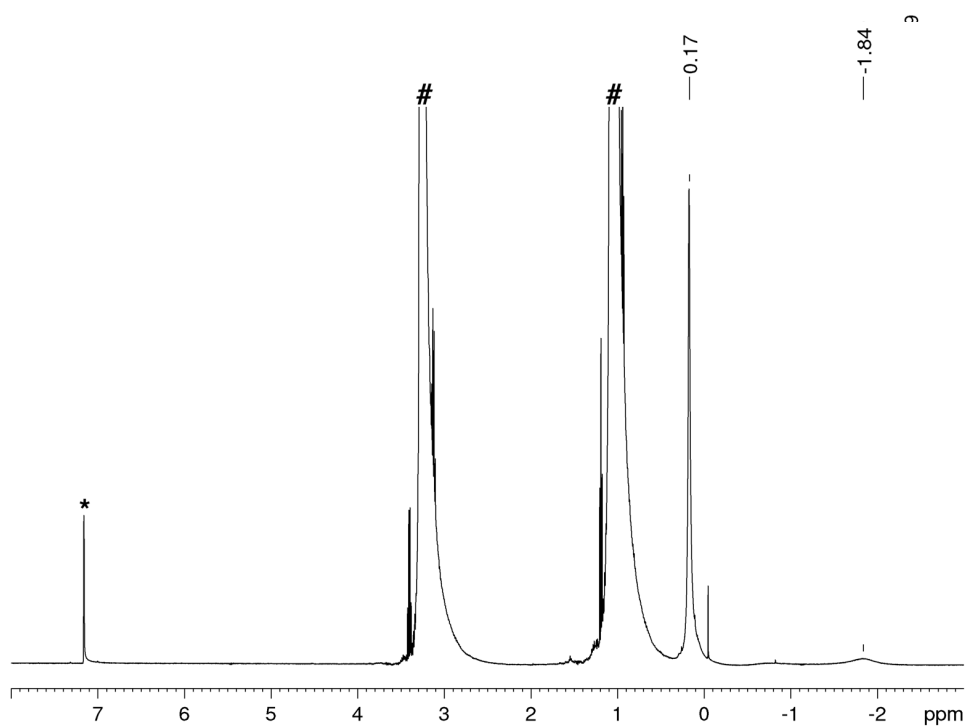


Figure S21. $^{13}\text{C}\{^1\text{H}\}$ NMR spectrum (126 MHz) of the reaction of LuCl_3 with 4 equivs. of $\text{LiCH}_2\text{SiMe}_3$ after workup in C_6D_6 at 26 °C. Solvent residual signal is marked with an asterisk, diethyl ether with #.

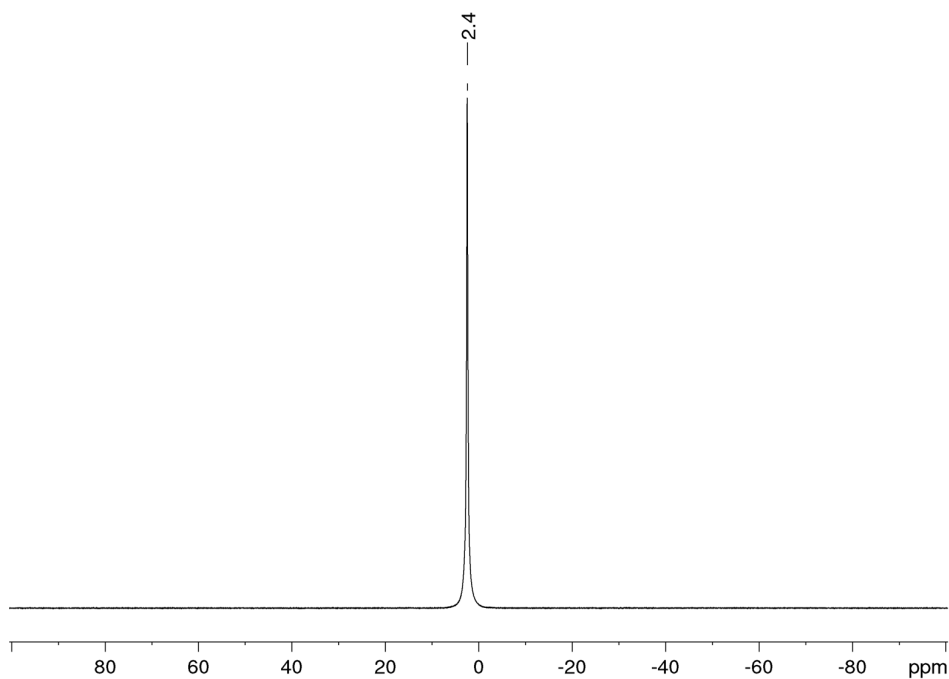


Figure S22. ^7Li NMR spectrum (194 MHz) of LuCl_3 with 4 equivs. of $\text{LiCH}_2\text{SiMe}_3$ after workup in C_6D_6 at 26 °C.

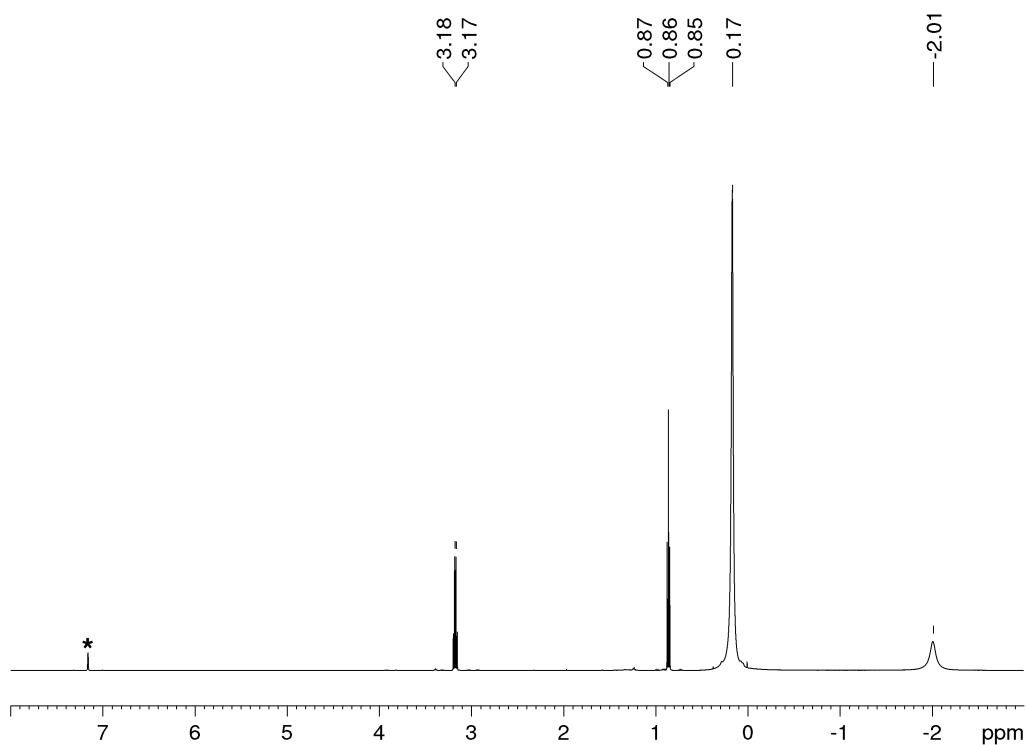


Figure S23. ^1H NMR spectrum (500 MHz) of the reaction of LuCl_3 with 4 equivs. of $\text{LiCH}_2\text{SiMe}_3$ after workup and addition of excess diethyl ether in C_6D_6 at 26 °C. Solvent residual signal is marked with an asterisk, diethyl ether with #.

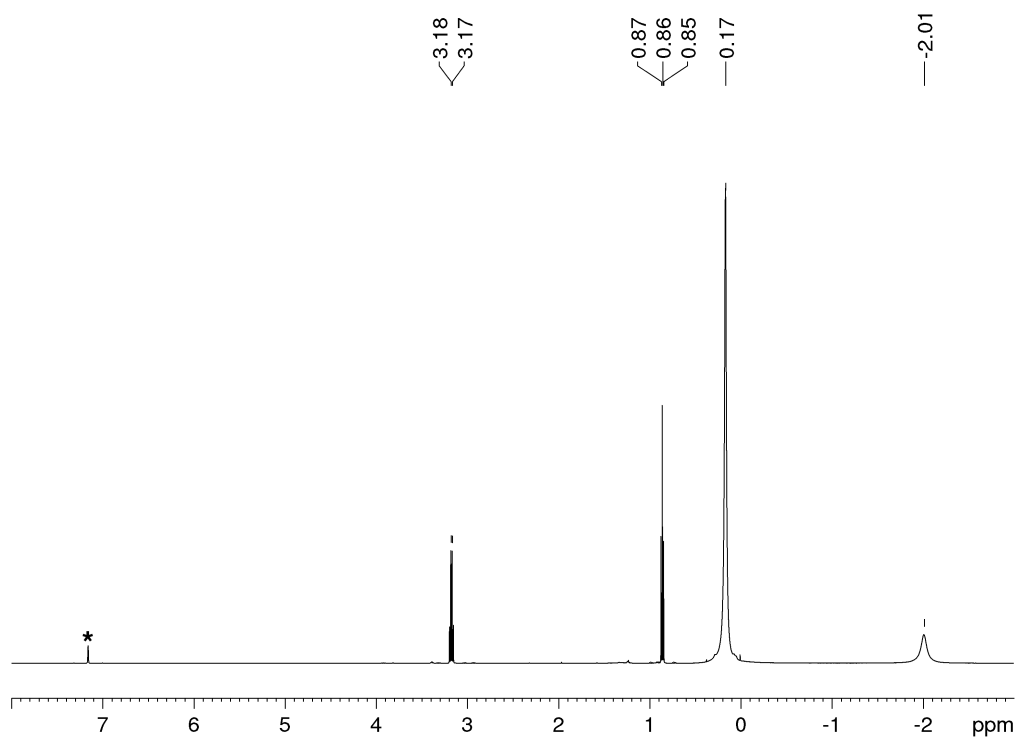


Figure S24. ^1H NMR spectrum (500 MHz) of the reaction of ScCl_3 with 6 equivs. of $\text{LiCH}_2\text{SiMe}_3$ after workup in C_6D_6 at 26 °C. Solvent residual signal is marked with an asterisk.

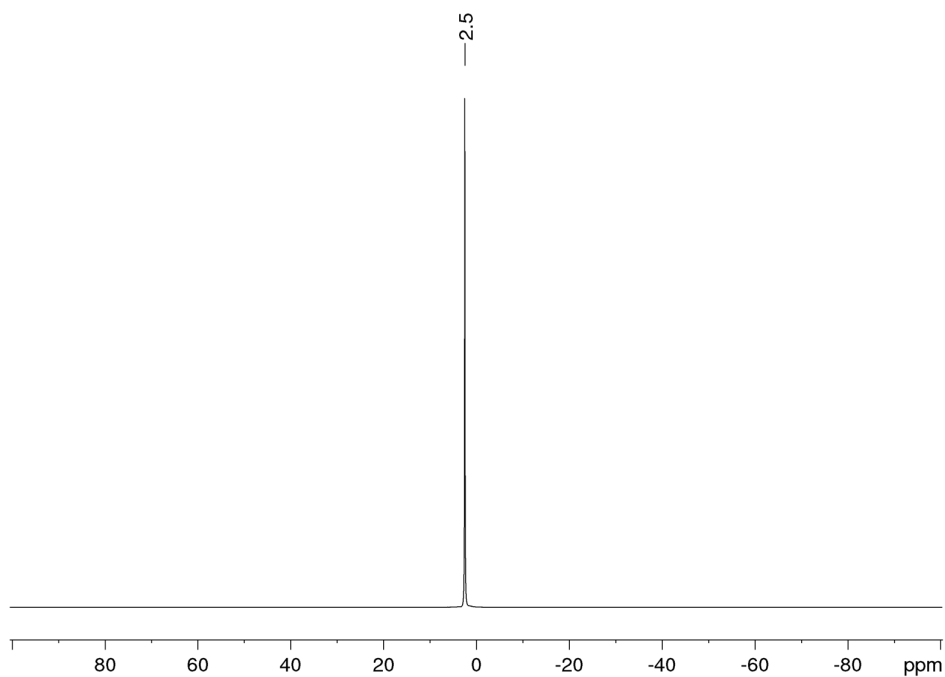


Figure S25. ${}^7\text{Li}$ NMR spectrum (194 MHz) of ScCl_3 with 6 equivs. of $\text{LiCH}_2\text{SiMe}_3$ after workup in C_6D_6 at 26 °C.

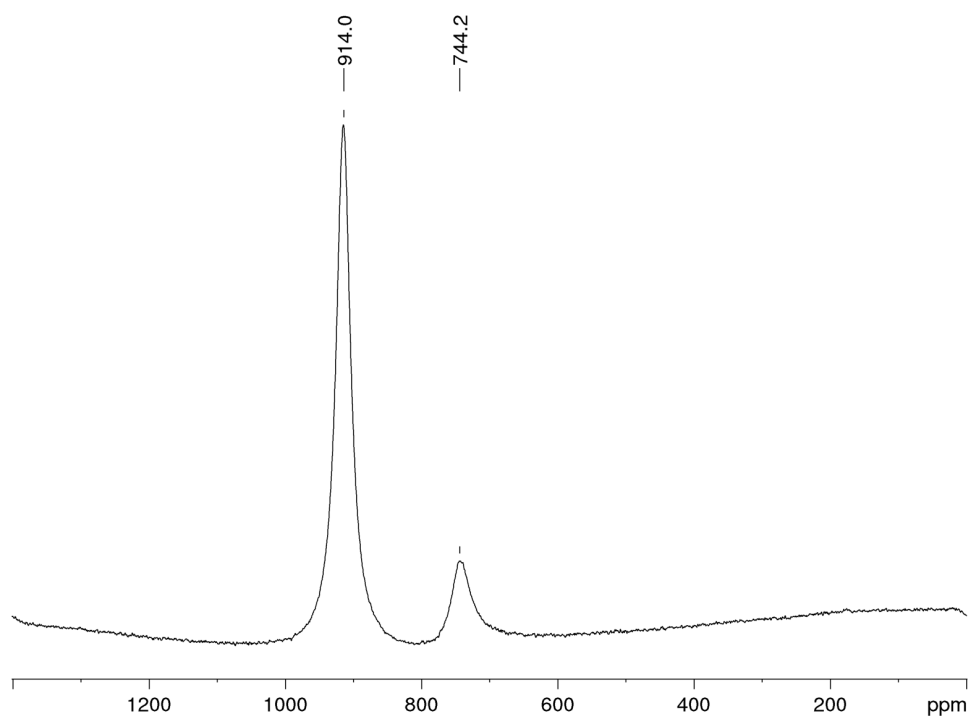


Figure S26. ${}^{45}\text{Sc}$ NMR spectrum (122 MHz) of ScCl_3 with 6 equivs. of $\text{LiCH}_2\text{SiMe}_3$ after workup in C_6D_6 at 26 °C.

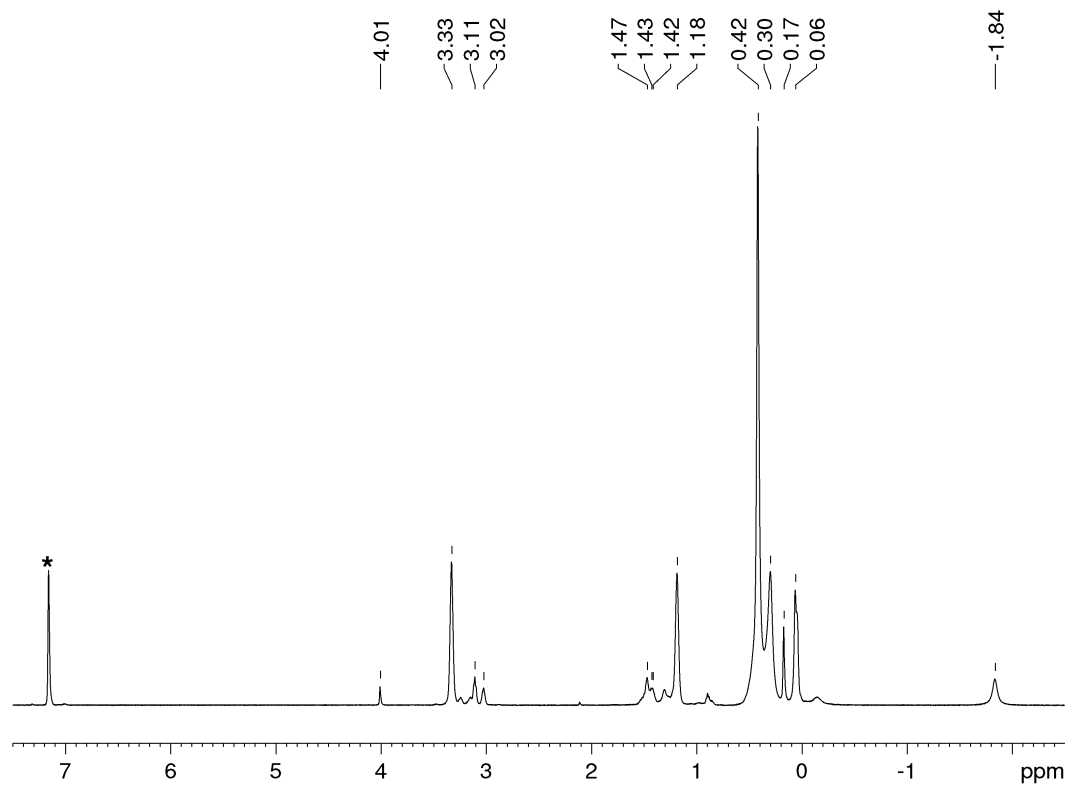


Figure S27. ^1H NMR spectrum (500 MHz) of the reaction of $\text{ScCl}_3(\text{thf})_3$ with 2.9 equivs. of $\text{LiCH}_2\text{SiMe}_3$ in C_6D_6 at 10°C . Solvent residual signal is marked with an asterisk.

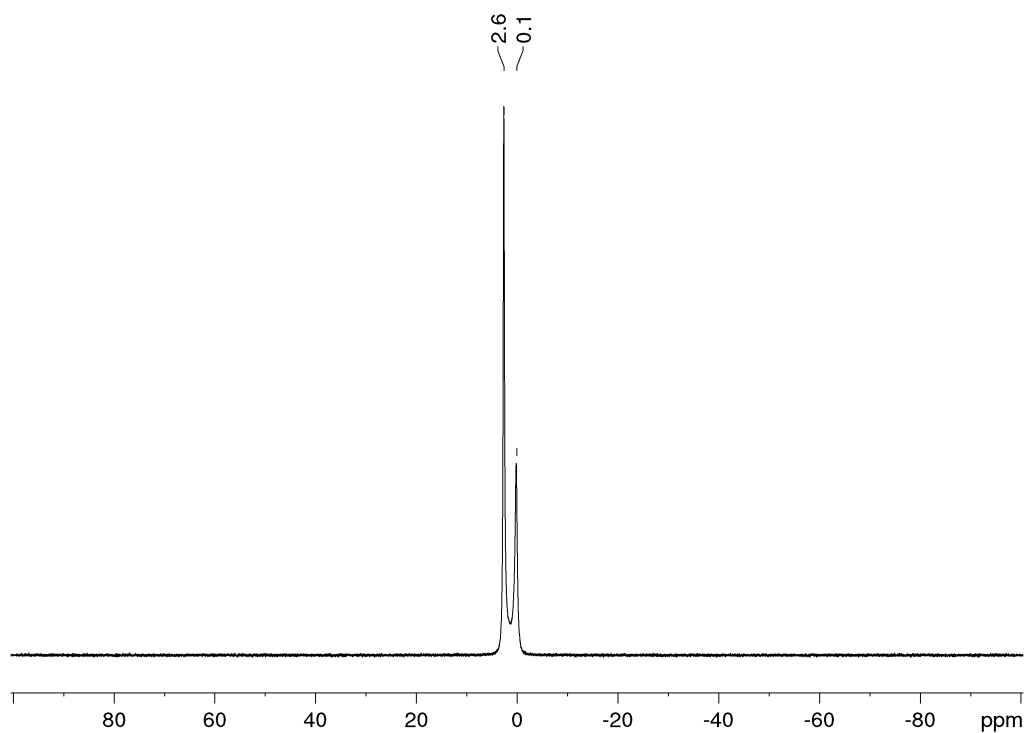


Figure S28. ^7Li NMR spectrum (194 MHz) of the reaction of $\text{ScCl}_3(\text{thf})_3$ with 2.9 equivs. of $\text{LiCH}_2\text{SiMe}_3$ in C_6D_6 at 10°C .

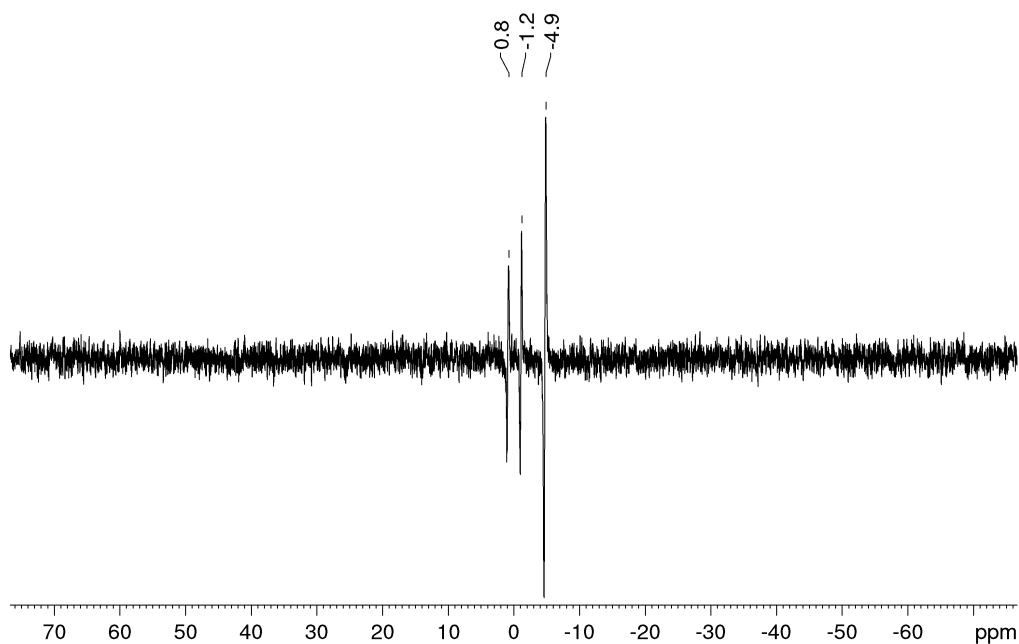


Figure S29. ^{29}Si INEPTND NMR spectrum (99 MHz) of the reaction of $\text{ScCl}_3(\text{thf})_3$ with 2.9 equivs. of $\text{LiCH}_2\text{SiMe}_3$ in C_6D_6 at 10°C .

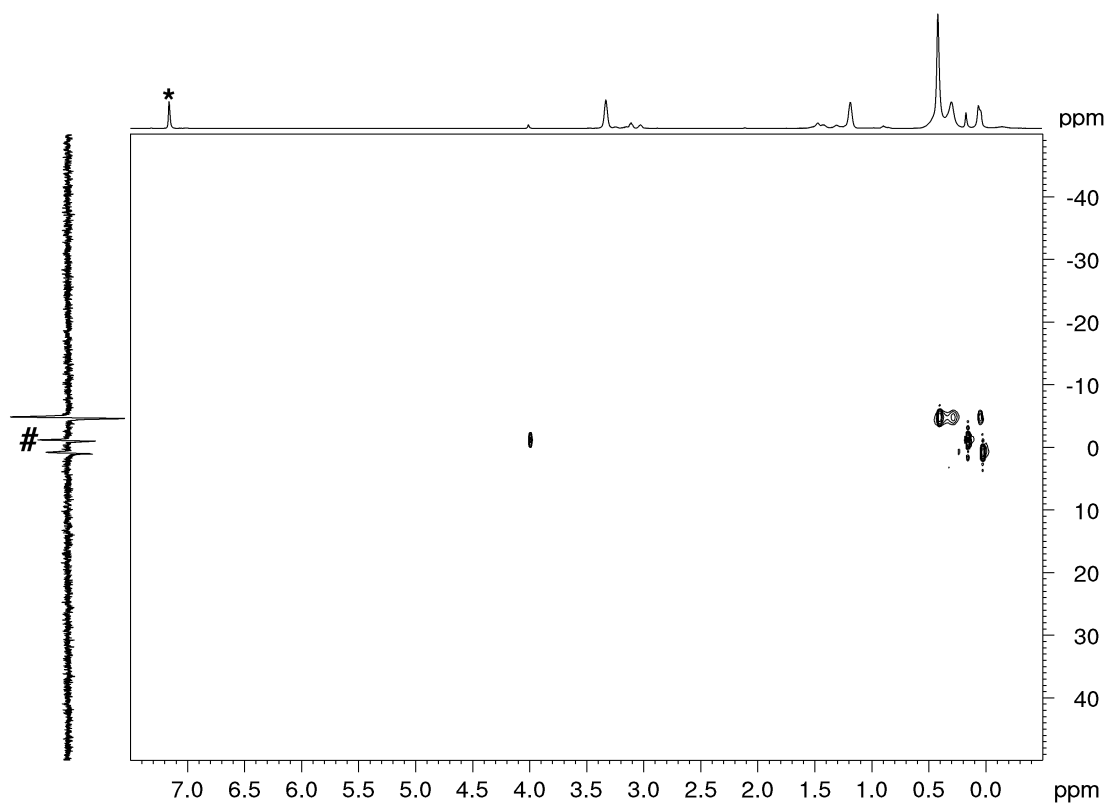


Figure S30. ^1H - ^{29}Si HSQC NMR spectrum (99 MHz) of the reaction of $\text{ScCl}_3(\text{thf})_3$ with 2.9 equivs. of $\text{LiCH}_2\text{SiMe}_3$ in C_6D_6 at 10°C . Solvent residual signal is marked with an asterisk, the resonance of $\text{Sc}(\text{CH}_2\text{SiMe}_3)_3(\text{thf})_2$ is marked with #.

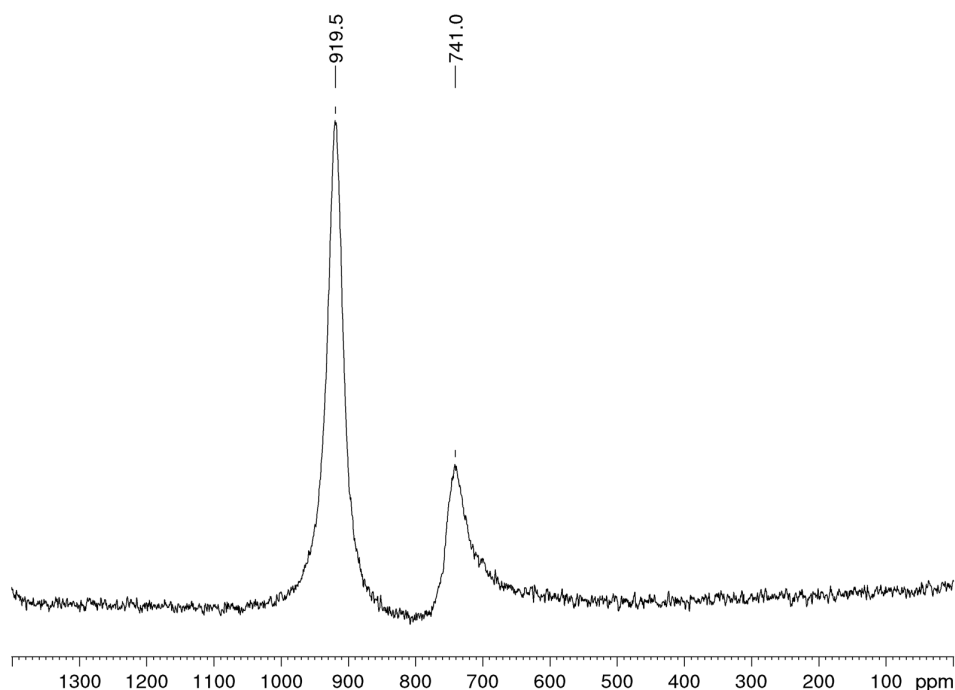


Figure S31. ^{45}Sc NMR spectrum (122 MHz) of the reaction of $\text{ScCl}_3(\text{thf})_3$ with 2.9 equivs. of $\text{LiCH}_2\text{SiMe}_3$ in C_6D_6 at 10 °C.

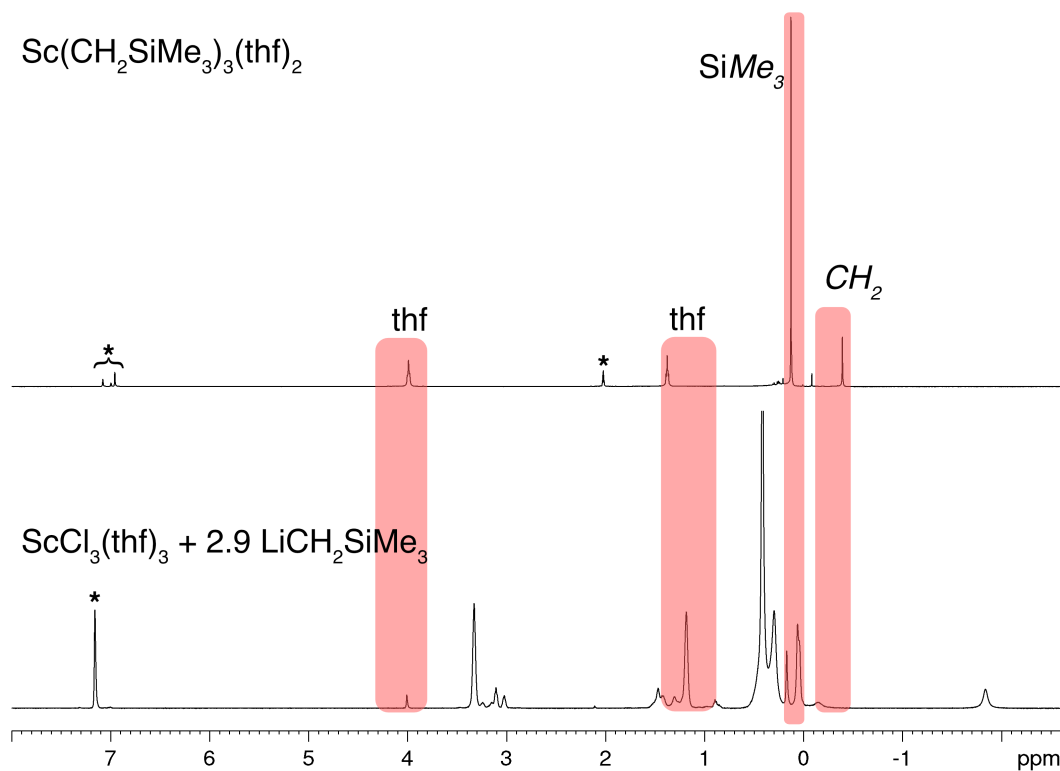


Figure S32. ^1H NMR spectra (500 MHz) of the reaction of $\text{ScCl}_3(\text{thf})_3$ with 2.9 equivs. of $\text{LiCH}_2\text{SiMe}_3$ in C_6D_6 compared with $\text{Sc}(\text{CH}_2\text{SiMe}_3)_3(\text{thf})_2$ in $[\text{D}_8]\text{toluene}$. Solvent residual signals are marked with asterisks.

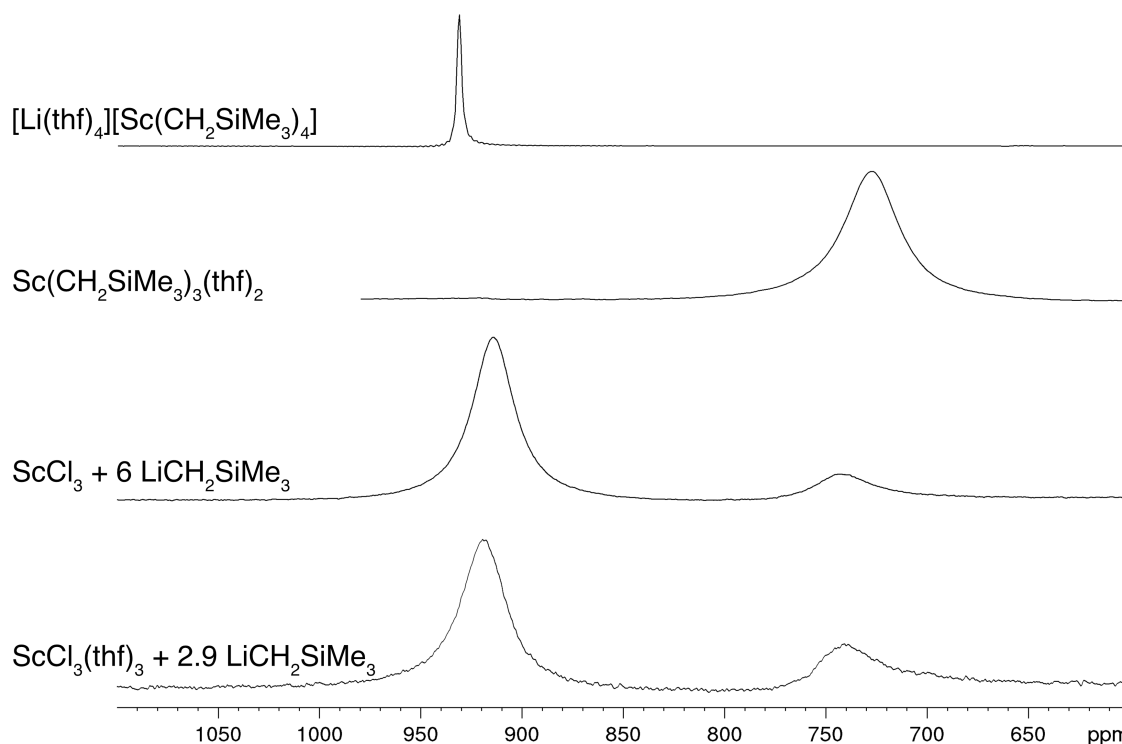


Figure S33. Stacked ^{45}Sc NMR spectra (122 MHz) of (from bottom to top) the reaction of $\text{ScCl}_3(\text{thf})_3$ with 2.9 equivs. of $\text{LiCH}_2\text{SiMe}_3$, ScCl_3 with 6 equivs. of $\text{LiCH}_2\text{SiMe}_3$, $\text{Sc}(\text{CH}_2\text{SiMe}_3)_3(\text{thf})_2$ and $[\text{Li}(\text{thf})_4][\text{Sc}(\text{CH}_2\text{SiMe}_3)_4]$ in C_6D_6 .

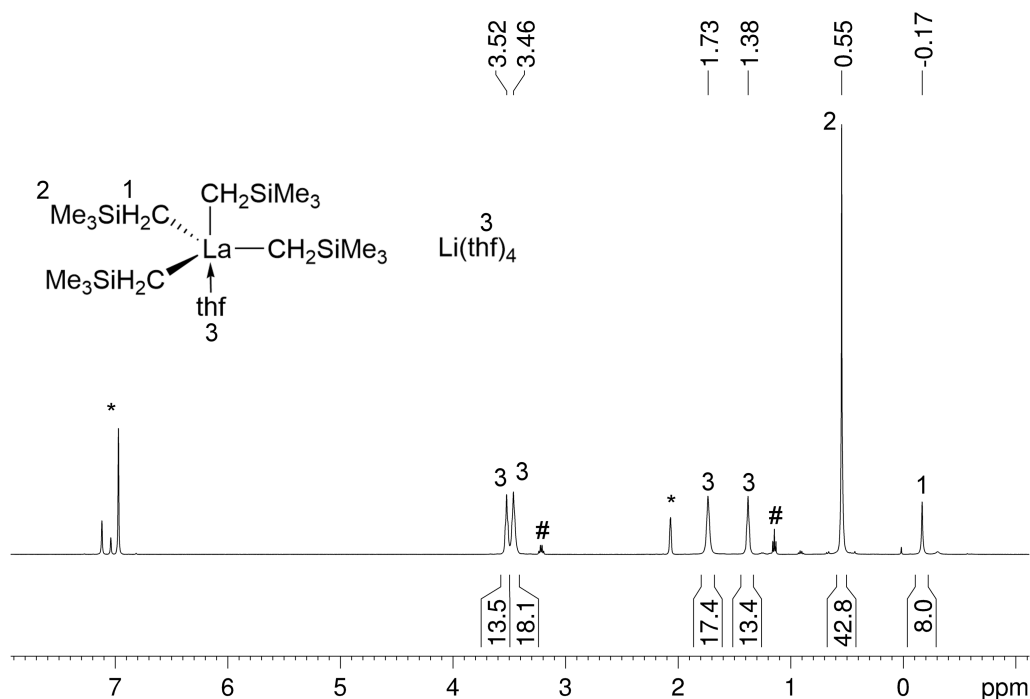


Figure S34. ^1H NMR spectrum of $[\text{Li}(\text{thf})_4][\text{La}(\text{CH}_2\text{SiMe}_3)_4(\text{thf})]$ (**3**) (500.13 MHz, $[\text{D}_8]\text{toluene}$, $-40\text{ }^\circ\text{C}$). The solvent residual signals are marked with asterisks. Residual Et_2O is marked #.

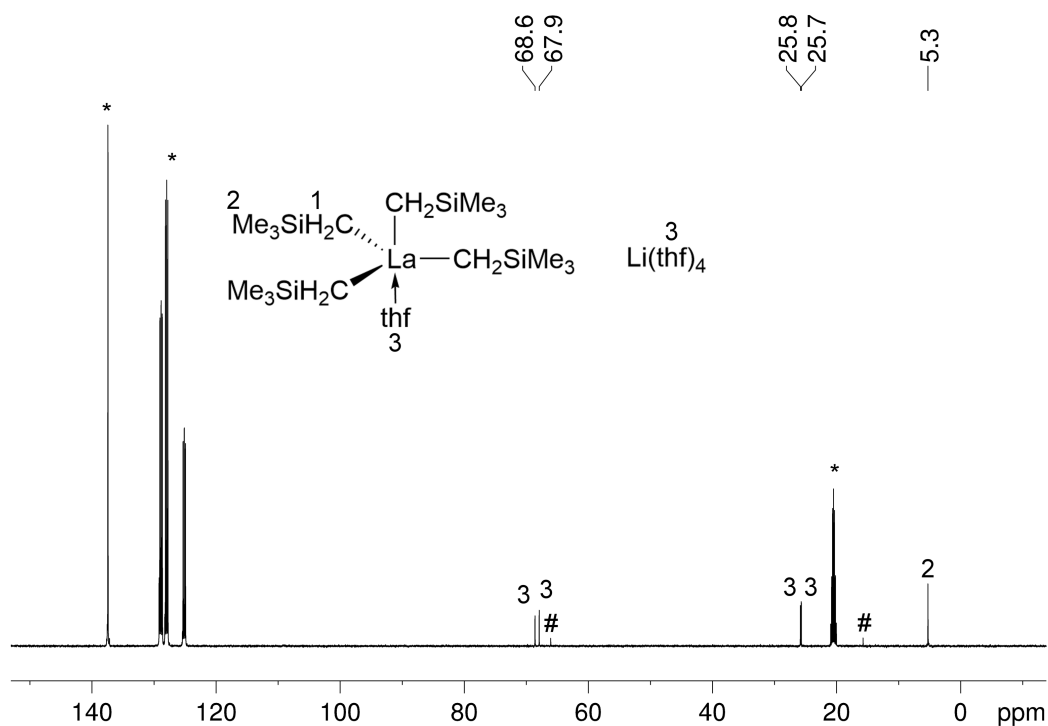


Figure S35. $^{13}C\{^1H\}$ NMR spectrum of $[Li(thf)_4][La(CH_2SiMe_3)_4(thf)]$ (**3**) (125.76 MHz, $[D_8]$ toluene, $-40^\circ C$). The solvent residual signals are marked with asterisks. Residual Et_2O is marked #.

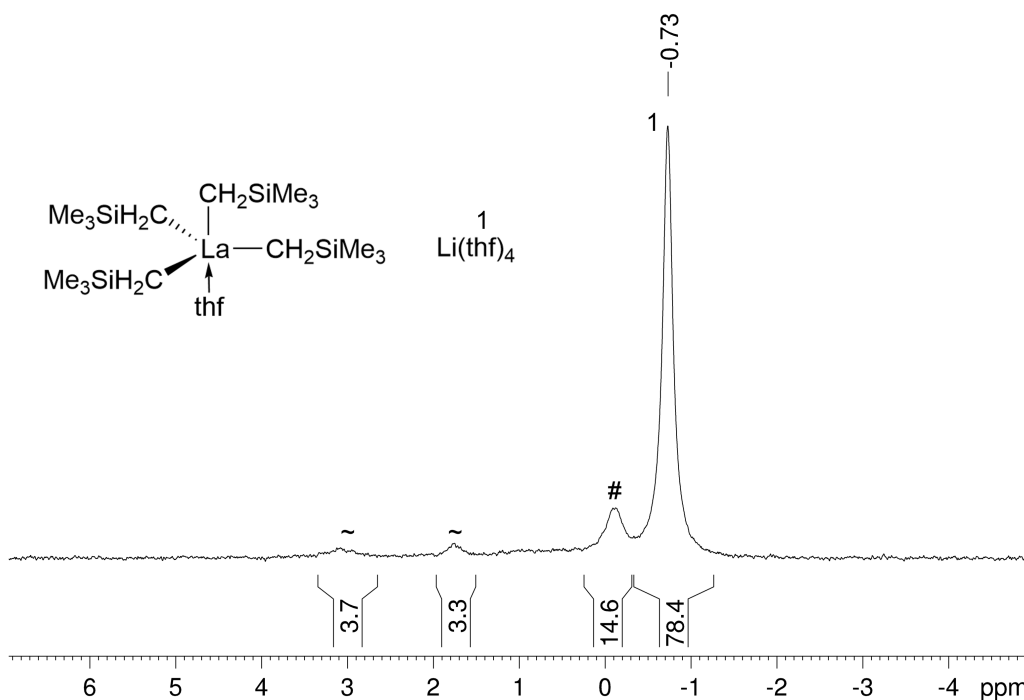


Figure S1. 7Li NMR spectrum of $[Li(thf)_4][La(CH_2SiMe_3)_4(thf)]$ (**3**) (194.37 MHz, $[D_8]$ toluene, $-40^\circ C$). LiCl is marked with # and unknown impurities are marked with ~.

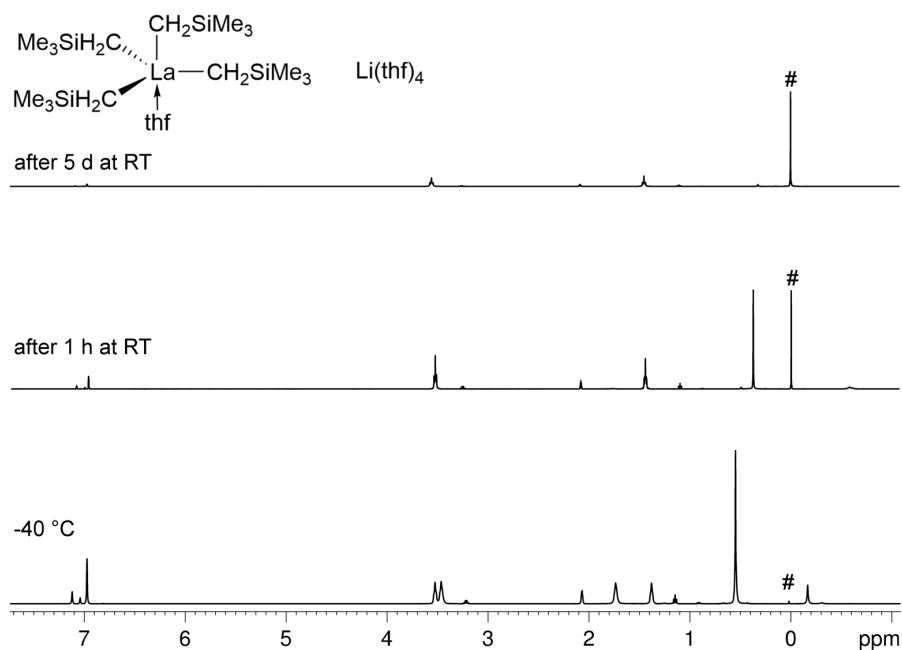


Figure S37. ^1H NMR spectra of $[\text{Li}(\text{thf})_4][\text{La}(\text{CH}_2\text{SiMe}_3)_4(\text{thf})]$ (**3**) at $-40\text{ }^\circ\text{C}$ (bottom) after 1 h at ambient temperature (middle) and after 5 d at ambient temperature (top), (bottom 500.13 MHz, $[\text{D}_8]$ toluene, $-40\text{ }^\circ\text{C}$), (middle 500.13 MHz, $[\text{D}_8]$ toluene, $26\text{ }^\circ\text{C}$), (top 400.11 MHz, $[\text{D}_8]$ toluene, $26\text{ }^\circ\text{C}$). SiMe_4 is marked with #.

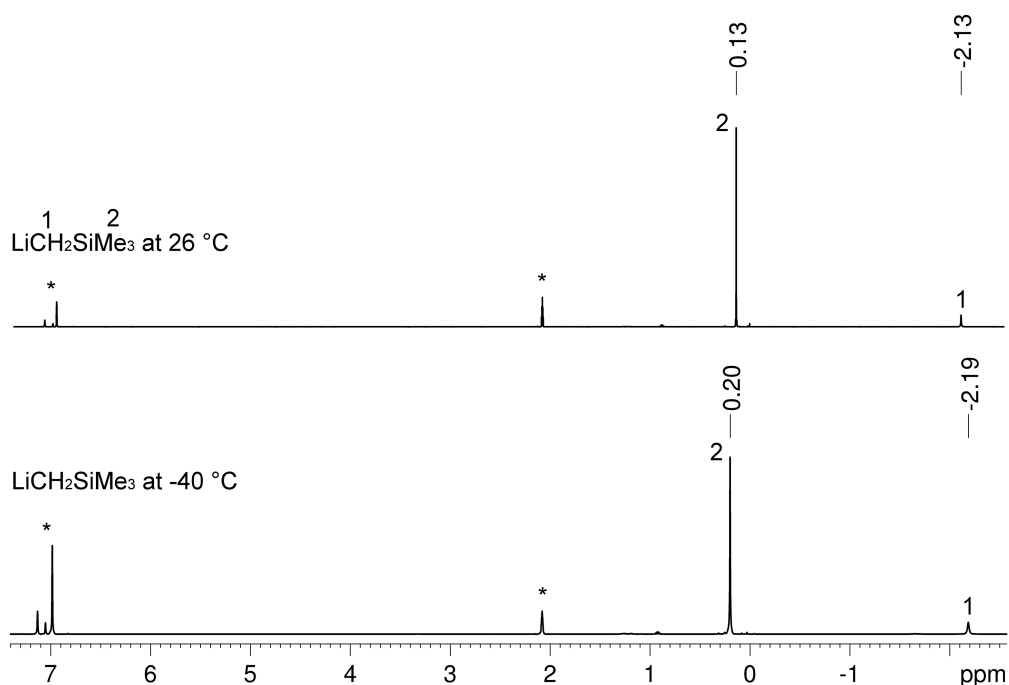


Figure S38. ^1H NMR spectra of $\text{LiCH}_2\text{SiMe}_3$ at $-40\text{ }^\circ\text{C}$ (bottom) and at ambient temperature (top), (bottom 500.13 MHz, $[\text{D}_8]$ toluene, $-40\text{ }^\circ\text{C}$), (top 500.13 MHz, $[\text{D}_8]$ toluene, $26\text{ }^\circ\text{C}$) solvent residual signals are marked with asterisks.

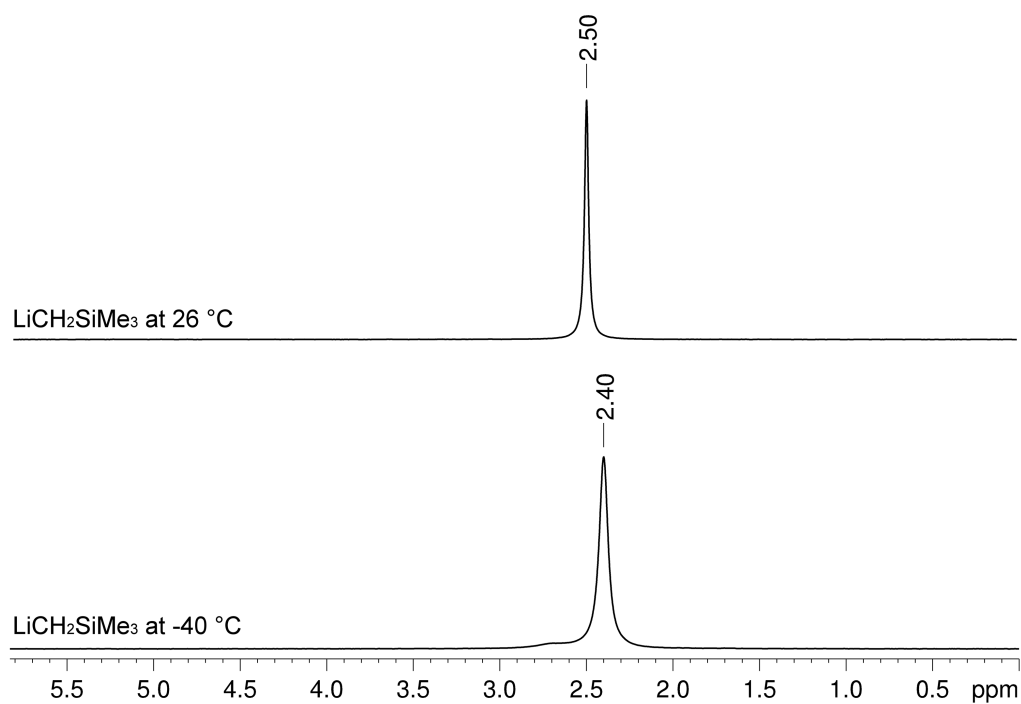


Figure S39. ^7Li NMR spectra of $\text{LiCH}_2\text{SiMe}_3$ at $-40\text{ }^\circ\text{C}$ (bottom, 194.37 MHz, $[\text{D}_8]\text{toluene}$) and at $26\text{ }^\circ\text{C}$ (top, 194.37 MHz, $[\text{D}_8]\text{toluene}$).

X-Ray Crystallography

Table S1. Crystallographic Data for Compound 1, 2 and 3

	1	2 ^[d]	3
formula	C ₂₄ H ₆₆ Li ₃ Si ₆ Y	C ₄₈ H ₁₂₀ Li ₂ O ₄ Sc ₂ Si ₈	C ₃₆ H ₈₄ LaLiO ₅ Si ₄
CCDC	2215408	2215407	2215409
M _r [g mol ⁻¹]	633.03	1089.95	855.24
colour	colourless	colourless	colourless
crystal dimensions [mm]	0.194 x 0.142 x 0.067	0.306 x 0.288 x 0.260	0.542 x 0.359 x 0.298
cryst syst	Monoclinic	Triclinic	Monoclinic
space group	Cc	P1	P2 ₁ /c
a [Å]	18.9631(17)	13.0921(6)	17.4785(18)
b [Å]	10.3876(10)	13.0811(6)	15.0572(16)
c [Å]	40.329(4)	21.0745(15)	20.279(2)
α [°]	90	90.0230(13)	90
β [°]	96.829(2)	90.093(14)	112.9880(10)
γ [°]	90	90.071(9)	90
V [Å ³]	7887.8(13)	3609.2(3)	4913.2(9)
Z	8	2	4
T [K]	100(2)	100(2)	100(2)
ρ _{calcd} [g cm ⁻³]	1.066	1.003	1.156
μ [mm ⁻¹]	1.672	0.353	0.999
F (000)	2736	1200	1824
θ range [°]	2.034/26.464	1.555/22.241	2.051/29.706
unique reflns	16149	13964	13924
collected reflns	53733	17319	84117
R ₁ ^[a] /wR ₂ (I>2θ) ^[b]	0.0433 / 0.0795	0.0894 / 0.2093	0.0349 / 0.0775
R ₁ ^[a] /wR ₂ (all data) ^[b]	0.0685 / 0.0875	0.1113 / 0.2272	0.0520 / 0.0868
GOF ^[c]	0.884	1.037	1.021

$$^{[c]} \text{GOF} = \left[\frac{\sum w(F_o^2 - F_c^2)^2}{(n_o - n_p)} \right]^{1/2}. \quad ^{[a]} \text{RI} = \frac{\sum (|F_o| - |F_c|)}{\sum |F_o|}, F_o > 4\sigma(F_o). \quad ^{[c]} \text{wR2} = \left\{ \frac{\sum [w(F_o^2 - F_c^2)^2]}{\sum [w(F_o^2)]} \right\}^{1/2}.$$

^[d] Metric seems to be tetragonal, but refinement was not possible (wR₂ = 0.70). The crystals had poor quality and only reflections up to 0.93 Å could be collected. Additional disorder was found but could not be resolved reliably due to the missing high resolution data.

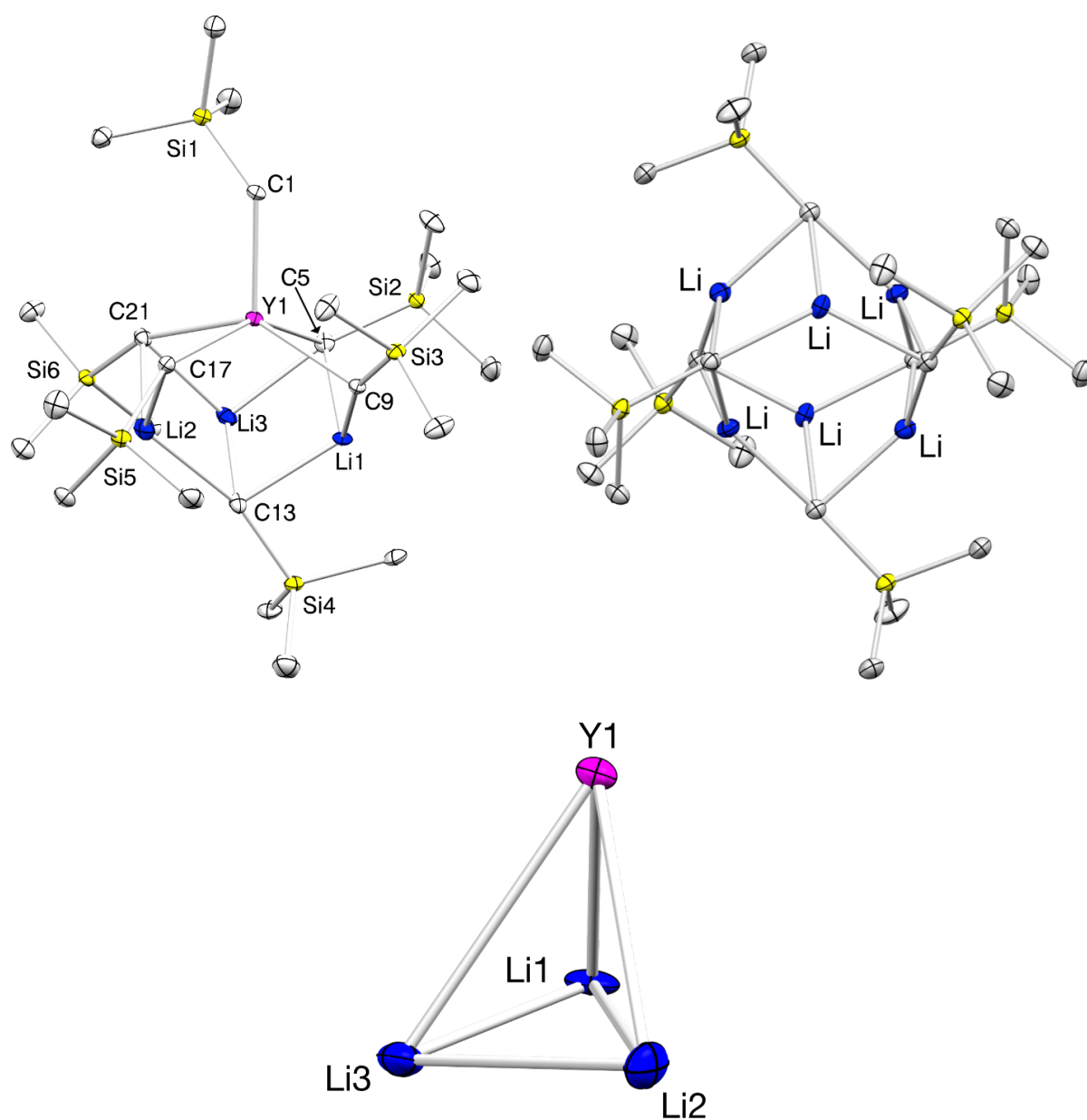


Figure S40. Comparison of the crystal structures of $\text{Li}_3\text{Y}(\text{CH}_2\text{SiMe}_3)_6$ (**1**, left) and hexameric $[\text{LiCH}_2\text{SiMe}_3]_6$ (right) (ellipsoids set to the 50 % probability level, hydrogen atoms omitted for clarity). Selected interatomic distances (Å) and angles (°) for complex **1**: Y1–C1 2.362(6), Y1–C5 2.628(7), Y1–C9 2.515(6), Y1–C17 2.467(7), Y1–C21 2.620(7), Y1–Li1 2.838(10), Y1–Li2 2.846(11), Y1–Li3 2.936(11), Li1–Li3 2.582(15), Li2–Li3 2.670(15), Li1–C5 2.259(14), Li1–C9 2.209(12), Li1–C13 2.244(12), Li2–C13 2.294(12), Li3–C13 2.163(13), Li2–C17 2.155(13), Li2–C21 2.267(13), Li3–C5 2.226(13), C1–Si1 1.842(6), C5–Si2 1.863(7), C9–Si3 1.861(7), C13–Si4 1.855(7), C17–Si5 1.858(7), C21–Si6 1.857(7); Y1–C1–Si1 128.4(3), Y1–C5–Si2 118.8(3), Y1–C5–Li1 70.5(3), Y1–C5–Li3 73.9(3), Y1–C9–Si3 120.3(3), Y1–C9–Li1 73.5(3), Y1–C17–Si5 153.8(4), Y1–C17–Li2 75.7(3), Y1–C21–Si6 159.0(3), Y1–C21–Li2 70.8(3), Y1–C21–Li3 74.6(3), Li1–Y1–Li2 81.0(3), Li1–Li3–Li2 89.3(5). Bottom: Illustration of distorted trigonal pyramid consisting of Li1–Li2–Li3–Y1 subunit of complex **1**.

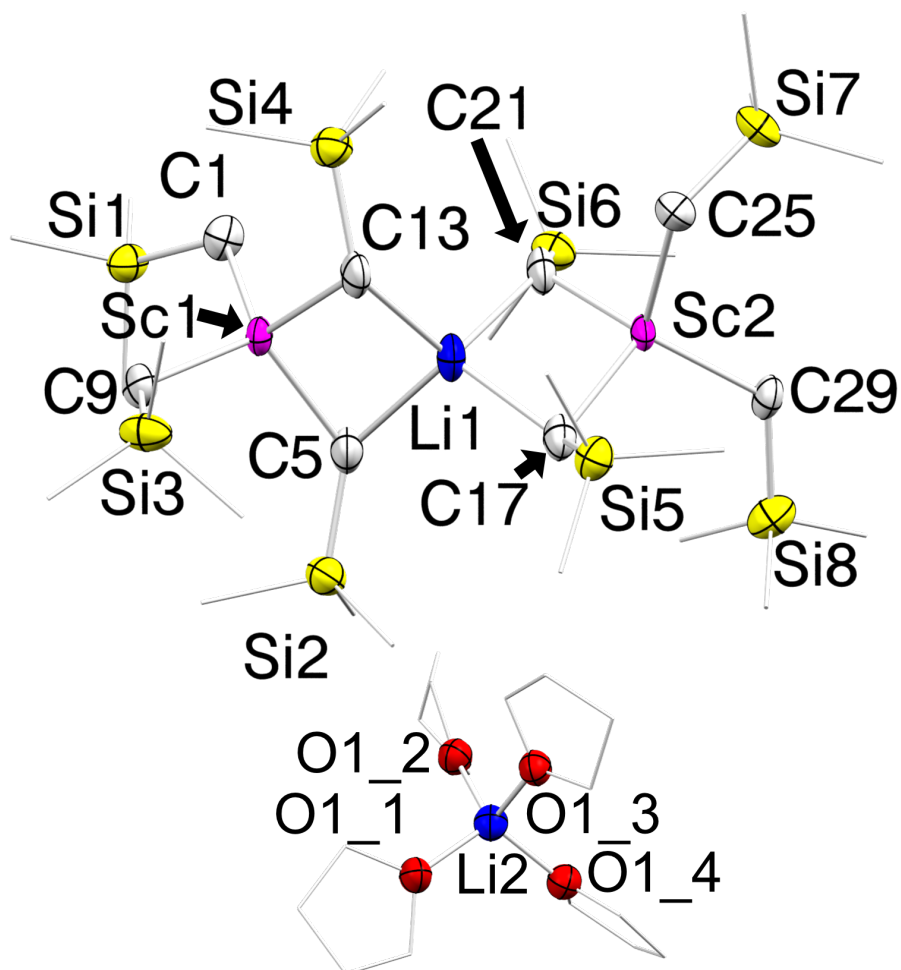


Figure S41. Crystal structure of one of the crystallographically independent molecules of $[\text{Li}(\text{thf})_4][\text{LiSc}_2(\text{CH}_2\text{SiMe}_3)_8]$ (**2**) (ellipsoids set to 50 % probability level). All hydrogen atoms and disorders were omitted for clarity. Carbon atoms of THF and the SiMe_3 groups were rendered as wireframes. Selected interatomic distances (Å) and angles ($^\circ$): Sc1–C1 2.27(3), Sc1–C5 2.344(14), Sc1–C9 2.24(3), Sc1–C13 2.169(14), Sc2–C17 2.190(14), Sc2–C21 2.348(17), Sc2–C25 2.29(3), Sc2–C29 2.22(3), C1–Si1 1.84(3), C5–Si2 1.867(16), C9–Si3 1.80(3), C13–Si4 1.914(14), C17–Si5 1.891(15), C21–Si6 1.882(18), C25–Si7 1.78(3), C29–Si8 1.87(3), Sc1 \cdots Li1 2.80(2), Sc2 \cdots Li1 2.82(2), Li2–O1_1 1.82(3), Li2–O1_2 1.92(4), Li2–O1_3 1.87(4), Li2–O1_4 1.89(4); Sc1–C1–Si1 119.7(15), Sc1–C5–Si2 132.4(7), Sc1–C9–Si3 125.5(16), Sc1–C13–Si4 112.8(7), Sc2–C17–Si5 113.2(6), Sc2–C21–Si6 129.4(8), Sc2–C25–Si7 121.7(18), Sc2–C29–Si8 123.3(14), Sc1–Li1–Sc2 165.7(10).

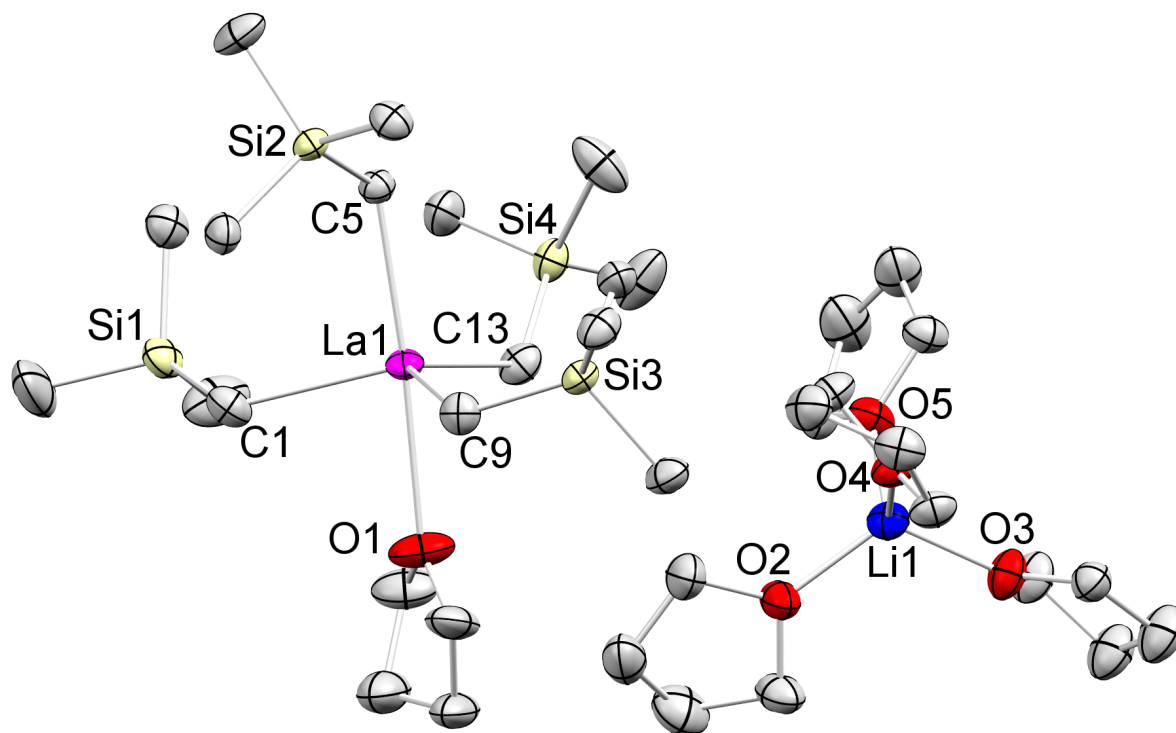


Figure S42. Crystal structure of $[\text{Li}(\text{thf})_4][\text{La}(\text{CH}_2\text{SiMe}_3)_4(\text{thf})]$ (**3**) (ellipsoids set to 50% probability level). Hydrogen atoms and disorders of the THF groups are omitted for clarity. Selected interatomic distances (Å) and angles (°): La1–C1 2.598(3), La1–C5 2.605(2), La1–C9 2.605(2), La1–C13 2.614(2), La1–O1 2.6895(18), C5–La1–O1 176.18(7), C1–La1–C5 96.29(8), C9–La1–C5 97.48(7), C13–La1–C5 104.11(8), C1–La1–C9 111.84(8), C9–La1–C13, 121.47(8), C1–La1–C13 118.72(8).

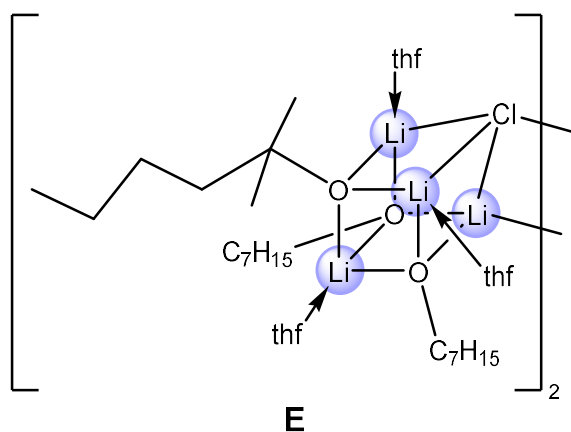
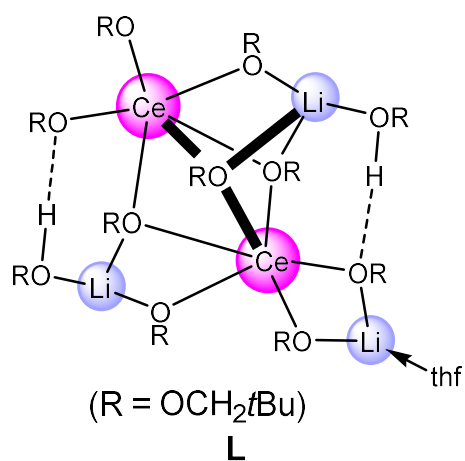
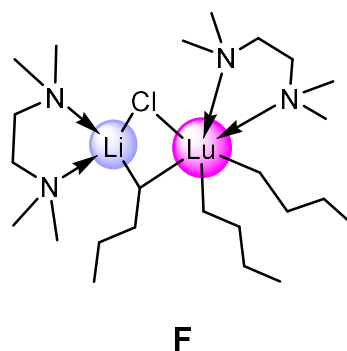
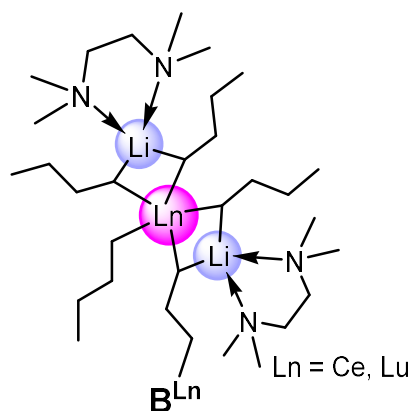
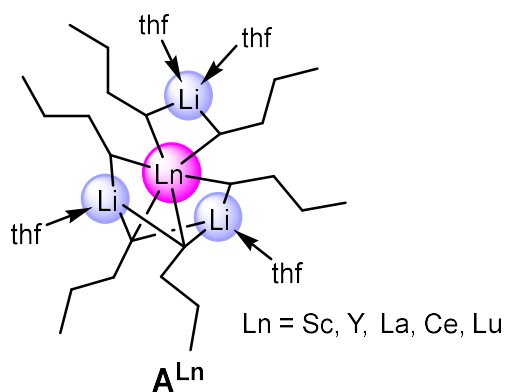
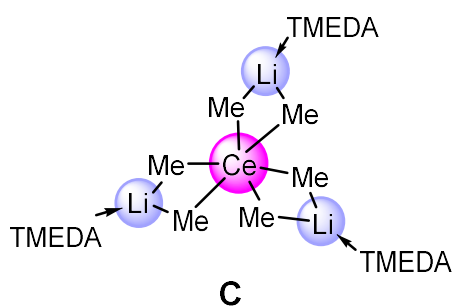
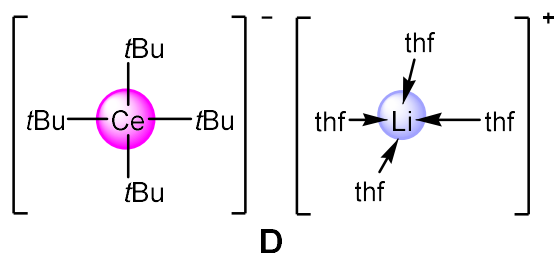
F

Appendix

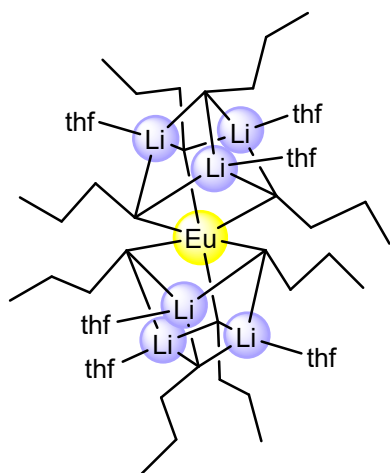
Structurally characterized complexes

On the following pages all X-ray structurally characterized compounds are listed as *ChemDraw* sketches.

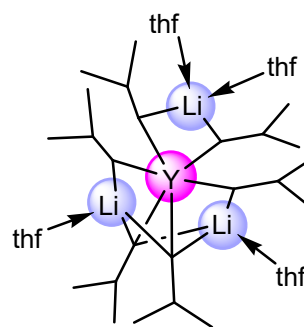
Paper I



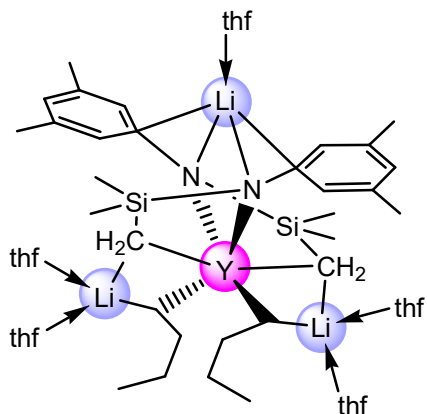
Paper II



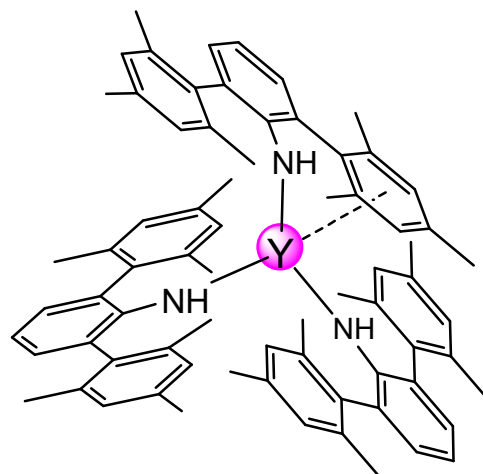
M



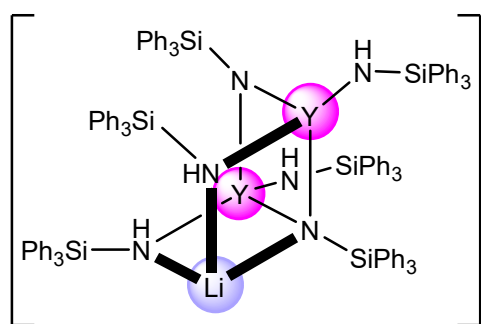
N



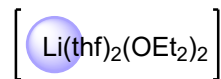
O



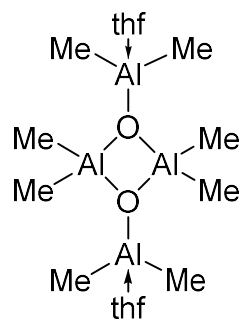
P



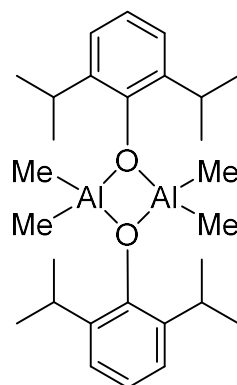
Q



Paper III

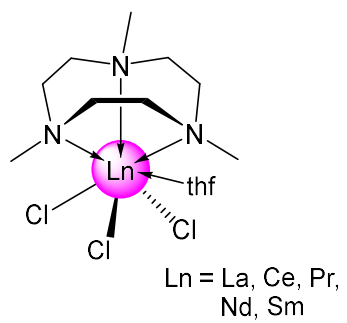


J

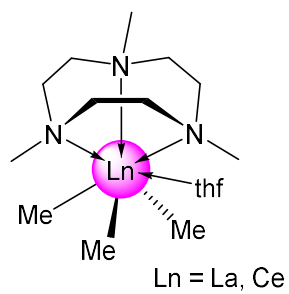


K

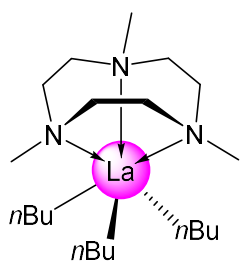
Paper IV



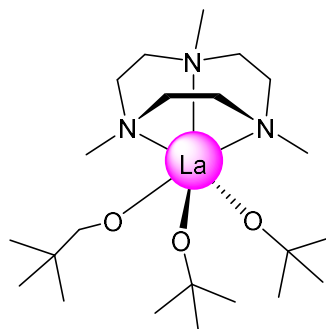
R



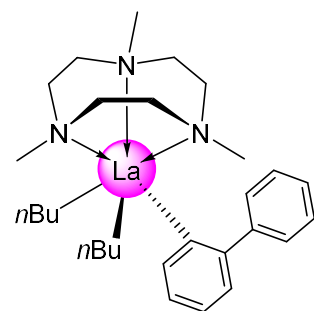
S



G^{Ln}

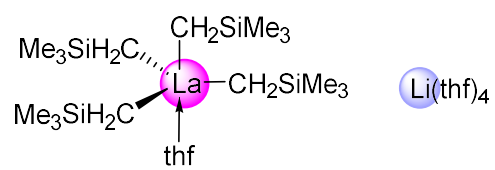


T



H

Paper V



I

Unpublished results

